

SUPRAMOLECULAR INTERACTIONS  
FROM SMALL-MOLECULE SELECTIVITY TO MOLECULAR CAPSULES

by

ARBIN RAJBANSHI

M.S., Tribhuvan University, Nepal, 2002

AN ABSTRACT OF A DISSERTATION

submitted in partial fulfillment of the requirements for the degree

DOCTOR OF PHILOSOPHY

Department of Chemistry  
College of Arts and Sciences

KANSAS STATE UNIVERSITY  
Manhattan, Kansas

2010

## Abstract

Supramolecular synthesis relies upon the creative and rational use of the common intermolecular forces and a proper understanding of these forces is critical for design and assembly of molecular building blocks into extended networks. The strength of seven substituted pyridines as hydrogen-bond acceptors was probed using a series of fifteen mono/dicarboxylic acids to demonstrate the interrelationship between the charge on the substrate and its ability to form co-crystals/salts. The higher charge in the acceptor led to proton transfer (100% yield) from the hydrogen bond donor to give a salt, whereas the lower charge led to co-crystals. This specificity observed for small molecules was extended to an investigation of selectivity in ditopic molecules. A series of nineteen hydrogen-bond donors, including fifteen carboxylic acids and four cyanoximes, were tested for binding preferences against ten ditopic ligands with variable charges. The overall supramolecular yield of 82% (9/11) proved a high degree of reliability in terms of best acceptor/donor approach, hence establishing the efficiency of the calculated charges as a guideline for molecular recognition processes.

Solubility and thermal properties of pharmaceutical drug mimics were altered via formation of co-crystals/salts. The ligands and their co-crystals/salts with five even-chain dicarboxylic acids were synthesized and their comparative solubility in pure water and in pH 6.8 buffer solution measured. Solubility enhancement to a degree of 9x is observed for pharmaceutical drug haloperidol, whereas decrease in solubility down to 81% is achieved for 2-amino-5-(3-pyridyl)pyrimidine (which has agrochemical significance). Also the thermal and solubility behavior of these co-crystals were shown to reflect the properties of their parent co-crystallizing agents, allowing for a modulation of physical properties.

Finally, the specificity and selectivity of the intermolecular interactions observed for small molecules were applied in the synthesis of hydrogen and halogen-bonded capsules. Several resorcinarene-based cavitands were synthesized and their upper rim decorated with acetamidopyridyl, aminopyrazinyl, 3-pyridyl, and 4-pyridyl moieties with hydrogen and halogen-bonding potentials. A homomeric hydrogen-bonded capsule was

formed with self-assembly of acetamidoethynylcavitand via N-H $\cdots$ O=C interactions, whereas a heteromeric halogen-bonded capsule, the very first of its kind, was formed with N $\cdots$ I halogen-bonded interaction between 3-pyridylcavitand and tetrafluoroiodo-substituted calixarene.

SUPRAMOLECULAR INTERACTIONS  
FROM SMALL-MOLECULE SELECTIVITY TO MOLECULAR CAPSULES

by

ARBIN RAJBANSHI

M.S., Tribhuvan University, Nepal, 2002

A DISSERTATION

submitted in partial fulfillment of the requirements for the degree

DOCTOR OF PHILOSOPHY

Department of Chemistry  
College of Arts and Sciences

KANSAS STATE UNIVERSITY  
Manhattan, Kansas

2010

Approved by:

Major Professor  
Prof. Christer B. Aakeröy

## Abstract

Supramolecular synthesis relies upon the creative and rational use of the common intermolecular forces and a proper understanding of these forces is critical for design and assembly of molecular building blocks into extended networks. The strength of seven substituted pyridines as hydrogen-bond acceptors was probed using a series of fifteen mono/dicarboxylic acids to demonstrate the interrelationship between the charge on the substrate and its ability to form co-crystals/salts. The higher charge in the acceptor led to proton transfer (100% yield) from the hydrogen bond donor to give a salt, whereas the lower charge led to co-crystals. This specificity observed for small molecules was extended to an investigation of selectivity in ditopic molecules. A series of nineteen hydrogen-bond donors, including fifteen carboxylic acids and four cyanoximes, were tested for binding preferences against ten ditopic ligands with variable charges. The overall supramolecular yield of 82% (9/11) proved a high degree of reliability in terms of best acceptor/donor approach, hence establishing the efficiency of the calculated charges as a guideline for molecular recognition processes.

Solubility and thermal properties of pharmaceutical drug mimics were altered via formation of co-crystals/salts. The ligands and their co-crystals/salts with five even-chain dicarboxylic acids were synthesized and their comparative solubility in pure water and in pH 6.8 buffer solution measured. Solubility enhancement to a degree of 9x is observed for pharmaceutical drug haloperidol, whereas decrease in solubility down to 81% is achieved for 2-amino-5-(3-pyridyl)pyrimidine (which has agrochemical significance). Also the thermal and solubility behavior of these co-crystals were shown to reflect the properties of their parent co-crystallizing agents, allowing for a modulation of physical properties.

Finally, the specificity and selectivity of the intermolecular interactions observed for small molecules were applied in the synthesis of hydrogen and halogen-bonded capsules. Several resorcinarene-based cavitands were synthesized and their upper rim decorated with acetamidopyridyl, aminopyrazinyl, 3-pyridyl, and 4-pyridyl moieties with

hydrogen and halogen-bonding potentials. A homomeric hydrogen-bonded capsule was formed with self-assembly of acetamidoethynylcavitand via N-H $\cdots$ O=C interactions, whereas a heteromeric halogen-bonded capsule, the very first of its kind, was formed with N $\cdots$ I halogen-bonded interaction between 3-pyridylcavitand and tetrafluoroiodo-substituted calixarene.

# Table of Contents

List of Figures .....	xvii
List of Tables .....	xxvii
Acknowledgements .....	xxxii
Dedication .....	xxxii
CHAPTER 1 - Supramolecular assembly and molecular recognition .....	1
1.1 Supramolecular Chemistry .....	1
1.1.1 Crystal Engineering .....	2
1.1.2 What is a hydrogen bond? .....	3
1.1.3 What is a halogen bond? .....	3
1.1.4 Synthons .....	4
1.2 Guidelines for hydrogen-bond driven synthesis .....	5
1.2.1 Co-crystals as a way of probing molecular interactions .....	5
1.2.2 Binary and ternary co-crystals .....	6
1.2.3 Establishing the hydrogen-bonding hierarchy .....	8
1.3 Changing properties of specialty chemicals via co-crystallization .....	10
1.3.1 Dissolution advantage .....	11
1.3.2 Hygroscopicity improvement .....	11
1.4 Hydrogen and halogen bonded cavitands .....	12
1.4.1 Molecular capsules .....	12
1.4.2 Calixarene capsules .....	13
1.4.3 Cavitand capsules .....	15
1.5 Goals .....	17
CHAPTER 2 - Mapping out the synthetic landscape of recrystallization, co-crystallization and salt formation .....	23
2.1 Introduction .....	23
2.2 Experimental .....	25
2.2.1 Synthesis of pyridyl compounds .....	26
2.2.1.1 Synthesis of 2-acetamidopyridine, <b>3</b> .....	26
2.2.1.2 Synthesis of 2-propioamido-5-bromopyridine, <b>4</b> .....	26

2.2.1.3 Synthesis of 2-acetamido-5-bromopyridine, <b>6</b> .....	27
2.2.1.4 Synthesis of 2-acetamido-3,5-dibromopyridine, <b>7</b> .....	27
2.2.2 Synthesis of co-crystals and salts.....	28
2.2.2.1 Synthesis of 2-aminopyridinium 4-cyanobenzoate, <b>1a</b> .....	28
2.2.2.2 Synthesis of 2-aminopyridinium 4-chlorobenzoate, <b>1c</b> .....	29
2.2.2.3 Synthesis of 2-aminopyridinium 2,6-difluorobenzoate, <b>1g</b> .....	29
2.2.2.4 Synthesis of 2-aminopyridinium pentafluorobenzoate, <b>1j</b> .....	29
2.2.2.5 Synthesis of bis(2-aminopyridinium) suberate, <b>1k</b> .....	29
2.2.2.6 Synthesis of bis(2-aminopyridinium) succinate, <b>1n</b> .....	30
2.2.2.7 Synthesis of bis(2-aminopyridinium) sebacate, <b>1o</b> .....	30
2.2.2.8 Synthesis of 2-amino-5-bromopyridinium 4-cyanobenzoate, <b>2a</b> .....	30
2.2.2.9 Synthesis of 2-amino-5-bromopyridinium 4-nitrobenzoate, <b>2e</b> .....	30
2.2.2.10 Synthesis of 2-acetamidopyridine/succinic acid (2:1), <b>3n</b> .....	30
2.2.2.11 Synthesis of 2-propiamido-5-bromopyridine/3,4-dichlorobenzoic acid (1:1), <b>4f</b> .....	31
2.2.2.12 Synthesis of 2-propiamido-5-bromopyridine/suberic acid (2:1), <b>4k</b> .....	31
2.2.2.13 Synthesis of 2-propiamido-5-bromopyridine/fumaric acid (2:1), <b>4m</b> .....	31
2.2.2.14 Synthesis of 2-propiamido-5-bromopyridine/succinic acid (2:1), <b>4n</b> .....	31
2.2.2.15 Synthesis of 2-propiamido-5-bromopyridine/sebacic acid (2:1), <b>4o</b> .....	32
2.2.2.16 Synthesis of 2-amino-3,5-dibromopyridine/3,5-dinitrobenzoic acid (1:1), <b>5i</b> .....	32
2.2.2.17 Synthesis of 2-amino-3,5-dibromopyridine/fumaric acid (2:1), <b>5m</b> .....	32
2.2.2.18 Synthesis of 2-acetamido-5-bromopyridine/succinic acid (2:1), <b>6n</b> .....	32
2.2.3 Electrostatic charges calculations .....	33
2.2.4 Single Crystal X-ray Crystallography.....	34
2.3 Results.....	34
2.3.1 Crystal structure of 2-propiamido-5-bromopyridine, <b>4</b> .....	39
2.3.2 Crystal structure of 2-acetamido-5-bromopyridine, <b>6</b> .....	39
2.3.3 Crystal structures of <b>1a</b> , <b>1c</b> , <b>1g</b> , <b>1j</b> , <b>1k</b> , and <b>1o</b> .....	41
2.3.4 Crystal structure of bis(2-aminopyridinium) succinate succinic acid, <b>1n</b> .....	43
2.3.5 Crystal structure of 2-amino-5-bromopyridinium 4-cyanobenzoate, <b>2a</b> .....	44



2.3.6	Crystal structure of 2-amino-5-bromopyridinium 4-nitrobenzoate, <b>2e</b> .....	45
2.3.7	Crystal structures of <b>3n</b> , <b>4f</b> , <b>4k</b> , <b>4o</b> , and <b>6n</b> .....	47
2.3.8	Crystal structures of <b>4m</b> and <b>4n</b> .....	49
2.3.9	Crystal structure of 2-amino-3,5-dibromopyridine/3,5-dinitrobenzoic acid, <b>5i</b> .....	50
2.3.10	Crystal structure of 2-amino-3,5-dibromopyridine/fumaric acid, <b>5m</b> .....	51
2.4	Discussion.....	52
2.4.1	Analysis of pyridine-carboxylic acid salts and co-crystals through FT-IR spectroscopy.....	52
2.4.2	Single crystal X-ray analysis of pyridine-carboxylic acid salts and co-crystals .....	54
2.4.3	Secondary hydrogen bonding and halogen bonding motifs.....	57
2.5	Conclusions.....	59
CHAPTER 3 - Measuring binding energies in solution using Isothermal Titration Calorimetry (ITC).....		
	Calorimetry (ITC).....	61
3.1	Introduction.....	61
3.1.1	Correlating solid-state binding with solution behavior.....	61
3.1.2	Isothermal Titration Calorimetry .....	62
3.2	Experimental.....	63
3.2.1	Electrostatic charges calculations .....	63
3.2.2	Synthesis of 2-acetamidopyridine.....	65
3.2.3	Co-crystal screening via IR spectroscopy.....	65
3.2.4	Single Crystal X-ray Crystallography.....	65
3.2.5	Instrumentation .....	66
3.2.6	General experimental procedure for binding studies by ITC.....	67
3.2.6.1	Binding study of 2-acetamidopyridine and benzoic acid.....	68
3.2.6.2	Binding study of 2-acetamidopyridine and 3-chlorobenzoic acid .....	68
3.2.6.3	Binding study of 2-acetamidopyridine and 3-(N,N-dimethyl)aminobenzoic acid.....	69
3.3	Results.....	69
3.3.1	Single crystal X-ray analysis of 2-acetamidopyridine : 3-N,N-dimethylbenzoic acid (1:1) .....	69

3.3.2 ITC spectra for thermodynamic study of dilution of 2-acetamidopyridine .....	69
3.3.3 ITC spectra for thermodynamic study of 2-acetamidopyridine and various benzoic acids.....	70
3.4 Discussion.....	72
3.4.1 Thermodynamic explanations for the co-crystal formation.....	72
3.5 Conclusions.....	75
CHAPTER 4 - Ditopic ligands as a probe to investigate selectivity in binary co-crystals/salts.....	78
4.1 Introduction.....	78
4.1.1 Selectivity prediction via AM1 calculations.....	79
4.1.2 Research goals .....	81
4.2 Experimental.....	83
4.2.1 Synthesis of ligands .....	83
4.2.1.1 Synthesis of 3-pyridylboronic acid, <b>8</b> .....	84
4.2.1.2 Synthesis of 2-amino-5-bromopyrimidine, <b>9</b> .....	84
4.2.1.3 Synthesis of 2-amino-5-(3-pyridyl)pyrimidine, <b>10</b> .....	85
4.2.1.4 Synthesis of 2-amino-4-methyl-5-bromopyrimidine, <b>11</b> .....	86
4.2.1.5 Synthesis of 2-amino-4-methyl-5-(3-pyridyl)pyrimidine, <b>12</b> .....	86
4.2.1.6 Synthesis of 2-amino-5-bromopyrazine, <b>13</b> and 2-amino-3,5-dibromopyrazine, <b>14</b> .....	87
4.2.1.7 Synthesis of 2-amino-5-(3-pyridyl)pyrazine, <b>15</b> .....	88
4.2.1.8 Synthesis of 2-acetamido-5-(3-pyridyl)pyridine, <b>16</b> .....	88
4.2.1.9 Synthesis of 2-acetamido-5-bromopyrimidine, <b>17</b> .....	89
4.2.1.10 Synthesis of 2-acetamido-5-(3-pyridyl)pyrimidine, <b>18</b> .....	90
4.2.1.11 Synthesis of 3-trimethylsilanylethynylpyridine, <b>19</b> .....	90
4.2.1.12 Synthesis of 3-ethynylpyridine, <b>20</b> .....	91
4.2.1.13 Synthesis of 2-acetamido-5-(3-pyridyl)ethynylpyridine, <b>21</b> .....	91
4.2.1.14 Synthesis of 2-amino-5-trimethylsilanylethynylpyridine, <b>22</b> .....	92
4.2.1.15 Synthesis of 2-amino-5-ethynylpyridine, <b>23</b> .....	93
4.2.1.16 Synthesis of 2-acetamido-5-(3-(2-aminopyridyl))ethynylpyridine, <b>24</b> ... 93	
4.2.1.17 Synthesis of 2-acetamido-5-trimethylsilanylethynylpyridine, <b>25</b> .....	95

4.2.1.18 Synthesis of 2-acetamido-5-ethynylpyridine, <b>26</b> .....	95
4.2.1.19 Synthesis of 2-amino-5-(3-(2-acetamidopyridyl))ethynylpyrazine, <b>27</b> ..	96
4.2.1.20 Synthesis of 2-acetamido-5-bromopyrazine, <b>28</b> .....	97
4.2.1.21 Synthesis of 2-acetamido-5-(3-(2-acetamidopyridyl))ethynylpyrazine, <b>29</b> .....	97
4.2.1.23 Synthesis of 2-amino-5-trimethylsilanylethynylpyrimidine, <b>30</b> .....	98
4.2.1.24 Synthesis of 2-amino-5-trimethylsilanylethynylpyrazine, <b>31</b> .....	99
4.2.1.25 Synthesis of 2-amino-5-(3-(2-aminopyrazino))ethynylpyrimidine, <b>32</b> ..	99
4.2.2 Synthesis of co-crystals and salts .....	101
4.2.2.1 Synthesis of 2-amino-5-(3-pyridyl)pyrimidine/4-chlorobenzoic acid (1:1), <b>10c</b> .....	101
4.2.2.2 Synthesis of 2-amino-5-(3-pyridinium)pyrimidine pentafluorobenzoate, <b>10j</b> .....	101
4.2.2.3 Synthesis of 2-amino-5-(3-pyridyl)pyrimidine/suberic acid (2:1), <b>10k</b> .	102
4.2.2.4 Synthesis of 2-amino-5-(3-pyridyl)pyrimidine/succinic acid (2:1), <b>10n</b>	102
4.2.2.5 Synthesis of 2-amino-5-(3-pyridyl)pyrimidine/sebacic acid (2:1), <b>10o</b> .	102
4.2.2.6 Synthesis of 2-amino-5-(3-pyridyl)pyrimidine/2-chlorocyanoxime (1:1), <b>10r</b> .....	102
4.2.2.7 Synthesis of 2-amino-4-methyl-5-(3-pyridyl)pyrimidine/succinic acid (2:1), <b>12n</b> .....	102
4.2.2.8 Synthesis of 2-amino-5-(3-pyridyl)pyrazine/4-nitrobenzoic acid (1:1), <b>15e</b> .....	103
4.2.2.9 Synthesis of 2-acetamido-5-(3-pyridyl)pyridine/cyanoxime (1:1), <b>16p</b> .	103
4.2.2.10 Synthesis of 2-amino-5-(3-(2-acetamido)pyridyl)ethynylpyridinium 3,5- dimethyl benzoate/ 3,5-dimethylbenzoic acid (1:1), <b>24h</b> .....	103
4.2.2.11 Synthesis of 2-amino-5-(3-(2-acetamido)pyridyl)ethynylpyridinium phthalate, <b>24l</b> .....	103
4.2.2.12 Synthesis of 2-amino-5-(3-(2-acetamido)pyridyl)ethynylpyrazine/3,5- dinitrobenzoic acid (1:1), <b>27i</b> .....	104
4.2.3 Electrostatic charges calculations .....	104
4.2.4 Single Crystal X-ray Crystallography .....	104

4.3 Results and Discussion .....	105
4.3.1 Characterization by FT-IR .....	105
4.3.2 Crystal Structures .....	108
4.3.2.1 Crystal structure of <b>10</b> and <b>12</b> .....	112
4.3.2.2 Crystal structure of 2-amino-5-(3-pyridyl)pyrazine, <b>15</b> .....	113
4.3.2.3 Crystal structure of 2-acetamido-5-(3-pyridyl)pyridine, <b>16</b> .....	113
4.3.2.4 Crystal structure of 2-acetamido-5-(3-pyridyl)ethynylpyridine, <b>21</b> .....	113
4.3.2.5 Crystal structure of 2-amino-5-(3-(2-acetamido)pyridyl)ethynylpyridine, <b>24</b> .....	114
4.3.2.6 Crystal structure of 2-amino-5-(3-(2-acetamido)pyridyl)ethynylpyrazine, <b>27</b> .....	114
4.3.2.7 Crystal structure of 2-amino-5-(3-pyridyl)pyrimidine/4-chlorobenzoic acid (1:1), <b>10c</b> .....	116
4.3.2.8 Crystal structure of 2-amino-5-(3-pyridinium)pyrimidine pentafluorobenzoate, <b>10j</b> .....	116
4.3.2.9 Crystal structure of <b>10k</b> and <b>10o</b> .....	117
4.3.2.10 Crystal structure of 2-amino-5-(3-pyridyl)pyrimidine/2-chlorocyanoxime (1:1), <b>10r</b> .....	118
4.3.2.11 Crystal structure of 2-amino-5-(3-pyridyl)pyrimidine/succinic acid (2:1), <b>10n</b> .....	119
4.3.2.12 Crystal structure of 2-amino-4-methyl-5-(3-pyridyl)pyrimidine/succinic acid (2:1), <b>12n</b> .....	120
4.3.2.13 Crystal structure of 2-amino-5-(3-pyridyl)pyrazine/4-nitrobenzoic acid (1:1), <b>15e</b> .....	121
4.3.2.14 Crystal structure of 2-acetamido-5-(3-pyridyl)pyridine/cyanoxime (1:1), <b>16p</b> .....	121
4.3.2.15 Crystal structure of 2-amino-5-(3-(2- acetamido)pyridyl)ethynylpyridinium 3,5-dimethylbenzoate/3,5-dimethylbenzoic acid (1:1), <b>24h</b> .....	122
4.3.2.16 Crystal structure of 2-amino-5-(3-(2- acetamido)pyridyl)ethynylpyridinium phthalate, <b>24l</b> .....	123

4.3.2.17 Crystal structure of 2-amino-5-(3-(2-acetamido)pyridyl)ethynylpyrazine /3,5-dinitrobenzoic acid (1:1), <b>27i</b> .....	123
4.3.3 Selectivity in the context of electrostatic potentials .....	124
4.3.4 Validity of Q values .....	128
4.5 Conclusions.....	130
CHAPTER 5 - Solubility enhancement via co-crystallization/salt-formation.....	132
5.1 Introduction.....	132
5.1.1 Co-crystal solubility ( $S_{cc}$ ) and solubility product ( $K_{sp}$ ).....	133
5.1.2 Research Goals.....	134
5.2 Experimental.....	136
5.2.1 Synthesis of APIs.....	136
5.2.2 Synthesis of co-crystals and salts.....	137
5.2.2.1 Synthesis of 2-acetamido-5-bromopyridine/succinic acid (2:1), <b>SR1-a</b> .....	137
5.2.2.2 Synthesis of 2-acetamido-5-bromopyridine/dodecanedioic acid (2:1), <b>SR1-e</b> .....	138
5.2.2.3 Synthesis of 2-propiamido-5-bromopyridine/succinic acid (2:1), <b>SR2-a</b> .....	138
5.2.2.4 Synthesis of 2-propiamido-5-bromopyridine/adipic acid (2:1), <b>SR2-b</b> .....	138
5.2.2.5 Synthesis of 2-propiamido-5-bromopyridine/suberic acid (2:1), <b>SR2-c</b> .....	138
5.2.2.6 Synthesis of 2-propiamido-5-bromopyridine/sebacic acid (2:1), <b>SR2-d</b> .....	139
5.2.2.7 Synthesis of 2-propiamido-5-bromopyridine/dodecanedioic acid (2:1), <b>SR2-e</b> .....	139
5.2.2.8 Synthesis of 2-amino-5-(3-pyridyl)pyrimidine/succinic acid (2:1), <b>SR3-a</b> .....	139
5.2.2.9 Synthesis of 2-amino-5-(3-pyridyl)pyrimidine/adipic acid (2:1), <b>SR3-b</b> .....	140
5.2.2.10 Synthesis of 2-amino-5-(3-pyridyl)pyrimidine/suberic acid (2:1), <b>SR3-c</b> .....	140
5.2.2.10 Synthesis of 2-amino-5-(3-pyridyl)pyrimidine/sebacic acid (2:1), <b>SR3-d</b> .....	140
5.2.2.11 Synthesis of 2-amino-5-(3-pyridyl)pyrimidine/dodecanedioic acid (2:1), <b>SR3-e</b> .....	140
5.2.2.12 Synthesis of haloperidol/succinate-suberic acid (1:1:1), <b>SR4-c</b> .....	141

5.2.3 Solubility studies.....	141
5.2.3.1 Determination of solubility standard curve for the ligand.....	141
5.2.3.2 Determination of solubility of co-crystals/salts.....	142
5.2.4 Single crystal X-ray crystallography.....	142
5.3 Results and Discussion.....	143
5.3.1 Crystal Structures.....	143
5.3.1.1 Crystal structure of APIs <b>SR1</b> , <b>SR2</b> , and <b>SR3</b> .....	146
5.3.1.2 Crystal structure of haloperidol, <b>SR4</b> .....	147
5.3.1.3 Crystal structures of <b>SR1-a</b> , <b>SR1-e</b> , <b>SR2-c</b> , <b>SR2-d</b> , and <b>SR2-e</b> .....	149
5.3.1.4 Crystal structures of <b>SR2-a</b> and <b>SR2-b</b> .....	150
5.3.1.5 Crystal structures of <b>SR3-a</b> .....	152
5.3.1.6 Crystal structures of <b>SR3-b</b> , <b>SR3-c</b> , <b>SR3-d</b> , and <b>SR3-e</b> .....	153
5.3.1.7 Crystal structures of <b>SR4-c</b> .....	155
5.3.2 Standard curves for the dissolution of API mimics.....	156
5.3.2.1 Standard curve for dissolution of <b>SR1</b> in deionized water.....	156
5.3.2.2 Standard curve for dissolution of <b>SR2</b> in deionized water.....	157
5.3.2.3 Standard curve for dissolution of <b>SR3</b> in pH 6.8 buffer.....	157
5.3.2.4 Standard curve for dissolution of <b>SR4</b> in pH 6.8 buffer solution.....	158
5.3.3 Equilibrium dissolution studies.....	158
5.3.3.1 Equilibrium dissolution of 2-acetamido-5-bromopyridine <b>SR1</b> co-crystals in water.....	158
5.3.3.2 Equilibrium dissolution of 2-propionamido-5-bromopyridine <b>SR2</b> co-crystals in water.....	159
5.3.3.3 Equilibrium dissolution of 2-amino-5-(3-pyridyl)pyrimidine <b>SR3</b> co- crystals in pH 6.8 buffer solution.....	161
5.3.3.4 Equilibrium dissolution of haloperidol <b>SR4</b> salts in pH 6.8 buffer solution .....	162
5.3.4 Effect of co-crystallizing agent properties on co-crystals and salts.....	164
5.4 Conclusions.....	166
CHAPTER 6 - From molecular recognition in cavitands to hydrogen and halogen-bonded capsules.....	169

6.1 Introduction.....	169
6.1.1 Hydrogen bonded cavitands.....	172
6.1.2 Halogen bonded cavitands .....	172
6.1.3 Research Goals.....	173
6.2 Experimental.....	174
6.2.1 Synthesis .....	174
6.2.1.1 Synthesis of C-pentylcalix[4]resorcinarene, <b>33</b> .....	174
6.2.1.2 Synthesis of C-pentyltetrabromocalix[4]resorcinarene, <b>34</b> .....	175
6.2.1.3 Synthesis of C-pentyltetrabromocavitand, <b>35</b> <sup>42</sup> .....	176
6.2.1.4 Synthesis of C-pentyltetraiodocavitand, <b>36</b> .....	177
6.2.1.5 Synthesis of C-pentyltetra-(2-acetamidopyridyl-5-ethynyl)cavitand, <b>37</b>	178
6.2.1.6 Synthesis of C-pentyl-1,3-di-(2-acetamidopyridyl-5-ethynyl)-2,4- dibromocavitand, <b>38</b> .....	179
6.2.1.7 Synthesis of C-pentyl-1,3-di(2-aminopyrazino-5-ethynyl)-2,4- diiodocavitand, <b>39</b> .....	180
6.2.1.8 Synthesis of C-pentyltetra(3-pyridyl)cavitand, <b>40</b> .....	181
6.2.1.9 Synthesis of C-pentyltetra(4-pyridyl)cavitand, <b>41</b> .....	181
6.2.2 Co-crystallizations of cavitands.....	182
6.2.2.1 Synthesis of tetra(2-acetamidopyridyl-5-ethynyl)cavitand co-crystals ..	182
6.2.2.2 Synthesis of C-pentyl-tetra(3-pyridyl)cavitand/1,4-diiodo- tetrafluorobenzene (1:2), <b>40a</b> .....	184
6.2.2.3 Synthesis of C-pentyl-tetra(4-pyridyl)cavitand/1,4-diiodo- tetrafluorobenzene (1:2), <b>41a</b> .....	185
6.2.2.4 Synthesis of C-pentyl-tetra(3-pyridyl)cavitand/halocalixarene (1:1), <b>40b</b> .....	185
6.3 Results and Discussion .....	185
6.3.1 Precursors and their functionalization .....	185
6.3.1.1 Crystal structure of C-pentyltetrabromocavitand, <b>35</b> .....	187
6.3.1.2 Crystal structure of C-pentyltetraiodocavitand, <b>36</b> .....	189
6.3.2 Quest for a hydrogen-bond driven capsule .....	191

6.3.2.1 Crystal structure of C-pentyltetra(2-acetamidopyridyl-5-ethynyl)cavitand, <b>37</b> .....	191
6.3.2.2 Crystal structure of C-pentyl-1,3-di(2-acetamidopyridyl-5-ethynyl)-2,4-dibromocavitand, <b>38</b> .....	194
6.3.3 Quest for halogen-bonded capsule.....	195
6.3.3.1 Crystal structure of C-pentyltetra(4-pyridyl)cavitand, <b>41</b> .....	195
6.3.3.2 Crystal structure of C-pentyltetra-(3-pyridyl)cavitand/1,4-diiidotetrafluorobenzene, <b>40a</b> .....	197
6.3.3.3 Crystal structure of C-pentyltetra-(4-pyridyl)cavitand/1,4-diiidotetrafluorobenzene, <b>41a</b> .....	198
6.3.3.4 Crystal structure of C-pentyltetra-(3-pyridyl)cavitand/calixarene, <b>40b</b> .	199
6.4 Conclusions.....	201
Appendix A - Crystal Structure Data.....	206
Appendix B - <sup>1</sup> H, <sup>13</sup> C NMR, and Mass Data.....	261



## List of Figures

Figure 1.1 Assembly of larger structures from smaller building blocks.....	1
Figure 1.2 Schematic of molecular recognition in smaller molecules to build larger structures. ....	2
Figure 1.3 General scheme for the formation of halogen bonds. <sup>12</sup> .....	3
Figure 1.4 Halogen bonding via N...I interactions.....	4
Figure 1.5 Examples of supramolecular synthons. ....	5
Figure 1.6 Schematic of re-crystallization (homomeric interaction) vs co-crystallization (heteromeric interaction).....	5
Figure 1.7 Hydrogen-bonded binary co-crystals .....	7
Figure 1.8 Ternary hydrogen-bonded co-crystal between isonicotinamide, 3,5-dinitrobenzoic acid, and 3,4-dimethoxycinnamic acid. ....	7
Figure 1.9 Schematic of the best hydrogen bond donor ( $D_1$ ) binding with best hydrogen bond acceptor ( $A_1$ ) and the second best hydrogen bond donor ( $D_2$ ) with second best hydrogen bond acceptor ( $A_2$ ). <sup>29</sup> .....	8
Figure 1.10 Molecular electrostatic potential surface of 2-amino-5-bromopyridine, calculated by using AM1 and a positive charge in vacuum as probe; blue (positive regions, $E_{\max}$ ), red (negative regions, $E_{\min}$ ), and green (neutral regions).....	10
Figure 1.11 Trimer unit of the itraconazole-succinic acid co-crystal. <sup>44</sup> .....	11
Figure 1.12 Self-assembling glycoluril-based dimeric capsules; <sup>53</sup> (a) “tennis ball” and (b) “softball” .....	12
Figure 1.13 (a) Homodimeric hydrogen-bonded capsule with carboxylic acid rim substituents (R = propyl); (b) Heterodimeric capsule with hydrogen bonding between a pyridyl functionalized monomer and a complementary carboxylic acid functionalized monomer, (R = octyl); (c) Urea-functionalized homodimeric capsule. ....	13
Figure 1.14 Giant hydrogen bonded capsule formed by self-assembly of six monomeric resorcinarenes units with eight water molecules.....	14

Figure 1.15 Charged capsule obtained via complementary interactions between two oppositely charged ammonium and carboxylate ions at the rim.....	15
Figure 1.16 Vase and kite conformation in Cram's cavitand due to folding of the quinoxaline arms. ....	15
Figure 1.17 Dimension and inner space in a series of capsules obtained by incorporating 0, 4, 8, and 12 glycoluril spacers in the imide-functionalized cavitands. ....	16
Figure 1.18 Dimeric molecular capsules based on resorcin[4]arene building blocks: (a) capsule held via charged hydrogen bonds, (b) a capsule with 2-aminopyrimidine as a linker to hold the cavitand sub-units, (c) a heterodimeric capsule formed via assembly of tetra(3-pyridyl)cavitand and tetracarboxyl cavitand.....	17
Figure 2.1 Formation of (a) 2-aminopyridinium carboxylate salt, .....	25
Figure 2.2 Library of pyridine-based hydrogen-bond acceptors. ....	25
Figure 2.3 AM1 calculations of charges on pyridyl-N on all the ligands under study. ....	34
Figure 2.4 Thermal ellipsoid plots (50 % probabilities) and labeling schemes for 2-propionamido-5-bromopyridine <b>4</b> , and 2-acetamido-5-bromopyridine <b>6</b> .....	39
Figure 2.5 Formation of 1-D strands of 2-propionamido-5-bromopyridine, <b>4</b> via N-H...O hydrogen bonding. ....	39
Figure 2.6 Formation of 1-D strands of 2-acetamido-5-bromopyridine, <b>6</b> via N-H...O hydrogen bonding. ....	40
Figure 2.7 Thermal ellipsoid plots (50 % probabilities) and labeling schemes for <b>1a-1o</b> .....	41
Figure 2.8 1-D strand formed through secondary N-H...O <sup>-</sup> hydrogen bonds in 2-aminopyrimidinium 4-cyanobenzoate, <b>1a</b> . ....	42
Figure 2.9 1-D strand formed through secondary N-H...O <sup>-</sup> hydrogen bonds in 2-aminopyrimidinium 4-chlorobenzoate, <b>1c</b> . ....	42
Figure 2.10 1-D strands of 2-aminopyridinium 2,6-difluorobenzoate, <b>1g</b> .....	42
Figure 2.11 1-D strands of 2-aminopyridinium pentafluorobenzoate, <b>1j</b> . ....	42
Figure 2.12 1-D strands of bis(2-aminopyridinium) suberate, <b>1k</b> . ....	43
Figure 2.13 1-D strands of bis(2-aminopyridinium) sebacate, <b>1o</b> . ....	43
Figure 2.14 1-D strands of bis(2-aminopyridinium) succinate succinic acid, <b>1n</b> . ....	44
Figure 2.15 Thermal ellipsoid plots (50 % probabilities) and labeling schemes for <b>2a</b> and <b>2e</b> .....	44

Figure 2.16 1-D strands of 2-amino-5-bromopyridinium 4-cyanobenzoate, <b>2a</b> .....	45
Figure 2.17 2-D network of 2-amino-5-bromopyridinium 4-nitrobenzoate, <b>2e</b> .....	46
Figure 2.18 Thermal ellipsoid plots (50 % probabilities) and labeling schemes for <b>3n</b> , <b>4f</b> , <b>4k</b> , <b>4m</b> , <b>4n</b> , <b>4o</b> , <b>5i</b> , <b>5m</b> , and <b>6n</b> .....	47
Figure 2.19 2:1 Co-crystal of 2-acetamidopyridine/succinic acid, <b>3n</b> .....	48
Figure 2.20 1:1 Co-crystal of 2-propiamido-5-bromopyridine/3,4-dichlorobenzoic acid, <b>4f</b> .....	48
Figure 2.21 2:1 Co-crystal of 2-propiamido-5-bromopyridine/suberic acid, <b>4k</b> .....	48
Figure 2.22 2:1 Co-crystal of 2-propiamido-5-bromopyridine/sebacic acid, <b>4o</b> .....	48
Figure 2.23 2:1 Co-crystal of 2-acetamido-5-bromopyridine/succinic acid, <b>6n</b> .....	49
Figure 2.24 2:1 Co-crystal of 2-propiamido-5-bromopyridine/fumaric acid, <b>4m</b> .....	49
Figure 2.25 2:1 Co-crystal of 2-propiamido-5-bromopyridine/succinic acid, <b>4n</b> exhibiting the four-component square-like system. ....	50
Figure 2.26 1:1 Co-crystal of 2-amino-3,5-dibromopyridine/3,5-dinitrobenzoic acid, <b>5i</b> . .....	50
Figure 2.27 2:1 Co-crystal of 2-amino-3,5-dibromopyridine/fumaric acid, <b>5m</b> .....	51
Figure 2.28 Crystal structure of 3-acetamidopyridine showing the 1D chain held by N- H...N interaction.....	54
Figure 2.29 Secondary motifs observed in the salts and co-crystals in the pyridine series. .....	58
Figure 3.1 The ligand and the acids under study (a) 2-acetamidopyridine (b) benzoic acid (c) 3-chlorobenzoic acid (d) 3-( <i>N,N</i> -dimethyl)aminobenzoic acid.....	62
Figure 3.2 The hydrogen bonding interaction between 2-acetamidopyridine (ligand) and 3-chlorobenzoic acid.....	63
Figure 3.3 AM1 calculations of charges on 2-acetamidopyridine and the acids under study.....	64
Figure 3.4 An isothermal titration calorimeter. ....	66
Figure 3.5 Spectrum showing endothermic nature of titration during the dilution of ligand.....	70
Figure 3.6 (a) ITC titration curve of 2-acetamidopyridine vs. benzoic acid; (b) thermodynamic fit parameters. ....	71

Figure 3.7 (a) ITC titration curve of 2-acetamidopyridine vs. 3-chlorobenzoic acid; (b) thermodynamic fit parameters. ....	71
Figure 3.8 (a) ITC titration curve for thermodynamic study of 2-acetamidopyridine vs. 3-(N,N-dimethyl)aminobenzoic acid; (b) thermodynamic fit parameters.....	72
Figure 3.9 (a) Homodimer of benzoic acid. (b) Homodimer of ligand, 2-acetamidopyridine. (c) Heterodimer between the benzoic acid and the ligand. ....	73
Figure 4.1 Schematic of selectivity of hydrogen-bond donors for ditopic ligands.....	78
Figure 4.2 Schematic of a donor molecule (D) binding to the best acceptor (A <sub>1</sub> ).....	79
Figure 4.3 Decreasing electrostatic potential in unsubstituted <i>N</i> -heterocycles and amino-substituted <i>N</i> -heterocycles. ....	80
Figure 4.4 A series of bifunctional ligands with two different hydrogen-bonding sites have been synthesized.....	82
Figure 4.5 A series of nineteen hydrogen-bond acceptors used for the study; monocarboxylic acids ( <b>a – j</b> ), dicarboxylic acids ( <b>k - o</b> ), and cyanoximes ( <b>p - s</b> ) ..	83
Figure 4.6 Thermal ellipsoid plots (50 % probabilities) and labeling schemes for the ditopic ligands <b>10</b> , <b>12</b> , <b>15</b> , <b>16</b> , <b>21</b> , <b>24</b> , and <b>27</b> .....	111
Figure 4.7 1-D arrangement in <b>10</b> formed via N-H···N hydrogen bonds. ....	112
Figure 4.8 1-D arrangement of <b>12</b> formed via N-H···N hydrogen bonds. ....	112
Figure 4.9 1-D chain in <b>15</b> formed via N-H···N hydrogen bonds.....	113
Figure 4.10 1-D strand of <b>16</b> connected via N-H···N hydrogen bonds.....	113
Figure 4.11 Four-component arrangement in the structure of <b>21</b> formed via N-H···O and N-H···N hydrogen bonds.....	114
Figure 4.12 2-D network of <b>24</b> formed via a series of N-H···N, N-H···O, and O-H···O hydrogen bonds. ....	114
Figure 4.13 2-D arrangement of <b>27</b> formed via N-H···N and N-H···O hydrogen bonds. ....	115
Figure 4.14 Thermal ellipsoid plots (50 % probabilities) and labeling schemes for the co-crystals ( <b>10c</b> , <b>10k</b> , <b>10n</b> , <b>10o</b> , and <b>10p</b> ) and salt ( <b>10j</b> ) of 2-amino-5-(3-pyridyl)pyrimidine <b>10</b> . ....	116
Figure 4.15 1-D ribbon of <b>10c</b> formed via O-H···N and N-H···N interactions.....	116
Figure 4.16 1-D ribbon of <b>10j</b> formed via N-H <sup>+</sup> ···O <sup>-</sup> and N-H···N interactions.....	117
Figure 4.17 2-D ribbon of <b>10k</b> formed via O-H···N and N-H···N interactions. ....	118

Figure 4.18 2-D ribbon of <b>10o</b> formed via O-H···N and N-H···N interactions.....	118
Figure 4.19 1-D ribbon of <b>10p</b> formed via O-H···N and N-H···N interactions. ....	118
Figure 4.20 2-D ribbon of <b>10n</b> connected via O-H···N and N-H···N interactions.....	119
Figure 4.21 Thermal ellipsoid plots (50 % probabilities) and labeling schemes for the co-crystals ( <b>12n</b> , <b>15e</b> , <b>16p</b> and <b>27i</b> ) and salts ( <b>24h</b> and <b>24l</b> ).....	120
Figure 4.22 2-D ribbon of <b>12n</b> formed via O-H···N and N-H···N interactions. ....	121
Figure 4.23 1-D ribbon of <b>15e</b> formed via O-H···N and N-H···O interactions.....	121
Figure 4.24 Co-crystal of <b>16p</b> with O-H···N interaction between cyanoxime and 16....	122
Figure 4.25 Two trimers of <b>24h</b> linked via N-H···O <sup>-</sup> interactions. ....	122
Figure 4.26 1-D chain in <b>24l</b> formed via a series of N-H <sup>+</sup> ···O <sup>-</sup> , N-H···O <sup>-</sup> , and N-H···O interactions.....	123
Figure 4.27 1-D network in <b>27i</b> formed via O-H···N and N-H···N interactions. ....	124
Figure 4.28 Electrostatic potential (kJ mol <sup>-1</sup> ) calculations on hydrogen-bond acceptors within the ditopic <i>N</i> -heterocycles. ....	125
Figure 4.29 Hydrogen-bonding interactions with the ligand in (a) <b>10o</b> (b) <b>10n</b> .....	127
Figure 4.30 Hydrogen-bonding interactions with the ligand in (a) <b>24h</b> (b) <b>24l</b> .....	127
Figure 5.1 Variation of melting points of even chain aliphatic dicarboxylic acids, (n = number of methylene groups in the chain) .....	134
Figure 5.2 The API mimics (Supramolecular reagents, <b>SR</b> ) under study for solubility.	136
Figure 5.3 List of aliphatic dicarboxylic acids used in the study.....	137
Figure 5.4 Thermal ellipsoid plots (50 % probabilities) and labeling schemes for 2-acetamido-5-bromopyridine <b>SR1</b> , 2-propionamido-5-bromopyridine <b>SR2</b> , and 2-amino-5-(3-pyridyl)pyrimidine <b>SR3</b> .....	146
Figure 5.5 1-D strands of ligands connected via N-H---O ( <b>SR1</b> and <b>SR2</b> ) and N-H---N ( <b>SR3</b> ) hydrogen bonds. ....	147
Figure 5.6 1-D strands of haloperidol <b>SR4</b> connected via O-H···N hydrogen bonding.	147
Figure 5.7 Thermal ellipsoid plots (50 % probabilities) and labeling schemes for <b>SR1-a</b> and <b>SR1-e</b> .....	148
Figure 5.8 Thermal ellipsoid plots (50 % probabilities) and labeling schemes for co-crystals of 2-propionamido-5-bromopyridine <b>SR2</b> .....	149
Figure 5.9 Primary hydrogen bonding in the crystal structure of <b>SR1-a</b> .....	149

Figure 5.10 Primary hydrogen bonding in the crystal structure of <b>SR1-e</b> .....	149
Figure 5.11 Primary hydrogen bonding in the crystal structure of <b>SR2-c</b> .....	150
Figure 5.12 Primary hydrogen bonding in the crystal structure of <b>SR2-d</b> .....	150
Figure 5.13 Primary hydrogen bonding in the crystal structure of <b>SR2-e</b> .....	150
Figure 5.14 1-D chain comprising of four component square-like architecture in <b>SR2-a</b> . .....	151
Figure 5.15 1-D chain comprising of four component square-like architecture in <b>SR2-b</b> . .....	151
Figure 5.16 Thermal ellipsoid plots (50 % probabilities) and labeling schemes for <b>SR3-a-e</b> .....	152
Figure 5.17 1-D sheets of <b>SR3-a</b> showing N-H---O, O-H---N, and N-H---N binding motifs. ....	153
Figure 5.18 2-D zigzag sheets of <b>SR3-b</b> showing O-H---N and N-H---N binding motifs. ....	154
Figure 5.19 2-D zigzag sheets of <b>SR3-c</b> showing O-H---N and N-H---N binding motifs. ....	154
Figure 5.20 2-D zigzag sheets of <b>SR3-d</b> showing O-H---N and N-H---N binding motifs. ....	154
Figure 5.21 2-D zigzag sheets of <b>SR3-e</b> showing O-H---N and N-H---N binding motifs. ....	155
Figure 5.22 Thermal ellipsoid plots (50 % probabilities) and labeling schemes for <b>SR4-c</b> . .....	155
Figure 5.23 2-D network of <b>SR4-c</b> showing N-H <sup>+</sup> ···O <sup>-</sup> , O-H···O <sup>-</sup> and O-H---O <sup>-</sup> binding motifs. ....	156
Figure 5.24 Solubility curves for dissolution of 2-acetamido-5-bromopyridine <b>SR1</b> in water after 48 hrs. (a) Wavelength vs. absorbance curve @244 nm in different concentrations (mM). (b) Standard curve for equilibrium solubility.....	156
Figure 5.25 Solubility curves for dissolution of 2-propionamido-5-bromopyridine <b>SR2</b> in water after 48 hrs. (a) Wavelength vs. absorbance curve @244 nm in different concentrations (mM). (b) Standard curve for equilibrium solubility.....	157

Figure 5.26 Solubility curves for dissolution of 2-amino-5-(3-pyridyl)pyrimidine <b>SR3</b> in pH 6.8 buffer water after 48 hrs. (a) Wavelength vs. absorbance curve @244 nm in different concentrations (mM). (b) Standard curve for equilibrium solubility. ....	157
Figure 5.27 Solubility curves for dissolution of haloperidol <b>SR4</b> in pH 6.8 buffer solution after 48 hrs. (a) Wavelength vs. absorbance curve @248 nm in different concentrations (mM). (b) Standard curve for equilibrium solubility.....	158
Figure 5.28 Comparative equilibrium solubilities of <b>SR1</b> and its co-crystals.....	158
Figure 5.29 Comparative equilibrium solubilities of <b>SR2</b> and its co-crystals.....	159
Figure 5.30 Comparative equilibrium solubilities of <b>SR3</b> and its co-crystals.....	161
Figure 5.31 Comparative equilibrium solubilities of <b>SR4</b> and its salts.....	162
Figure 5.32 Dependence of co-crystal/salt solubility on the solubility of co-crystallizing agents. ....	164
Figure 5.33 Dependence of thermal behavior of co-crystal ( <b>SR1-SR3</b> ) and salt ( <b>SR4</b> ) on the melting points of the co-crystallizing agents. ....	165
Figure 6.1 Schematic representation of the formation of functional capsules.....	170
Figure 6.2 Structural difference between resorcinarenes and cavitands.....	171
Figure 6.3 Structure of a resorcin[4]arene-based cavitand outlining its four parts of interest.....	171
Figure 6.4 (a) A complementary pair of 2-acetamido-5-bromopyridine in self-assembling hydrogen-bonding interaction. (b) Linker-assisted assembly.....	173
Figure 6.5 N---I halogen bonding between 1,4-diiidotetrafluorobenzene and 4,4'-bipyridyl-N-oxide. ....	174
Figure 6.6 FT-IR spectra of <b>37</b> and its co-crystal with 3,4-dichlorobenzoic acid. ....	183
Figure 6.7 Thermal ellipsoid plots (50 % probabilities) and labeling schemes for <b>35</b> and <b>35'</b> . ....	187
Figure 6.8 C-pentyltetrabromocavitand, with (a) ethyl acetate as guest, <b>35</b> ; (b) DMSO as guest, <b>35'</b> .....	187
Figure 6.9 Crystal packing in tetrabromocavitand molecule (a) <b>35</b> and (b) <b>35'</b> .....	188
Figure 6.10 Linking of cavitands pairs via Br---Br interactions, (a) <b>35</b> (b) <b>35'</b> . ....	189
Figure 6.11 Molecular structure and thermal ellipsoid plots (50 % probabilities) and labeling schemes for <b>36</b> .....	189

Figure 6.12 (a) An individual <i>C</i> -pentyltetraiodocavitand with acetonitrile guest, (b) Linking of two iodocavitands via an I---I interaction. ....	190
Figure 6.13 ‘Foot-in-mouth’ arrangement between iodocavitand molecules in <b>36</b> . ....	190
Figure 6.14 <i>C</i> -Pentyltetra(2-acetamidopyriyl-5-ethynyl)cavitand, <b>37</b> (a) thermal ellipsoid plots (50 % probabilities) and labeling schemes, (b) An individual cavitand. ....	191
Figure 6.15 Molecular structure and spacefilling diagram showing the capsular framework of <b>37</b> . ....	192
Figure 6.16 (a) Capsular framework of <b>37</b> (b) Distorted capsule upon 90° rotation w.r.t b. ....	193
Figure 6.17 <i>C</i> -Pentyl-1,3-di(2-acetamidopyriyl-5-ethynyl)-2,4-dibromocavitand, <b>38</b> ;..	194
Figure 6.18 Crystal packing of <b>38</b> revealing a linear 1D chain with ‘stacking of cones’ like architecture. ....	195
Figure 6.19 <i>C</i> -Pentyl(4-pyridyl)cavitand, <b>41</b> ; (a) thermal ellipsoid plots (50 % probabilities) and labeling schemes, (b) an individual cavitand. ....	196
Figure 6.20 (a) Individual cavitand <b>41</b> , with ethanol as guest molecules, (b) Linear arrangement of cavitands in crystallographic screw axis(hydrogen atoms removed for clarity). ....	196
Figure 6.21 Thermal ellipsoid plots (50 % probabilities) and labeling schemes of co-crystal of <i>C</i> -pentyltetra(3-pyridyl)cavitand and 1,4-diiodotetrafluorobenzene <b>40a</b> . ....	197
Figure 6.22 Halogen bonding in 3-pyridylcavitand with N---I interaction with 1,4-diiodotetrafluorobenzene <b>40a</b> . ....	197
Figure 6.23 Thermal ellipsoid plots (50 % probabilities) and labeling schemes of co-crystal of <i>C</i> -pentyltetra(4-pyridyl)cavitand and 1,4-diiodotetrafluorobenzene <b>41a</b> . ....	198
Figure 6.24 One-dimensional zigzag network of <b>41a</b> bonded via N---I interaction. ....	199
Figure 6.25 Structure of (a) <i>C</i> -pentyltetra-(3-pyridyl)cavitand, <b>40</b> (b) <i>t</i> -butyl-substituted halogen-derivatized calixarene. ....	199
Figure 6.26 Thermal ellipsoid plots (50 % probabilities) and labeling schemes of co-crystal of <i>C</i> -pentyltetra(3-pyridyl)cavitand and halogen-derivatized calixarene in a capsular framework <b>40b</b> . ....	200



Figure 6.27 Molecular structure and spacefill diagram showing the capsular framework of <b>40b</b> .....	201
Figure B.1 2-acetamidopyridine, <b>3</b> , <sup>1</sup> H.....	262
Figure B.2 2-propiamido-5-bromopyridine, <b>4</b> , <sup>1</sup> H & <sup>13</sup> C.....	263
Figure B.3 2-acetamido-5-bromopyridine, <b>6</b> , <sup>1</sup> H.....	264
Figure B.4 2-acetamido-3,5-dibromopyridine, <b>7</b> , <sup>1</sup> H.....	264
Figure B.5 3-pyridylbenzoic acid, <b>8</b> , <sup>1</sup> H.....	265
Figure B.6 2-amino-5-bromopyrimidine, <b>9</b> .....	266
Figure B.7 2-amino-5-(3-pyridyl)pyrimidine, <b>10</b> , <sup>1</sup> H & <sup>13</sup> C.....	267
Figure B.8 2-amino-4-methyl-5-bromopyrimidine, <b>11</b> , <sup>1</sup> H.....	268
Figure B.9 2-amino-4-methyl-5-(3-pyridyl)pyrimidine, <b>12</b> , <sup>1</sup> H.....	268
Figure B.10 2-amino-5-bromopyrazine, <b>13</b> , <sup>1</sup> H.....	269
Figure B.11 2-amino-3,5-dibromopyrazine, <b>14</b> , <sup>1</sup> H.....	269
Figure B.12 2-amino-5-(3-pyridyl)pyrazine, <b>15</b> , <sup>1</sup> H.....	270
Figure B.13 2-acetamido-5-(3-pyridyl)pyridine, <b>16</b> , <sup>1</sup> H.....	270
Figure B.14 2-acetamido-5-bromopyrimidine, <b>17</b> , <sup>1</sup> H.....	271
Figure B.15 2-acetamido-5-(3-pyridyl)pyrimidine, <b>18</b> .....	271
Figure B.16 2-acetamido-5-(3-pyridyl)pyrimidine, <b>18</b> , <sup>1</sup> H & <sup>13</sup> C.....	272
Figure B.17 TMS-protected 3-trimethylsilanylethynylpyridine, <b>19</b> , <sup>1</sup> H.....	273
Figure B.18 3-ethynylpyridine, <b>20</b> , <sup>1</sup> H.....	273
Figure B.19 2-acetamido-5-(3-pyridyl)ethynylpyridine, <b>21</b> , <sup>1</sup> H.....	274
Figure B.20 2-amino-5-trimethylsilanylethynylpyridine, <b>22</b> , <sup>1</sup> H.....	275
Figure B.21 2-amino-5-ethynylpyridine, <b>23</b> , <sup>1</sup> H.....	275
Figure B.22 2-acetamido-5-(3-(2-aminopyridyl))ethynylpyridine, <b>24</b> , <sup>1</sup> H.....	276
Figure B.23 2-acetamido-5-trimethylsilanylethynylpyridine, <b>25</b> , <sup>1</sup> H.....	277
Figure B.24 2-acetamido-5-ethynylpyridine, <b>26</b> , <sup>1</sup> H.....	277
Figure B.25 2-amino-5-(3-(2-acetamidopyridyl))ethynylpyrazine, <b>27</b> , <sup>1</sup> H & <sup>13</sup> C.....	278
Figure B.26 2-acetamido-5-bromopyrazine, <b>28</b> , <sup>1</sup> H.....	279
Figure B.27 2-acetamido-5-(3-(2-acetamidopyridyl))ethynylpyrazine, <b>29</b> , <sup>1</sup> H & <sup>13</sup> C....	280
Figure B.28 2-amino-5-trimethylsilanylethynylpyrimidine, <b>30</b> , <sup>1</sup> H.....	281
Figure B.29 2-amino-5-trimethylsilanylethynylpyrazine, <b>31</b> , <sup>1</sup> H.....	281

Figure B.30 2-amino-5-(3-(2-aminopyrazino))ethynylpyrimidine, <b>32</b> , <sup>1</sup> H & <sup>13</sup> C .....	282
Figure B.31 2-amino-5-ethynylprazine, <sup>1</sup> H .....	283
Figure B.32 C-Pentylbromocalix[4]resorcinarene, <b>34</b> , <sup>1</sup> H.....	284
Figure B.33 C-Pentyltetrabromocavitand, <b>35</b> , <sup>1</sup> H.....	285
Figure B.34 C-Pentyltetraprotiocavitand, <sup>1</sup> H.....	286
Figure B.35 C-Pentyltetraiodocavitand, <b>36</b> , <sup>1</sup> H & <sup>13</sup> C.....	287
Figure B.36 C-Pentyl-1,3-dibromo-2,4-diiodo-cavitand, <b>36'</b> , <sup>1</sup> H.....	288
Figure B.37 C-Pentyl-1,2-dibromo/diIodo-2,4-diprotiocavitand, <sup>1</sup> H .....	289
Figure B.38 C-Pentyl-triiodo-monoprotiocavitand, <sup>1</sup> H .....	290
Figure B.39 C-Pentyl-monobromo/iodo-triprotiocavitand, <sup>1</sup> H.....	291
Figure B.40 C-Pentyl-tetra-(2-acetamidopyridyl-5-ethynyl)cavitand, <b>37</b> , <sup>1</sup> H & <sup>13</sup> C.....	292
Figure B.41 C-Pentyl-1,3-di-(2-acetamidopyridyl-5-ethynyl)-2,4-bibromocavitand, <b>38</b> , <sup>1</sup> H & <sup>13</sup> C .....	293
Figure B.42 C-Pentyl-mono-(2-aminopyrazino-5-ethynyl)-tribromocavitand, <sup>1</sup> H.....	294
Figure B.43 C-Pentyl-mono-(2-aminopyrazino-5-ethynyl)-triiodocavitand, <sup>1</sup> H.....	295
Figure B.44 C-Pentyl-1,2-di(2-aminopyrazino-5-ethynyl)-3,4-diiodocavitand, <sup>1</sup> H .....	296
Figure B.45 C-Pentyl-1,3-di(2-aminopyrazino-5-ethynyl)-2,4-diiodocavitand, <b>39</b> , <sup>1</sup> H. 297	
Figure B.46 C-Pentyltetra(3-pyridyl)cavitand, <b>40</b> , <sup>1</sup> H.....	298
Figure 6.47 C-Pentyltetra(4-pyridyl)cavitand, <b>41</b> , <sup>1</sup> H & <sup>13</sup> C .....	299
Figure B.48 Mass Spectra of C-Pentyltetraiodocavitand, <b>36</b> .....	300
Figure B.49 Mass Spectra of C-Pentyltetra(4-pyridyl)cavitand, <b>41</b> .....	301

## List of Tables

Table 2.1 Summary of possible outcomes in a series of attempted co-crystallization reactions. ....	24
Table 2.2 CSD search on the ligands of interest in a series of pyridines.....	24
Table 2.3 Results in attempted co-crystallization reactions in pyridine series. ....	35
Table 2.4 IR stretching frequencies ( $\text{cm}^{-1}$ ) of salts and co-crystals under study. ....	36
Table 2.5 Hydrogen-bond geometries for the ligands, salts, and co-crystals under study. ....	37
Table 2.6 Summary of results in a series of attempted co-crystallization reactions. ....	53
Table 2.7 Comparison of bond distances and bond angles in salts and co-crystals.....	56
Table 2.8 Secondary structural motifs found in the pyridine series. ....	58
Table 3.1 AM1 calculations on the hydroxyl group and the carbonyl group in the carboxylic acids. ....	64
Table 3.2 IR stretching frequencies for three co-crystals of 2-acetamidopyridine.....	65
Table 3.3 Comparison of thermodynamic parameters for the complexation of three carboxylic acids co-crystallized with 2-acetamidopyridine <b>3</b> .....	72
Table 4.1 Results in attempted co-crystallization reactions in pyridine series.....	105
Table 4.2 IR stretching frequencies ( $\text{cm}^{-1}$ ) of salts and co-crystals of the ligands <b>10</b> , <b>12</b> , <b>15</b> , <b>16</b> , and <b>18</b> .....	106
Table 4.3 IR stretching frequencies ( $\text{cm}^{-1}$ ) of salts and co-crystals of the ligands <b>21</b> , <b>24</b> , <b>27</b> , <b>29</b> , and <b>32</b> .....	107
Table 4.4 Hydrogen-bond geometries for the ditopic ligands, and their salts and co-crystals. ....	109
Table 4.5 Charges on the nitrogen atoms assigned as the best hydrogen bond acceptor and second best acceptor in the ligands under study. ....	126
Table 4.6 Calculation of Q values from the combination of electrostatic potential of heterocyclic nitrogen and adjacent groups.....	129
Table 5.1 Physical properties of dicarboxylic acids with even number carbon atoms ...	135
Table 5.2 IR stretching frequencies ( $\text{cm}^{-1}$ ) of salts and co-crystals under study. ....	143

Table 5.3 Hydrogen-bond geometries for the ligands, salts, and co-crystals under study. .....	144
Table 5.4 Comparative solubilities of <b>SR1</b> and its co-crystals.....	159
Table 5.5 Comparative solubilities of <b>SR2</b> and its co-crystals.....	160
Table 5.6 Comparative solubilities of <b>SR3</b> and its co-crystals.....	162
Table 5.7 Comparative solubilities of <b>SR4</b> and its salts.....	163
Table 5.8 Comparative solubilities of co-crystallizing agents and its co-crystals/salts..	165
Table 5.9 Comparative melting points (°C) of co-crystallizing agents and its co- crystals/salts .....	166
Table 6.1 IR stretches in co-crystals of tetra(2-acetamidopyridyl-5-ethynyl)cavitand <b>37</b> .....	184
Table 6.2 Hydrogen-bond geometries for <b>37</b> and <b>38</b> .....	186
Table A.1 Crystal data and structure refinement for <b>4</b> .....	207
Table A.2 Crystal data and structure refinement for <b>6</b> .....	208
Table A.3 Crystal data and structure refinement for <b>1a</b> .....	209
Table A.4 Crystal data and structure refinement for <b>1c</b> .....	210
Table A.5 Crystal data and structure refinement for <b>1g</b> .....	211
Table A.6 Crystal data and structure refinement for <b>1j</b> .....	212
Table A.7 Crystal data and structure refinement for <b>1k</b> .....	213
Table A.8 Crystal data and structure refinement for <b>1n</b> .....	214
Table A.9 Crystal data and structure refinement for <b>1o</b> .....	215
Table A.10 Crystal data and structure refinement for <b>2a</b> .....	216
Table A.11 Crystal data and structure refinement for <b>2e</b> .....	217
Table A.12 Crystal data and structure refinement for <b>3n</b> .....	218
Table A.13 Crystal data and structure refinement for <b>4f</b> .....	219
Table A.14 Crystal data and structure refinement for <b>4k (SR2-c)</b> .....	220
Table A.15 Crystal data and structure refinement for <b>4m</b> .....	221
Table A.16 Crystal data and structure refinement for <b>4n (SR2-a)</b> .....	222
Table A.17 Crystal data and structure refinement for <b>4o (SR2-d)</b> .....	223
Table A.18 Crystal data and structure refinement for <b>5i</b> .....	224
Table A.19 Crystal data and structure refinement for <b>5m</b> .....	225

Table A.20 Crystal data and structure refinement for <b>6n (SR1-a)</b> .....	226
Table A.21 Crystal data and structure refinement for <b>10</b> .....	227
Table A.22 Crystal data and structure refinement for <b>10c</b> .....	228
Table A.23 Crystal data and structure refinement for <b>10j</b> .....	229
Table A.24 Crystal data and structure refinement for <b>10k</b> .....	230
Table A.25 Crystal data and structure refinement for <b>10n (SR3-a)</b> .....	231
Table A.26 Crystal data and structure refinement for <b>10o (SR3-d)</b> .....	232
Table A.27 Crystal data and structure refinement for <b>10r</b> .....	233
Table A.28 Crystal data and structure refinement for <b>12</b> .....	234
Table A.29 Crystal data and structure refinement for <b>12n</b> .....	235
Table A.30 Crystal data and structure refinement for <b>15</b> .....	236
Table A.31 Crystal data and structure refinement for <b>15e</b> .....	237
Table A.32 Crystal data and structure refinement for <b>16</b> .....	238
Table A.33 Crystal data and structure refinement for <b>16p</b> .....	239
Table A.34 Crystal data and structure refinement for <b>21</b> .....	240
Table A.35 Crystal data and structure refinement for <b>24</b> .....	241
Table A.36 Crystal data and structure refinement for <b>24h</b> .....	242
Table A.37 Crystal data and structure refinement for <b>24l</b> .....	243
Table A.38 Crystal data and structure refinement for <b>27</b> .....	244
Table A.39 Crystal data and structure refinement for <b>27i</b> .....	245
Table A.40 Crystal data and structure refinement for <b>35</b> .....	246
Table A.41 Crystal data and structure refinement for <b>35'</b> .....	247
Table A.42 Crystal data and structure refinement for <b>36</b> .....	248
Table A.43 Crystal data and structure refinement for <b>37</b> .....	249
Table A.44 Crystal data and structure refinement for <b>38</b> .....	250
Table A.45 Crystal data and structure refinement for <b>40a</b> .....	251
Table A.46 Crystal data and structure refinement for <b>40b</b> .....	252
Table A.47 Crystal data and structure refinement for <b>41</b> .....	253
Table A.48 Crystal data and structure refinement for <b>41a</b> .....	254
Table A.49 Crystal data and structure refinement for <b>SR1-e</b> .....	255
Table A.50 Crystal data and structure refinement for <b>SR2-b</b> .....	256

Table A.51 Crystal data and structure refinement for <b>SR2-e</b> .....	257
Table A.52 Crystal data and structure refinement for <b>SR3-b</b> .....	258
Table A.53 Crystal data and structure refinement for <b>SR3-e</b> .....	259
Table A.54 Crystal data and structure refinement for <b>SR4-c</b> .....	260

## Acknowledgements

My graduate years here at KSU, I consider myself very lucky to be surrounded by a group of supportive and enthusiastic people. They made my life much easier here coming from a different social background and trying to adjust to the new environment. I offer my regards to all who have supported me in my graduate years.

My first and foremost thanks go to my advisor Prof. Christer B. Aakeröy, whose encouragement, continual guidance and support enabled me to develop both as a person and as a better researcher. I am highly indebted for his support, valuable advices, and his patience with me all these five years of my graduate study. This thesis and my research would not have been possible without his help and support.

I would also like to thank my Ph.D. advisory committee Prof. Kenneth J. Klabunde, Prof. Stefan H. Bossmann, Prof. Om Prakash, and Prof. Larry A. Glasgow for the valuable time and input in my dissertation.

I am grateful to Dr. John Desper for the single-crystal X-ray data. His efforts and expertise at solving the crystal structures are highly commendable. Without the “cool” structures he generated for me, my thesis would have been very bland. I also thank Dr. Yasuaki Hiromasa for the MS data.

I owe my deepest gratitude to the people in the department for their assistance and making my life at KSU memorable, especially Dr. Yasmin Patell, Mr. Jim Hodgson, Ms. Linda Gibbs, Mrs. Mary L. Dooley, Ms. Earline Dikeman, Ms. Connie Cusimano, Mr. Tobe Eggers, Mr. Ronald L. Jackson, and Mr. Arlon Meek.

Special thanks go to all the Aakeröy group members past-and-present, for their continual support inside and outside the lab.

# **Dedication**

To Mom and Dad



# CHAPTER 1 - Supramolecular assembly and molecular recognition

## 1.1 Supramolecular Chemistry

*“Molecular chemistry, thus, has established its power over the covalent bond. The time has come to do the same for non-covalent intermolecular forces.”<sup>1</sup>*

- Jean-Marie Lehn

The rich structural diversity and complexity found in nature may be unraveled if we look into the simplicity present within. Nature uses molecules as building blocks to build a variety of complex architectures. Much of traditional chemistry focuses on covalent bonds whereas supramolecular chemistry deals with the weaker and reversible non-covalent interactions between molecules.<sup>1</sup> The study of these non-covalent interactions is of importance for many biological processes, which may even be an inspiration for supramolecular research.

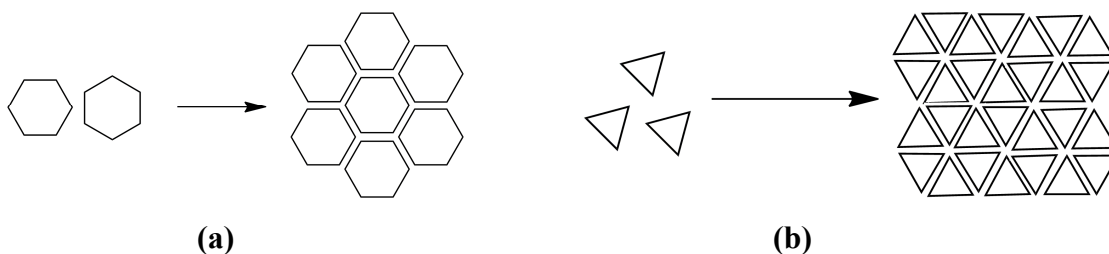


**Figure 1.1** Assembly of larger structures from smaller building blocks.

Ever since the works on host-guest chemistry and self-assembling systems, which led to a Nobel Prize in 1987 for Cram, Lehn, and Pedersen, the field of supramolecular chemistry has gained much attention and interest.<sup>2</sup> Also termed “chemistry beyond the molecules” supramolecular chemistry focuses on assembly of discrete molecular subunits into a larger target. The intermolecular forces responsible for the organization of these subunits include hydrogen bonding, halogen bonding, metal coordination, pi-pi stacking, and van der Waals interaction. Molecular recognition is a key aspect of supramolecular chemistry with a focus on molecular associations and determines how host molecules recognize guests in host-guest systems. Molecular recognition in the solid-state is

exemplified by the structure of a simple organic crystal which behaves as a supermolecule with the molecules in the crystal held together by non-covalent interactions.<sup>3</sup>

### 1.1.1 Crystal Engineering

*“The knowledge and control of intermolecular interactions is as vital to crystal synthesis as is control of the covalent bond is to molecular synthesis.”<sup>4</sup>*

- Jack David Dunitz

Crystal engineering is the design and synthesis of functional molecular solid-state structures from neutral or ionic building blocks using intermolecular interactions.<sup>5</sup> It focuses on the understanding of intermolecular interactions and connectivities which can later be utilized to control the solid state assembly of small molecular building blocks into extended architectures or supermolecules.<sup>6</sup> Valuable information related to molecular recognition, self-assembly, and the packing of the building blocks<sup>7</sup> help to identify bonding preferences and reliable synthons in crystals packing. Various intermolecular forces from strong, directional hydrogen bonds and halogen bonds, to the weak non-directional van der Waals’ forces are employed as the engineering tools to investigate the self-assembly of molecules in a crystal lattice.<sup>8</sup>

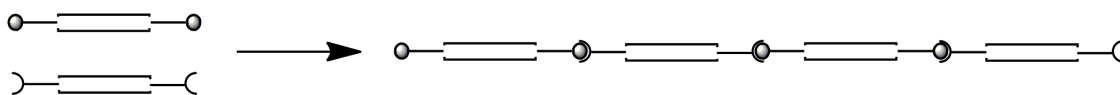


**Figure 1.2** Schematic of molecular recognition in smaller molecules to build larger structures.

### 1.1.2 What is a hydrogen bond?

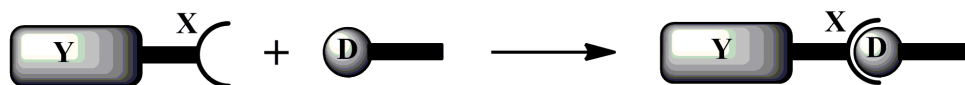
*“A hydrogen bond is an interaction that directs the association of a covalently bound hydrogen atom with one or more other atoms, groups of atoms, or molecules into an aggregate structure that is sufficiently stable to make it convenient for the chemist to consider it as an independent chemical species.”<sup>9</sup>*

Etter<sup>10</sup> put forth general guidelines for the formation of hydrogen bonds in organic molecules based on systematic structural studies of hydrogen-bonded crystals.

1. All good proton donors and acceptors are used in hydrogen bonding.<sup>11</sup>
2. Six-membered-ring intramolecular hydrogen bonds are preferentially formed to intermolecular hydrogen bonds.
3. The best proton donors and acceptors left after the formation of intramolecular hydrogen bonds, take part in intermolecular hydrogen bonding.

Etter suggested that the best hydrogen-bond donor and the best hydrogen-bond acceptor will preferentially form hydrogen bonds to one another. The most common hydrogen bond donors include carboxylic acids, amides, ureas, imides, anilines, phenols; whereas the hydrogen bond acceptors are typically acid and amide carbonyl groups, sulfoxides, nitroxides, phosphoryls, and amine nitrogens.<sup>10</sup>

### 1.1.3 What is a halogen bond?



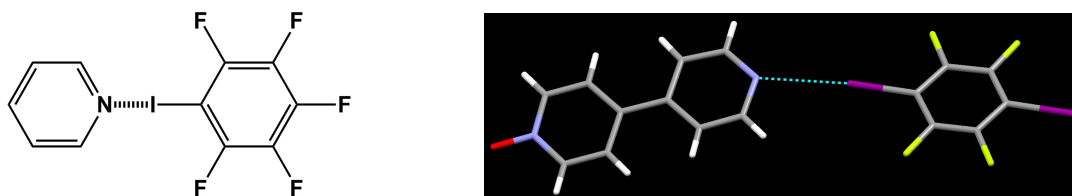
Y = C, N, halogen etc.

X = I, Br, Cl.

D = N, O, S, Se, Cl, Br, I, I<sup>-</sup>, Br<sup>-</sup>, Cl<sup>-</sup>, F<sup>-</sup>...

**Figure 1.3** General scheme for the formation of halogen bonds.<sup>12</sup>

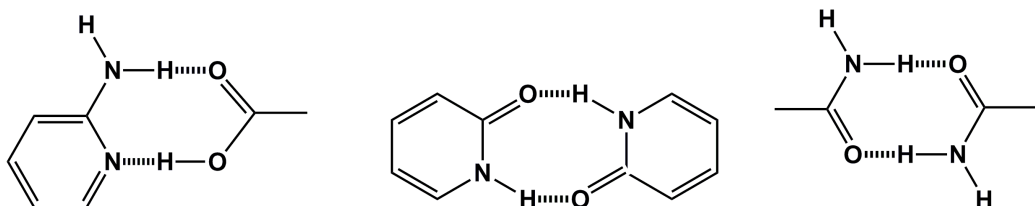
Halogen bonding is a non-covalent intermolecular interaction between halogen atoms (electrophilic) acting as halogen bond donors (D) and electron rich moieties like the nitrogen atom in pyridine acting as a halogen bond acceptor (X), (Figure 1.3).<sup>12</sup> Similar to hydrogen bonding (HB), halogen bonding (XB) also plays a major role in intermolecular recognition and self-assembly process.



**Figure 1.4** Halogen bonding via N...I interactions.<sup>13</sup>

### 1.1.4 Synthons

Supramolecular synthons are the “structural units within supermolecules which can be formed and/or assembled by known or conceivable intermolecular interaction.” The synthons, despite being smaller and less complex than its target molecule, contains most of the vital information inherent in the mutual recognition required to synthesize the supermolecules.<sup>14,15</sup> The use of synthons simplifies the understanding of the crystal structures by breaking down the complexity present in the supermolecules. The structures of benzoic acid, terephthalic acid, isophthalic acid, trimesic acid and adamantane-1,3,5,7-tetracarboxylic acid in zero-, one-, two- and three-dimensional arrangement contain the same carboxy dimer motif.<sup>16</sup>



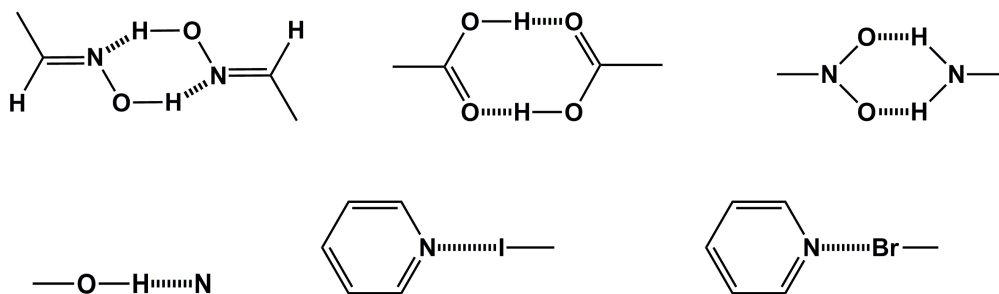


**Figure 1.5** Examples of supramolecular synthons.

## 1.2 Guidelines for hydrogen-bond driven synthesis

### 1.2.1 Co-crystals as a way of probing molecular interactions

The ability to convince two or more different molecules to co-exist within one crystalline lattice has become an important part of the synthesis of supramolecular solid-state architectures.<sup>17</sup> Co-crystallizations proceed without making or breaking covalent bonds, and rely on self-assembly processes that must overcome the innate structural ‘selfishness’ of molecules that makes re-crystallization such a powerful and versatile method of chemical purification. The fundamental aspects of co-crystal synthesis<sup>18</sup> offer unique opportunities for examining the balance and competition between intermolecular forces.<sup>19</sup>

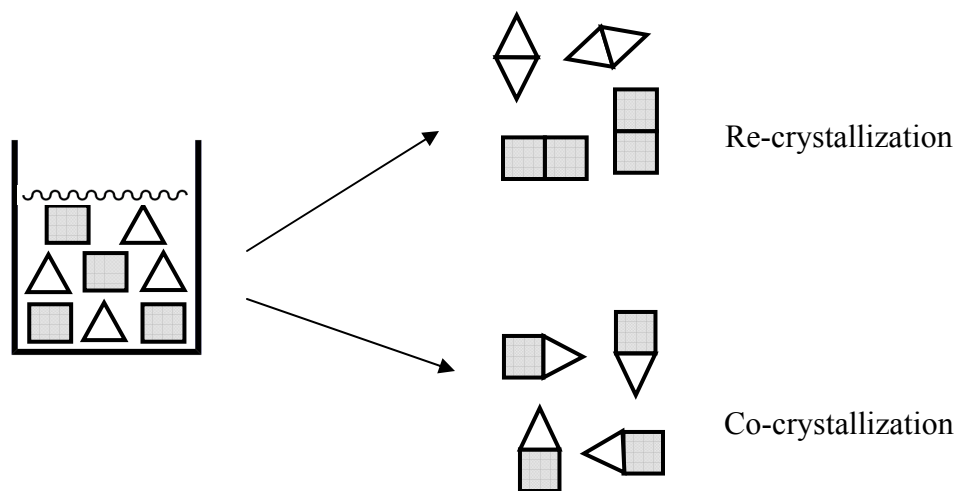
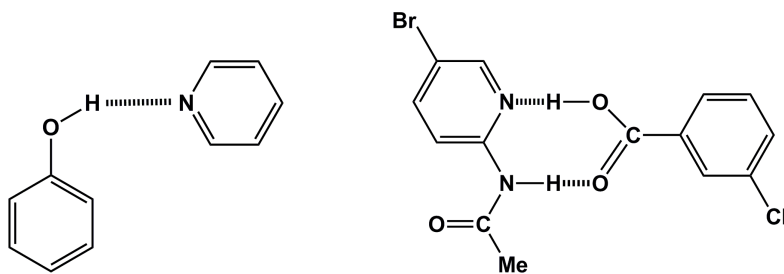


**Figure 1.6** Schematic of re-crystallization (homomeric interaction) vs co-crystallization (heteromeric interaction).

Co-crystals consist of a single crystalline phase with multiple components present in a given stoichiometric ratio. These different molecular components in the co-crystals interact via intermolecular interactions. The strength and directionality of the hydrogen bond make it the most important interaction in co-crystal formation. The commonly encountered hydrogen-bond interactions in co-crystals are O-H...O, O-H...N, N-H...O, N-H...N, C-H...N, C-H...O etc. with carboxylic acids, amines, amides, oximes, and alcohols. Halogen-bond interactions involve N-heterocycles (pyridine, pyrimidine, pyrazine, imidazole) with N...Br, N...I synthons. Co-crystals are prepared using solution-based evaporation,<sup>20</sup> cooling of heteromeric solution,<sup>21</sup> thermal microscopy (Kofler technique),<sup>22</sup> reaction crystallization method (RCM),<sup>23</sup> neat grinding,<sup>24</sup> liquid-assisted grinding, sublimation and growth from the melt<sup>25</sup> or slurry.<sup>26</sup> The mechanochemical methods of grinding have been demonstrated to provide better results;<sup>27</sup> however solution crystallization is commonly used especially to obtain single crystals for X-ray analysis.<sup>28</sup>

### 1.2.2 Binary and ternary co-crystals

By changing/modifying the hydrogen bonding sites in a molecule, we can change the way it binds to give various types of co-crystals. When molecules with single donor and single acceptor are mixed, usually 1:1 binary co-crystals are obtained with two different types of molecules in the same crystalline lattice, (Figure 1.7).



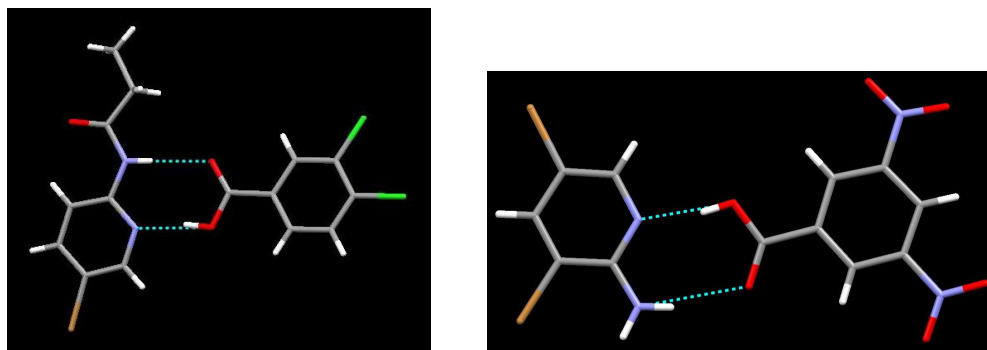


**Figure 1.7** Hydrogen-bonded binary co-crystals

However when a molecule has two donor/acceptor sites with variable hydrogen bonding potential, then it is possible to make ternary co-crystals, (Figure 1.8).

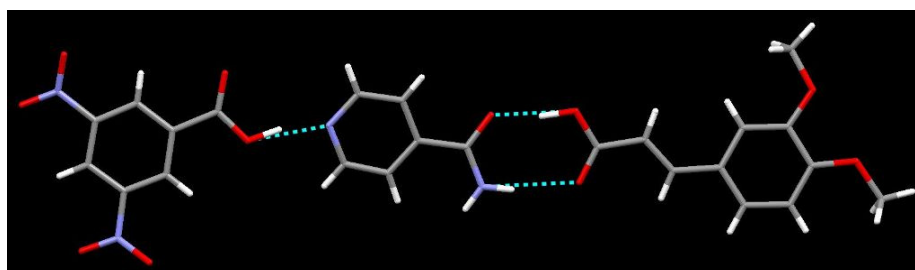
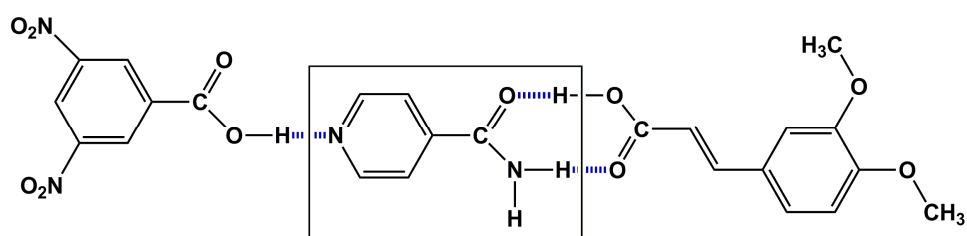


**Figure 1.8** Ternary hydrogen-bonded co-crystal between isonicotinamide, 3,5-dinitrobenzoic acid, and 3,4-dimethoxycinnamic acid.<sup>29</sup>

Hence a ternary co-crystal can be constructed by using an asymmetric hydrogen-bond acceptor and two different donors and vice-versa. The choice between the two asymmetric sites in the donor molecule depends on the comparative binding strength in these sites, as explained by Etter<sup>10</sup> “the best hydrogen-bond donor preferentially forms hydrogen bond with the best hydrogen-bond acceptor”, (Figure 1.9).

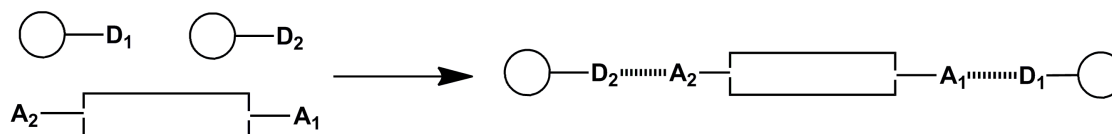


**Figure 1.9** Schematic of the best hydrogen bond donor ( $D_1$ ) binding with best hydrogen bond acceptor ( $A_1$ ) and the second best hydrogen bond donor ( $D_2$ ) with second best hydrogen bond acceptor ( $A_2$ ).<sup>29</sup>

### 1.2.3 Establishing the hydrogen-bonding hierarchy

In order to establish a hydrogen-bonding hierarchy of donors and acceptors in a system, the molecular behavior encountered and the underlying reasons need to be understood. Two approaches based on  $pK_a$  differences and molecular electrostatic potential are used to detail the general hierarchy in the hydrogen-bonded systems.

#### $\Delta pK_a$ rule

It was proposed that the formation of salts and co-crystals can be explained based on the  $pK_a$  difference between the donor and acceptor molecules.<sup>30</sup> The complete proton transfer from donors to acceptors leading to the charged species, and hence the salt formation is prompted by the difference in  $pK_a$  [ $\Delta pK_a = pK_a(\text{base}) - pK_a(\text{acid})$ ] values greater than 3, whereas if the difference is negative it exclusively forms co-crystals.<sup>31</sup> The predictability of formation of salt or co-crystal is low for the values in the range 0 to 3, where proton-sharing or mixed ionization states were encountered and hence cannot be assigned to either category and termed *salt-co-crystal continuum*. The co-crystallization of theophylline with various carboxylic acids in the  $\Delta pK_a$  ranges  $0 < \Delta pK_a < 2.5$  resulted in 16 salts, two co-crystals, and two mixed ionization states.<sup>30</sup>

#### Electrostatic potential

The  $\Delta pK_a$  approach is based on the transfer of proton and acts as a guideline for the prediction of salt and co-crystal formation, and is less of a measure of the hydrogen bonding strength of the acceptors and donors. Within a class of functional groups like pyridines and phenols, the  $pK_a$  approach correlates well with the trends in hydrogen bond



donor/acceptor strength; however the marked contradictions were seen for other functional groups.<sup>32</sup> e.g. thiols are more acidic than alcohols but are worse hydrogen-bond donors. Similarly, pyridine is more basic than DMSO, but is a worse hydrogen-bond acceptor. Hunter<sup>33</sup> came up with a new approach based on molecular electrostatic potentials (MEPs) to calculate the strength of hydrogen bond donors and acceptors in a wide range of functional groups. His approach was based on a purely electrostatic view of the hydrogen bond. The molecular electrostatic surface potential charges are determined by the effective charge on the nucleus, the location of the lone pair, and the van der Waals radius.

Considering the electrostatic nature of the hydrogen bond, the association constant ( $K$ ) for pairwise hydrogen-bonding interaction between two functional groups is given by the relationship.<sup>34</sup>

$$\log K = c_1\alpha_2\beta_2 + c_2 \qquad \text{Equation 1.1}$$

where  $c_1$  and  $c_2$  are constants that depend on the solvent and,  $\alpha_2$  and  $\beta_2$  are the functional group constants that relate to the hydrogen bonds donor and hydrogen-bond acceptor properties of the molecules.

The constant  $c_1$  is solvent-dependent and increases with a decrease in the polarity of the medium, whereas the constant  $c_2$  is relatively insensitive to solvent hence making it the fundamental property of interaction between two molecules. Hunter demonstrated that even at relatively low level of theory (semi empirical AM1), the calculated maxima and minima in the molecular electrostatic potential surface is well-correlated with the experimentally determined values of  $\alpha_2$  and  $\beta_2$ .<sup>33</sup>

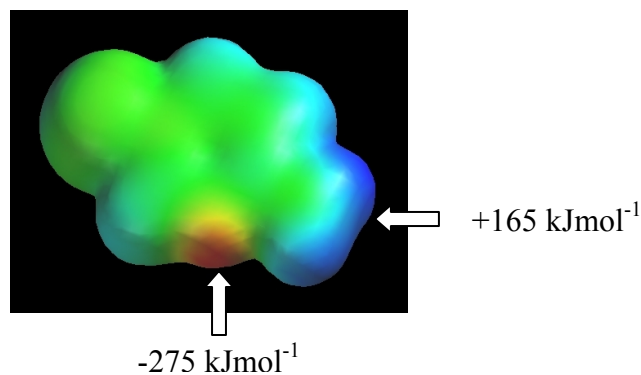


**Figure 1.10** Molecular electrostatic potential surface of 2-amino-5-bromopyridine, calculated by using AM1 and a positive charge in vacuum as probe; blue (positive regions,  $E_{\max}$ ), red (negative regions,  $E_{\min}$ ), and green (neutral regions).

The approach is extendable to include the hydrogen-bond strengths of donors and acceptors in solutions as well by using the normalization constant of  $52 \text{ kJ mol}^{-1}$  obtained from the theoretical-experimental correlations and the gas phase value of  $c_1$ , with some classes of functional groups like amides showing poor consistency ( $\pm 20\%$ ).<sup>33</sup>

$$\alpha = E_{\max}/52 \text{ kJmol}^{-1} \quad \beta = E_{\max}/52 \text{ kJmol}^{-1}$$

### 1.3 Changing properties of specialty chemicals via co-crystallization

Co-crystals represent new solid forms that can enable the modification of physicochemical properties such as solubility, stability, hygroscopicity, shelf-life, dissolution rate and biocompatibility of active pharmaceutical ingredients (APIs),<sup>35-36</sup> without tampering with their inherent pharmacological properties.<sup>37, 38, 39, 40</sup> Pharmaceutical co-crystals with their neutral components held together via non-covalent interactions have an advantage over their more common counterparts, the pharmaceutical salts, in being able to generate solid forms of APIs even when they do not contain any ionizable functional groups. Examples of pharmaceutical co-crystals are found in literature, with co-crystals of theophylline and phenobarbital<sup>41</sup>, caffeine and barbital<sup>42</sup>, caffeine and gentisic acid<sup>43</sup>, co-crystal of itraconazole with different carboxylic acids.<sup>44</sup> Childs and Rodriguez-Hornedo et. al. mentioned 50 co-crystals of piroxicam with 23 different carboxylic acids<sup>45</sup> and 35 co-crystals of carbamazepine with carboxylic acids, amides and amines.<sup>46</sup>

### 1.3.1 Dissolution advantage

The works of Childs<sup>47</sup> et. al. with antidepressant fluoxetine hydrochloride co-crystallized with carboxylic acids like benzoic acid, succinic acid and fumaric acid resulted in salt. The intrinsic dissolution studies showed approximately 3 times higher dissolution for 2:1 succinic acid complex, whereas for 1:1 benzoic acid complex the dissolution is reduced to half, and no change observed for 2:1 fumaric acid complex. Studies with norfloxacin (solubility 0.21 mg/mL) revealed 3 times increase in solubility with isonicotinamide co-crystal (0.59 mg/mL), whereas 20-45 times solubility increase is noted for salts with succinic, malonic, and maleic acids.<sup>48</sup> Similarly, 1:1 glutaric acid co-crystal of an extremely insoluble (<0.1 mg/mL) neuropathic drug, 2-[4-(4-chloro-2-fluorophenoxy)phenyl]pyrimidine-4-carboxamide showed 18 times greater intrinsic dissolution rate.<sup>49</sup> Furthermore, co-crystals of water-insoluble anti-fungal drug, itraconazole with succinic acid, L-malic acid, and L-tartaric acid showed 4- to 20-fold higher dissolution than that of the drug itself.<sup>44</sup>

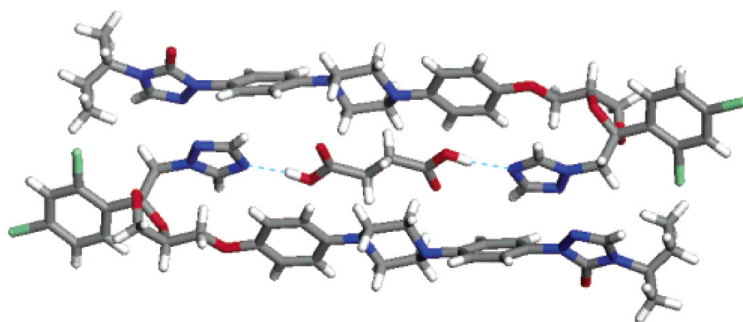


**Figure 1.11** Trimer unit of the itraconazole-succinic acid co-crystal.<sup>44</sup>

### 1.3.2 Hygroscopicity improvement

The co-crystal of caffeine with oxalic acid was found to be non-hygroscopic whereas the crystalline caffeine by itself absorbs moisture and forms a hydrate.<sup>50</sup> Similar stabilities to moisture were reported for co-crystals of carbamazepine with nicotinamide and saccharin.<sup>51</sup> Co-crystals of theophylline with oxalic acid, malonic acid, maleic acid, and glutaric acid failed to form any hydrates; the 2:1 co-crystal with oxalic acid was found to be stable even at 98% RH for 7 weeks.<sup>39d</sup>

## 1.4 Hydrogen and halogen bonded cavitands

The ability to trap or include guest molecules in a defined cavity of a larger host is an excellent example of host-guest chemistry. The potential for subsequent structural modification that will change the environment inside the cavity is very intriguing with the possibility of changing the properties of the trapped guests. The application of non-covalent reversible self-assembly processes dictated by ‘weak’ intermolecular interactions like hydrogen and halogen bonds to bind these two hosts together into a capsular framework opens a new world of molecular capsules. Newer dimensionless possibilities including selective delivery of guests, changing conditions for guests with reaction acceleration, as well as initiation of completely new reactions.<sup>52</sup>

### 1.4.1 Molecular capsules

Molecules that result in capsules should possess two important characteristics: they must be able to self-assemble and encapsulate the guest molecules. The self-assembly is pertinent to the self-complementary components based on the capsule components capable of reversible non-covalent interactions primarily hydrogen bonds. The subsequent encapsulation of the guest molecules depends on the complementarity of the guest size, shape and chemical surface with the host cavity.<sup>53</sup> Various types of molecular capsules that can self-assemble from smaller components using non-covalent interactions have been developed.<sup>54</sup>

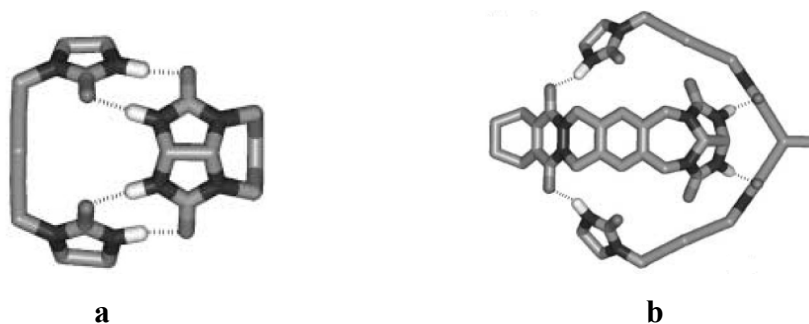


**Figure 1.12** Self-assembling glycoluril-based dimeric capsules;<sup>53</sup> (a) “tennis ball” and (b) “softball”

The first reversibly formed molecular capsule was named “tennis ball” with the monomer consisting of two self-complementary glycoluril subunits holding the tennis

ball (methane, ethane, ethylene, noble gases) via eight hydrogen bonds (C=O...H-N) in its tiny cavity ( $50 \text{ \AA}^3$ ), (Figure 1.12a).<sup>55</sup> Variation in the spacer led to a range of smaller and larger capsules (internal cavity  $240\text{-}320 \text{ \AA}^3$ ), termed “softballs”, (Figure 1.12b).<sup>56</sup>

### 1.4.2 Calixarene capsules

Calix[4]arenes and resorcin[4]arenes are commonly used for due to their architecture, straightforward synthesis, and the potential for derivatization at the rim with complementary functionalities suitable for non-covalent interactions for capsular assembly. The decoration of the calix[4]arene rim with hydrogen bond donor/acceptor groups has led to various capsular structures; self-complementary carboxylic acid groups produced a homomeric capsule held via four hydrogen bonds (Figure 1.13a),<sup>57</sup> whereas with pyridyl and carboxylic acid groups on opposing calixarene rims led to formation of heteromeric capsule (Figure 1.13b).<sup>58</sup> The more common urea-derivatized calixarene monomers self-assemble to give a dimeric capsule with a cavity of approx  $180 \text{ \AA}^3$  held via sixteen hydrogen bonds (Figure 1.13c).<sup>59</sup> The combination of different urea monomers resulted in mixtures of homo- and heterodimers.<sup>60</sup>

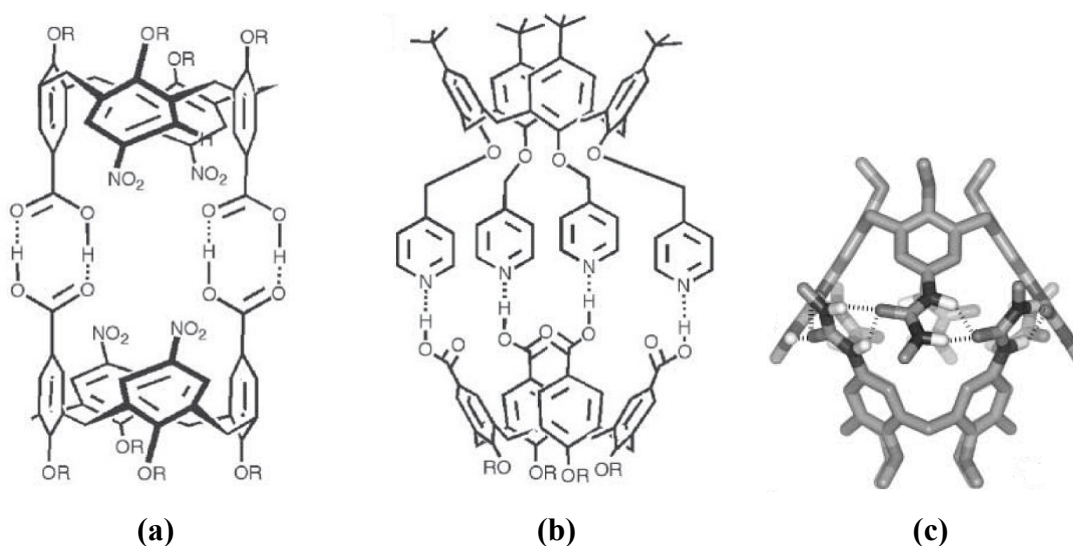


**Figure 1.13** (a) Homodimeric hydrogen-bonded capsule with carboxylic acid rim substituents (R = propyl); (b) Heterodimeric capsule with hydrogen bonding between a pyridyl functionalized monomer and a complementary carboxylic acid functionalized monomer, (R = octyl); (c) Urea-functionalized homodimeric capsule.

The limitation in guest size due to the smaller cavity of resorcinarenes capsule can be removed by (a) expanding the size of the macrocycle (calix[5]arene<sup>61</sup> and calyx[6]arene<sup>62</sup>) or (b) adding spacing units between the monomeric units (either covalently<sup>63</sup> or non-covalently<sup>64</sup>). McGillivray and Atwood<sup>65</sup> provided an alternative approach to create larger capsules by using multiple bowl fragments to create a giant capsular assembly. Their hexameric capsule consisted of a chiral arrangement of six resorcinarene subunits and eight water molecules with huge cavity 1375 Å<sup>3</sup> with 60 hydrogen bonds, (Figure 1.14).

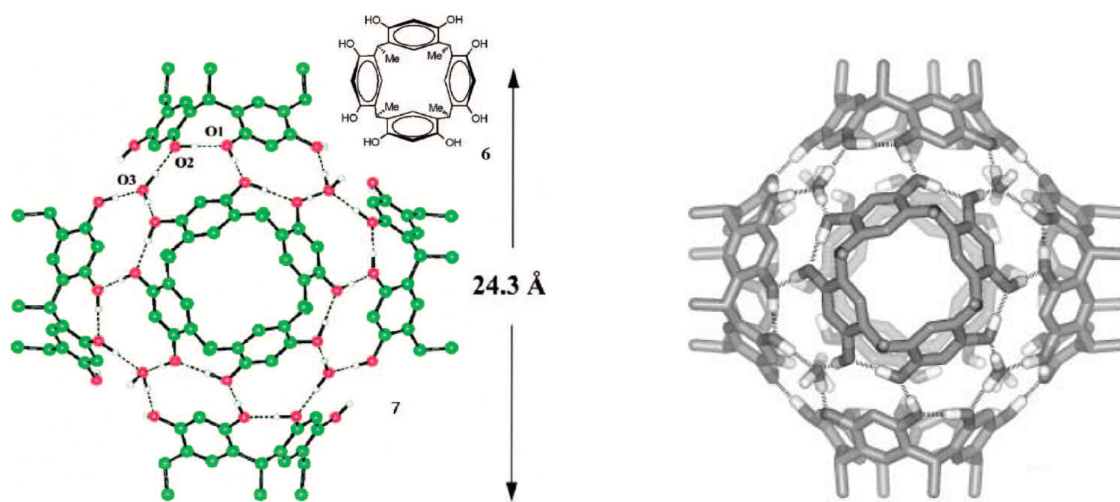


**Figure 1.14** Giant hydrogen bonded capsule formed by self-assembly of six monomeric resorcinarenes units with eight water molecules.

Specific examples of molecular capsules formed via self-assembly of calix[4]arenes equipped with oppositely charged functional groups in their upper rims are found in literature. 1:1 complexes of highly charged complementary building blocks based on ammonium (or amidinium) and phosphonate ions (tetracationic and tetraanionic) have high thermodynamic stability, and association constants  $K_a$  up to  $7 \times 10^5 \text{ M}^{-1}$  in methanol and  $>10^3 \text{ M}^{-1}$  in water.<sup>66</sup>

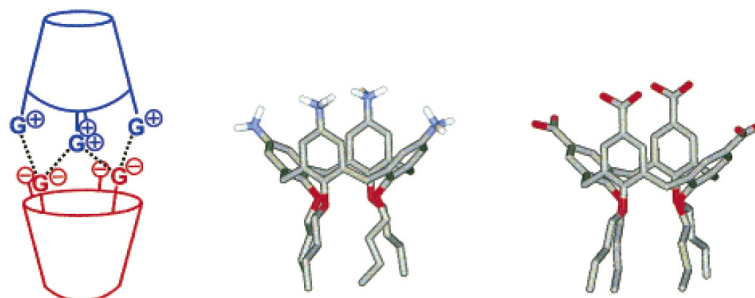


**Figure 1.15** Charged capsule obtained via complementary interactions between two oppositely charged ammonium and carboxylate ions at the rim.

### 1.4.3 Cavitand capsules

The structural rigidification by covalent modification of the hydroxyl arms of resorcinarenes result in cavitands. The transformation into cavitands exclude the conformational switching of resorcinarenes and allow them to hold their guests more tightly. Cram<sup>67</sup> synthesized a series of eighteen cavitands with deeper cavity and rigid surfaces, (Figure 1.16).

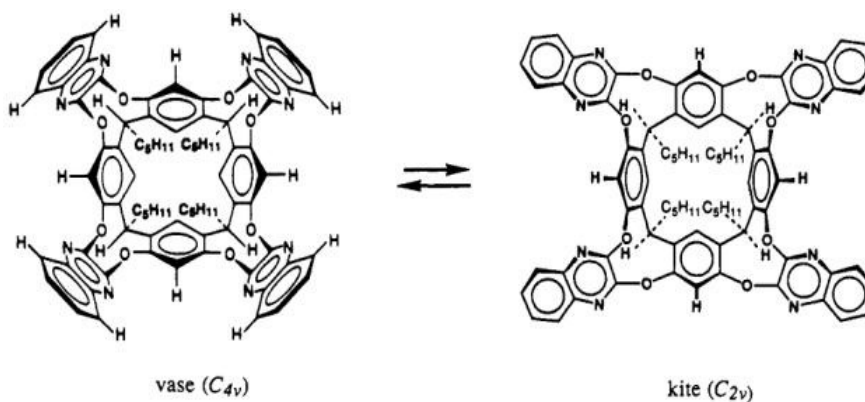


**Figure 1.16** Vase and kite conformation in Cram's cavitand due to folding of the quinoxaline arms.

Rebek<sup>68</sup> synthesized a vase-shaped cavitand with four imide functionalities on the rim which dimerizes through bifurcated hydrogen bonds to give a capsule. He showed that the size of this capsule can be increased by insertion of glycolurils units, which are a perfect fit, between the cavitand units, hence generating higher order capsules that can

hold larger-sized or larger number of guests, (Figure 1.17).<sup>69</sup> The glycoluril-based self-assembled molecular capsules were shown to stabilize reactive species or molecules in uncommon conformations via encapsulation as well as function as molecular reaction chamber for acceleration and catalysis of Diels-Alder reactions.<sup>70</sup>

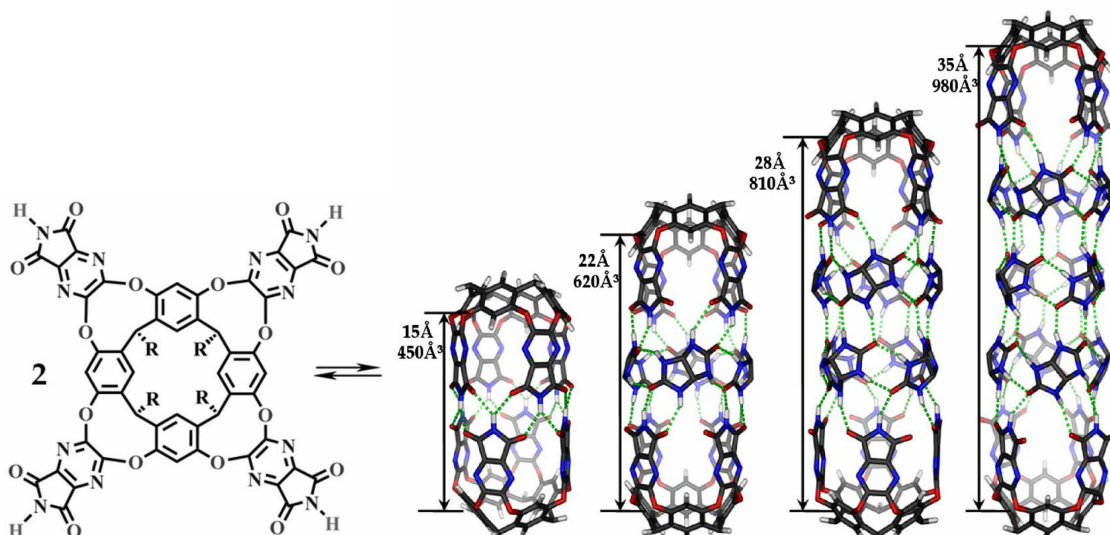


**Figure 1.17** Dimension and inner space in a series of capsules obtained by incorporating 0, 4, 8, and 12 glycoluril spacers in the imide-functionalized cavitanths.

Chapman and Sherman<sup>71</sup> utilized ionic hydrogen bonds to prepare capsules from hydroxyl-substituted resorcinarenes, (Figure 1.18 a). Kobayashi<sup>72</sup> et al. synthesized resorcinarenes based cavitanth functionalized with four carboxylic acid, held together by 2-aminopyrimidine acting as linker (Figure 1.18 b). They also integrated guest/ solvent-induced assembly of tetracarboxylcavitanth and tetra(3-pyridyl)cavitanth into a heterodimeric capsule held together via four intermolecular acid-pyridyl hydrogen bonds (Figure 1.18 c).<sup>73</sup>



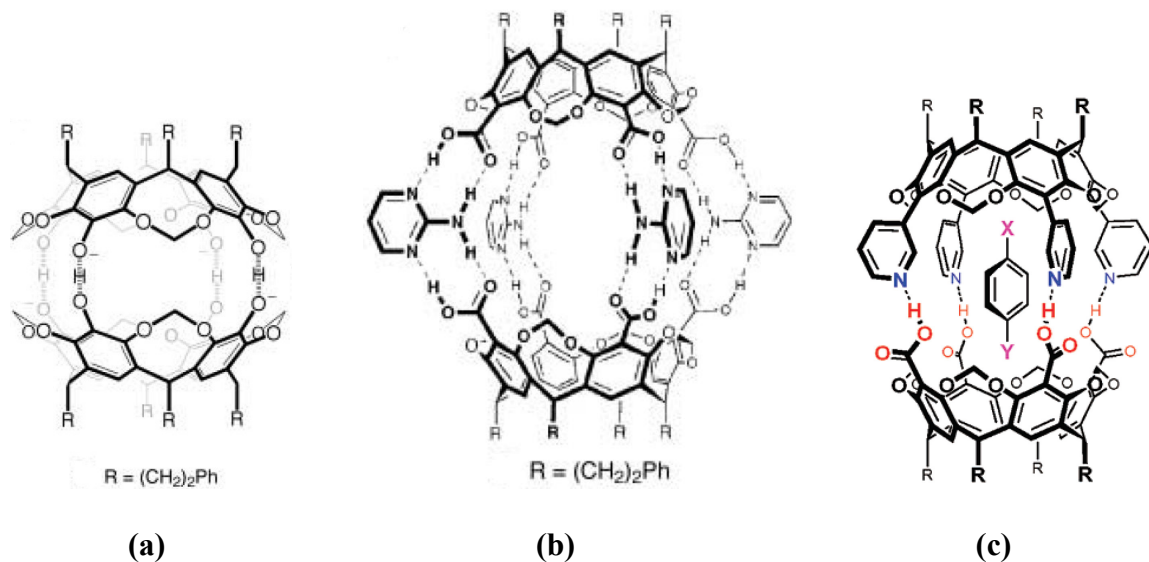


**Figure 1.18** Dimeric molecular capsules based on resorcin[4]arene building blocks: (a) capsule held via charged hydrogen bonds, (b) a capsule with 2-aminopyrimidine as a linker to hold the cavitand sub-units, (c) a heterodimeric capsule formed via assembly of tetra(3-pyridyl)cavitand and tetracarboxyl cavitand.

## 1.5 Goals

A proper understanding of intermolecular non-covalent interactions in self-assembly and molecular recognition processes will allow us to select proper components for the design of supramolecular networks as well as to modulate their physical properties. We will examine molecular recognition in small molecules at first and extend it into larger molecules to establish robust and versatile supramolecular synthetic methods. The understanding will be translated into the physical properties alteration of multi-component crystals as well as generation of capsular frameworks held via interplay of weak intermolecular interactions.

The goals pursued in this thesis are:

1. To establish a boundary defined by the molecular electrostatic surface potential charges to uncover the hierarchy of hydrogen-bonding strength in small-molecule pyridine family in terms of their capability to form salts and co-crystals with a series

- of mono/di-carboxylic acids. Molecular recognition in solution was also studied using isothermal titration calorimetry. (Chapter 2 and 3)
2. To investigate whether binding specificity in small molecules can be translated into binding selectivity in case of larger molecules. This will also test the Etter's approach that the best hydrogen-bond donor would bind with best hydrogen-bond acceptor in competitive conditions. We examined the competition between the acceptor sites in a family of ditopic coupled *N*-heterocycles comprising pyridine, pyrimidine, and pyrazine moieties with a series of mono/di-carboxylic acids and cyanoximes. (Chapter 4)
  3. To address the key questions concerning pharmaceutical co-crystals/salts: 1) Do co-crystals/salts offer any solubility alterations over its parent forms? ii) Is there any change in thermal behavior? iii) Can their crystal structure be related to the displayed molecular behavior? We synthesized co-crystals/salts of three drug mimics and a pharmaceutical drug and tested their thermal stability and solubility in water and buffer solutions. (Chapter 5)
  4. To assemble hydrogen and halogen-bond functionalized cavitands into molecular capsules. Various hydrogen and halogen-bond functionalized resorcinarenes-based cavitands were synthesized and their ability to co-crystallize as well as to self-assemble to give homodimeric and heterodimeric hydrogen and halogen-bonded capsules were studied. (Chapter 6)

## References

- <sup>1</sup> Lehn, J.-M. *Supramolecular Chemistry* **1995**, VCH, Weinheim.
- <sup>2</sup> Atwood, J. L.; Steed, J. W. *Encyclopedia of Supramolecular Chemistry* **2004**, CRC Press, Taylor & Francis Group, FL
- <sup>3</sup> Desiraju, G. R. *Angew. Chem. Int. Ed.* **2003**, 34(21), 2311
- <sup>4</sup> Dunitz, J. D. *Pure Appl. Chem.* **1991**, 63, 177.
- <sup>5</sup> Desiraju, G. R. *Angew. Chem. Int. Ed.* **2007**, 46, 8342.
- <sup>6</sup> (a) Desiraju, G. R. *Crystal Engineering: The Design of Organic Solids* **1989**, Elsevier, Amsterdam; (b) Aakeroy, C. B. *Acta Crystallogr. B53*, **1997**, 569.
- <sup>7</sup> (a) Desiraju, G. R. *The Crystal as a Supramolecular Entity. Perspectives in Supramolecular Chemistry* 1996, vol.2, Wiley, New York; (b) Dunitz, J. D. *Pure Appl. Chem.* **1991**, 63, 177; (c) Melendez, R. E.; Hamilton, A. D. *Top. Curr. Chem.* **1998**, 198, 97; (d) Braga, D.; Grepioni, F. *Acc. Chem. Res.* **2000**, 33, 601.
- <sup>8</sup> (a) Zaworotko, M. J. *Chem. Soc. Rev.* **1994**, 23, 283; (b) Russell, V. A.; Ward, M. D. *Chem. Mater.* **1996**, 8, 1654; (c) Ashton, P. R.; Fyfe, M. C. T.; Hickingbottom, S. K.; Menzer, S.; Stoddart, J. F.; White, A. J. P.; Williams, D. J. *Chem. Eur. J.* **1998**, 4, 577; (d) Steiner, T.; Desiraju, G. R. *Chem. Commun.* **1998**, 891.
- <sup>9</sup> Pauling, L. *The Nature of the Chemical Bond*, 3<sup>rd</sup> ed. **1960**, Cornell University Press, New York, pp 6.
- <sup>10</sup> (a) Etter, M. C. *Acc. Chem. Res.* **1990**, 23, 120; (b) Etter, M. C. *J. Phys. Chem.* **1991**, 95, 4601.
- <sup>11</sup> Donohue, J. *J. Phys. Chem.* **1952**, 56, 502.
- <sup>12</sup> Metrangolo, P.; Meyer, F.; Pilati, T.; Resnati, G.; Terraneo, G. *Angew. Chem. Int. Ed.* **2008**, 47, 6114.
- <sup>13</sup> Nate Schultheiss, private communication **NS0643**.
- <sup>14</sup> Nangia, A.; Desiraju, G. R. *Topics in Current Chemistry - Supramolecular Synthons and Pattern Recognition* **1998**, 198, Springer Verlag Berlin Heidelberg.
- <sup>15</sup> Reddy, D. S.; Craig, D. C.; Desiraju, G. R. *J. Am. Chem. Soc.* **1996**, 118(17), 4091.
- <sup>16</sup> Desiraju, G. R. *Angew. Chem. Int. Ed.* **1995**, 34, 2311.
- <sup>17</sup> Aakeröy, C. B.; Salmon, D. J. *CrystEngComm*, **2005**, 7, 439.
- <sup>18</sup> (a) Skovsgaard, S.; Bond, A. D. *CrystEngComm*, **2009**, 444; (b) Chadwick, K.; Davey, R.; Sadiq, G.; Cross, W.; Pritchard, R. *CrystEngComm*, **2009**, 412; (c) Aakeröy, C. B.; Desper, J.; Fasulo, M.; Hussain, I.; Levin, B.; Schultheiss, N. *CrystEngComm* **2008**, 1816; (e) Aakeröy, C. B.; Desper, J.; Helfrich, B. A.; Metrangolo, P.; Pilati, T.; Resnati, G.; Stevenazzi, A. *Chem. Commun.* **2007**, 4236.
- <sup>19</sup> Li, Z. J.; Abramov, Y.; Bordner, J.; Leonard, J.; Medek, A.; Trask, A. V. *J. Am. Chem. Soc.*, **2006**, 128, 8199.
- <sup>20</sup> Shattock, T.R.; Arora, K.K.; Vishweshwar, P.; Zaworotko, M. J. *Cryst Growth & Des* **2008**, 8, 4533.
- <sup>21</sup> Hickey, M. B.; Peterson, M. L.; Scoppettuolo, L. A.; Morrisette, S.L.; Vetter, A.; Guzman, H.; Remenar, J. F.; Zhang, Z.; Tawa, M.D.; Haley, S.; Zaworotko, M. J.; Almarsson, O. *Eur. J. Pharm. Biopharm.* **2007**, 67, 112.

- <sup>22</sup> McNamara, D. P.; Childs, S. L.; Giordano, J.; Iarriccio, A.; Cassidy, J.; Shet, M. S.; Mannion, R.; O'Donnell, E.; Park, A. *Pharm. Res.* **2006**, *23*, 1888.
- <sup>23</sup> (a) Nehm, S. J.; Rodriguez-Spong, B.; Rodriguez-Hornedo, N. *Cryst. Growth Des.* **2006**, *6*, 592; (b) Rodriguez-Hornedo, N.; Nehm, S. J.; Seefeldt, K. F.; Pagan-Torres, Y.; Falkiewicz, C. J. *Mol. Pharmaceutics* **2006**, *3*, 362.
- <sup>24</sup> (a) Chadwick, K.; Davey, R.; Cross, W. *CrystEngComm.* **2007**, *9*, 732; (b) Trask, A. V.; Jones, W. *Top. Curr. Chem.* **2005**, *254*, 41. (c) Karki, S.; Friscic, T.; Jones, W.; Motherwell, W. D. S. *Mol. Pharm.* **2007**, *4*, 347; (d) Trask, A. V.; Motherwell, W. D. S.; Jones, W. *Chem. Commun.* **2004**, 890.
- <sup>25</sup> Palmer, D. S.; Llinas, A.; Morao, I.; Day, G. M.; Goodman, J. M.; Glen, R. C.; Mitchell, J. B. O. *Mol. Pharm.* **2008**, *5*, 266; (b) Seefeldt, K.; Miller, J.; Alvarez-Nunez, F.; Rodriguez-Hornedo, N. *J. Pharm. Sci.* **2007**, *96*, 1147.
- <sup>26</sup> (a) Zhang, G. G. Z.; Henry, R. F.; Borchardt, T. B.; Lou, X. C. *J. Pharm. Sci.* **2007**, *96*, 990; (b) Takata, N.; Shiraki, K.; Takano, R.; Hayashi, Y.; Terada, K. *Cryst. Growth & Des.* **2008**, *8*, 3032.
- <sup>27</sup> Bernstein, J. *Nat. Mater.* **2005**, *4*, 427.
- <sup>28</sup> (a) Bis, J. A.; Vishweshwar, P.; Middleton, R. A.; Zaworotko, M. J. *Cryst. Growth & Des.* **2006**, *6*, 1048; (b) Fleishman, S. G.; Kuduva, S. S.; McMahon, J. A.; Moulton, B.; Rosa, D.; Bailey, W.; Rodriguez-Hornedo, N.; Zaworotko, M. J. *Cryst. Growth & Des.* **2003**, *3*, 909.
- <sup>29</sup> Aakeröy, C. B.; Beatty, A. M.; Helfrich, B. A. *Angew. Chem. Int. Ed.* **2001**, *40*(17), 3240.
- <sup>30</sup> (a) Johnson, S. L.; Rumon, K. A. *J. Phys. Chem.* **1965**, *69*, 74; (b) Huang, K-S.; Britton, D.; Etter, M. C.; Byrn, S. R. *J. Mater. Chem.* **1997**, *7*(5), 713; (c) Childs, S. L.; Stahly, G. P.; Park, A. *Mol. Pharm.* **2007**, *4*(3), 323.
- <sup>31</sup> Bhogala, B. R.; Basavoju, S.; Nangia, A. *CrystEngComm* **2005**, *7*, 551.
- <sup>32</sup> (a) Rubin, J.; Senkowski, B. Z.; Panson, G. S. *J. Phys. Chem.* **1964**, *68*, 1601; (b) Kamlet, M. J.; Gal, J. F.; Maria, P. C.; Taft, R.W. *J. Chem. Soc. Perkin Trans. 2* **1985**, 1583.
- <sup>33</sup> Hunter, C. A. *Angew. Chem. Int. Ed.* **2004**, *43*, 5310.
- <sup>34</sup> Abraham, M. H.; Platts, J. A. *J. Org. Chem.* **2001**, *66*, 3484.
- <sup>35</sup> (a) Stanton, M. K.; Bak, A. *Crystal Growth & Design*, **2008**, *8*, 3856; (b) Viertelhaus, M.; Hilfiker, R.; Blatter, F.; Neuburger, M. *Cryst. Growth Des.* **2009**, *9*, 2220; (c) Nehm, S. J.; Rodríguez-Spong, B.; Rodríguez-Hornedo, N. *Crystal Growth & Design*, **2006**, *6*, 592; (d) Schultheiss, N.; Newman, A. *Crys. Growth & Des.* **2009**, *9*, 2950.
- <sup>36</sup> Miroshnyk, I.; Mirza, S.; Sandler, N. *Expert Opinion on Drug Delivery* **2009**, *6*, 333.
- <sup>37</sup> Remenar, J. F.; Morissette, S. L.; Peterson, M. L.; Moulton, B.; MacPhee, J. M.; Guzmán, H. R.; Almarsson, Ö. *J. Am. Chem. Soc.* **2003**, *125*, 8456.
- <sup>38</sup> Walsh, R. D. B.; Bradner, M. W.; Fleischman, S.; Morales, L. A.; Moulton, B.; Rodríguez-Hornedo, N.; Zaworotko, M. J. *Chem. Commun.* **2003**, 186.
- <sup>39</sup> (a) Jones, W.; Motherwell, W. D. S.; Trask, A. V. *MRS Bull.* **2006**, *31*, 875; (b) Jayasankar, A.; Somwangthanaroj, A.; Shao, A. J.; Rodríguez-Hornedo, N. *Pharm. Res.* **2006**, *23*, 2381; (c) Steuber, H.; Zentgraf, M.; Gerlach, C.; Sotriffer, A.; Heine, A.; Klebe, G. *J. Mol. Biol.* **2006**, *363*, 174; (d) Trask, A. V.; Motherwell, W. D. S.;

- Jones, W. *Int. J. Pharm.* **2006**, *320*, 114; (e) Reddy, L. S.; Babu, N. J.; Nangia, A. *Chem. Commn.* **2006**, *13*, 1369.
- <sup>40</sup> (a) Fleischman, S. G.; Kuduva, S. S.; McMahon, J. A.; Moulton, B.; Bailey Walsh, R. D.; Rodriguez-Homedo, N.; Zaworotko, M. J. *Cryst. Growth. Des.* **2003**, *3*, 909; (b) Remenar, J. F.; Morissette, S. L.; Peterson, M. L.; Moulton, B.; MacPhee, J. M.; Guzman, H. R.; Almarsson, O. *J. Am. Chem. Soc.* **2003**, *125*, 8456; (c) Trask, A. V.; Motherwell, W. D. S., Jones, W. *Int. J. Pharm.* **2006**, *320*, 114; (d) Sun, C. C.; Hou, H. *Cryst. Growth Des.* **2008**, *8*, 1575.
- <sup>41</sup> Higgins, W. M.; Dunker, M. F. W. *J. Am. Pharm. Assoc.* **1944**, *33*, 310.
- <sup>42</sup> Craven, B. M.; Gartland, G. L. *J. Pharm. Sci.* **1970**, *59*, 1666.
- <sup>43</sup> Higuchi, T.; Pitman, I. H. *J. Pharm. Sci.* **1973**, *62*, 55.
- <sup>44</sup> Remenar, J. F.; Morissette, S. L.; Peterson, M. L.; Moulton, B.; MacPhee, J. M.; Guzman, H. R.; Almarsson, O. *J. Am. Chem. Soc.* **2003**, *125*, 8456.
- <sup>45</sup> Childs, S. L.; Hardcastle, K. I. *Cryst. Growth & Des.* **2007**, *7*, 1291.
- <sup>46</sup> Childs, S. L.; Rodriguez-Hornedo, N.; Reddy, L. S.; Jayasankar, A.; Maheshwari, C.; McCausland, L.; Shipplett, R.; Stahly, B. C. *CrystEngComm.* **2008**, *10*, 856.
- <sup>47</sup> Childs, S. L.; Chyall, L. J.; Dunlap, J. T.; Smolenskaya, V. N.; Stahly, B. C.; Stahly, G. P. *J. Am. Chem. Soc.* **2004**, *126*, 13335.
- <sup>48</sup> Basavoju, S.; Bostrm, D.; Velaga, S. P. *Cryst. Growth & Des.* **2006**, *6*(12), 2699.
- <sup>49</sup> McNamara, D. P.; Childs, S. L.; Giordano, J.; Iarriccio, A.; Cassidy, J.; Shet, M. S.; Mannion, R.; O'Donnell, E.; Park, A. *Pharm. Res.* **2006**, *23*, 1888.
- <sup>50</sup> Trask, A. V.; Motherwell, W. D. S.; Jones, W. *Cryst. Growth Des.* **2005**, *5*, 1013.
- <sup>51</sup> Swarbrick, J.; Boylan, J. C. *Encyclopedia of pharmaceutical technology* **2007**, 3<sup>rd</sup> ed. Vol. 1, New York, Informa Healthcare USA, Inc.
- <sup>52</sup> Chen, J.; Rebek, J., Jr. *Org. Lett.* **2002**, *4*, 327.
- <sup>53</sup> Hof, F.; Craig, S. L.; Nuckolls, C.; Rebek, J. *Angew. Chem. Int. Ed.* **2002**, *41*, 1488.
- <sup>54</sup> (a) Conn, M. M.; Rebek, J. *Chem.Rev.* **1997**, *97*, 1647; (b) Heinz, T.; Rebek, J. *Nature* **1998**, *394*, 764; (c) Prins, L. J.; Huskens, J.; de Jong, F.; Timmermann, P.; Reinhoudt, D. N. *Nature* **1999**, *398*, 498; (d) Rivera, J. M.; Craig, S. L.; Marti'n, T.; Rebek, J. *Angew. Chem., Int. Ed.* **2000**, *39*, 2130.
- <sup>55</sup> (a) Wyler, R.; de Mendoza, J.; Rebek, Jr., J. *Angew. Chem.* **1993**, *105*, 1820; (b) Branda, N.; Wyler, R.; Rebek, Jr., J. *Science* **1994**, *263*, 1267.
- <sup>56</sup> (a) Branda, N.; Grotzfeld, R. M.; Valdes, C.; Rebek, Jr., J. *J. Am. Chem. Soc.* **1995**, *117*, 85; (b) Rivera, J. M.; Martin, T.; Rebek, Jr., J. *J. Am. Chem. Soc.* **1998**, *120*, 819.
- <sup>57</sup> Struck, O.; Verboom, W.; Smeets, W. J. J.; Spek, A. L.; Reinhoudt, D. N. *J. Chem. Soc. Perkin Trans.* **1997**, *2*, 223.
- <sup>58</sup> (a) Koh, K.; Araki, A.; Shinkai, S. *Tetrahedron Lett.* **1994**, *35*, 8255; (b) Vreekamp, R. H.; Verboom, W.; Reinhoudt, D. N. *J. Org. Chem.* **1996**, *61*, 4282.
- <sup>59</sup> Shimizu, K. D.; Rebek, Jr., J. *Proc. Natl. Acad. Sci. USA* **1995**, *92*, 12403.
- <sup>60</sup> (a) Mogck, O.; Bohmer, V.; Vogt, W. *Tetrahedron* **1996**, *52*, 8489. (b) Castellano, R. K.; Kim, B. H.; Rebek, Jr. *J. Am. Chem. Soc.* **1997**, *119*, 12671.
- <sup>61</sup> Yanase, M.; Haino, T.; Fukazawa, Y. *Tetrahedron Lett.* **1999**, *40*, 2781.
- <sup>62</sup> (a) Arduini, A.; Domiano, L.; Ogliosi, L.; Pochini, A.; Secchi, A.; Ungaro, R. *J. Org. Chem.* **1997**, *62*, 7866. (b) Rincon, A. M.; Prados, P.; de Mendoza, J. *Eur. J. Org. Chem.* **2002**, 640. (c) Arduini, A.; Ferdani, R.; Pochini, A.; Secchi, A.; Ugozzoli, F.;

- 
- Sheldrick, G. M.; Prados, P.; Gonzalez, J. J.; de Mendoza, J. J. *Supramol. Chem.* **2002**, *2*, 85.
- <sup>63</sup> Heinz, T.; Rudkevich, D. M.; Rebek, Jr. J. *Nature (London)* **1998**, *394*, 764.
- <sup>64</sup> (a) Cho, Y. L.; Rudkevich, D. M.; Rebek, Jr. J. *J. Am. Chem. Soc.* **2000**, *122*, 9868. (b) MacGillivray, L. R.; Diamente, P. R.; Reid, J. L.; Ripmeester, J. A. *Chem. Commun.* **2000**, 359. (c) Murayama, K.; Aoki, K. *Chem. Commun.* **1998**, 607. (d) Rose, K. N.; Barbour, L. J.; Orr, G. W.; Atwood, J. L. *Chem. Commun.* **1998**, 407. (e) Shivanyuk, A.; Rissanen, K.; Kolehmainen, E. *Chem. Commun.* **2000**, 1107. (f) Shivanyuk, A.; Friese, J. C.; Doring, S.; Rebek, Jr. J. *J. Org. Chem.* **2003**, *68*, 6489.
- <sup>65</sup> MacGillivray, L. R.; Atwood, J. L. *Nature* **1997**, *389*, 469.
- <sup>66</sup> Zadnard, R.; Schrader, T.; Grawe, T.; Kraft, A. *Org. Lett.* **2002**, *4*(10), 1687.
- <sup>67</sup> Cram, D. J.; Choi, H.-J.; Bryant, J. A.; Knobler, C. B. *J. Am. Chem. Soc.* **1992**, *114*, 7748.
- <sup>68</sup> Heinz, T.; Rudkevich, D. M.; Rebek, Jr., J. *Nature* **1998**, *394*, 764.
- <sup>69</sup> Ajami, D.; Rebek, J. *Supramolecular Chem.* **2009**, *21*(1-2), 103.
- <sup>70</sup> (a) Rebek, Jr., J. *Chem. Soc. Rev.* **1996**, 255; (b) Conn, M. M.; Rebek, Jr., J. *Chem. Rev.* **1997**, *97*, 1647; (c) Rebek, Jr., J. *Acc. Chem. Res.* **1999**, *32*, 278; (d) Rebek, Jr., J. *Chem. Commun.* **2000**, 637.
- <sup>71</sup> Chapman, R. G.; Sherman, J. C. *J. Am. Chem. Soc.* **1998**, *120*, 9818.
- <sup>72</sup> Kobayashi, K.; Shirasaka, T.; Horn, E.; Furukawa, N.; Yamaguchi, K.; Sakamoto, S. *Chem. Commun.* **2000**, 41.
- <sup>73</sup> Kobayashi, K.; Ishii, K.; Sakamoto, S.; Shirasaka, T.; Yamaguchi, K. *J. Am. Chem. Soc.* **2003**, *125*, 10615.

## CHAPTER 2 - Mapping out the synthetic landscape of recrystallization, co-crystallization and salt formation

### 2.1 Introduction

The synthetic method of choice for co-crystal synthesis typically employs a combination of complementary hydrogen-bond functionalities that reside on different molecular entities, and a key aspect of this approach is that heteromeric interactions (resulting in co-crystallization) need to be more favorable than homomeric interactions (which simply lead to recrystallization).<sup>1</sup> Our operating strategy for supramolecular synthesis of binary co-crystals will be that if we can control the binding affinity between different molecules bearing complementary hydrogen-bond moieties, then we can manipulate the balance between homomeric and heteromeric interactions.

Most hydrogen bonds are primarily electrostatic in nature and centers on the Coulombic attraction between an acidic hydrogen atom and a suitable acceptor atom with surplus negative charge.<sup>2</sup> Therefore, it makes sense to focus on controlling the balance between electrostatic charges when developing versatile and modular synthetic strategies for hydrogen-bond driven assembly of co-crystals.<sup>3</sup> By simply adding (through covalent synthesis) suitable electron-donating/withdrawing groups to a molecule, we can dial-in the electrostatic charge on the acidic proton of the hydrogen-bond donor site. An increase in charge difference will increase the strength of the hydrogen bond which, in turn, will increase the chances of co-crystal formation (as long as the primary hydrogen-bond donor and acceptor sites are located on different molecules).<sup>4</sup> Hunter has demonstrated how molecular electrostatic potential (MEP) surface calculations can be used to assign relative hydrogen-bond donor/acceptor strengths of various chemical functionalities,<sup>2</sup> and we will employ this approach for quantifying the electrostatic charge on individual atoms within molecules. Prevailing definitions of the term ‘co-crystal’ state that such a compound only contain electrically neutral components<sup>5</sup> and therefore in addition to controlling the efficiency of the assembly process, the supramolecular yield, we must also ensure that we actually produce the targeted co-crystal, and not a salt, Table 2.1.

**Table 2.1** Summary of possible outcomes in a series of attempted co-crystallization reactions.

Reactants	Driving force	Products
$A_{\text{soln}} + D_{\text{soln}}$	Homomeric interactions dominate	$A(s) + D(s)$ Recrystallization
	Heteromeric interactions dominate	$[A \cdots D](s)$ Co-crystallization
	Proton transfer	$[A]^{n+}[D]^{n-}(s)$ Salt formation

The goal of this study is to map out the synthetic landscape that determines the solid-state outcome of the reactions between a series of Brønsted-Lowry acids and bases. The reactivity of each component will be examined using co-crystallization reactions, and rationalized in the context of electrostatic charges on individual hydrogen-bond donor/acceptor sites.

Our model system comprises a library of aliphatic and aromatic carboxylic acids as the hydrogen-bond donor, and a series of substituted aminopyridine-based molecules as the hydrogen-bond acceptor. The rationale behind the choice of base was based upon existing crystallographic data from the Cambridge Structural Database.<sup>6</sup>

**Table 2.2** CSD search on the ligands of interest in a series of pyridines.

	Ligands	Hits	Salts	Co-crystals
<b>1</b>	2-aminopyridine	35	33	2
<b>2</b>	2-amino-5-bromopyridine	1	1	0
<b>3</b>	2-acetamidopyridine	8	0	8
<b>4</b>	2-propionamido-5-bromopyridine	0	0	0
<b>5</b>	2-amino-3,5-dibromopyridine	0	0	0
<b>6</b>	2-acetamido-5-bromopyridine	0	0	0
<b>7</b>	2-acetamido-3,5-dibromopyridine	0	0	0

A CSD search for crystal structures containing 2-aminopyridine and a carboxylic acid resulted in 35 hits, 33 of which were salts. A similar search for 2-acetamidopyridine and carboxylic acids yielded eight hits, all of which were co-crystals. The latter base has the same chemical and geometric complementarity towards a carboxylic acid as does 2-aminopyridine, but it is significantly less basic, and the pyridyl nitrogen atom has a substantially lower electrostatic charge. The fact that the difference in electrostatic



charge on the two pyridyl-compounds lead to dramatically different products (33/35 salts vs 8/8 co-crystals), Table 2.2, indicates that this type of molecule can offer a test-bed for examining the parameters that govern hydrogen-bond driven co-crystal synthesis.

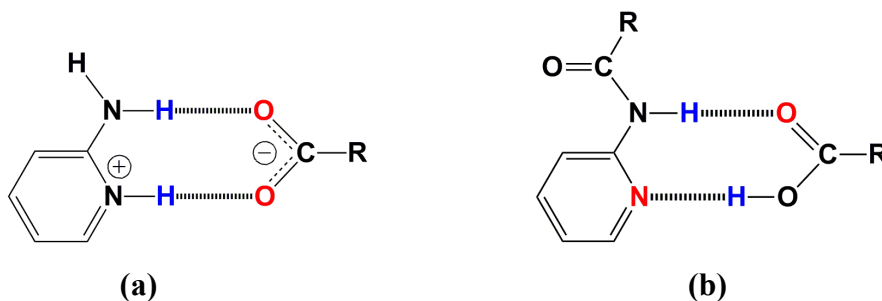


**Figure 2.1** Formation of (a) 2-aminopyridinium carboxylate salt, (b) 2-acetamidopyridine carboxylic acid co-crystal.

Through covalent synthesis we can produce a specific charge on the pyridyl nitrogen atom and subsequently establish if there are defined boundaries between recrystallization/co-crystallization/salt-formation that can be understood and predicted a priori using MEPS derived charges and a simple electrostatic view of hydrogen-bonds.

## 2.2 Experimental

We employed seven pyridine-based molecules as hydrogen-bond acceptors, Figure 2.2. All of them have the same primary binding moiety comprising an N/N-H hydrogen-bond donor/acceptor site and the electrostatic charge on the pyridyl nitrogen atom is modulated through covalent substitutions that do not create any steric impediments to binding.

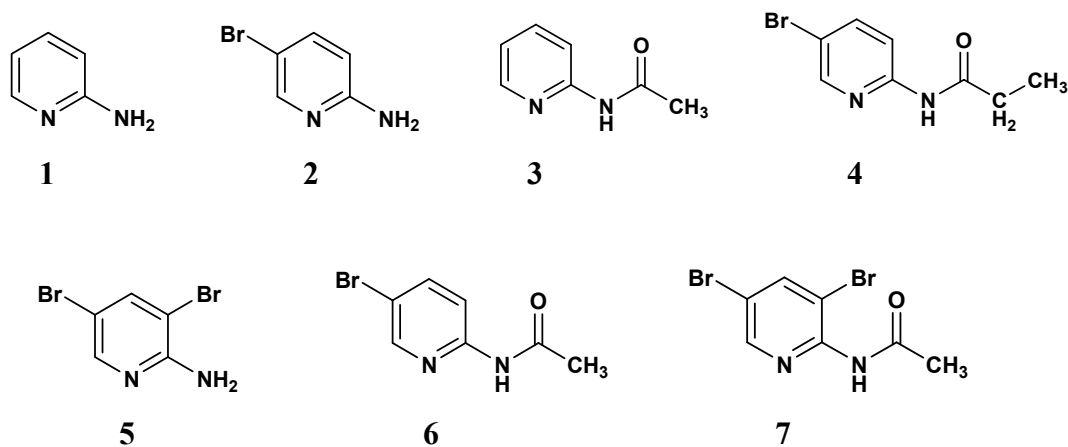
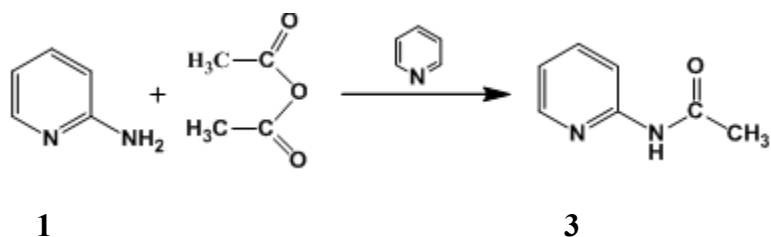


**Figure 2.2** Library of pyridine-based hydrogen-bond acceptors.

### 2.2.1 Synthesis of pyridyl compounds

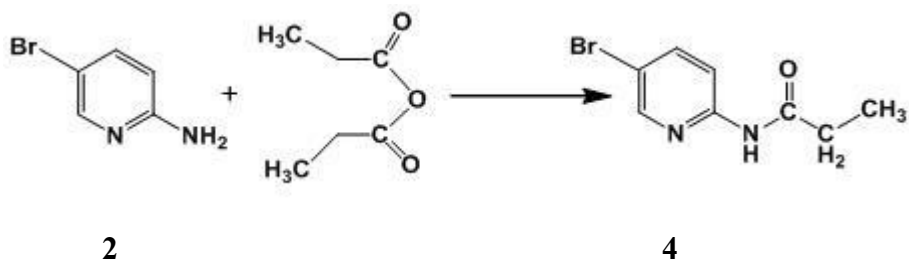
All carboxylic acids and the ligands 2-aminopyridine **1**, 2-amino-5-bromopyridine **2**, and 2-amino-3,5-dibromopyridine **5** were purchased from Aldrich and used without further purification. Acetamido-substituted pyridines were synthesized following previously reported methods.<sup>7</sup> The determinations of melting points were carried out on Fisher-Johns melting point apparatus and are uncorrected. Compounds were prepared for infrared spectroscopic (IR) analysis as a mixture in KBr. <sup>1</sup>H NMR and <sup>13</sup>C NMR spectra were recorded on a Varian Unity plus 200 MHz spectrometer in CDCl<sub>3</sub>.

#### 2.2.1.1 Synthesis of 2-acetamidopyridine, **3**



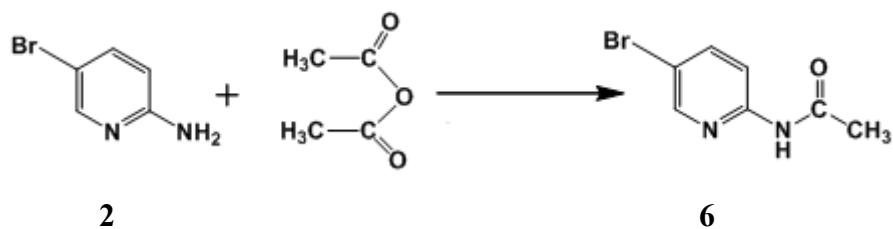
The synthesis of 2-acetamidopyridine **3** was carried out by a previously reported method.<sup>7</sup> 2-Aminopyridine **1** (1.0 g, 10.6 mmol) was dissolved in a mixture of pyridine (4 mL) and acetic anhydride (5 mL). The resulting solution was stirred at room temperature for 24 hours. Water (20 mL) was added to the mixture and the solution evaporated to dryness. Upon recrystallization with ethyl acetate, large colorless crystals were obtained. Yield 80%, M. P. 73-75 °C; IR (KBr pellet)  $\nu$  1695 cm<sup>-1</sup> (C=O, s), 1533 cm<sup>-1</sup> (Amide II, s); <sup>1</sup>H NMR ( $\delta$ H; 200 MHz, CDCl<sub>3</sub>): 9.05 (NH, br), 8.26 (2H, overlap), 7.72 (1H, dt), 7.05 (1H, dt), 2.21 (3H, s).

#### 2.2.1.2 Synthesis of 2-propioamido-5-bromopyridine, **4**



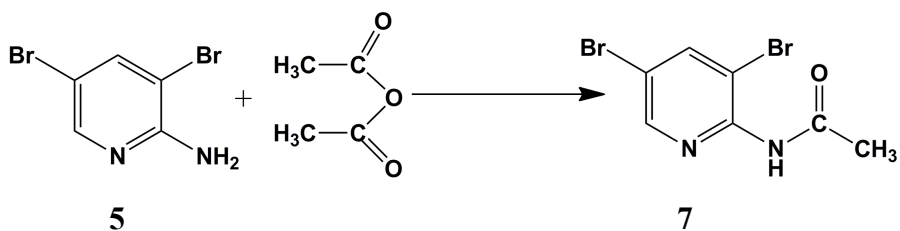
2-Amino-5-bromopyridine **2** (5.0 g, 28.9 mmol) was dissolved in propionic anhydride (5 mL). The mixture was refluxed at 65°C for 1 hr. The excess of propionic anhydride and propionic acid produced was removed via vacuum distillation to obtain a white powder. Upon recrystallization from ethyl acetate, white needle shaped crystals were obtained. Yield 95%, M. P. 140-143 °C; IR (KBr pellet)  $\nu$  3241  $\text{cm}^{-1}$  (N—H, br), 1667  $\text{cm}^{-1}$  (C=O, s), 1566  $\text{cm}^{-1}$  (Amide II, s) ;  $^1\text{H}$  NMR ( $\delta\text{H}$ ; 200 MHz,  $\text{CDCl}_3$ ): 8.31 (1H, d), 8.17 (1H, d), 7.95 (NH, br), 7.8 (1H, dd), 2.44(2H, q), 1.25 (3H, t);  $^{13}\text{C}$  NMR ( $\delta\text{C}$ ; 200 MHz,  $\text{CDCl}_3$ ): 172.71, 150.49, 148.54, 141.03, 115.63, 114.53, 30.82, 9.45.

### 2.2.1.3 Synthesis of 2-acetamido-5-bromopyridine, **6**



2-Amino-5-bromopyridine **2** (3.47g, 20.00 mmol) was dissolved in acetic anhydride (5 mL) added dropwise. The mixture was heated under reflux at 60°C for 30 mins. Excess acetic anhydride and acetic acid produced were removed via vacuum distillation to obtain a white powder. Upon recrystallization from methanol, white needle shaped crystals were obtained. Yield 85%, M. P. 176-178 °C; IR (KBr pellet)  $\nu$  3242  $\text{cm}^{-1}$  (N—H, br), 1670  $\text{cm}^{-1}$  (C=O, s), 1538  $\text{cm}^{-1}$  (Amide II, s);  $^1\text{H}$  NMR ( $\delta\text{H}$ ; 200 MHz,  $\text{CDCl}_3$ ): 8.32 (1H, d), 8.2 (1H, s), 8.13 (NH, br), 7.8 (1H, dd), 2.21 (3H, s);  $^{13}\text{C}$  NMR ( $\delta\text{C}$ ; 200 MHz,  $\text{CDCl}_3$ ): 168.99, 150.44, 148.57, 141.1, 115.67, 114.69, 24.87.

### 2.2.1.4 Synthesis of 2-acetamido-3,5-dibromopyridine, **7**



2-Amino-3,5-dibromopyridine **5** (2.00 g, 7.94 mmol) was dissolved in acetic anhydride (3 mL). The mixture was refluxed at 50°C for 30 mins. The acetic acid was removed via vacuum distillation to obtain a mixture of 2-acetamido-3,5-dibromopyridine **7**, 2-bisacetamido-3,5-dibromopyridine, and the starting material. Purification was carried out via column chromatography with hexane: ethyl acetate (7:3) as eluant. Upon recrystallization in acetonitrile, white needle shaped crystals were obtained. Yield 40%, M. P. 165-168 °C; IR (KBr pellet)  $\nu$  1678  $\text{cm}^{-1}$  (C=O, s), 1510  $\text{cm}^{-1}$  (Amide II, s);  $^1\text{H}$  NMR ( $\delta\text{H}$ ; 200 MHz,  $\text{CDCl}_3$ ): 8.39(1H, d), 8.02(1H, d), 7.86(NH, br), 2.43(3H, s);  $^{13}\text{C}$  NMR ( $\delta\text{C}$ ; 200 MHz,  $\text{CDCl}_3$ ).

### 2.2.2 Synthesis of co-crystals and salts

Each of the seven pyridyl compounds was subjected to co-crystallization reactions with fifteen different carboxylic acids. There were ten monocarboxylic acids: 4-cyanobenzoic acid (**a**), 3-hydroxybenzoic acid (**b**), 4-chlorobenzoic acid (**c**), 4-fluorobenzoic acid (**d**), 4-nitrobenzoic acid (**e**), 3,4-dichlorobenzoic acid (**f**), 2,6-difluorobenzoic acid (**g**), 3,5-dimethylbenzoic acid (**h**), 3,5-dinitrobenzoic acid (**i**), pentafluorobenzoic acid (**j**) and five dicarboxylic acids: suberic acid (**k**), phthalic acid (**l**), fumaric acid (**m**), succinic acid (**n**), and sebacic acid (**o**). A mixture of aliphatic and aromatic carboxylic acids, weak and strong, were included in the set in order to remove any inadvertent bias arising from the nature of the carboxylic acids.

Stoichiometric amounts of base and acid, either 1:1 (monoacids) or 2:1 (diacids) were dissolved separately in suitable solvents and mixed together. The resulting solution was warmed and allowed to stand for slow evaporation at room temperature. The resulting precipitates were initially examined using IR spectroscopy. Reactions that produced suitable crystals were characterized using single-crystal X-ray diffraction (eighteen such samples were obtained).

#### 2.2.2.1 Synthesis of 2-aminopyridinium 4-cyanobenzoate, **1a**

2-Aminopyridine (0.015 g, 0.160 mmol) was dissolved in 5mL of ethyl acetate. To this solution was added 4-cyanobenzoic acid (0.023 g, 0.160 mmol) in 5 mL of ethyl acetate. The resulting solution was warmed and allowed to stand for slow evaporation at

room temperature. Colorless, rod-shaped crystals were obtained after 4 days. M. P. 191–194°C; IR (KBr pellet)  $\nu$  2433  $\text{cm}^{-1}$ , 1976  $\text{cm}^{-1}$  ( $\text{O}^{\cdot}\dots\text{H-N}^+$ , br), 1655  $\text{cm}^{-1}$  ( $\text{COO}^{\cdot}$ , s)

#### **2.2.2.2 Synthesis of 2-aminopyridinium 4-chlorobenzoate, 1c**

2-Aminopyridine (0.015 g, 0.160 mmol) was dissolved in 5 mL of ethyl acetate. To this solution was added 4-chlorobenzoic acid (0.025 g, 0.160 mmol) in 5 mL of ethyl acetate. The resulting solution was warmed and allowed to stand for slow evaporation at room temperature. Colorless, block-shaped crystals were obtained after 4 days. M. P. 148–150°C; IR (KBr pellet)  $\nu$  2518  $\text{cm}^{-1}$ , 1947  $\text{cm}^{-1}$  ( $\text{O}^{\cdot}\dots\text{H-N}^+$ , br), 1670  $\text{cm}^{-1}$  ( $\text{COO}^{\cdot}$ , s)

#### **2.2.2.3 Synthesis of 2-aminopyridinium 2,6-difluorobenzoate, 1g**

2-Aminopyridine (0.015 g, 0.160 mmol) was dissolved in 5 mL of ethyl acetate. To this solution was added 2,6-difluorobenzoic acid (0.025 g, 0.160 mmol) in 5 mL of ethyl acetate. The resulting solution was warmed and allowed to stand for slow evaporation at room temperature. Colorless, hexagon-shaped crystals were obtained after 3 days. M. P. 158–160°C; IR (KBr pellet)  $\nu$  2564  $\text{cm}^{-1}$ , 2022  $\text{cm}^{-1}$  ( $\text{O}^{\cdot}\dots\text{H-N}^+$ , br), 1617  $\text{cm}^{-1}$  ( $\text{COO}^{\cdot}$ , s)

#### **2.2.2.4 Synthesis of 2-aminopyridinium pentafluorobenzoate, 1j**

2-Aminopyridine (0.015 g, 0.160 mmol) was dissolved in 5 mL of ethyl acetate. To this solution was added pentafluorobenzoic acid (0.034 g, 0.160 mmol) in 5 mL of ethyl acetate. The resulting solution was warmed and allowed to stand for slow evaporation at room temperature. Colorless, block-shaped crystals were obtained after 3 days. M. P. 168–170°C; IR (KBr pellet)  $\nu$  2598  $\text{cm}^{-1}$ , 2022  $\text{cm}^{-1}$  ( $\text{O}^{\cdot}\dots\text{H-N}^+$ , br), 1593  $\text{cm}^{-1}$  ( $\text{COO}^{\cdot}$ , s)

#### **2.2.2.5 Synthesis of bis(2-aminopyridinium) suberate, 1k**

2-Aminopyridine (0.015 g, 0.160 mmol) was dissolved in 5 mL of ethyl acetate. To this solution was added suberic acid (0.014 g, 0.080 mmol) in 5 mL of ethyl acetate. The resulting solution was warmed and allowed to stand for slow evaporation at room temperature. Colorless, needle-shaped crystals were obtained after 4 days. M. P. 112–115°C; IR (KBr pellet)  $\nu$  2741  $\text{cm}^{-1}$ , 2016  $\text{cm}^{-1}$  ( $\text{O}^{\cdot}\dots\text{H-N}^+$ , br), 1502  $\text{cm}^{-1}$  ( $\text{COO}^{\cdot}$ , s)

#### **2.2.2.6 Synthesis of bis(2-aminopyridinium) succinate, 1n**

2-Aminopyridine (0.015 g, 0.160 mmol) was dissolved in 5 mL of ethyl acetate. To this solution was added succinic acid (0.01 g, 0.08 mmol) in 5 mL of ethyl acetate. The resulting solution was warmed and allowed to stand for slow evaporation at room temperature. Colorless, needle-like crystals were obtained after 4 days. M. P. 162–165 °C; IR (KBr pellet)  $\nu$  2495  $\text{cm}^{-1}$ , 1964  $\text{cm}^{-1}$  ( $\text{O}^{\cdot}\dots\text{H-N}^+$ , br), 1656  $\text{cm}^{-1}$  ( $\text{COO}^-$ , s).

#### **2.2.2.7 Synthesis of bis(2-aminopyridinium) sebacate, 1o**

2-Aminopyridine (0.015 g, 0.160 mmol) was dissolved in 5 mL of ethyl acetate. To this solution was added sebacic acid (0.016 g, 0.080 mmol) in 5 mL of ethyl acetate. The resulting solution was warmed and allowed to stand for slow evaporation at room temperature. Colorless, plate-like crystals were obtained after 4 days. M. P. 98–100 °C; IR (KBr pellet)  $\nu$  2370  $\text{cm}^{-1}$ , 1936  $\text{cm}^{-1}$  ( $\text{O}^{\cdot}\dots\text{H-N}^+$ , br), 1661  $\text{cm}^{-1}$  ( $\text{COO}^-$ , s).

#### **2.2.2.8 Synthesis of 2-amino-5-bromopyridinium 4-cyanobenzoate, 2a**

A solution of 2-amino-5-bromopyridine (0.030 g, 0.173 mmol) in 5 mL of acetonitrile was mixed with 4-cyanobenzoic acid (0.026 g, 0.173 mmol) in 5 mL of acetonitrile and allowed to stand at room temperature for slow evaporation. Colorless, block-shaped crystals were obtained after 4 days. M. P. 143–145 °C; IR (KBr pellet)  $\nu$  2363  $\text{cm}^{-1}$ , 1983  $\text{cm}^{-1}$  ( $\text{O}^{\cdot}\dots\text{H-N}^+$ , br), 1671  $\text{cm}^{-1}$  ( $\text{COO}^-$ , s).

#### **2.2.2.9 Synthesis of 2-amino-5-bromopyridinium 4-nitrobenzoate, 2e**

A solution of 2-amino-5-bromopyridine (0.030 g, 0.173 mmol) in 5 mL of acetonitrile was mixed with 4-nitrobenzoic acid (0.029 g, 0.173 mmol) in 5 mL of acetonitrile and allowed to stand at room temperature for slow evaporation. Yellow colored, flat crystals were obtained after 5 days. M. P. 172–174 °C; IR (KBr pellet)  $\nu$  2712  $\text{cm}^{-1}$ , 1945  $\text{cm}^{-1}$  ( $\text{O}^{\cdot}\dots\text{H-N}^+$ , br), 1649  $\text{cm}^{-1}$  ( $\text{COO}^-$ , s).

#### **2.2.2.10 Synthesis of 2-acetamidopyridine/succinic acid (2:1), 3n**

A solution of 2-acetamidopyridine (0.027 g, 0.200 mmol) and succinic acid (0.012 g, 0.100 mmol) in 10 mL of ethanol was boiled and allowed to stand at room temperature for slow evaporation. Colorless prisms were afforded after one week. M. P.

165—167°C; IR (KBr pellet)  $\nu$  2450  $\text{cm}^{-1}$ , 1870  $\text{cm}^{-1}$  (O—H...N, br), 1706  $\text{cm}^{-1}$  (C=O, s), 1550  $\text{cm}^{-1}$  (Amide II, s).

#### **2.2.2.11 Synthesis of 2-propiamido-5-bromopyridine/3,4-dichlorobenzoic acid (1:1), 4f**

A solution of 2-propiamido-5-bromopyridine (0.030 g, 0.131 mmol) in 5 mL of acetonitrile was mixed with 3,4-dichlorobenzoic acid (0.025 g, 0.131 mmol) in 5 mL of acetonitrile and allowed to stand at room temperature for slow evaporation. Colorless, thin, needle-shaped crystals were obtained after 4 days. M. P. 170—172°C; IR (KBr pellet)  $\nu$  2474  $\text{cm}^{-1}$ , 1923  $\text{cm}^{-1}$  (O—H...N, br), 1705  $\text{cm}^{-1}$  (C=O, s), 3259  $\text{cm}^{-1}$  (N—H amide, s), 1570  $\text{cm}^{-1}$  (Amide II, s).

#### **2.2.2.12 Synthesis of 2-propiamido-5-bromopyridine/suberic acid (2:1), 4k**

A solution of 2-propiamido-5-bromopyridine (0.030 g, 0.131 mmol) in 5 mL of acetonitrile was mixed with suberic acid (0.012 g, 0.066 mmol) in 5 mL of acetonitrile and allowed to stand at room temperature for slow evaporation. Colorless, block-shaped crystals were obtained after 6 days. M. P. 118—120°C; IR (KBr pellet)  $\nu$  2597  $\text{cm}^{-1}$ , 1816  $\text{cm}^{-1}$  (O—H...N, br), 1700  $\text{cm}^{-1}$  (C=O, s), 3255  $\text{cm}^{-1}$  (N—H amide, s), 1565  $\text{cm}^{-1}$  (Amide II, s).

#### **2.2.2.13 Synthesis of 2-propiamido-5-bromopyridine/fumaric acid (2:1), 4m**

A solution of 2-propiamido-5-bromopyridine (0.030 g, 0.131 mmol) in 5 mL of acetonitrile was mixed with fumaric acid (0.008 g, 0.066 mmol) in 5 mL of acetonitrile and allowed to stand at room temperature for slow evaporation. Colorless, thin, needle-shaped crystals were obtained after 5 days. M. P. 176—180°C; IR (KBr pellet)  $\nu$  2456  $\text{cm}^{-1}$ , 1867  $\text{cm}^{-1}$  (O—H...N, br), 1705  $\text{cm}^{-1}$  (C=O, s), 3254  $\text{cm}^{-1}$  (N—H amide, s), 1550  $\text{cm}^{-1}$  (Amide II, s).

#### **2.2.2.14 Synthesis of 2-propiamido-5-bromopyridine/succinic acid (2:1), 4n**

A solution of 2-propiamido-5-bromopyridine (0.030 g, 0.131 mmol) in 5 mL of acetonitrile was mixed with succinic acid (0.008 g, 0.066 mmol) in 5 mL of acetonitrile and allowed to stand at room temperature for slow evaporation. Colorless, rod-shaped crystals were obtained after 7 days. M. P. 150—151°C; IR (KBr pellet)  $\nu$  2529  $\text{cm}^{-1}$ ,

1863  $\text{cm}^{-1}$  (O—H...N, br), 1702  $\text{cm}^{-1}$  (C=O, s), 3259  $\text{cm}^{-1}$  (N—H amide, s), 1580  $\text{cm}^{-1}$  (Amide II, s).

#### **2.2.2.15 Synthesis of 2-propionamido-5-bromopyridine/sebacic acid (2:1), 4o**

A solution of 2-propionamido-5-bromopyridine (0.030 g, 0.131 mmol) in 5 mL of acetonitrile was mixed with sebacic acid (0.013 g, 0.066 mmol) in 5 mL of acetonitrile and allowed to stand at room temperature for slow evaporation. Colorless, block-shaped crystals were obtained after 5 days. M. P. 115—117°C; IR (KBr pellet)  $\nu$  2609  $\text{cm}^{-1}$ , 1901  $\text{cm}^{-1}$  (O—H...N, br), 1697  $\text{cm}^{-1}$  (C=O, s), 3250  $\text{cm}^{-1}$  (N—H amide, s), 1560  $\text{cm}^{-1}$  (Amide II, s).

#### **2.2.2.16 Synthesis of 2-amino-3,5-dibromopyridine/3,5-dinitrobenzoic acid (1:1), 5i**

A solution of 2-amino-3,5-dibromopyridine (0.015 g, 0.060 mmol) in 5 mL of ethanol was mixed with 3,5-dinitrobenzoic acid (0.013 g, 0.060 mmol) in 5 mL of ethanol. The mixture was allowed to stand at room temperature for slow evaporation. Light brown colored, rod-shaped crystals were obtained after 4 days. M. P. 150—152°C; IR (KBr pellet)  $\nu$  2550  $\text{cm}^{-1}$ , 1890  $\text{cm}^{-1}$  (O—H...N, br), 1697  $\text{cm}^{-1}$  (C=O, s), 3477  $\text{cm}^{-1}$  (N—H amine, s).

#### **2.2.2.17 Synthesis of 2-amino-3,5-dibromopyridine/fumaric acid (2:1), 5m**

A solution of 2-amino-3,5-dibromopyridine (0.015 g, 0.060 mmol) in 5 mL of ethanol was mixed with 2,4-dinitrobenzoic acid (0.004 g, 0.030 mmol) in 5 mL of ethanol. The mixture was allowed to stand at room temperature for slow evaporation. Light brown colored, needle-shaped crystals were obtained after 5 days. M. P. 198—200°C; IR (KBr pellet)  $\nu$  2398  $\text{cm}^{-1}$ , 1930  $\text{cm}^{-1}$  (O—H...N, br), 1696  $\text{cm}^{-1}$  (C=O, s), 3437  $\text{cm}^{-1}$  (N—H amine, s).

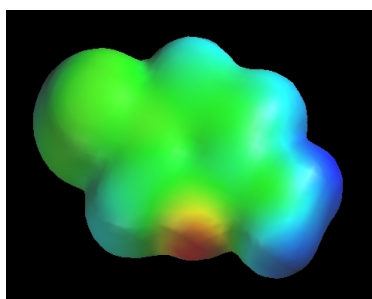
#### **2.2.2.18 Synthesis of 2-acetamido-5-bromopyridine/succinic acid (2:1), 6n**

A solution of 2-acetamido-5-bromopyridine (0.03 g, 0.14 mmol) in 5 mL of ethyl acetate was mixed with fumaric acid (0.008 g, 0.070 mmol) in 5 mL of ethyl acetate. The mixture was allowed to stand at room temperature for slow evaporation. Colorless, thin, rod-shaped crystals were obtained after 4 days. M. P. 158—160°C; IR (KBr pellet)  $\nu$  2452  $\text{cm}^{-1}$ , 1870  $\text{cm}^{-1}$  (O—H...N, br), 1707  $\text{cm}^{-1}$  (C=O, s), 1560  $\text{cm}^{-1}$  (Amide II, s).

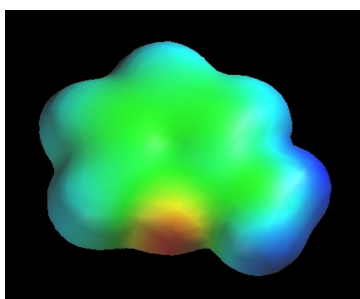


### 2.2.3 Electrostatic charges calculations

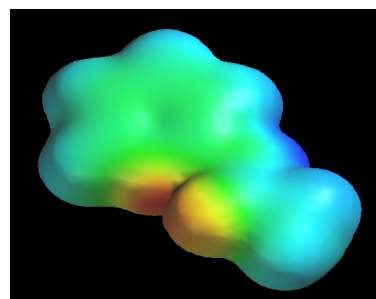
The magnitude of electrostatic charge on hydrogen-bond donors and acceptors in these molecules were obtained using semi-empirical AM1 calculations.<sup>8</sup> Values for individual atoms are obtained by probing the MEPS (0.002 e/au isosurface, from AM1 calculations) with a point charge. For example, the 2-aminopyridine with its strongly electron donating amino group has higher charge (-288 kJ/mol) on the pyridyl-N than the pyridyl nitrogen atom in 2-acetamidopyridine (-260 kJ/mol).



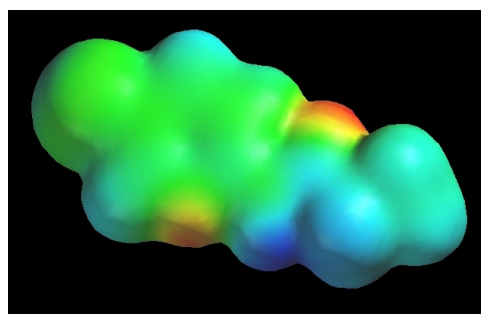
2-aminopyridine, **1**  
(-288 kcal/mol)



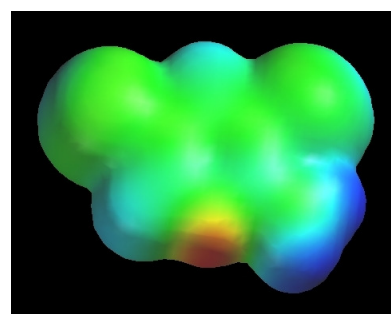
2-amino-5-bromopyridine, **2**  
(-275 kcal/mol)



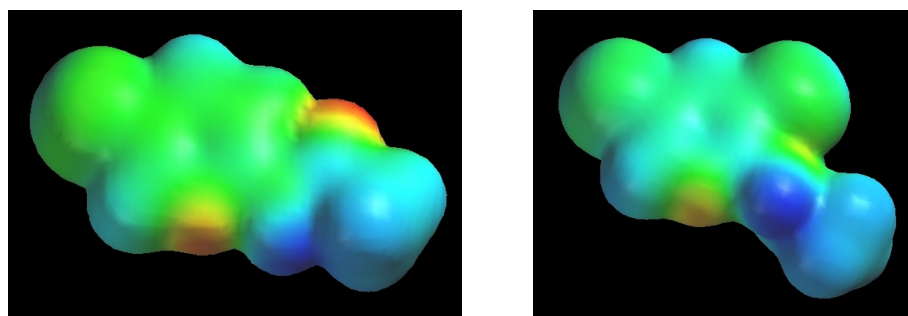
2-acetamidopyridine, **3**  
(-260 kcal/mol)



2-propionamido-5-bromopyridine, **4**  
(-244 kcal/mol)



2-amino-3,5-dibromopyridine, **5**  
(-237 kcal/mol)



2-acetamido-5-bromopyridine, **6**  
(-230 kcal/mol)

2-acetamido-3,5-dibromopyridine, **7**  
(-220 kcal/mol)

**Figure 2.3** AM1 calculations of charges on pyridyl-N on all the ligands under study.

#### *2.2.4 Single Crystal X-ray Crystallography*

X-ray data were collected on a Bruker SMART APEX or a SMART 1000 diffractometer using Mo K $\alpha$  radiation and, where noted, were corrected for absorption using the multiscan procedure implemented by SADABS. Data were collected using SMART. The relevant X-ray data are summarized in Table 2.5 and labeling schemes and thermal ellipsoids for all structures are shown in Figures 2.4, 2.7, 2.15, and 2.18.

### **2.3 Results**

Each pyridyl compound was allowed to react with the same set of 15 carboxylic acids. The solids from all 105 (7 x 15) reactions were screened by IR spectroscopy in order to establish if the result was a co-crystallization, salt formation or a recrystallization.<sup>9</sup> The outcome of this analysis is displayed in Table 2.3. The IR stretching frequencies of interest of all the salts and co-crystals under study is listed in Table 2.4.

**Table 2.3** Results in attempted co-crystallization reactions in pyridine series.

	<b>Ligands</b>	<b>Salts</b>	<b>Co-crystals</b>	<b>No Reaction</b>	<b>Supramol. yield %</b>
<b>1</b>	2-aminopyridine	15	0	0	100
<b>2</b>	2-amino-5-bromopyridine	15	0	0	100
<b>3</b>	2-acetamidopyridine	0	13	2	87
<b>4</b>	2-propionamido-5-bromopyridine	0	14	1	93
<b>5</b>	2-amino-3,5-dibromopyridine	0	12	3	80
<b>6</b>	2-acetamido-5-bromopyridine	0	11	4	73
<b>7</b>	2-acetamido-3,5-dibromopyridine	0	1	14	7

A total of 20 crystal structures are obtained, out of which two are of the ligands by themselves, nine are co-crystals, and nine are salts. The co-crystals and salts are either in 1:1 or 2:1 stoichiometry

**Table 2.4** IR stretching frequencies (cm<sup>-1</sup>) of salts and co-crystals under study.

	Acids							
		1	2	3	4	5	6	7
		2-amino pyridine	2-amino-5-bromopyridine	2-acetamido pyridine	2-propionimido-5-bromopyridine	2-amino-3,5-dibromopyridine	2-acetamido-5-bromopyridine	2-acetamido-3,5-dibromopyridine
<b>a</b>	4-Cyano benzoic acid	1376, 1531, 1655, 1976, 2433	1364, 1475, 1671, 1983, 2363	1702, 1942, 2444	1698, 1893, 2546	1707, 1867, 2433	1701, 1902, 2553	no reaction
<b>b</b>	3-Hydroxy benzoic acid	1365, 1555, 1668, 1970, 2524	1398, 1525, 1915, 2478	1691, 1873, 2478	1674, 1830, 2584	1724, 1890, 2627	1688, 1866, 2584	no reaction
<b>c</b>	4-Chloro benzoic acid	1382, 1540, 1670, 1947, 2518	1394, 1500, 1670, 1983, 2550	1713, 1930, 2450	1705, 1889, 2460	1685, 1873, 2484	no reaction	no reaction
<b>d</b>	4-Fluoro benzoic acid	1376, 1548, 1595, 1966, 2461	1402, 1515, 1650, 1863, 2426	1702, 1862, 2415	1710, 1879, 2553	1698, 1868, 2461	1711, 1870, 2549	no reaction
<b>e</b>	4-Nitrobenzoic acid	1348, 1554, 1990, 2524	1337, 1512, 1649, 1945, 2712	1702, 1919, 2455	1698, 1859, 2542	1696, 1890, 2444	no reaction	no reaction
<b>f</b>	3,4-Dichloro benzoic acid	1371, 1542, 1982, 2478	1330, 1500, 1633, 1880, 2354	1708, 1936, 2455	1705, 1923, 2474	1697, 1879, 2495	1714, 1926, 2409	no reaction
<b>g</b>	2,6-Difluoro benzoic acid	1376, 1601, 1617, 2022, 2564	1335, 1510, 1652, 1929, 2357	1740, 1944, 2433	1710, 1885, 2409	1702, 1839, 2490	1713, 1862, 2524	no reaction
<b>h</b>	3,5-Dimethylbenzoic acid	1375, 1505, 2008, 2386	1325, 1486, 1641, 1874, 2443	1696, 1868, 2480	1698, 1857, 2518	1690, 1845, 2587	1708, 1873, 2598	no reaction
<b>i</b>	3,5-Dinitro benzoic acid	1350, 1548, 1670, 1982, 2735	1350, 1539, 1671, 2011, 2470	1725, 1959, 2550	1716, 1821, 2527	1698, 1890, 2553	1716, 1896, 2774	1691, 1919, 2455
<b>j</b>	Pentafluoro benzoic acid	1359, 1593, 2022, 2598	1371, 1601, 1670, 1997, 2410	1724, 1873, 2513	1720, 1866, 2439	no reaction	1711, 1926, 2518	no reaction
<b>k</b>	Duberic acid	1338, 1502, 2016, 2741	1330, 1490, 1650, 1927, 2422	1711, 1869, 2500	1700, 1816, 2597	1702, 1890, 2655	no reaction	no reaction
<b>l</b>	Phthalic acid	1390, 1561, 1671, 1979, 2480	1355, 1535, 1671, 1961, 2520	1730, 1945, 2478	no reaction	1695, 1953, 2541	no reaction	no reaction
<b>m</b>	Fumaric acid	1379, 1483, 1992, 2490	1325, 1495, 1645, 1874, 2364	1710, 1845, 2440	1705, 1867, 2456	1697, 1930, 2398	1707, 1870, 2452	no reaction
<b>n</b>	Succinic acid	1376, 1542, 1656, 1964, 2495	1340, 1475, 1670, 1991, 2525	1706, 1870, 2450	1702, 1863, 2529	1702, 1873, 2421	1703, 1870, 2540	no reaction
<b>o</b>	Sebacic acid	1312, 1500, 1661, 1936, 2370	1312, 1505, 1628, 1932, 2456	1709, 1895, 2454	1697, 1901, 2609	no reaction	1711, 1861, 2539	no reaction

A summary of the crystallographic information for the salts and co-crystals are presented in the Appendix A and all the hydrogen-bond geometries are listed in Table 2.5.

**Table 2.5** Hydrogen-bond geometries for the ligands, salts, and co-crystals under study.

Structure	D-H...A	d(D-H)/Å	d(H...A)/Å	d(D...A)/Å	<(DHA)/°
<b>4<sup>i</sup></b>	N(17)-H(17)...O(17)#1	0.84(4)	2.05(4)	2.858(3)	161(3)
<b>6<sup>ii</sup></b>	N172-H172...O171#1	0.86(3)	2.10(2)	2.946(2)	167(2)
	N171-H171...O172	0.80(3)	2.13(3)	2.925(2)	174(2)
<b>1a<sup>iii</sup></b>	N(11)-H(11)...O(21)	0.96(2)	1.73(2)	2.6835(16)	175.6(19)
	N(12)-H(12A)...O(22)	0.90(2)	1.87(3)	2.7743(18)	174(2)
	N(12)-H(12B)...O(22)#1	0.85(2)	2.01(2)	2.8329(18)	163(2)
<b>1c<sup>iv</sup></b>	N(11)-H(11)...O(21)	0.94(2)	1.78(2)	2.7253(15)	174.9(18)
	N(12)-H(12A)...O(22)	0.92(2)	1.85(2)	2.7631(16)	179(2)
	N(12)-H(12B)...O(21)#1	0.89(2)	1.95(2)	2.8381(15)	176.0(18)
<b>1g<sup>v</sup></b>	N(11)-H(11)...O(21)	0.926(15)	1.730(15)	2.6531(11)	174.2(13)
	N(12)-H(12A)...O(22)	0.874(16)	2.026(16)	2.8790(12)	165.0(14)
	N(12)-H(12B)...O(21)#1	0.885(16)	1.937(16)	2.8139(12)	170.5(14)
<b>1j<sup>vi</sup></b>	N(11)-H(11)...O(21)	0.926(15)	1.783(15)	2.7037(11)	172.4(14)
	N(12)-H(12A)...O(22)	0.871(16)	1.973(16)	2.8256(12)	165.7(14)
	N(12)-H(12B)...O(21)#1	0.866(15)	1.977(15)	2.8388(12)	173.3(14)
<b>1k<sup>vii</sup></b>	N(11)-H(11)...O(21)	0.945(12)	1.675(12)	2.6166(9)	174.1(11)
	N(12)-H(12A)...O(22)	0.893(14)	1.875(14)	2.7639(10)	173.5(12)
	N(12)-H(12B)...O(22)#2	0.890(13)	1.941(13)	2.7876(9)	158.5(12)
<b>1n<sup>viii</sup></b>	N(11)-H(11)...O(21)	0.958(13)	1.742(13)	2.6981(9)	174.9(12)
	N(12)-H(12A)...O(22)	0.885(14)	1.985(14)	2.8526(10)	166.2(14)
	N(12)-H(12B)...O(22)#3	0.858(15)	2.078(15)	2.9222(10)	168.0(13)
	O(31)-H(31)...O(21)	0.886(15)	1.699(15)	2.5806(9)	172.6(14)
<b>1o<sup>ix</sup></b>	N(11)-H(11)...O(21)	1.007(12)	1.574(12)	2.5786(9)	174.3(10)
	N(12)-H(12A)...O(22)	0.915(13)	1.912(14)	2.8224(10)	172.7(12)
	N(12)-H(12B)...O(22)#2	0.901(13)	2.009(13)	2.8641(10)	158.0(11)
<b>2a<sup>x</sup></b>	N(11)-H(11)...O(21)	0.85(3)	1.79(3)	2.627(3)	171(2)
	N(12)-H(12A)...O(22)	0.71(3)	2.11(3)	2.817(2)	172(3)
	N(12)-H(12B)...O(21)#1	0.91(2)	2.10(3)	2.954(2)	154(2)
<b>2e<sup>xi</sup></b>	N(11)-H(11)...O(21)	1.03(3)	1.60(4)	2.614(3)	170(3)
	N(12)-H(12A)...O(22)	0.84(4)	2.03(4)	2.829(3)	161(4)
	N(12)-H(12B)...O(21)#1	0.94(4)	2.21(4)	3.061(3)	151(3)
<b>3n<sup>xii</sup></b>	O(31)-H(31)...N(11)	0.930(16)	1.716(16)	2.6421(10)	173.7(14)
	N(12)-H(12)...O(32)	0.861(14)	2.016(14)	2.8743(10)	174.7(11)
<b>4f<sup>xiii</sup></b>	N(12)-H(12)...O(22)	0.83(2)	2.09(2)	2.9242(16)	174.0(18)
	O(21)-H(21)...N(11)	0.90(2)	1.74(2)	2.6274(16)	170(2)

Structure	D-H...A	d(D-H)/Å	d(H...A)/Å	d(D...A)/Å	<(DHA)/°
<b>4k</b> <sup>xiv</sup>	O(21)-H(21)...N(11)	0.77(2)	1.98(2)	2.7538(19)	174(2)
	N(12)-H(12)...O(22)	0.75(2)	2.12(2)	2.8686(19)	177(2)
<b>4m</b> <sup>xv</sup>	N(16)-H(16)...O(22)	0.76(2)	2.12(2)	2.8818(18)	174(2)
	O(21)-H(21)...N(11)	0.73(2)	1.93(2)	2.6537(18)	168(2)
<b>4n</b> <sup>xvi</sup>	O311-H311...N111	0.84	1.87	2.705(12)	171.6
	O312-H312...N112	0.84	1.87	2.705(12)	174.1
	O313-H313...N113	0.84	1.85	2.689(14)	172.9
	O314-H314...N114	0.84	1.84	2.677(13)	177.8
	N171-H171...O321	0.88	2.02	2.874(17)	162.3
	N172-H172...O322	0.88	2.06	2.887(15)	156.7
	N173-H173...O323	0.88	2.06	2.917(18)	163.0
	N174-H174...O324	0.88	2.06	2.921(18)	166.2
	O341-H341...N211	0.84	1.84	2.672(12)	169.5
	O342-H342...N212	0.84	1.88	2.711(11)	171.2
	O343-H343...N213	0.84	1.88	2.714(12)	173.1
	O344-H344...N214	0.84	1.86	2.699(13)	176.2
	N271-H271...O331	0.88	2.02	2.878(16)	164.8
	N272-H272...O332	0.88	2.00	2.867(16)	169.3
	N273-H273...O333	0.88	2.03	2.900(18)	170.1
N274-H274...O334	0.88	2.07	2.926(18)	163.1	
<b>4o</b> <sup>xvii</sup>	O(31)-H(31)...N(11)	0.77(2)	1.99(2)	2.7522(17)	174(2)
	N(12)-H(12)...O(32)	0.82(2)	2.01(2)	2.8209(17)	169(2)
<b>5i</b> <sup>xviii</sup>	O211-H211...N111	0.83(3)	1.76(4)	2.580(3)	170(3)
	O212-H212...N112	1.19(3)	1.35(3)	2.538(3)	173(3)
	N121-H12A1...O221	0.85(4)	2.21(4)	3.030(3)	161(3)
	N122-H12A2...O222	0.93(4)	2.03(4)	2.946(3)	170(3)
	N121-H12B1...O232	0.89(4)	2.20(4)	3.034(3)	157(3)
	N122-H12B2...O231#1	0.94(3)	2.22(3)	2.958(3)	135(3)
<b>5m</b> <sup>xix</sup>	O(21)-H(21)...N(11)	0.839(16)	1.758(17)	2.5855(12)	168.3(15)
	N(12)-H(12A)...O(22)	0.814(16)	2.145(16)	2.9510(13)	170.7(14)
	N(12)-H(12B)...O(22)#2	0.812(15)	2.272(14)	2.9839(11)	146.5(14)
<b>6n</b> <sup>xx</sup>	O(21)-H(21)...N(11)	0.73(4)	1.99(4)	2.716(4)	174(5)
	N(12)-H(12)...O(22)	0.77(4)	2.13(4)	2.900(4)	171(4)

i) #1 x-1/2,y,-z+3/2 ii) #1 x+1,y+1,z iii) #1 -x+1,y-1/2,-z+1 iv) #1 x-1/2,-y+1,z-1/2 v) #1 -x+3/2,y+1/2,z vi) #1 x,-y+1/2,z-1/2 vii) #1 -x,-y+2,-z #2 -x+1/2,y-1/2,-z+1/2 viii) #1 -x+1,-y,-z+1 #2 -x,-y+2,-z+1 #3 -x+1,y-1/2,-z+3/2 ix) #1 -x,-y+2,-z #2 -x+1/2,y-1/2,-z+1/2 x) #1 x-1/2,-y+1,z xi) #1 x,y-1,z xii) #1 -x+1,-y,-z; xiii) n/a xiv) #1 -x-1,-y+1,-z xv) #1 -x-1,-y+1,-z+1 xvi) n/a xvii) #1 -x,-y+1,-z+1 xviii) #1 x+1,y,z+1 xix) #1 -x+1,-y,-z+1 #2 -x+1,y+1/2,-z+3/2 xx) #1 -x-1,-y,-z

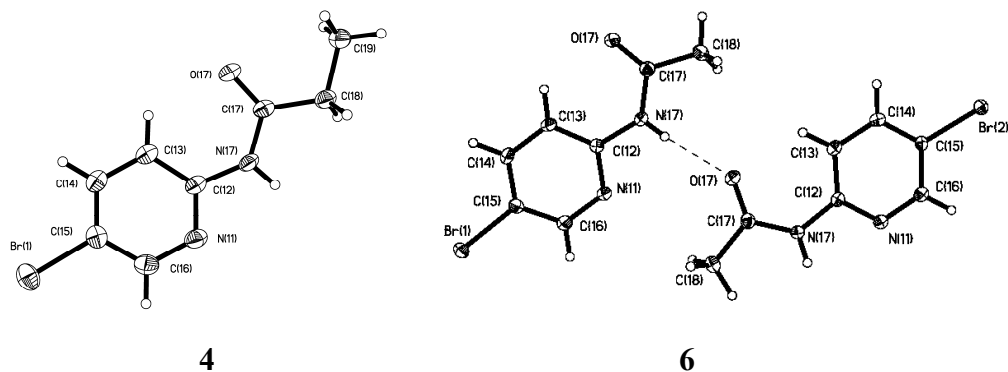


**Figure 2.4** Thermal ellipsoid plots (50 % probabilities) and labeling schemes for 2-propionamido-5-bromopyridine **4**, and 2-acetamido-5-bromopyridine **6**.

### 2.3.1 Crystal structure of 2-propionamido-5-bromopyridine, **4**

The crystal structure of **2** shows one molecule within the asymmetric unit, with the extension of the molecular architecture showing the ligands forming zigzag 1-D strands via self-complementary N-H $\cdots$ O hydrogen bonds (N17 $\cdots$ O17, 2.858(3) Å), Figure 2.5.

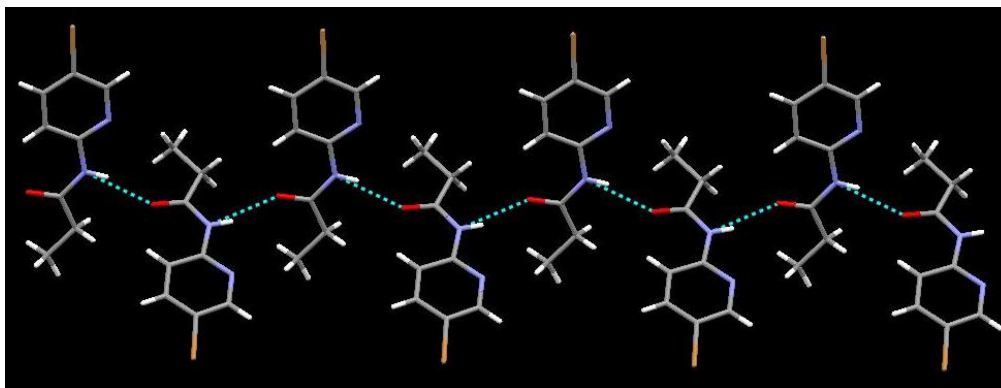


**Figure 2.5** Formation of 1-D strands of 2-propionamido-5-bromopyridine, **4** via N-H $\cdots$ O hydrogen bonding.

### 2.3.2 Crystal structure of 2-acetamido-5-bromopyridine, **6**

The crystal structure of **1** shows one molecule within the asymmetric unit, with the extension of the molecular architecture showing the ligands forming zigzag 1-D strands via self-complementary N-H $\cdots$ O hydrogen bonds (N17 $\cdots$ O17, 2.946(2) Å), Figure 2.6.

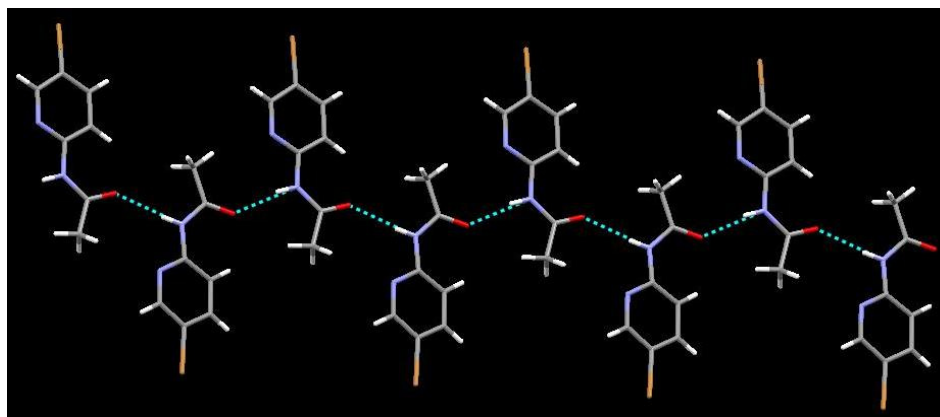
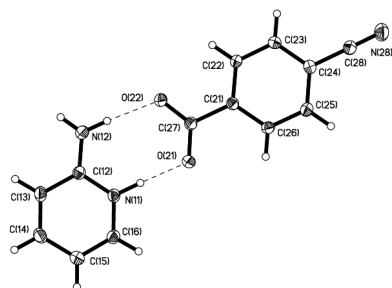
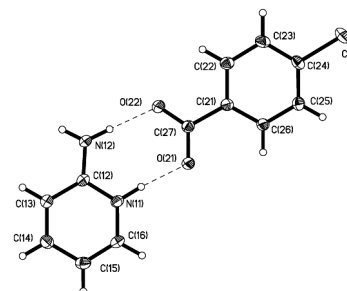


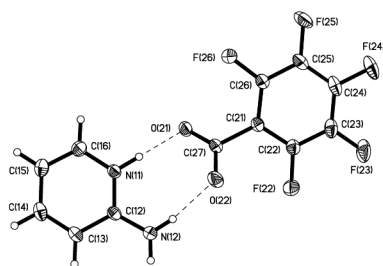
**Figure 2.6** Formation of 1-D strands of 2-acetamido-5-bromopyridine, **6** via N-H $\cdots$ O hydrogen bonding.



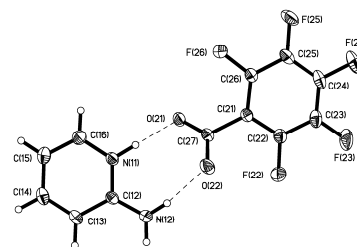
**1a**



**1c**



**1g**



**1j**



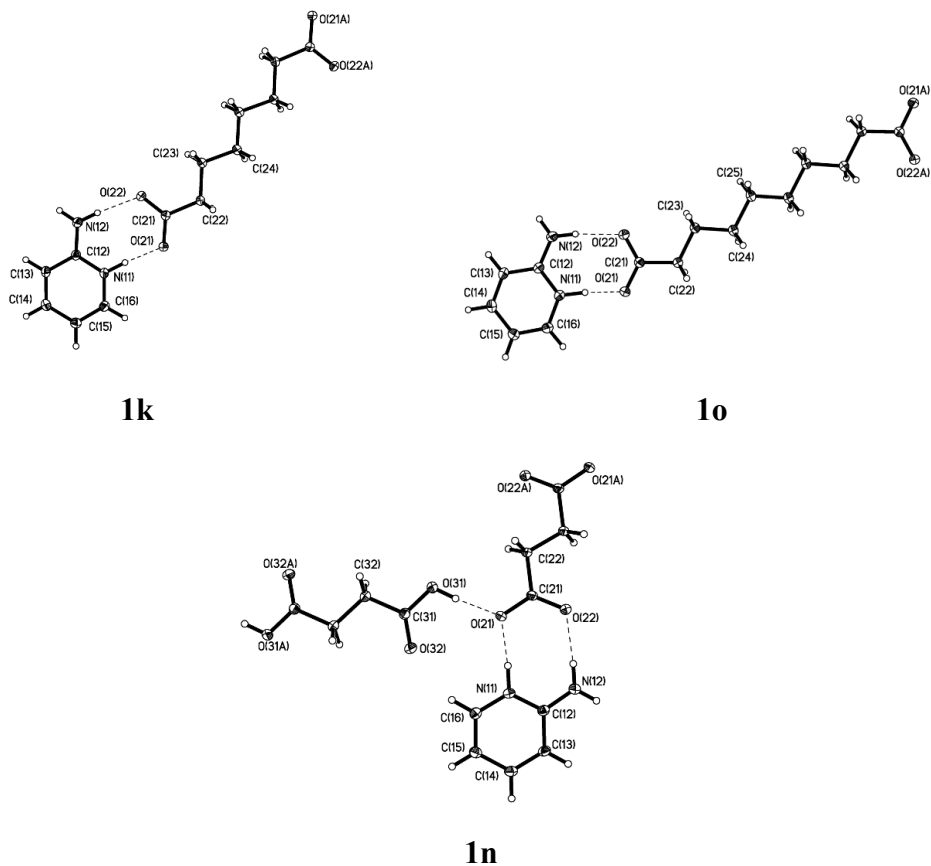


**Figure 2.7** Thermal ellipsoid plots (50 % probabilities) and labeling schemes for **1a-1o**.

### 2.3.3 Crystal structures of **1a**, **1c**, **1g**, **1j**, **1k**, and **1o**

The crystal structures of **1a**, **1c**, **1g**, and **1j** show an 1:1 ionic salt comprising a protonated ligand 2-aminopyridinium ion and a 4-cyanobenzoate ion, 4-chlorobenzoate ion, 2,6-difluorobenzoate ion, and pentafluorobenzoate ion respectively; whereas the crystal structures of **1k** and **1o** reveal 2:1 ionic salts consisting of two 2-aminopyridinium ions and a suberate or sebacate ion respectively connected via hydrogen-bonding interactions between aminopyridinium and carboxylate moieties. The primary synthons in these structures are charge-assisted  $\text{N-H}^+\cdots\text{O}^-$  and  $\text{N-H}\cdots\text{O}^-$  hydrogen bonds. These individual 1:1 or 2:1 ion pairs are further connected to the neighboring ion pairs via  $\text{N-H}\cdots\text{O}$  hydrogen bonds between the *anti*-amino proton and the carboxylate oxygen atom to give a cross-linked network, Figure 2.8 – 2.13.

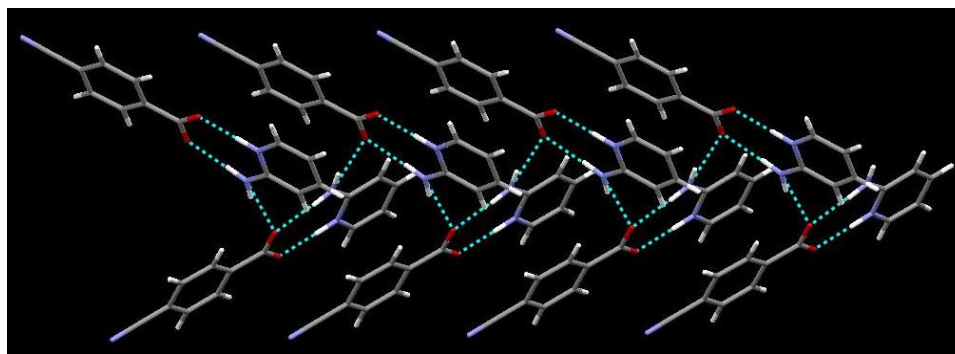


**Figure 2.8** 1-D strand formed through secondary N–H···O<sup>-</sup> hydrogen bonds in 2-aminopyrimidinium 4-cyanobenzoate, **1a**.

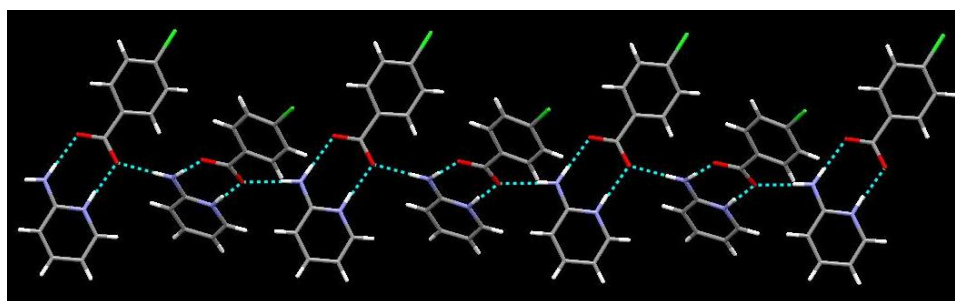


**Figure 2.9** 1-D strand formed through secondary N–H···O<sup>-</sup> hydrogen bonds in 2-aminopyrimidinium 4-chlorobenzoate, **1c**.

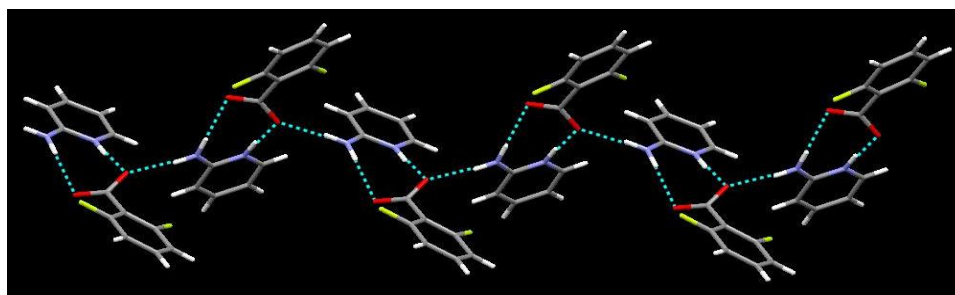


**Figure 2.10** 1-D strands of 2-aminopyridinium 2,6-difluorobenzoate, **1g**.

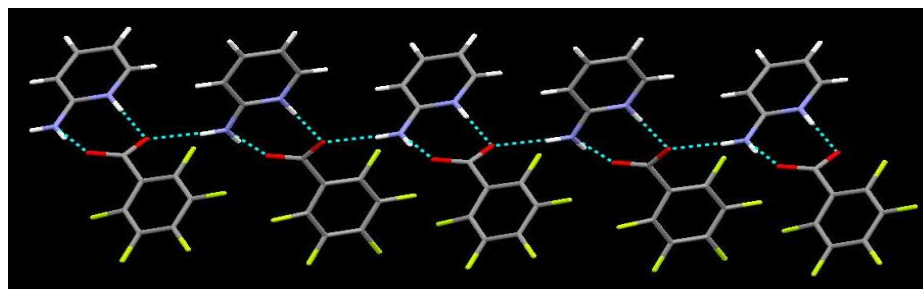


**Figure 2.11** 1-D strands of 2-aminopyridinium pentafluorobenzoate, **1j**.

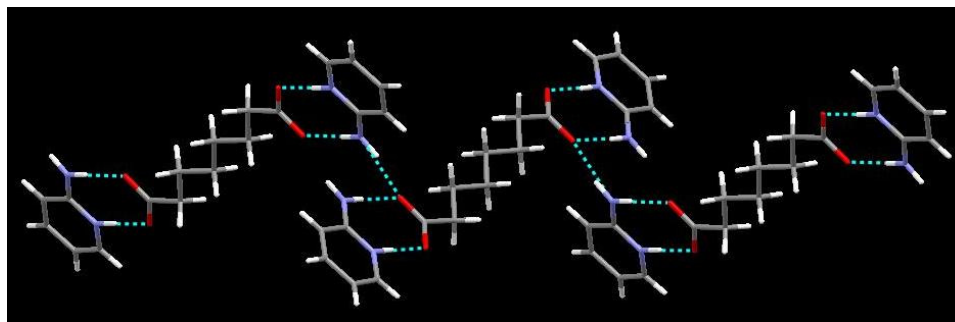


**Figure 2.12** 1-D strands of bis(2-aminopyridinium) suberate, **1k**.

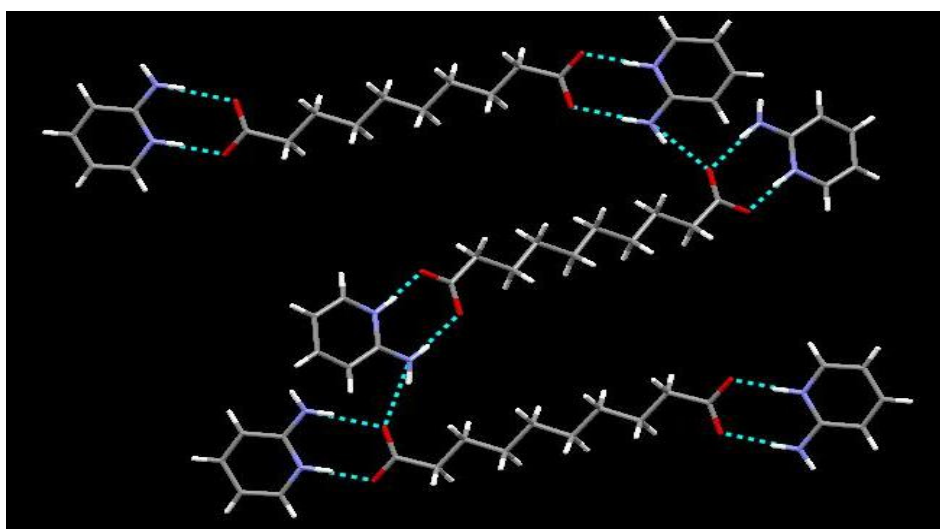


**Figure 2.13** 1-D strands of bis(2-aminopyridinium) sebacate, **1o**.

### **2.3.4 Crystal structure of bis(2-aminopyridinium) succinate succinic acid, *1n***

The crystal structure of *1n* is an interesting exception to the complexes obtained from 2-aminopyridine. The main motif consists of 2:1 protonated 2-aminopyridine linked with a succinate ion via charge-assisted  $\text{N-H}^+\cdots\text{O}^-$  and  $\text{N-H}\cdots\text{O}$  hydrogen bonds with  $\text{N}(11)\text{-H}(11)\cdots\text{O}(21)$  and  $\text{N}(12)\text{-H}(12\text{A})\cdots\text{O}(22)$  distances of  $2.6981(9)\text{\AA}$  and  $2.8526(10)\text{\AA}$  respectively, which are further connected to the next ion pair via  $\text{N-H}\cdots\text{O}$  hydrogen bonds between the *anti*-amino proton and the carboxylate oxygen atom,  $\text{N}(12)\text{-H}(12\text{B})\cdots\text{O}(21)$  with  $2.9222(10)$ , similar to the previous complexes. In addition, there is a free carboxylic acid which is connected to the carboxylate ion moiety via complementary

O–H $\cdots$ O $^-$  hydrogen-bond interactions to extend into 2-D network, O(31)-H(31)...O(21) with bond distance 2.5806(9), Figure 2.14.

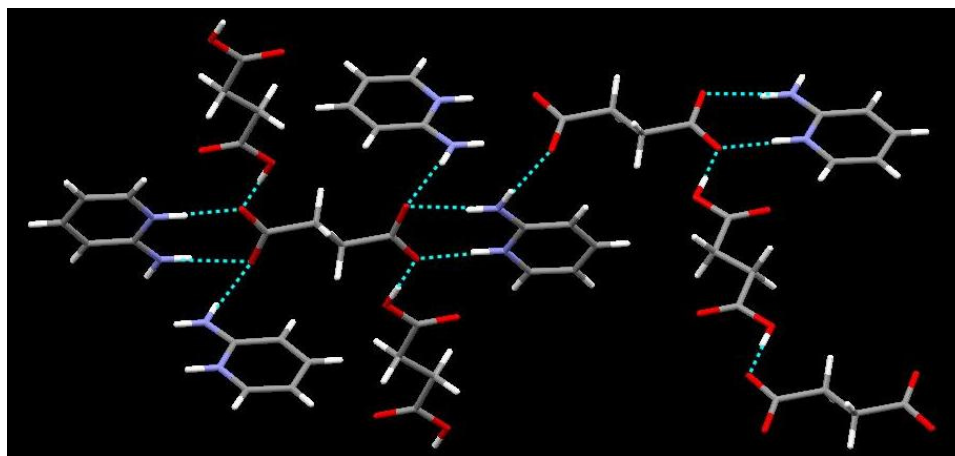


**Figure 2.14** 1-D strands of bis(2-aminopyridinium) succinate succinic acid, **1n**.

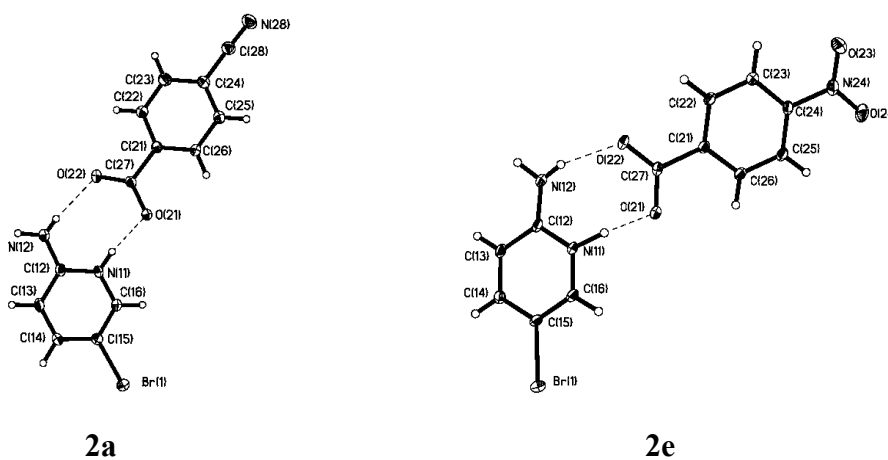


**Figure 2.15** Thermal ellipsoid plots (50 % probabilities) and labeling schemes for **2a** and **2e**.

### 2.3.5 Crystal structure of 2-amino-5-bromopyridinium 4-cyanobenzoate, **2a**

The crystal structure of **2a** displays 1:1 architecture with similar connectivities as seen for the salts of 2-aminopyridine. The asymmetric unit consists of one protonated 2-amino-5-bromopyridinium ion and 4-cyanobenzoate ion as the primary synthon connected via charge-assisted N–H $^+$  $\cdots$ O $^-$  and N–H $\cdots$ O $^-$  hydrogen bonds with N(11)–

H(11)...O(21) and N(12)–H(12A)...O(22) distances of 2.627(3) Å and 2.817(2) Å respectively. Secondary N–H...O<sup>−</sup> hydrogen bonds, N(12)–H(12B)...O(21) with 2.954(2) Å exists between the *anti*-amino proton and the carboxylate oxygen atom, resulting in the extension of the network, Figure 2.16.

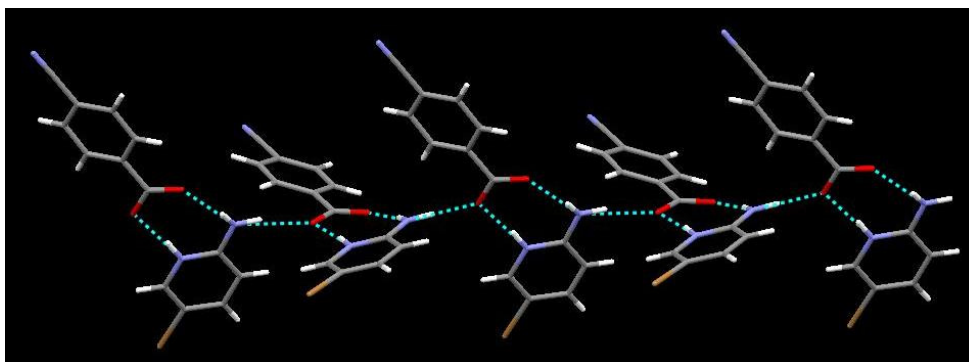


**Figure 2.16** 1-D strands of 2-amino-5-bromopyridinium 4-cyanobenzoate, **2a**.

### 2.3.6 Crystal structure of 2-amino-5-bromopyridinium 4-nitrobenzoate, **2e**

The crystal structure of **2e** displays 1:1 architecture similar to **2a** with one protonated 2-amino-5-bromopyridinium ion and a 4-nitrobenzoate ion connected via charge-assisted N–H<sup>+</sup>...O<sup>−</sup> and N–H...O<sup>−</sup> hydrogen bonds with N(11)–H(11)...O(21) and N(12)–H(12A)...O(22) distances of 2.614(3) Å and 2.829(3) Å respectively and secondary N–H...O<sup>−</sup> hydrogen bonds, N(12)–H(12B)...O(21) with 3.061(3) Å between the *anti*-amino proton and the neighboring carboxylate oxygen atom to form a 2-D network. The bromine atom in this case, in contrast to **2a**, is actively involved in formation of halogen bond between the nitro-oxygen atom of the nitrobenzoic acid via N–O...Br interaction, hence binding the hetero-dimers together into chain-like sheets which in turn were held together via N–H...O<sup>−</sup> secondary interactions, Figure 2.17.

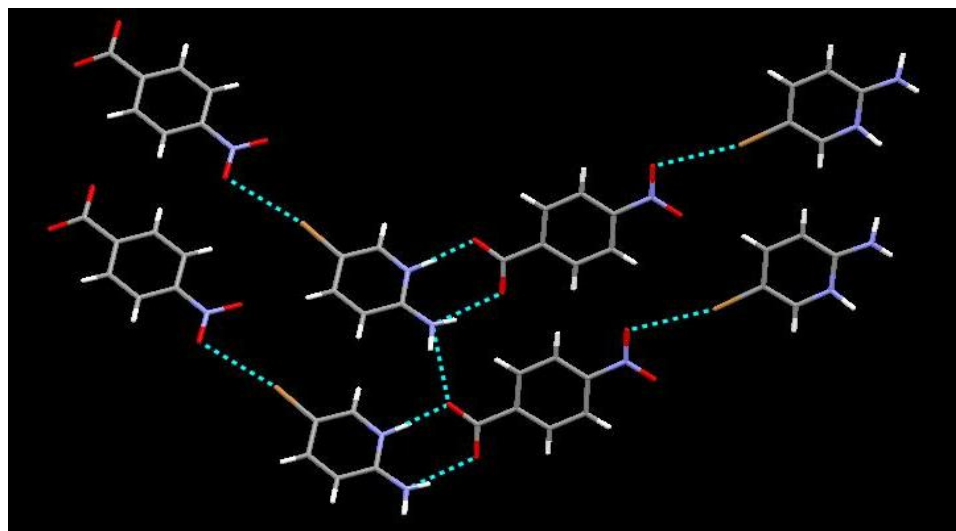
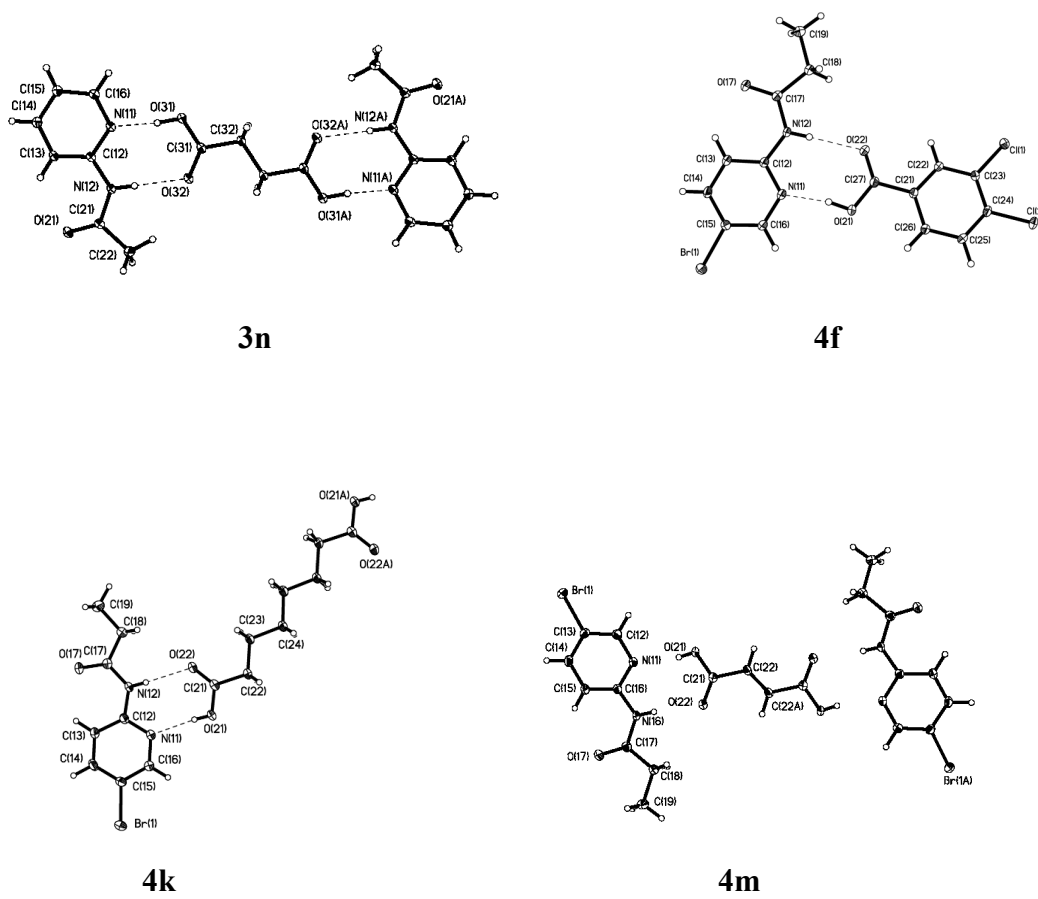
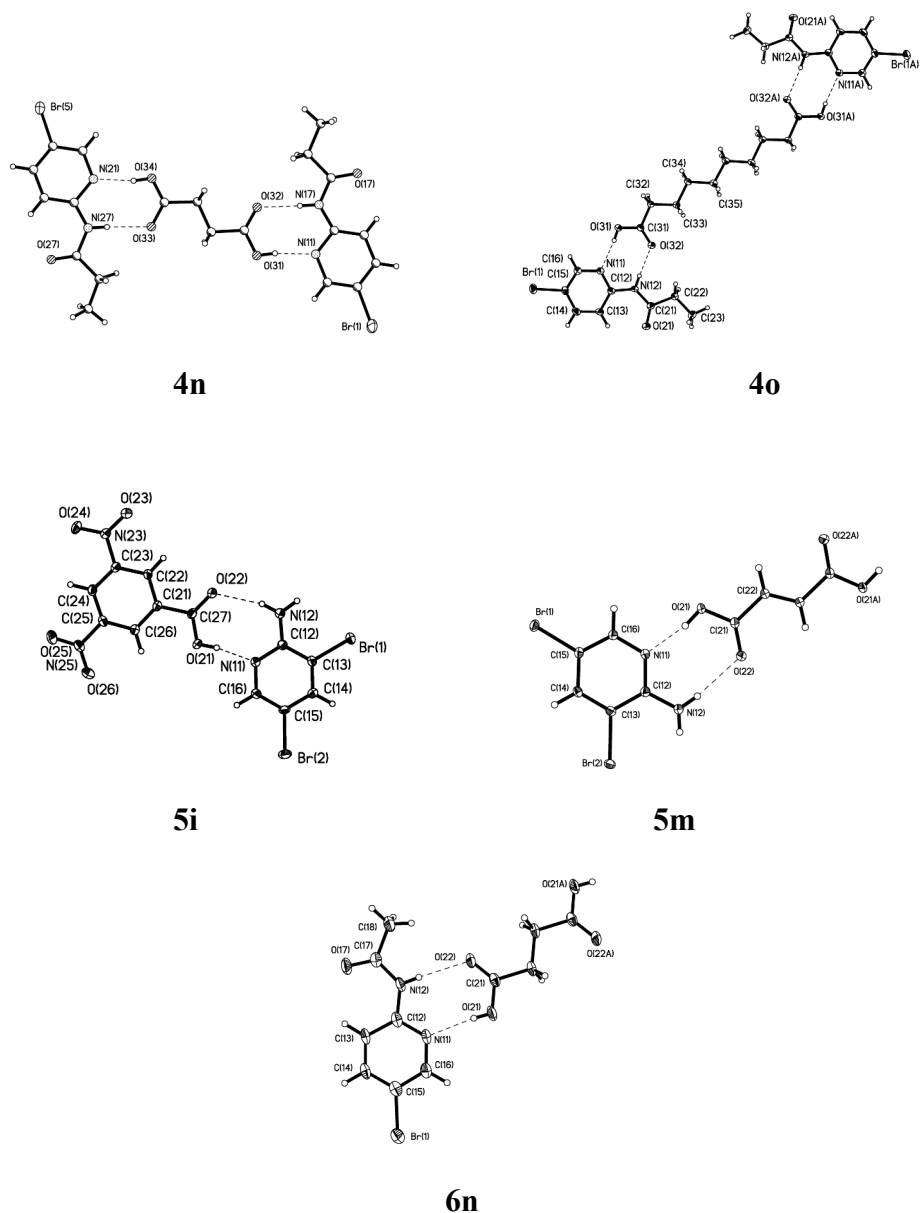


Figure 2.17 2-D network of 2-amino-5-bromopyridinium 4-nitrobenzoate, **2e**.





**Figure 2.18** Thermal ellipsoid plots (50 % probabilities) and labeling schemes for **3n**, **4f**, **4k**, **4m**, **4n**, **4o**, **5i**, **5m**, and **6n**.

### 2.3.7 Crystal structures of **3n**, **4f**, **4k**, **4o**, and **6n**

The crystal structures of **3n**, **4k**, **4o** and **6n** show 2:1 co-crystal (1:1 co-crystal for **4f**) comprising of the neutral ligand and one acid molecule connected via hydrogen bonding interactions in the asymmetric unit. The primary synthons in these structures are N–H···O and N···H–O hydrogen bonds. The bromine atom present in the ligand does not contribute in the interaction, Figure 2.19 – 2.23.

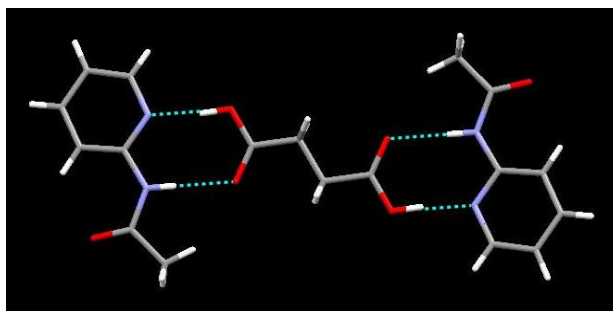


**Figure 2.19** 2:1 Co-crystal of 2-acetamidopyridine/succinic acid, **3n**.

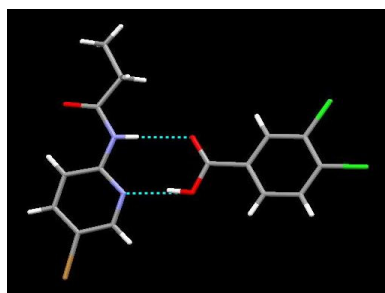


**Figure 2.20** 1:1 Co-crystal of 2-propionamido-5-bromopyridine/3,4-dichlorobenzoic acid, **4f**

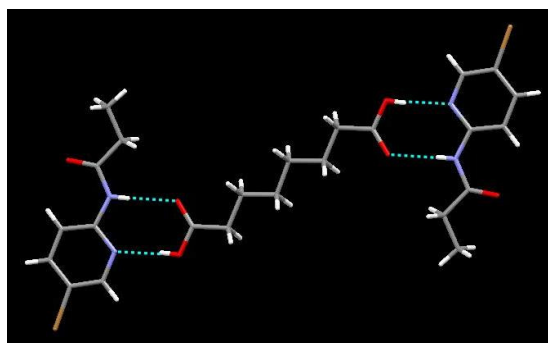


**Figure 2.21** 2:1 Co-crystal of 2-propionamido-5-bromopyridine/suberic acid, **4k**.

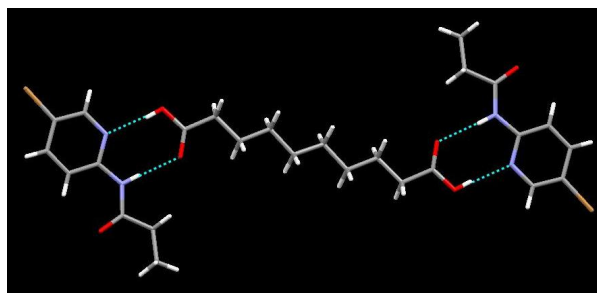


**Figure 2.22** 2:1 Co-crystal of 2-propionamido-5-bromopyridine/sebacic acid, **4o**.



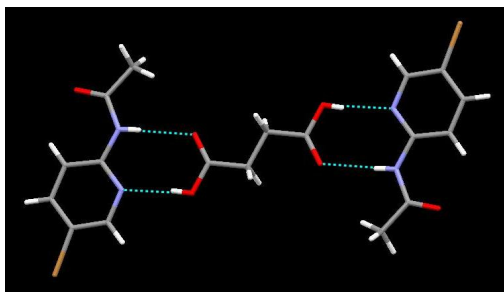


**Figure 2.23** 2:1 Co-crystal of 2-acetamido-5-bromopyridine/succinic acid, **6n**.

### 2.3.8 Crystal structures of **4m** and **4n**

The crystal structure of **4m** and **4n** displays a primary motif composed of the ligand 2-propionamido-5-bromopyridine and the fumaric acid or succinic acid in a 2:1 ratio. The primary synthons in these structures are  $\text{N-H}\cdots\text{O}$  and  $\text{N}\cdots\text{H-O}$  hydrogen bonds between the propionamidopyridine moieties and the carboxylic acid. The secondary  $\text{Br}\cdots\text{O-H}$  interaction between the carboxylic O-H and the bromine atom from the ligand extend the architecture into a four-component square, Figure 2.24 – 2.25.

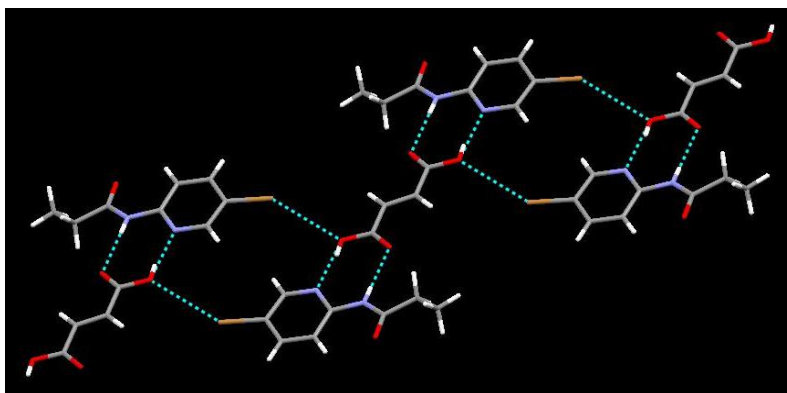


**Figure 2.24** 2:1 Co-crystal of 2-propionamido-5-bromopyridine/fumaric acid, **4m**.

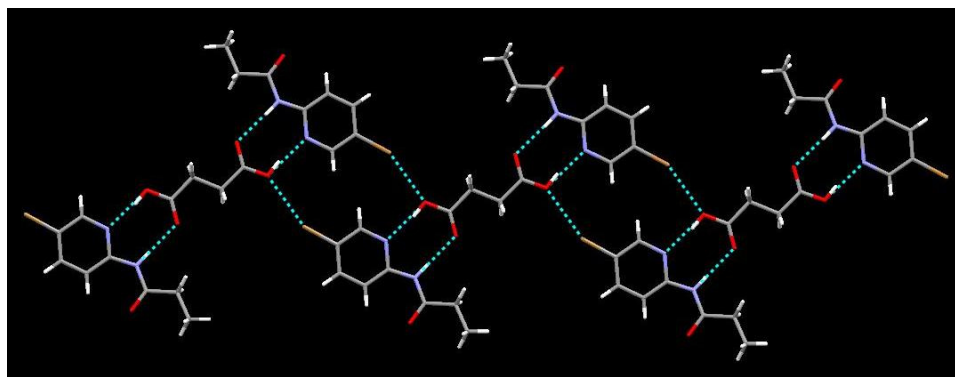


**Figure 2.25** 2:1 Co-crystal of 2-propionamido-5-bromopyridine/succinic acid, **4n** exhibiting the four-component square-like system.

### 2.3.9 Crystal structure of 2-amino-3,5-dibromopyridine/3,5-dinitrobenzoic acid, **5i**

The crystal structure of **5i** displays a 1:1 co-crystal with 2-amino-3,5-dibromopyridine and 3,5-dinitrobenzoic acid connected via N–H···O and N···H–O hydrogen bonds. The *anti*-amino proton in the ligand interacts with the nitro group of the carboxylic acid via N–H···O=N interaction to extend the architecture. This secondary interaction is further augmented by a halogen bond Br···O=C interaction between one of the bromine atoms in the ligand and the carbonyl oxygen atom in the acid, whereas the second Br atom remains inactive. An interesting feature in this crystal structure is the intermolecular N=O···O=N interaction between two dinitrobenzoic acids, Figure 2.26.

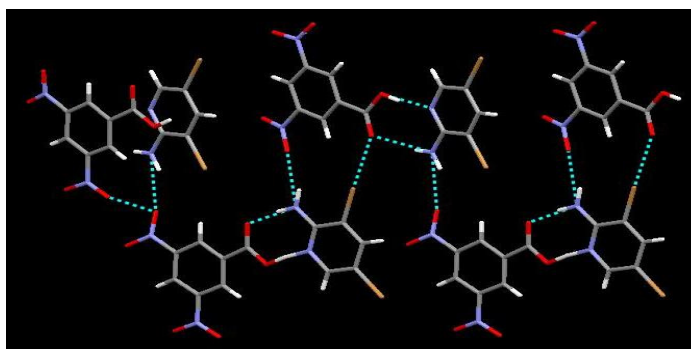


**Figure 2.26** 1:1 Co-crystal of 2-amino-3,5-dibromopyridine/3,5-dinitrobenzoic acid, **5i**.

### 2.3.10 Crystal structure of 2-amino-3,5-dibromopyridine/fumaric acid, **5m**

The crystal structure of **5m** displays 2:1 co-crystal with 2-amino-3,5-dibromopyridine and fumaric acid as the primary synthon connected via N–H···O and N···H–O hydrogen bonds. The *anti*-amino proton in the ligand interacts with the carbonyl oxygen atom from the neighbouring carboxylic acid via N–H···O=C interaction. Halogen bonding Br···O–H is seen between one of the bromine atoms in the ligand and the hydroxyl oxygen atom in the acid, whereas the second Br atom remains inactive, Figure 2.27.

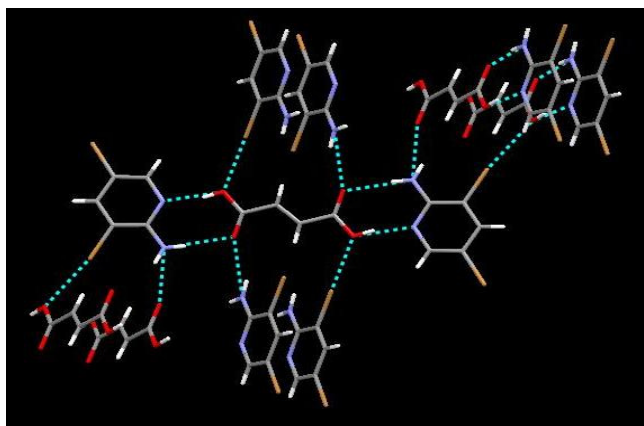


**Figure 2.27** 2:1 Co-crystal of 2-amino-3,5-dibromopyridine/fumaric acid, **5m**.

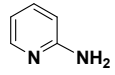
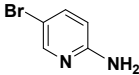
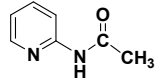
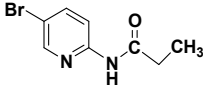
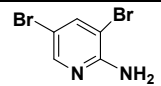
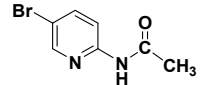
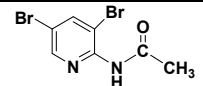
## 2.4 Discussion

### *2.4.1 Analysis of pyridine-carboxylic acid salts and co-crystals through FT-IR spectroscopy*

The distinction between salt and co-crystal was based on the specific stretches and shifting of carbonyl stretches between free and ligand-bonded carboxylic acids. In general, a free monomeric C=O stretch for aromatic carboxylic acids is seen around 1760  $\text{cm}^{-1}$  whereas a dimeric C=O stretch is seen around 1720-1706  $\text{cm}^{-1}$ . The presence/absence of broad stretches near 1950 and 2450  $\text{cm}^{-1}$  are indicative of intermolecular O—H---N(heterocycle) hydrogen bonds and will only appear in salts and co-crystals, and not in physical mixtures of the two reagents.<sup>10</sup> The characteristic difference in the IR spectrum between the salt and co-crystal lies in the position of the C=O stretch, which in case of a co-crystal (containing a neutral carboxylic acid) is seen as a strong band near 1700  $\text{cm}^{-1}$  in view of the intact COOH moiety and a weak C—O stretch near 1275  $\text{cm}^{-1}$ . The salts containing the carboxylate anion however, show a strong asymmetrical COO<sup>-</sup> stretch around 1650-1550  $\text{cm}^{-1}$  and a weaker symmetrical stretch around 1400  $\text{cm}^{-1}$  (absent in co-crystals).<sup>10</sup> In the case where no reaction has taken place between the two reactants, the IR spectrum of the resulting solid is simply a superimposition of the IR spectra of the two components with no new bands.

An analysis of the infrared spectra obtained for the combination of different carboxylic acids, **a-o**, with each of the seven ligands, **1-7**, showed that out of 105, 30 resulted in salts (28%), 51 gave co-crystals (49%), and 24 produced no reaction (23%). All attempted reactions between a carboxylic acid and any of the two ligands **1** and **2** resulted exclusively in salts. These results correlate well with the charge calculation on these molecules since the presence of a strongly electron-donating amino group in the ring raises the charge on the pyridyl-N and hence boosts its capability to remove a proton from the acid resulting in two charged species. Even though the presence of a weakly electron withdrawing bromine in the ligand **2** decreases the charge on the pyridyl nitrogen atom (to -275 kJ/mol), it is still sufficiently basic to produce salts in every case.

**Table 2.6** Summary of results in a series of attempted co-crystallization reactions.

		charge (kJ mol <sup>-1</sup> )	salt	co-crystal	no reaction	%	
1		-288	15	0	0	100	salt
2		-275	15	0	0	100	
3		-260	0	13	2	87	co-crystal
4		-244	0	14	1	93	
5		-237	0	12	3	80	
6		-230	0	11	4	73	
7		-220	0	1	14	7	none

None of the less basic ligands (**3 - 6**) produced salts but instead were capable of producing co-crystals with varying degree of success. These results are also in complete agreement with the trend suggested by AM1 charge calculations for these ligands. The ligand **3** and **4** with third and fourth priority in the charge order gave 13 and 14 co-crystals (87% and 93% supramolecular yield). These results can be explained in terms of reduced electron donating capability of acetamido and propionamido moieties compared to the amino group. The ligand **5** with two bromines in the ring further decreases the electron density; hence the low charge on the pyridyl-N. This is implicated in the decreased ability to form intermolecular interactions (80% supramolecular yield). The ligand **7** with lowest charge has the least ability to form intermolecular interactions (7% supramolecular yield).

#### 2.4.2 Single crystal X-ray analysis of pyridine-carboxylic acid salts and co-crystals

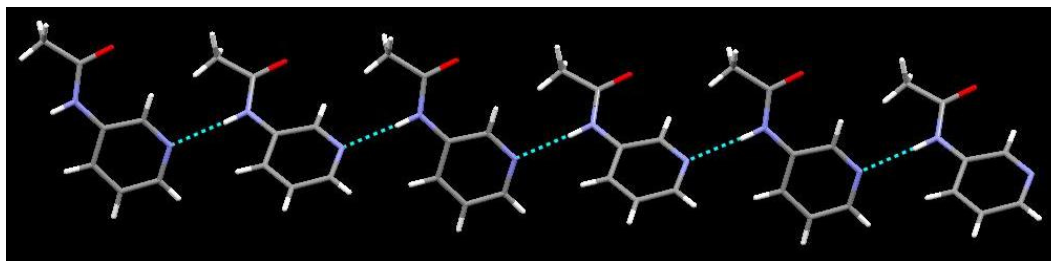


**Figure 2.28** Crystal structure of 3-acetamidopyridine showing the 1D chain held by N-H...N interaction.<sup>11</sup>

The single crystal X-ray structures of the ligands under study, 2-propionamido-5-bromopyridine **4** and 2-acetamido-5-bromopyridine **6** show one dimensional chain structure with the two entities held together via N-H...O hydrogen bond interactions, Figure 2.5 – 2.6. However, the structurally closely-related ligand 3-acetamidopyridine exhibit similar 1D chain structure but are held by N-H...N hydrogen bonds, figure 2.28. One explanation may be the steric hindrance due to the bromine atom, which require the molecules to be as possible hence shifting the hydrogen bonding pattern from N-H...N to N-H...O. There is no reported crystal structures available for 2-acetamido or 4-acetamidopyridine and bromosubstituted 3-acetamido or 4-acetamidopyridines to make a comparison of binding preferences with the change in the position of the acetamido group relative to the pyridyl nitrogen.

Out of 18 crystal structures studied from the co-crystallization experiment, 9 were co-crystals (50%), 8 were salts (44%) and 1 (6%) came out to be complex with ionic/co-crystal pair. The stoichiometries for the salts and co-crystals were as expected; with one ligand and one carboxylic acid (1:1) for monocarboxylic acids and with two ligands and one carboxylic acid (2:1) in the asymmetric unit for dicarboxylic acids. A summary of all the crystallographic information for the salts and co-crystals was given in Table 2.5.

All crystal structures revealed the primary hydrogen bonding motif as O—H---N(Py) and C=O---H—N in co-crystals and C—O<sup>-</sup>---H—N<sup>+</sup>(Py) and C—O<sup>-</sup>---H—N in salts. In the ligands containing the amino group, **1a**, **1c**, **1g**, **1j**, **1k**, **1n**, **1o**, **2a**, and **2e**, the second proton from the amino group (not involved in the primary interaction) interacts with C—O<sup>-</sup> from acid. In addition, Br---O—N interaction is seen for **2e**. A surprising

case is **1n** which is a complex between 2-aminopyridine and succinic acid. In addition to the ionic interaction ( $\text{C—O}^- \cdots \text{H—N}^+(\text{Py})$ ) and ( $\text{C—O}^- \cdots \text{H—N}$ ) between the 2-aminopyridinium moiety and the carboxylate moiety, there exists  $\text{C—O}^- \cdots \text{H—O}$  (free acid) interaction. So this particular case can be treated as a complex with ionic/co-crystal pair. No secondary interactions were seen for the crystal structures **3n**, **4f**, **4k**, **4n**, **4o**, **6n**. For crystals **4m** and **5m**,  $\text{Br} \cdots \text{O—H}$  interaction is seen. For **5m**, the second NH proton interacts with carbonyl oxygen whereas the second Br atom is inactive. For **5i**,  $\text{Br} \cdots \text{O=C}$  interaction is seen, whereas the second Br is inactive. An interesting feature in this crystal structure is the intermolecular  $\text{N=O} \cdots \text{O=N}$  interaction between two dinitrobenzoic acids along with  $\text{N=O} \cdots \text{H—N}$  interaction with the remaining NH proton from the amino group.

Comparison of crystal data for salts and co-crystals shows that the average ratio of carbonyl  $\text{C=O}$  bond distance to  $\text{C—OH}$  bond distance in co-crystals is 1.08 Å, whereas the ratio of  $\text{C—O}^-$  bond distance for the carboxylate anion is 1.02 Å. Similarly, the average  $\text{C—OH} \cdots \text{N(py)}$  bond length in co-crystals is 2.665 Å, whereas the average  $\text{C—O}^- \cdots \text{H—N}^+(\text{py})$  bond length in salts is 2.656 Å. The average  $\text{C=O} \cdots \text{HNR}$  bond length in co-crystals is 2.908 Å and  $\text{C—O}^- \cdots \text{HNR}$  is 2.814 Å. The average  $\text{C—N—C}$  pyridyl bond angle in carboxylic acid is 119.482° and that in  $\text{C—NH}^+ \text{—C}$  is 122.40°, Table 2.7. These are the expected results, since the stronger binding of the carboxylate anion to the protonated pyridine compound would lead to stronger and hence shorter bond compared to the weaker, neutral hydrogen bonding found in co-crystals.

As seen in the Table 2.2, a charge of -275 or higher resulted in salts whereas charges in between -260 to -230 resulted in a decreasing trend in an ability to form co-crystals, and a charge of -220 resulted in a physical mixture only. Based upon these results, a cut-off point in terms of electrostatic charge on the molecule may be drawn for the formation of salts and co-crystals, or any interaction at all.

Studies also revealed that in our case, the co-crystal formation is driven entirely by the charge in the py-N (ligand) and not by the carboxylic acid. The choice of the same 15 carboxylic acid used aid to create homogeneity in the experiment with the trend showing no link with the type of acid used. The stronger acid, 4-nitrobenzoic acid (**e**)

gave a physical mixture with 2-acetamido-5-bromopyridine (**6**), whereas a weaker acid, 3-hydroxybenzoic acid (**c**) gave co-crystal.

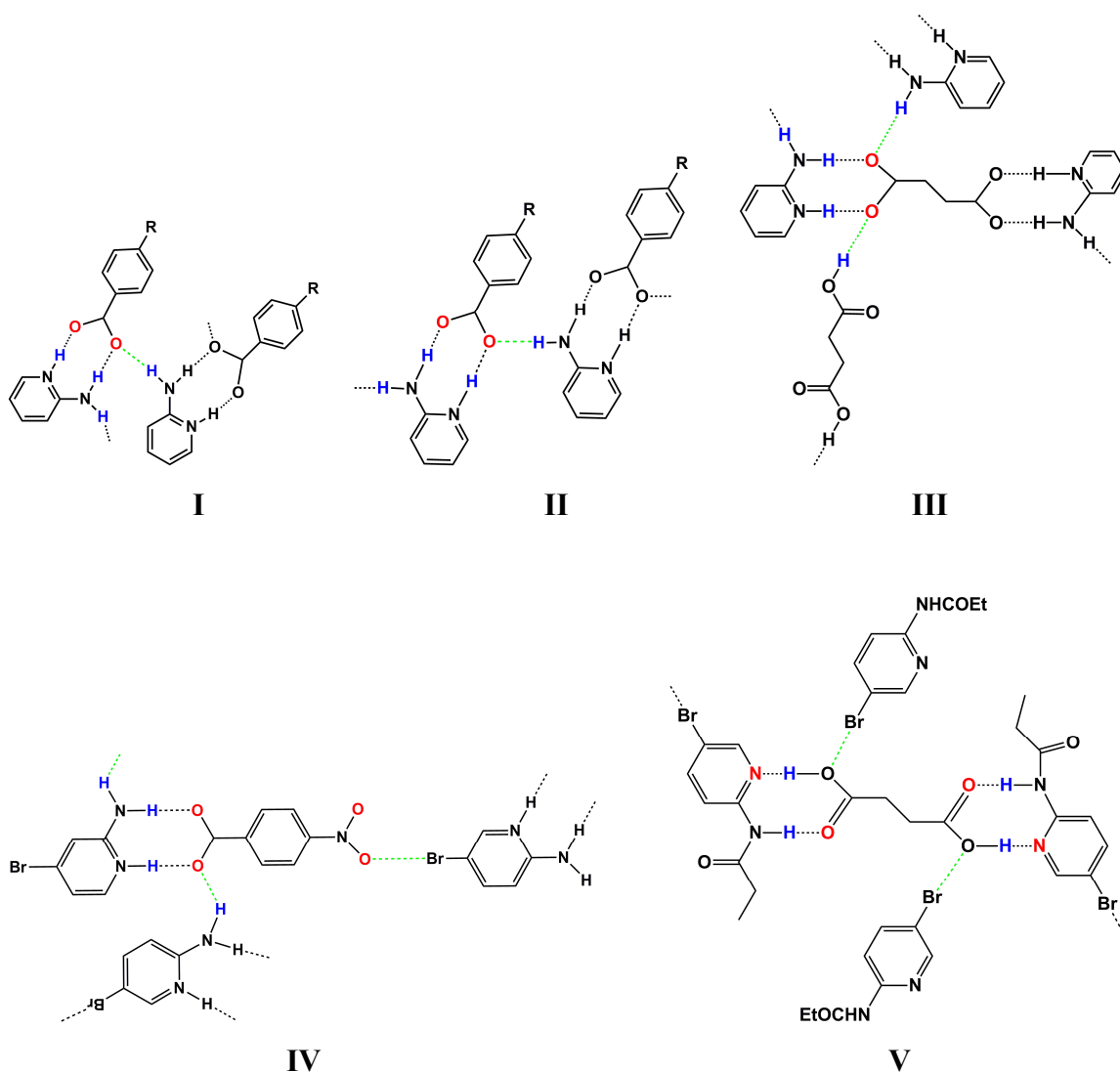
**Table 2.7** Comparison of bond distances and bond angles in salts and co-crystals

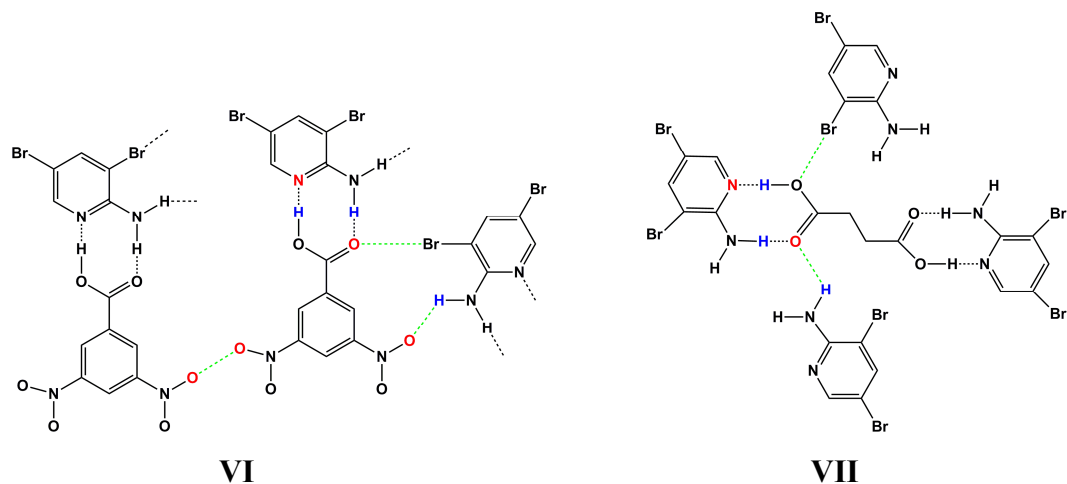
	C–OH	C=O	ratio	C–O <sup>-</sup> --- H–N+(py)	C–O <sup>-</sup> --- H–NR]	ratio	COH --- N(py)	C=O- -- HNR	C–O <sup>-</sup> --- H–N+(py)	C–O <sup>-</sup> - -- H–NR	C–N–C	C–NH <sup>+</sup> –C
<b>1a</b>	x	x	x	1.257	1.261	0.997	x	x	2.684	2.774	x	122.53
<b>1c</b>	x	x	x	1.27	1.255	1.012	x	x	2.725	2.763	x	122.25
<b>1g</b>	x	x	x	1.262	1.233	1.024	x	x	2.653	2.879	x	122.75
<b>1j</b>	x	x	x	1.258	1.234	1.019	x	x	2.704	2.826	x	122.59
<b>1k</b>	x	x	x	1.264	1.25	1.011	x	x	2.617	2.764	x	122.06
<b>1n</b>	x	x	x	1.278	1.245	1.027	x	x	2.698	2.853	x	122.71
<b>1o</b>	x	x	x	1.27	1.247	1.018	x	x	2.579	2.822	x	121.71
<b>2a</b>	x	x	x	1.277	1.233	1.036	x	x	2.627	2.817	x	122.3
<b>2e</b>	x	x	x	1.267	1.252	1.012	x	x	2.614	2.829	x	122.7
<b>3n</b>	1.314	1.226	1.072	x	x	x	2.642	2.874	x	x	118.8	x
<b>4f</b>	1.319	1.226	1.076	x	x	x	2.628	2.924	x	x	119.2	x
<b>4k</b>	1.32	1.216	1.086	x	x	x	2.754	2.868	x	x	118.7	x
<b>4m</b>	1.306	1.215	1.075	x	x	x	2.654	2.882	x	x	119.1	x
<b>4n</b>	1.311	1.205	1.088	x	x	x	2.677	2.92	x	x	120	x
<b>4o</b>	1.316	1.21	1.088	x	x	x	2.752	2.821	x	x	118.54	x
<b>5i</b>	1.311	1.212	1.082	x	x	x	2.58	3.03	x	x	121.1	x
<b>5m</b>	1.305	1.224	1.066	x	x	x	2.585	2.951	x	x	120.8	x
<b>6n</b>	1.313	1.214	1.082	x	x	x	2.716	2.9	x	x	119.1	x
<b>Avg</b>			1.079			1.017	2.665	2.908	2.656	2.814	119.482	122.4



### 2.4.3 Secondary hydrogen bonding and halogen bonding motifs

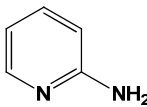
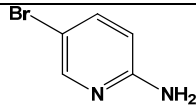
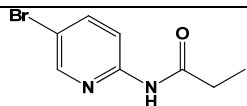
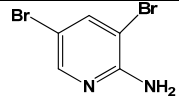
In addition to the primary hydrogen bonding motifs found in the crystal structures of the salts and co-crystals of the pyridine series under study, there exists another set of interactions which comprises both hydrogen and halogen bonding interactions that assists in extension of the architecture of these molecules. The secondary hydrogen bonding interaction here involves N-H...O<sup>-</sup>, N-H...O, and O-H...O<sup>-</sup> synthons. The halogen bonding secondary interaction involves a halogen atom (bromine atom in this case) as the halogen bond donor, and highly electronegative oxygen atom as the halogen bond acceptor. We identified seven different types of motifs, Figure 2.28, and the frequency of occurrence of each motif is summarized in Table 2.8.





**Figure 2.29** Secondary motifs observed in the salts and co-crystals in the pyridine series.

**Table 2.8** Secondary structural motifs found in the pyridine series.

Ligand	Carboxylic acid	Structure	Secondary structural motif
	4-Cyanobenzoic acid	<b>1a</b>	<b>I</b>
	4-Chlorobenzoic acid	<b>1c</b>	<b>II</b>
	2,6-Difluorobenzoic acid	<b>1g</b>	<b>II</b>
	Pentafluorobenzoic acid	<b>1j</b>	<b>II</b>
	Suberic acid	<b>1k</b>	<b>I</b>
	Succinic acid	<b>1n</b>	<b>III</b>
	Sebacic acid	<b>1o</b>	<b>I</b>
	4-Cyanobenzoic acid	<b>2a</b>	<b>II</b>
	4-Nitrobenzoic acid	<b>2e</b>	<b>IV</b>
	Fumaric acid	<b>4m</b>	<b>V</b>
	Succinic acid	<b>4n</b>	<b>V</b>
	3,5-Dinitrobenzoic acid	<b>5i</b>	<b>VI</b>
	Fumaric acid	<b>5m</b>	<b>VII</b>

## 2.5 Conclusions

Our experimental results successfully demonstrated the relationship between the charge and the potential of a compound to form intermolecular hydrogen bonds. The higher charges in a molecule corresponded with the formation of salt via proton transfer, whereas the lower charges lead to interaction between neutral moieties to give co-crystals, and the least charges resulted in no interaction between the moieties. It proves that charge in the molecule plays a huge role in their ability to exhibit intermolecular interactions.

## References

- <sup>1</sup> (a) Skovsgaard, S.; Bond, A. D. *CrystEngComm*. **2009**, 444; (b) Chadwick, K.; Davey, R.; Sadiq, G.; Cross, W.; Pritchard, R. *CrystEngComm*, **2009**, 412; (c) Aakeröy, C. B.; Desper, J.; Fasulo, M.; Hussain, I.; Levin, B.; Schultheiss, N. *CrystEngComm*. **2008**, 1816; (d) Aakeröy, C. B.; Desper, J.; Helfrich, B.A.; Metrangolo, P.; Pilati, T.; Resnati, G.; Stevenazzi, A. *Chem. Commun.*, **2007**, 4236.
- <sup>2</sup> (a) Hunter, C. A. *Angew. Chem. Int. Ed.* **2004**, 43, 5310. (b) Henry, M.; Hosseini, M. W. *New J. Chem.* **2004**, 28, 897.
- <sup>3</sup> (a) Aakeröy, C. B.; Salmon, D. J.; Smith, M. M.; Desper, J. *Crystal Growth & Design*, **2006**, 6, 1033; (b) Aakeröy, C. B.; Desper, J.; Fasulo, M. E. *CrystEngComm*. **2006**, 586.
- <sup>4</sup> Aakeröy, C. B.; Rajbanshi, A.; Desper, J. *CrystEngComm*. **2010**. (submitted)
- <sup>5</sup> Aakeröy, C. B.; Salmon, D. J. *CrystEngComm*. **2005**, 7, 439.
- <sup>6</sup> Cambridge Structural Database ConQuest version 1.8.
- <sup>7</sup> (a) Sollogoub, M.; Fox, K. R.; Powers, V. E. C.; Brown, T. *Tetrahedron Letters*, **2002**, 43, 3121; (b) Li, C.; Rittmann, L. S.; Tsiftoglou, A. S.; Bhargava, K. K.; Sartorelli, A. *C. J. Med. Chem.* **1978**, 21, 874; (c) Aakeröy, C. B.; Hussain, I.; Desper, J. *Cryst. Growth & Des.* **2006**, 6, 474.
- <sup>8</sup> Charge calculations for the structures **a—g** were performed using Spartan '04 (Wavefunction, Inc. Irvine, CA). All seven molecules were optimized using AM1, with the maxima and minima in the electrostatic potential surface (0.002 e au<sup>-1</sup> isosurface) determined using a positive point charge in the vacuum as a probe.
- <sup>9</sup> Brittain, H.G. *Cryst. Growth & Design* **2009**, 9, 2492.
- <sup>10</sup> Silverstein, R.M.; Bassler, G. C.; Morrill, T.C. *Spectroscopic Identification of Organic Compounds*, **1991**, John Wiley and Sons, New York.
- <sup>11</sup> Aakeröy, C. B., Forbes, S., Desper, J, Kansas State University (Unpublished Data).

# CHAPTER 3 - Measuring binding energies in solution using Isothermal Titration Calorimetry (ITC)

## 3.1 Introduction

### *3.1.1 Correlating solid-state binding with solution behavior*

The formation of a co-crystal determines thermodynamic events that lead to an overall decrease in the energy (stabilization) of the system. The bringing together of two neutral molecular entities via weak non-covalent interactions may result in release of energy to give an energy-minimum stable compound. The amount of energy released may be correlated to the strength of the intermolecular interaction.<sup>1</sup> The most experimentally observable thermodynamic quantity occurring during the conversion of a free (unbound) to the bound state is heat (enthalpy).<sup>2</sup> Calorimetry is the measurement of energy changes that occur during a chemical process in the form of heat released (exothermic) or heat absorbed (endothermic).<sup>3</sup> Various calorimetric methods have been devised to measure the energy change during a reaction, the most common being Differential Scanning calorimetry (DSC) and isothermal titration calorimetry (ITC).<sup>4</sup> In DSC, the temperature of a sample is increased linearly as a function of time, whereas the sample is maintained at a constant temperature in ITC.

In Chapter 2, we correlated the charges in a molecule to the capability to form co-crystals in a range of pyridine compounds. In this chapter we tend to seek if this solid-state behavior is reflected in solution as well. The study was carried out with 2-acetamidopyridine as the model compound due to its highly effective co-crystallizing capability<sup>5</sup> (Table 2.3 'c') and good aqueous solubility. Three carboxylic acids with variable charges were chosen as co-crystallizing agents pertaining to the deduction that differences in charges relate to the differences in interactions.

### 3.1.2 Isothermal Titration Calorimetry

Isothermal titration calorimetry (ITC) is a thermodynamic technique used in the study of intermolecular interactions between two species in solution. The interaction between two molecular species results in either gain or loss of energy (heat). The amount of heat lost during the process is a measure of strength of interaction between these species. This can be analyzed in terms of thermodynamic parameters like enthalpy change ( $\Delta H$ ), entropy change ( $\Delta S$ ), which further can be resolved into Gibbs free energy changes ( $\Delta G$ ) of the system. The binding constants ( $K_a$ ) and binding stoichiometry ( $N$ ) can also be calculated.<sup>6,7,8</sup> (Eq 3.1 – 3.2)

$$\Delta G = - RT \ln K_a \quad (\text{where, } R = \text{Gas constant, } T = \text{Absolute temperature}) \quad \text{Equation 3.1}$$

$$\Delta G = \Delta H - T \Delta S \quad \text{Equation 3.2}$$

ITC experiments are more commonly used to determine thermodynamic parameters of biochemical interactions, usually in the study of small drug molecules with larger macromolecules like protein, DNA.<sup>9</sup> Currently, it is also being used to study complex formation in pharmaceutical applications and binding reactions in biochemical systems.<sup>9, 10, 11</sup> In our studies, we will employ ITC experiments<sup>2, 12</sup> to determine the enthalpy change during the binding of different acids with our ligand, and hence interpreting the strength of binding.

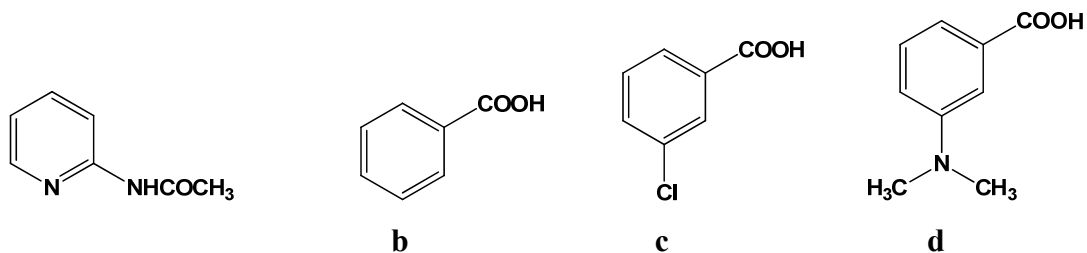


**Figure 3.1** The ligand and the acids under study (a) 2-acetamidopyridine (b) benzoic acid (c) 3-chlorobenzoic acid (d) 3-(*N,N*-dimethyl)aminobenzoic acid.

Our study comprises: a) dilution study of the ligand, b) dilution study of the acid, and c) titration of the ligand and acid.<sup>2</sup> The calorimeter measures the extent of binding of

a molecule to another molecule using the heat of interaction as the probe. The binding of the ligand and the acid is thermodynamically favorable process.<sup>2</sup> Energy is released during the titration in the form of heat, resulting in a more stable ligand-acid complex held together via hydrogen bonds. The magnitude of heat energy released during the titration is an indication of the stability of the complex, which will be measured by the calorimeter and expressed in thermodynamic terms.

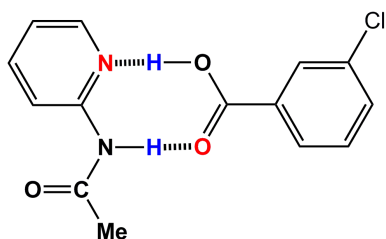
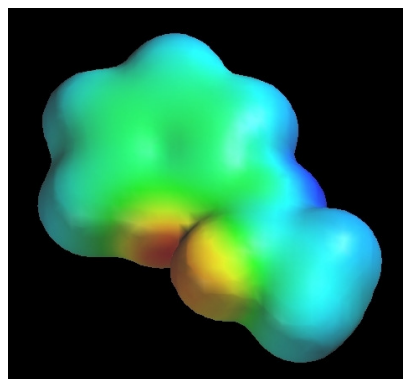


**Figure 3.2** The hydrogen bonding interaction between 2-acetamidopyridine (ligand) and 3-chlorobenzoic acid.

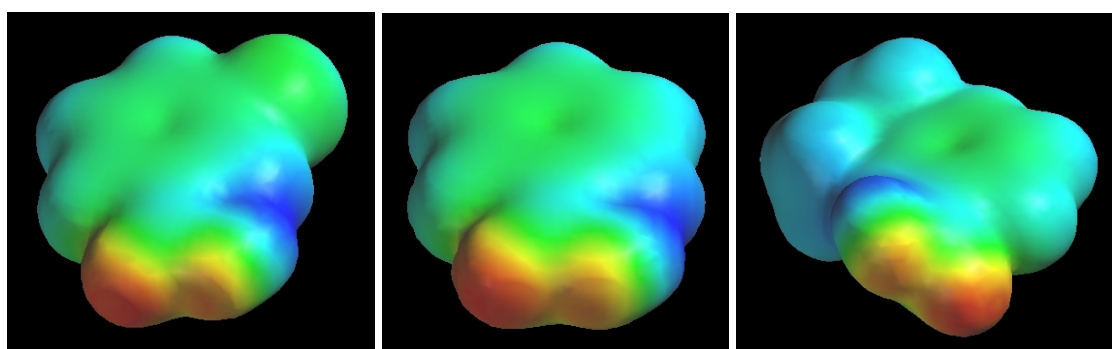
## 3.2 Experimental

### 3.2.1 *Electrostatic charges calculations*

The magnitude of electrostatic charge on hydrogen-bond donors and acceptors in these molecules were obtained using semi-empirical AM1 calculations. Values for individual atoms are obtained by probing the MEPS (0.002 e/au isosurface, from AM1 calculations) with a point charge.<sup>13</sup> For example, 3-chlorobenzoic acid with its electron withdrawing chloro group has lower charge (-285 kJ/mol) on the carbonyl oxygen atom than that in benzoic acid (-298 kJ/mol). (Fig 3.3)



2-acetamidopyridine



3-chlorobenzoic acid

benzoic acid

3-(*N,N*-dimethyl)aminobenzoic acid

**Figure 3.3** AM1 calculations of charges on 2-acetamidopyridine and the acids under study.

**Table 3.1** AM1 calculations on the hydroxyl group and the carbonyl group in the carboxylic acids.

	AM1 calc. (kJ/mol)	
	-OH	C=O
<b>3-Chlorobenzoic acid</b>	190	-285
<b>Benzoic acid</b>	180	-298
<b>3-(<i>N,N</i>-dimethyl)aminobenzoic acid</b>	171	-309

The presence of an electron withdrawing chloro group in the benzene ring decreases the electron density on the carbonyl oxygen hence a lesser charge of -285 kJ/mol is observed compared to -298 kJ/mol for unsubstituted benzoic acid. For the same reason, there is a higher positive charge on the acidic proton 190 kJ/mol compared to the 180 kJ/mol in the benzoic acid. The opposite argument applies to 3-(*N,N*-



dimethyl)aminobenzoic acid, where the electron donating effects of the methyl group increases the electron density in the ring and hence in the carbonyl oxygen where the charge on the oxygen is raised to -309 kJ/mol. The charge on hydroxyl proton however is reduced to 171 kJ/mol, making it a weaker acid compared to benzoic acid.

### 3.2.2 Synthesis of 2-acetamidopyridine

All three carboxylic acids used for our experiment were purchased from Aldrich and used without further purification. The ligand under study, 2-acetamidopyridine was synthesized according to the previous described method (section 2.2.1.1)

### 3.2.3 Co-crystal screening via IR spectroscopy

The ability of the carboxylic acids chosen for our study to form co-crystals was determined by screening via IR spectroscopy. All the acids formed co-crystal with 2-acetamidopyridine as evidenced by the presence of broad stretches near 1950 and 2450  $\text{cm}^{-1}$ , indicative of intermolecular O—H---N(heterocycle) hydrogen bonds and as a strong band for C=O near 1700  $\text{cm}^{-1}$  indicative of an intact -COOH moiety and a weak C—O stretch near 1275  $\text{cm}^{-1}$ .<sup>14</sup>

**Table 3.2** IR stretching frequencies for three co-crystals of 2-acetamidopyridine.

Ligand/3-chlorobenzoic acid ( $\text{cm}^{-1}$ )	3219, 2390, 1883, 1700, 1584
Ligand/benzoic acid ( $\text{cm}^{-1}$ )	3224, 2410, 1855, 1699, 1609
Ligand/3-( <i>N,N</i> -dimethyl) aminobenzoic acid ( $\text{cm}^{-1}$ )	3007, 2472, 1871, 1699, 1610

### 3.2.4 Single Crystal X-ray Crystallography

X-ray data were collected on a Bruker SMART APEX or a SMART 1000 diffractometer using Mo  $\text{K}\alpha$  radiation and, where noted, were corrected for absorption using the multiscan procedure implemented by SADABS. Data were collected using SMART.

### 3.2.5 Instrumentation

The titrations were performed on a VP-ITC isothermal titration calorimeter, (*MicroCal Inc.*, Northampton, MA).

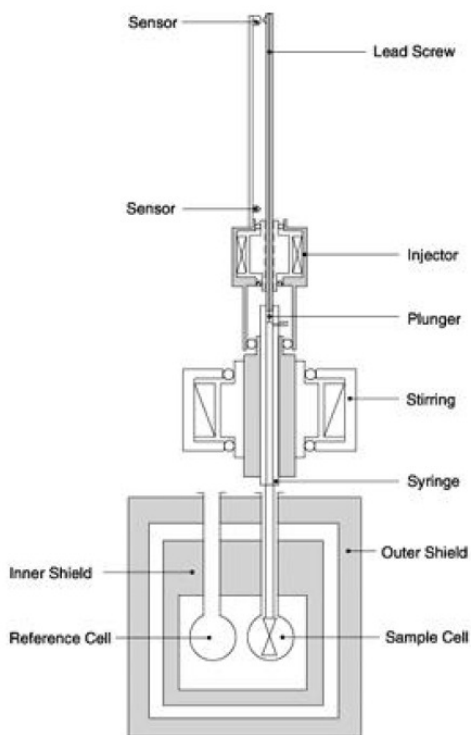


**Figure 3.4** An isothermal titration calorimeter.

A typical isothermal titration calorimeter consists of an injector system, an adiabatic shield, and two identical cells as reference and sample cells made of a thermal conducting material. The cells are elongated tube-like with 1.4 ml bulbs where the samples are introduced via long-needled syringes. Heaters are arranged around the cells with special thermoelectric device to detect and measure the temperature differences between the two cells ( $\Delta T$ ).<sup>8</sup> (Figure 3.4) Both cells are maintained at a constant and identical temperature at least 5 °C above that of the surroundings. The reference cell is filled with water and the sample cell is injected with the ligand solution. At the start of the experiment, a constant power of less than 1 milliwatt is applied to the reference cell.

This activates the cell feedback circuit (thermopile/thermocouple system) activating the heater in the sample cell and driving  $\Delta T$  back to 0. Hence it insures that whatever change in temperature is seen in the sample cell, the heat is supplied or decreased accordingly to retain the thermal equilibrium between the two cells.<sup>2</sup> Exothermic reactions result in an increase in the sample cell temperature, hence the feedback power needs to be decreased in the sample cell to maintain same temperature in both cells. Endothermic reactions decreases the sample cell temperature, hence feedback power needs to be increased.<sup>8, 15</sup>

### ***3.2.6 General experimental procedure for binding studies by ITC***

The samples were degassed at the start of the experiment to minimize any discrepancies resulting from the presence of air bubbles, as they may lead to abnormal data collection.<sup>2</sup> The MicroCal instrument is allowed to warm up and then set at 30 °C. The sample cell was filled with 1.3 mL of water or acid solution using a syringe with an elongated needle. The instrument was then allowed to stabilize for about 30 minutes. Then 100 $\mu$ L syringe was filled with the degassed ligand solution and fitted in the sample cell. The instrument is again allowed to stabilize, until the baseline is acceptable. The ligand solution is then injected into the sample cell in aliquots of 10 $\mu$ L for a total of 10 injections. All the injections were carried out with automatically-set computerized instructions. Each aliquot of ligand solution is injected over a time span of 60 seconds with 300 seconds interval between injections to allow for the system to stabilize after each injection. High concentration of the ligand compared to the acid is used (50 times more ligand in terms of moles) so as to make sure that all of the acid molecules available are bonded to the ligand. The heat change patterns can then be analyzed to determine the ligand/acid binding ratio in terms of moles as well as the thermodynamic parameters to find the stability of the binding interaction. All reactions were performed at room temperature with the instrument set at 30 °C.

*a) Dilution of the Ligand:* The dilution effects on 2-acetamidopyridine was studied to adjust for the effect of ligand dilution on complexation with acid. The sample cell was filled with degassed water and the ligand solution was injected into the cell over time.

The reaction was found to be slightly endothermic and the data obtained was later subtracted from ligand-acid titration data to adjust for the dilution of ligand.

*b) Dilution of the Acid:* The thermodynamics of dilution of benzoic acids were studied by injecting degassed pure water into the acid solution in the sample cell. Data obtained showed that the effect of dilution is minimal for the acid and hence neglected for further studies.

*c) Titration of Ligand with Acid:* The aqueous substituted benzoic acid was filled into the sample cell. The system was then allowed to stabilize, after which the aqueous 2-acetamidopyridine solution was injected into it. The data obtained showed that the ligand-acid binding is exothermic in nature. The data was adjusted for dilution of ligand and analyzed using the software *Origin ITC*.

Data analysis and data fit procedures were done using the software *MicroCal Origin ITC*. The signals from the experiment are plotted in  $\mu\text{cal}/\text{sec}$  as a function of time, interpreting the power needed to maintain the reference and sample cell at the same temperature. The number of pulses corresponds to the heat released/absorbed with injection of the ligand. These can be integrated to obtain the total heat change per injection.

### ***3.2.6.1 Binding study of 2-acetamidopyridine and benzoic acid***

1.3 mL of 0.044mM aqueous benzoic acid was filled into the sample cell. The instrument was allowed to stabilize and then 12mM aqueous 2-acetamidopyridine solution was injected into it in aliquots of 10 $\mu\text{L}$  for a total of 10 injections using the automatic computerized instructions. The heat change patterns were recorded and analyzed.

### ***3.2.6.2 Binding study of 2-acetamidopyridine and 3-chlorobenzoic acid***

1.3 mL of 0.044mM aqueous 3-chlorobenzoic acid was filled into the sample cell. The instrument was allowed to stabilize and then 12mM aqueous 2-acetamidopyridine solution was injected into it in aliquots of 10 $\mu\text{L}$  for a total of 10 injections using the

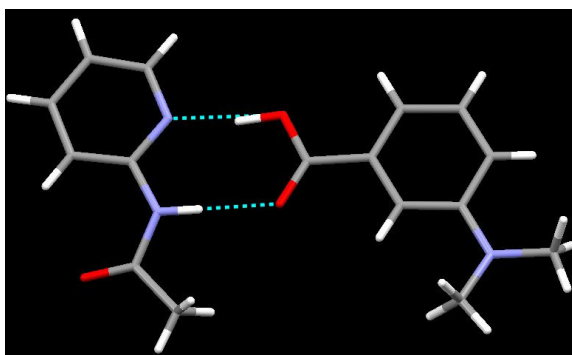
automatic computerized instructions. The heat change patterns were recorded and analyzed.

### ***3.2.6.3 Binding study of 2-acetamidopyridine and 3-(N,N-dimethyl)aminobenzoic acid***

1.3 mL of 0.044mM aqueous 3-(N,N-dimethyl)aminobenzoic acid was filled into the sample cell. The instrument was allowed to stabilize and then 12mM aqueous 2-acetamidopyridine solution was injected into it in aliquots of 10 $\mu$ L for a total of 10 injections using the automatic computerized instructions. The heat change patterns were recorded and analyzed.

## **3.3 Results**

### ***3.3.1 Single crystal X-ray analysis of 2-acetamidopyridine : 3-N,N-dimethylbenzoic acid (1:1)***



Crystal structure of 2-acetamidopyridine:3-N,N-dimethylbenzoic acid (1:1) co-crystal showing the binding motif.<sup>16</sup>

Crystal structure of 2-acetamidopyridine with 3-N,N-dimethylbenzoic acid shows the binding motif as N-H $\cdots$ O and O-H $\cdots$ N hydrogen bonds. Similar binding motifs can be expected for other two carboxylic acids used for our experiment.

### ***3.3.2 ITC spectra for thermodynamic study of dilution of 2-acetamidopyridine***

The dilution of the ligand, 2-acetamidopyridine was found to be slightly endothermic, the peaks of which remained constant through consecutive injections. This data was later subtracted from ligand-acid titration data to adjust for the dilution of

ligand. (Fig. 3.5) Similar but even less endothermic peaks were observed for dilution of the carboxylic acids, which are termed insignificant and are discarded.

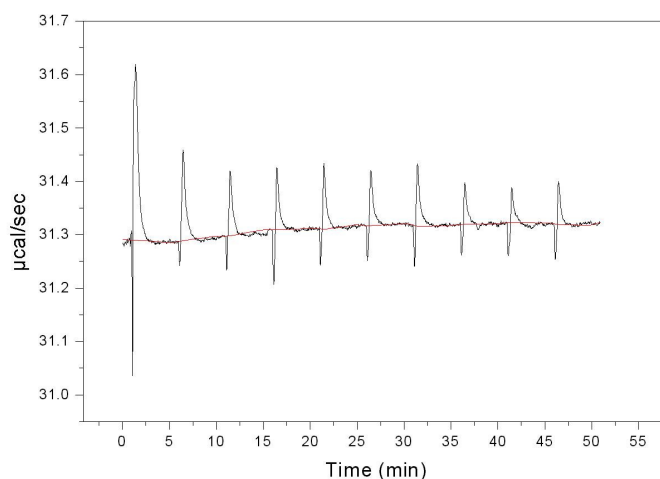


**Figure 3.5** Spectrum showing endothermic nature of titration during the dilution of ligand.

### ***3.3.3 ITC spectra for thermodynamic study of 2-acetamidopyridine and various benzoic acids***

The ITC study comprises of titration, injection of 2-acetamidopyridine into the aqueous solution of the acid in the sample cell. The initial injection of the ligand results in the binding of most of the injected ligand, and hence maximum heat is generated in the process as seen by the exothermic nature of the curve. On subsequent injections of the ligand solutions, however less and less of the acid molecules are available for binding with the injected ligand and hence reduces the amount of heat liberated. Eventually, with continual injection of the ligand no more acid molecules are available for binding and no further heat release is observed.

The heat exchange resulting from each individual injection is then integrated with respect to time and plotted against molar ratio of the two components. These are fitted using the appropriate binding models using the software *Origin/ITC* to calculate enthalpy change ( $\Delta H$ ), equilibrium association or dissociation constant ( $K$ ), entropy ( $\Delta S$ ), and stoichiometry. The free energy change ( $\Delta G$ ) can be calculated, from the values of  $\Delta H$  and

$\Delta S$  are known. (Equation 3.4) All the thermodynamic parameters obtained from the ITC experiment of 2-acetamidopyridine are given in Table 3.3.

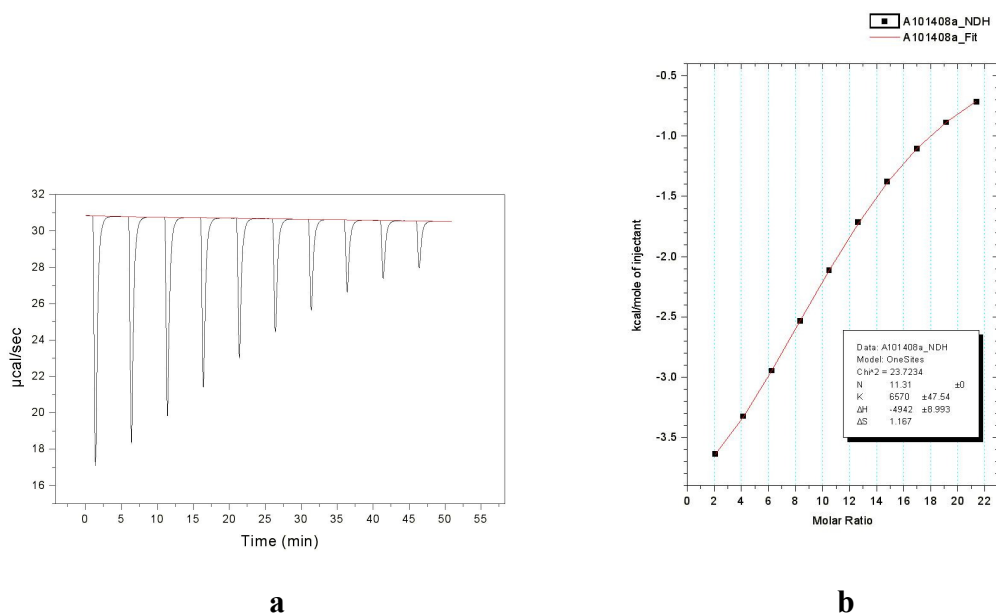


**Figure 3.6** (a) ITC titration curve of 2-acetamidopyridine vs. benzoic acid; (b) thermodynamic fit parameters.

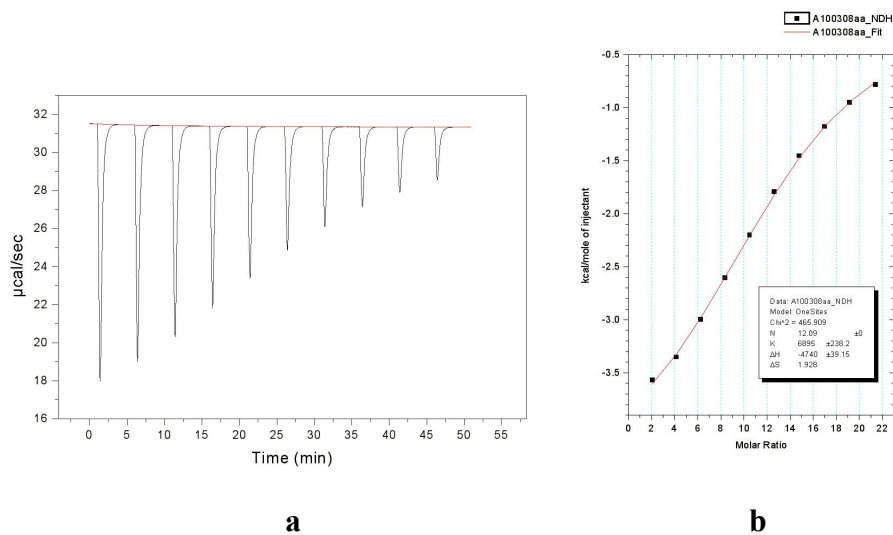


**Figure 3.7** (a) ITC titration curve of 2-acetamidopyridine vs. 3-chlorobenzoic acid; (b) thermodynamic fit parameters.

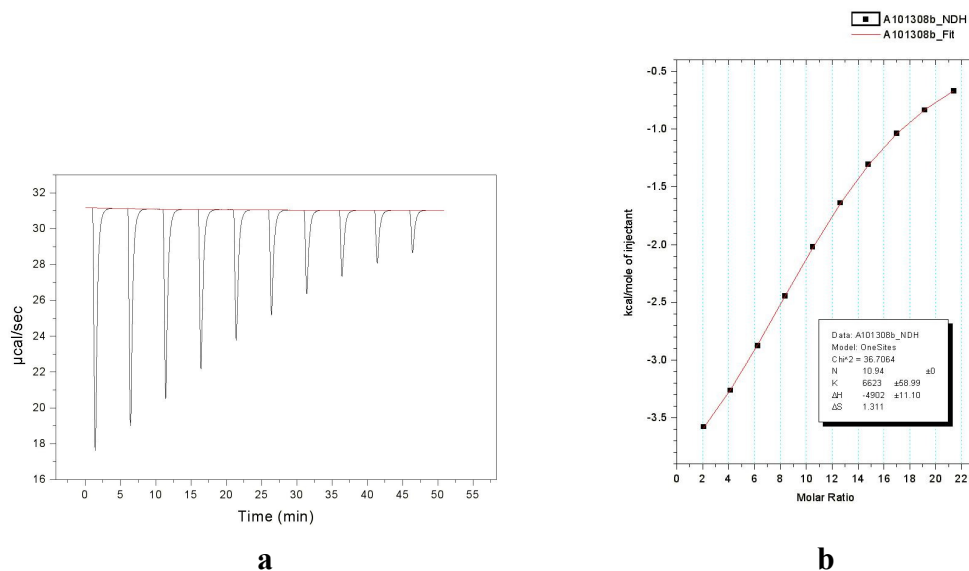


**Figure 3.8** (a) ITC titration curve for thermodynamic study of 2-acetamidopyridine vs. 3-(N,N-dimethyl)aminobenzoic acid; (b) thermodynamic fit parameters.

### 3.4 Discussion

#### 3.4.1 Thermodynamic explanations for the co-crystal formation

**Table 3.3** Comparison of thermodynamic parameters for the complexation of three carboxylic acids co-crystallized with 2-acetamidopyridine **3**.

	3-Chlorobenzoic acid	Benzoic acid	3-(N,N)-dimethylbenzoic acid
pKa <sup>17</sup>	3.83	4.20	5.10
K	6895 ± 238	6570 ± 48	6623 ± 59
ΔH (cal/mol)	-4740 ± 39	-4942 ± 9	-4902 ± 11
ΔS (cal/mol)	1.93	1.17	1.31
ΔG (cal/mol)	-5324.3	-5295.7	-5299.3

In solid state, the hydrogen-bonding patterns are well-defined; however in solutions the patterns are less-easily established. Studies show that in concentrated solutions, the molecules may occur as dimers whereas chains may be preferred in



concentrated solutions. The case is even more complicated for solvents with high dielectric constants like water that may favor more polar conformers.<sup>18</sup> The formation of dimers is a hydrophobic effect. The non-polar compounds in aqueous solutions tend to aggregate as dimers or chains.

Very few examples of benzoic acid dimers in aqueous solution<sup>19</sup> are available in literature with inconsistent data for cyclic and non-cyclic species,<sup>20</sup> whereas dimerization of benzoic acids is a common event in non-polar solvents and gaseous phase. Dimers of benzoic acid were reported in alcohol-water mixture.<sup>21</sup> The binding energy in benzoic acids were found to be 5.0 (CCl<sub>4</sub>), 4-8 (benzene), and 6.3 kcal/mole (CHCl<sub>3</sub>) as cyclic dimers.<sup>20</sup> Similarly, the amide-amide intermolecular hydrogen bond formation exists in aqueous solution<sup>22</sup> with the intrinsic binding energy of 5.7 kcal/mol. This dimerization is driven by a favorable energy change associated with the release of water molecules from amide NH and CO groups which are involved during hydrogen bond formation.<sup>23, 24</sup> Hence both the ligand and benzoic acids are considered to exist as dimers in aqueous solutions.

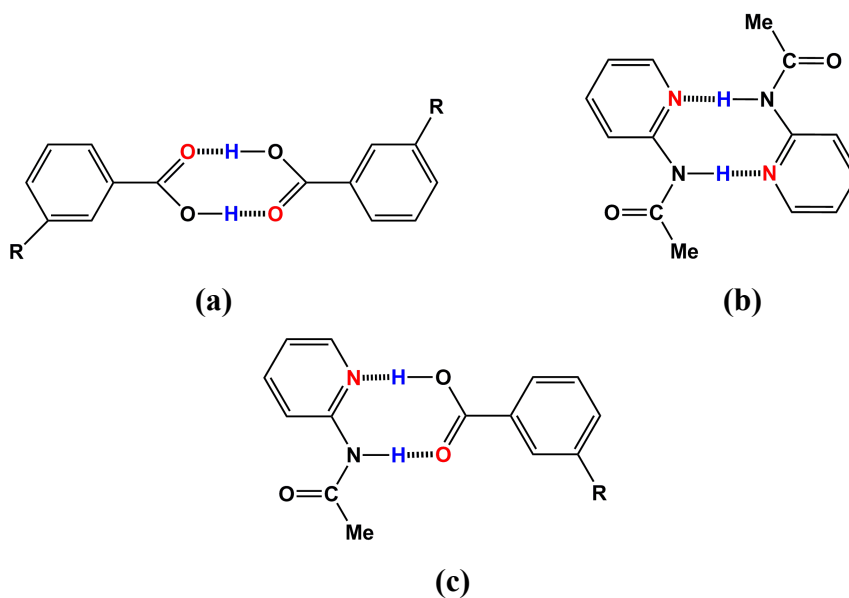


**Figure 3.9** (a) Homodimer of benzoic acid. (b) Homodimer of ligand, 2-acetamidopyridine. (c) Heterodimer between the benzoic acid and the ligand.

The mixing together of these two 1:1 dimer solutions would result in the dissociation of the homomeric linkage in favor of the heteromeric dimers. Such structural binding motif is more robust than the homomeric binding motifs.<sup>25</sup> Calorimetric binding

studies on antibiotic ristocetin showed that the ligand binding even induces the dissociation of antibiotic dimers.<sup>26</sup>

In order for a heteromeric dimer between 2-acetamidopyridine and benzoic acids to form, the water molecules surrounding the dimers need to be removed and the dimer has to be broken down into monomers. This process is endothermic and entropy favorable. The formation of heteromeric dimer between the free ligand and acid occurs which again gets surrounded by the water molecules. This process involves formation of new bonds, an exothermic process and entropy unfavorable. The thermodynamic effects observed are the net effect of the breaking of old hydrogen bonds in homomeric dimer and formation of new hydrogen bonds in heteromeric dimers. We also need to understand that the heat studies for binding reactions is difficult and only qualitative studies can be found due to contributions from many equilibria conditions in the overall heat effect.<sup>27</sup>

The thermodynamic results obtained from our experiments showed the lowest enthalpy change value for 3-chlorobenzoic acid and comparable values for benzoic acid and 3-(*N,N*)-dimethylbenzoic acid. This is in contrast to our prediction of highest enthalpy value for 3-chlorobenzoic acid in part due to the electron-withdrawing effect imparted by the chloro group and hence stronger binding, with higher amount of energy release. Comparatively higher entropy change is observed for 3-chlorobenzoic acid which may account for the low enthalpic gain. However, the overall entropy effects is very small as the number of homodimers at the start and the number of heterodimers formed at the end stays the same during the process. The association constant (*K*) is highest for 3-chlorobenzoic acid which supports our hypothesis. This factor may be taken as the major factor as other thermodynamic events entropy and free energy are dependent on the association constant.

In these circumstances, the best thermodynamic parameter to study would be the Gibbs free energy of association which takes in consideration both enthalpic and entropic factors. Many physical properties of a compound like hydrophobic, electronic and steric substituent constants, as well as the biological activities themselves, are related to the Gibbs energy<sup>28</sup>. It seems logical therefore, to set up scales of hydrogen bonding strengths using Gibbs energies rather than enthalpies.<sup>1</sup> The more negative the value of  $\Delta G$ , the more favorable the process would be and more would be the energy release. Here, the

value of  $\Delta G$  is lowest for 3-chlorobenzoic acid which is as expected whereas the values for other two acids are comparable. However, these values for all three carboxylic acids are still very close to each other. This suggests that the polarity of the solvent used may be playing a dominating role, as the polar solvent water with high dielectric constant 78 (300K) is used as solvent,<sup>29</sup> which itself competitively interact with the ligands/acids and the co-crystals.

In addition, our experimental value of 5.3 kcal/mol fits well with the expected values for a normal hydrogen bond (ca 5 kcal/mol).<sup>30</sup> The strength of heteromeric acid-amide hydrogen bonding interaction is still dubious, whereas homodimeric N-H---O=C bond in urea is in the range of 4-15 kcal/mole.<sup>31</sup> However it should be noted that very little work if any, has been done to investigate the thermodynamic properties of co-crystallization of small molecules in aqueous medium. Our work may be the very first systematic work in investigating the solution behavior during co-crystallization of various benzoic acids with substituted pyridines.

### 3.5 Conclusions

The experimental results are consistent with the observations from the solid-state behavior (chapter 2). The strength and potential of co-crystallization is found to depend on the charges on the ligand and not on the co-crystallizing agents. There is a need to repeat the experiment with a single carboxylic acid and varying the ligands with different charges to further supplement our results. In our case, we were unable to do so due to solubility restrictions of the ligands. Also, the strength of the intermolecular interaction in terms of hydrogen bonding in co-crystals can be explained in thermodynamic terms to some extent. However, due to competitive contributions from the solvent, the solvation factors needs to be considered. However, due to experimental limitations, we were unable to run the experiment in different solvents to figure out the extent of solvent effects on the thermodynamics factors during co-crystallization.

## References

- <sup>1</sup> (a) Laurence, C.; Berthelot, M. *Perspectives in Drug Discovery and Design*, **2000**, *18*, 39; (b) Joesten, M.D. and Schaad, L.J., *Hydrogen Bonding*, Marcel Dekker, **1974**, New York.
- <sup>2</sup> O'Brien, R.; Ladbury, J. E.; Chowdhry, B. Z. *Protein-Ligand Interactions; Hydrodynamics and Calorimetry: A Practical Approach*, Chapter 10 Isothermal Titration Calorimetry of biomolecules, **2000**, Oxford University Press, New York.
- <sup>3</sup> Swarbrick, J., Boylan J. C. *Encyclopedia of Pharmaceutical Technology*, Volume 1, 3<sup>rd</sup> Ed., Informa Healthcare USA, Inc.
- <sup>4</sup> Privalov, P. L., Dragan, A. I. *Biophysical Chemistry*, **2007**, *126*, 16.
- <sup>5</sup> Aakeröy, C. B.; Hussain, I.; Desper, J. *Crystal Growth & Design* **2006**, *6(2)*, 474.
- <sup>6</sup> [http://en.wikipedia.org/wiki/Isothermal\\_Titration\\_Calorimetry](http://en.wikipedia.org/wiki/Isothermal_Titration_Calorimetry)
- <sup>7</sup> Banerjee, M.; Poddar, A.; Mitra, G.; Surolia, A.; Owa, T.; Bhattacharyya, B. *J. Med. Chem.* **2005**, *48*, 547.
- <sup>8</sup> Wiseman, T.; Williston, S.; Brandts, J. F.; Lin, L. N. *Analytical Biochemistry*, **1989**, *179*, 131.
- <sup>9</sup> Saboury, A. A. *J. Therm. Anal. Cal.* **2004**, *77*, 997.
- <sup>10</sup> Dan, F.; Hamed, M. H.; Grolier, J-P. E. *Journal of Thermal Analysis and Calorimetry*, **2006**, *85*, 531.
- <sup>11</sup> Markoa, N.; Hallen, D. *Analytical Biochemistry*, **2004**, *331*, 77.
- <sup>12</sup> (a) Heerklotz, H. H.; Binder, H.; Epand, R. M. *Biophysical journal* **1999**, *76*, 2606; (b) Rowe, E. S.; Zhang, F.; Leung, T. W.; Parr, J. S.; Guy, P. T. *Biochemistry*, **1998**, *37*, 2430; (c) Trandum, C.; Westh, P.; Jorgensen, K.; Mouritsen, O. G. *J. Phys. Chem. B* **1999**, *103*, 4751; (d) Brogan, A. P.; Widger, W. R.; Bensadek, D.; Riba-Garcia, I.; Gaskell, S. J.; Kohn, H. *J. Am. Chem. Soc.* **2005**, *127*, 2741.
- <sup>13</sup> Charge calculations for the ligand and the carboxylic acids studied were performed using Spartan '04 (Wavefunction, Inc. Irvine, CA). All molecules were optimized using AM1, with the maxima and minima in the electrostatic potential surface (0.002 e au<sup>-1</sup> isosurface) determined using a positive point charge in the vacuum as a probe.
- <sup>14</sup> Silverstein, R.M.; Bassler, G. C.; Morrill, T.C. *Spectroscopic Identification of Organic Compounds*, **1991**, John Wiley and Sons, New York.
- <sup>15</sup> VP-ITC Microcalorimeter User's Manual, MicroCal Inc., Northampton, MA, USA. **2001**
- <sup>16</sup> CSD structure KEFBED
- <sup>17</sup> Brown, H.C. et al., in Braude, E.A. and F.C. Nachod *Determination of Organic Structures by Physical Methods*, 1955, Academic Press, New York.
- <sup>18</sup> Etter, M. C. *Acc. Chem. Res.* **1990**, *23(4)*, 120.
- <sup>19</sup> (a) Strong, L. E.; Brummel, C. L.; Ryther, R.; Radford, J. R.; Pethybridge, A. D. *Journal of Solution Chemistry* **1988**, *17(12)*, 1145; (b) Sagarik, K.; Rode, B. M. *Chemical Physics* **2000**, *260*, 159.
- <sup>20</sup> Pimentel, G. C.; McClellan, A. L. *The Hydrogen Bond* **1960**, W. H. Freeman and company, San Francisco and London, 206-225.
- <sup>21</sup> Bruno, G.; Randaccio, L. *Acta Cryst.* **1980**, *B36*, 1711.
- <sup>22</sup> Robertson, E. G.; Hockridge, M. R.; Jelfs, P. D.; Simons, J. P. *Phys. Chem. Chem. Phys.*, **2001**, *3*, 786.

- 
- <sup>23</sup> Williams, D. H.; Cox, J. P. L.; Doig, A. J.; Gardner, M.; Gerhard, U.; Kaye, P. T.; Lal, A. R.; Nicholls, I. A.; Salter, C. J.; Mitchell, R. C. *J. Am. Chem. Soc.* **1991**, *113*, 7020.
- <sup>24</sup> Doig, A. J.; Williams, D. H. *J. Am. Chem. Soc.* **1992**, *114*, 338.
- <sup>25</sup> Etter, M. C.; Frankenbach, G. M. *Chem. Mater.* **1989**, *1*, 10.
- <sup>26</sup> Cooper, A.; McAuley-Hecht, K. *Philos. Trans. R. Soc. London A*, **1993**, *345*, 23.
- <sup>27</sup> Wang, R.; Schmiedel, H.; Paulke, B. R. *Colloid Polym Sci.* **2004**, *283*, 91.
- <sup>28</sup> Hansch, C.A. *Acc. Chem. Res.* **1969**, *2*, 232.
- <sup>29</sup> Smith, P. E.; van Gunsteren, W. F. *J. Chem. Phys.* **1994**, *100*(4), 3169.
- <sup>30</sup> Perrin, C. L.; Nielson, J. B. *Annu. Rev. Phys. Chem.* **1997**, *48*, 511.
- <sup>31</sup> Desiraju, G. R.; Steiner, T. *The Weak Hydrogen Bond: In Structural Chemistry and Biology.* **2001**, International Union of Crystallography, Oxford Science Publications.

# CHAPTER 4 - Ditopic ligands as a probe to investigate selectivity in binary co-crystals/salts

## 4.1 Introduction

A co-crystallization<sup>1</sup> process is an interplay between intermolecular interactions involving mainly hydrogen bonding,<sup>2</sup> halogen bonding,<sup>3</sup> and  $\pi$ - $\pi$  interactions.<sup>4</sup> The most common of these interactions remains the hydrogen bond which brings along its strength and directionality.<sup>5</sup> Co-crystallization via hydrogen-bond interactions requires the interaction between two complementary hydrogen-bond donors and hydrogen-bond acceptors. During the process, commonly occurring synthons e.g. acid-acid and amide-amide homosynthons are disrupted to form acid-amide heterosynthons.<sup>6</sup> In the presence of a single acceptor and single donor molecule, the case is straightforward with 1:1 co-crystal/salt formed. However, the presence of two acceptors complicates the case and predicting binding preferences becomes even more challenging, (Figure 4.1).

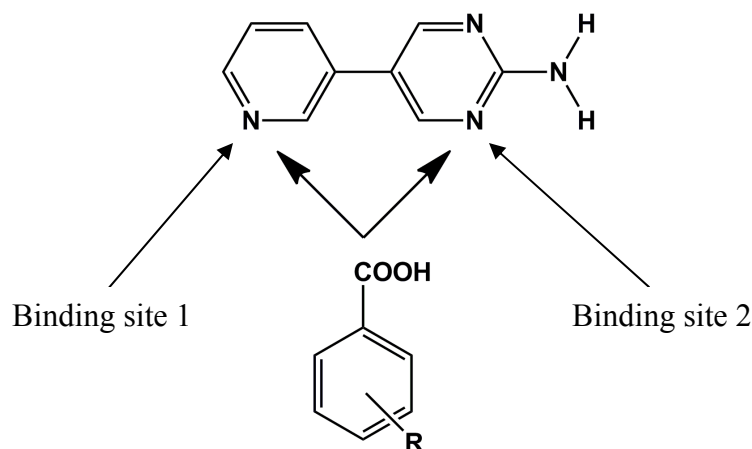


**Figure 4.1** Schematic of selectivity of hydrogen-bond donors for ditopic ligands.

A systematic study of hydrogen bonding patterns in various crystal structures led Etter<sup>7</sup> to suggest that in a mix of multiple hydrogen-bond donors and acceptors, the best hydrogen-bond donor will prefer the best hydrogen-bond acceptor and so on. Hence in our system with two acceptors and a single donor molecule, the interaction should occur

selectively between the donor molecule and the better acceptor, (Figure 4.2). The reliability of this approach was tested with a series of new ditopic ligands comprising two competing acceptor sites equipped with pyridine, pyrimidine, and pyrazine moieties. These N-heterocycles have different strength and binding abilities which would probe the selectivity of the donor. To bring further variability in the choice of acceptors, the amino- and acetamido- substituents were equipped on these N-heterocyclic sites competing for a single donor.

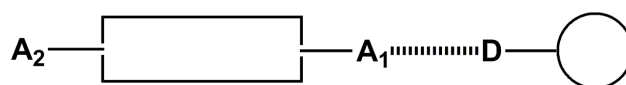


**Figure 4.2** Schematic of a donor molecule (D) binding to the best acceptor (A<sub>1</sub>).

#### ***4.1.1 Selectivity prediction via AM1 calculations***

Electrostatic potential surface calculations provide important information regarding the binding strength of hydrogen-bonding entities.<sup>8</sup> In Chapter 2, we have shown that the AM1-based electrostatic charge calculation is very successful in ranking binding potential of hydrogen-bond donors and acceptors. This specificity observed for the small molecules is further extended to investigate the selectivity in ditopic molecules in this chapter.

Our ditopic testing system consists of a combination of two entities selected from unsubstituted pyridyl and amino/acetamido-substituted *N*-heterocycles. These groups by themselves have the capability to engage in hydrogen-bond interactions with hydrogen-bond donors like carboxylic acids via the commonly encountered *N*-heterocycle/carboxylic acid heterosynthon.<sup>9</sup> The assembly of these two moieties together within the same building block will test their comparative binding strengths against a single donor. A CSD search on the selectivity within the coupled *N*-heterocycles revealed that no such studies have been done to date.<sup>10</sup>

AM1 calculations of the electrostatic potential of the nitrogen atom in unsubstituted pyridines, pyrimidines, and pyrazines follow a decreasing trend, (Figure 4.3). These charges can be enhanced by incorporating electron donating amino/acetamido groups in the ring; however this addition will also introduce complexity in our ligands by converting a one-point interacting group to two point interactions with probable contributions from auxiliary groups.

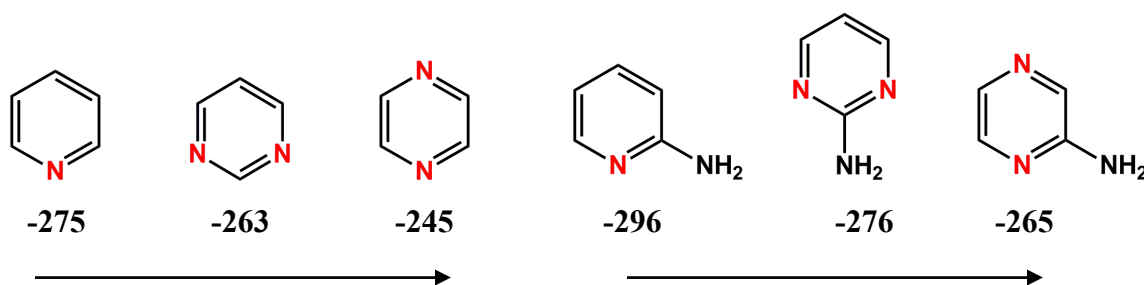
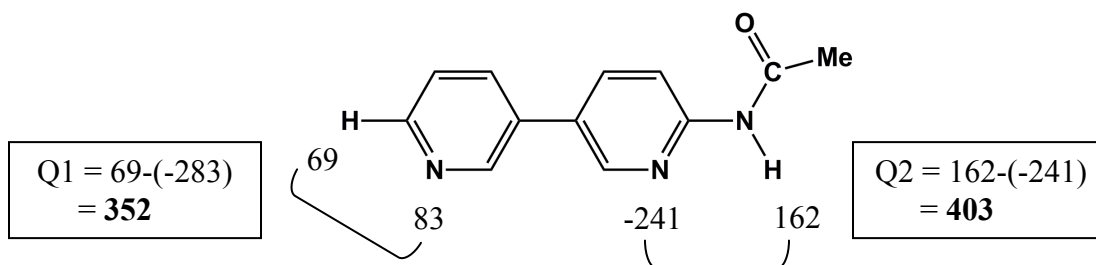


**Figure 4.3** Decreasing electrostatic potential in unsubstituted *N*-heterocycles and amino-substituted *N*-heterocycles.

With the assumption that the two point donors like carboxylic acids might favor two-point interactions with the acceptor molecules, we set out to include the auxiliary group contributions in calculating the total charge on the acceptor sites as a measure of its binding potential. A combined hydrogen-bonding ability value, *Q* is introduced, which is the sum of the electrostatic potential surfaces for the hydrogen bonding entities in binding site.

$$Q = A1 - (A2)$$

Where *A1* is the maximum positive potential and *A2* is the minimum negative potential.

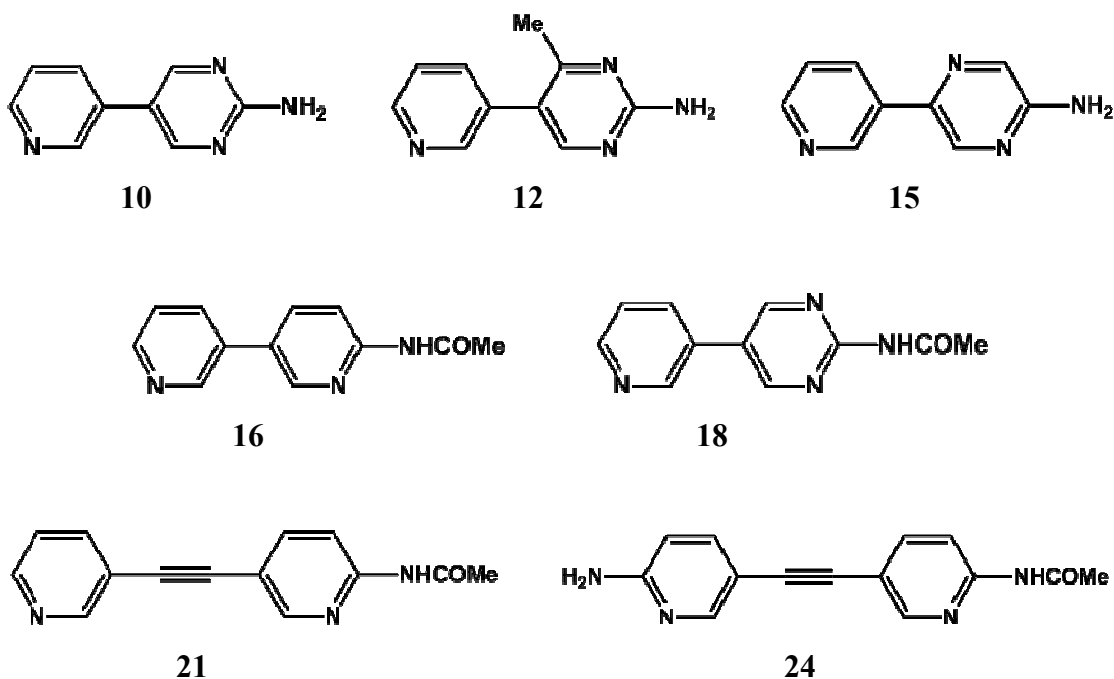


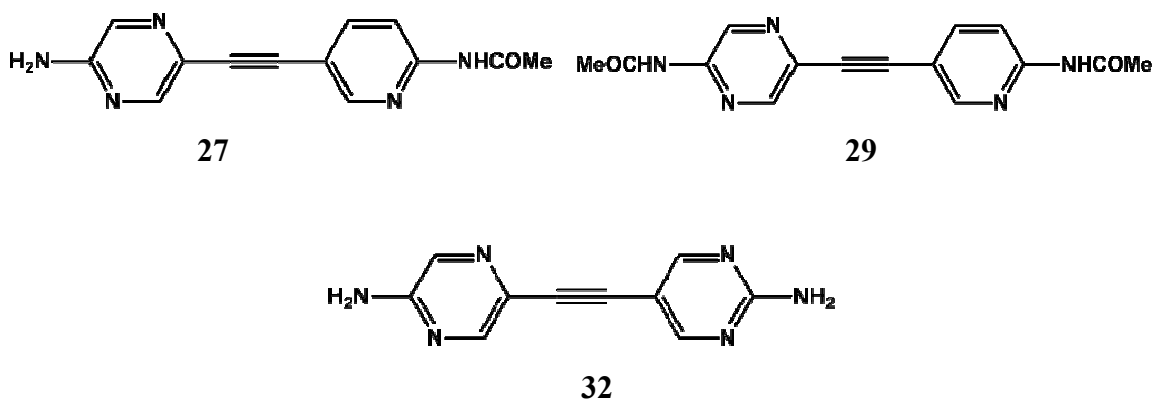


For two point interactions, Q values were assigned to each binding site with the magnitude of the Q value reflecting the binding ability of a particular site. The comparison of the Q values for the two sites in the ditopic molecule is expected to act as a guideline in binding selectivity. Using 2-acetamido-5-(3-pyridyl) pyridine as an example, the two binding sites have either C-H or N-H as auxiliary groups. Each site is assigned a Q value; and in this particular case, the acetamidopyridyl site with Q2 (403) is predicted to have higher binding over the site with Q1 (352).

#### 4.1.2 Research goals

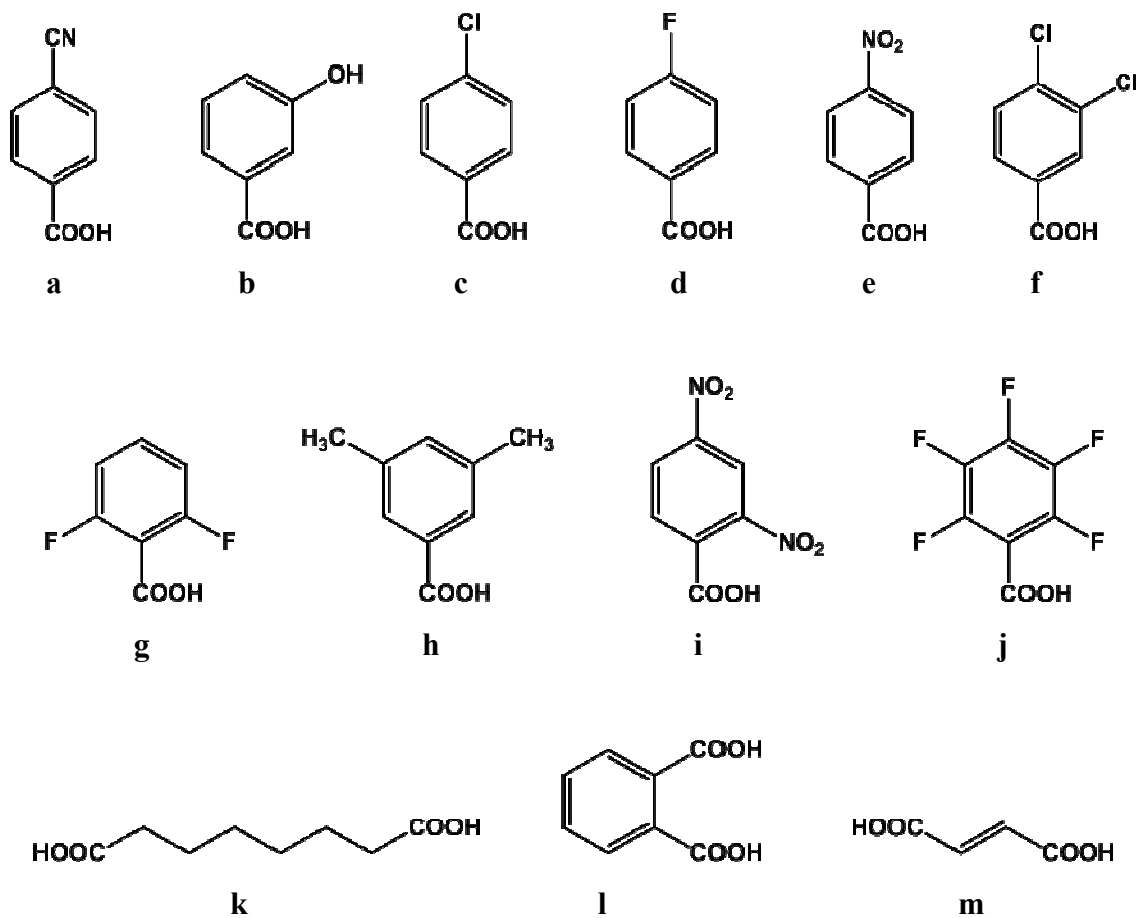
We propose that electrostatic potentials may be used to determine selectivity in ditopic ligands containing two comparable binding sites. To investigate our hypothesis, we designed and synthesized a series of ditopic *N*-heterocyclic ligands (a combination of pyridine, pyrimidine, and pyrazine) capable of interacting with hydrogen bond donors, (Figure 4.4). The electrostatic potential of each binding sites in these ditopic ligands is calculated and ranked with the assumption that the donor will pair with the best hydrogen bond acceptor.





**Figure 4.4** A series of bifunctional ligands with two different hydrogen-bonding sites have been synthesized.

The hypothesis was tested with the introduction of a series of hydrogen bond donors ranging from monocarboxylic acids, dicarboxylic acids, and cyanoximes (Figure 4.5) with the assumption that a donor should prefer to bind to the best acceptor site in the ditopic ligand.



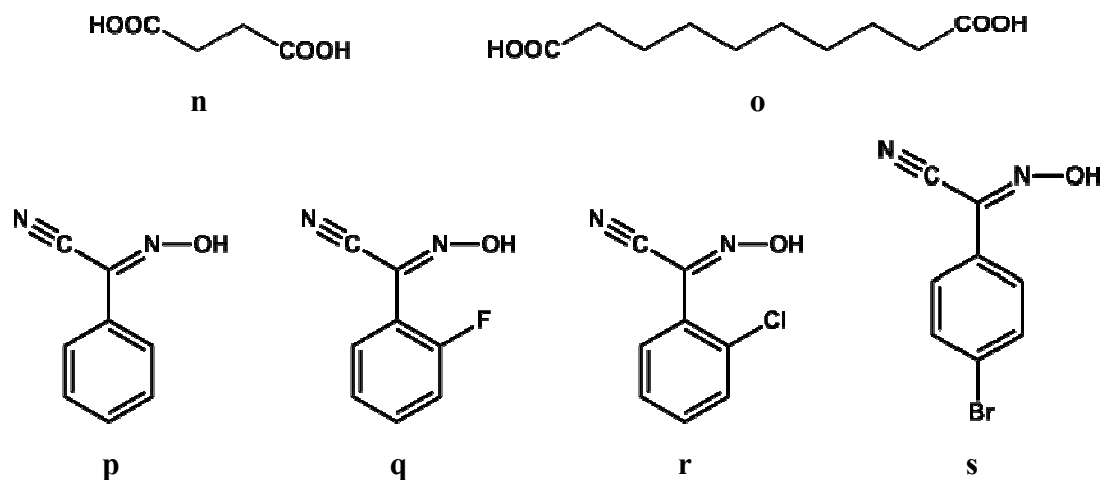


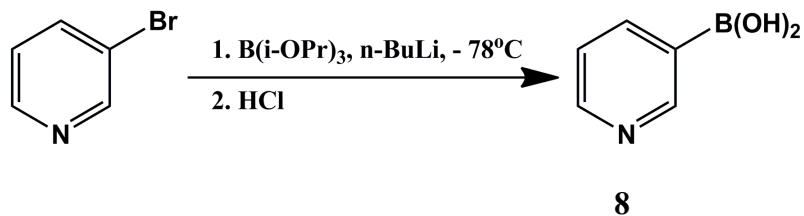
**Figure 4.5** A series of nineteen hydrogen-bond acceptors used for the study; monocarboxylic acids (**a – j**), dicarboxylic acids (**k – o**), and cyanoximes (**p – s**).

## 4.2 Experimental

### 4.2.1 Synthesis of ligands

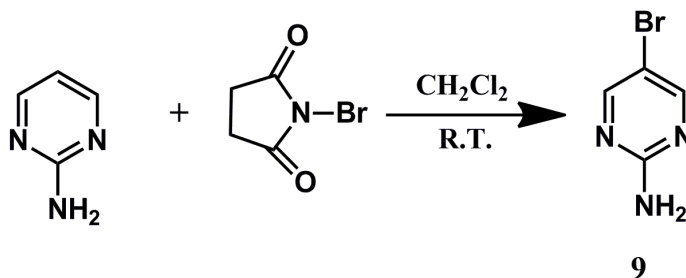
All chemicals, unless otherwise noted, were purchased from Aldrich and used without further purification. Trimethylsilylacetylene was purchased from GFS chemicals. The catalysts, *bis*(triphenylphosphine)palladium(II) dichloride and Tetrakis(triphenylphosphine)palladium(0), were purchased from Strem chemicals. Column chromatography was carried out on silica gel (150 Å pore size) from Analtech Inc. Melting points were determined on a Fisher-Johns melting point apparatus and are uncorrected.  $^1\text{H}$  and  $^{13}\text{C}$  NMR spectra were collected on a Varian Unity plus 200 MHz or 400 MHz spectrometer in  $\text{CDCl}_3$  or  $d_6\text{-DMSO}$ . The infrared (IR) spectrum was collected on ThermoScientific Nicolet 380 FT-IR spectrometer, either directly or as a KBr mixture.

#### 4.2.1.1 Synthesis of 3-pyridylboronic acid, 8<sup>11</sup>



Dry THF (200 mL) was added to a round-bottom flask kept in a dry ice/acetone bath (-78 °C). Dinitrogen was bubbled through the solution and the flask closed with a rubber stopper. The dinitrogen atmosphere was maintained inside the flask along with continuous stirring. 3-Bromopyridine (9.65 mL, 0.10 mol) was added to it via syringe, followed by tri-isopropylborate (27.70 mL, 0.12 mol). Then n-butyllithium (75.00 mL, 0.12 mol, ca. 1.6 M solution in hexanes) was added dropwise via syringe over 1 hr. The mixture was stirred for additional 30 mins with the temperature maintained at about -78 °C. The dry ice/acetone bath was then removed and the mixture allowed to warm to -20 °C when 2N HCl (200 mL) was added to it. When the mixture attained room temperature, the aqueous layer was separated using a separating funnel. The aqueous layer was stirred and its pH adjusted to 7 by adding 5N NaOH, whereupon a white ppt. was obtained. It was filtered and air dried. (8.83 g, 72%). M. P. >250 °C; <sup>1</sup>H NMR (δH; 200 MHz, CD<sub>3</sub>OD): 8.52 (s, 1H), 8.43 (d, 1H), 8.22 (d, J = 8.0 Hz, 1H), 7.51 (d, J = 6.0 Hz, 1H).

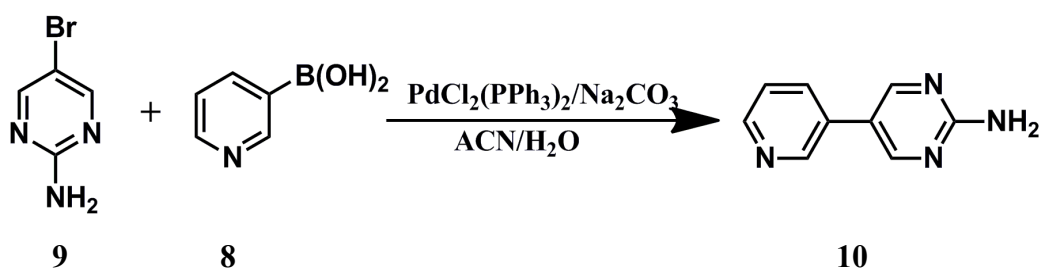
#### 4.2.1.2 Synthesis of 2-amino-5-bromopyrimidine, 9



A solution of *N*-bromosuccinimide (11.0 g, 61.8 mmol) in methylene chloride (200 mL) was added dropwise to the solution of 2-aminopyrimidine (5.0 g, 52.6 mmol) in methylene chloride (100 mL) kept over an ice bath. After addition, the ice bath was removed and the reaction mixture was stirred at room temperature for 1 hr. The reaction

was monitored by TLC and upon completion, was quenched with 10% sodium bicarbonate and 10% sodium sulfite solution. The mixture was filtered and the precipitate washed with water twice and dried. The filtrate was extracted with methylene chloride and dried over anhydrous magnesium sulfate. The solvent was removed on a rotary evaporator to obtain the product as yellowish-white powder. (8.7 g, 95.6 %). M.P. > 250 °C; <sup>1</sup>H NMR (δH; 200 MHz, CDCl<sub>3</sub>): 8.31 (s, 2H), 5.09 (br, 2H).

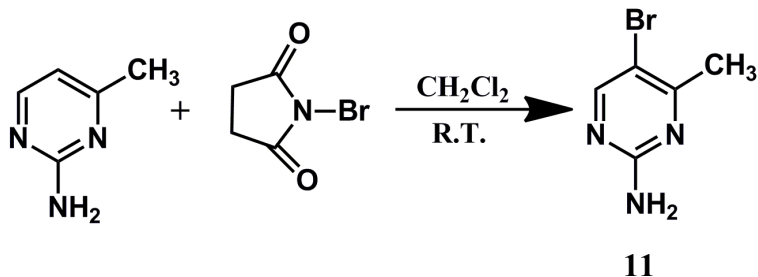
#### 4.2.1.3 Synthesis of 2-amino-5-(3-pyridyl)pyrimidine, 10



2-Amino-5-bromopyrimidine **9** (0.65 g, 3.74 mmol), 3-pyridylboronic acid **8** (0.55 g, 4.47 mmol), and sodium carbonate (0.22 g, 2.08 mmol) were added to a round bottom flask. Acetonitrile (15 mL) and water (15 mL) were added and dinitrogen was bubbled through the mixture for 10 minutes. *Bis*(triphenylphosphine)palladium(II) dichloride (0.055 g, 0.078 mmol, 2.1 mol%) was added and dinitrogen bubbled through for 5 more minutes. The apparatus was fitted with a condenser and the mixture was refluxed at 80 °C under dinitrogen atmosphere. The reaction was monitored by TLC and upon completion (36 hrs) was cooled to room temperature. The solution was then diluted with ethyl acetate (50 mL), washed with (3 x 50 mL) and saturated aqueous sodium chloride solution (1 x 50 mL). The organic layer was separated and dried over anhydrous magnesium sulfate. The solvent was removed on a rotary evaporator and the residue was chromatographed on silica with hexane: ethyl acetate (1:1) mixture as eluant. The product was obtained as a yellowish white solid. The product was then recrystallized from ethyl acetate to obtain colorless block-shaped crystals. (0.48 g, 75 %). M.P. 192 – 195 °C; <sup>1</sup>H NMR (δH; 400 MHz, CDCl<sub>3</sub>): 8.78 (s, 1H), 8.63 (s, 1H), 8.54 (s, 2H), 7.79 (d, J = 8.0 Hz, 1H), 7.39 (d, 1H), 5.31 (br, 2H); <sup>13</sup>C NMR (δH; 200 MHz, CDCl<sub>3</sub>): 193.95,

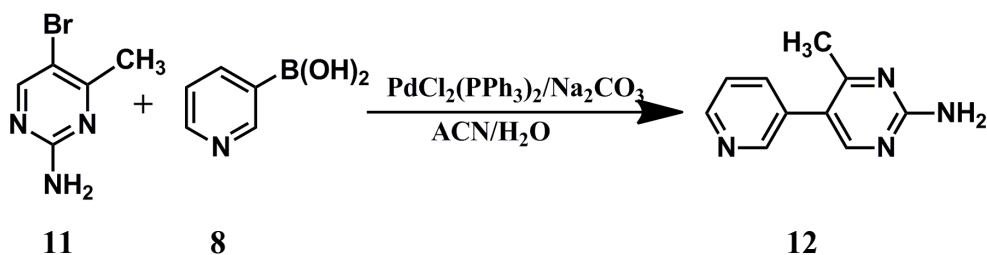
156.73, 149.02, 147.39, 133.50, 131.30, 124.00, 121.96; FT-IR:  $\nu$  3313, 3150, 1659, 1596  $\text{cm}^{-1}$ .

#### 4.2.1.4 Synthesis of 2-amino-4-methyl-5-bromopyrimidine, **11**



N-bromosuccinimide (6.0 g, 33.7 mmol) in methylene chloride was added drop wise to 2-amino-4-methylpyrimidine (3.0 g, 27.5 mmol) dissolved in methylene chloride (100 mL), cooled in an ice bath. The ice bath was removed and the reaction mixture was stirred at room temperature for 1 hr. The reaction was monitored by TLC and upon completion, was quenched with 10% sodium bicarbonate and 10% sodium sulfite solution. The mixture was filtered and the precipitate washed with water twice and dried. The filtrate was extracted with methylene chloride and dried over anhydrous magnesium sulfate. The solvent was removed on a rotary evaporator to obtain the product as yellowish-white powder. (4.50 g, 88 %). M. P. 200 – 202  $^{\circ}\text{C}$ ;  $^1\text{H}$  NMR ( $\delta\text{H}$ ; 400 MHz, DMSO- $d_6$ ): 8.206 (s, 1H), 6.783 (br, 2H), 2.312 (s, 3H); IR ( $\text{cm}^{-1}$ ):  $\nu$  3314, 3146, 1655, 1548, 1473, 1209, 1041, 787.

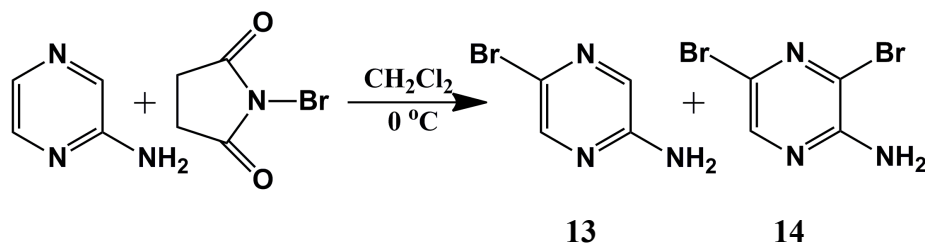
#### 4.2.1.5 Synthesis of 2-amino-4-methyl-5-(3-pyridyl)pyrimidine, **12**



2-Amino-4-methyl-5-bromopyrimidine **11** (1.00 g, 5.32 mmol), 3-pyridylboronic acid **8** (0.8 g, 6.5 mmol), and sodium carbonate (0.7 g, 6.6 mmol) were added to a round bottom flask. Acetonitrile (35 mL) and water (35 mL) were added and dinitrogen was bubbled through the mixture for 10 minutes. *Bis*(triphenylphosphine)palladium(II) dichloride (0.09 mg, 0.13 mmol, 2.4 mol%) was added and dinitrogen bubbled through

for 5 more minutes. The apparatus was fitted with a condenser and the mixture was refluxed at 80 °C under a dinitrogen atmosphere. The reaction was monitored by TLC and upon completion (36 hrs) was cooled to room temperature. The solution was diluted with ethyl acetate (100 mL), washed with (3 x 100 mL) and saturated aqueous sodium chloride solution (1 x 100 mL). The organic layer was separated and dried over anhydrous magnesium sulfate. The solvent was removed on a rotary evaporator and the residue was chromatographed on silica with hexane: ethyl acetate mixture as eluant. The product was obtained as an off-white powder. The product is then recrystallized from ethyl acetate to obtain colorless flake-like crystals, (0.60 g, 61 %). M. P. 202 – 204 °C; <sup>1</sup>H NMR (δH; 400 MHz, CDCl<sub>3</sub>): 8.63 (s, 1H), 8.58 (s, 1H), 8.14 (s, 2H), 7.62 (d, J = 8.0 Hz, 1H), 7.4 (s, 1H), 5.26 (br, 2H), 2.35 (s, 3H); FT-IR (cm<sup>-1</sup>): ν 3284, 3126, 1660, 1581.

#### 4.2.1.6 Synthesis of 2-amino-5-bromopyrazine, **13** and 2-amino-3,5-dibromopyrazine, **14**

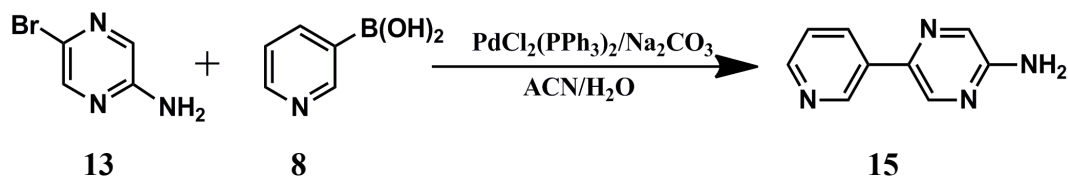


A solution of *N*-bromosuccinimide (1.2 g, 6.7 mmol) in methylene chloride was added dropwise to 2-aminopyrazine (0.5 g, 5.3 mmol) dissolved in methylene chloride cooled at 0 °C. The reaction mixture was stirred at 5-10 °C for 1 hr. The reaction was monitored by TLC and upon completion, was quenched with 10% sodium bicarbonate and 10% sodium sulfite solution. The mixture was filtered and the precipitate washed with water twice and dried. The filtrate was extracted with methylene chloride and dried over anhydrous magnesium sulfate. The solvent was removed on a rotary evaporator and the residue was chromatographed on silica with hexane: ethyl acetate 4:6 mixture as eluant. The product **13** was isolated as a yellowish-white powder and the product **14** as a white powder. The products were then recrystallized from ethyl acetate.

Product **13** (2-amino-5-bromopyrazine), (0.51 g, 56%). M. P. 105-107 °C; <sup>1</sup>H NMR (δH; 200 MHz, CDCl<sub>3</sub>): 8.09 (s, 1H), 7.78 (s, 1H), 4.64 (br, 2H).

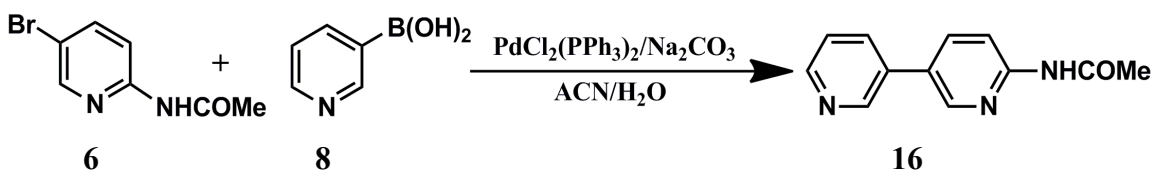
Product **14** (2-amino-3,5-dibromopyrazine), (0.12 g, 10%). M. P. 111-113 °C; <sup>1</sup>H NMR (δH; 200 MHz, CDCl<sub>3</sub>): 8.05 (s, 1H), 5.05 (br, 2H).

#### 4.2.1.7 Synthesis of 2-amino-5-(3-pyridyl)pyrazine, **15**



2-Amino-5-bromopyrazine **13** (1.00 g, 5.75 mmol), 3-pyridylboronic acid **8** (0.8 g, 6.5 mmol), and sodium carbonate (0.7 g, 6.6 mmol) were added to a round bottom flask. Acetonitrile (35 mL) and water (35 mL) were added and dinitrogen was bubbled through the mixture for 10 minutes. *Bis*(triphenylphosphine)palladium(II) dichloride (90 mg, 0.13 mmol, 2.3 mol%) was added and dinitrogen bubbled through for 5 more minutes. The apparatus was fitted with a condenser and the mixture was refluxed at 80 °C under dinitrogen atmosphere. The reaction was monitored by TLC and upon completion (36 hrs) was cooled to room temperature. The solution was then diluted with ethyl acetate (100 mL), washed with (3 x 100 mL) and saturated aqueous sodium chloride solution (1 x 100 mL). The organic layer was separated and dried over anhydrous magnesium sulfate. The solvent was removed on a rotary evaporator and the residue was chromatographed on silica with hexane: ethyl acetate (6:4) mixture as eluant. The product was obtained as white powder. The product was recrystallized from ethyl acetate to give colorless crystals, (0.74 g, 75 %). M. P. 210 – 212 °C; <sup>1</sup>H NMR (δH; 400 MHz, CDCl<sub>3</sub>): 9.12 (s, 1H), 8.61 (s, 1H), 8.49 (s, 1H), 8.18 (s, 1H), 8.10 (s, 1H), 7.38 (s, 1H), 4.75 (br, 2H); FT-IR (cm<sup>-1</sup>): *v* 3351, 3304, 3116, 1642, 1584.

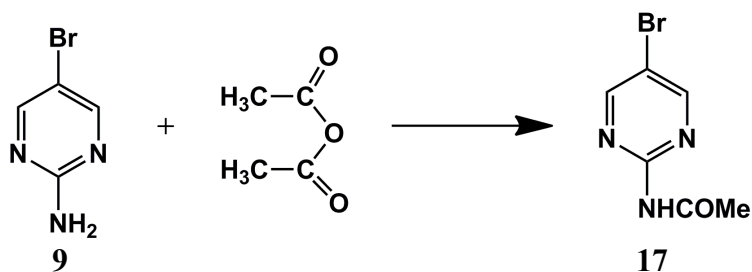
#### 4.2.1.8 Synthesis of 2-acetamido-5-(3-pyridyl)pyridine, **16**





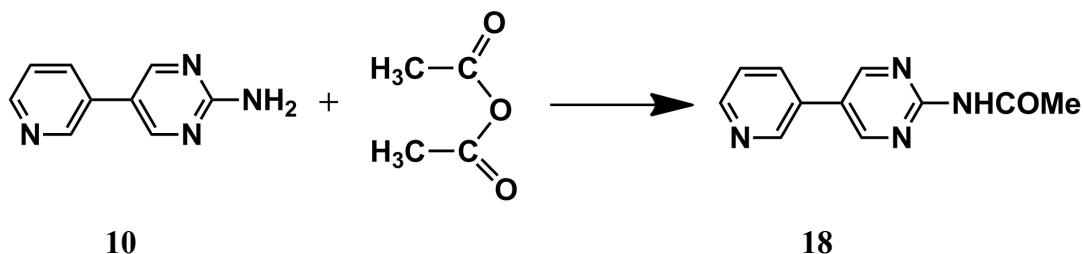
2-Acetamido-5-bromopyridine, **6** (1.2 g, 5.5 mmol), 3-pyridylboronic acid **8** (0.8 g, 6.5 mmol), and sodium carbonate (0.7 g, 6.6 mmol) were added to a round bottom flask. Acetonitrile (35 mL) and water (35 mL) were added and dinitrogen was bubbled through the mixture for 10 minutes. *Bis*(triphenylphosphine)palladium(II) dichloride (90 mg, 0.13 mmol, 2.4 mol%) was added and dinitrogen bubbled for 5 more minutes. The apparatus was fitted with a condenser and the mixture was refluxed at 80 °C under dinitrogen atmosphere. The reaction was monitored by TLC and upon completion (40 hrs) was cooled to room temperature. The solution was then diluted with ethyl acetate (100 mL), washed with (3 x 100 mL) and saturated aqueous sodium chloride solution (1 x 100 mL). The organic layer was separated and dried over anhydrous magnesium sulfate. The solvent was removed on a rotary evaporator and the residue was chromatographed on silica with hexane: ethyl acetate (6:4) mixture as eluant. The product was obtained as an off-white powder. The product was recrystallized from ethyl acetate to obtain colorless prism-shaped crystals, (0.45 g, 40 %). M.p. 179 – 181 °C; <sup>1</sup>H NMR (δH; 200 MHz, CDCl<sub>3</sub>): 8.85 (s, 1H), 8.64 (s, 1H), 8.51 (s, 1H), 8.31 (d, 1H), 8.07 (br, NH), 7.90 (t, 2H), 7.41 (t, 1H), 2.26 (s, 3H); FT-IR (cm<sup>-1</sup>): *v* 3176, 3002, 1688, 1568, 1523.

#### 4.2.1.9 Synthesis of 2-acetamido-5-bromopyrimidine, **17**



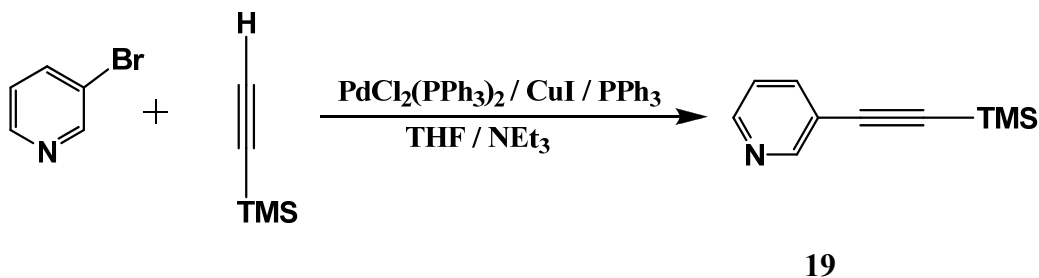
2-Amino-5-bromopyridine **9** (4 g, 23 mmol) was dissolved in acetic anhydride (20 mL) added dropwise. The mixture was heated under reflux at 80°C for 2 hrs. Excess acetic anhydride and acetic acid produced were removed via vacuum distillation to obtain a white powder. Upon recrystallization from acetone, the product **17** was obtained as an off-white powder, (4.5 g, 91%). Decomposed at 175 °C; <sup>1</sup>H NMR (δH; 400 MHz, CDCl<sub>3</sub>): 8.63 (s, 2H), 8.52 (br, NH), 2.48 (s, 3H). FT-IR *v* 3114 cm<sup>-1</sup> (N—H, br), 1695 cm<sup>-1</sup> (C=O, s), 1564 cm<sup>-1</sup> (Amide II, s).

#### 4.2.1.10 Synthesis of 2-acetamido-5-(3-pyridyl)pyrimidine, 18



2-Amino-5-(3-pyridyl)pyrimidine **10** (1.0 g, 5.8 mmol) was dissolved in acetic anhydride (5 mL) which was added dropwise. The mixture was heated under reflux at 80°C for 3 hrs with continuous monitoring by TLC. Excess acetic anhydride and acetic acid produced were removed via vacuum distillation to obtain a white powder. Upon recrystallization from ethyl acetate, the product **18** was obtained as colorless flake-like crystals, (0.8 g, 65%,). M. P. 240 – 242 °C; <sup>1</sup>H NMR (δH; 400 MHz, CDCl<sub>3</sub>): 9.02 (br, NH), 8.15 (br, 3H), 8.70 (d, 1H), 7.87 (d, 1H) 7.47 (s, 1H), 2.56 (s, 3H). <sup>13</sup>C NMR (400 MHz, CDCl<sub>3</sub>): 169.08, 157.35, 156.25, 149.23, 147.34, 133.91, 129.85, 125.31, 124.05, 24.78; FT-IR (cm<sup>-1</sup>) ν 3208, 3123, 2977, 2934, 1681.

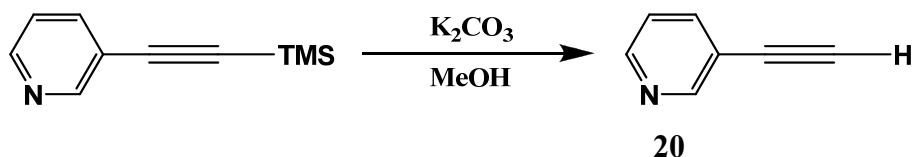
#### 4.2.1.11 Synthesis of 3-trimethylsilylanylethynylpyridine, 19



3-Bromopyridine (5.00 g, 31.65 mmol), trimethylsilylacetylene (3.97 g, 40.40 mmol), copper(I) iodide (0.17 g, 0.89 mmol), triphenylphosphine (0.60 g, 2.29 mmol), and *bis*(triphenylphosphine)palladium(II) dichloride (0.60 g, 0.86 mmol) were added to a round bottom flask. Tetrahydrofuran (65 mL) and triethylamine (65 mL) were added and dinitrogen bubbled through the resultant mixture for 10 minutes. The apparatus was fitted with a condenser and the mixture refluxed at 75 °C under dinitrogen atmosphere. The reaction was monitored by TLC and upon completion (48 hrs) was cooled to room temperature. The solution was then diluted with ethyl acetate (100 mL), washed with (3 x

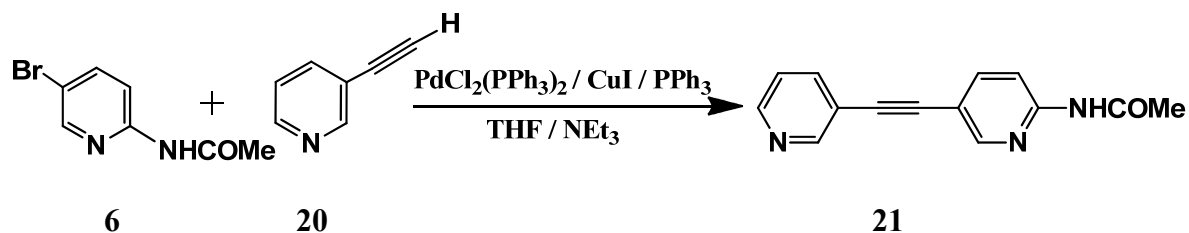
100 mL) and saturated aqueous sodium chloride solution (1 x 100 mL). The organic layer was separated and dried over anhydrous magnesium sulfate. The solvent was removed on a rotary evaporator and the residue was chromatographed on silica with hexane: ethyl acetate (6:4) mixture as eluant. The product was isolated as a light brown colored oil, (5.0 g, 91 %). <sup>1</sup>H NMR (δH; 400 MHz, CDCl<sub>3</sub>): 8.66 (s, 1H), 8.48 (d, J = 4.2Hz, 1H), 7.70 (d, J = 8.0 Hz, 1H), 7.19 (t, J = 6.8 Hz, 1H), 0.24 (s, 9H).

#### 4.2.1.12 Synthesis of 3-ethynylpyridine, 20



3-trimethylsilyl ethynylpyridine **19** (2.04 g, 11.66 mmol) and potassium carbonate (1.75 g, 17.85 mmol) were stirred in methanol (60 mL) at room temperature for 2 hours. The solution was then diluted with ethyl ether (100 mL) and washed with water (4 x 100 mL). The solvent was removed on a rotary evaporator and the residue/product **20** obtained as a light brown colored oil, (0.88 g, 74 %). <sup>1</sup>H NMR (δH; 200 MHz, CDCl<sub>3</sub>): 8.73 (s, 1H), 8.57 (d, J = 2.4Hz, 1H), 7.77 (d, J = 3.8Hz, 1H), 7.26 (t, J = 3.8Hz, 1H), 3.22 (s, 1H).

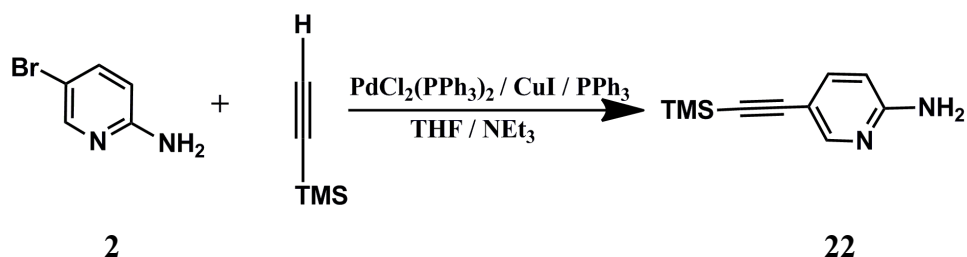
#### 4.2.1.13 Synthesis of 2-acetamido-5-(3-pyridyl)ethynylpyridine, 21



2-Acetamido-5-bromopyridine **6** (1.09 g, 5.06 mmol), 3-ethynylpyridine (0.50 g, 4.85 mmol) **20**, copper(I) iodide (0.025 g, 0.131 mmol), triphenylphosphine (0.11 g, 0.42 mmol), and *bis*(triphenylphosphine)palladium(II) dichloride (0.11 g, 0.16 mmol) were added to a round bottom flask. Tetrahydrofuran (15 mL) and triethylamine (15 mL) were added and dinitrogen bubbled through the resultant mixture for 10 minutes. The apparatus was fitted with a condenser and the mixture refluxed at 70 °C under a

dinitrogen atmosphere. The reaction was monitored by TLC and upon completion (36 hrs) was cooled to room temperature. The solution was diluted with ethyl acetate (100 mL), washed with (3 x 100 mL) and saturated aqueous sodium chloride solution (1 x 100 mL). The organic layer was separated and dried over anhydrous magnesium sulfate. The solvent was removed on a rotary evaporator and the residue was chromatographed on silica with hexane: ethyl acetate (1:1) mixture as eluant. The product **21** was isolated as a light brown colored solid, and recrystallized from ethyl acetate. (0.67 g, 65 %). M. P. 195 – 197 °C; <sup>1</sup>H NMR (δH; 400 MHz, DMSO-d<sub>6</sub>): 10.765 (s, NH), 8.760 (s, 1H), 8.602 (s, 1H), 8.543 (s, 1H), 8.140 (s, 1H), 7.989 (s, 1H), 7.968 (s, 1H), 7.480 (s, 1H), 2.117 (s, 3H); FT-IR (cm<sup>-1</sup>): *v* 3259, 3007, 2218, 1701, 1671, 1513, 1297.

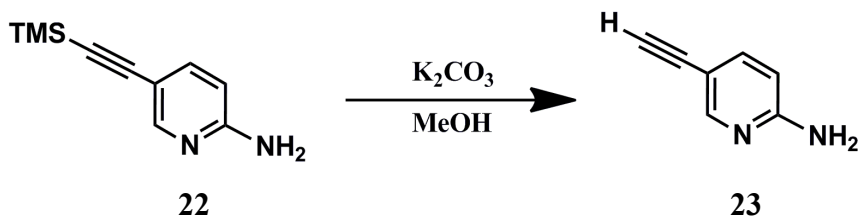
#### 4.2.1.14 Synthesis of 2-amino-5-trimethylsilanylethynylpyridine, **22**



2-Amino-5-bromopyridine **2** (5.0 g, 28.9 mmol), trimethylsilylacetylene (3.97 g, 40.4 mmol), copper(I) iodide (0.17 g, 0.89 mmol), triphenylphosphine (0.60 g, 2.29 mmol), and *bis*(triphenylphosphine)palladium(II) dichloride (0.60 g, 0.86 mmol, 3 mol%) were added to a round bottom flask. Tetrahydrofuran (100 mL) and triethylamine (100 mL) were added and dinitrogen bubbled through the resultant mixture for 10 minutes. The apparatus was fitted with a condenser and the mixture refluxed at 75 °C under a dinitrogen atmosphere. The reaction was monitored by TLC and upon completion (48 hrs) was cooled to room temperature. The solution was then diluted with ethyl acetate (100 mL), washed with (3 x 100 mL) and saturated aqueous sodium chloride solution (1 x 100 mL). The organic layer was separated and dried over anhydrous magnesium sulfate. The solvent was removed on a rotary evaporator and the residue was chromatographed on silica with hexane: ethyl acetate (1:1) mixture as eluant to obtain a light brown colored powder. Upon recrystallization from methylene chloride, colorless crystals were

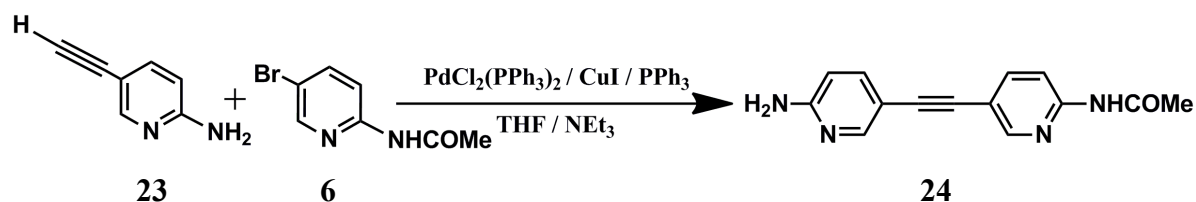
obtained, (3.9 g, 71 %).  $^1\text{H NMR}$  ( $\delta\text{H}$ ; 200 MHz,  $\text{CDCl}_3$ ): 8.21(s, 1H), 7.49 (d,  $J = 8.0$  Hz, 1H), 6.42 (d,  $J = 8.0$  Hz, 1H), 4.61 (br, 2H), 0.24 (s, 9H).

#### 4.2.1.15 Synthesis of 2-amino-5-ethynylpyridine, **23**



2-Amino-5-trimethylsilyl ethynylpyridine **22** (1.3 g, 6.8 mmol) and potassium carbonate (1.00 g, 7.23 mmol) were stirred in methanol (25 mL) at room temperature for 2 hours. The solution was then diluted with ethyl ether (50 mL) and washed with water (4 x 50 mL). The solvent was removed on a rotary evaporator and the residue/product **23** was obtained as a light brown colored powder, (0.62 g, 79%).  $^1\text{H NMR}$  ( $\delta\text{H}$ ; 200 MHz,  $\text{CDCl}_3$ ): 8.24 (s, 1H), 7.52 (d,  $J = 8.0$  Hz, 1H), 6.44 (d,  $J = 8.0$  Hz, 1H), 4.62 (br, 2H), 3.07 (s, 1H).

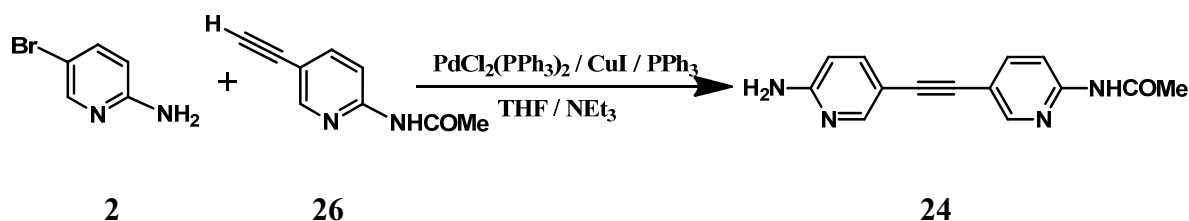
#### 4.2.1.16 Synthesis of 2-acetamido-5-(3-(2-aminopyridyl)ethynyl)pyridine, **24**



2-Acetamido-5-bromopyridine **6** (0.55 g, 2.56 mmol), 2-amino-5-ethynylpyridine **23** (0.35 g, 2.97 mmol), copper(I) iodide (0.013 g, 0.066 mmol), triphenylphosphine (0.055 g, 0.210 mmol), and *bis*(triphenylphosphine)palladium(II) dichloride (0.055 g, 0.080 mmol) were added to a round bottom flask. Tetrahydrofuran (10 mL) and triethylamine (10 mL) were added and dinitrogen bubbled through the resultant mixture for 10 minutes. The apparatus was fitted with a condenser and the mixture refluxed at 70 °C under a dinitrogen atmosphere. The reaction was monitored by TLC and upon completion (36 hrs) was cooled to room temperature. The solution was then diluted with ethyl acetate (20 mL), washed with (3 x 20 mL) and saturated aqueous sodium chloride

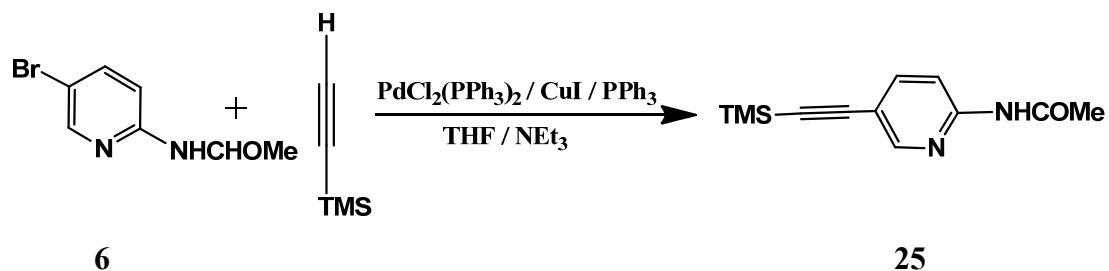
solution (1 x 20 mL). The organic layer was separated and dried over anhydrous magnesium sulfate. The solvent was removed on a rotary evaporator and the residue was chromatographed on silica with hexane: ethyl acetate (1:1) mixture as eluant. The product **24** was isolated as a light brown colored solid and recrystallized from ethyl acetate, (0.35 g, 55 %). M.P. 236 – 238 °C; <sup>1</sup>H NMR (δH; 200 MHz, DMSO): 10.66 (br, 1H), 8.43 (s, 1H), 8.13 (s, 2H), 7.85 (d, 1H), 7.48 (d, 2H), 6.45 (br, 2H), 2.10 (s, 3H); FT-IR (cm<sup>-1</sup>): ν 3463, 3283, 3116, 1696, 1628, 1606.

*Alternate method*



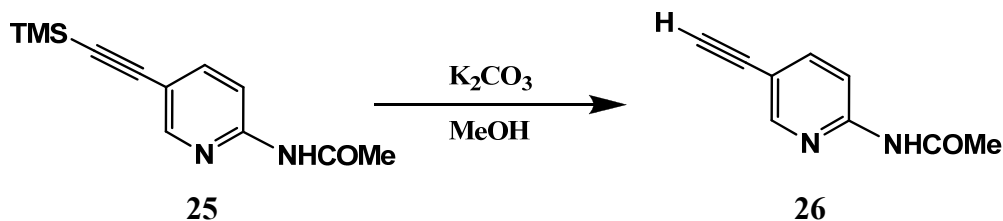
2-Amino-5-bromopyridine **2** (0.35 g, 2.02 mmol), 2-acetamido-5-ethynylpyridine **26** (0.25 g, 1.56 mmol), copper(I) iodide (0.009 g, 0.047 mmol), triphenylphosphine (0.04 g, 0.15 mmol), and *bis*(triphenylphosphine)palladium(II) dichloride (0.04 g, 0.06 mmol) were added to a round bottom flask. Tetrahydrofuran (10 mL) and triethylamine (10 mL) were added and dinitrogen bubbled through the resultant mixture for 10 minutes. The apparatus was fitted with a condenser and the mixture refluxed at 70 °C under a dinitrogen atmosphere. The reaction was monitored by TLC and upon completion (36 hrs) was cooled to room temperature. The solution was then diluted with ethyl acetate (50 mL), washed with (3 x 50 mL) and saturated aqueous sodium chloride solution (1 x 50 mL). The organic layer was separated and dried over anhydrous magnesium sulfate. The solvent was removed on a rotary evaporator and the residue was chromatographed on silica with hexane: ethyl acetate (1:1) mixture as eluant. The product **24** was isolated as a light brown colored solid and recrystallized from ethyl acetate. (0.24 g, 60 %). <sup>1</sup>H NMR (δH; 200 MHz, DMSO): 10.66 (br, 1H), 8.43 (s, 1H), 8.13 (s, 2H), 7.85 (d, 1H), 7.48 (d, 2H), 6.45 (br, 2H), 2.10 (s, 3H).

#### 4.2.1.17 Synthesis of 2-acetamido-5-trimethylsilanylethynylpyridine, 25



2-Acetamido-5-bromopyridine **6** (4.14 g, 19.26 mmol), trimethylsilylacetylene (2.65 g, 26.93 mmol), copper(I) iodide (0.12 g, 0.63 mmol), triphenylphosphine (0.40 g, 1.53 mmol), and *bis*(triphenylphosphine)palladium(II) dichloride (0.40 g, 0.57 mmol, 3 mol%) were added to a round bottom flask. Tetrahydrofuran (50 mL) and triethylamine (50 mL) were added and dinitrogen bubbled through the resultant mixture for 10 minutes. The apparatus was fitted with a condenser and the mixture refluxed at 75 °C under dinitrogen atmosphere. The reaction was monitored by TLC and upon completion (48 hrs) was cooled to room temperature. The solution was then diluted with ethyl acetate (100 mL), washed with (3 x 100 mL) and saturated aqueous sodium chloride solution (1 x 100 mL). The organic layer was separated and dried over anhydrous magnesium sulfate. The solvent was removed on a rotary evaporator and the residue was chromatographed on silica with hexane: ethyl acetate (6:4) mixture as eluant to obtain a light brown colored powder. Upon recrystallization from methylene chloride : hexane (1:2), colorless flaky crystals were obtained, (3.35 g, 75 %). <sup>1</sup>H NMR (δH; 200 MHz, CDCl<sub>3</sub>): 8.36 (br, NH), 8.12 (s, 2H), 7.75 (d, J = 10.0 Hz, 1H), 2.22 (s, 3H), 0.26 (s, 9H).

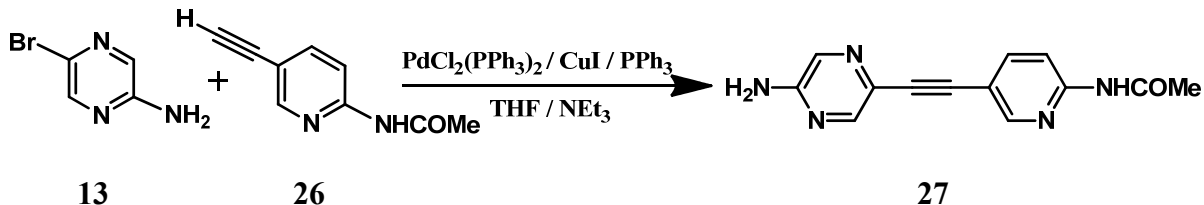
#### 4.2.1.18 Synthesis of 2-acetamido-5-ethynylpyridine, 26



2-Acetamido-5-trimethylsilanylethynylpyridine **25** (1.69 g, 7.28 mmol) and potassium carbonate (1.05 g, 7.60 mmol) were stirred in methanol (30 mL) at room temperature for 2 hours. The solution was then diluted with ethyl ether (100 mL) and

washed with water (4 x 100 mL). The solvent was removed on a rotary evaporator and the product **26** was obtained as a light brown colored powder, (0.85 g, 73%). <sup>1</sup>H NMR ( $\delta$ H; 200 MHz, CDCl<sub>3</sub>): 8.39 (s, 1H), 8.19 (d, J = 8.0 Hz, 1H), 8.02 (br, NH), 7.79 (dd, J = 12.0 Hz, 1H), 3.17 (s, 1H), 2.23 (s, 3H).

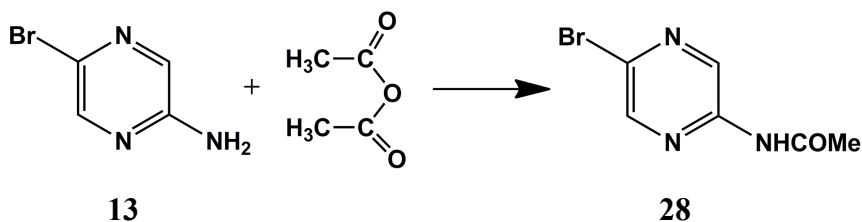
#### 4.2.1.19 Synthesis of 2-amino-5-(3-(2-acetamidopyridyl)ethynylpyrazine, **27**



A mixture of 2-amino-5-bromopyrazine **13** (0.52 g, 3.00 mmol), 2-acetamido-5-ethynylpyridine **26** (0.50 g, 3.13 mmol), copper(I) iodide (0.018 g, 0.094 mmol), triphenylphosphine (0.08 g, 0.30 mmol), and *bis*(triphenylphosphine)palladium(II) dichloride (0.08 g, 0.12 mmol) were added to a round bottom flask. Tetrahydrofuran (20 mL) and triethylamine (20 mL) were added and dinitrogen bubbled through the resultant mixture for 10 minutes. The apparatus was fitted with a condenser and the mixture refluxed at 70 °C under a dinitrogen atmosphere. The reaction was monitored by TLC and upon completion (48 hrs) was cooled to room temperature. The solution was then diluted with ethyl acetate (50 mL), washed with (3 x 50 mL) and saturated aqueous sodium chloride solution (1 x 50 mL). The organic layer was separated and dried over anhydrous magnesium sulfate. The solvent was removed on a rotary evaporator and the residue was chromatographed on silica with hexane: ethyl acetate (2:8) mixture as eluant. The product was washed with methanol and filtered to obtain a white solid, which was recrystallized from ethyl acetate. (0.64 g, 84 %). Decomposes at 200 °C. <sup>1</sup>H NMR ( $\delta$ H; 200 MHz, DMSO): 10.69 (br, NH), 8.45 (s, 1H), 8.15 (s, 1H), 8.10 (s, 1H), 7.94 (s, 1H), 7.89 (s, 1H), 6.94 (br, 2H), 2.12 (s, 3H); ( $\delta$ C; 400 MHz, DMSO-*d*<sub>6</sub>): 169.78, 154.91, 151.66, 146.00, 140.76, 124.94, 114.33, 113.09, 112.47, 89.74, 85.88. FT-IR (cm<sup>-1</sup>):  $\nu$  3390, 3294, 3125, 1688, 1666.

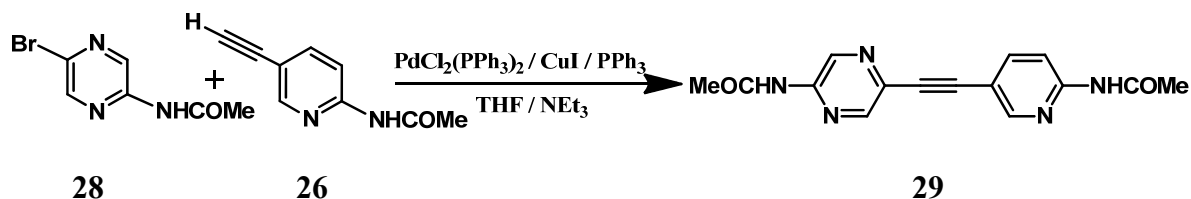


#### 4.2.1.20 Synthesis of 2-acetamido-5-bromopyrazine, 28



2-Amino-5-bromopyrazine **13** (2.0 g, 11.5 mmol) was dissolved in acetic anhydride (10 mL) which was added dropwise. The mixture was heated under reflux at 80°C for 2 hrs. Excess acetic anhydride and acetic acid produced were removed via vacuum distillation to obtain a white powder. Upon recrystallization from ethyl acetate, the product **28** was obtained as a white powder, (2.0 g, 81%). M.P. 198 – 201 °C; <sup>1</sup>H NMR (δH; 200 MHz, CDCl<sub>3</sub>): 9.33 (s, 1H), 8.34 (s, 1H), 7.83 (br, NH), 2.27(s, 3H). FT-IR ν 3273 cm<sup>-1</sup> (N—H, br), 1671 cm<sup>-1</sup> (C=O, s), 1528 cm<sup>-1</sup> (Amide II, s).

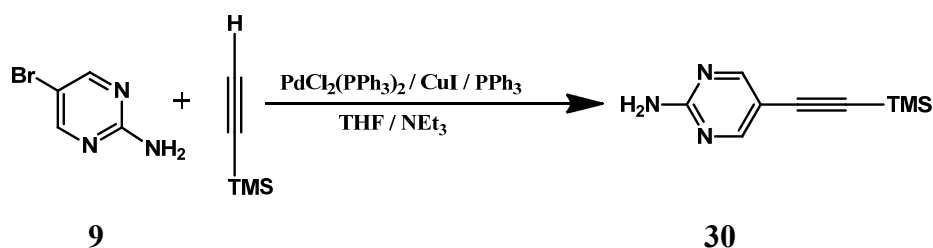
#### 4.2.1.21 Synthesis of 2-acetamido-5-(3-(2-acetamidopyridyl)ethynyl)pyrazine, 29



A mixture of 2-acetamido-5-bromopyrazine **28** (0.33 g, 1.52 mmol), 2-acetamido-5-ethynylpyridine **26** (0.26 g, 1.63 mmol), copper(I) iodide (0.009 g, 0.047 mmol), triphenylphosphine (0.04 g, 0.15 mmol), and *bis*(triphenylphosphine)palladium(II) dichloride (0.04 g, 0.06 mmol) were added to a round bottom flask. Tetrahydrofuran (10 mL) and triethylamine (10 mL) were added and dinitrogen bubbled through the resultant mixture for 10 minutes. The apparatus was fitted with a condenser and the mixture refluxed at 70 °C under a dinitrogen atmosphere. The reaction was monitored by TLC and upon completion (48 hrs) was cooled to room temperature. The solution was diluted with ethyl acetate (25 mL), washed with (3 x 25 mL) and saturated aqueous sodium chloride solution (1 x 25 mL). The organic layer was separated and dried over anhydrous magnesium sulfate. The solvent was removed on a rotary evaporator and the residue was chromatographed on silica with hexane: ethyl acetate (2:8) mixture as eluant. The

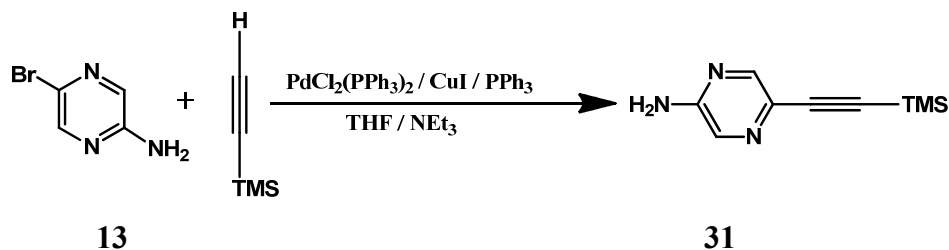
product was washed with methanol and filtered to obtain a white solid, which was recrystallized from ethyl acetate. (0.23 g, 53 %). M.P. 182 – 184 °C;  $^1\text{H}$  NMR ( $\delta\text{H}$ ; 400 MHz, DMSO- $d_6$ ): 10.97 (br, NH), 10.66 (br, NH), 9.12 (s, 1H), 8.59 (s, 1H), 8.41 (s, 1H), 8.04 (s, 1H), 7.98 (s, 1H), 2.13 (s, 3H), 2.08 (s, 3H); ( $\delta\text{C}$ ; 400 MHz, DMSO- $d_6$ ): 169.45, 155.30, 150.87, 147.91, 140.40, 131.92, 114.76, 112.98, 104.19. FT-IR ( $\text{cm}^{-1}$ ):  $\nu$  3230, 3068, 1660, 1571.

#### 4.2.1.23 Synthesis of 2-amino-5-trimethylsilanylethynylpyrimidine, 30



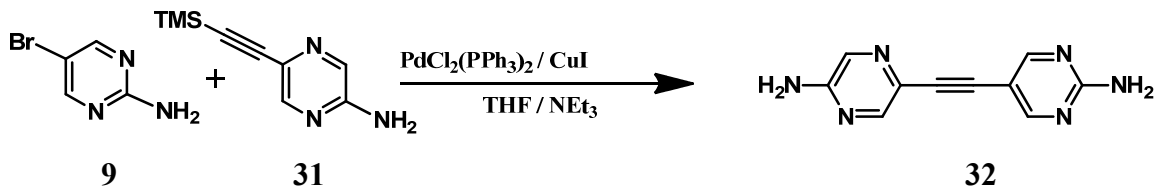
A mixture of 2-amino-5-bromopyrimidine **9** (2.5 g, 14.5 mmol), trimethylsilylacetylene (2.0 g, 20.3 mmol), copper(I) iodide (0.085 g, 0.45 mmol), triphenylphosphine (0.30 g, 1.15 mmol), and *bis*(triphenylphosphine)palladium(II) dichloride (0.30 g, 0.43 mmol, 3 mol%) were added to a round bottom flask. Tetrahydrofuran (50 mL) and triethylamine (50 mL) were added and dinitrogen bubbled through the resultant mixture for 10 minutes. The apparatus was fitted with a condenser and the mixture refluxed at 75 °C under dinitrogen atmosphere. The reaction was monitored by TLC and upon completion (48 hrs) was cooled to room temperature. The solution was then diluted with ethyl acetate (50 mL), washed with (3 x 50 mL) and saturated aqueous sodium chloride solution (1 x 50 mL). The organic layer was separated and dried over anhydrous magnesium sulfate. The solvent was removed on a rotary evaporator and the residue was chromatographed on silica with hexane: ethyl acetate mixture as eluant to obtain a light brown colored powder. Upon recrystallization from methylene chloride, colorless crystals were obtained, (2.2 g, 80 %).  $^1\text{H}$  NMR ( $\delta\text{H}$ ; 400 MHz,  $\text{CDCl}_3$ ): 8.40 (s, 2H), 5.21 (br, 2H), 0.26 (s, 9H).

#### 4.2.1.24 Synthesis of 2-amino-5-trimethylsilanylethynylpyrazine, **31**



A mixture of 2-amino-5-bromopyrazine **13** (2.5 g, 14.5 mmol), trimethylsilylacetylene (2.0 g, 20.3 mmol), copper(I) iodide (0.085 g, 0.45 mmol), triphenylphosphine (0.30 g, 1.15 mmol), and *bis*(triphenylphosphine)palladium(II) dichloride (0.30 g, 0.43 mmol, 3 mol%) were added to a round bottom flask. Tetrahydrofuran (50 mL) and triethylamine (50 mL) were added and dinitrogen bubbled through the resultant mixture for 10 minutes. The apparatus was fitted with a condenser and the mixture refluxed at 75 °C under dinitrogen atmosphere. The reaction was monitored by TLC and upon completion (48 hrs) was cooled to room temperature. The solution was then diluted with ethyl acetate (50 mL), washed with water (3 x 50 mL) and saturated aqueous sodium chloride solution (1 x 50 mL). The organic layer was separated and dried over anhydrous magnesium sulfate. The solvent was removed on a rotary evaporator and the residue was chromatographed on silica with hexane: ethyl acetate mixture as eluant to obtain a dark brown colored powder, (2.4 g, 87 %).  $^1\text{H}$  NMR ( $\delta\text{H}$ ; 200 MHz,  $\text{CDCl}_3$ ): 8.16 (s, 1H), 7.94 (s, 1H), 4.80 (br, 2H), 0.26 (s, 9H).

#### 4.2.1.25 Synthesis of 2-amino-5-(3-(2-aminopyrazino))ethynylpyrimidine, **32**<sup>12</sup>



A mixture of 2-amino-5-trimethylsilanylethynylpyrazine, **31** (1.30 g, 6.95 mmol), 2-amino-5-bromopyrimidine, **9** (1.21 g, 6.95 mmol), copper (I) iodide (0.131 g, 0.689 mmol), triethylamine (1.39 g, 14.47 mmol), and ethylene glycol dimethyl ether (145 mL) was placed in a round bottom flask. *Tetrakis*(triphenylphosphine)palladium (0) (0.413 g, 0.358 mmol) was added and dinitrogen bubbled through for 10 mins. The solution was



chromatographed on silica with hexane: ethyl acetate: methanol mixture as eluant to obtain light brown colored powder. It was washed with hot water (3 x 100 mL) and then dried, (1.5 g, 95 %). M. P. >280 °C. <sup>1</sup>H NMR (δH; 200 MHz, DMSO-d<sub>6</sub>): 8.40 (s, 2H), 8.08 (s, 1H), 7.85 (s, 1H), 7.16 (br, 2H), 6.89 (br, 2H); <sup>13</sup>C NMR (δC; 400 MHz, DMSO-d<sub>6</sub>): 161.89, 160.14, 154.50, 145.34, 132.48, 125.18, 105.75, 89.94, 84.08, 57.52, 23.09, 19.23.

#### ***4.2.2 Synthesis of co-crystals and salts***

Each of the ten ligands under study was allowed to react with the same set of 19 co-crystallizing agents comprising of ten monocarboxylic acids, five dicarboxylic acids and four cyanoximes. The solubility of the ligands range from highly soluble to very poorly soluble in a variety of solvents including ethyl acetate, nitrobenzene, methylene chloride, chloroform, acetonitrile, ethanol, and methanol. The low solubility of some of the ligands prompted the change of co-crystallization technique from slow evaporation at room temperature to methanol-assisted solvent-drop grinding (**18**, **27**, **29**, and **32**).

##### ***4.2.2.1 Synthesis of 2-amino-5-(3-pyridyl)pyrimidine/4-chlorobenzoic acid (1:1), 10c***

2-amino-5-(3-pyridyl)pyrimidine (0.010 g, 0.058 mmol) was dissolved in 5mL of ethyl acetate. To this solution was added 4-chlorobenzoic acid (0.009 g, 0.058 mmol) in 5 mL of ethyl acetate. The resulting solution was warmed and allowed to stand for slow evaporation at room temperature. Colorless, plate-like crystals were obtained after 3 days. M. P. 160–162°C; FT-IR (cm<sup>-1</sup>) ν 3298, 2375, 1830, 1691.

##### ***4.2.2.2 Synthesis of 2-amino-5-(3-pyridinium)pyrimidine pentafluorobenzoate, 10j***

2-amino-5-(3-pyridyl)pyrimidine (0.010 g, 0.058 mmol) was dissolved in 5mL of ethyl acetate. To this solution was added pentafluorobenzoic acid (0.012 g, 0.058 mmol) in 5 mL of ethyl acetate. The resulting solution was warmed and allowed to stand for slow evaporation at room temperature. Colorless, plate-like crystals were obtained after 3 days. M. P. 156–158°C; FT-IR (cm<sup>-1</sup>) ν 3092, 2446, 1930, 1695.

#### **4.2.2.3 Synthesis of 2-amino-5-(3-pyridyl)pyrimidine/suberic acid (2:1), 10k**

2-amino-5-(3-pyridyl)pyrimidine (0.010 g, 0.058 mmol) was dissolved in 5mL of ethyl acetate. To this solution was added suberic acid (0.005 g, 0.029 mmol) in 5 mL of ethyl acetate. The resulting solution was warmed and allowed to stand for slow evaporation at room temperature. Colorless crystals were obtained after 3 days. M. P. 150°C; FT-IR ( $\text{cm}^{-1}$ )  $\nu$  3301, 3150, 2410, 1912, 1687.

#### **4.2.2.4 Synthesis of 2-amino-5-(3-pyridyl)pyrimidine/succinic acid (2:1), 10n**

2-amino-5-(3-pyridyl)pyrimidine (0.010 g, 0.058 mmol) was dissolved in 5mL of ethyl acetate. To this solution was added succinic acid (0.004 g, 0.029 mmol) in 5 mL of ethyl acetate. The resulting solution was warmed and allowed to stand for slow evaporation at room temperature. Colorless rod-like crystals were obtained after 3 days. M. P. 188–189°C; FT-IR ( $\text{cm}^{-1}$ )  $\nu$  3325, 3163, 2387, 1871, 1697.

#### **4.2.2.5 Synthesis of 2-amino-5-(3-pyridyl)pyrimidine/sebacic acid (2:1), 10o**

2-amino-5-(3-pyridyl)pyrimidine (0.010 g, 0.058 mmol) was dissolved in 5mL of ethyl acetate. To this solution was added sebacic acid (0.006 g, 0.029 mmol) in 5 mL of ethyl acetate. The resulting solution was warmed and allowed to stand for slow evaporation at room temperature. Colorless, rod-like crystals were obtained after 3 days. M. P. 143–145°C; FT-IR ( $\text{cm}^{-1}$ )  $\nu$  3325, 3137, 2475, 1947, 1688.

#### **4.2.2.6 Synthesis of 2-amino-5-(3-pyridyl)pyrimidine/2-chlorocyanoxime (1:1), 10r**

2-amino-5-(3-pyridyl)pyrimidine (0.010 g, 0.058 mmol) was dissolved in 5mL of ethyl acetate. To this solution was added 2-chlorocyanoxime (0.010 g, 0.058 mmol) in 5 mL of ethyl acetate. The resulting solution was warmed and allowed to stand for slow evaporation at room temperature. Light yellow colored, block-like crystals were obtained after 3 days. M. P. 175–177°C; FT-IR ( $\nu$ ,  $\text{cm}^{-1}$ ) 3299, 3147, 2462, 1861, 1661.

#### **4.2.2.7 Synthesis of 2-amino-4-methyl-5-(3-pyridyl)pyrimidine/succinic acid (2:1), 12n**

2-amino-4-methyl-5-(3-pyridyl)pyrimidine (0.004 g, 0.021 mmol) was dissolved in 5mL of ethyl acetate/acetonitrile/ethanol (1:1:1). To this solution was added succinic acid (0.002 g, 0.011 mmol) in 5 mL of ethyl acetate. The resulting solution was warmed and allowed to stand for slow evaporation at room temperature. Yellowish plate-like

crystals were obtained after 3 days. M. P. 160–162°C; FT-IR ( $\nu$ ,  $\text{cm}^{-1}$ ) 3291, 3122, 2472, 1877, 1703.

#### **4.2.2.8 Synthesis of 2-amino-5-(3-pyridyl)pyrazine/4-nitrobenzoic acid (1:1), 15e**

2-amino-5-(3-pyridyl)pyrazine (0.010 g, 0.058 mmol) was dissolved in 5 mL of ethyl acetate/methanol (1:1). To this solution was added 4-nitrobenzoic acid (0.010 g, 0.058 mmol) in 5 mL of ethyl acetate. The resulting solution was warmed and allowed to stand for slow evaporation at room temperature. Yellowish needle-shaped crystals were obtained after 3 days. M. P. 208–210°C; FT-IR ( $\nu$ ,  $\text{cm}^{-1}$ ) 3445, 3343, 2435, 1928, 1689.

#### **4.2.2.9 Synthesis of 2-acetamido-5-(3-pyridyl)pyridine/cyanoxime (1:1), 16p**

2-acetamido-5-(3-pyridyl)pyridine (0.030 g, 0.141 mmol) was dissolved in 5 mL of ethyl acetate. To this solution was added cyanoxime (0.021 g, 0.141 mmol) in 5 mL of ethyl acetate. The resulting solution was warmed and allowed to stand for slow evaporation at room temperature. Colorless crystals were obtained after 3 days. M. P. 140–142°C; IR (KBr pellet)  $\nu$   $\text{cm}^{-1}$  3263, 2452, 1896, 1696.

#### **4.2.2.10 Synthesis of 2-amino-5-(3-(2-acetamido)pyridyl)ethynylpyridinium 3,5-dimethyl benzoate/ 3,5-dimethylbenzoic acid (1:1), 24h**

2-amino-5-(3-(2-acetamido)pyridyl)ethynylpyridine (0.030 g, 0.119 mmol) was dissolved in 5 mL of ethyl acetate. To this solution was added 3,5-dimethylbenzoic acid, (0.018 g, 0.119 mmol) in 5 mL of ethyl acetate. The resulting solution was warmed and allowed to stand for slow evaporation at room temperature. Colorless crystals were obtained after 3 days. M. P. 177–180°C; IR (KBr pellet)  $\nu$   $\text{cm}^{-1}$  3340, 3034, 2504, 1885, 1678.

#### **4.2.2.11 Synthesis of 2-amino-5-(3-(2-acetamido)pyridyl)ethynylpyridinium phthalate, 24l**

2-amino-5-(3-(2-acetamido)pyridyl)ethynylpyridine (0.030 g, 0.119 mmol) was dissolved in 5 mL of ethyl acetate. To this solution was added phthalic acid (0.010 g, 0.059 mmol) in 5 mL of ethyl acetate. The resulting solution was warmed and allowed to stand for slow evaporation at room temperature. Colorless crystals were obtained after 3 days. M. P. 175–176°C; IR (KBr pellet)  $\nu$   $\text{cm}^{-1}$  3199, 3010, 2474, 2003, 1690.

#### 4.2.2.12 *Synthesis of 2-amino-5-(3-(2-acetamido)pyridyl)ethynylpyrazine/3,5-dinitrobenzoic acid (1:1), 27i*

2-amino-5-(3-(2-acetamido)pyridyl)ethynylpyrazine (0.010 g, 0.040 mmol) was dissolved in 5 mL of ethyl acetate/ethanol/DMSO (1:1:0.5). To this solution was added 3,5-dinitrobenzoic acid (0.008 g, 0.040 mmol) in 5 mL of ethyl acetate. The resulting solution was warmed and allowed to stand for slow evaporation at room temperature. Yellowish needle-shaped crystals were obtained after 3 days. Decomposed at 180 °C; IR (KBr pellet)  $\nu$  cm<sup>-1</sup> 3375, 3094, 2435, 1871, 1687.

#### 4.2.3 *Electrostatic charges calculations*

The magnitude of the electrostatic potential on the hydrogen-bond donors and acceptors in these molecules were obtained using semi-empirical AM1 calculations.<sup>13</sup> Values for individual atoms are obtained by probing the MEPS (0.002 e/au isosurface, from AM1 calculations) with a point charge. Depending upon the values obtained for the nitrogen atoms in the pyridine/pyrimidine/pyrazine molecules, the best hydrogen acceptor and second best hydrogen acceptor was assigned to be the one with the highest charge and second highest charge respectively. For example, the 2-amino-5-(3-pyridyl)pyrimidine **10** has one pyridyl-N and two pyrimidyl-N atoms. The two highest charges on the nitrogen atoms were identified using the software and duly assigned best hydrogen bond acceptor and second best acceptor. Hence the pyridyl-N with the highest charge (-277 kJ/mol) was assigned the best hydrogen bond acceptor and pyrimidyl-N with the second higher charge (-260 kJ/mol) was assigned second best acceptor.

#### 4.2.4 *Single Crystal X-ray Crystallography*

X-ray data were collected on a Bruker SMART APEX or a SMART 1000 diffractometer using Mo K $\alpha$  radiation and, where noted, were corrected for absorption using the multiscan procedure implemented by SADABS. Data were collected using SMART. The relevant X-ray data are summarized in Table 4.4 and labeling schemes and thermal ellipsoids for all structures are shown in Figures 4.6, 4.14, and 4.21.



## 4.3 Results and Discussion

### 4.3.1 Characterization by FT-IR

The solids obtained from the co-crystallization of each of the ten ligands with 19 co-crystallizing agents (ten monocarboxylic acids, five dicarboxylic acids and four cyanoximes), a total of 190 (10 x 19), were screened using IR spectroscopy. The outcome of this analysis is displayed in Table 4.1. The IR stretching frequencies of interest of all the salts and co-crystals under study is listed in Table 4.1 and 4.2.

The distinction between the salt, neutral co-crystal, and no reaction was done by identifying the characteristics band stretches and shifting of carbonyl stretches in free and bonded acids via IR spectroscopy. The presence/absence of broad absorption bands in the regions near 1950 and 2450  $\text{cm}^{-1}$  indicates intermolecular O—H---N(heterocycle) hydrogen bonds. The appearance of a sharp stretch around 1700  $\text{cm}^{-1}$  and a weak stretch near 1275  $\text{cm}^{-1}$  indicates intact C=O in co-crystals, whereas a strong stretch around 1650-1550  $\text{cm}^{-1}$  and a weaker symmetrical stretch around 1400  $\text{cm}^{-1}$  indicates  $\text{COO}^-$  in salts.<sup>14</sup>

**Table 4.1** Results in attempted co-crystallization reactions in pyridine series

Ligands	10	12	15	16	18	21	24	27	29	32
Salt & co-crystal	19/19	16/19	15/19	19/19	6/19	14/19	17/19	9/19	5/19	6/19
Yield %	100	84	79	100	32	74	89	47	26	32

The results indicate high supramolecular yields in terms of formation of salts and co-crystals for the ligands **10**, **12**, **15**, **16**, **21** and **24**; whereas for the remaining ligands the yield is poor. This may have been due to the poor solubility of the ligands themselves. The co-crystallization for the ligands **18**, **27**, **29** and **32** were carried out via solvent-drop grinding due to their minimal solubility in traditional solvents, hence could not be carried out via evaporation at room temperature. In addition, the carboxylic acid/carboxylate stretching which is the basis of differentiation between salts and co-crystals is very elusive here. The salts **10j**, **24h**, and **24l** display carbonyl stretching at 1695, 1678, 1690  $\text{cm}^{-1}$  instead of the expected carboxylate stretching at 1650-1550  $\text{cm}^{-1}$ . Hence, within this system of coupled ditopic heterocyclic ligands, the IR data is inconclusive in distinguishing between the salts and the co-crystals formed.

**Table 4.2 IR stretching frequencies (cm<sup>-1</sup>) of salts and co-crystals of the ligands 10, 12, 15, 16, and 18.**

		<b>10</b>	<b>12</b>	<b>15</b>	<b>16</b>	<b>18</b>
<b>a</b>	4-cyanobenzoic acid	3449, 3311, 2370, 1888, 1701	3304, 3152, 2491, 1905, 1701	3420, 3201, 2374, 1882, 1699	3449, 3254, 2408, 1936, 1694	3309, 2930, 2441, 1939, 1683
<b>b</b>	3-hydroxybenzoic acid	3477, 3346, 2457, 1949, 1692	3305, 3171, 2477, 1880, 1686	n/a	3422, 3255, 2496, 1844, 1701	3312, 2934, 2469, 1934, 1681
<b>c</b>	4-chlorobenzoic acid	3298, 2375, 1830, 1691	n/a	3383, 3201, 2368, 1869, 1687	3435, 3255, 2439, 1879, 1695	n/a
<b>d</b>	4-fluorobenzoic acid	3400, 3321, 2459, 1920, 1700	3317, 3132, 2558, 1878, 1670	3380, 3204, 2418, 1923, 1686	3435, 3256, 2443, 1918, 1694	n/a
<b>e</b>	4-nitrobenzoic acid	3414, 3318, 2370, 1920, 1701	3415, 3117, 2391, 1900, 1701	3445, 3343, 2435, 1928, 1689	3449, 3299, 2448, 1945, 1699	3116, 2924, 2366, 1940, 1692
<b>f</b>	3,4-dichlorobenzoic acid	3330, 3184, 2373, 1922, 1699	3280, 3117, 2422, 1896, 1656	3315, 3202, 2362, 1869, 1693	3440, 3255, 2439, 1905, 1698	n/a
<b>g</b>	2,6-difluorobenzoic acid	3293, 3163, 2492, 1942, 1716	3300, 3156, 2479, 1922, 1720	3323, 3212, 2360, 1900, 1701	3422, 3249, 2521, 1884, 1697	n/a
<b>h</b>	3,5-dimethylbenzoic acid	3322, 3154, 2607, 1811, 1683	3320, 3192, 2532, 1812, 1683	n/a	3444, 2496, 1892, 1707	n/a
<b>i</b>	3,5-dinitrobenzoic acid	3280, 3118, 2484, 1938, 1716	3262, 2988, 2370, 1968, 1680	n/a	3445, 3217, 2453, 1961, 1679	n/a
<b>j</b>	pentafluorobenzoic acid	3092, 2446, 1930, 1695	3326, 2918, 2468, 1928, 1682	n/a	3431, 3043, 2448, 1879, 1707	n/a
<b>k</b>	suberic acid	3303, 3166, 2413, 1904, 1687	3310, 3134, 2493, 1901, 1701	3433, 3309, 2437, 1871, 1693	3457, 3255, 2474, 1923, 1698	n/a
<b>l</b>	phthalic acid	3309, 3140, 2480, 1869, 1694	3445, 3332, 2366, 1845, 1686	3311, 3119, 2435, 1865, 1688	3431, 3241, 2505, 1874, 1695	3295, 2940, 2509, 1920, 1684
<b>m</b>	fumaric acid	3463, 3319, 2394, 1864, 1683	3290, 3121, 2429, 1866, 1699	3343, 3172, 2541, 1928, 1725	3422, 3255, 2527, 1888, 1698	3388, 2926, 2492, 1965, 1684
<b>n</b>	succinic acid	3325, 3163, 2387, 1871, 1697	3291, 3122, 2472, 1877, 1703	3414, 3336, 2456, 1905, 1725	3479, 3246, 2448, 1923, 1698	3362, 2925, 2524, 1948, 1685
<b>o</b>	sebacic acid	3325, 3137, 2475, 1947, 1688	3307, 3147, 2492, 1925, 1693	3405, 3310, 2458, 1871, 1692	3259, 2487, 1918, 1702	n/a
<b>p</b>	cyanoxime	3416, 3323, 2562, 1781, 1667	3419, 3329, 2534, 1627	3335, 3212, 2439, 1867, 1682	3263, 2452, 1896, 1696	n/a
<b>q</b>	2-fluorocyanoxime	3414, 3326, 2530, 1777, 1668	3418, 3332, 2534, 1776, 1629	3321, 3214, 2432, 1789, 1634	3475, 3294, 2474, 1861, 1702	n/a
<b>r</b>	2-chlorocyanoxime	3299, 3147, 2462, 1861, 1661	n/a	3332, 3111, 2395, 1826, 1627	3431, 3250, 2452, 1918, 1694	n/a
<b>s</b>	4-bromocyanoxime	3304, 3156, 2455, 1888, 1661	n/a	3337, 3207, 2438, 1900, 1644	3444, 3285, 2487, 1866, 1698	n/a

**Table 4.3 IR stretching frequencies ( $\text{cm}^{-1}$ ) of salts and co-crystals of the ligands 21, 24, 27, 29, and 32.**

		21	24	27	29	32
a	4-cyanobenzoic acid	3422, 3056, 2474, 1905, 1702	3282, 2745, 1973, 1681	3304, 2944, 2513, 1939, 1687	3242, 3057, 2548, 1953, 1686	n/a
b	3-hydroxybenzoic acid	3249, 3053, 2607, 1870, 1693	3464, 3116, 2492, 1843, 1695	n/a	n/a	n/a
c	4-chlorobenzoic acid	3440, 3030, 2439, 1893, 1714	3423, 3217, 2533, 1873, 1696	n/a	n/a	n/a
d	4-fluorobenzoic acid	3427, 3074, 2540, 1914, 1699	3423, 3199, 2498, 1902, 1692	3301, 2943, 2556, 1924, 1674	n/a	n/a
e	4-nitrobenzoic acid	3435, 3052, 2417, 1905, 1707	3255, 2363, 1941, 1696	3387, 3296, 2552, 1959, 1687	n/a	3016, 2411, 1939, 1702
f	3,4-dichlorobenzoic acid	3435, 3065, 2465, 1888, 1716	3393, 2486, 1926, 1690	3315, 2943, 2509, 1871, 1691	3240, 3091, 2570, 1930, 1673	n/a
g	2,6-difluorobenzoic acid	3440, 3065, 2470, 1888, 1702	3415, 2461, 1919, 1690	n/a	n/a	n/a
h	3,5-dimethylbenzoic acid	3436, 3035, 2512, 1856, 1706	3340, 3034, 2504, 1885, 1678	n/a	3228, 3042, 2519, 1851, 1703	n/a
i	3,5-dinitrobenzoic acid	3413, 2465, 1932, 1716	3340, 3075, 2515, 1979, 1673	3375, 3094, 2435, 1871, 1687	3093, 2829, 2539, 1851, 1699	3312, 3091, 2463, 1855, 1702
j	pentafluorobenzoic acid	n/a	3325, 3075, 2509, 2032, 1684	3390, 3296, 2455, 1912, 1686	3241, 3066, 2521, 1887, 1696	n/a
k	suberic acid	n/a	3464, 3193, 2486, 1932, 1696	n/a	n/a	3310, 3152, 2500, 1904, 1704
l	phthalic acid	n/a	3199, 3010, 2474, 2003, 1690	3389, 3157, 2615, 1924, 1687	n/a	3313, 2944, 2504, 1990, 1703
m	fumaric acid	3440, 3049, 2489, 1875, 1706	3323, 3034, 2439, 1985, 1684	3390, 3155, 2536, 1900, 1667	n/a	3307, 3161, 2464, 1882, 1702
n	succinic acid	n/a	3235, 2384, 2002, 1674	3390, 3160, 2525, 1932, 1687	n/a	3307, 2963, 2533, 1900, 1693
o	sebacic acid	n/a	3452, 3211, 2474, 1908, 1702	n/a	n/a	n/a
p	cyanoxime	3368, 2525, 1911, 1707	3455, 3180, 2530, 1810, 1685	n/a	n/a	n/a
q	4-fluorocyanoxime	3450, 3063, 2471, 1902, 1707	3420, 3222, 2547, 1856, 1713	n/a	n/a	n/a
r	4-chlorocyanoxime	3436, 2471, 1911, 1702	n/a	n/a	n/a	n/a
s	4-bromocyanoxime	3444, 2536, 1839, 1702	n/a	n/a	n/a	n/a

### *4.3.2 Crystal Structures*

A total of 19 crystal structures were obtained, out of which seven are of the ligands by themselves, nine are co-crystals, and three are salts. Out of twelve co-crystals/salts, ten were obtained with carboxylic acids and two with cyanoximes. The co-crystals and salts with the dicarboxylic acids are in 2:1 stoichiometry, while monocarboxylic acids and cyanoximes display 1:1 stoichiometry.

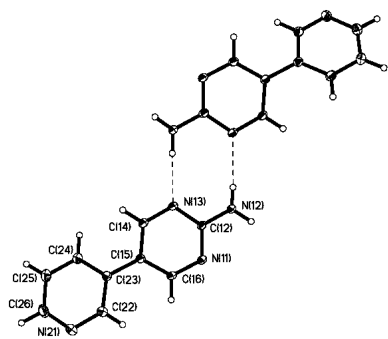
A summary of the crystallographic information for the salts and co-crystals are presented in the Appendix A and all the hydrogen-bond geometries are listed in Table 4.4.

**Table 4.4** Hydrogen-bond geometries for the ditopic ligands, and their salts and co-crystals.

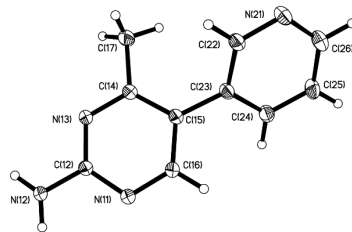
Structure	D-H...A	d(D-H)/Å	d(H...A)/Å	d(D...A)/Å	<(DHA)/°
<b>10<sup>i</sup></b>	N121-H12A1...N132	0.90(2)	2.15(2)	3.0507(17)	174(2)
	N122-H12A2...N131	0.90(2)	2.13(2)	3.0288(17)	174(2)
	N121-H12B1...N112#1	0.91(2)	2.12(2)	3.0301(17)	176(2)
	N122-H12B2...N111#2	0.87(2)	2.18(2)	3.0466(17)	175(2)
<b>12<sup>ii</sup></b>	N(12)-H(12A)...N(13)#1	0.876(14)	2.124(14)	2.9948(12)	172.4(13)
	N(12)-H(12B)...N(11)#2	0.889(14)	2.145(14)	3.0278(12)	171.6(12)
<b>15<sup>iii</sup></b>	N(12)-H(12A)...N(21)#1	0.885(19)	2.13(2)	3.0067(18)	172.9(17)
	N(12)-H(12B)...N(14)#2	0.87(2)	2.40(2)	3.239(2)	162.7(16)
<b>16<sup>iv</sup></b>	N371-H371...N212#1	0.88	2.19	3.064(2)	169.4
	N372-H372...N211	0.88	2.20	3.071(3)	171.6
<b>21<sup>v</sup></b>	N(32)-H(32)...O(18)	0.83(3)	2.07(3)	2.879(3)	166(3)
	N(12)-H(12)...N(41)#1	0.87(3)	2.14(3)	3.007(3)	176(3)
<b>24<sup>vi</sup></b>	N221-H22A1...O(1S)	0.894(16)	2.133(16)	2.9502(13)	151.6(13)
	N222-H22A2...O(1S)	0.895(15)	2.107(16)	2.9953(12)	172.1(14)
	N221-H22B1...N112#1	0.895(16)	2.169(16)	3.0625(13)	176.2(14)
	N222-H22B2...N111#2	0.904(16)	2.122(16)	3.0253(13)	176.3(13)
	N121-H121...N212#2	0.894(16)	2.220(16)	3.1055(13)	170.4(13)
	N122-H122...N211#1	0.882(15)	2.213(15)	3.0899(13)	172.6(13)
	O(1S)-H(1A)...O182#3	0.889(16)	1.884(17)	2.7661(12)	171.2(15)
	O(1S)-H(1B)...O181#4	0.852(17)	1.958(17)	2.8073(12)	174.1(15)
<b>27<sup>vii</sup></b>	N(22)-H(22A)...N(11)#1	0.932(14)	2.132(14)	3.0615(11)	174.9(12)
	N(22)-H(22B)...O(18)#2	0.938(13)	2.145(13)	3.0117(11)	153.0(11)
	N(12)-H(12)...N(21)#3	0.922(13)	2.185(13)	3.1010(11)	171.8(11)
<b>10c<sup>viii</sup></b>	O(31)-H(31)...N(21)	0.96(2)	1.67(2)	2.6274(16)	179(2)
	N(12)-H(12A)...N(11)#1	0.92(2)	2.19(2)	3.0998(16)	172.9(15)
	N(12)-H(12B)...N(13)#2	0.912(19)	2.05(2)	2.9650(16)	176.1(15)
<b>10j<sup>ix</sup></b>	N(21)-H(21)...O(31)	1.022(16)	2.690(15)	3.3299(12)	120.7(11)
	N(12)-H(12A)...N(11)#1	0.860(16)	2.122(16)	2.9778(12)	173.4(15)
	N(12)-H(12B)...N(13)#2	0.897(16)	2.094(17)	2.9848(13)	172.4(15)
<b>10k<sup>x</sup></b>	O(31)-H(31)...N(21)	0.95(2)	1.70(2)	2.6516(16)	174.9(17)
	N(12)-H(12A)...N(13)#2	0.873(18)	2.188(19)	3.0603(18)	177.7(17)
	N(12)-H(12B)...N(11)#3	0.903(19)	2.120(19)	3.0222(18)	176.1(15)
<b>10n<sup>xi</sup></b>	O(51)-H(51)...N(11)	0.98(3)	1.64(3)	2.618(2)	174(3)
	O(54)-H(54)...N(31)	0.98(3)	1.69(3)	2.662(2)	171(3)
	N(12)-H(12A)...O(52)	0.92(3)	1.96(3)	2.873(3)	171(3)
	N(12)-H(12B)...N(41)#1	0.97(3)	2.01(3)	2.973(3)	173(2)
	N(32)-H(32A)...O(55)	1.03(3)	1.86(3)	2.871(3)	168(2)
	N(32)-H(32B)...N(21)#2	0.93(3)	2.12(3)	3.038(3)	171(3)

Structure	D-H...A	d(D-H)/Å	d(H...A)/Å	d(D...A)/Å	<(DHA) <sup>o</sup>
<b>10o<sup>xiii</sup></b>	O(31)-H(31)...N(21)	0.919(19)	1.741(19)	2.6509(13)	170.2(16)
	N(12)-H(12A)...N(11)#2	0.907(15)	2.150(15)	3.0546(13)	175.3(13)
	N(12)-H(12B)...N(13)#3	0.917(16)	2.101(16)	3.0176(14)	177.6(14)
<b>10p<sup>xiii</sup></b>	O(37)-H(37)...N(21)	0.94(3)	1.72(3)	2.644(2)	169(2)
	N(12)-H(12A)...N(11)#1	0.89(2)	2.16(2)	3.045(2)	173(2)
	N(12)-H(12B)...N(13)#2	0.92(2)	2.13(2)	3.041(2)	175(2)
<b>12n<sup>xiv</sup></b>	O(31)-H(31)...N(21)	0.999(17)	1.698(17)	2.6910(14)	171.7(15)
	N(12)-H(12A)...N(11)#2	0.924(16)	2.167(16)	3.0789(15)	168.9(13)
	N(12)-H(12B)...N(13)#3	0.889(16)	2.096(17)	2.9779(15)	171.3(14)
<b>15e<sup>xv</sup></b>	O(31)-H(31)...N(21)	0.84	1.73	2.566(4)	175.1
	N(12)-H(12A)...O(31)#1	0.88	2.12	2.981(4)	165.4
	N(12)-H(12B)...O(34)#2	0.88	2.18	3.051(4)	168.3
<b>16p<sup>xvi</sup></b>	O(37)-H(37)...N(21)	0.994(15)	1.610(15)	2.6037(11)	178.0(13)
	N(12)-H(12)...N(11)#1	0.903(13)	2.327(13)	3.2280(11)	175.0(11)
<b>24h<sup>xvii</sup></b>	N(12)-H(12)...O(32)	0.904(19)	1.92(2)	2.8212(17)	173.6(17)
	N(21)-H(21)...O(41)	0.96(2)	1.58(2)	2.532(2)	173(2)
	N(22)-H(22A)...O(42)	0.90(2)	1.97(2)	2.867(2)	173.6(19)
	O(31)-H(31)...N(11)	0.82(2)	1.90(2)	2.7067(17)	171(2)
	N(22)-H(22B)...O(42)#1	0.89(2)	1.98(2)	2.863(2)	169.4(19)
<b>24n<sup>xviii</sup></b>	N(12)-H(12)...O(38)#1	0.88	2.05	2.916(2)	166.2
	N(21)-H(21)...O(51)	0.99(2)	1.64(2)	2.592(2)	160(2)
	N(22)-H(22A)...O(52)	0.88	2.01	2.848(2)	157.9
	N(22)-H(22B)...O(54)#2	0.88	2.06	2.877(2)	154.1
	N(32)-H(32)...O(53)#3	0.88	2.18	3.035(2)	165.0
	N(41)-H(41)...O(53)	0.87(3)	1.76(3)	2.622(2)	173(3)
	N(42)-H(42A)...O(52)	0.88	2.15	2.973(2)	155.4
N(42)-H(42B)...O(54)#2	0.88	2.32	3.181(3)	166.4	
<b>27i<sup>xix</sup></b>	N(22)-H(22A)...N(11)#1	0.97(3)	1.98(3)	2.957(3)	177(2)
	O(31)-H(31)...N(24)	0.98(3)	1.63(3)	2.599(3)	166(2)
	N(12)-H(12)...N(21)#2	0.89(3)	2.22(3)	3.108(3)	177(2)

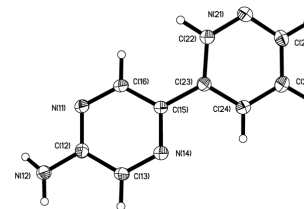
(i) #1 x+1,y,z+1 #2 x-1,y,z-1 (ii) #1 -x+1,y-1/2,-z+3/2 #2 -x+1,y+1/2,-z+3/2 (iii) #1 x,y-1,z #2 x-1/2,-y+1/2,z-1/2 (iv) #1 x+1,y,z-1 (v) #1 -x+1,-y,-z+1 (vi) #1 -x,-y,-z #2 -x+2,-y+1,-z+2 #3 -x-1,-y,-z #4 x-1,y,z-1 (vii) #1 x,y-1,z #2 x,-y+1,z-1/2 #3 x,y+1,z (viii) #1 -x,y-1/2,-z+3/2 #2 -x,y+1/2,-z+3/2 (ix) #1 -x+3,-y,-z+1 #2 -x+3,-y-1,-z+1 (x) #1 -x-1,-y-1,-z #2 -x+2,-y,-z+1 #3 -x+3,-y+1,-z+1 (xi) #1 x-1,-y+1/2,z-1/2 #2 x+1,-y+3/2,z+1/2 (xii) #1 -x+3,-y-1,-z #2 -x,-y,-z+1 #3 -x-1,-y+1,-z+1 (xiii) #1 -x+1,y+1/2,-z+5/2 #2 -x+1,y-1/2,-z+5/2 (xiv) #1 -x+1,-y+2,-z+1 #2 -x,y-1/2,-z+3/2 #3 -x,y+1/2,-z+3/2 (xv) #1 -x,-y,-z #2 x-1,y-2,z-1 (xvi) #1 -x+1,-y,-z+1 (xvii) #1 x+1/2,-y+3/2,z+1/2 (xviii) #1 x+2,y+1,z-1 #2 -x,-y,-z+1 #3 -x,-y,-z+2 (xix) #1 x-2,y,z-1 #2 x+2,y,z+1



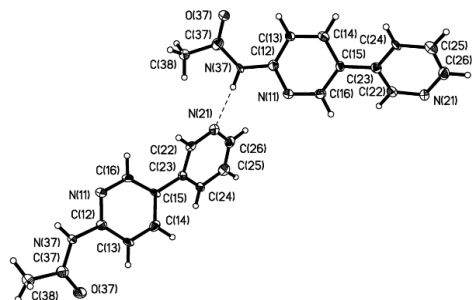
10



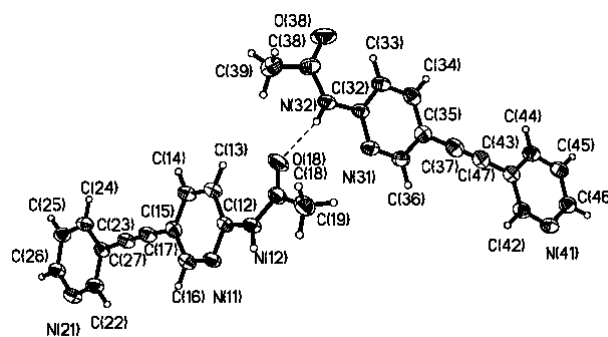
12



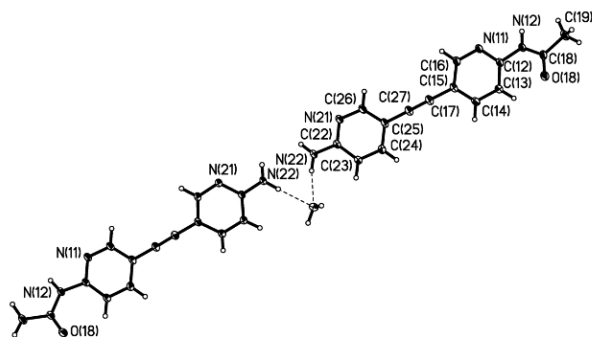
15



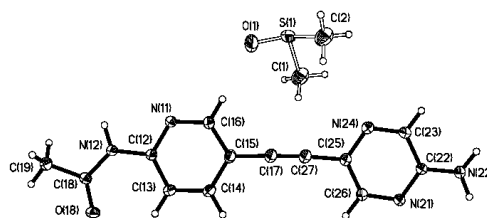
16



21



24



27

**Figure 4.6** Thermal ellipsoid plots (50 % probabilities) and labeling schemes for the ditopic ligands 10, 12, 15, 16, 21, 24, and 27.

#### 4.3.2.1 Crystal structure of 10 and 12

The crystal structures of the ditopic ligands 2-amino-5-(3-pyridyl)pyrimidine **10** and 2-amino-4-methyl-5-(3-pyridyl)pyrimidine **12** show similar packing with 1-D chains resulting from two self-complementary N-H $\cdots$ N hydrogen bonds between the amino groups and the pyrimidinyl nitrogens on either side. The consecutive pyridyl-N atoms on the chains are positioned in anti- arrangement in **10** and syn- arrangement in **12**, (Figure 4.7 – 4.8).

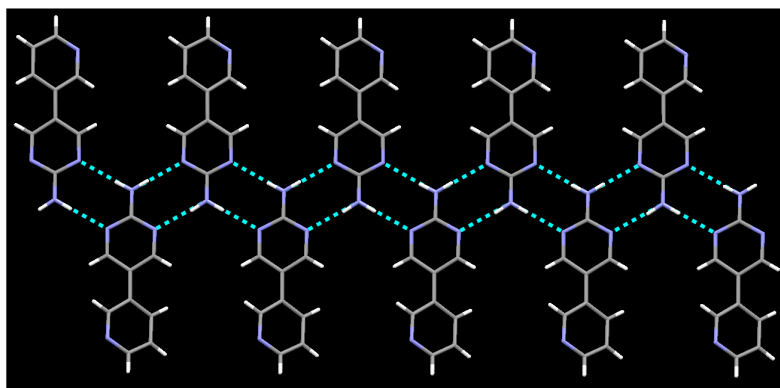


**Figure 4.7** 1-D arrangement in **10** formed via N-H $\cdots$ N hydrogen bonds.

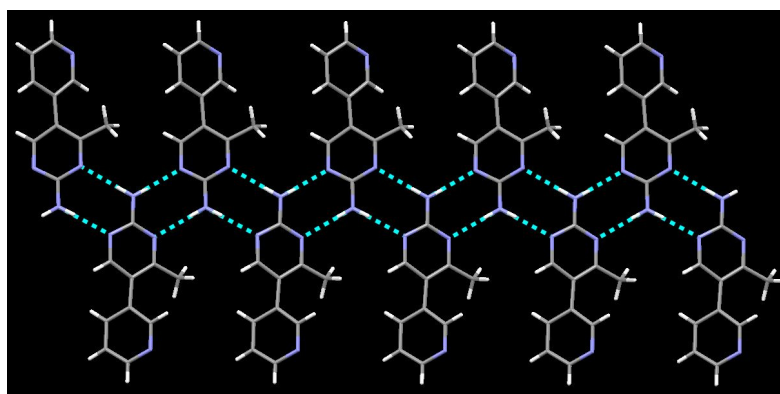


**Figure 4.8** 1-D arrangement of **12** formed via N-H $\cdots$ N hydrogen bonds.



#### 4.3.2.2 Crystal structure of 2-amino-5-(3-pyridyl)pyrazine, 15

The crystal structure of **15** shows 1-D strands formed via two self-complementary N-H $\cdots$ N hydrogen bonds (N(12)-H(12A) $\cdots$ N(21), 3.0067(18) Å) and (N(12)-H(12B) $\cdots$ N(14), 3.239(2) Å) between the pyridyl-N and the amino N-H in the neighboring ligands arranged in a parallel manner, (Figure 4.9).

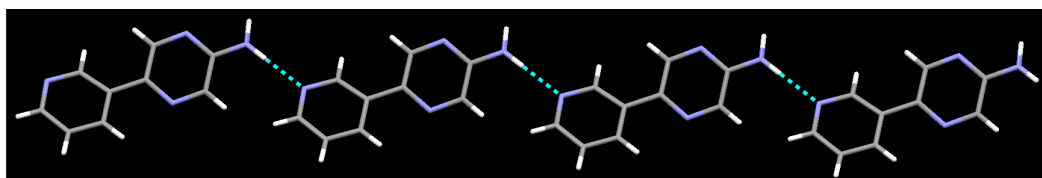


**Figure 4.9** 1-D chain in **15** formed via N-H $\cdots$ N hydrogen bonds.

#### 4.3.2.3 Crystal structure of 2-acetamido-5-(3-pyridyl)pyridine, 16

The crystal structure of **16** shows zigzag 1-D strands formed via two self-complementary N-H $\cdots$ N hydrogen bonds (N371-H371 $\cdots$ N212, 3.064(2) Å) and (N372-H372 $\cdots$ N211, 3.071(3) Å) between the pyridyl-N and the acetamido N-H in the neighboring ligands, (Figure 4.10).

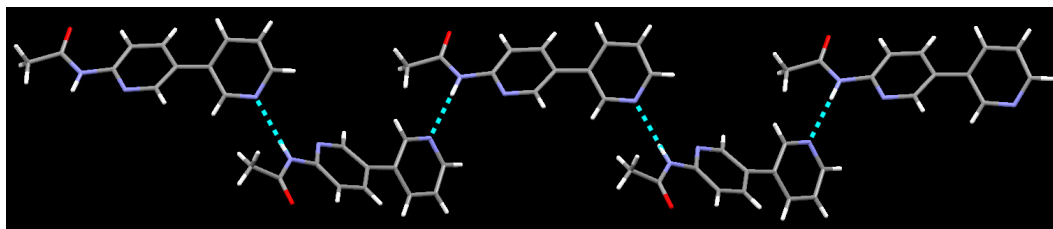


**Figure 4.10** 1-D strand of **16** connected via N-H $\cdots$ N hydrogen bonds.

#### 4.3.2.4 Crystal structure of 2-acetamido-5-(3-pyridyl)ethynylpyridine, 21

The crystal structure of **21** shows a four-component assembly linked via N-H $\cdots$ O hydrogen bonds (N(32)-H(32) $\cdots$ O(18), 2.879(3) Å) and N-H $\cdots$ N hydrogen bonds (N(12)-H(12) $\cdots$ N(41)1, 3.007(3) Å) between the acetamido N-H and carbonyl oxygen, and the acetamido N-H and pyridyl-N respectively, (Figure 4.11).

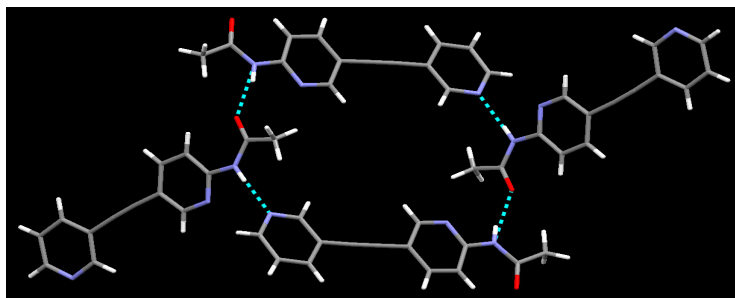


**Figure 4.11** Four-component arrangement in the structure of **21** formed via N-H $\cdots$ O and N-H $\cdots$ N hydrogen bonds.

#### 4.3.2.5 Crystal structure of 2-amino-5-(3-(2-acetamido)pyridyl)ethynylpyridine, **24**

The crystal structure of **24** consists of primary motif formed via three N-H $\cdots$ N interactions; two resulting from amino N-H and pyridyl-N interactions, and one from acetamido N-H and pyridyl-N interaction with two of its neighbors to give a 1-D chain. The chain is further extended by water molecules via two N-H $\cdots$ O between the amino N-H and water molecules, and two O-H $\cdots$ O interactions between carbonyl oxygens and water molecules to form a 2-D network, (Figure 4.12).

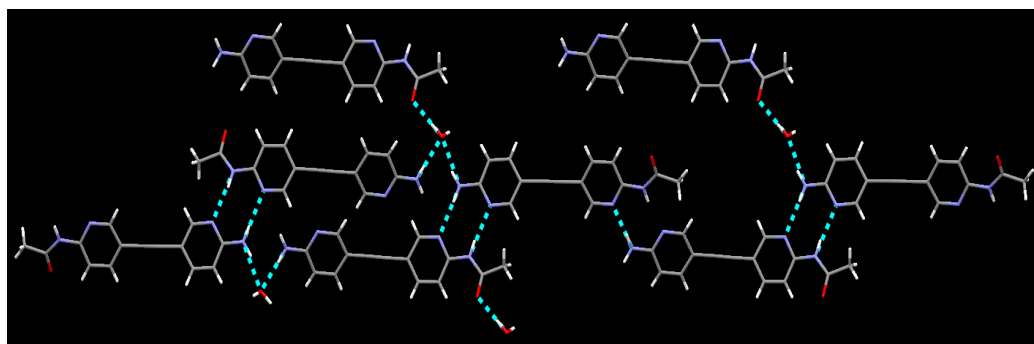


**Figure 4.12** 2-D network of **24** formed via a series of N-H $\cdots$ N, N-H $\cdots$ O, and O-H $\cdots$ O hydrogen bonds.

#### 4.3.2.6 Crystal structure of 2-amino-5-(3-(2-acetamido)pyridyl)ethynylpyrazine, **27**

The crystal structure of **27** consists of primary motif formed via two N-H $\cdots$ N hydrogen bonds between amino N-H and pyridyl-N (N(22)-H(22A)...N(11), 174.9(12) Å); and acetamido N-H and pyridyl-N (N(12)-H(12)...N(21), 3.1010(11) Å). In addition,

two N-H...O hydrogen bonds between amino N-H and carbonyl oxygen (N(22)-H(22B)...O(18), 3.0117(11) Å) are also present, (Figure 4.13).

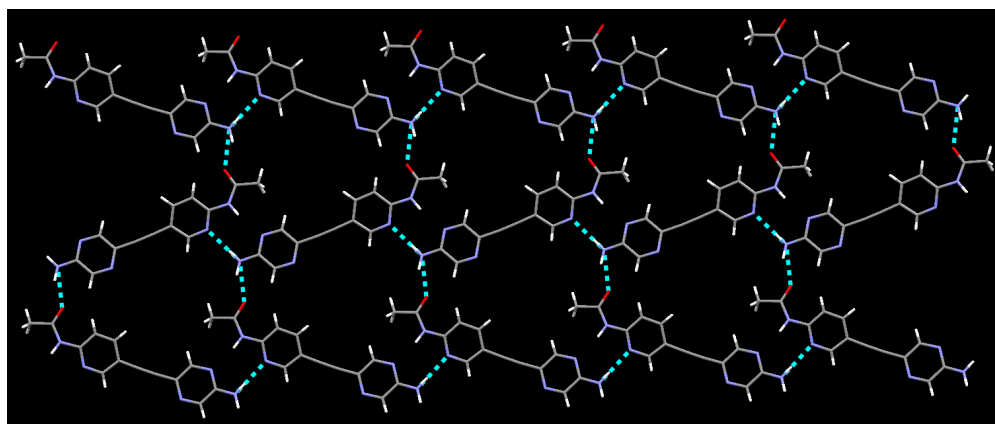
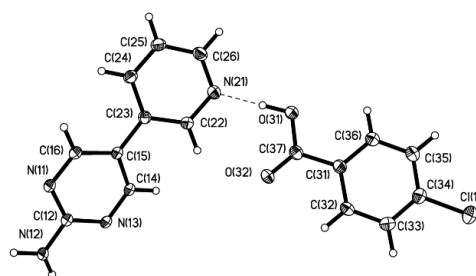
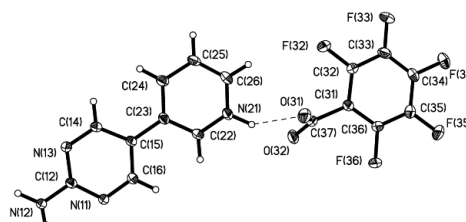


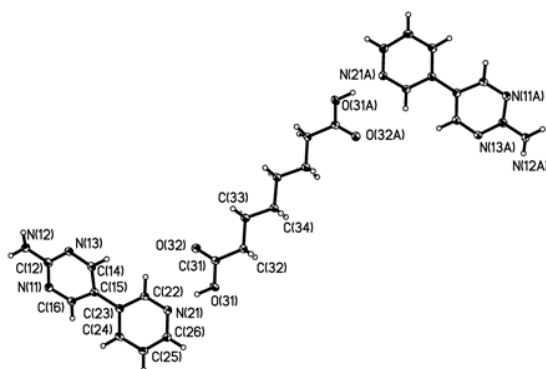
**Figure 4.13** 2-D arrangement of **27** formed via N-H...N and N-H...O hydrogen bonds.



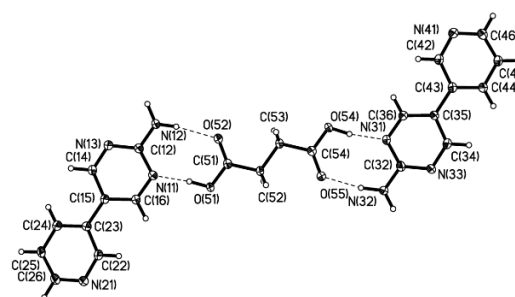
**10c**



**10j**



**10k**



**10n**

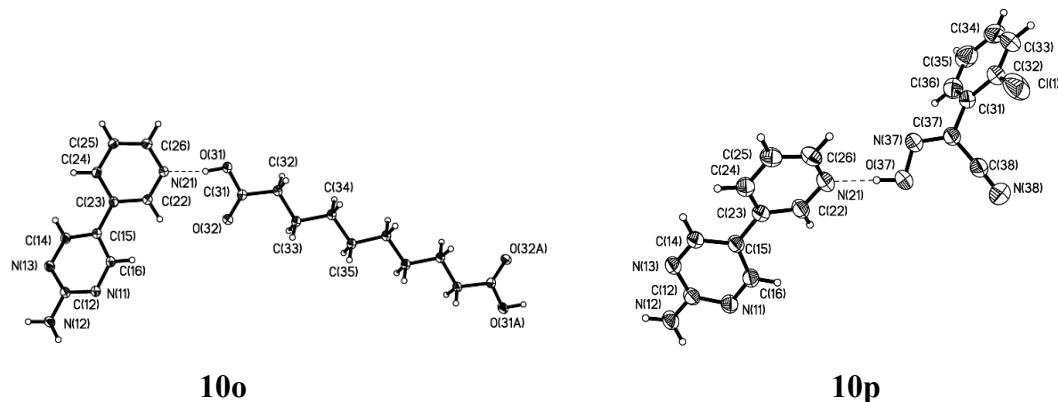


**Figure 4.14** Thermal ellipsoid plots (50 % probabilities) and labeling schemes for the co-crystals (**10c**, **10k**, **10n**, **10o**, and **10p**) and salt (**10j**) of 2-amino-5-(3-pyridyl)pyrimidine **10**.

#### 4.3.2.7 Crystal structure of 2-amino-5-(3-pyridyl)pyrimidine/4-chlorobenzoic acid (1:1), **10c**

The crystal structure of **10c** shows a 1:1 co-crystal with 2-amino-5-(3-pyridyl)pyrimidine and 4-chlorobenzoic acid connected via O-H $\cdots$ N hydrogen bonds (O(31)-H(31)...N(21), 2.6274(16) Å) between the hydroxyl group of the acid and the pyridyl-N of **10**. The aminopyrimidine moiety is engaged in N-H $\cdots$ N interactions with its neighboring ligands to give a 1-D ribbon, (Figure 4.15).

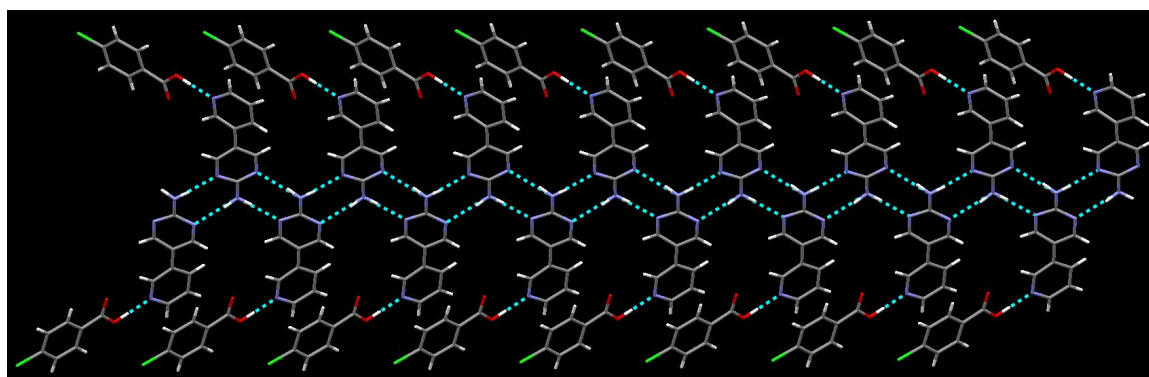
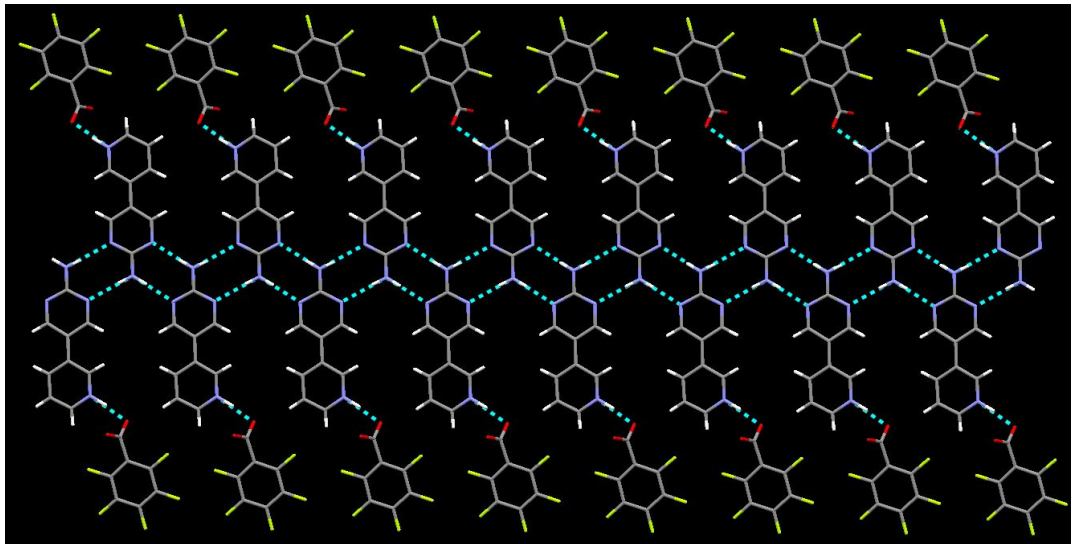


**Figure 4.15** 1-D ribbon of **10c** formed via O-H $\cdots$ N and N-H $\cdots$ N interactions.

#### 4.3.2.8 Crystal structure of 2-amino-5-(3-pyridinium)pyrimidine pentafluorobenzoate, **10j**

The crystal structure of **10j** displays a similar 1:1 architecture as observed for **10c**. However, the loss of proton from the pentafluorobenzoic acid gives rise to a ionic salt with

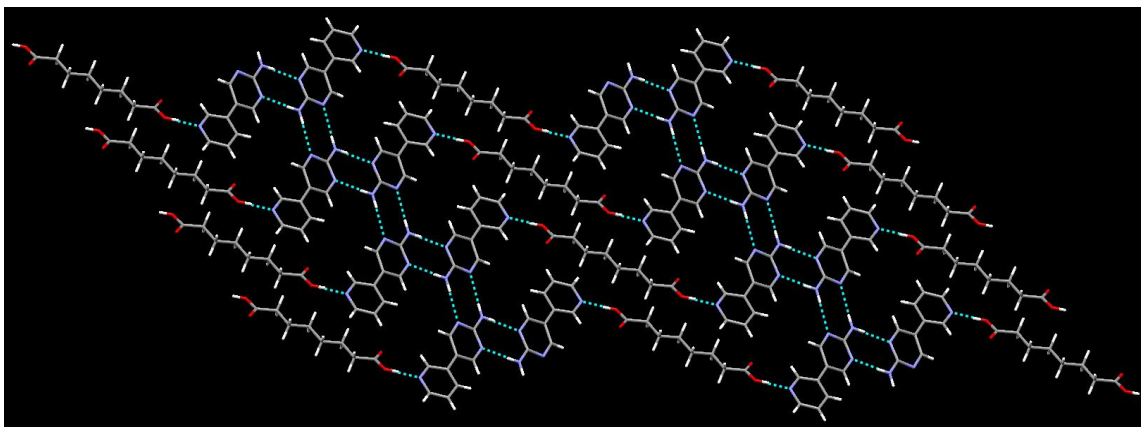
$\text{N-H}^+\cdots\text{O}^-$  interactions ( $\text{N}(21)\text{-H}(21)\cdots\text{O}(31)$ , 3.3299(12) Å) between the pyridinium and the carboxylate oxygen. The aminopyrimidine moiety is engaged in  $\text{N-H}\cdots\text{N}$  interactions with its neighboring ligands to give a 1-D ribbon, (Figure 4.16).



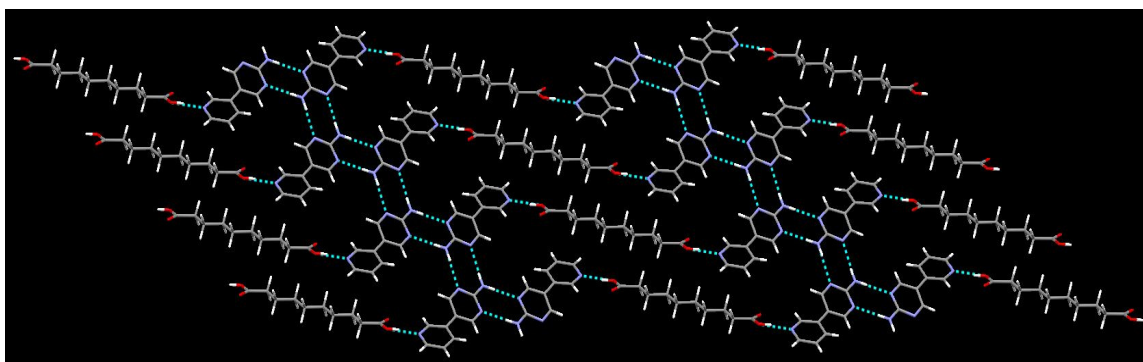
**Figure 4.16** 1-D ribbon of **10j** formed via  $\text{N-H}^+\cdots\text{O}^-$  and  $\text{N-H}\cdots\text{N}$  interactions.

#### 4.3.2.9 Crystal structure of **10k** and **10o**

The crystal structures of **10k** and **10o** show 2:1 co-crystals comprising of the neutral ligand **10** and suberic acid or sebacic acid molecule connected via hydrogen bonding interactions. The primary synthons in these structures are  $\text{O-H}\cdots\text{N}$  hydrogen bonds which are extended into interlinking ribbon to give a 2-D network via  $\text{N-H}\cdots\text{N}$  interactions between the aminopyrimidine moieties, (Figure 4.17 - 4.18).



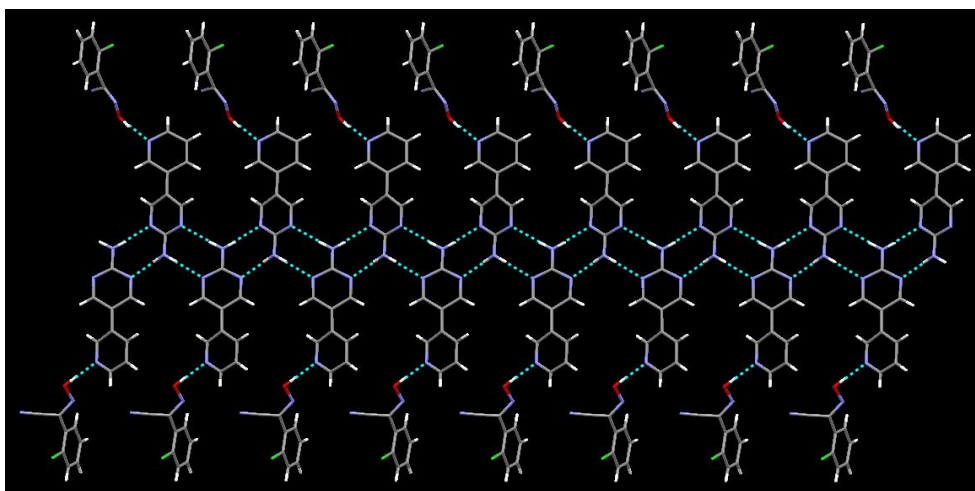
**Figure 4.17** 2-D ribbon of **10k** formed via O-H $\cdots$ N and N-H $\cdots$ N interactions.



**Figure 4.18** 2-D ribbon of **10o** formed via O-H $\cdots$ N and N-H $\cdots$ N interactions.

#### **4.3.2.10** *Crystal structure of 2-amino-5-(3-pyridyl)pyrimidine/2-chlorocyanoxime (1:1), 10r*

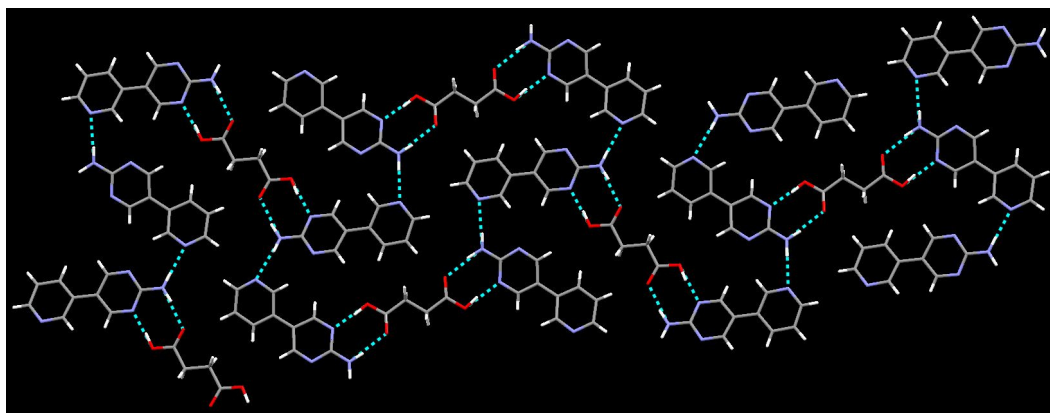
The crystal structure of **10p** shows a 1:1 co-crystal similar to **10c**, with the ligand 2-amino-5-(3-pyridyl)pyrimidine **10** and chlorocyanoxime connected via O-H $\cdots$ N hydrogen bonds (O(37)-H(37)...N(21), 2.644(2) Å) between the hydroxyl group of the cyanoxime and the pyridyl-N of **10**. The aminopyrimidine moiety is engaged in N-H $\cdots$ N interactions with its neighboring ligands to give a 1-D ribbon, (Figure 4.19).



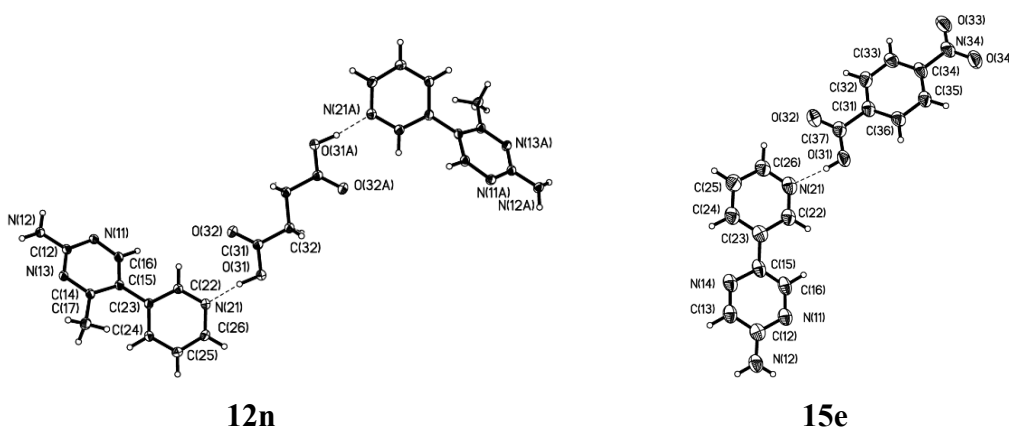
**Figure 4.19** 1-D ribbon of **10p** formed via O-H $\cdots$ N and N-H $\cdots$ N interactions.

#### 4.3.2.11 Crystal structure of 2-amino-5-(3-pyridyl)pyrimidine/succinic acid (2:1), **10n**

The crystal structure of **10n** shows a 2:1 co-crystal comprising of the neutral ligand **10** and succinic acid molecule connected via hydrogen bonding interactions. This structure is different from other co-crystals/salts structure of **10** in the binding mode of the co-crystallizing agent. Here, the acid binds with the aminopyrimidine moiety rather than with the pyridine. The primary synthons in these structures are O–H···N and N–H···O hydrogen bonds between the succinic acid and the aminopyrimidinium-NH moieties. The architecture is extended into 2-D ribbons via N–H···N interactions between the anti-proton of the aminopyrimidine and the pyridyl-N, (Figure 4.20).



**Figure 4.20** 2-D ribbon of **10n** connected via O–H···N and N–H···N interactions.



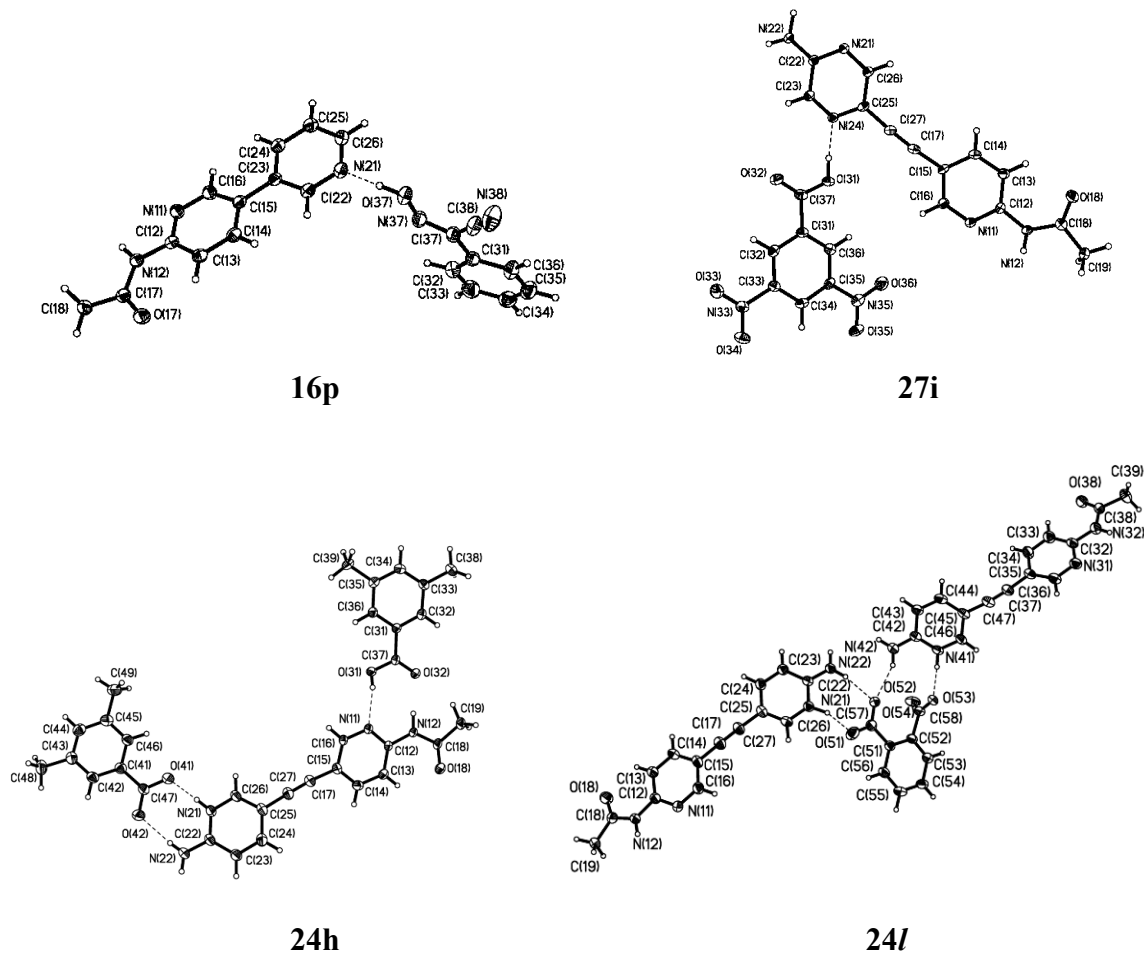


**Figure 4.21** Thermal ellipsoid plots (50 % probabilities) and labeling schemes for the co-crystals (**12n**, **15e**, **16p** and **27i**) and salts (**24h** and **24l**).

#### 4.3.2.12 Crystal structure of 2-amino-4-methyl-5-(3-pyridyl)pyrimidine/succinic acid (2:1), **12n**

The crystal structure of **12n** shows a 2:1 co-crystal comprising of the neutral ligand **12** and succinic acid molecule connected via hydrogen bonding interactions. The primary synthons in these structures are O–H $\cdots$ N hydrogen bonds (O(31)-H(31) $\cdots$ N(21), 2.6910(14) Å). The architecture is extended into chains, which are interlinked to give a 2-D network via N–H $\cdots$ N interactions between the aminopyrimidine moieties, (Figure 4.22).



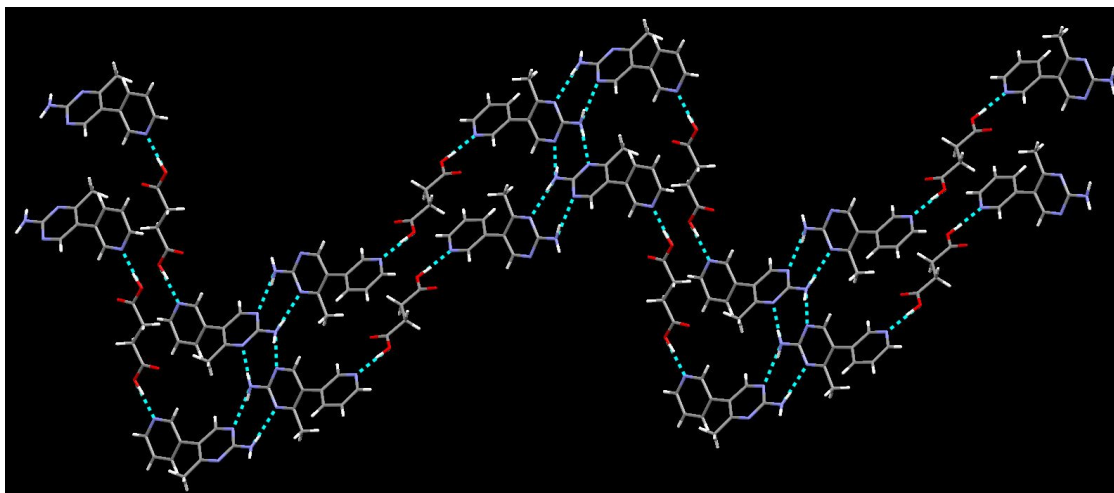


**Figure 4.22** 2-D ribbon of **12n** formed via O-H $\cdots$ N and N-H $\cdots$ N interactions.

#### 4.3.2.13 Crystal structure of 2-amino-5-(3-pyridyl)pyrazine/4-nitrobenzoic acid (1:1), **15e**

The crystal structure of **15e** shows a 1:1 co-crystal with the ligand 2-amino-5-(3-pyridyl)pyrazine and 4-nitrobenzoic acid connected via O-H $\cdots$ N hydrogen bond (O(31)-H(31) $\cdots$ N(21), 2.566(4) Å) between the hydroxyl group of the acid and the pyridyl-N of **15** as the primary motif. The amino group of the aminopyrazine moiety is engaged in two N-H $\cdots$ O interactions with hydroxyl oxygen and the nitro-oxygen of the nitrobenzoic acid, resulting in a four-component ribbon-like chain, (Figure 4.23).

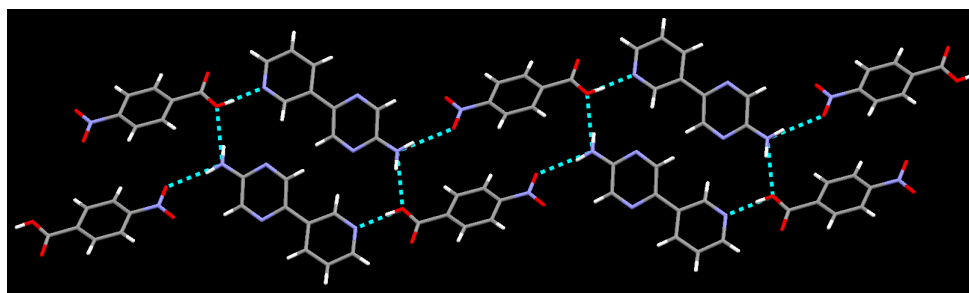
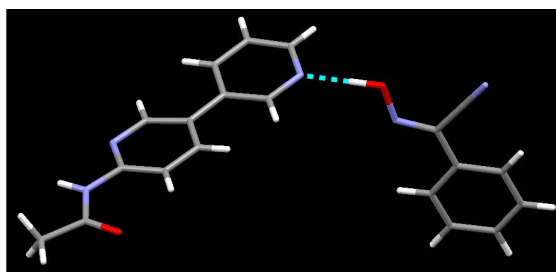


**Figure 4.23** 1-D ribbon of **15e** formed via O-H $\cdots$ N and N-H $\cdots$ O interactions.

#### 4.3.2.14 Crystal structure of 2-acetamido-5-(3-pyridyl)pyridine/cyanoxime (1:1), **16p**

The crystal structure of **16p** shows a 1:1 co-crystal with the ligand 2-acetamido-5-(3-pyridyl)pyridine **16** and cyanoxime connected via O-H $\cdots$ N hydrogen bonds (O(37)-

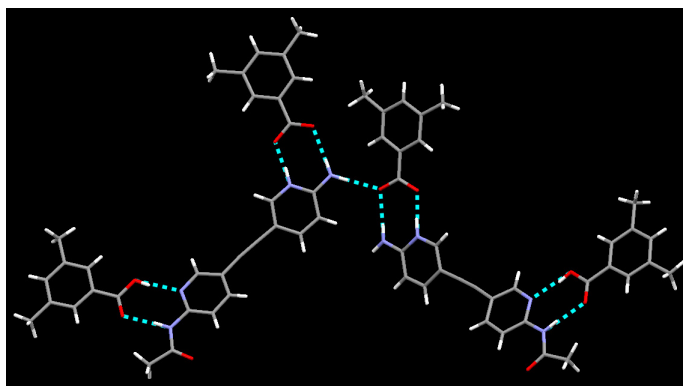
H(37)...N(21), 2.6037(11) Å) between the hydroxyl group of the cyanoxime and the pyridyl-N of **16**, (Figure 4.24).



**Figure 4.24** Co-crystal of **16p** with O-H...N interaction between cyanoxime and **16**.

#### 4.3.2.15 Crystal structure of 2-amino-5-(3-(2-acetamido)pyridyl)ethynylpyridinium 3,5-dimethylbenzoate/3,5-dimethylbenzoic acid (1:1), **24h**

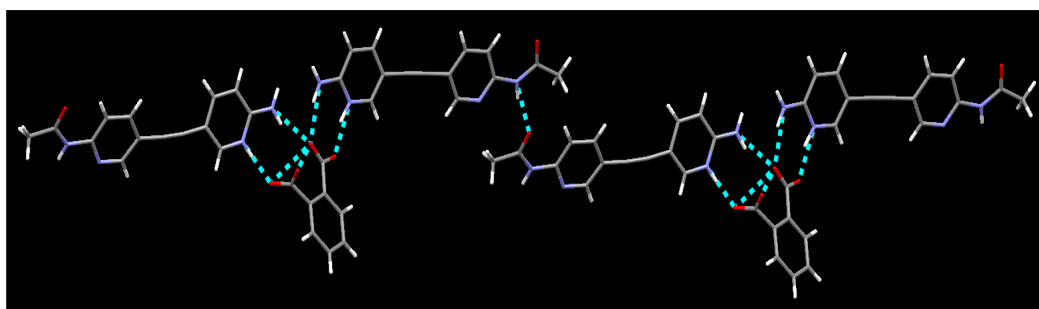
The crystal structure of **24h** show a 1:1:1 salt/co-crystal complex of 2-amino-5-(3-(2-acetamido)pyridyl)ethynylpyridinium with one molecule of 3,5-dimethylbenzoate and one molecule of 3,5-dimethylbenzoic acid. The primary motifs are, (i) charged N-H<sup>+</sup>...O<sup>-</sup> and N-H...O<sup>-</sup> interactions between the aminopyridinium moiety of the ligand and 3,5-dimethylbenzoate ion; (ii) neutral O-H...N and N-H...O interactions between the acetamidopyridyl moiety of the ligand and 3,5-dimethylbenzoic acid. These trimers are further linked to neighboring complexes via N-H...O<sup>-</sup> interactions between the anti-proton of the aminopyridine moiety and the neighboring carboxylate ion, (Figure 4.25).



**Figure 4.25** Two trimers of **24h** linked via N-H...O<sup>-</sup> interactions.

#### 4.3.2.16 Crystal structure of 2-amino-5-(3-(2-acetamido)pyridyl)ethynylpyridinium phthalate, **24l**

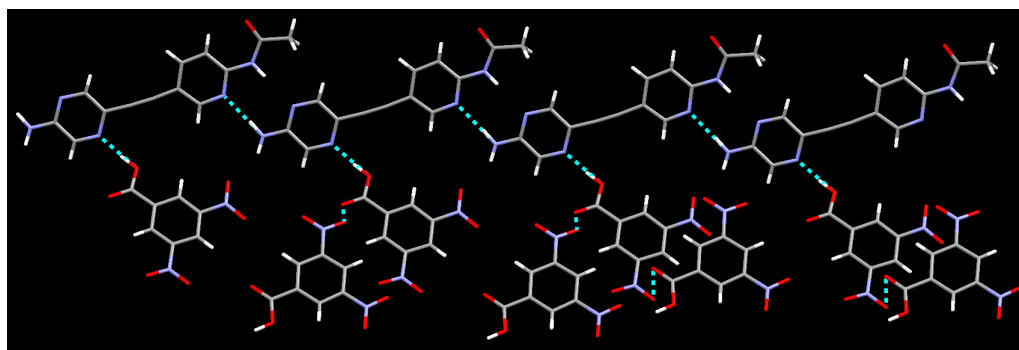
The crystal structure of **24l** display a 2:1 salt with two molecules of 2-amino-5-(3-(2-acetamido)pyridyl)ethynylpyridinium with one phthalate ion. The primary motifs are  $\text{N-H}^+\cdots\text{O}^-$  and  $\text{N-H}\cdots\text{O}^-$  interactions between the aminopyridinium moiety of the ligand and phthalate ion. These ionic complexes are extended into a 1-D network via neutral  $\text{N-H}\cdots\text{O}$  interactions between the acetamidopyridyl moieties of two neighboring ligands, (Figure 4.26).



**Figure 4.26** 1-D chain in **24l** formed via a series of  $\text{N-H}^+\cdots\text{O}^-$ ,  $\text{N-H}\cdots\text{O}^-$ , and  $\text{N-H}\cdots\text{O}$  interactions.

#### 4.3.2.17 Crystal structure of 2-amino-5-(3-(2-acetamido)pyridyl)ethynylpyrazine /3,5-dinitrobenzoic acid (1:1), **27i**

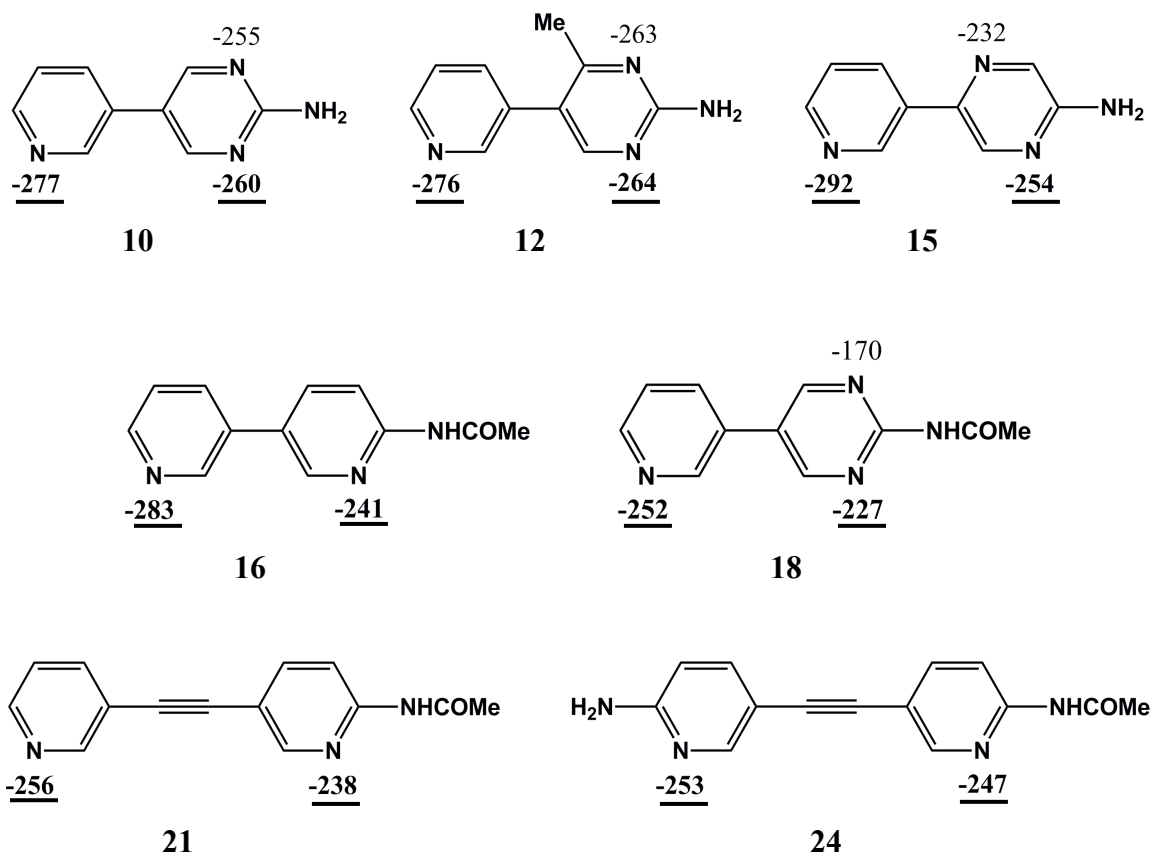
The crystal structure of **27i** show a 1:1 co-crystal with the ligand 2-amino-5-(3-(2-acetamido)pyridyl)ethynylpyrazine **27** and 3,5-dinitrobenzoic acid connected via  $\text{O-H}\cdots\text{N}$  hydrogen bond ( $\text{O}(31)\text{-H}(31)\cdots\text{N}(24)$ , 2.599(3) Å) between the hydroxyl group of the acid and the pyrazinyl-N of **27** as the primary motif. The  $\text{N-H}\cdots\text{N}$  interactions between the amino-NH of the aminopyrazine moiety and the pyridyl-N results in 1-D extension of the network. In addition, an interesting  $\text{O}\cdots\text{O}$  interaction is seen between the carboxyl-O and nitro-O of two neighboring dinitrobenzoic acids, (Figure 4.27).



**Figure 4.27** 1-D network in **27i** formed via O-H...N and N-H...N interactions.

### 4.3.3 Selectivity in the context of electrostatic potentials

The charges on the heterocyclic nitrogen atoms in pyridine, pyrimidine, and/or pyrazine moieties in each ligand were used to rank the best hydrogen bond acceptor and second best hydrogen bond acceptor.



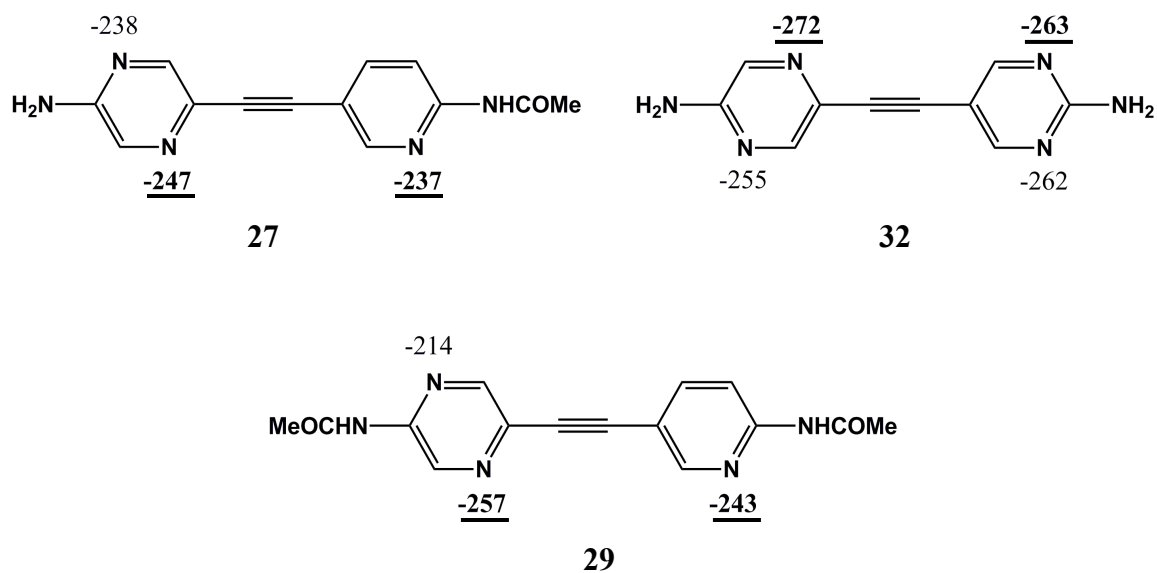


**Figure 4.28** Electrostatic potential ( $\text{kJ mol}^{-1}$ ) calculations on hydrogen-bond acceptors within the ditopic *N*-heterocycles.

Out of the 12 crystal structures analyzed, the hydrogen bond donor was found to selectively bind with the best hydrogen bond acceptor in ten cases (supramolecular yield, 83%), with the second best acceptor in one case **10n** (supramolecular yield, 9%), and one case **24h** the donors could not distinguish between the two acceptor sites and binds with both acceptors, (Table 4.5).

**Table 4.5** Charges on the nitrogen atoms assigned as the best hydrogen bond acceptor and second best acceptor in the ligands under study.

#		A1	A2	$\Delta A$	$\sqrt{\quad}$	% Yield
<b>10</b>	2-amino-5-(3-pyridyl)pyrimidine	-277	-260	17	5/6	83
<b>12</b>	2-amino-4-methyl-5-(3-pyridyl) pyrimidine	-276	-264	12	1/1	100
<b>15</b>	2-amino-5-(3-pyridyl)pyrazine	-292	-254	38	1/1	100
<b>16</b>	2-acetamido-5-(3-pyridyl)pyridine	-283	-241	42	1/1	100
<b>18</b>	2-acetamido-5-(3-pyridyl)pyrimidine	-252	-227	25	n/a	-
<b>21</b>	2-acetamido-5-(3-pyridyl)ethynylpyridine	-256	-238	18	n/a	-
<b>24</b>	2-acetamido-5-(3-(2-aminopyridyl))ethynylpyridine	-253	-247	6	1/2	50
<b>27</b>	2-amino-5-(3-(2-acetamidopyridyl))ethynylpyrazine	-247	-237	10	1/1	100
<b>29</b>	2-acetamido-5-(3-(2-acetamidopyridyl))ethynylpyrazine	-257	-243	14	n/a	-
<b>32</b>	2-amino-5-(3-(2-aminopyrazino))ethynylpyrimidine	-272	-263	9	n/a	-

All electrostatic potential charges are in  $\text{kJ mol}^{-1}$

A1 (best hydrogen bond acceptor)

A2 (second best hydrogen bond acceptor)

$\Delta A$   $|A1 - A2|$

$\sqrt{\quad}$  Donors binding with best hydrogen-bond acceptors.

% Yield (supramolecular yield)

The first six ligands (**10**, **12**, **15**, **16**, **18**, and **21**) consist of two unequal acceptor sites; the pyridyl binding site is a one-point acceptor, whereas the amino/acetamido substituted pyridyl, pyrimidyl, or pyrazinyl binding sites are two-point acceptors. This may lead to an assumption that the one-point donors like cyanoximes would favor the one-point acceptors in the pyridyl moiety, and the two-point donors like carboxylic acids would favor the second binding site. However it was found that the donor, irrespective of their “binding-points” largely prefers the acceptor site (the pyridyl group in this case) with the higher electrostatic potential.

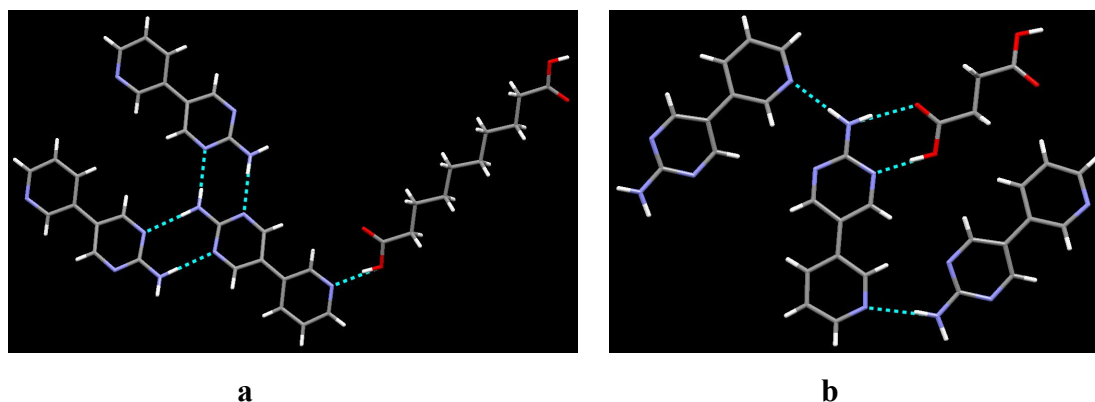


**Figure 4.29** Hydrogen-bonding interactions with the ligand in (a) **10o** (b) **10n**

The selectivity for the pyridyl group may have arisen due to the advantage in the overall number of hydrogen bonds achieved with the choice of the best acceptor. The analysis can be done by comparing the co-crystals of 2-amino-5-(3-pyridyl)pyrimidine **10** which displayed both binding to the best acceptor (5 instances) and second best acceptor (1 instance). In the co-crystals **10k** and **10o** with suberic acid and sebacic acid, the ligand **10** is involved in the formation of five hydrogen bonds (one with the carboxylic acid, four with the neighboring ligands), (Figure 4.29a). However, in the co-crystal **10n** with succinic acid, the ligand **10** is involved in four hydrogen bonds only (two with the carboxylic acid, two with the neighboring ligands), (Figure 4.29b). This extra stability furnished by the additional hydrogen bond on binding to the best acceptor might have favored the binding of the hydrogen bond donors to the best acceptors.

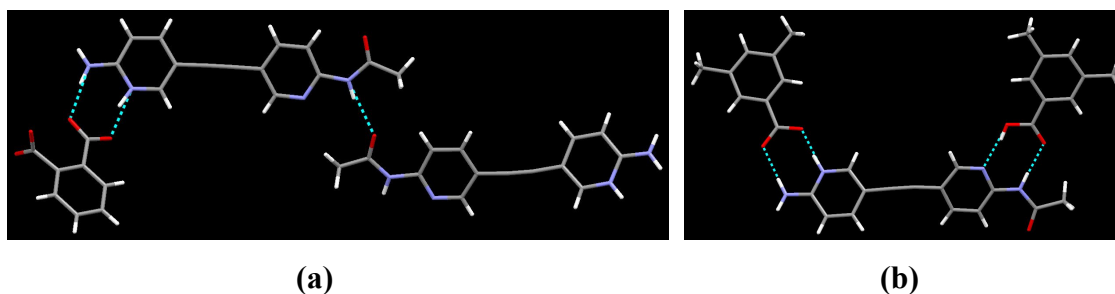


**Figure 4.30** Hydrogen-bonding interactions with the ligand in (a) **24h** (b) **24l**

Out of the twelve crystal structures, nine were co-crystals, two were salts and one a salt-co-crystal complex. The cyanoximes with higher potential to form co-crystals than salts gave co-crystals with the expected binding to the best hydrogen bond acceptor in

both cases (**10r** and **16p**). The two salts were obtained with pentafluorobenzoic acid (**10j**) and phthalic acid (**24l**). Out of the six complexes obtained from **10**, the high tendency of pentafluorobenzoic acid to lose proton resulted in the formation of salt **10j**, whereas the remaining five complexes are co-crystals. Both solids obtained with **24** are salts. The salt **24l** contains two protonated ligands with aminopyridinium ions bound with a phthalate ion via  $\text{N-H}^+\cdots\text{O}^-$  and  $\text{N-H}\cdots\text{O}^-$  interactions. The free acetamidopyridyl moiety in the ligand interacts via neutral  $\text{N-H}\cdots\text{O}$  bonds with the acetamido group of a neighboring ligand, (Figure 4.30a). Another complex **24h** of the same ligand with 3,5-dimethylbenzoic acid displays an ionic interaction on one side with the aminopyridinium ion binding with the dimethylbenzoate ion, whereas the other side consisting of acetamidopyridine moiety forms a co-crystal with the neutral acid, hence resulting in an interesting salt-co-crystal complex, (4.30b). This type of behavior at the aminopyridine site is not completely unexpected, as the CSD database<sup>15</sup> search shows that out of 105 structures containing the aminopyridyl moiety and carboxylic acid/carboxylate ion only five structures are co-crystals whereas 100/105 are salts. This observation in **24h** may also be influenced by the small difference ( $6 \text{ kJ mol}^{-1}$ ) in the electrostatic potential between these two acceptor sites, which may be too small to be distinguish between the two binding sites, (Table 4.5).

#### 4.3.4 Validity of *Q* values

The *Q* values for the two individual hydrogen binding sites in the ligands are calculated by including the participation of the groups adjacent to the heterocycle-*N* atom. The electrostatic contribution from the adjacent N-H or C-H groups in addition that of the pyridyl/pyrimidyl/pyrazinyl nitrogen atom itself is used for the calculation of the *Q* value. The larger value of *Q* may implicate the higher ability to binding, and hence the particular site may be considered as the better hydrogen bonding site.

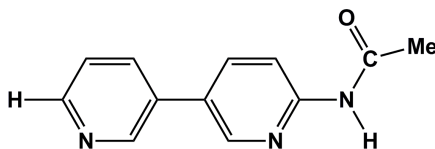




**Table 4.6** Calculation of Q values from the combination of electrostatic potential of heterocyclic nitrogen and adjacent groups

		Het-N/CH	Q1	Het-N/NH	Q1'	Het-N/NH	Q2	√
<b>10</b>	2-amino-5-(3-pyridyl)pyrimidine	277/66	343	x	x	260/48	308	5/6
<b>12</b>	2-amino-4-methyl-5-(3-pyridyl)pyrimidine	276/71	347	x	x	264/144	408	0/1
<b>15</b>	2-amino-5-(3-pyridyl)pyrazine	292/59	351	x	x	254/146	400	0/1
<b>16</b>	2-acetamido-5-(3-pyridyl)pyridine	283/69	352	x	x	241/162	403	0/1
<b>18</b>	2-acetamido-5-(3-pyridyl)pyrimidine	252/77	329	x	x	227/104	331	n/a
<b>21</b>	2-acetamido-5-(3-pyridyl)ethynylpyridine	256/82	338	x	x	238/99	337	n/a
<b>24</b>	2-acetamido-5-(3-(2-aminopyridyl))ethynylpyridine	x	x	253/145	398	247/89	336	1/2
<b>27</b>	2-amino-5-(3-(2-acetamido)pyridyl)ethynylpyrazine	247/124	371	238/170	408	237/90	327	1/1
<b>29</b>	2-acetamido-5-(3-(2-acetamido)pyridyl)ethynylpyrazine	257/7	264	241/185	426	243/94	337	n/a
<b>32</b>	2-amino-5-(3-(2-aminopyrazino))ethynylpyrimidine	272/104	376	255/158	413	263/140	403	n/a

Q1 (sum of charges on Het-N and C-H at site 1)

Q1' (sum of charges on Het-N and N-H at site 1)

Q2 (sum of charges on Het-N and N-H at site 2)

√ (number of times the donor binds with best hydrogen bond donor in accordance to Q values)

The Q values at both ends of the ligand were calculated. For pyrimidine and pyrazine moieties with two heterocyclic nitrogens, two different Q values were assigned based on the nature of the adjacent groups (C-H or N-H), (Table 4.6). Hence for each ditopic ligand two Q values are assigned (Q1/Q1' and Q2) and based on these values the best hydrogen bond acceptor and second best acceptor were identified. However, the results show that the selectivity based on Q values is only followed for the ligand **10**. The six crystal structures obtained for co-crystals/salts of **10** reveals that at five instances the hydrogen bond donor binds with the best hydrogen bond acceptor as assigned by the Q

value, which consists of four carboxylic acids and one cyanoxime (one-point donor). The crystal structure of **24h** has the donor acid binding with both acceptor sites, which can be better explained by the minimal charge differences between the acceptor nitrogen atoms rather than by the differences between the Q values. The co-crystal **27i** displayed the acid binding with the Q value-assigned better hydrogen bond donor; however it failed to distinguish between the two Q1 values (Q1 and Q1' for two heterocyclic nitrogens in pyrazine) and was found to bind with Q1 (371) over Q1' (408). This shows that Q values are not suitable for determining the selectivity in these ditopic ligands.

## 4.5 Conclusions

The results showed that the selectivity of hydrogen bond donors in the choice of hydrogen bond acceptors can be exploited by using the electrostatic potential calculations as shown by the overall supramolecular yield of 83% (10/12) in terms of best acceptor/donor approach. Hence electrostatic potential charges can be used as reliable guidelines in the prediction of binding preferences in the presence of two or more different binding sites.

## References

- <sup>1</sup> (a) Lehn, J. M.; Mascal, M.; DeCian, A.; Fischer, J. *Chem. Commun.* **1990**, 479; (b) Almarsson, Ö.; Zaworotko, M. J. *Chem Commun.* **2004**, 1889; (c) Vishweshwar, P.; Thaimattam, R.; Jaskolski, M.; Desiraju, G. R. *Chem. Commun.* **2002**, 1830; (d) Aakeröy, C. B.; Desper, J.; Helfrich, B. A. *CrystEngComm.* **2004**, *6*, 19; (e) Bhogala, B. R.; Basavoju, S.; Nangia, A. *Cryst. Growth Des.* **2005**, *5*, 1683.
- <sup>2</sup> (a) Desiraju, G. R. *Acc. Chem. Res.* **2002**, *35*, 565; (b) Lehn, J.-M. *Science* **2002**, *295*, 2400; (c) Aakeröy, C. B.; Beatty, A. M. *Aust. J. Chem.* **2001**, *54*, 409.
- <sup>3</sup> (a) Metrangolo, P.; Neukirch, H.; Pilati, T.; Resnati, G. *Acc. Chem. Res.* **2005**, *38*, 386; (b) Metrangolo, P.; Pilati, T.; Resnati, G.; Stevenazzi, A. *Chem. Commun.* **2004**, 1492.
- <sup>4</sup> Barooah, N.; Sarma, R. J.; Baruah, J. B. *CrystEngComm.* **2006**, *8*, 608.
- <sup>5</sup> (a) Aakeröy, C. B.; Desper, J.; Urbina, J. F. *CrystEngComm* **2005**, *31*, 193; (b) Aakeröy, C. B.; Beatty, A. M.; Helfrich, B. A. *J. Am. Chem. Soc.* **2002**, *124*, 14425; (c) Vakerio, G.; Raos, G.; Meille, S. V.; Metrangolo, P.; Resnati, G. *J. Phys. Chem. A.* **2000**, *104*, 1617.
- <sup>6</sup> Babu, J.; Reddy, L. S.; Nangia, A. *Molecular Phamaceutics.* **2007**, *4*(3), 417.
- <sup>7</sup> (a) Etter, M. C. *Acc. Chem. Res.* **1990**, *23*, 120; (b) Etter, M. C. *J. Phys. Chem.* **1991**, *95*, 4601.
- <sup>8</sup> (a) Hunter, C. A. *Angew. Chem. Int. Ed.* **2004**, *43*, 5310; (b) Henry, M.; Hosseini, M. W. *New J. Chem.* **2004**, *28*, 897.
- <sup>9</sup> (a) Aakeröy, C. B.; Desper, J.; Scott, B. M. T. *Chem. Commun.* **2006**, 1445; (b) Aakeröy, C. B.; Desper, J.; Leonard, B.; Urbina, J. F. *CrystEngComm.* **2005**, *5*, 865.
- <sup>10</sup> CSD search carried out on ConQuest Version 1.12. Search was directed at finding out comparative studies performed of coupled *N*-heterocycles.
- <sup>11</sup> Li, W.; Nelson, D. P.; Jensen, M. S.; Hoerner, R. S.; Cai, D.; Larsen, R. D.; Reider, P. *J. J. Org. Chem.* **2002**, *67*, 5394.
- <sup>12</sup> Cosford, N. D.; Roppe, J. R.; Tehrani, L. R.; Smith, N. D.; Stearns, B.; Huang, D.; Wang, B. *U.S. Pat. Appl. Publ.* **2005**, 21 pp.
- <sup>13</sup> Charge calculations were performed using Spartan '04 (Wavefunction, Inc. Irvine, CA). All molecules were optimized using AM1, with the maxima and minima in the electrostatic potential surface (0.002 e au<sup>-1</sup> isosurface) determined using a positive point charge in the vacuum as a probe.
- <sup>14</sup> Silverstein, R.M.; Bassler, G. C.; Morrill, T.C. *Spectroscopic Identification of Organic Compounds* **1991**, John Wiley and Sons, New York.
- <sup>15</sup> CSD search carried out on ConQuest Version 1.12. Search was oriented at finding the structures containing aminopyridine moiety associated with either carboxylic acid (co-crystal) or carboxylate ion (salt).

# CHAPTER 5 - Solubility enhancement via co-crystallization/salt-formation

## 5.1 Introduction

One of the major challenges in the pharmaceutical industry during drug development and formulation is the need to optimize poor biopharmaceutical properties of an active pharmaceutical ingredient (API). The identification of the optimum solid form in terms of solubility, dissolution rate, mechanical properties, thermal stability etc. is essential before it can be marketed.<sup>1, 2</sup> Due to these problems, very few drugs being discovered every year actually make it to the market (1/10,000).<sup>3</sup> One of the major challenges is the improvement of the solubility of these pharmaceutical drug candidates.<sup>4</sup> Various techniques are in use to enhance the solubility of a pharmaceutical drug candidate including salt formation,<sup>6</sup> reduced particle size,<sup>7</sup> cosolvents,<sup>8</sup> micronization,<sup>9</sup> micellar solutions,<sup>10</sup> lipid-based systems<sup>11</sup> etc. Another approach gaining attention is pharmaceutical co-crystallizations,<sup>12</sup> where the API is allowed to complex with one or more molecules in the crystal lattice via non-covalent interactions.<sup>13, 14</sup>

Co-crystallization techniques have a proven ability to improve the physicochemical properties of a drug molecule such as solubility<sup>15, 16</sup> and stability<sup>17</sup>. However, this technique differs from the more widely used salt formation technique in that no ionic species are formed during the process. The neutral molecules used are held together via non-covalent interactions without making or breaking of covalent bonds.<sup>18</sup> In brief, no proton transfer occurs during co-crystallization process and hence it may be a significant factor in improving the solubility of neutral compounds and weak acids and bases which lack the potential to form a salt.<sup>19</sup>

### 5.1.1 Co-crystal solubility ( $S_{cc}$ ) and solubility product ( $K_{sp}$ )

Co-crystal solubility ( $S_{cc}$ ) is a function of the solubility product ( $K_{sp}$ ), which is the product of the concentration of API and co-crystallizing agent in solution.<sup>20</sup> For a binary co-crystal  $A_aB_b$  that does not ionize or form complexes in the solution, the solubility of the co-crystal is defined by the chemical equilibrium of the solid co-crystal with the solution.<sup>5</sup>



Where A is the API, B is the co-crystallizing agent, and subscripts 'a' and 'b' are the stoichiometric number of molecules of A and B in the complex.

The corresponding equilibrium constant is given by

$$K_{eq} = \frac{a_A^a a_B^b}{a_{AB}} \quad \text{Equation 5.2}$$

$K_{eq}$  is proportional to the thermodynamic activity product of the co-crystal components.

Taking solid co-crystal activity as unity ( $a_{AB(s)} = 1$ ) and assuming the activity coefficients of A and B equal unity for low solute levels, the co-crystal solubility can be described by the solubility product.

$$K_{sp} = a_A^a a_B^b \sim [A]^a [B]^b \quad \text{Equation 5.3}$$

Where  $K_{sp}$  is the solubility product of the co-crystal, [A] and [B] are the molar concentration of the co-crystal components at equilibrium.

On dissolution of a 1:1 co-crystal in a pure solvent into individual components without complexation or ionization to form a saturated solution. Considering the equilibrium reaction above, the mass balance for [A] =  $aS_{AaBb}$  and [B] =  $bS_{AaBb}$  can be substituted in **Equation 6.3** to provide the co-crystal solubility.

$$S_{AaBb} = \sqrt[a+b]{(K_{sp}/a^a b^b)} \quad \text{Equation 5.4}$$

### 5.1.2 Research Goals

The melting points and enthalpies of pharmaceutical crystals are the indicators of their ideal solubility. These readily measurable properties are associated with crystal lattice energy that must be overcome for dissolution to occur.<sup>5, 21</sup> The incorporation of compounds with predictable properties and crystal packing into the crystal lattice of an API should bring a predictable change in the properties of the API.

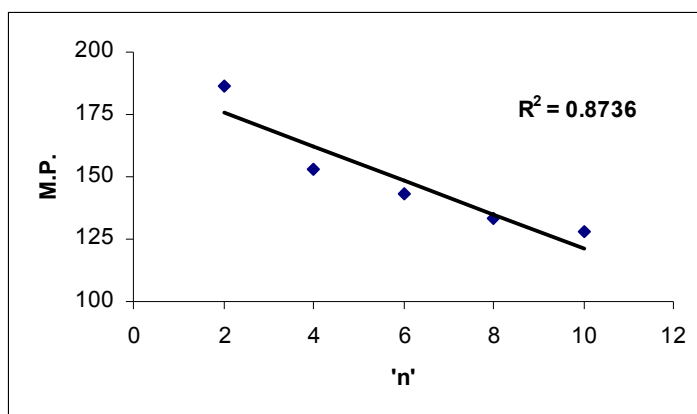


**Figure 5.1** Variation of melting points of even chain aliphatic dicarboxylic acids, (n = number of methylene groups in the chain)

A series of 5 aliphatic dicarboxylic acids with even number of carbon chains were chosen for our study, (Table 5.1). The choice of even-chain dicarboxylic acids was done on the basis of their systematic change in physical properties compared to their odd-chain analogues.<sup>22</sup> The melting points of these even-numbered aliphatic dicarboxylic acids decreases with the increasing number of methylene groups in the chain (Figure 5.1); whereas for the odd-numbered diacids the melting points are significantly lower due to the differences in crystal structure/packing.<sup>23</sup> Since the crystal structure translates to the physical properties of a compound, this might be beneficial for fine-tuning the solubility behavior of our API mimics.

**Table 5.1** Physical properties of dicarboxylic acids with even number carbon atoms

<i>Diacids</i>	<i>Formula</i>	<i>M.W.</i>	$\lambda_{max}$ (nm)	<i>M.P. (°C)</i>	<i>Aq. Solubility</i>	<i>pKa1/pKa2</i>
Succinic Acid	C <sub>4</sub> H <sub>6</sub> O <sub>4</sub>	118.09	203.4	185 – 187	76.6 mg/mL <sup>24</sup>	4.16/5.61
Adipic Acid	C <sub>6</sub> H <sub>10</sub> O <sub>4</sub>	146.14	208	151-154	22.1 mg/mL <sup>25</sup>	4.43/5.41
Suberic Acid	C <sub>8</sub> H <sub>14</sub> O <sub>4</sub>	174.20	206.6	141-144	8.9 mg/mL <sup>24</sup>	4.53/5.5 <sup>26</sup>
Sebacic Acid	C <sub>10</sub> H <sub>18</sub> O <sub>4</sub>	202.25	255.6	131-135	0.25 mg/mL <sup>26</sup>	4.72/5.45 <sup>26</sup>
Dodecanedioic Acid	C <sub>12</sub> H <sub>22</sub> O <sub>4</sub>	230.3	261.4	128	0.004 mg/mL <sup>24</sup>	-

Four API mimics were chosen for our study; 3 small molecules with pyridine and pyrimidine backbone and one known-pharmaceutical drug. Pyridines are used as precursors to agrochemicals and pharmaceuticals in view of their high biological activities,<sup>27</sup> whereas pyrimidines are present as nucleobases in RNA and DNA. All these molecules are known to form co-crystals.<sup>28</sup> Haloperidol is an antipsychotic drug used for the treatment of acute psychosis, delirium, and schizophrenia.<sup>29</sup> The presence of the acetamido and propiamido group in 2-acetamido/propiamido-5-bromopyridine with an N/N-H hydrogen-bond donor/acceptor site provide them with better potential to form hydrogen bonds with various co-crystallizing agents. The presence of pyridyl and pyrimidyl nitrogen, amino group in 2-amino-5-(3-pyridyl)pyrimidine; and the piperidinyl-N and hydroxyl group in haloperidol also have hydrogen-bond forming ability. We expect that the predictable pattern exhibited by the chosen series of dicarboxylic acids will be reflected in the properties of the co-crystals upon their incorporation in the crystal lattice of the API mimics.

Our studies have three main objectives:

- 1) Alter the API solubility via co-crystallization.
- 2) Measure equilibrium solubility changes in co-crystals against the API mimics in water and pH 6.8 buffer.
- 3) Determine solubility changes upon salt formation.

## 5.2 Experimental

All five aliphatic dicarboxylic acids and the drug haloperidol were purchased from Aldrich and used without further purification. The pH 6.8 buffer solution was prepared by dissolving calculated weights of sodium hydrogen phosphate, sodium dihydrogen phosphate, and sodium chloride in deionized water. The determinations of melting points were carried out on Fisher-Johns melting point apparatus and are uncorrected.

### 5.2.1 Synthesis of APIs

The molecules under study range from small-molecule API mimics (2-acetamido-5-bromopyridine, 2-propionamido-5-bromopyridine) to larger 2-amino-5-(3-pyridyl)pyrimidine and haloperidol. 2-acetamido-5-bromopyridine **SR1**, 2-propionamido-5-bromopyridine **SR2**, and 2-amino-5-(3-pyridyl)pyrimidine **SR3** were synthesized as described in the section 2.2.1.1 (ligand **6**), 2.2.1.2 (ligand **4**), and 4.2.1.3 (ligand **10**) respectively.  $^1\text{H}$  NMR and  $^{13}\text{C}$  NMR spectra were recorded on a Varian Unity plus 200 MHz and 400 MHz spectrometer in  $\text{CDCl}_3$  and DMSO.

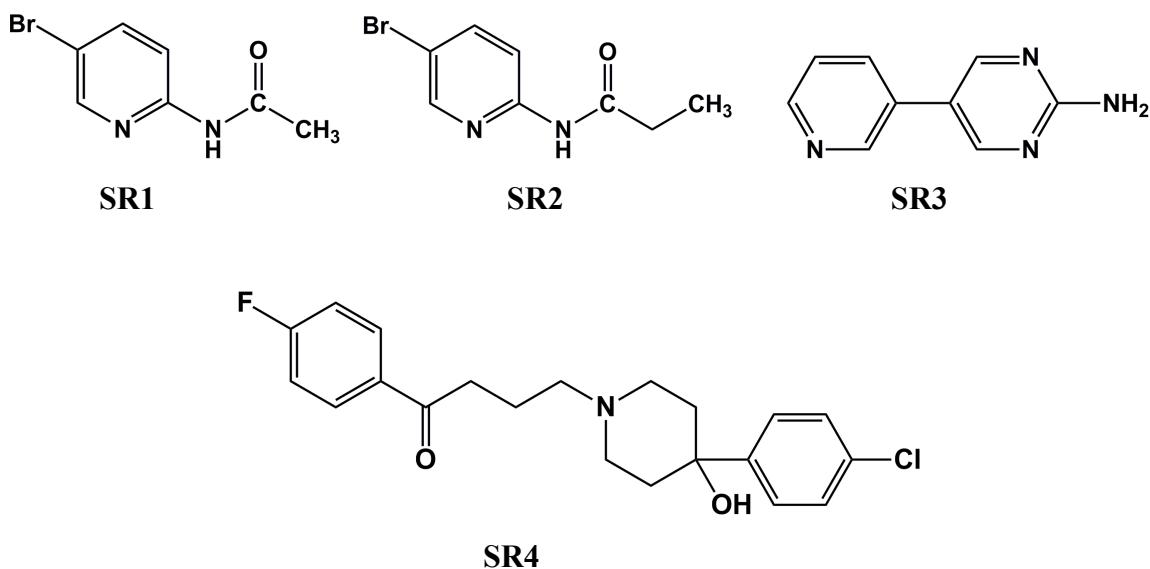


**Figure 5.2** The API mimics (Supramolecular reagents, **SR**) under study for solubility



### 5.2.2 Synthesis of co-crystals and salts

All API mimics 2-acetamido-5-bromopyridine **SR1**, 2-propionamido-5-bromopyridine **SR2**, 2-amino-5-(3-pyridyl)pyrimidine **SR3** and the drug haloperidol **SR4** were allowed to co-crystallize with the five aliphatic dicarboxylic acids with even number of carbon atoms; succinic acid (C<sub>4</sub>H<sub>6</sub>O<sub>4</sub>) **a**, adipic acid (C<sub>6</sub>H<sub>10</sub>O<sub>4</sub>) **b**, suberic acid (C<sub>8</sub>H<sub>14</sub>O<sub>4</sub>) **c**, sebacic acid (C<sub>10</sub>H<sub>18</sub>O<sub>4</sub>) **d**, and dodecanedioic acid (C<sub>12</sub>H<sub>22</sub>O<sub>4</sub>) **e**.

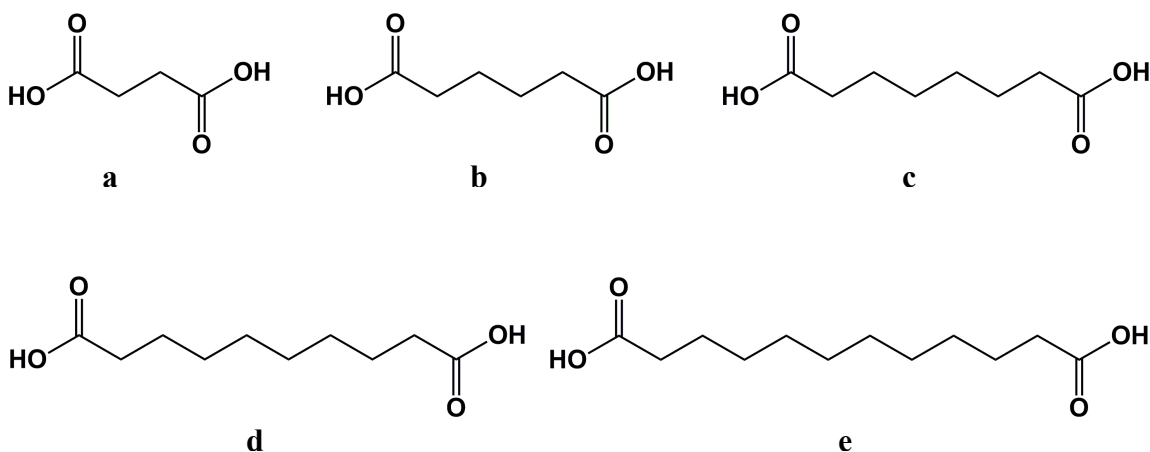


**Figure 5.3** List of aliphatic dicarboxylic acids used in the study.

The general procedure followed for the synthesis of co-crystals/salts involves refluxing stoichiometric amounts of ligand and acid in a suitable solvent, which was immediately cooled, the product filtered, dried and then subjected to IR screening. For structure and binding preferences determination, single crystals were grown from suitable solvents via slow evaporation at room temperature and were characterized using single-crystal X-ray diffraction.

#### 5.2.2.1 Synthesis of 2-acetamido-5-bromopyridine/succinic acid (2:1), *SR1-a*

A mixture of 2-acetamido-5-bromopyridine (0.20 g, 0.93 mmol) and succinic acid (0.055 g, 0.465 mmol) in ethanol was refluxed at 40 °C for 1 hr. The solution was immediately cooled to room temperature, whereupon the product crystallizes out. It was filtered and dried. For X-ray diffraction purposes, single crystals were grown by slow evaporation of an ethanolic solution at room temperature. Colorless, thin, rod-shaped

crystals were obtained after 4 days. M. P. 158—161°C; IR  $\nu$  2452  $\text{cm}^{-1}$ , 1870  $\text{cm}^{-1}$  (O—H...N, br), 1707  $\text{cm}^{-1}$  (C=O, s), 1560  $\text{cm}^{-1}$  (Amide II, s).

#### **5.2.2.2 Synthesis of 2-acetamido-5-bromopyridine/dodecanedioic acid (2:1), SR1-e**

A mixture of 2-acetamido-5-bromopyridine (0.20 g, 0.93 mmol) and dodecanedioic acid (0.107 g, 0.465 mmol) in ethanol was refluxed at 40 °C for 1 hr. The solution was immediately cooled to room temperature, whereupon the product crystallizes out. It was filtered and dried. For X-ray diffraction purposes, single crystals were grown by slow evaporation of an ethanolic solution at room temperature. Colorless, rod-shaped crystals were obtained after 4 days. M. P. 118—120°C; IR  $\nu$  2496  $\text{cm}^{-1}$ , 1847  $\text{cm}^{-1}$  (O—H...N, br), 1699  $\text{cm}^{-1}$  (C=O, s), 1577  $\text{cm}^{-1}$  (Amide II, s).

#### **5.2.2.3 Synthesis of 2-propionamido-5-bromopyridine/succinic acid (2:1), SR2-a**

A mixture of 2-propionamido-5-bromopyridine (0.20 g, 0.87 mmol) and succinic acid (0.052 g, 0.437 mmol) in ethanol was refluxed at 40 °C for 1 hr. The solution was immediately cooled to room temperature, whereupon the product crystallizes out. It was filtered and dried. For X-ray diffraction purposes, single crystals were grown by slow evaporation of an ethanolic solution at room temperature. Colorless, rod-shaped crystals were obtained after 3 days. M. P. 150°C; IR  $\nu$  2529  $\text{cm}^{-1}$ , 1863  $\text{cm}^{-1}$  (O—H...N, br), 1702  $\text{cm}^{-1}$  (C=O, s), 3259  $\text{cm}^{-1}$  (N—H amide, s), 1580  $\text{cm}^{-1}$  (Amide II, s).

#### **5.2.2.4 Synthesis of 2-propionamido-5-bromopyridine/adipic acid (2:1), SR2-b**

A mixture of 2-propionamido-5-bromopyridine (0.20 g, 0.87 mmol) and adipic acid (0.064 g, 0.437 mmol) in ethanol was refluxed at 40 °C for 1 hr. The solution was immediately cooled to room temperature, whereupon the product crystallizes out. It was filtered and dried. For X-ray diffraction purposes, single crystals were grown by slow evaporation of an ethanolic solution at room temperature. Colorless, rod-shaped crystals were obtained after 3 days. M. P. 132—134°C; IR  $\nu$  2476  $\text{cm}^{-1}$ , 1904  $\text{cm}^{-1}$  (O—H...N, br), 1687  $\text{cm}^{-1}$  (C=O, s), 3260  $\text{cm}^{-1}$  (N—H amide, s), 1536  $\text{cm}^{-1}$  (Amide II, s).

#### **5.2.2.5 Synthesis of 2-propionamido-5-bromopyridine/suberic acid (2:1), SR2-c**

A mixture of 2-propionamido-5-bromopyridine (0.20 g, 0.87 mmol) and suberic acid (0.076 g, 0.437 mmol) in ethanol was refluxed at 40 °C for 1 hr. The solution was

immediately cooled to room temperature, whereupon the product crystallizes out. It was filtered and dried. For X-ray diffraction purposes, single crystals were grown by slow evaporation of an ethanolic solution at room temperature. Colorless crystals were obtained after 3 days. M. P. 120°C; IR  $\nu$  2597  $\text{cm}^{-1}$ , 1816  $\text{cm}^{-1}$  (O—H...N, br), 1700  $\text{cm}^{-1}$  (C=O, s), 3255  $\text{cm}^{-1}$  (N—H amide, s), 1565  $\text{cm}^{-1}$  (Amide II, s).

#### ***5.2.2.6 Synthesis of 2-propiamido-5-bromopyridine/sebacic acid (2:1), SR2-d***

A mixture of 2-propiamido-5-bromopyridine (0.20 g, 0.87 mmol) and sebacic acid (0.088 g, 0.437 mmol) in ethanol was refluxed at 40 °C for 1 hr. The solution was immediately cooled to room temperature, whereupon the product crystallizes out. It was filtered and dried. For X-ray diffraction purposes, single crystals were grown by slow evaporation of an ethanolic solution at room temperature. Colorless, block-shaped crystals were obtained after 3 days. M. P. 115—117°C; IR  $\nu$  2609  $\text{cm}^{-1}$ , 1901  $\text{cm}^{-1}$  (O—H...N, br), 1697  $\text{cm}^{-1}$  (C=O, s), 3250  $\text{cm}^{-1}$  (N—H amide, s), 1560  $\text{cm}^{-1}$  (Amide II, s).

#### ***5.2.2.7 Synthesis of 2-propiamido-5-bromopyridine/dodecanedioic acid (2:1), SR2-e***

A mixture of 2-propiamido-5-bromopyridine (0.20 g, 0.87 mmol) and dodecanedioic acid (0.101 g, 0.437 mmol) in ethanol was refluxed at 40 °C for 1 hr. The solution was immediately cooled to room temperature, whereupon the product crystallizes out. It was filtered and dried. For X-ray diffraction purposes, single crystals were grown by slow evaporation of an ethanolic solution at room temperature. Colorless, block-shaped crystals were obtained after 3 days. M. P. 108—110°C; IR  $\nu$  2533  $\text{cm}^{-1}$ , 1847  $\text{cm}^{-1}$  (O—H...N, br), 1697  $\text{cm}^{-1}$  (C=O, s), 1534  $\text{cm}^{-1}$  (Amide II, s).

#### ***5.2.2.8 Synthesis of 2-amino-5-(3-pyridyl)pyrimidine/succinic acid (2:1), SR3-a***

A mixture of 2-propiamido-5-bromopyridine (0.20 g, 1.16 mmol) and succinic acid (0.069 g, 0.581 mmol) in ethanol was refluxed at 40 °C for 1 hr. The solution was immediately cooled to room temperature, whereupon the product crystallizes out. It was filtered and dried. For X-ray diffraction purposes, single crystals were grown by slow evaporation of an ethanolic solution at room temperature. Colorless, block-shaped crystals were obtained after 3 days. M. P. 188—189°C; IR  $\nu$  2378  $\text{cm}^{-1}$ , 1887  $\text{cm}^{-1}$  (O—H...N, br), 1697  $\text{cm}^{-1}$  (C=O, s), 3166  $\text{cm}^{-1}$  (N—H amide, s), 1605  $\text{cm}^{-1}$  (Amide II, s).

#### **5.2.2.9 Synthesis of 2-amino-5-(3-pyridyl)pyrimidine/adipic acid (2:1), SR3-b**

A mixture of 2-propionamido-5-bromopyridine (0.20 g, 1.16 mmol) and adipic acid (0.085 g, 0.581 mmol) in ethanol was refluxed at 40 °C for 1 hr. The solution was immediately cooled to room temperature, whereupon the product crystallizes out. It was filtered and dried. For X-ray diffraction purposes, single crystals were grown by slow evaporation of an ethanolic solution at room temperature. Colorless, block-shaped crystals were obtained after 3 days. M. P. 160—161°C; IR  $\nu$  2476  $\text{cm}^{-1}$ , 1892  $\text{cm}^{-1}$  (O—H $\cdots$ N, br), 1695  $\text{cm}^{-1}$  (C=O, s), 1596  $\text{cm}^{-1}$  (Amide II, s).

#### **5.2.2.10 Synthesis of 2-amino-5-(3-pyridyl)pyrimidine/suberic acid (2:1), SR3-c**

A mixture of 2-propionamido-5-bromopyridine (0.20 g, 1.16 mmol) and sebacic acid (0.102 g, 0.581 mmol) in ethanol was refluxed at 40 °C for 1 hr. The solution was immediately cooled to room temperature, whereupon the product crystallizes out. It was filtered and dried. For X-ray diffraction purposes, single crystals were grown by slow evaporation of an ethanolic solution at room temperature. Colorless crystals were obtained after 3 days. M. P. 150°C; IR  $\nu$  2410  $\text{cm}^{-1}$ , 1912  $\text{cm}^{-1}$  (O—H $\cdots$ N, br), 1687  $\text{cm}^{-1}$  (C=O, s), 1593  $\text{cm}^{-1}$  (Amide II, s).

#### **5.2.2.10 Synthesis of 2-amino-5-(3-pyridyl)pyrimidine/sebacic acid (2:1), SR3-d**

A mixture of 2-propionamido-5-bromopyridine (0.20 g, 1.16 mmol) and sebacic acid (0.118 g, 0.581 mmol) in ethanol was refluxed at 40 °C for 1 hr. The solution was immediately cooled to room temperature, whereupon the product crystallizes out. It was filtered and dried. For X-ray diffraction purposes, single crystals were grown by slow evaporation of an ethanolic solution at room temperature. Colorless, rod-shaped crystals were obtained after 3 days. M. P. 143—145°C; IR  $\nu$  2406  $\text{cm}^{-1}$ , 1904  $\text{cm}^{-1}$  (O—H $\cdots$ N, br), 1695  $\text{cm}^{-1}$  (C=O, s), 1557  $\text{cm}^{-1}$  (Amide II, s).

#### **5.2.2.11 Synthesis of 2-amino-5-(3-pyridyl)pyrimidine/dodecanedioic acid (2:1), SR3-e**

A mixture of 2-propionamido-5-bromopyridine (0.20 g, 1.16 mmol) and dodecanedioic acid (0.134 g, 0.581 mmol) in ethanol was refluxed at 40 °C for 1 hr. The solution was immediately cooled to room temperature, whereupon the product crystallizes out. It was filtered and dried. For X-ray diffraction purposes, single crystals

were grown by slow evaporation of an ethanolic solution at room temperature. Colorless, block-shaped crystals were obtained after 3 days. M. P. 140—142°C; IR  $\nu$  2415  $\text{cm}^{-1}$ , 1904  $\text{cm}^{-1}$  (O—H $\cdots$ N, br), 1695  $\text{cm}^{-1}$  (C=O, s), 1590  $\text{cm}^{-1}$  (Amide II, s).

#### ***5.2.2.12 Synthesis of haloperidol/succinate-suberic acid (1:1:1), SR4-c***

A mixture of haloperidol (0.50 g, 1.33 mmol) and suberic acid (0.232 g, 0.437 mmol) in methylene chloride was refluxed at 50 °C for 1 hr. The solution was immediately cooled to room temperature, whereupon the product crystallizes out. It was filtered and dried. For X-ray diffraction purposes, single crystals were grown by slow evaporation of an ethyl acetate solution at room temperature. Colorless, block-shaped crystals were obtained after 3 days. M. P. 130—132°C; IR  $\nu$  3322  $\text{cm}^{-1}$ , 2525  $\text{cm}^{-1}$ , 1932  $\text{cm}^{-1}$ , 1704  $\text{cm}^{-1}$ , 1679  $\text{cm}^{-1}$ , 1544  $\text{cm}^{-1}$ .

### ***5.2.3 Solubility studies***

Solubility studies involve the determination of a solubility standard curve of the ligand using UV spectroscopy and then calculating the concentration of the ligand on dissolution of the co-crystal. Studies were carried out in a neutral aqueous medium as well as in pH 6.8 buffer solution.

#### ***5.2.3.1 Determination of solubility standard curve for the ligand***

A known mass of the API mimic was allowed to stir in a known volume of deionized water/buffer solution kept over a water bath at room temperature (20-22 °C) for 24 hrs, 48 hrs, and 72 hrs to determine the time for dissolution to reach equilibrium. After each trial, the stirred solution was filtered and the solution concentration was calculated. The solubility was found to increase from 24 hrs to 48 hrs, but no significant difference is noted between 48 hrs and 72 hrs. Hence it was assumed that the solution attained equilibrium concentration at 48 hrs, and so all studies were performed at 48 hrs.

The filtered equilibrium solution of the ligand was subjected to serial dilutions and the absorbance recorded via UV spectroscopy. Absorbance data at  $\lambda_{\text{max}}$  were then plotted against the corresponding concentrations to obtain the standard curve for the

ligand. While choosing the  $\lambda_{\max}$  for the ligand, care was taken as not to overlap it with the  $\lambda_{\max}$  from the aliphatic dicarboxylic acids used as co-crystallizing agents.

#### ***5.2.3.2 Determination of solubility of co-crystals/salts***

The co-crystals/salts of each API mimic was stirred separately in deionized water/buffer solution over water bath at room temp. Aliquots were drawn at 48 hrs, filtered, and the filtrate subjected to UV analysis. The absorbance of the solution at the wavelength corresponding to the  $\lambda_{\max}$  for the ligand is noted and the standard curve for the ligand is employed to calculate the equilibrium concentration of the ligand. The concentrations obtained were plotted for comparative study of solubility.

#### ***5.2.4 Single crystal X-ray crystallography***

X-ray data were collected on a Bruker SMART APEX or a SMART 1000 diffractometer using Mo K $\alpha$  radiation and, where noted, were corrected for absorption using the multiscan procedure implemented by SADABS. Data were collected using SMART. The relevant X-ray data are summarized in Table 5.3 and labeling schemes and thermal ellipsoids for all structures are shown in Figures 5.3, 5.6, 5.7, 5.15, and 5.20.

## 5.3 Results and Discussion

**Table 5.2** IR stretching frequencies ( $\text{cm}^{-1}$ ) of salts and co-crystals under study.

	Acids	co-crystals			salt
		SR1	SR2	SR3	SR4
		2-acetamido-5-bromopyridine	2-propiamido-5-bromopyridine	2-amino-5-(3-pyridyl)pyrimidine	haloperidol
<b>a</b>	<b>Succinic acid</b>	3237, 2452, 1870, 1707, 1520	3259, 2529, 1863, 1702, 1580	3322, 3166, 2378, 1887, 1697, 1605	3281, 2431, 1904, 1679, 1589
<b>b</b>	<b>Adipic acid</b>	3241, 2556, 1831, 1687, 1515	3260, 2476, 1904, 1687, 1536	3301, 3126, 2476, 1892, 1695, 1596	3154, 2443, 1945, 1703, 1687, 1573
<b>c</b>	<b>Suberic acid</b>	3248, 2513, 1851, 1704, 1531	3255, 2597, 1816, 1700, 1565	3301, 3150, 2410, 1912, 1687, 1593	3322, 2525, 1932, 1704, 1679, 1544
<b>d</b>	<b>Sebacic acid</b>	3256, 2484, 1863, 1704, 1536	3250, 2609, 1901, 1697, 1560	3289, 3150, 2406, 1904, 1695, 1557	3334, 2521, 1928, 1711, 1683, 1507
<b>e</b>	<b>Dodecanedioic acid</b>	3244, 2496, 1847, 1699, 1520	3269, 2512, 1863, 1704, 1531	3305, 3146, 2415, 1904, 1695, 1590	3204, 2509, 1894, 1700, 1691, 1587

### 5.3.1 Crystal Structures

A summary of the crystallographic information for the salts and co-crystals are presented in the Appendix A and all the hydrogen-bond geometries are listed in Table 5.3.

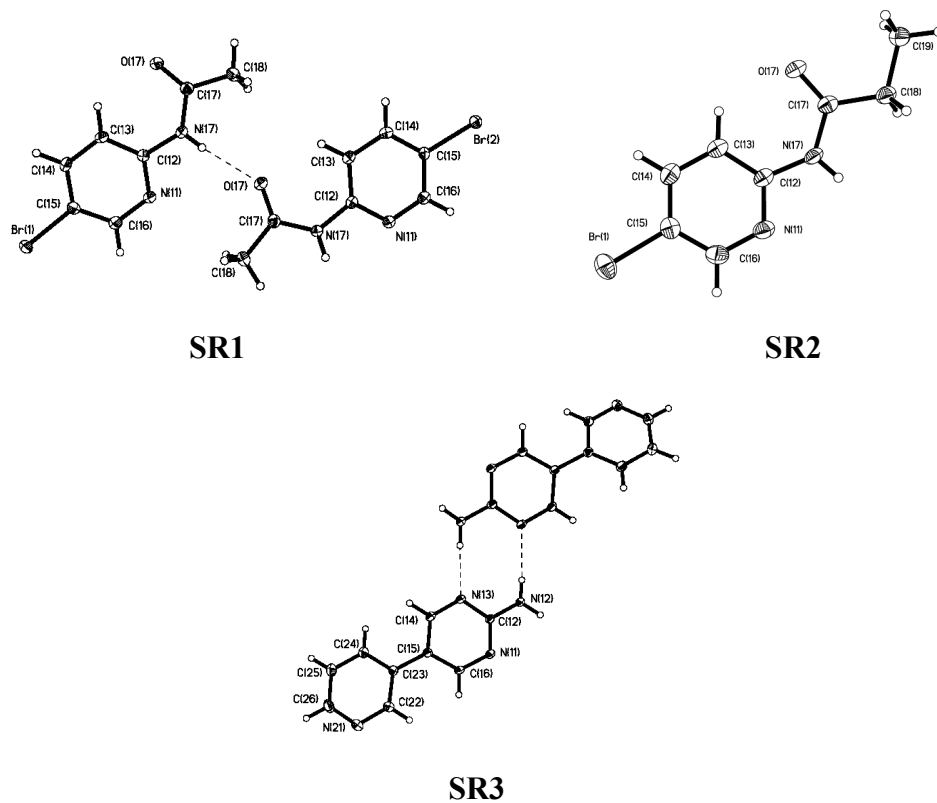
**Table 5.3** Hydrogen-bond geometries for the ligands, salts, and co-crystals under study.

Structure	D-H...A	d(D-H)/Å	d(H...A)/Å	d(D...A)/Å	<(DHA)/°
<b>SR1<sup>i</sup></b>	N172-H172...O171#1	0.86(3)	2.10(2)	2.946(2)	167(2)
	N171-H171...O172	0.80(3)	2.13(3)	2.925(2)	174(2)
<b>SR2<sup>ii</sup></b>	N(17)-H(17)...O(17)#1	0.84(4)	2.05(4)	2.858(3)	161(3)
<b>SR3<sup>iii</sup></b>	N121-H12A1...N132	0.90(2)	2.15(2)	3.0507(17)	174(2)
	N122-H12A2...N131	0.90(2)	2.13(2)	3.0288(17)	174(2)
	N121-H12B1...N112#1	0.91(2)	2.12(2)	3.0301(17)	176(2)
	N122-H12B2...N111#2	0.87(2)	2.18(2)	3.0466(17)	175(2)
<b>SR1-a<sup>iv</sup></b>	O(21)-H(21)...N(11)	0.73(4)	1.99(4)	2.716(4)	174(5)
	N(12)-H(12)...O(22)	0.77(4)	2.13(4)	2.900(4)	171(4)
<b>SR1-e<sup>v</sup></b>	N(12)-H(12)...O(22)	0.97(4)	1.91(4)	2.870(3)	173(3)
	O(21)-H(21)...N(11)	0.83(4)	1.94(4)	2.737(3)	159(4)
<b>SR2-a<sup>vi</sup></b>	O311-H311...N111	0.84	1.87	2.705(12)	171.6
	O312-H312...N112	0.84	1.87	2.705(12)	174.1
	O313-H313...N113	0.84	1.85	2.689(14)	172.9
	O314-H314...N114	0.84	1.84	2.677(13)	177.8
	N171-H171...O321	0.88	2.02	2.874(17)	162.3
	N172-H172...O322	0.88	2.06	2.887(15)	156.7
	N173-H173...O323	0.88	2.06	2.917(18)	163.0
	N174-H174...O324	0.88	2.06	2.921(18)	166.2
	O341-H341...N211	0.84	1.84	2.672(12)	169.5
	O342-H342...N212	0.84	1.88	2.711(11)	171.2
	O343-H343...N213	0.84	1.88	2.714(12)	173.1
	O344-H344...N214	0.84	1.86	2.699(13)	176.2
	N271-H271...O331	0.88	2.02	2.878(16)	164.8
	N272-H272...O332	0.88	2.00	2.867(16)	169.3
	N273-H273...O333	0.88	2.03	2.900(18)	170.1
	N274-H274...O334	0.88	2.07	2.926(18)	163.1
<b>SR2-b<sup>vii</sup></b>	N(12)-H(12)...O(21)	0.86(2)	2.01(2)	2.8720(19)	173(2)
	O(22)-H(22)...N(11)	0.74(3)	1.94(3)	2.6697(19)	170(3)
<b>SR2-c<sup>viii</sup></b>	O(21)-H(21)...N(11)	0.77(2)	1.98(2)	2.7538(19)	174(2)
	N(12)-H(12)...O(22)	0.75(2)	2.12(2)	2.8686(19)	177(2)
<b>SR2-d<sup>ix</sup></b>	O(31)-H(31)...N(11)	0.77(2)	1.99(2)	2.7522(17)	174(2)
	N(12)-H(12)...O(32)	0.82(2)	2.01(2)	2.8209(17)	169(2)
<b>SR2-e<sup>x</sup></b>	N(12)-H(12A)...O(32)	0.81(2)	2.04(2)	2.8561(17)	178(2)
	O(31)-H(31)...N(11)	0.71(3)	2.03(3)	2.7405(17)	173(3)
<b>SR3-a<sup>xi</sup></b>	O(51)-H(51)...N(11)	0.98(3)	1.64(3)	2.618(2)	174(3)
	O(54)-H(54)...N(31)	0.98(3)	1.69(3)	2.662(2)	171(3)
	N(12)-H(12A)...O(52)	0.92(3)	1.96(3)	2.873(3)	171(3)
	N(12)-H(12B)...N(41)#1	0.97(3)	2.01(3)	2.973(3)	173(2)
	N(32)-H(32A)...O(55)	1.03(3)	1.86(3)	2.871(3)	168(2)
	N(32)-H(32B)...N(21)#2	0.93(3)	2.12(3)	3.038(3)	171(3)



Structure	D-H...A	d(D-H)/Å	d(H...A)/Å	d(D...A)/Å	<(DHA)/°
<b>SR3-b</b> <sup>xii</sup>	O(31)-H(31)...N(21)	0.91(2)	1.76(2)	2.6714(15)	174.8(19)
	N(12)-H(12B)...N(13)#2	0.885(18)	2.113(18)	2.9965(16)	176.2(16)
	N(12)-H(12A)...N(11)#3	0.896(18)	2.161(18)	3.0554(16)	176.6(16)
<b>SR3-c</b> <sup>xiii</sup>	O(31)-H(31)...N(21)	0.95(2)	1.70(2)	2.6516(16)	174.9(17)
	N(12)-H(12A)...N(13)#2	0.873(18)	2.188(19)	3.0603(18)	177.7(17)
	N(12)-H(12B)...N(11)#3	0.903(19)	2.120(19)	3.0222(18)	176.1(15)
<b>SR3-d</b> <sup>xiv</sup>	O(31)-H(31)...N(21)	0.919(19)	1.741(19)	2.6509(13)	170.2(16)
	N(12)-H(12A)...N(11)#2	0.907(15)	2.150(15)	3.0546(13)	175.3(13)
	N(12)-H(12B)...N(13)#3	0.917(16)	2.101(16)	3.0176(14)	177.6(14)
<b>SR3-e</b> <sup>xv</sup>	O(31)-H(31)...N(21)	0.90(2)	1.76(2)	2.6486(13)	169.4(19)
	N(12)-H(12A)...N(11)#2	0.864(15)	2.179(16)	3.0400(14)	173.9(15)
	N(12)-H(12B)...N(13)#3	0.891(16)	2.118(16)	3.0095(14)	178.5(14)
<b>SR4-c</b> <sup>xvi</sup>	N(21)-H(21)...O(51)	0.905(13)	1.825(14)	2.7120(11)	165.7(12)
	O(41)-H(41)...O(52)	0.883(16)	1.749(16)	2.5730(11)	154.2(14)
	O(24)-H(24)...O(52)#3	0.793(16)	2.030(16)	2.7661(11)	154.2(15)

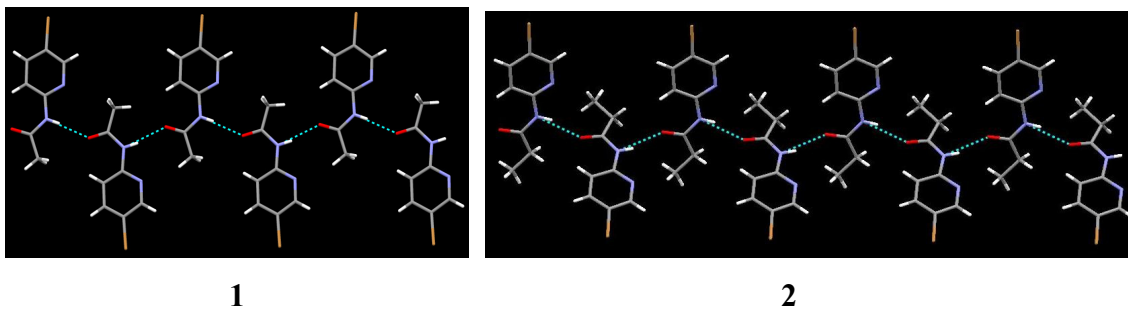
i) #1 x+1,y+1,z ii) #1 x-1/2,y,-z+3/2 iii) #1 x+1,y,z+1 #2 x-1,y,z-1 iv) #1 -x-1,-y,-z v) #1 -x+3,-y+2,-z  
vi) n/a vii) #1 -x+2,-y,-z+2 viii) #1 -x-1,-y+1,-z ix) #1 -x,-y+1,-z+1 x) #1 -x-2,-y,-z+1 xi) #1 x-1,-  
y+1/2,z-1/2 #2 x+1,-y+3/2,z+1/2 xii) #1 -x+1,-y+2,-z+1 #2 -x,y-1/2,-z+3/2 #3 -x,y+1/2,-z+3/2 xiii) #1 -  
x-1,-y-1,-z #2 -x+2,-y,-z+1 #3 -x+3,-y+1,-z+1 xiv) #1 -x+3,-y-1,-z #2 -x,-y,-z+1 #3 -x-1,-y+1,-z+1 xv)  
#1 -x-1,-y+3,-z #2 -x+2,-y+1,-z+1 #3 -x+3,-y,-z+1 xvi) #1 -x,-y+2,-z+1 #2 -x+1,-y,-z #3 x+1,y,z

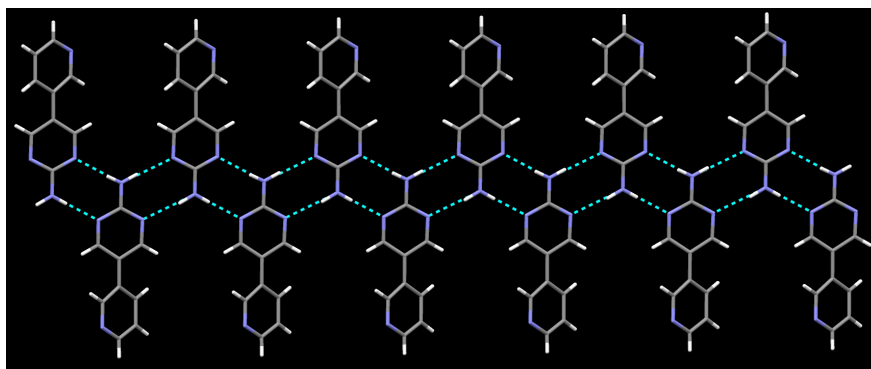


**Figure 5.4** Thermal ellipsoid plots (50 % probabilities) and labeling schemes for 2-acetamido-5-bromopyridine **SR1**, 2-propionamido-5-bromopyridine **SR2**, and 2-amino-5-(3-pyridyl)pyridine **SR3**.

### 5.3.1.1 Crystal structure of APIs **SR1**, **SR2**, and **SR3**.

The crystal structures of the APIs 2-acetamido-5-bromopyridine **SR1**, 2-propionamido-5-bromopyridine **SR2**, 2-amino-5-(3-pyridyl)pyridine **SR3** are described in the sections 2.3.1, 2.3.2, and 4.3.2.1 respectively, (Figure 5.5).





3

**Figure 5.5** 1-D strands of ligands connected via N-H---O (SR1 and SR2) and N-H---N (SR3) hydrogen bonds.

### 5.3.1.2 Crystal structure of haloperidol, SR4<sup>30</sup>

The crystal structure of SR4 shows the molecules of haloperidol connected via intermolecular interaction between the hydroxyl group of one haloperidol to piperidinyln of neighboring haloperidol through O-H---N hydrogen bonds giving rise to stacked 1-D strands, (Figure 5.6).

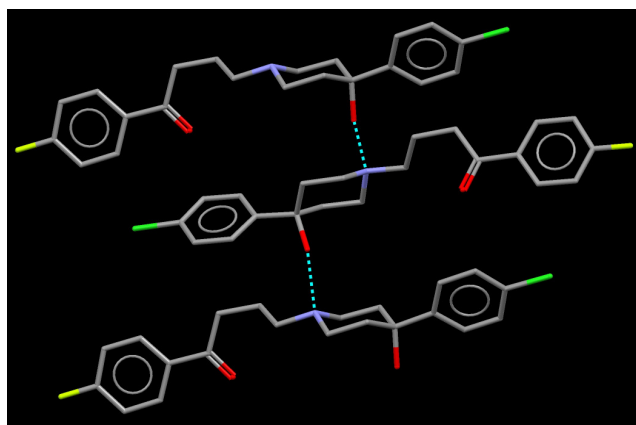
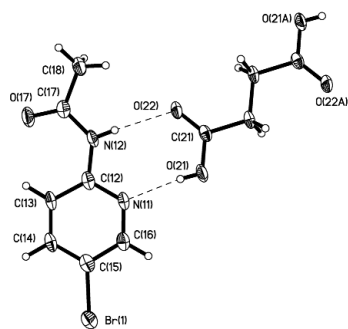
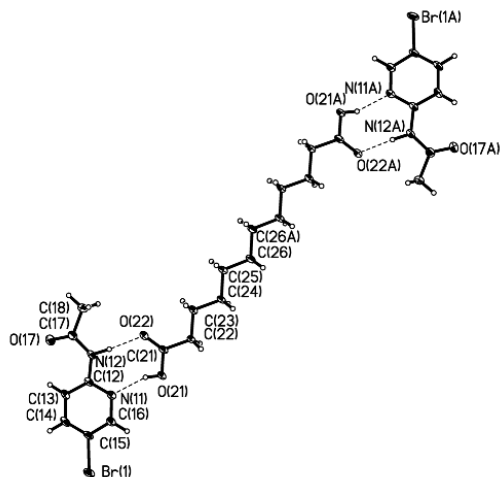


**Figure 5.6** 1-D strands of haloperidol SR4 connected via O-H...N hydrogen bonding.

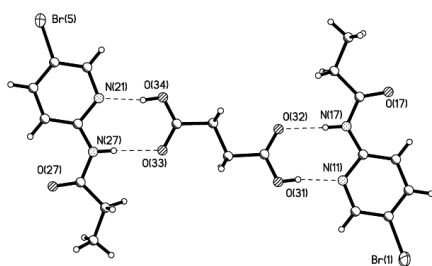


SR1-a

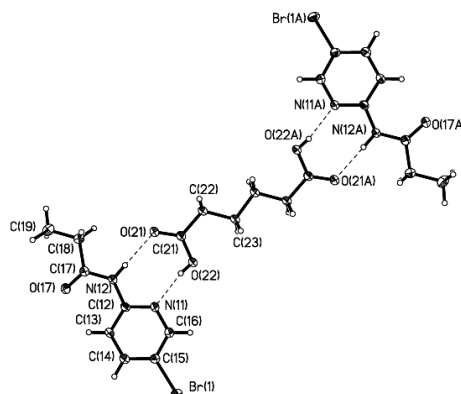


SR1-e

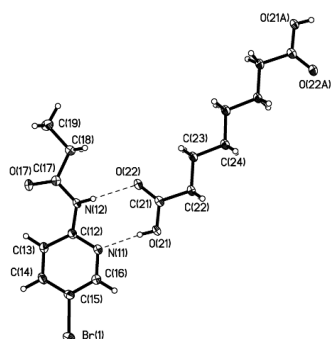
**Figure 5.7** Thermal ellipsoid plots (50 % probabilities) and labeling schemes for **SR1-a** and **SR1-e**.



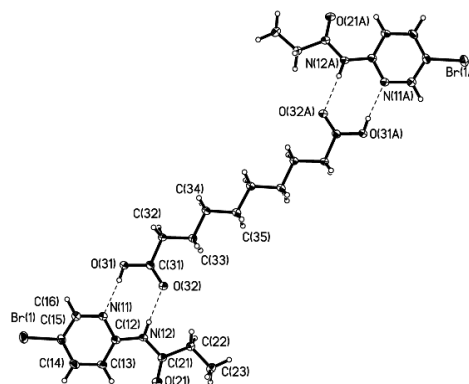
SR2-a



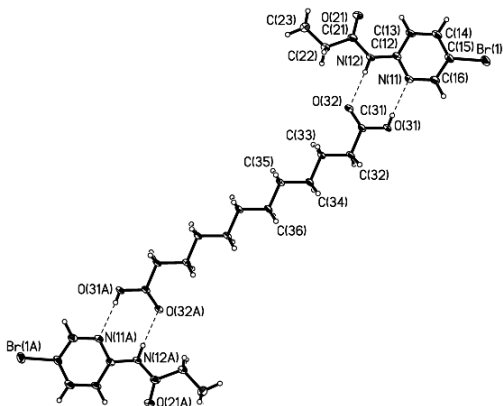
SR2-b



SR2-c



SR2-d



**SR2-e**

**Figure 5.8** Thermal ellipsoid plots (50 % probabilities) and labeling schemes for co-crystals of 2-propiamido-5-bromopyridine **SR2**.

### 5.3.1.3 Crystal structures of *SR1-a*, *SR1-e*, *SR2-c*, *SR2-d*, and *SR2-e*

The crystal structures of **SR1-a**, **SR1-e**, **SR2-c**, **SR2-d** and **SR2-e** show 2:1 co-crystals comprising of the neutral API mimic and one diacid connected via the primary synthons  $\text{N-H}\cdots\text{O}$  and  $\text{N}\cdots\text{H-O}$  hydrogen bonds. The bromine atom present in the ligand does not contribute in any significant interaction, Figure 5.9 – 5.13.

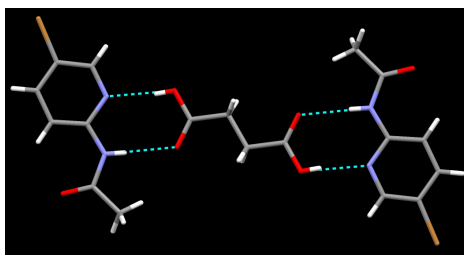


**Figure 5.9** Primary hydrogen bonding in the crystal structure of **SR1-a**.

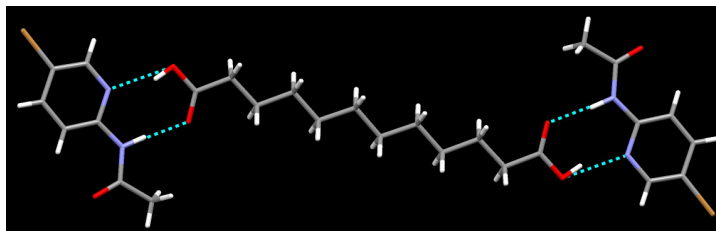


**Figure 5.10** Primary hydrogen bonding in the crystal structure of **SR1-e**.

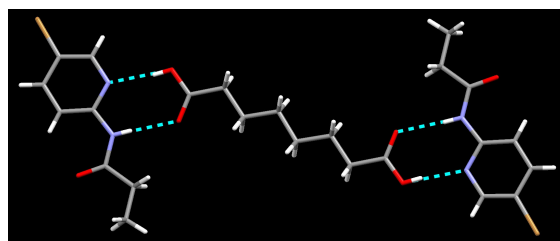


**Figure 5.11** Primary hydrogen bonding in the crystal structure of **SR2-c**.

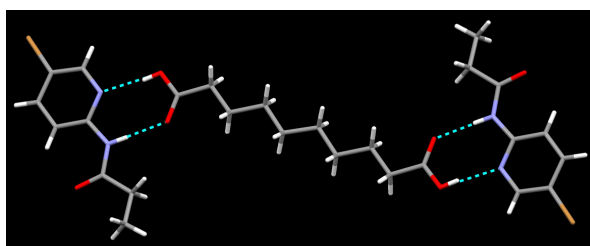


**Figure 5.12** Primary hydrogen bonding in the crystal structure of **SR2-d**.

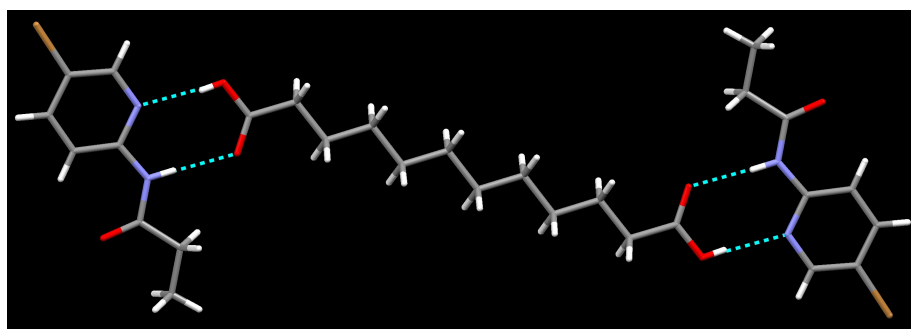


**Figure 5.13** Primary hydrogen bonding in the crystal structure of **SR2-e**.

#### **5.3.1.4** *Crystal structures of SR2-a and SR2-b*

The crystal structures of **SR2-a** and **SR2-b** display primary motifs composed of the ligand 2-propionamido-5-bromopyridine and the succinic acid or adipic acid in a 2:1 ratio. The primary synthons in these structures are  $\text{N-H}\cdots\text{O}$  and  $\text{N}\cdots\text{H}-\text{O}$  hydrogen bonds between the propionamidopyridine moieties and the carboxylic acid. The secondary  $\text{Br}\cdots\text{O}-\text{H}$  interaction between the carboxylic O-H and the bromine atom from the ligand extend the architecture into a ribbon-like structure, (Figure 5.14 – 5.15).

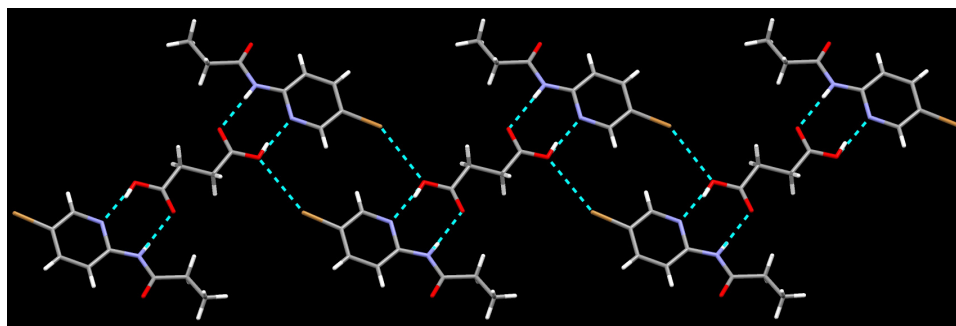


**Figure 5.14** 1-D chain comprising of four component square-like architecture in **SR2-a**.

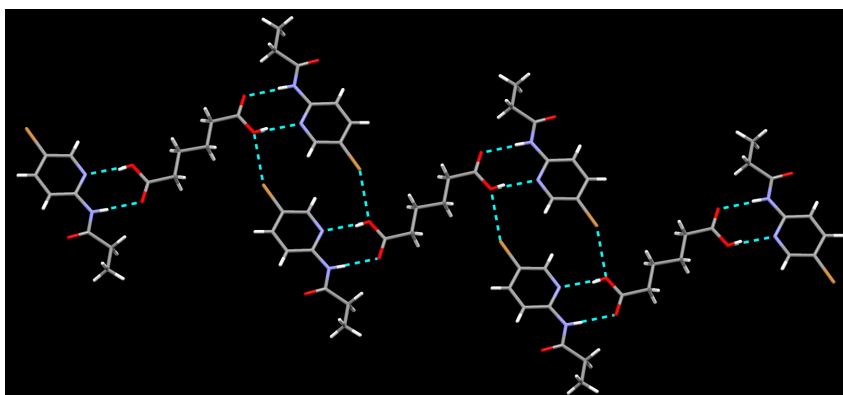


**Figure 5.15** 1-D chain comprising of four component square-like architecture in **SR2-b**.

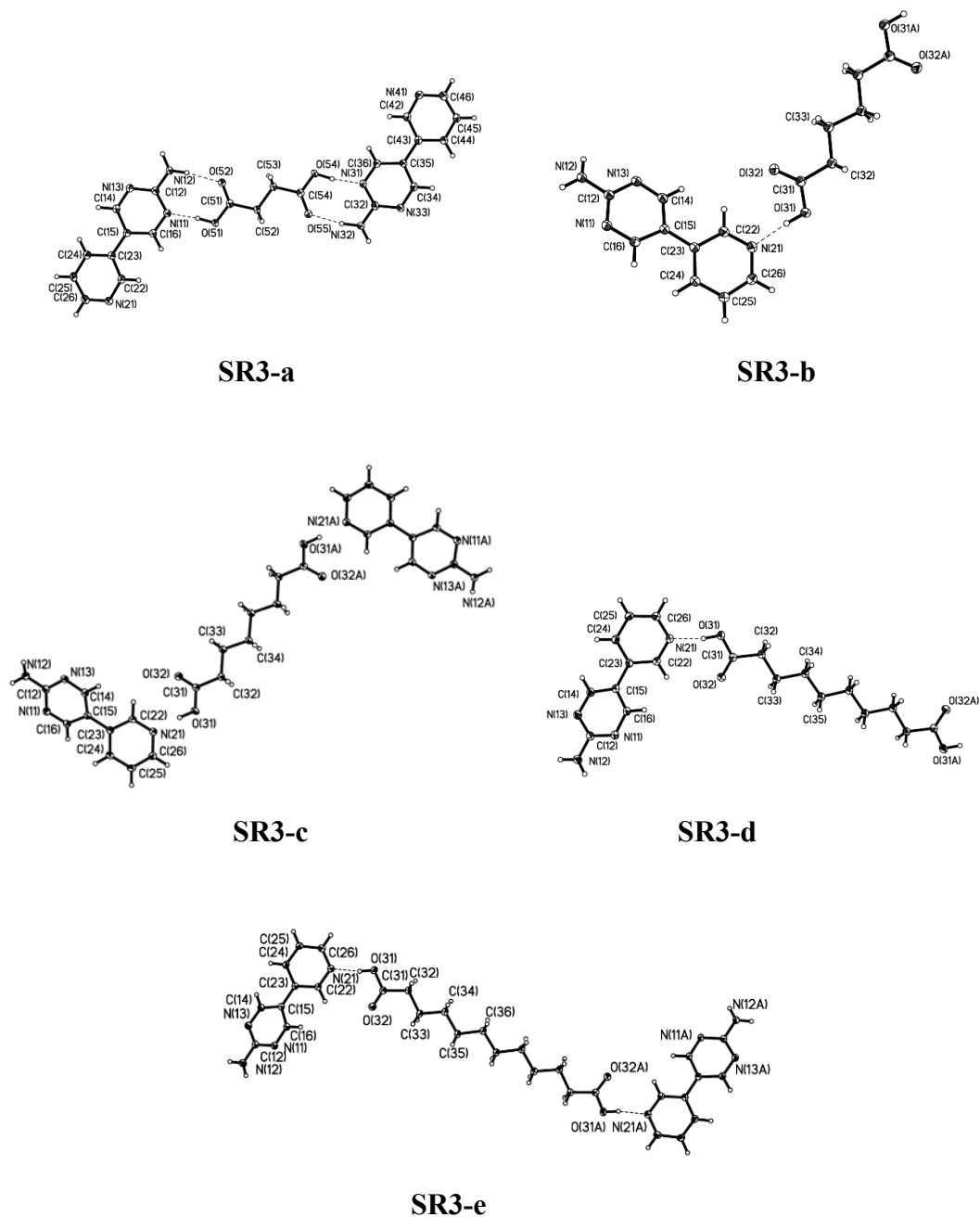


**Figure 5.16** Thermal ellipsoid plots (50 % probabilities) and labeling schemes for **SR3-a-e**.

### 5.3.1.5 Crystal structures of *SR3-a*

The crystal structure of **SR3-a** displays a primary motif composed of the ligand 2-amino-5-(3-pyridyl)pyrimidine and succinic acid. The primary synthons are the O–H···N interaction between the hydroxyl proton of the acid and the pyrimidyl-N of the ligand, and a N–H···O interaction between the amino proton of the pyrimidine moiety and the



carbonyl oxygen of the acid. The motif is extended via N–H···N interactions between the anti-amino N–H and pyridyl–N to give a zigzag network, (Figure 5.17).

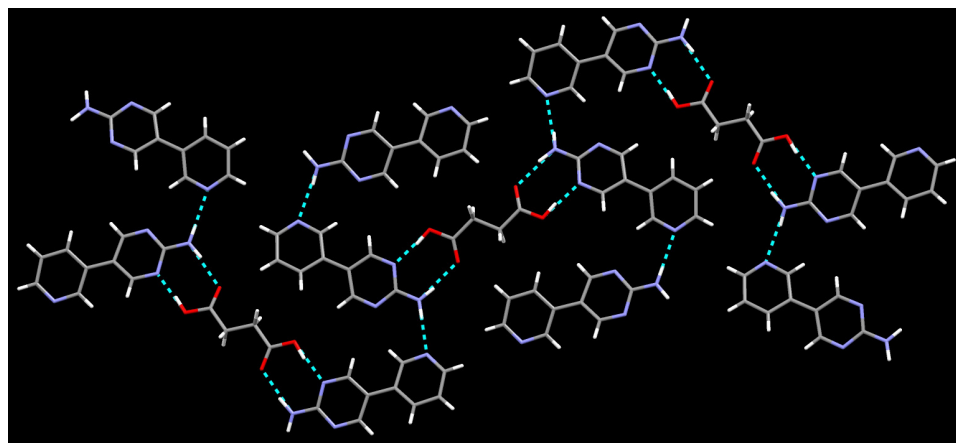


**Figure 5.17** 1-D sheets of **SR3-a** showing N–H···O, O–H···N, and N–H···N binding motifs.

#### **5.3.1.6 Crystal structures of *SR3-b*, *SR3-c*, *SR3-d*, and *SR3-e***

The crystal structure of **SR3-b**, **SR3-c**, **SR3-d** and **SR3-e** displays a primary motif composed of the ligand 2-amino-5-(3-pyridyl)pyrimidine and adipic acid, suberic acid, sebacic acid, or dodecanedioic acid. The primary synthons in these structures are O–H···N hydrogen bond between the hydroxyl proton of the acid and the pyridyl–N of the ligand. The motif is extended into 2-D network via self-complementary N–H···N interactions between the amino N–H and pyrimidyl–N of neighboring aminopyrimidine moieties, (Figure 5.18 – 5.20).

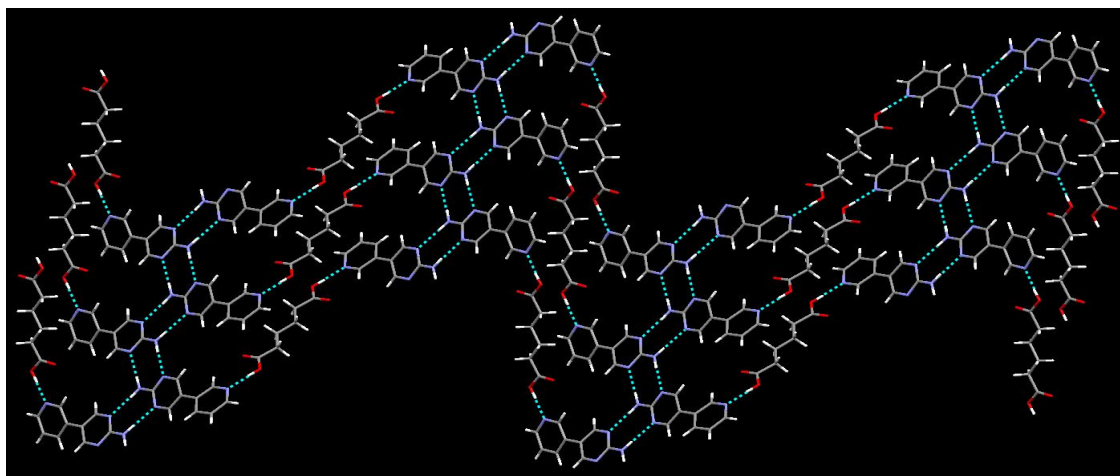


**Figure 5.18** 2-D zigzag sheets of **SR3-b** showing O-H---N and N-H---N binding motifs.

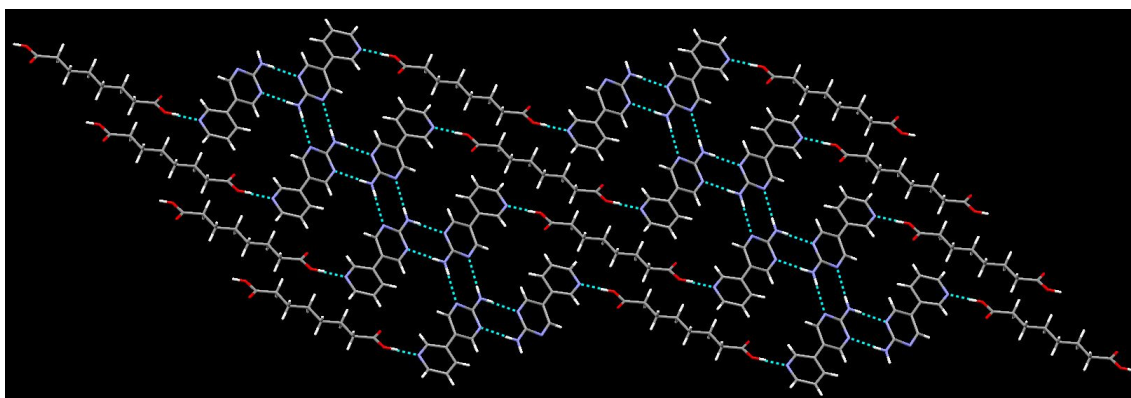


**Figure 5.19** 2-D zigzag sheets of **SR3-c** showing O-H---N and N-H---N binding motifs.

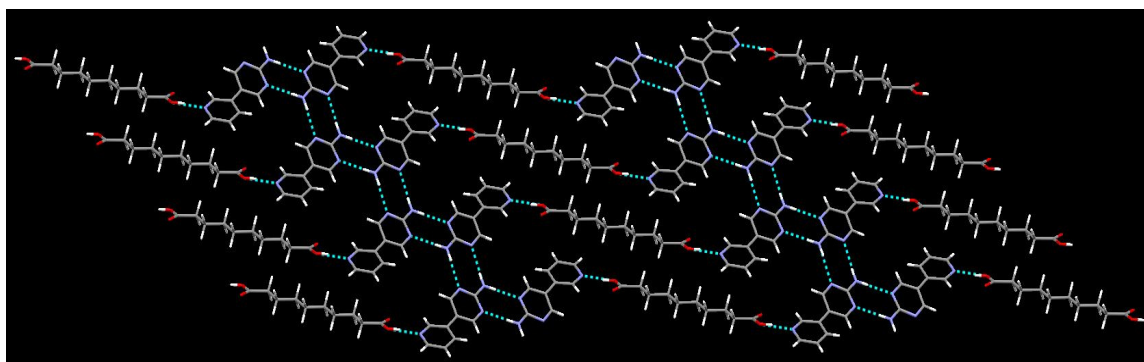


**Figure 5.20** 2-D zigzag sheets of **SR3-d** showing O-H---N and N-H---N binding motifs.

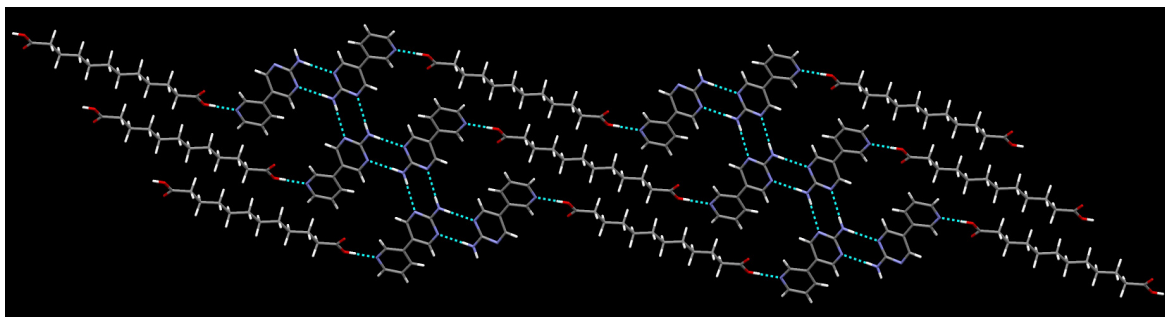


**Figure 5.21** 2-D zigzag sheets of SR3-e showing O-H...N and N-H...N binding motifs.

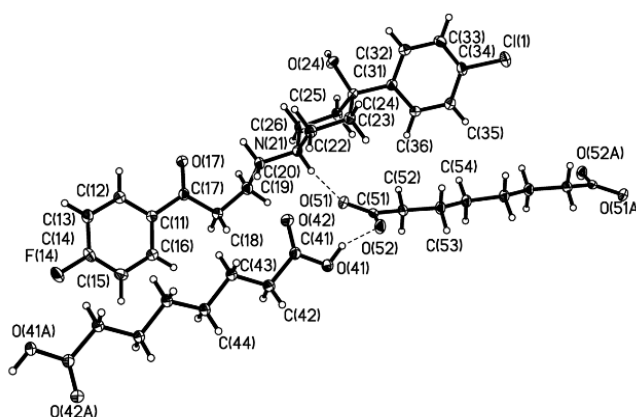


**Figure 5.22** Thermal ellipsoid plots (50 % probabilities) and labeling schemes for SR4-c.

### 5.3.1.7 Crystal structures of SR4-c

The crystal structure of SR4-c displays a primary motif composed of protonated haloperidol linked with a succinate ion via charge-assisted N-H<sup>+</sup>...O<sup>-</sup> and O-H...O<sup>-</sup> hydrogen bonds with N(21)-H(21)...O(51) and O(24)-H(24)...O(52) distances of 2.7120(11) and 2.7661(11) Å, respectively. In addition, there is a free carboxylic acid which is connected to the carboxylate ion moiety via complementary O-H...O<sup>-</sup> hydrogen-bond interactions producing a 2-D network, (Figure 5.23).

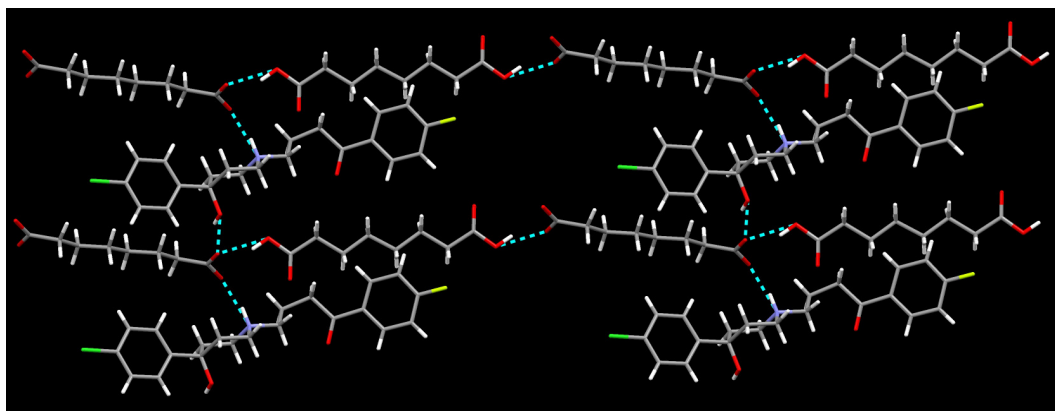


**Figure 5.23** 2-D network of SR4-c showing N–H<sup>+</sup>···O<sup>-</sup>, O–H···O<sup>-</sup> and O–H---O<sup>-</sup> binding motifs.

### 5.3.2 Standard curves for the dissolution of API mimics

#### 5.3.2.1 Standard curve for dissolution of SR1 in deionized water

The equilibrium solubility of 2-acetamido-5-bromopyridine SR1 in deionized water at 48 hrs was found to be 0.5100 mg/mL ( $\pm 0.0091$ ).

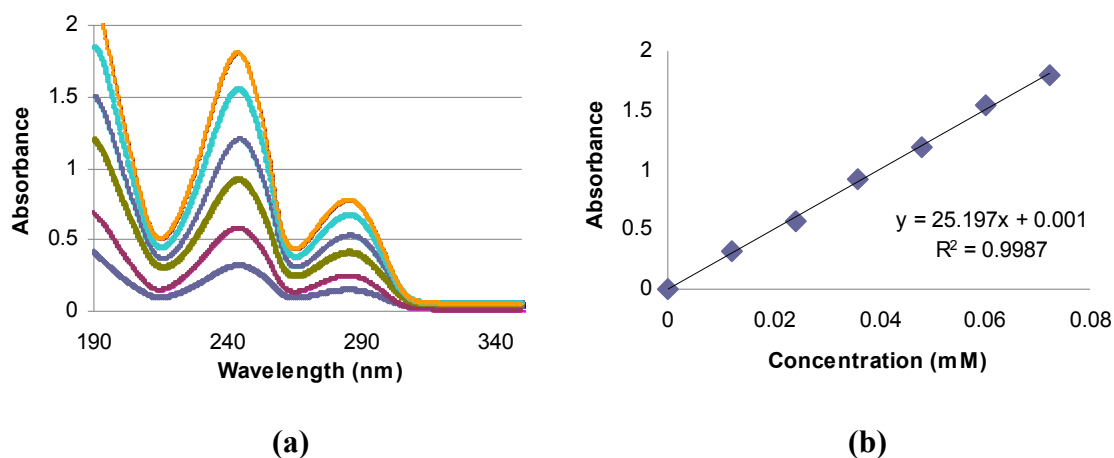


**Figure 5.24** Solubility curves for dissolution of 2-acetamido-5-bromopyridine SR1 in water after 48 hrs. (a) Wavelength vs. absorbance curve @244 nm in different concentrations (mM). (b) Standard curve for equilibrium solubility.

### 5.3.2.2 Standard curve for dissolution of SR2 in deionized water

The equilibrium solubility of 2-propiamido-5-bromopyridine **SR2** in deionized water at 48 hrs is found to be 0.3395 mg/mL ( $\pm 0.0139$ ).

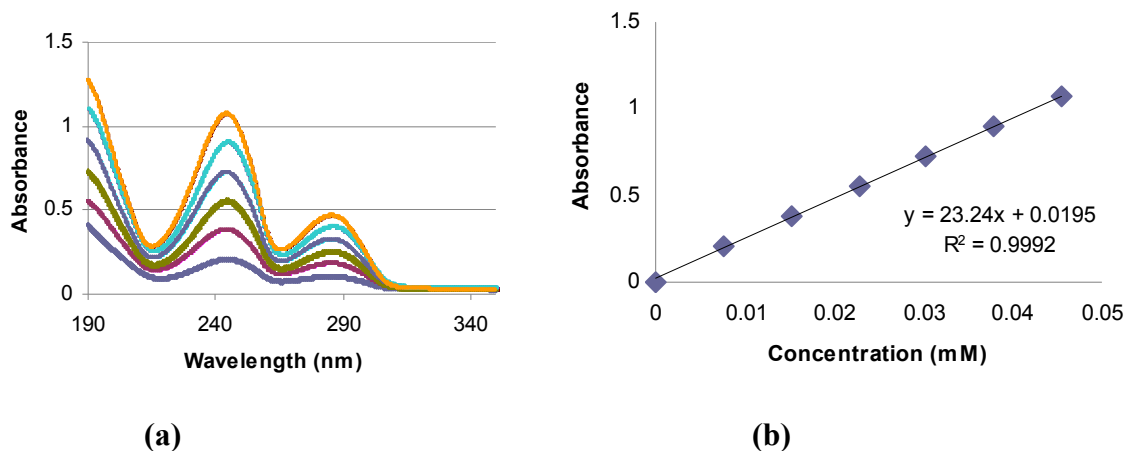


**Figure 5.25** Solubility curves for dissolution of 2-propiamido-5-bromopyridine **SR2** in water after 48 hrs. (a) Wavelength vs. absorbance curve @244 nm in different concentrations (mM). (b) Standard curve for equilibrium solubility.

### 5.3.2.3 Standard curve for dissolution of SR3 in pH 6.8 buffer

The equilibrium solubility of 2-amino-5-(3-pyridyl)pyrimidine **SR3** in pH 6.8 buffer solution at 48 hrs is found to be 3.7540 mg/mL ( $\pm 0.1018$ ).

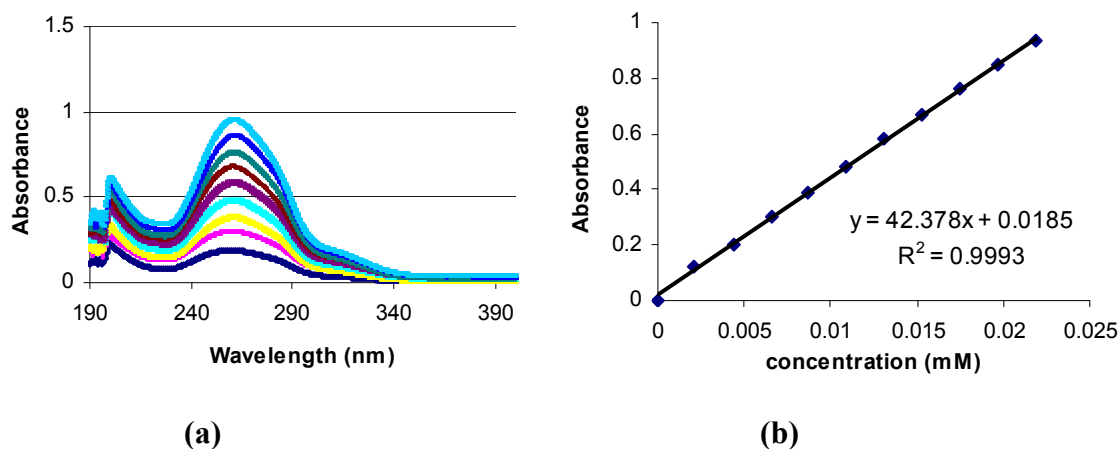


**Figure 5.26** Solubility curves for dissolution of 2-amino-5-(3-pyridyl)pyrimidine **SR3** in pH 6.8 buffer water after 48 hrs. (a) Wavelength vs. absorbance curve @244 nm in different concentrations (mM). (b) Standard curve for equilibrium solubility.

### 5.3.2.4 Standard curve for dissolution of SR4 in pH 6.8 buffer solution

The equilibrium solubility of haloperidol **SR4** in pH 6.8 buffer solution at 48 hrs is found to be 0.0738 mg/mL ( $\pm 0.0039$ ).

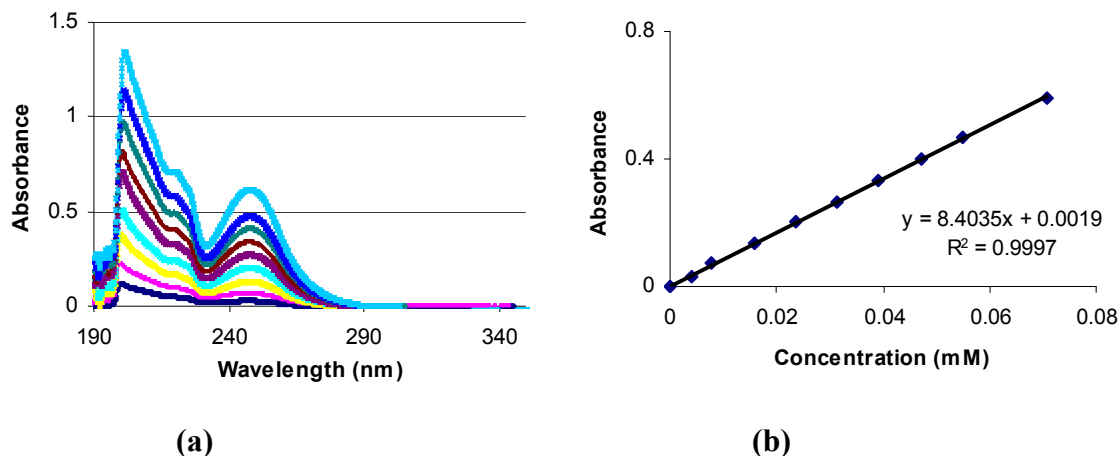


**Figure 5.27** Solubility curves for dissolution of haloperidol **SR4** in pH 6.8 buffer solution after 48 hrs. (a) Wavelength vs. absorbance curve @248 nm in different concentrations (mM). (b) Standard curve for equilibrium solubility.

### 5.3.3 Equilibrium dissolution studies

#### 5.3.3.1 Equilibrium dissolution of 2-acetamido-5-bromopyridine (SR1) co-crystals in water

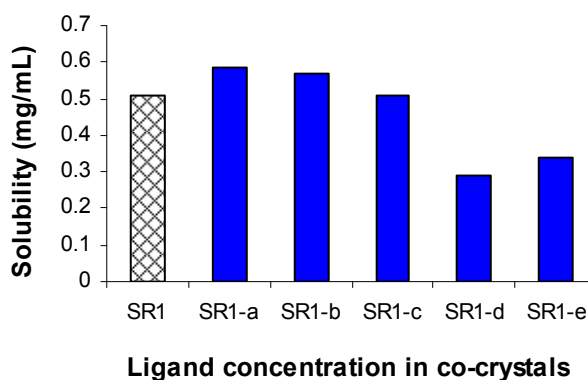


**Figure 5.28** Comparative equilibrium solubilities of **SR1** and its co-crystals.

The results show that there is slight change in solubility of 2-acetamido-5-bromopyridine upon co-crystallization with succinic and adipic acid, whereas a decrease in solubility is observed with sebacic acid and dodecanedioic acid, (Table 5.4). This

minimal solubility change can be explained on the basis of the crystal packing of these co-crystals. Both crystal structures of **SR1-a** and **SR1-e** show similar crystal packing with each of the acid binding with two APIs in a zero-dimensional architecture, (Figure 5.9-5.10). Since there is no extension of network beyond the periphery of these three molecules, the solubility enhancement is not expected to change much.

**Table 5.4** Comparative solubilities of **SR1** and its co-crystals.

Key	Sample	Solubility (mg/mL)	Change in solubility
API	SR1	0.510 ± 0.0091	-
API + Succinic acid	SR1-a	0.5872 ± 0.0107	+15%
API + Adipic acid	SR1-b	0.5703± 0.0059	+12%
API + Suberic acid	SR1-c	0.5071± 0.0058	-6%
API + Sebacic acid	SR1-d	0.2903± 0.0073	-43%
API + Dodecanedioic acid	SR1-e	0.3387± 0.0161	-34%

### 5.3.3.2 Equilibrium dissolution of 2-propionamido-5-bromopyridine (SR2) co-crystals in water

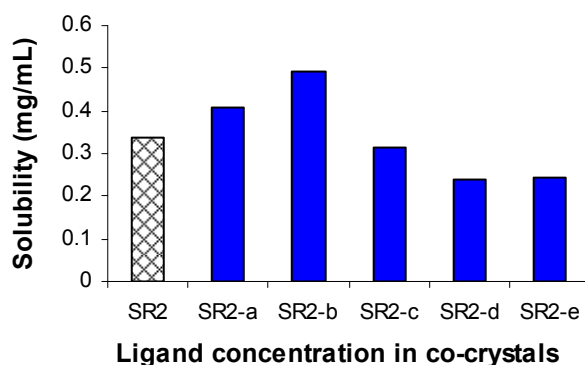


**Figure 5.29** Comparative equilibrium solubilities of **SR2** and its co-crystals.

The solubility of the API mimic 2-propionamido-5-bromopyridine itself is almost half compared to the solubility of homologous API 2-acetamido-5-bromopyridine. This might be due to the presence of a methylene group which reduces its solubility in an

aqueous environment. There is slight increase in solubility (+46%) of co-crystals of 2-propionamido-5-bromopyridine compared to that of 2-acetamido-5-bromopyridine (+15%). Again, the solubility gain is seen with co-crystallizing agents succinic and adipic acid, whereas with sebacic acid and dodecanedioic acid a decrease in solubility is noted, (Table 5.5). Upon investigation of the crystal structures, a crystal packing similar to the ones observed for the co-crystals of 2-acetamido-5-bromopyridine is seen for the co-crystals **SR2-c**, **SR2-d**, and **SR2-e**, a zero-dimensional architecture with no propagation of network in space, (Figure 5.11-5.13). However for the co-crystals **SR2-a** and **SR2-b** there is extension of network in one-dimensional space (Figure 5.14-5.15), which might have contributed to a slightly higher aqueous solubility. The lower solubility seen for the co-crystals with sebacic acid and dodecanedioic acid is attributed to the lower aqueous solubility of the co-crystallizing agents themselves.

**Table 5.5** Comparative solubilities of **SR2** and its co-crystals.

Key	Sample	Solubility (mg/mL)	Change in solubility
API	SR2	0.3395± 0.0111	-
API + Succinic acid	SR2-a	0.4073± 0.0113	+20%
API + Adipic acid	SR2-b	0.4939± 0.0028	+46%
API + Suberic acid	SR2-c	0.3143± 0.0166	-7%
API + Sebacic acid	SR2-d	0.2378± 0.0296	-30%
API + Dodecanedioic acid	SR2-e	0.2433± 0.0033	-28%



### 5.3.3.3 Equilibrium dissolution of 2-amino-5-(3-pyridyl)pyrimidine (SR3) co-crystals in pH 6.8 buffer solution

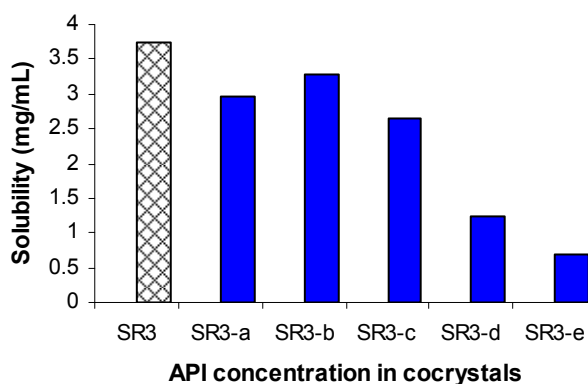


**Figure 5.30** Comparative equilibrium solubilities of **SR3** and its co-crystals.

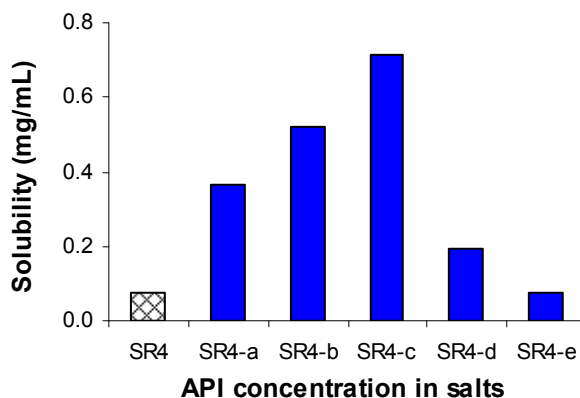
The slight improvement in aqueous solubility for the co-crystals observed for one-dimensional network over zero-dimensional network for the previous APIs prompted us to choose an API capable of propagating the network into 1D or 2D space. The choice of the API 2-amino-5-(3-pyridyl)pyrimidine was made on the basis of its observed ability to form extended 1D networks, hence it may play a role in determining whether the network extension would actually help in altering the aqueous solubility of an API. In addition, the experiments were run in a pH 6.8 buffer solution to cancel out any change in acidity/basicity during the studies.

For the co-crystals of 2-amino-5-(3-pyridyl)pyrimidine, an overall decrease in solubility is observed, (Table 5.6). A decreasing trend in aqueous solubility is seen in the co-crystal series from adipic acid to dodecanedioic acid (-13% to -81%). The succinic acid co-crystal shows an offset from this trend, possibly due to its different crystal packing compared to the ones from the other carboxylic acids, (Figure 5.17). This again, highlights the role of crystal packing in the overall solubility of a compound. The decrease in solubility observed for the co-crystals may be due to the high solubility of the API (3.75 mg/mL) itself. Hence, a proper choice of API with lower solubility and proper co-crystallizing agents may give co-crystals with an extended 1D or 2D network.

**Table 5.6 Comparative solubilities of SR3 and its co-crystals.**

Key	Sample	Solubility (mg/mL)	Change in solubility
API	SR3	3.7540 ± 0.1018	-
API + Succinic acid	SR3-a	2.9578 ± 0.0897	-21%
API + Adipic acid	SR3-b	3.2723 ± 0.0430	-13%
API + Suberic acid	SR3-c	2.6382 ± 0.0646	-30%
API + Sebacic acid	SR3-d	1.2481 ± 0.0502	-67%
API + Dodecanedioic acid	SR3-e	0.6976 ± 0.0789	-81%

#### 5.3.3.4 Equilibrium dissolution of haloperidol (SR4) salts in pH 6.8 buffer solution

**Figure 5.31** Comparative equilibrium solubilities of **SR4** and its salts.

The solubility experiments were carried out with an API with the least solubility (0.0738 mg/mL) among all the API mimics tried so far. Co-crystallization was attempted with this API with the same series of co-crystallizing agents. Haloperidol has a highly basic piperidine-N and a hydroxyl group capable of hydrogen bonding. Out of the three haloperidol complexes (all salts) in the CSD search, one is with an organic compound (saccharin), whereas the remaining were with HCl and HBr. The co-crystallization was carried out in chloroform in an effort to limit proton transfer during the process, however

the results show that the piperidine-N is basic enough to pull the proton from the carboxylic acid even in non-polar chloroform as solvent to give salts/complexes.

Almost all salt/complexes show considerable increase in aqueous solubility compared to the API, (Table 5.7). The highest increase is seen for the complex of the API with suberic acid (867%) whereas for dodecanedioic acid the solubility remained similar to that of API. A parabolic curve is observed for the solubility of the complexes with the solubility increasing from succinic to suberic acid along the series and then decreasing to dodecanedioic acid. This observation may be explained considering the solubility of the co-crystallizing agents complexed with haloperidol (0.0738 mg/mL). From Table 5.1, we see that the solubility of aliphatic dicarboxylic acids decreases from succinic acid (76.6 mg/mL) to suberic acid (8.9 mg/mL) and dodecanedioic acid (0.004 mg/mL). The high solubility difference between succinic acid and the API (haloperidol) may have triggered rapid dissociation of the complex in water. This might have perturbed the equilibrium between the undissociated complex and the dissociated moieties, hence tilting the equilibrium toward more undissociated complex and hence lower solubility is observed for succinic acid complex. The suberic acid with intermediate aqueous solubility might be the right fit on sustaining the equilibrium hence resulting in the highest solubility.

**Table 5.7** Comparative solubilities of SR4 and its salts.

Key	Sample	Solubility (mg/mL)	Change in solubility
API (Haloperidol)	SR4	0.0738 ± 0.0039	-
API + Succinic acid	SR4-a	0.3665 ± 0.0126	+397%
API + Adipic acid	SR4-b	0.5192 ± 0.0237	+604%
API + Suberic acid	SR4-c	0.7133 ± 0.0237	+867%
API + Sebacic acid	SR4-d	0.1952 ± 0.0107	+165%
API + Dodecanedioic acid	SR4-e	0.0759 ± 0.0069	+3%

### 5.3.4 Effect of co-crystallizing agent properties on co-crystals and salts

The solubility and thermal behavior of co-crystals and salts were found to reflect the properties of the co-crystallizing agent they were complexed with. A successful translation of the co-crystallizing agent properties into the API mimics is achieved by their incorporation into their crystalline lattice of the API mimics.

The solubility of the co-crystallizing agents decrease with the increase in molecular weight, the succinic acid having the highest and the dodecanedioic acid having the lowest solubility. The co-crystals of **SR1** and **SR2** with these co-crystallizing acids follow a similar trend with the solubilities decreasing from the co-crystals generated from succinic acid to the dodecanedioic acid. A slight decrease in solubility of succinic acid co-crystal with **SR3** resulting from a different crystal packing compared to other co-crystal in the series. The salts generated from haloperidol **SR4** with the co-crystallizing agent sing a completely different tune, marking the unpredictability of the salt properties, (Figure 5.32).

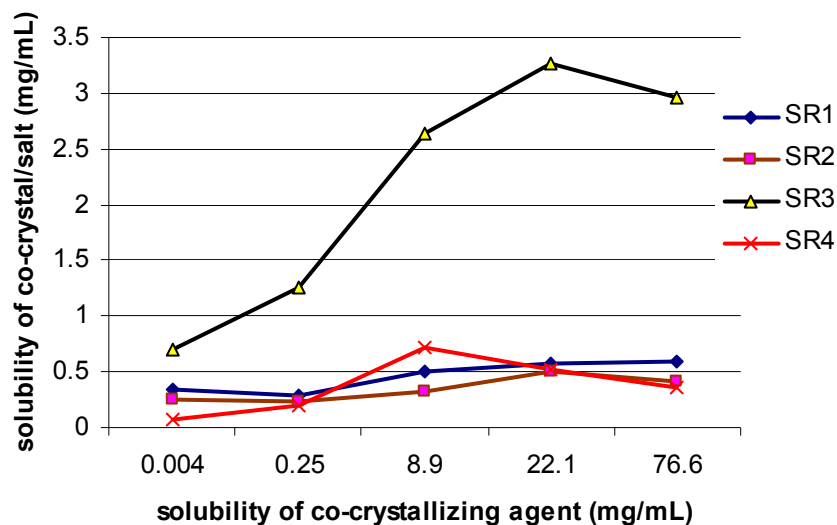


**Figure 5.32** Dependence of co-crystal/salt solubility on the solubility of co-crystallizing agents.

**Table 5.8** Comparative solubilities of co-crystallizing agents and its co-crystals/salts

Diacids		SR1	SR2	SR3	SR4
Dodecanedioic acid	0.004	0.3387	0.2433	0.6976	0.0759
Sebacic acid	0.25	0.2903	0.2378	1.2481	0.1952
Suberic acid	8.9	0.5071	0.3143	2.6382	0.7133
Adipic acid	22.1	0.5703	0.4939	3.2723	0.5192
Succinic acid	76.6	0.5872	0.4073	2.9578	0.3665

Similarly, the melting points of the co-crystallizing agent decreases with the increase in the molecular weight, the succinic acid having the highest and the dodecanedioic acid having the lowest melting point in the series. The co-crystals of the **SR1**, **SR2**, and **SR3** depict the same trend with the co-crystal generated from succinic acid having the highest melting point and that from dodecanedioic acid having the lowest melting point. The salts however, again show an unpredictable behavior, failing to show any relationship with the properties of the co-crystallizing agents from which they are generated, (Figure 5.33).

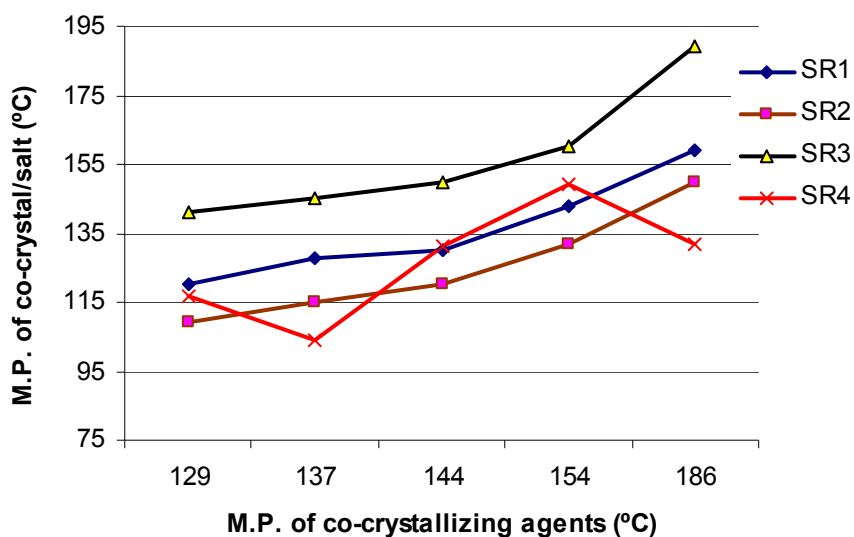


**Figure 5.33** Dependence of thermal behavior of co-crystal (SR1-SR3) and salt (SR4) on the melting points of the co-crystallizing agents.

**Table 5.9** Comparative melting points (°C) of co-crystallizing agents and its co-crystals/salts

<b>Diacids</b>		<b>SR1</b>	<b>SR2</b>	<b>SR3</b>	<b>SR4</b>
Dodecanedioic acid	129	120	109	141	117
Sebacic acid	137	128	115	145	104
Suberic acid	144	130	120	150	131
Adipic acid	154	143	132	160	149
Succinic acid	186	159	150	189	132

## 5.4 Conclusions

Our experimental results successfully show that the solubility of an API can be altered via co-crystallization. The co-crystallizing agents and the crystal packing are found to be the major determinants in altering the solubility. Higher aqueous solubility was observed for the co-crystals obtained from the co-crystallizing agent with higher solubility (Figure 5.32), as long as the solubility difference between the co-crystallizing agent and the API is not large enough to disturb the equilibrium (as seen for haloperidol). Also, the extension of network in the co-crystals showed higher alteration in solubility (**SR2-a-b** and **SR3-a-e**). Hence if we need higher solubility enhancement for an API (desired by pharmaceutical industries), the co-crystallizing agents with higher solubility needs to be chosen whereas for decreasing the solubility (desired by agrochemicals), the co-crystallizing agents with lower solubility needs to be chosen. Similarly, to generate co-crystals with higher melting point requires co-crystallizing agents to have higher melting points.

## References

- <sup>1</sup> Sun, C.C.; Hou, H. *Cryst Growth Des*, **2008**, *8*, 1575.
- <sup>2</sup> (a) Kerns, E. H.; Di, L. *Drug-like Properties: Concepts, Structure Design and Methods: from ADME to Toxicity Optimization*; **2008**, Elsevier: Amsterdam, pp 7-9; (b) Basavoju, S.; Bostrom, D.; Velaga, S. P. *Pharm. Res.* **2008**, *25*, 530.
- <sup>3</sup> (a) *Pharmaceutical Industry Profile 2006*, PhRMA: Washington, DC; (b) Ramanathan, R. *Mass Spectrometry in Drug Metabolism and Pharmacokinetics*, **2009**, pp 1-4, Wiley: Hoboken, NJ.
- <sup>4</sup> Chaumeil, J. C. *Exp. Clin. Pharmacol.* **1998**, *20*, 211.
- <sup>5</sup> (a) Good, D. J.; Rodriguez-Hornedo, N. *Cryst. Growth Des.* **2009**, *9*(5), 2252; (b) Nehm, S. J.; Rodriguez-Spong, B.; Rodriguez-Hornedo, N. *Cryst. Growth Des.* **2006**, *6*(2), 592.
- <sup>6</sup> Agharkar, S.; Lindenbaum, S.; Higuchi, T. *J. Pharm. Sci.* **1976**, *65*, 747.
- <sup>7</sup> Liversidge, G. G.; Cundy, K. C. *Int. J. of Pharmaceutics* **1995**, *125*(1), 91.
- <sup>8</sup> Aim, K.; Dannenfelser, R.-M.; Zielinski, J.; Wang, B. *J. Pharm. Sci.* **2004**, *93*, 2244.
- <sup>9</sup> (a) Li, N.; DeGennaro, M. D.; Liebenberg, W.; Tiedt, L. R.; Zahr, A. S.; Pishko, M. V.; de Villiers, M. M. *Pharmazie.* **2006**, *61*, 595; (b) Rasenack, N.; Muller, B. W. *Pharm. Res.* **2002**, *19*, 1894.
- <sup>10</sup> (a) Torchillin, V. P. *Pharm. Res.* **2007**, *24*, 1; (b) Rajewski, R. A.; Stella, V. J. *J. Pharm. Sci.* **1996**, *85*, 1142; (c) Humberstone, A. J.; Charman, W. N. *Adv. Drug Delivery Rev.* **1997**, *25*, 103; (d) Kataoka, K.; Harada, A.; Nagasaki, Y. *Adv. Drug Delivery Rev.* **2001**, *47*(1), 113.
- <sup>11</sup> (a) Rane, S. S.; Anderson, B. D. *Adv. Drug Delivery Rev.* **2008**, *60*, 638; (b) Spornath, A.; Aserin, A. *Adv. Coll. Interface Sci.* **2006**, *47*, 128; (c) Kogan, A.; Garti, N. *Adv. Coll. Interface Sci.* **2006**, *369*, 123; (d) Wasan, K. M.; Constantinides, P. P. *Adv. Drug Deliv. Rev.* **2004**, *56*, 1239; (e) Hauss, D. J. *Adv. Drug Deliv. Rev.* **2007**, *59*, 667; (f) Constantinides, P. P. *Pharm. Res.* **1995**, *12*, 1561; (g) Lawrence, M. J.; Rees, G. D. *Adv. Drug Deliv. Rev.* **2000**, *45*, 89; (h) Strickley, R. G. *Pharm. Res.* **2004**, *21*, 201; (i) New, R. R. C.; Kirby, C. J. *Adv. Drug Deliv. Rev.* **1997**, *25*, 59; (j) Wasan, K. M. *Drug Dev. Ind. Pharm.* **2001**, *27*, 267.
- <sup>12</sup> (a) Bak, A.; Gore, A.; Yanez, E.; Stanton, M.; Tufekcic, S.; Syed, R.; Akrami, A.; Rose, M.; Surapaneni, S.; Bostick, T.; King, A.; Neervannan, S.; Ostovic, D.; Koparkar, A. *J. Pharm. Sci.* **2008**, *97*(9), 3942; (b) Hickey, M. B.; Peterson, M. L.; Scoppettuolo, L. A.; Morrisette, S. L.; Vetter, A.; Guzman, H.; Remenar, J. F.; Zhang, Z.; Tawa, M. D.; Haley, S.; Zaworotko, M. J.; Almarsson, O. *Eur. J. Pharm. Biopharm.* **2007**, *67* (1), 112; (c) McNamara, D. P.; Childs, S. L.; Giordano, J.; Iarriccio, A.; Cassidy, J.; Shet, M. S.; Mannion, R.; O'Donnell, E.; Park, A. *Pharm. Res.* **2006**, *23* (8), 1888; (d) Remenar, J. F.; Peterson, M. L.; Stephens, P. W.; Zhang, Z.; Zimenkov, Y.; Hickey, M. B. *Mol. Pharm.* **2007**, *4* (3), 386.
- <sup>13</sup> Vishweshwar, P.; McMahan, J. A.; Bis, J. A.; Zaworotko, M.J. *J Pharm Sci*, **2006**, *95*, 499.
- <sup>14</sup> Liao, X.; Gautam, M.; Grill, A.; Zhu, H. J. *Journal of Pharmaceutical Sciences*, **2010**, *99*(1), 246.
- <sup>15</sup> Shiraki, K.; Takata, N.; Takano, R.; Hayashi, Y.; Terada, K. *Pharm. Res.* **2008**, *25*(11), 2581.

- 
- <sup>16</sup> (a) Childs, S. L.; Chyall, L. J.; Dunlap, J. T.; Smolenskaya, V. N.; Stahly, B. C.; Stahly, G. P. *J. Am. Chem. Soc.* **2004**, *126*, 13335; (b) Remenar, J. F.; Morissette, S. L.; Peterson, M. L.; Moulton, B.; MacPhee, J. M.; Guzman, H. R.; Almarsson, O. *J. Am. Chem. Soc.* **2003**, *125*, 8456; (c) McNamara, D. P.; Childs, S. L.; Giordano, J.; Iarriccio, A.; Cassidy, J.; Shet, M. S.; Mannion, R.; O'Donnell, E.; Park, A. *Pharm. Res.* **2006**, *23*(8), 1888.
- <sup>17</sup> (a) Trask, A. V.; Motherwell, W. D. S.; Jones, W. *Cryst. Growth Des.* **2005**, *5*, 1013; (b) Trask, A. V.; Motherwell, W. D.; Jones, W. *Int. J. Pharm.* **2006**, *320*, 114.
- <sup>18</sup> (a) Aakeröy, C. B.; Desper, J.; Urbina, J. F. *Chem. Commun.* **2005**, 2820; (b) Aakeröy, C. B.; Salmon, D. J. *CrystEngComm.* **2005**, *7*, 439; (c) Vishweshwar, P.; McMahon, J. A.; Bis, J. A.; Zaworotko, M. J. *J. Pharm. Sci.* **2006**, *95*(3), 499.
- <sup>19</sup> Childs, S. L.; Stahly, G. P.; Park, A. *Mol. Pharm.* **2007**, *4*, 323.
- <sup>20</sup> Nehm, S. J.; Rodriguez-Spong, B.; Rodriguez-Hornedo, N. *Cryst. Growth Des.* **2006**, *6* (2), 592.
- <sup>21</sup> (a) Grant, D. J. W.; Higuchi, T., *Solubility Behavior of Organic Compounds* **1990**, Wiley, New York. (b) Yalkowsky, S. H. *Solubility and Solubilization in Aqueous Media* **1999**, American Chemical Society: Washington, D.C., pp.61.
- <sup>22</sup> (a) Thalladi, V. R.; Nusse, M.; Boese, R. *J. Am. Chem. Soc.* **2000**, *122*, 9227; (b) Vishweshwar, P.; Nangia, A.; Lynch, V. M. *Cryst. Growth Des.* **2003**, *3*, 783.
- <sup>23</sup> Aakeröy, C. B.; Forbes, S.; Desper, J. *J. Am. Chem. Soc.* **2009**, *131*(47), 17048.
- <sup>24</sup> Mitchell, B. E.; Jurs, P. C. *J. Chem. Inf. Comput. Sci.* **1998**, *38*, 489.
- <sup>25</sup> Ran, Y.; Jain, N.; Yalkowsky, S. H. *J. Chem. Inf. Comput. Sci.* **2001**, *41*(5), 1208.
- <sup>26</sup> Bretti, C.; Crea, F.; Foti, C.; Sammartano, S. *J. Chem. Eng. Data* **2006**, *51*(5), 1660.
- <sup>27</sup> Higashio, Y.; Shoji, T. *Applied Catalysis A: General* **2004**, *260*(2), 251.
- <sup>28</sup> Aakeröy, C. B.; Rajbanshi, A.; Desper, J. *CrystEngComm.* **2010** (submitted).
- <sup>29</sup> Tollefson, G. D.; Beasley Jr., C. M.; Tran, P. V.; Street, J. S.; Krueger, J. A.; Tamura, R. N.; Graffeo, K. A.; Thieme, M. E. *Am. J. Psychiatry* **1997** *154*(4), 457.
- <sup>30</sup> CSD database structure HALDOL.



# CHAPTER 6 - From molecular recognition in cavitands to hydrogen and halogen-bonded capsules

## 6.1 Introduction

Molecular recognition processes are common in nature and are responsible for the formation of complex biological structures as well as for their unique behavior.<sup>1</sup> This process is a delicate balance between shape, size, and functional complementarities and governs whether any individual molecules can self-assemble to give larger architectures.<sup>2</sup> An understanding of molecular recognition and self-assembly processes is vital in the development of new strategies in supramolecular chemistry.<sup>1,3</sup> Utilization of self-assembly processes in designing strategies to bring together two self-complementary architectures to form a capsular structure has gained extensive attention in the past two decades.<sup>4</sup> Nano-sized molecular capsules with a well-defined inner cavity find applications in various fields including selective binding, separation, and sensing of small molecules and ions,<sup>5</sup> use as reaction chamber,<sup>6</sup> control of reactivity,<sup>7</sup> in catalysis, stabilization of reactive intermediates,<sup>8</sup> as chiral receptor,<sup>9</sup> gas encapsulation,<sup>10</sup> social isomerization<sup>11</sup> etc.

Various molecular capsules have been synthesized employing a range of molecular interactions such as strong ionic interactions,<sup>12</sup> covalent interaction to give rigid covalent capsules,<sup>13</sup> weaker non-covalent intermolecular interaction especially hydrogen bonds,<sup>14</sup> metal-ligand interactions,<sup>15</sup> combination of covalent and hydrogen bonds,<sup>16</sup> combination of metal ion coordination and intermolecular interaction, and hydrophobic effects.<sup>17</sup> The use of non-covalent interactions like hydrogen bonding (HB) or halogen bonding (XB) has an advantage in the ease of formation and the reversibility of the capsule. This expands the applications of molecular capsules in selective delivery of drugs where the relative ease of closing and opening of the capsular framework simplifies the drug delivery in a controlled manner.

The most common reversible-capsule synthesis is based on the self-assembly of resorcinarenes.<sup>18,19</sup> The incorporation of appropriate molecular recognition entities on these structures leads to self-assembly to form capsules of different shapes and sizes. The incorporation of self-complementary entities may result in the formation of a homomeric capsule, whereas two complementary entities on two different hosts may give a heteromeric capsule. The two containers can also be brought together into the formation of a capsule using a linker with a complementary functionality, (Figure 6.1).

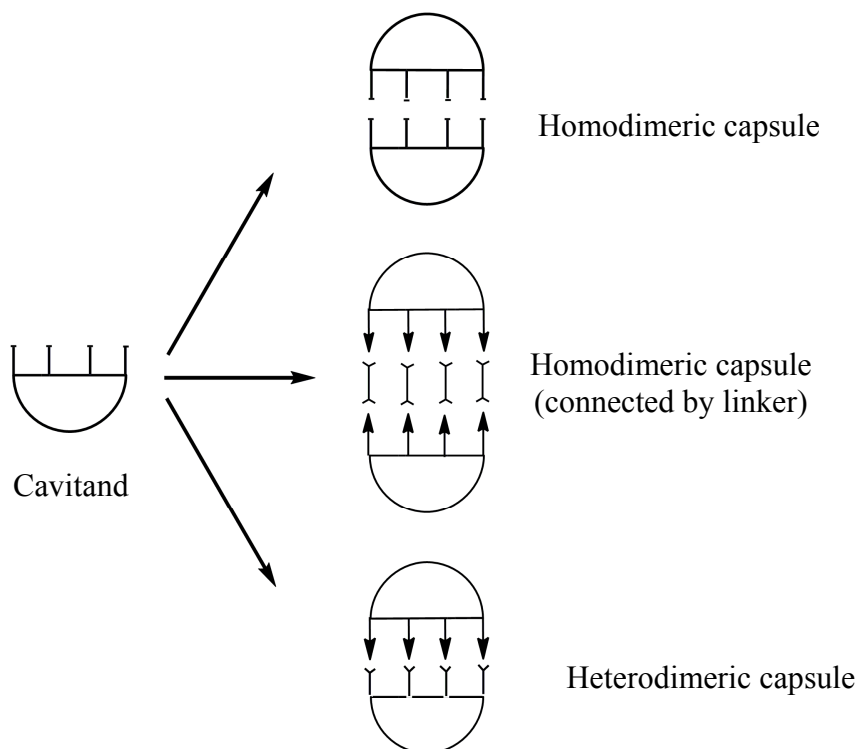


**Figure 6.1** Schematic representation of the formation of functional capsules.

Molecular capsules can also encapsulate two or more similar guests within the cavity of homodimeric (symmetrical) capsule and two or more different guests within the cavity of heterodimeric (asymmetrical) capsule. However, heterodimeric assembly requires two halves to be complementary with different inner environments in order to selectively incorporate different guests.

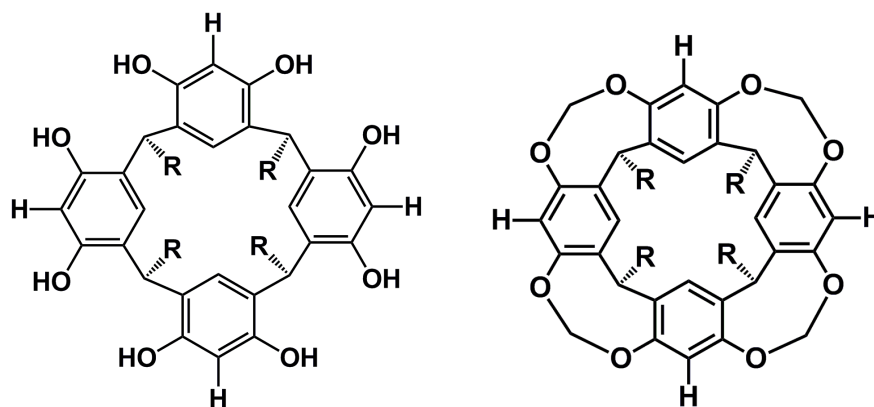


**Figure 6.2** Structural difference between resorcinarenes and cavitands.

Resorcinarene-based cavitands were introduced by Cram in the early 1980s.<sup>19, 20</sup> Its bowl-shaped curvature, large extended surfaces for intermolecular interactions is a suitable for the incorporation of guest molecules with different shapes and sizes. The rigidity garnered by the condensation of the hydroxyl groups provides a stable wall to keep the guest molecules inside the cavity, (Figure 6.3). In addition, the potential to functionalize as well as to deepen the cavity makes it a desirable choice for host-guest chemistry.

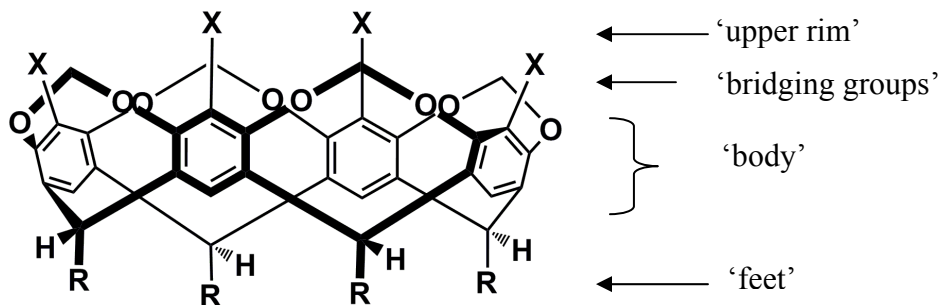


**Figure 6.3** Structure of a resorcin[4]arene-based cavitand outlining its four parts of interest.

A typical resorcinarene-based cavitand is broadly composed of four parts. The four evenly-placed sterically hindered aromatic positions at the rim of the cavity, termed the ‘upper rim’<sup>21</sup> and the methylene bridge<sup>22</sup> between the adjacent benzene rings, are suitable locales for functionalization. Both areas can be decorated with various functional moieties to vary the depth of the cavity as well as to impart specific properties to the cavitands. The ‘bridging groups’ are responsible for reducing flexibility of the molecule, hence erasing the possibility of different conformations. The middle part comprising the

cavity is termed ‘body’. It consists of an inner cavity lined with  $sp^2$ -hybridized atoms (benzene) with  $\Pi$ -bonds coating the surface. It hence behaves like a thin layer of negative charge which is suitable for trapping electron deficient guests.<sup>23</sup> The lower end, termed ‘feet’, is usually the place where modifications are carried out to alter the solubility.<sup>24</sup> Our synthetic focus will be on functionalizing the ‘upper rim’ and incorporating pentyl ‘feet’ for solubilization in organic solvents.

### ***6.1.1 Hydrogen bonded cavitands***

Hydrogen bonding is the major non-covalent interaction employed in self-assembly studies.<sup>14</sup> Current approaches towards the synthesis of hydrogen bonded cavitands involve functionalizing the methylene bridge<sup>25, 26</sup> or the aromatic ring<sup>27</sup> to impart the hydrogen bonding capabilities to the cavitand. Homodimeric,<sup>25</sup> heterodimeric<sup>27</sup> and linker-assisted homomeric<sup>25</sup> hydrogen-bonded capsules with various shapes and sizes were reported. The hydrogen bond donors like  $-\text{COOH}$ ,  $-\text{OH}$ ,  $-\text{NH}_2$ ,  $-\text{NOH}$ ,  $-\text{NHCOR}$  and the hydrogen bond acceptors pyridyl-N,  $\text{OCOOR}$  are being used in the capsules with the major binding motifs as  $\text{O-H}\cdots\text{N}$ ,  $\text{N-H}\cdots\text{O}$ ,  $\text{O-H}\cdots\text{O}$  bonding interactions.

### ***6.1.2 Halogen bonded cavitands***

Halogen bonding<sup>28</sup> has emerged as a promising supramolecular synthetic tool in the field of noncovalent synthesis because of its high strength, specificity, and directionality.<sup>29</sup> It consists of a halogen atom acting as electron pair acceptor (electrophilic species) and an electron rich moiety as the electron pair donor, with the strength of the halogen bond increasing in the order  $\text{Cl} < \text{Br} < \text{I}$ .<sup>30</sup> Halogen bonds are equipped with comparable binding strengths and directionality and pH endurance advantages over the better-known hydrogen bond.<sup>31</sup> It has applications in the self-assembly in liquid crystals,<sup>32</sup> controlling properties of conducting and magnetic molecular materials<sup>33</sup>, separating enantiomeric mixtures and isomers,<sup>34</sup> controlling solid state reactivity,<sup>35</sup> molecular folding and other biopharmacological properties,<sup>36</sup> and anion binding.<sup>37</sup> Halogen bonding also has the potential to form molecular capsules, however there are no known examples of halogen bonded capsules in the literature to date.

### 6.1.3 Research Goals

Our studies employ resorcinarene-based cavitands and probe their potential to form self-assembled or linker-assisted hydrogen and halogen-bond directed molecular capsules. By incorporating suitable/complementary hydrogen-bonding motifs on a cavitand, self-assembly can bring the two cavitands together with or without a linker into a dimeric hydrogen-bonded capsular assembly. 2-acetamidopyridine and 2-aminopyrazine moieties with a known potential to self-assemble were decorated on the upper rim of a cavitand and their potential to self-assemble via hydrogen bond to form capsular structures were probed.

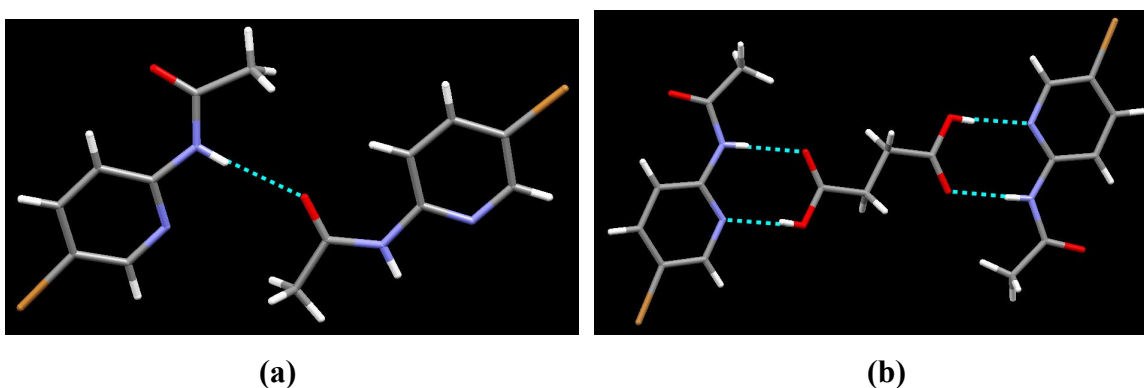


**Figure 6.4** (a) A complementary pair of 2-acetamido-5-bromopyridine in self-assembling hydrogen-bonding interaction. (b) Linker-assisted assembly.

Similarly, the formation of a halogen-bonding capsule requires halogen bond donors and halogen bond acceptors. The incorporation of a pyridyl group with a proven potential to act as halogen bond acceptor onto the ‘upper rim’ provides an opportunity to bring together two cavitands with the help of a halogen-bond donor linker. The tetrafluorobromobenzene<sup>38</sup> and tetrafluorodiodobenzene<sup>39</sup> moieties are known to form robust halogen bonding with nitrogen in pyridine and piperazine moieties. Hence, the use of tetrafluorodiodobenzene as a linker should enable the two pyridyl-substituted cavitands to come together via N---I halogen bonding into a capsular framework given the appropriate geometry of the molecules. 3-Pyridyl and 4-pyridyl moieties were decorated on the upper rim of the cavitand via standard Suzuki Miyaura cross-coupling reactions and tested for their ability to form co-crystals as well as linker-assisted homodimeric capsules with 1,4-diiodo-tetrafluorobenzene. In addition, the possibility of

formation of a heterodimeric halogen-bonded capsule was studied with pyridylcavitands and a halogen-substituted calixarene molecule.

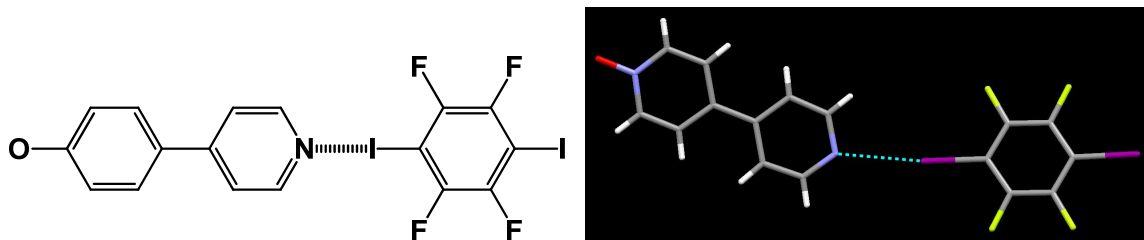


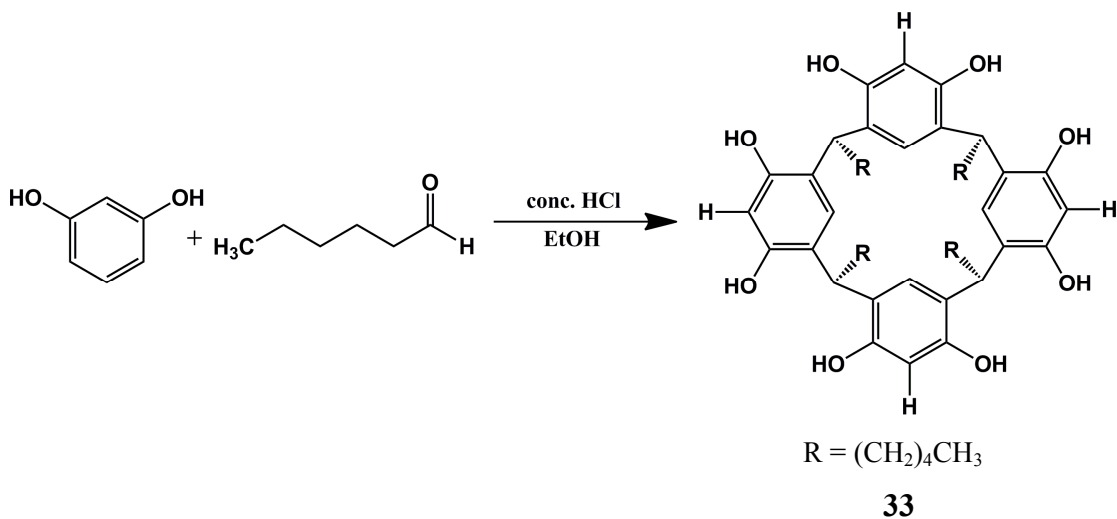
**Figure 6.5** N---I halogen bonding between 1,4-diiodotetrafluorobenzene and 4,4'-bipyridyl-N-oxide.<sup>40</sup>

## 6.2 Experimental

### 6.2.1 Synthesis

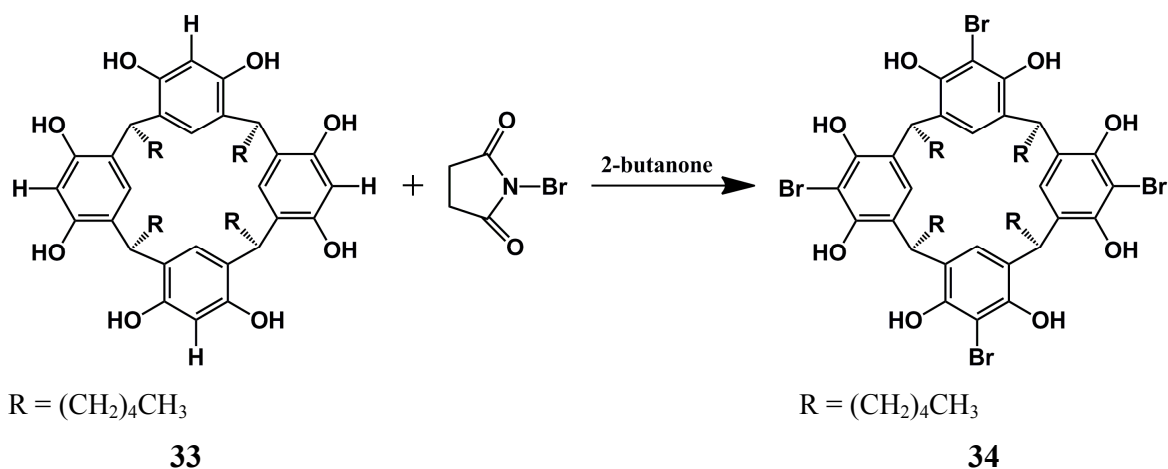
All chemicals were purchased from Aldrich and Strem chemicals and used without further purification. The determinations of melting points were carried out on Fisher-Johns melting point apparatus and are uncorrected. <sup>1</sup>H NMR and <sup>13</sup>C NMR spectra were recorded on a Varian Unity plus 200 MHz or 400 MHz spectrometer in CDCl<sub>3</sub> or D<sub>6</sub>-DMSO. Compounds were prepared for infrared spectroscopic (IR) analysis as a mixture in KBr. MALDI-TOF / TOF-MS was carried out on a Bruker Daltonics Ultraflex TOF/TOF.

#### 6.2.1.1 Synthesis of C-pentylcalix[4]resorcinarene, 33<sup>41</sup>



A mixture of resorcinol (5.100 g, 0.045 mol), hexanal (4.550 g, 0.045 mol) and ethanol (45 mL) was placed in a round bottom flask. Conc. HCl (7.25 mL) was added to it at 0 °C under dinitrogen atmosphere. The apparatus was fitted with a condenser and the mixture was refluxed at 70 °C for 10 hours. The reaction was monitored by TLC and upon completion was cooled to room temperature. It was then diluted with water to obtain a yellowish precipitate with a sweet, fruity smell. It was filtered and the precipitate washed with warm water until the filtrate is pH neutral. The white precipitate obtained was then dried, (8 g, 91%). M.P. >280 °C. <sup>1</sup>H NMR (δH; 400 MHz, DMSO-d<sub>6</sub>): 8.86 (s, 8H), 7.15 (s, 4H), 6.14 (s, 4H), 4.21 (t, J = 7.6Hz, 4H), 2.00 – 2.02 (m, 8H), 1.16 – 1.25 (m, 24H), 0.83 (t, J = 6.4Hz, 12H).

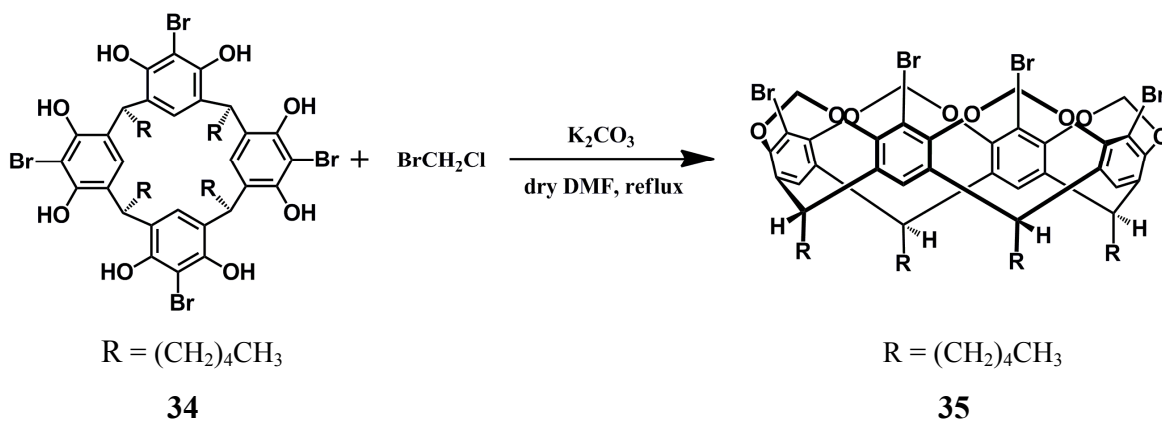
### 6.2.1.2 Synthesis of *C*-pentyltetrabromocalix[4]resorcinarene, **34**<sup>42, 43</sup>



*C*-Pentylcalix[4]resorcinarene **33** (5.0 g, 6.5 mmol) was placed in a round bottom flask and 2-butanone (40 mL) was added to it. The reaction mixture was stirred until all of **33** was dissolved. The solution was cooled below 10 °C by keeping over ice bath. The reaction flask was wrapped with aluminum foil, and under dark conditions *N*-bromosuccinimide (6.9 g, 39 mmol) was added to it in small portions so that the temperature of the reaction mixture remained below 10 °C. After the addition of NBS, the reaction mixture was allowed to stir at room temperature for 12 hrs. The precipitate obtained was filtered, washed with cold acetone (25 mL), then cold water (3 x 50 mL), and again with cold acetone (25 mL). The product was then dried in oven overnight to

obtain a white solid. (5.7 g, 81%) M. P. >300 °C; <sup>1</sup>H NMR (δH; 200 MHz, DMSO-d<sub>6</sub>): 9.10 (s, 8H), 7.35 (s, 4H), 4.34 (t, J = 8.0Hz, 4H), 2.17 (br, 8H), 1.27 (br, 24H), 0.84 (br, 12H).

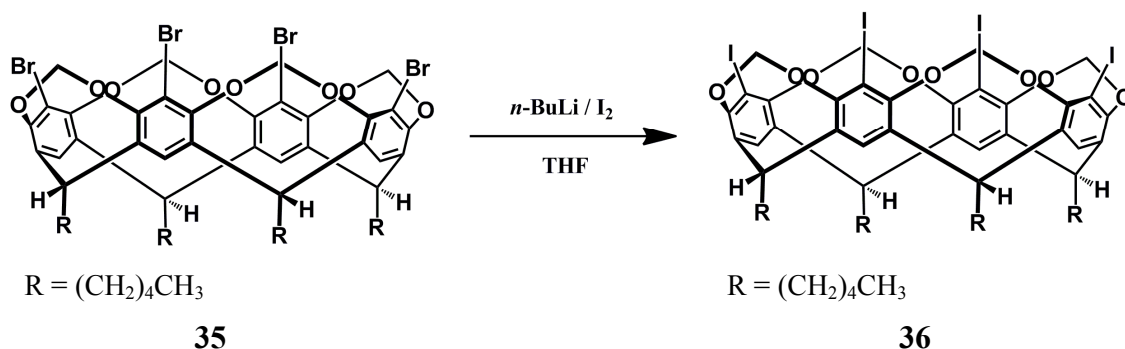
### 6.2.1.3 Synthesis of C-pentyltetrabromocavitand, **35**<sup>42</sup>



C-Pentyltetrabromocalix[4]resorcinarene, **34** (15.0 g, 13.8 mmol) was placed in a three-necked round-bottomed flask fitted with a mechanical stirrer and a reflux condenser. Anhydrous DMF (225 mL) was added and the mixture was stirred under dinitrogen until all of **34** was dissolved. K<sub>2</sub>CO<sub>3</sub> (30.0 g, 215.5 mmol) was added to the reaction mixture and was further stirred. The first portion of bromochloromethane (4.0 mL, 63 mmol) was then added carefully into the reaction mixture. It was refluxed at 40 °C under a dinitrogen atmosphere for 24 hrs with vigorous stirring. The second portion of bromochloromethane (4.0 mL) was added into the reaction mixture and refluxed at 65 °C for another 24 hrs. Similarly, the third and fourth portion of bromochloromethane (4.0 mL) was added after every 24 hrs under reflux. After 24 hrs of reflux after addition of the fourth portion, the mechanical stirrer and the heating were turned off and the reaction mixture allowed to cool to room temperature for additional 48 hrs. The product was then filtered and the precipitate washed with DMF (2 x 25 mL) followed by water (3 x 100 mL) and methanol (2 x 30 mL) and dried to obtain white powder, (11.75 g, 75 %). M. P. >280 °C; <sup>1</sup>H NMR (δH; 200 MHz, CDCl<sub>3</sub>): 7.04 (s, 4H), 5.97 (d, J = 8.0Hz, 4H), 4.86 (t, J = 8.0Hz, 4H), 4.40 (d, J = 8.0Hz, 4H), 2.19 – 2.22 (br, 8H), 1.39 (br, 24H), 0.92 (m, 12H).



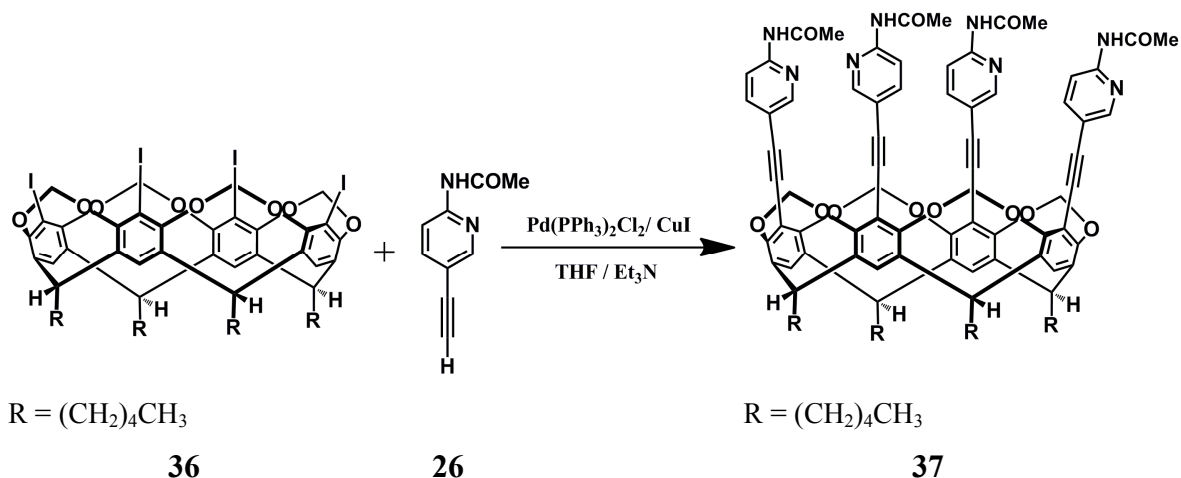
#### 6.2.1.4 Synthesis of *C*-pentyltetraiodocavitand, **36**



*C*-Pentyltetrabromocavitand **35** (2.0 g, 1.8 mmol) was placed in a round bottomed flask and warmed to 50 °C with stirring for about 30 mins. Dry, freshly distilled THF (50 mL) was added to it and the solution cooled to -78 °C using dry ice/acetone bath. The reaction mixture was stirred under dinitrogen and *n*-butyllithium (6.0 equiv., 6.6 mL, ca. 1.6 M solution in hexanes) was rapidly added using syringe. After stirring for 1 hr, iodine (3.6 g, 14.2 mmol in THF (5 mL)) was added. The cooling bath was removed and the reaction mixture was allowed to warm to room temperature. The stirring was continued for 2 hrs and then the reaction mixture was cooled to 0 °C using ice bath and quenched with a saturated aqueous sodium thiosulfate solution. The aqueous phase was extracted with ethyl acetate (3 x 75 mL), washed with brine and dried with magnesium sulfate. The solvent was removed on a rotary evaporator to obtain a white residue. It was purified by column chromatography using a hexanes/dichloromethane mixture as the eluent, whereupon small amounts of *C*-pentyl-1,3-dibromo-2,4-diiodocavitand, **36'** was also isolated. The product **36** was further purified by recrystallization with dichloromethane yielding a white powder, (1.70 g, 73 %). M. P. >280 °C; <sup>1</sup>H NMR (δH; 200 MHz, CDCl<sub>3</sub>): 7.07 (s, 4H), 5.98 (d, J = 6.0Hz, 4H), 4.86 (t, J = 8.0 Hz, 4H), 4.32 (d, 6.0Hz, 4H), 2.22 – 2.19 (m, 8H), 1.39 (br, 24H), 0.92 (t, J = 7Hz, 12 H); <sup>13</sup>C NMR (δH; 200 MHz, CDCl<sub>3</sub>): 155.03, 138.80, 120.85, 98.90, 93.25, 38.14, 32.06, 30.23, 27.61, 22.84, 14.27.

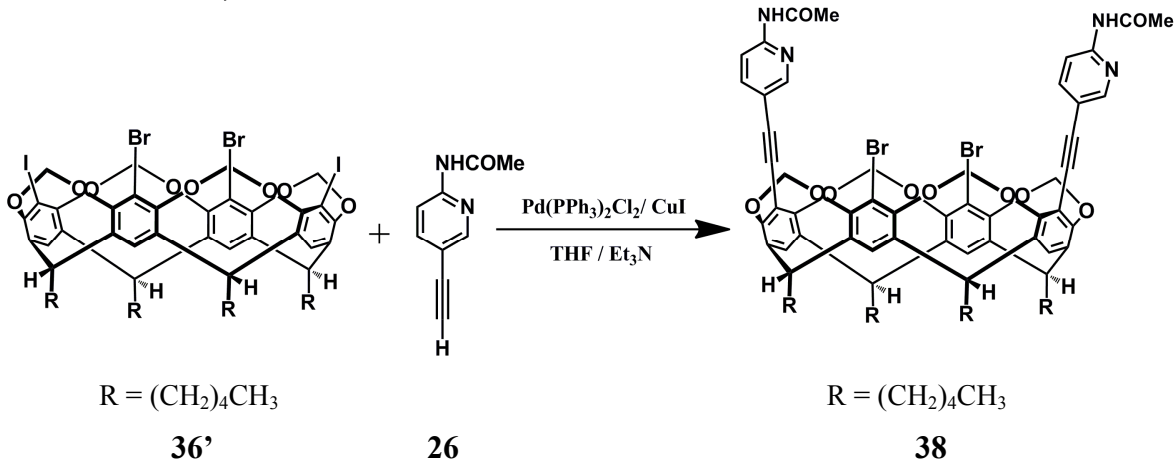
The product **36'** was further purified by recrystallization with dichloromethane yielding a white powder, (0.25 g). M. P. >280 °C; <sup>1</sup>H NMR (δH; 200 MHz, CDCl<sub>3</sub>): 7.05(d, J = 6.0Hz, 4H), 5.98 (d, J = 8.0Hz, 4H), 4.86 (t, J = 8.0 Hz, 4H), 4.37 (d, 6.0Hz, 4H), 2.19 – 2.22 (m, 8H), 1.39 (br, 24H), 0.92 (t, J = 7Hz, 12 H).

### 6.2.1.5 Synthesis of C-pentyltetra-(2-acetamidopyridyl-5-ethynyl)cavitand, 37



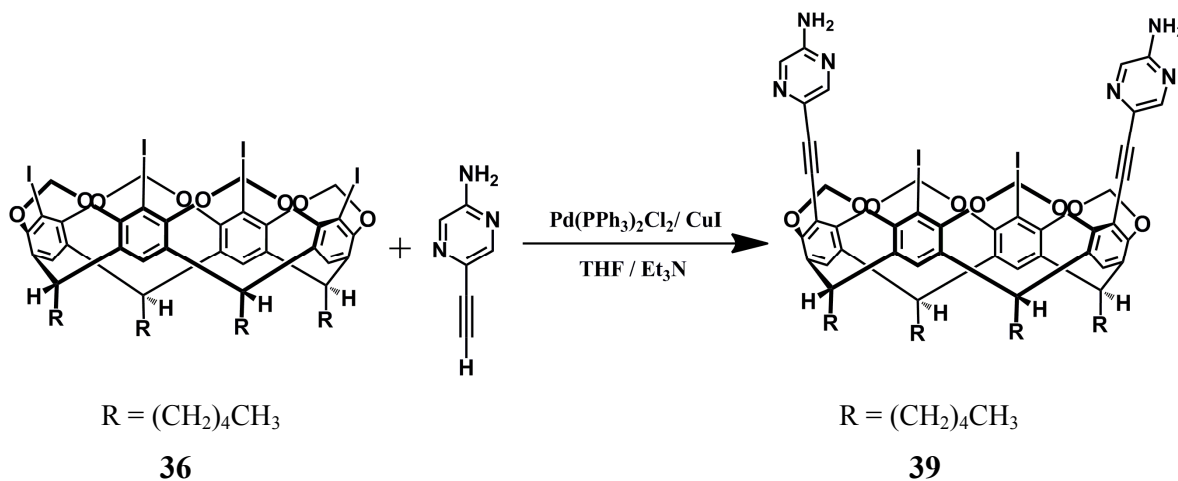
C-Pentyltetraiodocavitand **36** (0.20 g, 0.15 mmol) was placed in a round bottomed flask and warmed to 50 °C with stirring for about 30 mins to remove moisture. 2-acetamido-5-ethynylpyridine **26** (0.14 g, 0.88 mmol), *bis*(triphenylphosphine)palladium (II) dichloride (0.010 g, 0.014 mmol), triphenylphosphine (0.004 g, 0.016 mmol), and copper(I) iodide (0.002 g, 0.010 mmol) was added along with dry, freshly distilled THF (10 mL) and triethylamine (5 mL). Dinitrogen was bubbled through the mixture for 10 minutes and refluxed at 70 °C under dinitrogen. The reaction was monitored by TLC and upon completion (36 hrs) was cooled to room temperature. The solution was then diluted with ethyl acetate (100 mL), washed with (3 x 100 mL) and saturated aqueous sodium chloride solution (1 x 100 mL). The organic layer was separated and dried over anhydrous magnesium sulfate. The solvent was removed on a rotary evaporator and the residue was chromatographed on silica with hexane/ethyl acetate/methanol mixture as eluant. The product was isolated as a white colored solid, which was recrystallized from ethyl acetate. (125 mg, 58 %). M. P. >285 °C; <sup>1</sup>H NMR (δH; 200 MHz, CDCl<sub>3</sub>): 9.14 (br, 4 NH), 8.27 (s, 4H), 8.22 (s, 4H), 7.74 (d, J = 8.0 Hz, 4H), 7.12 (s, 4 H), 6.01 (d, J = 6.0 Hz, 4H), 4.86 (t, J = 8Hz, 4H), 4.59 (d, 6.0 Hz, 4H), 2.25 (s, 12H), 2.18 – 2.21 (m, 8H), 1.41 – 1.27 (m, 24H), 0.93 (m, 12 H); <sup>13</sup>C NMR (δH; 200 MHz, CDCl<sub>3</sub>): 169.45, 155.44, 151.11, 150.04, 141.24, 138.73, 120.71, 115.81, 113.96, 112.95, 94.26, 83.92, 36.72, 32.02, 29.66, 27.61, 24.84, 22.84, 14.26. IR (KBr pellet):  $\nu$  (cm<sup>-1</sup>) 3293, 2930, 2863, 1697, 1573, 1517, 1368, 1292, 974. MALDI-TOF / TOF-MS *m/z* 1448 ([**25** + Na]<sup>+</sup>)

6.2.1.6 Synthesis of *C*-pentyl-1,3-di-(2-acetamidopyridyl-5-ethynyl)-2,4-dibromocavitand, **38**



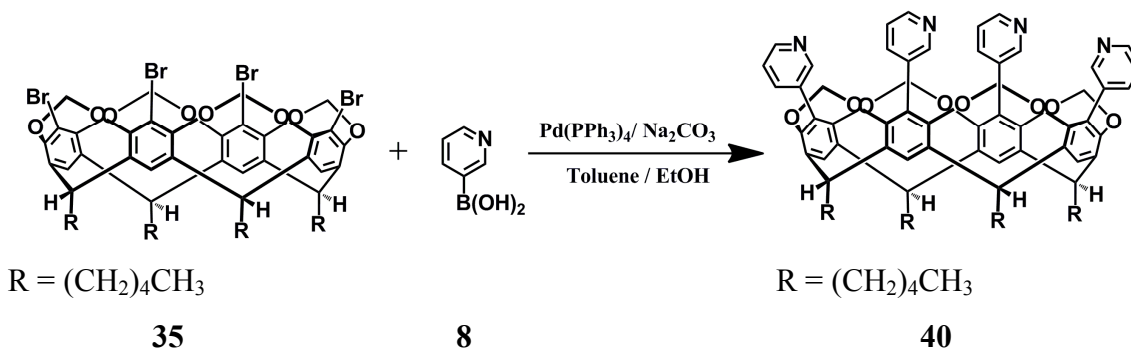
*C*-Pentyl-1,3-dibromo-2,4-diiodocavitand **36'** (0.200 g, 0.163 mmol) was placed in a round bottomed flask and warmed to 50 °C with stirring for 30 minutes to remove moisture. 2-Acetamido-5-ethynylpyridine **26** (0.075 g, 0.470 mmol), *bis*(triphenylphosphine)palladium (II) dichloride (0.005 g, 0.007 mmol), triphenylphosphine (0.002 mg, 0.008 mmol), and copper(I) iodide (0.001 mg, 0.005 mmol) was added to it along with dry, freshly distilled THF (5 mL) and triethylamine (3 mL). Dinitrogen was bubbled through the mixture for 10 minutes and refluxed at 70 °C under dinitrogen. The reaction was monitored by TLC and upon completion (36 hrs) was cooled to room temperature. The solution was then diluted with ethyl acetate (100 mL), washed with (3 x 100 mL) and saturated aqueous sodium chloride solution (1 x 100 mL). The organic layer was separated and dried over anhydrous magnesium sulfate. The solvent was removed on a rotary evaporator and the residue was chromatographed on silica with hexane/ethyl acetate/methanol mixture as eluant. The product was isolated as a white solid, which was recrystallized from ethyl acetate. (100 mg, 48 %). M. P. >285 °C; <sup>1</sup>H NMR (δH; 200 MHz, CDCl<sub>3</sub>): 8.34 (s, 2 NH), 8.18 (d, 2H), 8.03 (s, 2H), 7.73 (d, J = 8.0 Hz, 2H), 7.08 (d, J = 4.0 Hz, 4 H), 6.00 (d, J = 8.0 Hz, 4H), 4.86 (t, J = 6.0 Hz, 4H), 4.51 (d, 8.0 Hz, 4H), 2.23 (s, 14H), 1.40 (m, 24H), 0.93 (m, 12 H); <sup>13</sup>C NMR (δH; 200 MHz, CDCl<sub>3</sub>): 155.44, 152.21, 150.66, 141.05, 139.63, 138.56, 113.30, 37.29, 32.04, 29.83, 27.60, 24.97, 22.84, 14.25. MALDI-TOF / TOF-MS *m/z* 1290 ([**26** + Na]<sup>+</sup>).

### 6.2.1.7 Synthesis of C-pentyl-1,3-di(2-aminopyrazino-5-ethynyl)-2,4-diiodocavitand, 39



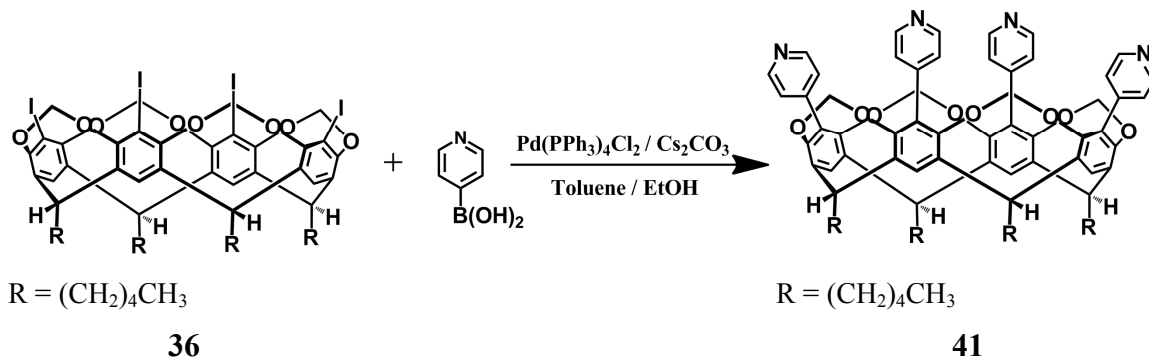
C-Pentryltetraiodocavitand **36** (2.0 g, 1.5 mmol) was placed in a round bottomed flask and warmed to 50 °C with stirring for about 30 mins to remove moisture. 2-amino-5-ethynylpyrazine (0.90 g, 7.56 mmol), *bis*(triphenylphosphine)palladium (II) dichloride (0.020 g, 0.028 mmol), triphenylphosphine (0.020 g, 0.080 mmol), and copper(I) iodide (0.008 g, 0.040 mmol) was added to it along with dry, freshly distilled THF (20 mL) and triethylamine (20 mL). Dinitrogen was bubbled through the mixture for 10 minutes and it was refluxed at 70 °C under a dinitrogen atmosphere. The reaction was monitored by TLC and upon completion (36 hrs) was cooled to room temperature. The solution was then diluted with ethyl acetate (100 mL), washed with (3 x 100 mL) and saturated aqueous sodium chloride solution (1 x 100 mL). The organic layer was separated and dried over anhydrous magnesium sulfate. The solvent was removed on a rotary evaporator and the residue was chromatographed on silica with hexane/dichloromethane/ethyl acetate mixture as eluant to remove the impurities. The product was isolated as a white colored solid, which was recrystallized from ethyl acetate. M. P. >285 °C; <sup>1</sup>H NMR (δH; 200 MHz, CDCl<sub>3</sub>): 8.15 (s, 2H), 7.98 (s, 2H), 7.08 (br, 4H), 6.02 (d, J = 8.0 Hz, 4H), 4.86 (t, J = 8Hz, 4H+2NH<sub>2</sub>), 4.48 (d, 6.0 Hz, 4H), 2.21 (s, J=6.0 Hz, 8H), 1.40 (m, 24H), 0.93 (m, 12 H).

### 6.2.1.8 Synthesis of *C*-pentyltetra(3-pyridyl)cavitand, **40**<sup>44</sup>



A mixture of *C*-pentyltetrabromocavitand **35** (2.0 g, 1.8 mmol) and *tetrakis*-triphenylphosphine palladium (II) (0.420 g, 0.362 mmol) were added to a round bottom flask under a stream of dinitrogen. Toluene (30 mL), ethanol (20 mL) and aqueous sodium bicarbonate (100 mg, 5 mL) were all purged with dinitrogen before being added to the round bottom flask along with 3-pyridylboronic acid **8** (2.80 g, 22.76 mmol). The reaction mixture was refluxed for 72 hours under a dinitrogen atmosphere. Upon completion of the reaction, the mixture was cooled to room temperature and diluted with water (100 mL). The aqueous phase was washed with dichloromethane (3 x 100 mL) and dried with magnesium sulfate. The solvent was removed using rotary evaporator and the residue obtained was purified by column chromatography using ethanol/ethyl acetate mixture as eluant over silica. The product was isolated as a white crystalline solid (1.50 g, 76%). M.P. >280 °C; <sup>1</sup>H NMR (δH; 400 MHz, CDCl<sub>3</sub>): 8.408 (br, 4H), 8.244 (s, 4H), 7.39(s, 8H), 7.183 (br, 4H), 5.243 (br, 4H), 4.881(s, 4H), 4.234 (s, 4H), 2.376 (m, 8H), 1.481 (m, 24H), 0.962 (t, 12H).

### 6.2.1.9 Synthesis of *C*-pentyltetra(4-pyridyl)cavitand, **41**

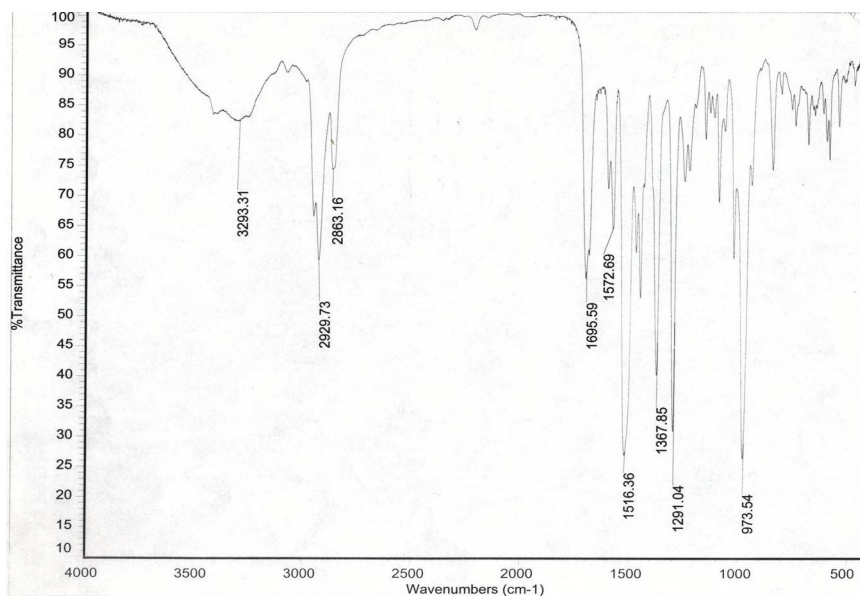


C-Pentyltetraiodocavitand **36** (0.80 g, 0.61 mmol) was placed in a round bottom flask. It was heated to 50 °C under a stream of dinitrogen for 30 mins with stirring. Toluene (20 mL), ethanol (10 mL) and cesium carbonate (150 mg, 0.46 mmol) were all purged with dinitrogen before being added to the round bottom flask in dinitrogen atmosphere. *Tetrakis*-triphenylphosphine palladium (II) (420 mg, 0.362 mmol) was added to the reaction mixture followed by 4-pyridylboronic acid (0.80 g, 6.52 mmol). The reaction mixture was refluxed at 80 °C for 72 hours under dinitrogen. Upon completion of the reaction, the mixture was cooled to room temperature and diluted with water (100 mL). The aqueous phase was washed with dichloromethane (3 x 100 mL) and dried with magnesium sulfate. The solvent was removed using rotary evaporator and the residue obtained was purified by column chromatography using ethanol/ethyl acetate/traces of Et<sub>3</sub>N mixture as eluant over silica. The product was isolated as a white powder (0.30 g, 45%). M.P. >280 °C; <sup>1</sup>H NMR (δH; 200 MHz, CDCl<sub>3</sub>): 8.58 (d, J = 6.0 Hz, 8H), 7.37 (s, 4H), 6.98 (d, J = 6.0 Hz, 8H), 5.29 (d, J = 6.0 Hz, 4H), 4.84 (t, J = 8.0 Hz, 4H), 4.23 (d, 8.0 Hz, 4H), 2.34 (m, 8H), 1.46 (m, 24H), 0.96 (t, J = 7Hz, 12 H); <sup>13</sup>C NMR (δH; 200 MHz, CDCl<sub>3</sub>): 152.17, 149.46, 142.02, 138.00, 126.83, 124.91, 120.85, 100.39, 43.23, 37.01, 31.99, 30.24, 27.58, 22.68, 14.14. MALDI-TOF / TOF-MS *m/z* 1124 ([**30** + H]<sup>+</sup>).

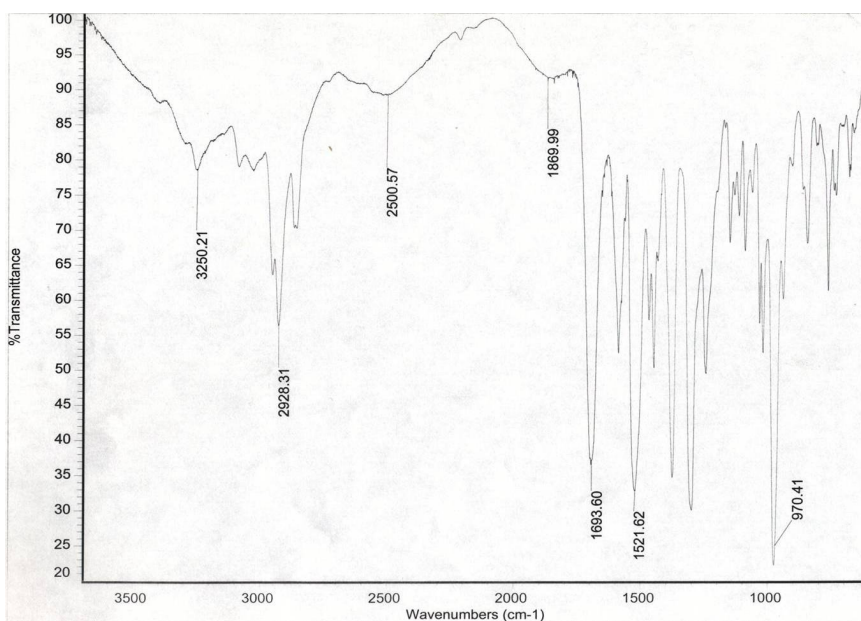
## 6.2.2 Co-crystallizations of cavitands

### 6.2.2.1 Synthesis of tetra(2-acetamidopyridyl-5-ethynyl)cavitand co-crystals

Co-crystallizations of tetra(2-acetamidopyridyl-5-ethynyl)cavitand was attempted with 20 different co-crystallizing agents to probe the molecular recognition abilities, which can later be interpreted into its potential to form hydrogen-bonded molecular capsules. However we were unable to grow suitable crystals for single-crystal X-ray crystallography for any of the co-crystals screened via IR spectroscopy. The co-crystals of **37** exhibited the characteristic O-H---N stretches around 1850 and 2550 cm<sup>-1</sup>, and free C=O stretch in 1700 cm<sup>-1</sup> region, (Figure 6.6).



FT-IR spectra of tetra(2-acetamidopyridyl-5-ethynyl)cavitand



FT-IR spectra of co-crystal of tetra(2-acetamidopyridyl-5-ethynyl)cavitand and 3,4-dichlorobenzoic acid

**Figure 6.6** FT-IR spectra of **37** and its co-crystal with 3,4-dichlorobenzoic acid.

**Table 6.1** IR stretches in co-crystals of tetra(2-acetamidopyridyl-5-ethynyl)cavitand **37**

	Co-crystallizing agents	IR stretches
1	4-Cyanobenzoic acid	3246, 2549, 1866, 1703, 1540
2	3-Hydroxybenzoic acid	3272, 2580, 1870, 1685, 1530
3	4-Chlorobenzoic acid	n/a
4	4-Fluorobenzoic acid	3246, 2540, 1883, 1694, 1513
5	4-Nitrobenzoic acid	3259, 2554, 1857, 1698, 1526
6	3,4-Dichlorobenzoic acid	3250, 2501, 1870, 1694, 1522
7	2,6-Difluorobenzoic acid	3246, 2540, 1874, 1702, 1510
8	3,5-Dimethylbenzoic acid	3250, 2606, 1839, 1680, 1525
9	2,4-Dinitrobenzoic acid	3395, 2496, 1945, 1698, 1531
10	Pentafluorobenzoic acid	3250, 2527, 1914, 1698, 1526
11	Suberic acid	n/a
12	Phthalic acid	n/a
13	Fumaric acid	n/a
14	Succinic acid	n/a
15	Sebacic acid	n/a
16	Cyanoxime	n/a
17	4-Fluorocyanoxime	n/a
18	4-Chlorocyanoxime	n/a
19	4-Bromocyanoxime	n/a
20	4-Carboxyphenylcavitand pentyl	3418, 2523, 1866, 1694, 1517

#### 6.2.2.2 Synthesis of C-pentyl-tetra(3-pyridyl)cavitand/1,4-diiodo-tetrafluorobenzene (1:2), **40a**

C-Pentyl-tetra(3-pyridyl)cavitand **40** (0.020 g, 0.0178 mmol) was dissolved in 5mL of acetonitrile. To this solution was added 1,4-diiodo-tetrafluorobenzene (0.029 g, 0.0712 mmol) in 5 mL of ethanol. The resulting solution was warmed and allowed to stand for slow evaporation at room temperature. Colorless, block-shaped crystals were obtained after 4 days. M. P. >280°C; IR  $\nu$  (cm<sup>-1</sup>) 2928 (C-N stretch), 1463 (C-I stretch), 1251, 1084, 971, 944 (C-I bend), 584.



### **6.2.2.3 Synthesis of *C*-pentyl-tetra(4-pyridyl)cavitand/1,4-diiodo-tetrafluorobenzene (1:2), 41a**

*C*-Pentyl-tetra(4-pyridyl)cavitand **41** (0.020 g, 0.0178 mmol) was dissolved in 5 mL of acetonitrile. To this solution was added 1,4-diiodo-tetrafluorobenzene (0.029 g, 0.0712 mmol) in 5 mL of ethanol. The resulting solution was warmed and allowed to stand for slow evaporation at room temperature. Colorless, cubic crystals were obtained after 4 days. M. P. >300 °C; IR  $\nu$  (cm<sup>-1</sup>) 2925 (C-N stretch), 1603, 1460 (C-I stretch), 1216, 1086, 976, 942 (C-I bend), 584.

### **6.2.2.4 Synthesis of *C*-pentyl-tetra(3-pyridyl)cavitand/halocalixarene<sup>45</sup> (1:1), 40b**

*C*-Pentyl-tetra(3-pyridyl)cavitand **40** (0.006 g, 0.0053 mmol) was dissolved in 5 mL of ethanol. To this solution was added *C*-ethoxy-4-iodo-tetrafluorobenzene-*tert*-butylcalixarene (0.010 g, 0.0052 mmol) in 5 mL of ethanol. The resulting solution was warmed and allowed to stand for slow evaporation at room temperature. Colorless, rectangular crystals were obtained after 4 days. M. P. 185 - 187 °C; IR  $\nu$  (cm<sup>-1</sup>) 2928 (C-N stretch), 1727, 1480 (C-I stretch), 1241, 1106, 970, 948 (C-I bend), 583.

## **6.3 Results and Discussion**

### **6.3.1 Precursors and their functionalization**

The synthesis of hydrogen- and halogen-bonded capsules started with the challenge of decorating the functionalizable upper rim with moieties having robust hydrogen or halogen bonding sites. The starting point was the condensation of resorcinol with hexanal to obtain the cyclic calix[4]resorcinarene. The upper rim was then brominated with *N*-bromosuccinimide and rigidity imparted to the structure by linking the hydroxyl arms using bromochloromethane to obtain a bromocavitand. Until this step the yield was good, and the product bromocavitand can be used for functionalization via cross-coupling reactions. However, for some coupling reactions a better leaving group is required, hence a further conversion into the iodocavitand was needed.

The complications started from the conversion of *C*-pentyltetrabromocavitand into the iodocavitand. The process uses a moisture-sensitive reagent, *n*-butyllithium which requires a completely dry environment. The replacement of bromine atoms with

iodine may be hindered in the presence of moisture to yield protio-cavitands. Also, *n*-butyllithium itself may be ruined by moisture. The synthesis of *C*-pentyltetraiodocavitand itself resulted in a mixture of cavitands with varying degrees of substitution. Along with the desired tetrasubstituted product, 1,3-disubstituted, 1,2-disubstituted, trisubstituted and monosubstituted products were obtained. The purification via column chromatography was tedious and with low to moderate yields. Upon complete isolation and characterization, palladium-catalyzed Sonogashira and Suzuki Miyaura cross-coupling reactions were carried out, again with various substitution products.

**Table 6.2** Hydrogen-bond geometries for **37** and **38**.

Structure	D-H...A	d(D-H)/Å	d(H...A)/Å	d(D...A)/Å	<(DHA)/°
<b>37</b> <sup>i</sup>	N362-H362...O384#1	0.88	2.05	2.920(4)	170.6
	N363-H363...O382#1	0.88	1.98	2.852(4)	173.1
	N364-H364...O161#2	0.88	2.23	3.070(4)	159.2
<b>38</b> <sup>ii</sup>	N322-H322...O121#2	0.88	2.03	2.903(4)	175.0

(i) #1 -x+1,-y+1,-z #2 -x+1,-y,-z (ii) #1 x,-y+3/2,z #2 -x+1,-y+1,-z

### 6.3.1.1 Crystal structure of *C*-pentyltetrabromocavitand, **35**

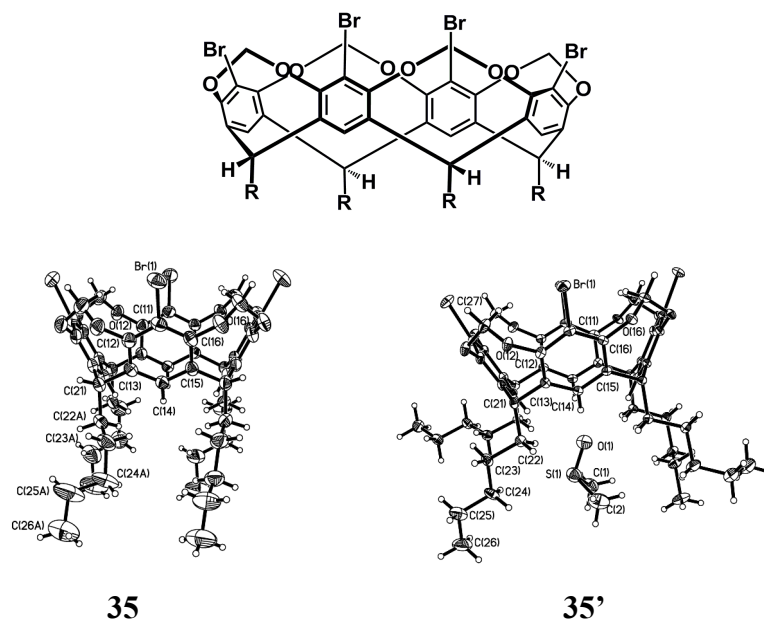


**Figure 6.7** Thermal ellipsoid plots (50 % probabilities) and labeling schemes for **35** and **35'**.

Two crystal structures of tetrabromocavitands were obtained with ethyl acetate (**35**) and DMSO (**35'**) as guest molecules lying in the lower rim as well as near the upper rim of the cavitand (**35**). Previous crystal structures of **35** have dichloromethane and acetonitrile as guest molecules residing around the lower rim of the cavitand.<sup>44</sup>

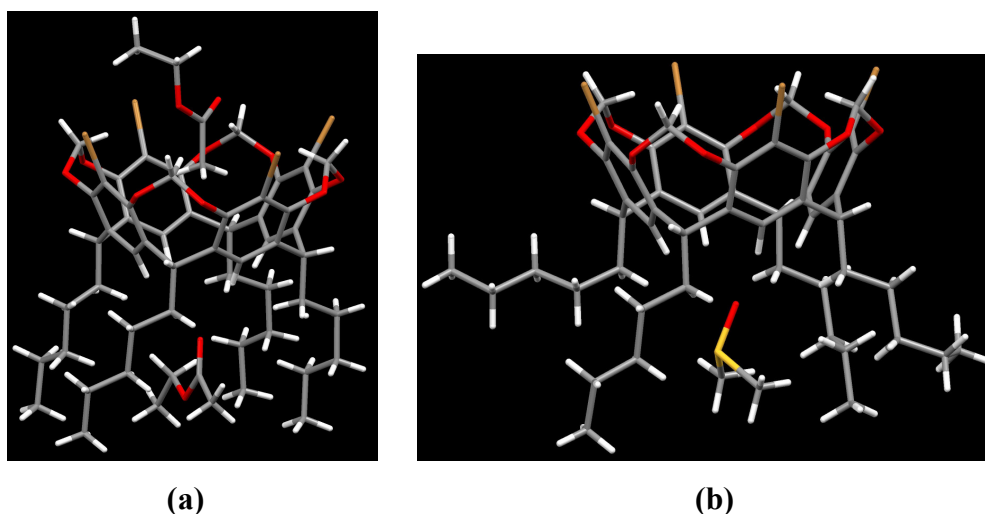


**Figure 6.8** *C*-pentyltetrabromocavitand, with (a) ethyl acetate as guest, **35**; (b) DMSO as guest, **35'**.

The crystal structures **35** and **35'** have certain similarities as well as dissimilarities. In line with the previous reported structures, these structures have their pentyl 'feet' residing inside the cavity of the other. In the structure of **35**, two 'feet' of a cavitand are dipping into the upper rim of a neighboring cavitand (Figure 6.9a), whereas in structure **35'**, only one of the pentyl feet of the cavitand resides in the cavity of a neighboring cavitand, (Figure 6.9b).

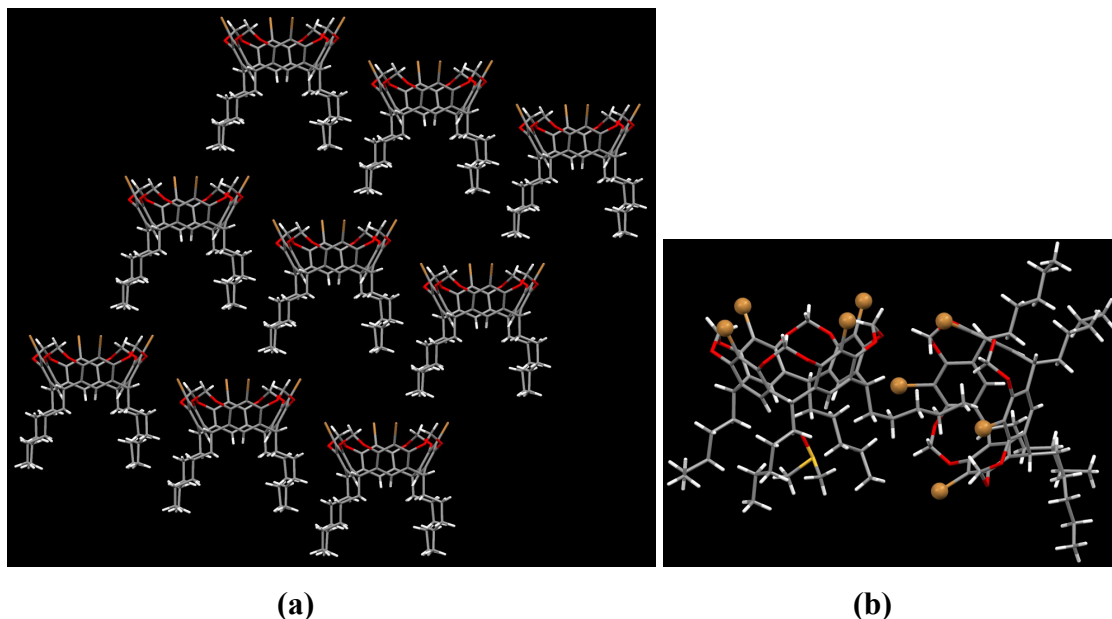


**Figure 6.9** Crystal packing in tetrabromocavitand molecule (a) **35** and (b) **35'**.

Another difference between these two crystal structures is the Br---Br interaction between the neighboring cavitand molecules. Both structures have two cavitand molecules in an inverted/alternate arrangement interacting via Br---Br interaction; however, the crystal structure **35** consists of two symmetry related pairs of Br---Br interactions (3.592 Å) whereas for **35'** only a single Br---Br interaction (3.405 Å) is observed, (Figure 6.10).

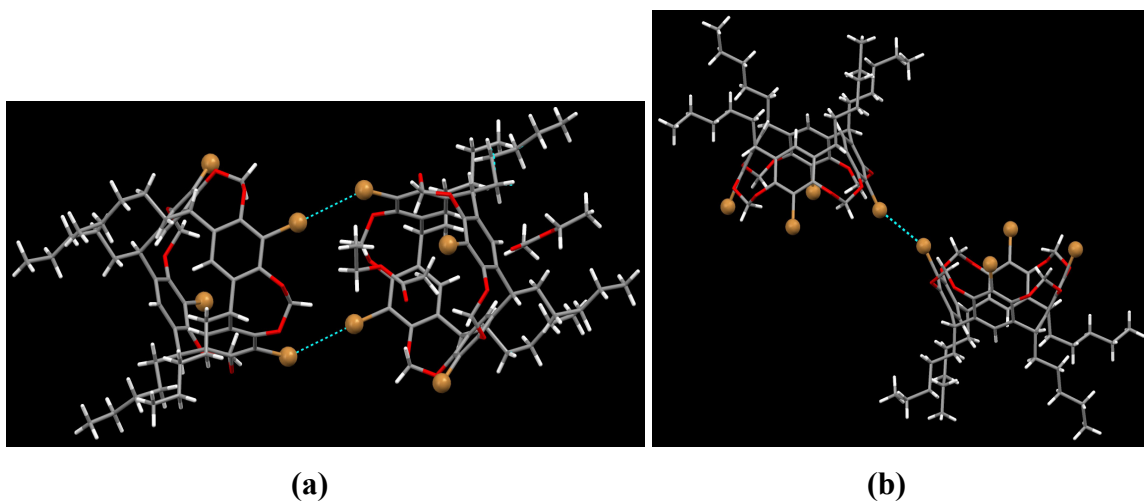


**Figure 6.10** Linking of cavitands pairs via Br---Br interactions, (a) **35** (b) **35'**.

### 6.3.1.2 Crystal structure of *C*-pentyltetraiodocavitand, **36**

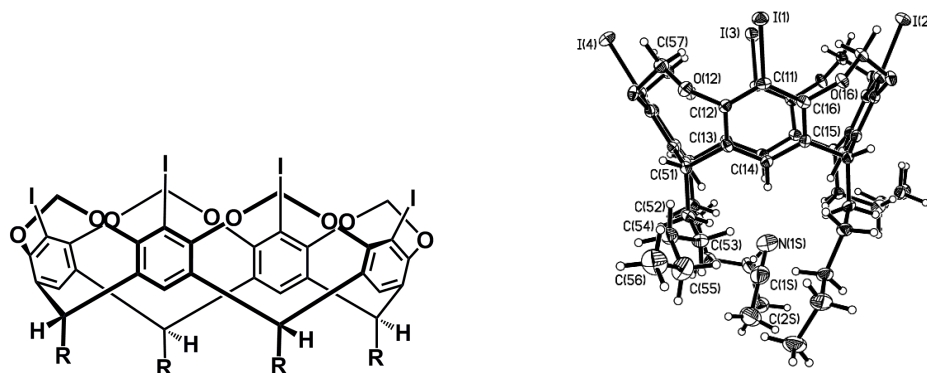
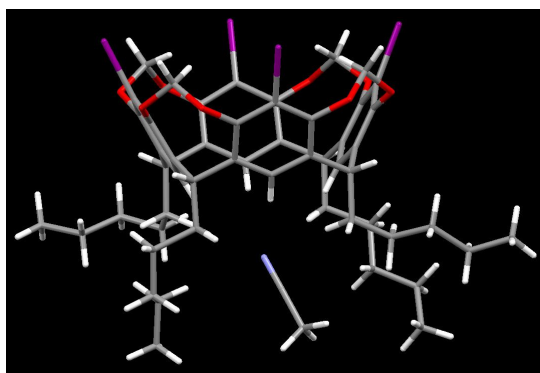
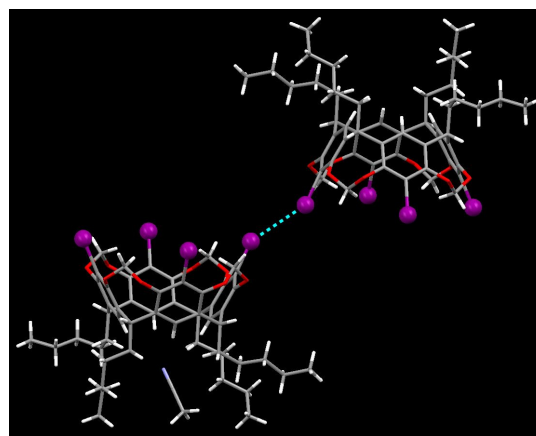


**Figure 6.11** Molecular structure and thermal ellipsoid plots (50 % probabilities) and labeling schemes for **36**

The crystal structure of iodocavitand, **36** revealed one acetonitrile molecule residing as guest between the ‘feet’ of the host with the nitrile end pointing upwards towards the cavity, (Figure 6.12a).



(a)



(b)

**Figure 6.12** (a) An individual *C*-pentyltetraiodocavitand with acetonitrile guest, (b) Linking of two iodocavitands via an I...I interaction.

A typical ‘foot-in-mouth’ arrangement is seen in the extended architecture of **36**, with one pentyl ‘foot’ of an iodocavitand residing inside the upper rim of a neighboring iodocavitand molecule, (Figure 6.13). A single I...I interaction (3.636 Å) between the iodine atoms of two individual iodocavitand molecules was observed, (Figure 6.12b).

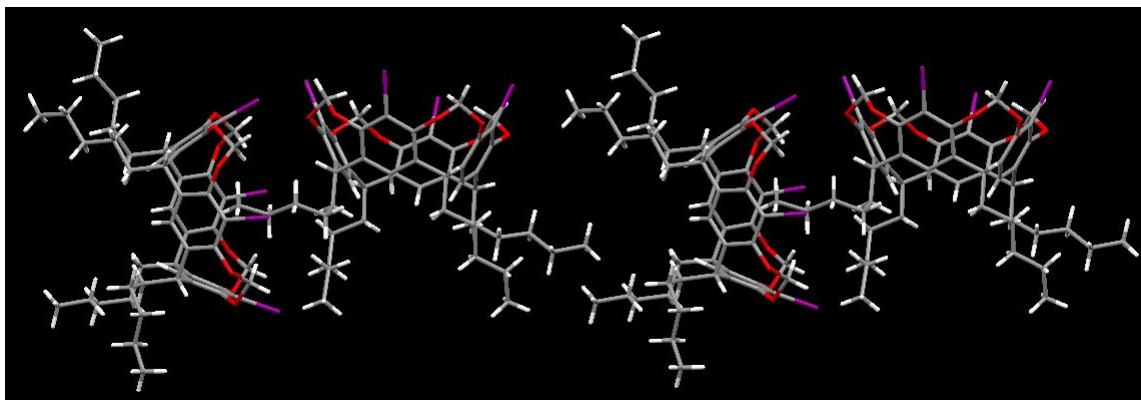


**Figure 6.13** ‘Foot-in-mouth’ arrangement between iodocavitand molecules in **36**.

### 6.3.2 Quest for a hydrogen-bond driven capsule

Standard Sonogashira cross-coupling reactions were employed to impart hydrogen bonding capabilities to the cavitands. Tetraiodocavitands were used for the purpose and acetamidopyridine and aminopyrazine moieties were incorporated into the upper rim of the cavitand.

#### 6.3.2.1 Crystal structure of *C*-pentyltetra(2-acetamidopyridyl-5-ethynyl)cavitand, **37**

*C*-Pentyltetra-(2-acetamidopyridyl-5-ethynyl)cavitand, **37** was synthesized using Sonogashira cross-coupling conditions with 2-acetamido-5-ethynylpyridine under basic conditions. The main purpose of incorporating the ethynyl group is to give more depth to the cavitand hence enabling it to trap larger guest molecules. Again various degrees of substitution were observed with the major product being the desired tetrasubstituted cavitand. The product was purified using silica-gel column chromatography and recrystallized from a mixture of solvents (methanol/ethanol/ethyl acetate/toluene).

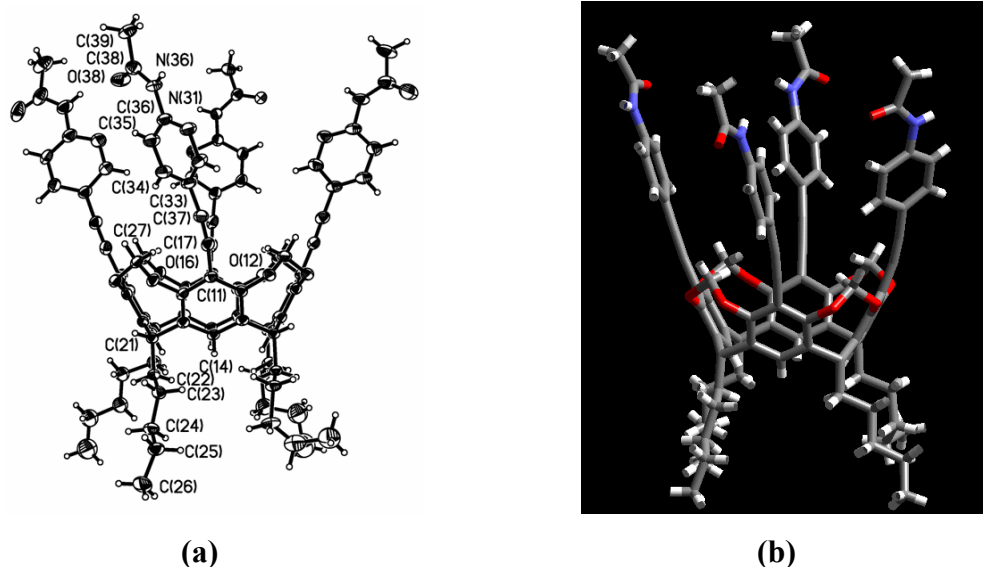


**Figure 6.14** *C*-Pentyltetra(2-acetamidopyridyl-5-ethynyl)cavitand, **37** (a) thermal ellipsoid plots (50 % probabilities) and labeling schemes, (b) An individual cavitand.

The crystal structure determination of **37** revealed the presence of solvent molecules inside the cavity as well as near the upper rim of the cavitand. A toluene

molecule was found seated deep inside the cavity whereas two ethanol molecules and one methanol molecule was found lying near the upper rim of the cavitand. A single disordered ethyl acetate was found near the ‘feet’ of the cavitand.

Upon extension of the architecture, it was found that the upper rims of two *C*-pentyltetra(2-acetamidopyridyl-5-ethynyl)cavitands come together via hydrogen bonding interactions to give a capsular structure. The capsular framework is held together via a total of four N-H---O interactions (NH group of acetamido group of one cavitand with O=C group of complementary cavitand) between three “arms” of each cavitand. The ethanol and methanol molecules engage in multiple hydrogen bonds with each other and with the N-H group of the remaining “arm” of both cavitands in the capsule, (Figure 6.15).

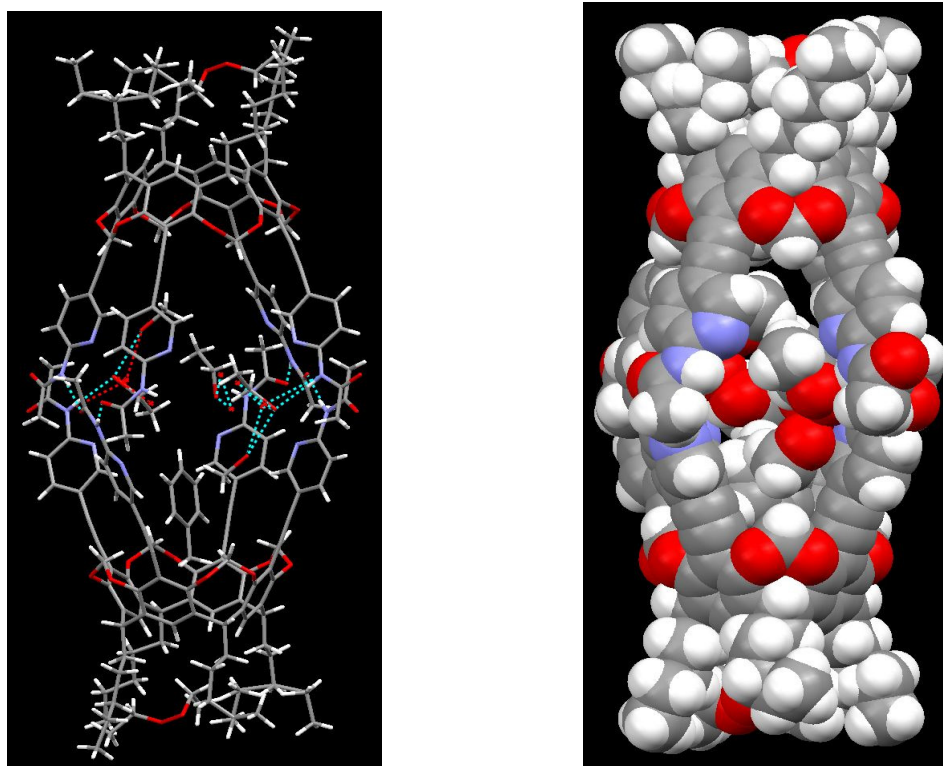
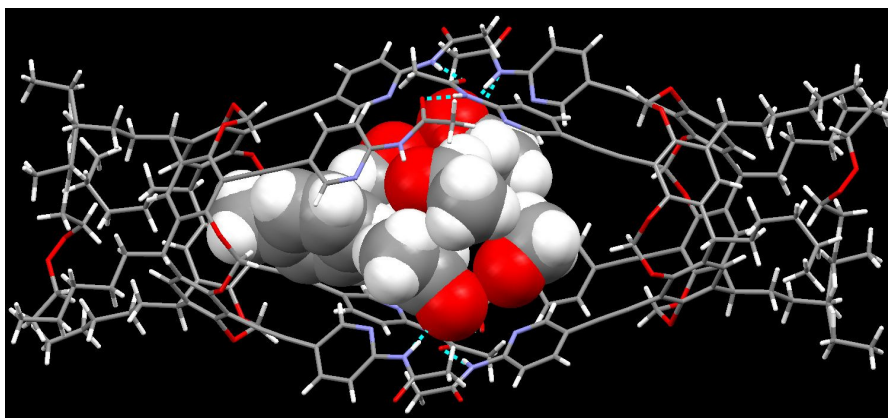


**Figure 6.15** Molecular structure and spacefilling diagram showing the capsular framework of **37**.

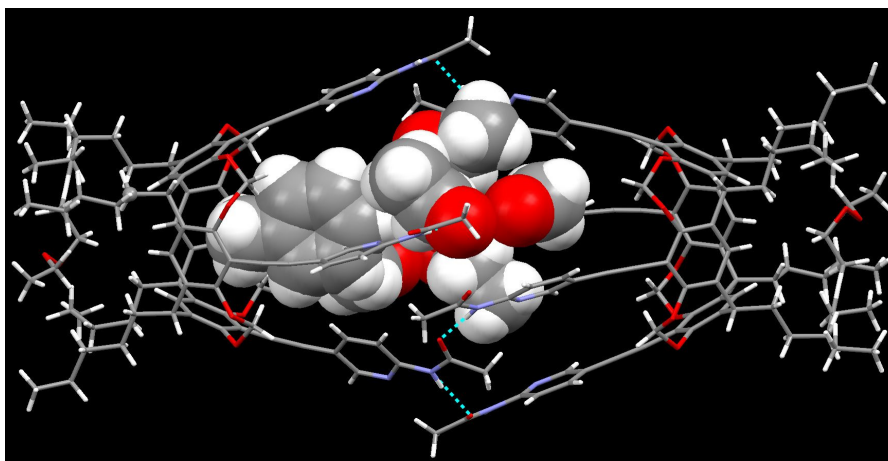
The hydrogen-bonded capsule included three ethanol molecules, two methanol molecules, and one toluene molecule inside its cavity. The length of the capsule (distance between the lower ends of the aromatic ring in the “body” of the cavitand) is 22 Å, whereas the maximum width is found to be 15 Å. Upon closer observation and



rotating 90° wrt b, however it was found that the framework is not a perfect capsule, but rather a distorted one, (Figure 6.16).



(a)



(b)

**Figure 6.16** (a) Capsular framework of **37** (b) Distorted capsule upon 90° rotation w.r.t b.

Similar synthesis using 2-amino-5-ethynylpyrazine was attempted (amino-substituted was used due to hydrolysis of acetamido group of acetamidopyrazine in reaction medium), which however only yielded disubstituted products, (Section 6.2.1.7). Unfortunately for these cavitands, single crystals were not obtained for structure determination.

### 6.3.2.2 Crystal structure of *C*-pentyl-1,3-di(2-acetamidopyridyl-5-ethynyl)-2,4-dibromocavitand, **38**

*C*-Pentyl-1,3-di(2-acetamidopyridyl-5-ethynyl)-2,4-dibromocavitand, **38** was synthesized following standard Sonogashira coupling procedures from 1,3-dibromo-2,4-diodocavitand with moderate yields (48%). The crystal structure determination of **38** revealed the presence of disordered acetone molecules along the upper rim.

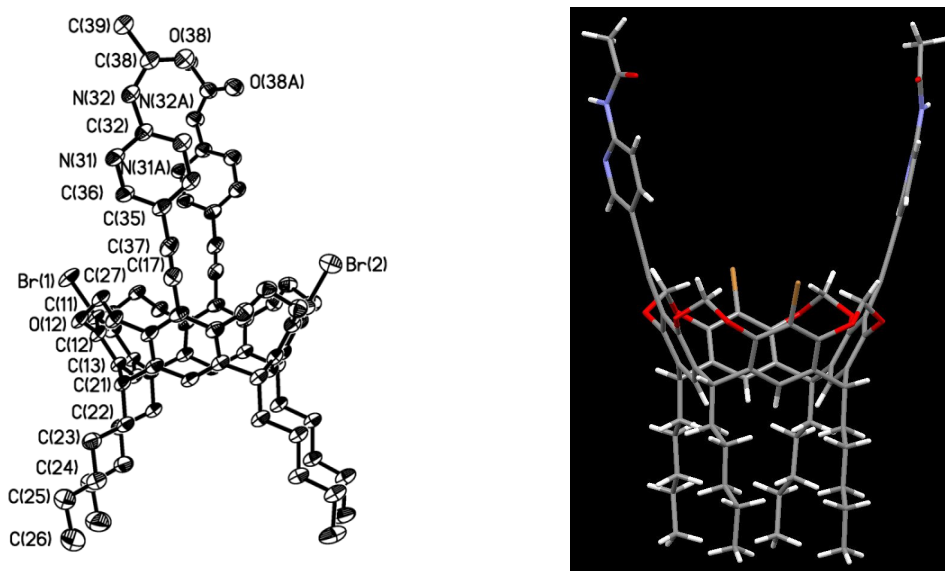


**Figure 6.17** *C*-Pentyl-1,3-di(2-acetamidopyridyl-5-ethynyl)-2,4-dibromocavitand, **38**; (a) thermal ellipsoid plots (50 % probabilities) and labeling schemes, (b) An individual cavitand.

Each cavitand molecule is connected to two inverted neighbors via two N-H...O (2.026 Å) hydrogen bonding between the NH group of the acetamido moiety in the “arm” and the oxygen atom in the methylene bridge on both sides to give extended 1D chain. The two individual chains are arranged such that the ‘feet’ of the cavitands in the upper chain lies in the cavity of the ones in the lower chain to give a ‘stacking of cones’ kind of arrangement, (Figure 6.18).

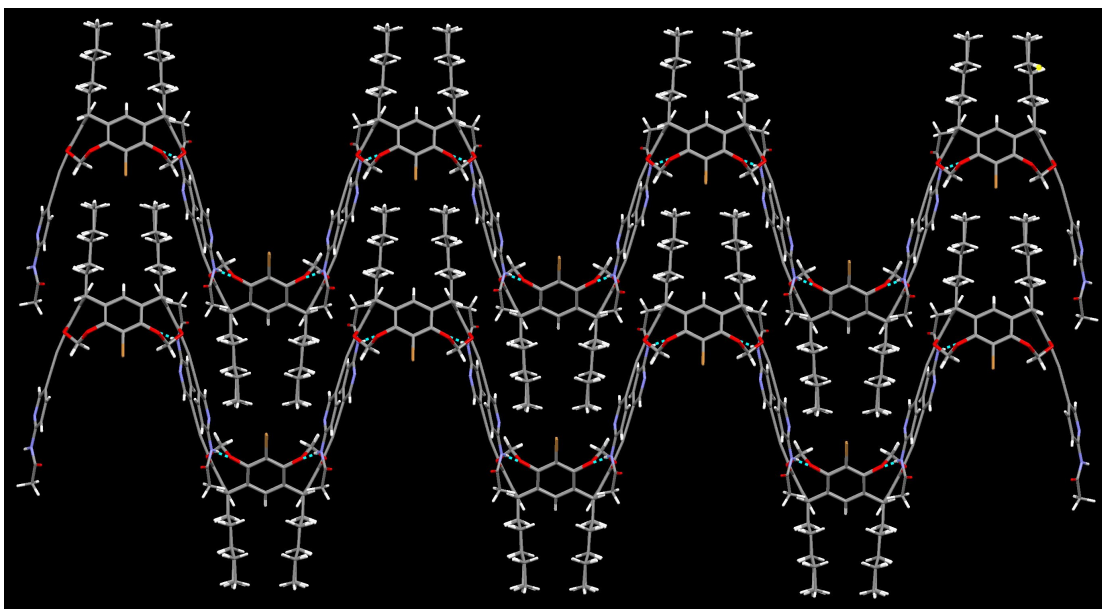


**Figure 6.18** Crystal packing of **38** revealing a linear 1D chain with ‘stacking of cones’ like architecture.

### 6.3.3 Quest for halogen-bonded capsule

Halogen-bond driven capsules require two cavitand molecules with halogen bonding potential to come together via heteromeric interactions. Unlike hydrogen-bond driven capsules, it is not possible to bring two cavitands together via homomeric interaction to form a capsule, hence a linker is needed to bind these frameworks. The heteromeric capsule however omits the need for a linker, but unfortunately our attempts at forming a heteromeric halogen bond driven capsule using 3-pyridyl or 4-pyridyl functionalized capsule with bromo- or iodo-cavitand failed to yield any suitable crystals.

#### 6.3.3.1 Crystal structure of C-pentyltetra(4-pyridyl)cavitand, **41**

Previous studies aimed at incorporating halogen bonding moieties on a cavitand resulted in the synthesis of C-pentyltetra(3-pyridyl)cavitand.<sup>44</sup> With the outward pointing pyridyl-N in 3-pyridylcavitand it may be impossible to bring in another cavitand molecule together into a capsular framework without any structural modifications. However, if a 4-pyridylcavitand with the pyridyl-N pointing upwards, there is a possibility to bring in another cavitand molecule using a linker into a capsular framework.

The synthesis of a 4-pyridylcavitand started with a standard Suzuki-Miyaura coupling reaction using tetrabromocavitand as the precursor. A reasonable yield of the product is not obtained, which prompted us to make few modifications along with the change of precursor to tetraiodocavitand to obtain moderate yields (45%).

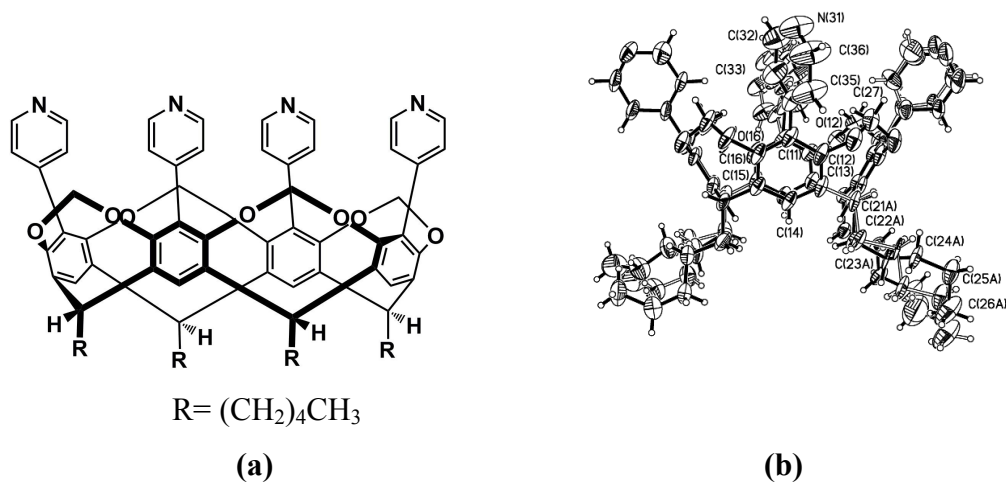


**Figure 6.19** C-Pentyl(4-pyridyl)cavitand, **41**; (a) thermal ellipsoid plots (50 % probabilities) and labeling schemes, (b) an individual cavitand.

The crystal structure determination of **41** revealed the presence of two ethanol molecules as guests along the upper rim of the cavitand, (Figure 6.20a). The extension of the network revealed the crystal packing with cavitands arranged in two layers of cavitands, (Figure 6.20b).

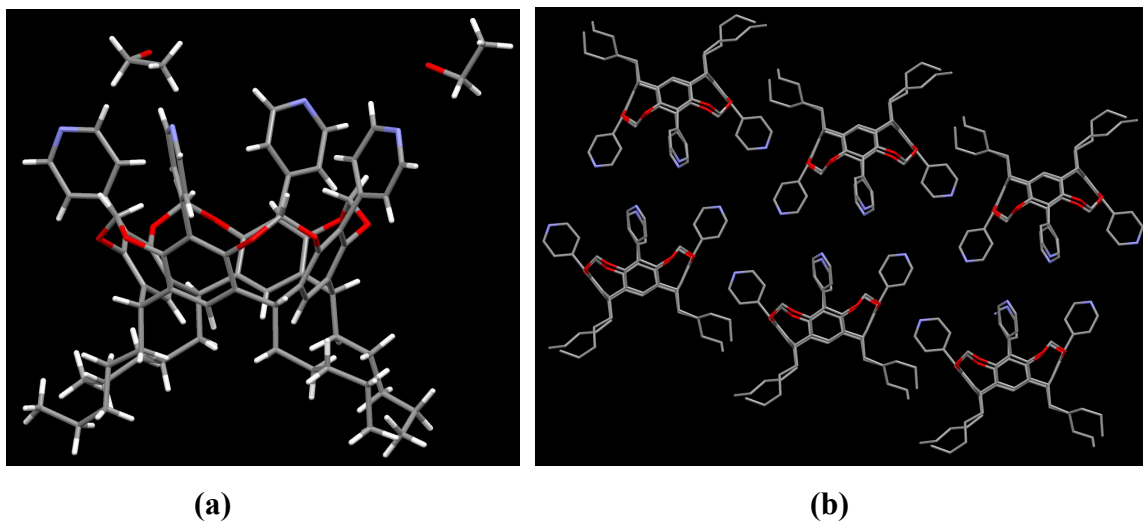


**Figure 6.20** (a) Individual cavitand **41**, with ethanol as guest molecules, (b) Linear arrangement of cavitands in crystallographic screw axis (hydrogen atoms removed for clarity).

### 6.3.3.2 Crystal structure of *C*-pentyltetra-(3-pyridyl)cavitand/1,4-diodotetrafluorobenzene, 40a

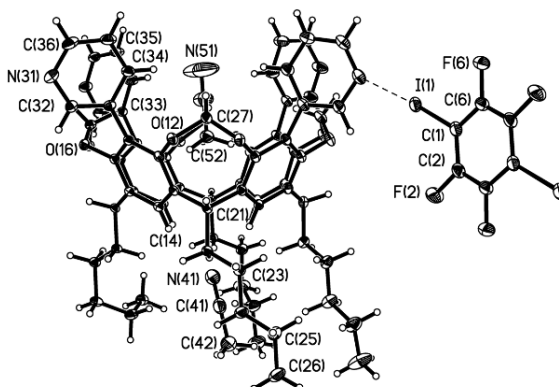


**Figure 6.21** Thermal ellipsoid plots (50 % probabilities) and labeling schemes of co-crystal of *C*-pentyltetra(3-pyridyl)cavitand and 1,4-diodotetrafluorobenzene.

The co-crystallization of *C*-pentyltetra(3-pyridyl)cavitand was carried out with 1,4-diodotetrafluorobenzene as a linker in acetonitrile. The crystal structure showed a 2:1 halogen-bonded co-crystal comprising 1,4-diodotetrafluorobenzene linked with two tetra(3-pyridyl)cavitand via an N---I interaction, (2.809 Å). Two acetonitrile molecules are present, one inside the cavity with the methyl group pointing towards the cavity and the other along the ‘feet’ of the cavitand with the cyano group pointing towards the cavity, (Figure 6.22). It is however surprising that the remaining three pyridyl ‘arms’ remain inactive.

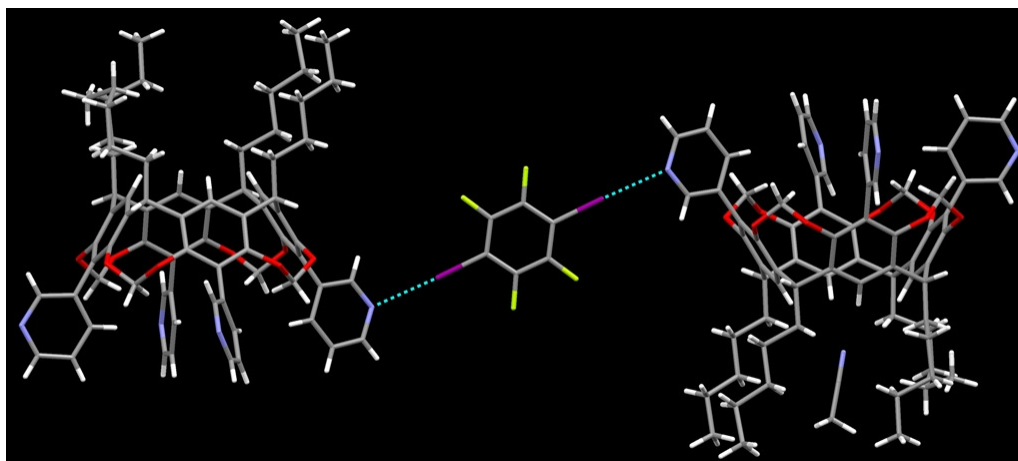


**Figure 6.22** Halogen bonding in 3-pyridylcavitand with N---I interaction with 1,4-diodotetrafluorobenzene 40a.

### 6.3.3.3 Crystal structure of *C*-pentyltetra-(4-pyridyl)cavitand/1,4-diiodotetrafluorobenzene, 41a

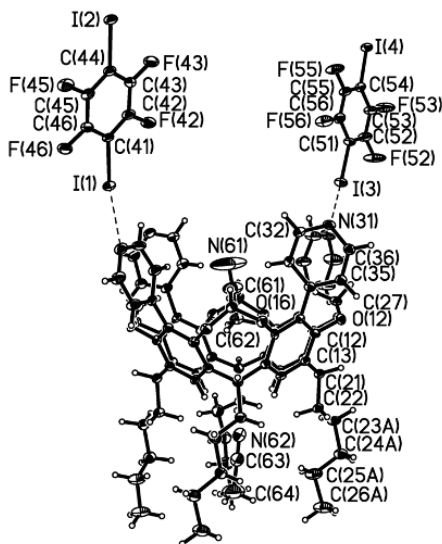


**Figure 6.23** Thermal ellipsoid plots (50 % probabilities) and labeling schemes of co-crystal of *C*-pentyltetra(4-pyridyl)cavitand and 1,4-diiodotetrafluorobenzene **41a**.

The co-crystallization of *C*-pentyltetra(4-pyridyl)cavitand was carried out with 1,4-diiodotetrafluorobenzene as a linker in acetonitrile. The crystal structure showed each of the pyridyl group in the “arms” halogen bonded to the diiodotetrafluorobenzene via N--I interactions (2.751 Å). Two acetonitrile molecules are present as guests, one inside the cavity with the methyl group pointing towards the cavity and the other along the ‘feet’ of the cavitand with the cyano group pointing towards the cavity, (Figure 6.23). Upon extension of the network, it was observed that each of the set of two adjacent diiodotetrafluorobenzenes bonded to the pyridylcavitand, in turn binds to two neighboring pyridyl cavitands, hence resulting in a zigzag 1D chain structure, (Figure 6.24).

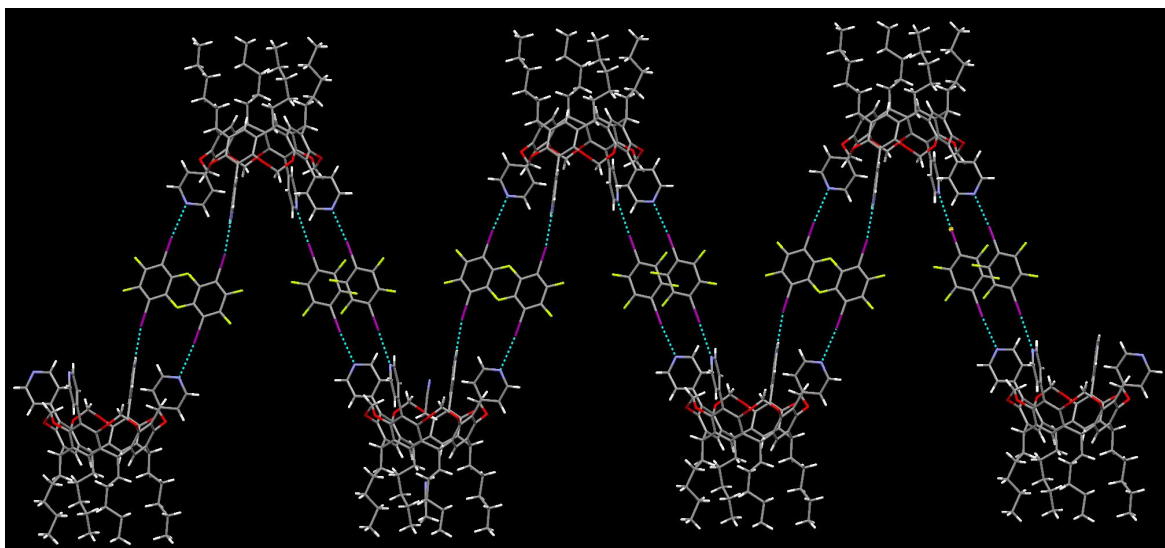


**Figure 6.24** One-dimensional zigzag network of **41a** bonded via N...I interaction.

#### 6.3.3.4 Crystal structure of C-pentyltetra-(3-pyridyl)cavitand/calixarene, **40b**

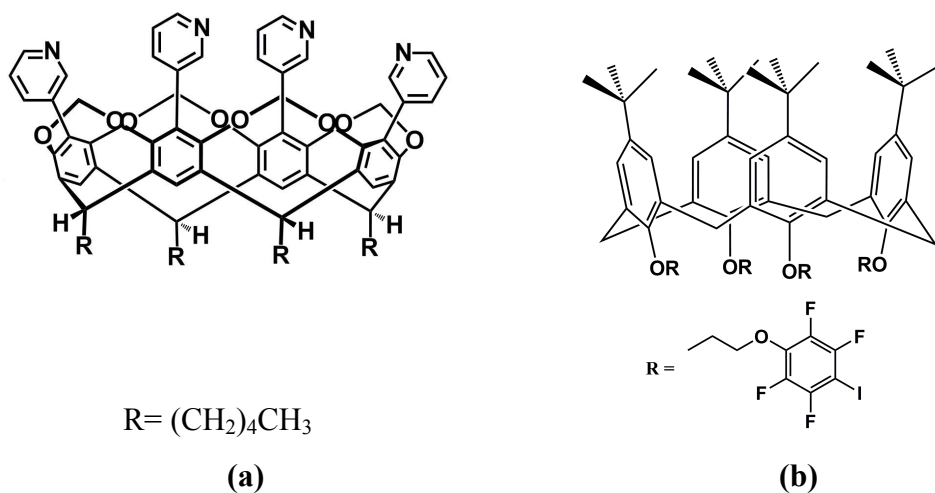


**Figure 6.25** Structure of (a) C-pentyltetra-(3-pyridyl)cavitand, **40** (b) t-butyl-substituted halogen-derivatized calixarene.

C-Pentyltetra-(3-pyridyl)cavitand was co-crystallized with a halogen functionalized substituted calixarene<sup>45</sup> to obtain a halogen bonded capsule.

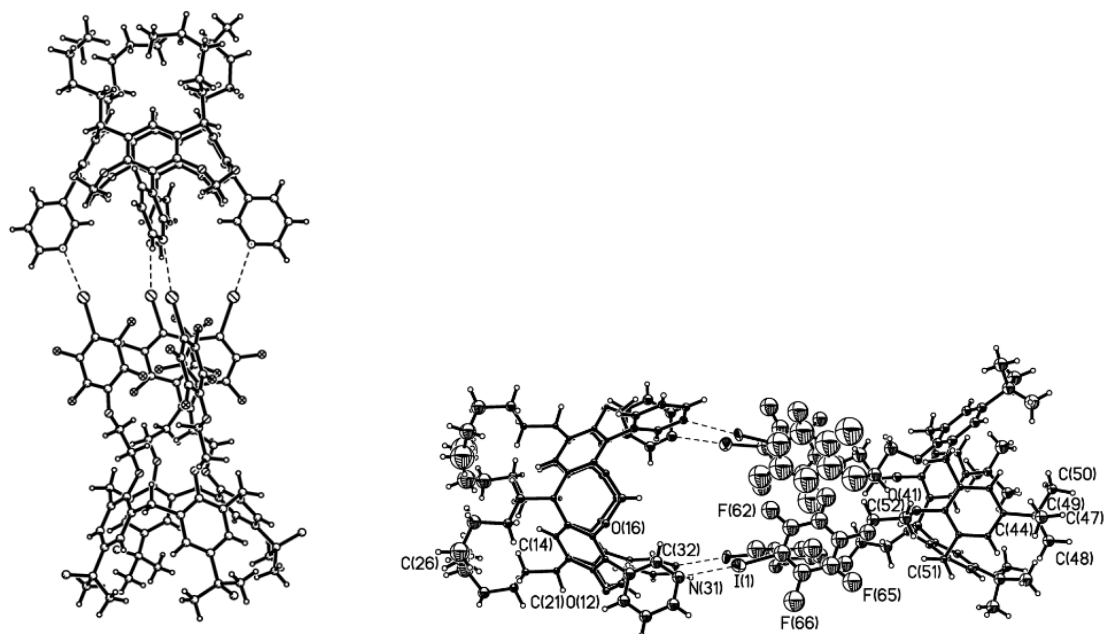


**Figure 6.26** Thermal ellipsoid plots (50 % probabilities) and labeling schemes of co-crystal of C-pentyltetra(3-pyridyl)cavitand and halogen-derivatized calixarene in a capsular framework.

The crystal structure of **40b** shows one tetra(3-pyridyl)cavitand and one halo-substituted calixarene molecule interacting via N---I halogen bonds to give a capsular framework. It contains one acetonitrile molecule lying along the t-butyl end of the calixarene with the methyl group pointing towards the interior of the cavity. Each of the four pyridyl-N from the cavitand is linked with iodines in the substituted calixarene with N---I bond distances of 2.780, 2.867, 2.875, and 2.876 Å. The interior of the capsule is shaped like a ‘vase’ with the length of 16 Å and maximum width of 10 Å, the wider part being the cavity of the cavitand which tapers into the calixarene, (Figure 6.27).



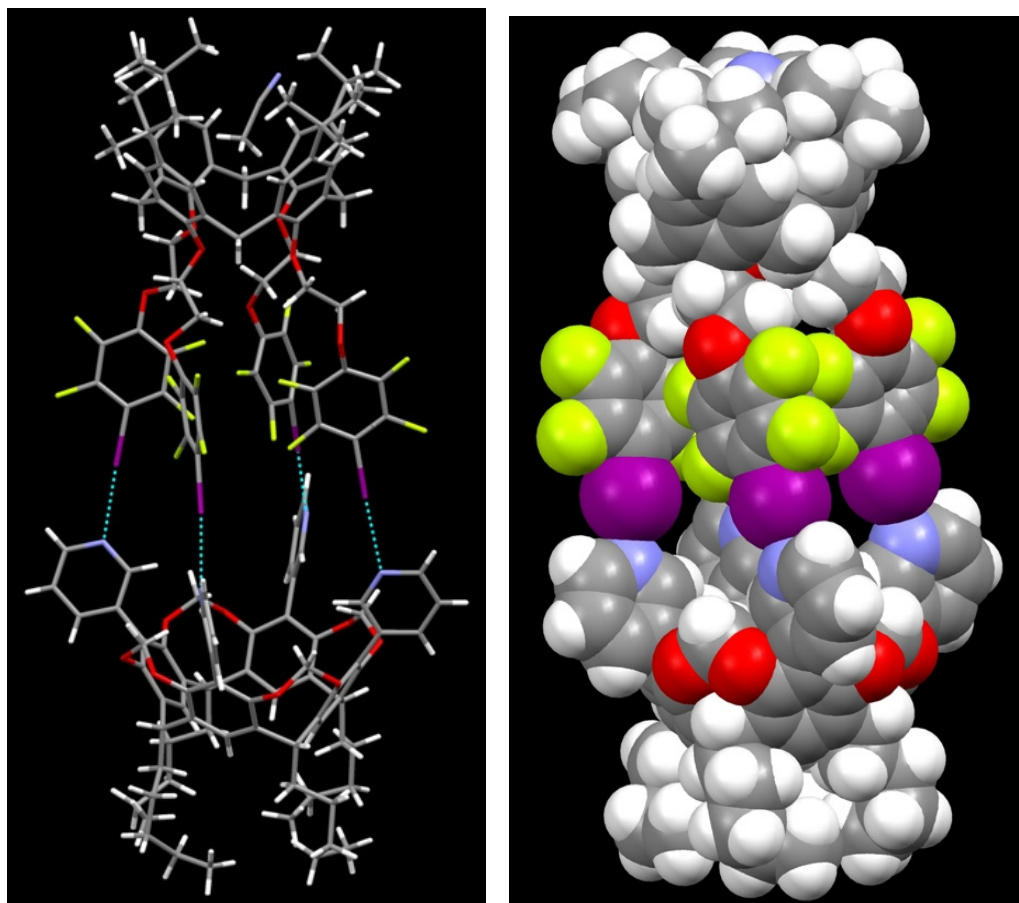


**Figure 6.27** Molecular structure and spacefill diagram showing the capsular framework of **40b**.

## 6.4 Conclusions

Our studies show that resorcinarene-based cavitands can be utilized as building blocks to craft the assembly of discrete molecular capsules via both hydrogen bonds and halogen bonds. The capability of functionalization via palladium (0 and II) catalyzed Suzuki-Miyaura or Sonogashira cross-coupling reactions to furnish variety of cavitands with wide variations in structure and characteristics is very appealing. The bromo/iodocavitand can act as a point for heterodimeric capsule formation or can be further functionalized to generate cavitands with specific properties.

The addition of ethynyl groups adds to the depth of the cavitand and also increases the electron density in the walls bounding the interior of the cavity, hence enabling it to capture electron deficient and larger-sized guests. The incorporation of substituted pyridines, pyrazine as well as pyrimidine moieties allowed us to manipulate the binding capabilities as well as to increase the probability of forming symmetric as well as asymmetric dimeric capsules via hydrogen bonding and even halogen bonding with or without the help of a suitable linker.

Decorating the upper rim of the cavitand with appropriate functionalities also gives an opportunity to explore the probability of trapping two different guests in the interior of two complementary cavitands (electron-deficient and electron-rich cavitands), and bringing them in close contact in a heterodimeric capsule.

## References

- <sup>1</sup> Whitesides, G. M.; Mathias, J. P.; Seto, C. T. *Science*, **1991**, 29(254), 1312.
- <sup>2</sup> (a) Lehn, J.-M. *Supramolecular Chemistry: concepts and perspectives* 1995, VCH: Weinheim; (b) Steed, J. W.; Atwood, J. L. *Supramolecular Chemistry* 2000, John Wiley and Sons: Ltd., Chichester.
- <sup>3</sup> Lehn, J. M. *Angew. Chem., Int. Ed.* **2003**, 29, 1304.
- <sup>4</sup> Rebek, J., Jr. *Angew. Chem., Int. Ed.* **2005**, 44, 2068.
- <sup>5</sup> Castellano, R. K.; Craig, S. L.; Nuckolls, C.; Rebek, J., Jr. *J. Am. Chem. Soc.* **2000**, 122, 7876.
- <sup>6</sup> Chen, J.; Rebek, J., Jr. *Org. Lett.* **2002**, 4, 327.
- <sup>7</sup> (a) Fujita, M.; Umemoto, K.; Yoshizawa, M.; Fujita, N.; Kusukawa, T.; Biradha, K. *Chem. Commun.* **2001**, 509; (b) Yoshizawa, M.; Kusukawa, T.; Fujita, M.; Yamaguchi, K. *J. Am. Chem. Soc.* **2000**, 122, 6311; (c) Kang, J. M.; Santamaría, J.; Hilmersson, G.; Rebek, J., Jr. *J. Am. Chem. Soc.* **1998**, 120, 7389; (d) Chen, J.; Körner, S.; Craig, S. L.; Rudkevich, D. M.; Rebek, J., Jr. *Nature* **2002**, 415.
- <sup>8</sup> (a) Kusukawa, T.; Fujita, M. *J. Am. Chem. Soc.* **1999**, 121, 1397; (b) Körner, S. K.; Tucci, F. C.; Rudkevich, D. M.; Heinz, T.; Rebek, J., Jr. *Chem. Eur. J.* **2000**, 6, 187.
- <sup>9</sup> Scarso, A.; Shivanyuk, A.; Hayashida, O.; Rebek, J., Jr. *J. Am. Chem. Soc.* **2003**, 125, 6239.
- <sup>10</sup> Ajami, D.; Rebek, J., Jr. *Angew. Chem., Int. Ed.* **2008**, 47, 6059.
- <sup>11</sup> Ajami, D.; Rebek, J., Jr. *Proc. Natl. Acad. Sci. U.S.A.* **2007**, 104, 16000.
- <sup>12</sup> (a) Fujita, M.; Umemoto, K.; Yoshizawa, M.; Fujita, N.; Kusukawa, T.; Biradha, K. *Chem. Commun.* **2001**, 509; (b) Olenyuk, B.; Whiteford, J. A.; Fechtenkotter, A.; Stang, P. J. *Nature* **1999**, 398, 796; (c) Baxter, P. N. W.; Lehn, J.-M.; Baum, G.; Fenske, D. *Chem. Eur. J.* **1999**, 5, 102; (d) Baxter, P. N. W.; Lehn, J.-M.; Kneisel, B. O.; Baum, G.; Fenske, D. *Chem. Eur. J.* **1999**, 5, 113; (e) Fox, O. D.; Dalley, N. K.; Harrison, R. G. *J. Am. Chem. Soc.* **1998**, 120, 7111.
- <sup>13</sup> (a) Sherman, J. C. *Tetrahedron.* **1995**, 51, 3395; (b) Rebek, J., Jr. *Angew. Chem., Int. Ed.* **2005**, 44, 2068; (c) Chen, J.; Rebek, J., Jr. *Org. Lett.* **2002**, 4, 327; (d) Scarso, A.; Shivanyuk, A.; Hayashida, O.; Rebek, J., Jr. *J. Am. Chem. Soc.* **2003**, 125, 6239; (e) Scarso, A.; Shivanyuk, A.; Rebek, J., Jr. *J. Am. Chem. Soc.* **2003**, 125, 13981; (f) Ajami, D.; Rebek, J., Jr. *J. Am. Chem. Soc.* **2006**, 128, 15038; (g) Ajami, D.; Rebek, J., Jr. *Angew. Chem., Int. Ed.* **2008**, 47, 6059.
- <sup>14</sup> (a) Ajami, D.; Rebek, J., Jr. *J. Org. Chem.* **2009**, 74, 6584; (b) Avram, L.; Cohen, Y. *J. Am. Chem. Soc.* **2004**, 126, 11556; (c) Shivanyuk, A.; Rebek, J., Jr. *Chem. Commun.* **2001**, 2424; (d) MacGillivray, L. R.; Atwood, J. L. *Nature* **1997**, 389, 469; (e) Kobayashi, K.; Ishii, K.; Sakamoto, S.; Shirasaka, T.; Yamaguchi, K. *J. Am. Chem. Soc.* **2003**, 125, 10615; (f) Gonzalez, J. J.; Ferdani, R.; Albertini, E.; Blasco, J. M.; Arduini, A.; Pochini, A.; Prados, P.; de Mendoza, J. *Chem. Eur. J.* **2000**, 6, 73; (g) Scarso, A.; Pellizzaro, L.; De Lucchi, O.; Linden, A.; Fabris, F. *Angew. Chem., Int. Ed.* **2007**, 46, 4972.
- <sup>15</sup> (a) Yoshizawa, M.; Tamura, M.; Fujita, M. *Science* **2006**, 312, 251; (b) Ziegler, M.; Brumaghim, J. L.; Raymond, K. N. *Angew. Chem., Int. Ed.* **2000**, 39, 4119.
- <sup>16</sup> Chapman, R. G.; Sherman, J. C. *J. Am. Chem. Soc.* **1998**, 120, 9818.

- 
- <sup>17</sup> Kaanumalle, L. S.; Gibb, C. L. D.; Gibb, B. C.; Ramamurthy, V. *J. Am. Chem. Soc.* **2005**, *127*, 3674.
- <sup>18</sup> Rebek, J. *Angew. Chem. Int. Ed.* **2005**, *44*, 2068.
- <sup>19</sup> Moran, J. R.; Karbach, S.; Cram, D. J. *J. Am. Chem. Soc.* **1982**, *104*, 5826.
- <sup>20</sup> Cram, D. J.; Cram, J. M. *Container Molecules and Their Guests* 1994, Royal Society of Chemistry, Cambridge.
- <sup>21</sup> (a) Cram, D. J.; Stewart, K. D.; Goldberg, I.; Trueblood, K. N. *J. Am. Chem. Soc.* **1985**, *107*, 2574; (b) Barrett, E. S.; Irwin, J. L.; Turner, P.; Sherburn, M. S. *J. Org. Chem.* **2001**, *66*, 8227.
- <sup>22</sup> (a) Cram, D. J.; Choi, H.-J.; Bryant, J. R.; Knobler, C. B. *J. Am. Chem. Soc.* **1992**, *114*, 7748; (b) Hooley, R. J.; Biro, S. M.; Rebek, J. *Angew. Chem., Int. Ed.* **2006**, *45*, 3517.
- <sup>23</sup> (a) Barrett, E. S.; Irwin, J. L.; Turner, P.; Sherburn, M. S.; *J. Org. Chem.* **2001**, *66*, 8227; (b) Purse, B. W.; Rebek, J.; *PNAS*, **2005**, *102*, 31.
- <sup>24</sup> (a) Tunstad, L. M.; Tucker, J. A.; Dalcanale, E.; Weiser, J.; Bryant, J. A.; Sherman, J. C.; Helgeson, R. C.; Knobler, C. B.; Cram, D. J. *J. Org. Chem.* **1989**, *54*, 1305; (b) Mezo, A. R.; Sherman, J. C. *J. Org. Chem.* **1998**, *63*, 6824.
- <sup>25</sup> Ajami, D.; Rebek, Jr. *J. Supramol. Chem.* **2009**, *21*(1-2), 103.
- <sup>26</sup> (a) Zuidema, E.; Sarmentero, M. A.; Bo, C.; Ballester, P. *Chem. Eur. J.* **2008**, *14*, 7285; (b) Srinivasan, K.; Laughrey, Z. R.; Gibb, B. C. *Eur. J. Org. Chem.* **2008**, 3265; (c) Botta, B.; Cassani, M.; D'Acquarica, I.; Subissati, D.; Zappia, G.; Monache, G. D. *Current Org. Chem.* **2005**, *9*, 1167.
- <sup>27</sup> (a) Kitagawa, H.; Kawahata, M.; Kitagawa, R.; Yamada, Y.; Yamanaka, M.; Yamaguchi, K.; Kobayashi, K. *Tetrahedron* **2009**, *65*, 7234; (b) Schroder, T.; Brodbeck, R.; Letzel, M. C.; Mix, A.; Schnatwinkel, B.; Tonigold, M.; Volkmer, D.; Mattay, J. *Tet. Lett.* **2008**, *49*, 5939; (c) Zhu, S. S.; Staats, H.; Brandhorst, K.; Grunenberg, J.; Gruppi, F.; Dalcanale, E.; Lutzen, A.; Rissanen, K.; Schalley, C. A. *Angew. Chem. Int. Ed.* **2008**, *47*, 788; (d) Irwin, J. L.; Sherburn, M. S. *J. Org. Chem.* **2000**, *65*, 5846.
- <sup>28</sup> Metrangolo, P.; Resnati, G.; Arman, H. D. *Halogen Bonding: Fundamentals and Applications* **2008**, Springer, Berlin.
- <sup>29</sup> (a) Metrangolo, P.; Resnati, G. *Chem.; Eur. J.* **2001**, *7*, 2511; (b) Metrangolo, P.; Neukirch, H.; Pilati, T.; Resnati, G. *Acc. Chem. Res.* **2005**, *38*, 386; (c) Metrangolo, P.; Pilati, T.; Resnati, G. *CrystEngComm* **2006**, *8*, 946.
- <sup>30</sup> Metrangolo, P.; Meyer, F.; Pilati, T.; Resnati, G.; Terraneo, G. *Angew. Chem. Int. Ed.* **2008**, *47*, 6114.
- <sup>31</sup> Metrangolo, P.; Resnati, G. *Science* **2008**, *321*, 918.
- <sup>32</sup> Awwadi, F. F.; Willet, R. D.; Peterson, K. A.; Twamley, B. *Chem. Eur. J.* **2006**, *12*, 8952.
- <sup>33</sup> Fourmigu, M.; Batail, P. *Chem. Rev.* **2004**, *104*, 5379.
- <sup>34</sup> Takeuchi, T.; Minato, Y.; Masayoshi, M.; Shinmori, H. *Tetrahedron Lett.* **2005**, *46*, 9025.
- <sup>35</sup> (a) Marras, G.; Metrangolo, P.; Meyer, F.; Pilati, T.; Resnati, G.; Vij, A. *New J. Chem.* **2006**, *30*, 1397; (b) Caronna, T.; Liantonio, R.; Logothetis, T. A.; Metrangolo, P.; Pilati, T.; Resnati, G. *J. Am. Chem. Soc.* **2004**, *126*, 4500.
- <sup>36</sup> (a) Adler, M.; Kochanny, M. J.; Ye, B.; Rumennik, G.; Light, D. R.; Biancalana, S.;

- 
- Whitlow, M. *Biochemistry* **2002**, *41*, 15514; (b) Auffinger, P.; Hays, F. A.; Westhof, E.; Ho, P. S. *Proc. Natl. Acad. Sci. USA* **2004**, *101*, 16789; (c) Jiang, Y.; Alcaraz, A. A.; Chen, J. M.; Kobayashi, H.; Lu, Y. J.; Snyder, J. P. *J. Med. Chem.* **2006**, *49*, 1891.
- <sup>37</sup> (a) Mele, A.; Metrangolo, P.; Neukirch, H.; Pilati, T.; Resnati, G. *J. Am. Chem. Soc.* **2005**, *127*, 14972; (b) Minguez Espallargas, G.; Brammer, L.; van de Streek, J.; Shankland, K.; Florence, A. J.; Adams, H. *J. Am. Chem. Soc.* **2006**, *128*, 9584.
- <sup>38</sup> Shirman, T.; Lamere J-F.; Shimon, L. J. W.; Gupta, T.; Martin, J. M. L.; Boom, E. *Crystal Growth & Design* **2008**, *8*(8), 3066.
- <sup>39</sup> (a) Raatikainen, K.; Huuskonen, J.; Lahtinen, M.; Metrangolo, P.; Rissanen, K. *Chem. Commun.* **2009**, 2160; (b) Metrangolo, P.; Meyer, F.; Pilati, T.; Proserpio, D. M.; Resnati, G. *Chem. Eur. J.* **2007**, *13*, 5765.
- <sup>40</sup> Aakeröy, C. B.; Schultheiss, N.; Desper, J. *Unpublished*
- <sup>41</sup> Aoyama, Y.; Tanaka, Y.; Sugahara, S. *J. Am. Chem. Soc.* **1989**, *111*, 2167.
- <sup>42</sup> Liu, X.; Warmuth, R. *Nature Protocols.* **2007**, *2*(3), 1288.
- <sup>43</sup> Bryant, J. A.; Blanda, M. T.; Vincenti, M.; Cram, D. J. *J. Am. Chem. Soc.* **1991**, *113*, 2167.
- <sup>44</sup> Aakeröy, C. B.; Schultheiss, N.; Desper, J. *Org. Lett.* **2006**, *8* (12), 2607.
- <sup>45</sup> The compound haloxalixarene was supplied by Giuseppe Resnati and Pierangelo Metrangolo, University of Milano, Italy.

## **Appendix A - Crystal Structure Data**

**Table A.1** Crystal data and structure refinement for **4**

Identification code	ar0912m	
Empirical formula	C <sub>8</sub> H <sub>9</sub> Br N <sub>2</sub> O	
Formula weight	229.08	
Temperature	120(2) K	
Wavelength	0.71073 Å	
Crystal system	Orthorhombic	
Space group	Pbca	
Unit cell dimensions	a = 9.3809(8) Å	α = 90°.
	b = 8.3436(7) Å	β = 90°.
	c = 22.7825(18) Å	γ = 90°.
Volume	1783.2(3) Å <sup>3</sup>	
Z	8	
Density (calculated)	1.707 g/cm <sup>3</sup>	
Absorption coefficient	4.562 mm <sup>-1</sup>	
F(000)	912	
Crystal size	0.22 x 0.18 x 0.12 mm <sup>3</sup>	
Theta range for data collection	2.81 to 31.62°.	
Index ranges	-13 ≤ h ≤ 13, -12 ≤ k ≤ 12, -33 ≤ l ≤ 33	
Reflections collected	36371	
Independent reflections	2983 [R(int) = 0.0871]	
Completeness to theta = 31.62°	99.4 %	
Absorption correction	None	
Max. and min. transmission	0.6105 and 0.4335	
Refinement method	Full-matrix least-squares on F <sup>2</sup>	
Data / restraints / parameters	2983 / 0 / 113	
Goodness-of-fit on F <sup>2</sup>	1.073	
Final R indices [I > 2σ(I)]	R1 = 0.0436, wR2 = 0.0994	
R indices (all data)	R1 = 0.0803, wR2 = 0.1167	
Largest diff. peak and hole	0.798 and -0.594 e.Å <sup>-3</sup>	

**Table A.2** Crystal data and structure refinement for **6**

Identification code	ar0708m	
Empirical formula	C7 H7 Br N2 O	
Formula weight	215.06	
Temperature	120(2) K	
Wavelength	0.71073 Å	
Crystal system	Triclinic	
Space group	P-1	
Unit cell dimensions	a = 3.8683(3) Å	$\alpha = 81.734(3)^\circ$ .
	b = 8.6800(7) Å	$\beta = 88.723(3)^\circ$ .
	c = 22.5717(18) Å	$\gamma = 85.962(3)^\circ$ .
Volume	748.09(10) Å <sup>3</sup>	
Z	4	
Density (calculated)	1.909 g/cm <sup>3</sup>	
Absorption coefficient	5.431 mm <sup>-1</sup>	
F(000)	424	
Crystal size	0.25 x 0.10 x 0.10 mm <sup>3</sup>	
Theta range for data collection	0.91 to 31.19°.	
Index ranges	-5 ≤ h ≤ 5, -12 ≤ k ≤ 12, -26 ≤ l ≤ 32	
Reflections collected	13566	
Independent reflections	4521 [R(int) = 0.0283]	
Completeness to theta = 31.19°	92.6 %	
Absorption correction	None	
Max. and min. transmission	0.6127 and 0.3438	
Refinement method	Full-matrix least-squares on F <sup>2</sup>	
Data / restraints / parameters	4521 / 0 / 207	
Goodness-of-fit on F <sup>2</sup>	0.982	
Final R indices [I > 2σ(I)]	R1 = 0.0304, wR2 = 0.0668	
R indices (all data)	R1 = 0.0489, wR2 = 0.0739	
Largest diff. peak and hole	0.678 and -0.553 e.Å <sup>-3</sup>	



**Table A.3** Crystal data and structure refinement for **1a**

Identification code	ar0908m	
Empirical formula	C <sub>13</sub> H <sub>11</sub> N <sub>3</sub> O <sub>2</sub>	
Formula weight	241.25	
Temperature	120(2) K	
Wavelength	0.71073 Å	
Crystal system	Monoclinic	
Space group	P2(1)	
Unit cell dimensions	a = 8.3508(5) Å	α = 90°.
	b = 6.9219(4) Å	β = 102.214(4)°.
	c = 10.4152(6) Å	γ = 90°.
Volume	588.41(6) Å <sup>3</sup>	
Z	2	
Density (calculated)	1.362 g/cm <sup>3</sup>	
Absorption coefficient	0.095 mm <sup>-1</sup>	
F(000)	252	
Crystal size	0.24 x 0.18 x 0.12 mm <sup>3</sup>	
Theta range for data collection	3.51 to 32.58°.	
Index ranges	-12 ≤ h ≤ 12, -8 ≤ k ≤ 10, -15 ≤ l ≤ 14	
Reflections collected	7738	
Independent reflections	2293 [R(int) = 0.0237]	
Completeness to theta = 32.58°	99.7 %	
Absorption correction	None	
Max. and min. transmission	0.9887 and 0.9775	
Refinement method	Full-matrix least-squares on F <sup>2</sup>	
Data / restraints / parameters	2293 / 1 / 172	
Goodness-of-fit on F <sup>2</sup>	1.051	
Final R indices [I > 2σ(I)]	R1 = 0.0380, wR2 = 0.1018	
R indices (all data)	R1 = 0.0439, wR2 = 0.1064	
Absolute structure parameter	0.4(11)	
Largest diff. peak and hole	0.333 and -0.180 e.Å <sup>-3</sup>	

**Table A.4** Crystal data and structure refinement for **1c**

Identification code	ar0815m	
Empirical formula	C <sub>12</sub> H <sub>11</sub> Cl N <sub>2</sub> O <sub>2</sub>	
Formula weight	250.68	
Temperature	120(2) K	
Wavelength	0.71073 Å	
Crystal system	Monoclinic	
Space group	Pn	
Unit cell dimensions	a = 6.6153(14) Å	α = 90°.
	b = 7.9832(17) Å	β = 99.763(5)°.
	c = 11.143(3) Å	γ = 90°.
Volume	579.9(2) Å <sup>3</sup>	
Z	2	
Density (calculated)	1.436 g/cm <sup>3</sup>	
Absorption coefficient	0.320 mm <sup>-1</sup>	
F(000)	260	
Crystal size	0.20 x 0.12 x 0.08 mm <sup>3</sup>	
Theta range for data collection	3.15 to 31.50°.	
Index ranges	-9 ≤ h ≤ 9, -11 ≤ k ≤ 11, -15 ≤ l ≤ 16	
Reflections collected	6842	
Independent reflections	3349 [R(int) = 0.0191]	
Completeness to theta = 25.00°	99.7 %	
Absorption correction	None	
Max. and min. transmission	0.9749 and 0.9388	
Refinement method	Full-matrix least-squares on F <sup>2</sup>	
Data / restraints / parameters	3349 / 2 / 163	
Goodness-of-fit on F <sup>2</sup>	1.087	
Final R indices [I > 2σ(I)]	R1 = 0.0297, wR2 = 0.0771	
R indices (all data)	R1 = 0.0322, wR2 = 0.0790	
Absolute structure parameter	0.02(4)	
Largest diff. peak and hole	0.292 and -0.188 e.Å <sup>-3</sup>	

**Table A.5** Crystal data and structure refinement for **1g**

Identification code	ar0902m	
Empirical formula	C <sub>12</sub> H <sub>10</sub> F <sub>2</sub> N <sub>2</sub> O <sub>2</sub>	
Formula weight	252.22	
Temperature	120(2) K	
Wavelength	0.71073 Å	
Crystal system	Orthorhombic	
Space group	Pbca	
Unit cell dimensions	a = 9.0887(5) Å	α = 90°.
	b = 11.5417(7) Å	β = 90°.
	c = 20.9156(13) Å	γ = 90°.
Volume	2194.0(2) Å <sup>3</sup>	
Z	8	
Density (calculated)	1.527 g/cm <sup>3</sup>	
Absorption coefficient	0.128 mm <sup>-1</sup>	
F(000)	1040	
Crystal size	0.25 x 0.25 x 0.15 mm <sup>3</sup>	
Theta range for data collection	3.01 to 31.50°.	
Index ranges	-6 ≤ h ≤ 13, -16 ≤ k ≤ 16, -29 ≤ l ≤ 30	
Reflections collected	35383	
Independent reflections	3553 [R(int) = 0.0401]	
Completeness to theta = 31.50°	97.1 %	
Absorption correction	None	
Max. and min. transmission	0.9810 and 0.9687	
Refinement method	Full-matrix least-squares on F <sup>2</sup>	
Data / restraints / parameters	3553 / 0 / 172	
Goodness-of-fit on F <sup>2</sup>	1.065	
Final R indices [I > 2σ(I)]	R1 = 0.0393, wR2 = 0.1079	
R indices (all data)	R1 = 0.0494, wR2 = 0.1139	
Largest diff. peak and hole	0.379 and -0.213 e.Å <sup>-3</sup>	

**Table A.6** Crystal data and structure refinement for **1j**

Identification code	ar0905m	
Empirical formula	C <sub>12</sub> H <sub>7</sub> F <sub>5</sub> N <sub>2</sub> O <sub>2</sub>	
Formula weight	306.20	
Temperature	120(2) K	
Wavelength	0.71073 Å	
Crystal system	Monoclinic	
Space group	P2(1)/c	
Unit cell dimensions	a = 12.1134(12) Å	α = 90°.
	b = 9.0910(9) Å	β = 114.822(4)°.
	c = 11.9721(13) Å	γ = 90°.
Volume	1196.6(2) Å <sup>3</sup>	
Z	4	
Density (calculated)	1.700 g/cm <sup>3</sup>	
Absorption coefficient	0.168 mm <sup>-1</sup>	
F(000)	616	
Crystal size	0.20 x 0.16 x 0.12 mm <sup>3</sup>	
Theta range for data collection	2.91 to 32.58°.	
Index ranges	-18 ≤ h ≤ 18, -13 ≤ k ≤ 12, -18 ≤ l ≤ 15	
Reflections collected	15805	
Independent reflections	4348 [R(int) = 0.0258]	
Completeness to theta = 32.58°	99.9 %	
Absorption correction	None	
Max. and min. transmission	0.9801 and 0.9671	
Refinement method	Full-matrix least-squares on F <sup>2</sup>	
Data / restraints / parameters	4348 / 0 / 199	
Goodness-of-fit on F <sup>2</sup>	1.027	
Final R indices [I > 2σ(I)]	R1 = 0.0407, wR2 = 0.1168	
R indices (all data)	R1 = 0.0498, wR2 = 0.1234	
Largest diff. peak and hole	0.493 and -0.236 e.Å <sup>-3</sup>	

**Table A.7** Crystal data and structure refinement for **1k**

Identification code	ar0904m	
Empirical formula	C <sub>18</sub> H <sub>26</sub> N <sub>4</sub> O <sub>4</sub>	
Formula weight	362.43	
Temperature	120(2) K	
Wavelength	0.71073 Å	
Crystal system	Monoclinic	
Space group	P2(1)/n	
Unit cell dimensions	a = 8.8279(6) Å	α = 90°.
	b = 5.6026(4) Å	β = 94.946(3)°.
	c = 18.5118(11) Å	γ = 90°.
Volume	912.17(10) Å <sup>3</sup>	
Z	2	
Density (calculated)	1.320 g/cm <sup>3</sup>	
Absorption coefficient	0.095 mm <sup>-1</sup>	
F(000)	388	
Crystal size	0.25 x 0.20 x 0.15 mm <sup>3</sup>	
Theta range for data collection	2.21 to 32.58°.	
Index ranges	-11 ≤ h ≤ 13, -8 ≤ k ≤ 7, -28 ≤ l ≤ 20	
Reflections collected	11583	
Independent reflections	3225 [R(int) = 0.0206]	
Completeness to theta = 32.58°	97.1 %	
Absorption correction	None	
Max. and min. transmission	0.9859 and 0.9767	
Refinement method	Full-matrix least-squares on F <sup>2</sup>	
Data / restraints / parameters	3225 / 0 / 127	
Goodness-of-fit on F <sup>2</sup>	1.109	
Final R indices [I > 2σ(I)]	R1 = 0.0386, wR2 = 0.1088	
R indices (all data)	R1 = 0.0436, wR2 = 0.1164	
Largest diff. peak and hole	0.433 and -0.266 e.Å <sup>-3</sup>	

**Table A.8** Crystal data and structure refinement for **1n**

Identification code	ar0909m	
Empirical formula	C <sub>9</sub> H <sub>12</sub> N <sub>2</sub> O <sub>4</sub>	
Formula weight	212.21	
Temperature	120(2) K	
Wavelength	0.71073 Å	
Crystal system	Monoclinic	
Space group	P2(1)/c	
Unit cell dimensions	a = 10.0946(9) Å	α = 90°.
	b = 5.1454(5) Å	β = 104.255(3)°.
	c = 18.9656(17) Å	γ = 90°.
Volume	954.76(15) Å <sup>3</sup>	
Z	4	
Density (calculated)	1.476 g/cm <sup>3</sup>	
Absorption coefficient	0.117 mm <sup>-1</sup>	
F(000)	448	
Crystal size	0.35 x 0.25 x 0.15 mm <sup>3</sup>	
Theta range for data collection	2.08 to 32.57°.	
Index ranges	-10 ≤ h ≤ 15, -6 ≤ k ≤ 7, -28 ≤ l ≤ 28	
Reflections collected	10173	
Independent reflections	3337 [R(int) = 0.0197]	
Completeness to theta = 30.00°	99.0 %	
Absorption correction	None	
Max. and min. transmission	0.9826 and 0.9601	
Refinement method	Full-matrix least-squares on F <sup>2</sup>	
Data / restraints / parameters	3337 / 0 / 148	
Goodness-of-fit on F <sup>2</sup>	1.025	
Final R indices [I > 2σ(I)]	R1 = 0.0387, wR2 = 0.1092	
R indices (all data)	R1 = 0.0436, wR2 = 0.1149	
Largest diff. peak and hole	0.489 and -0.269 e.Å <sup>-3</sup>	

**Table A.9** Crystal data and structure refinement for **1o**

Identification code	ar0816m	
Empirical formula	C <sub>20</sub> H <sub>30</sub> N <sub>4</sub> O <sub>4</sub>	
Formula weight	390.48	
Temperature	120(2) K	
Wavelength	0.71073 Å	
Crystal system	Monoclinic	
Space group	P2(1)/n	
Unit cell dimensions	a = 8.2382(6) Å	α = 90°.
	b = 7.3603(5) Å	β = 102.979(3)°.
	c = 17.7902(11) Å	γ = 90°.
Volume	1051.16(12) Å <sup>3</sup>	
Z	2	
Density (calculated)	1.234 g/cm <sup>3</sup>	
Absorption coefficient	0.087 mm <sup>-1</sup>	
F(000)	420	
Crystal size	0.25 x 0.25 x 0.20 mm <sup>3</sup>	
Theta range for data collection	2.35 to 31.51°.	
Index ranges	-9 ≤ h ≤ 12, -9 ≤ k ≤ 10, -26 ≤ l ≤ 26	
Reflections collected	12489	
Independent reflections	3494 [R(int) = 0.0206]	
Completeness to theta = 31.51°	99.9 %	
Absorption correction	None	
Max. and min. transmission	0.9828 and 0.9786	
Refinement method	Full-matrix least-squares on F <sup>2</sup>	
Data / restraints / parameters	3494 / 0 / 136	
Goodness-of-fit on F <sup>2</sup>	1.091	
Final R indices [I > 2σ(I)]	R1 = 0.0400, wR2 = 0.1100	
R indices (all data)	R1 = 0.0474, wR2 = 0.1159	
Largest diff. peak and hole	0.430 and -0.307 e.Å <sup>-3</sup>	

**Table A.10** Crystal data and structure refinement for **2a**

Identification code	ar0709m	
Empirical formula	C <sub>13</sub> H <sub>10</sub> Br N <sub>3</sub> O <sub>2</sub>	
Formula weight	320.15	
Temperature	120(2) K	
Wavelength	0.71073 Å	
Crystal system	Orthorhombic	
Space group	Pca2(1)	
Unit cell dimensions	a = 12.3903(8) Å	α = 90°.
	b = 5.6871(3) Å	β = 90°.
	c = 18.0290(11) Å	γ = 90°.
Volume	1270.41(13) Å <sup>3</sup>	
Z	4	
Density (calculated)	1.674 g/cm <sup>3</sup>	
Absorption coefficient	3.237 mm <sup>-1</sup>	
F(000)	640	
Crystal size	0.25 x 0.20 x 0.10 mm <sup>3</sup>	
Theta range for data collection	3.29 to 33.17°.	
Index ranges	-18 ≤ h ≤ 19, -8 ≤ k ≤ 5, -27 ≤ l ≤ 27	
Reflections collected	22901	
Independent reflections	4830 [R(int) = 0.0752]	
Completeness to theta = 33.17°	99.8 %	
Absorption correction	Semi-empirical from equivalents	
Max. and min. transmission	0.7379 and 0.4984	
Refinement method	Full-matrix least-squares on F <sup>2</sup>	
Data / restraints / parameters	4830 / 1 / 181	
Goodness-of-fit on F <sup>2</sup>	0.991	
Final R indices [I > 2σ(I)]	R1 = 0.0331, wR2 = 0.0735	
R indices (all data)	R1 = 0.0409, wR2 = 0.0756	
Absolute structure parameter	-0.006(7)	
Largest diff. peak and hole	1.329 and -0.641 e.Å <sup>-3</sup>	



**Table A.11** Crystal data and structure refinement for **2e**

Identification code	ar0719m	
Empirical formula	C <sub>12</sub> H <sub>10</sub> Br N <sub>3</sub> O <sub>4</sub>	
Formula weight	340.14	
Temperature	120(2) K	
Wavelength	0.71073 Å	
Crystal system	Monoclinic	
Space group	P2(1)/c	
Unit cell dimensions	a = 7.9727(5) Å	α = 90°.
	b = 6.2956(4) Å	β = 90.580(4)°.
	c = 24.6286(15) Å	γ = 90°.
Volume	1236.12(13) Å <sup>3</sup>	
Z	4	
Density (calculated)	1.828 g/cm <sup>3</sup>	
Absorption coefficient	3.344 mm <sup>-1</sup>	
F(000)	680	
Crystal size	0.20 x 0.20 x 0.15 mm <sup>3</sup>	
Theta range for data collection	1.65 to 32.58°.	
Index ranges	-12 ≤ h ≤ 10, -9 ≤ k ≤ 9, -37 ≤ l ≤ 37	
Reflections collected	18835	
Independent reflections	4299 [R(int) = 0.0328]	
Completeness to theta = 32.58°	95.3 %	
Absorption correction	None	
Max. and min. transmission	0.6339 and 0.5544	
Refinement method	Full-matrix least-squares on F <sup>2</sup>	
Data / restraints / parameters	4299 / 0 / 190	
Goodness-of-fit on F <sup>2</sup>	1.198	
Final R indices [I > 2σ(I)]	R1 = 0.0478, wR2 = 0.1243	
R indices (all data)	R1 = 0.0562, wR2 = 0.1281	
Largest diff. peak and hole	1.785 and -1.655 e.Å <sup>-3</sup>	

**Table A.12** Crystal data and structure refinement for **3n**

Identification code	ih0519	
Empirical formula	C <sub>18</sub> H <sub>22</sub> N <sub>4</sub> O <sub>6</sub>	
Formula weight	390.40	
Temperature	100(2) K	
Wavelength	0.71073 Å	
Crystal system	Monoclinic	
Space group	P2(1)/n	
Unit cell dimensions	a = 9.1172(8) Å	α = 90°.
	b = 9.2969(8) Å	β = 92.694(2)°.
	c = 10.6430(9) Å	γ = 90°.
Volume	901.12(13) Å <sup>3</sup>	
Z	2	
Density (calculated)	1.439 g/cm <sup>3</sup>	
Absorption coefficient	0.110 mm <sup>-1</sup>	
F(000)	412	
Crystal size	0.33 x 0.27 x 0.24 mm <sup>3</sup>	
Theta range for data collection	2.88 to 30.04°.	
Index ranges	-12 ≤ h ≤ 12, -11 ≤ k ≤ 13, -14 ≤ l ≤ 14	
Reflections collected	9947	
Independent reflections	2600 [R(int) = 0.0298]	
Completeness to theta = 30.04°	98.9 %	
Absorption correction	None	
Refinement method	Full-matrix least-squares on F <sup>2</sup>	
Data / restraints / parameters	2600 / 0 / 134	
Goodness-of-fit on F <sup>2</sup>	1.134	
Final R indices [I > 2σ(I)]	R1 = 0.0447, wR2 = 0.1217	
R indices (all data)	R1 = 0.0475, wR2 = 0.1249	
Extinction coefficient	0.010(3)	
Largest diff. peak and hole	0.498 and -0.374 e.Å <sup>-3</sup>	

**Table A.13** Crystal data and structure refinement for **4f**

Identification code	ar0801m	
Empirical formula	C15 H13 Br Cl2 N2 O3	
Formula weight	420.08	
Temperature	120(2) K	
Wavelength	0.71073 Å	
Crystal system	Triclinic	
Space group	P-1	
Unit cell dimensions	a = 3.9019(2) Å	$\alpha = 73.128(3)^\circ$ .
	b = 12.5454(8) Å	$\beta = 86.428(3)^\circ$ .
	c = 16.9260(10) Å	$\gamma = 85.881(3)^\circ$ .
Volume	790.08(8) Å <sup>3</sup>	
Z	2	
Density (calculated)	1.766 g/cm <sup>3</sup>	
Absorption coefficient	2.955 mm <sup>-1</sup>	
F(000)	420	
Crystal size	0.25 x 0.10 x 0.05 mm <sup>3</sup>	
Theta range for data collection	2.60 to 30.51°	
Index ranges	-5 ≤ h ≤ 5, -17 ≤ k ≤ 17, -24 ≤ l ≤ 24	
Reflections collected	16452	
Independent reflections	4701 [R(int) = 0.0293]	
Completeness to theta = 30.51°	97.3 %	
Absorption correction	None	
Max. and min. transmission	0.8663 and 0.5254	
Refinement method	Full-matrix least-squares on F <sup>2</sup>	
Data / restraints / parameters	4701 / 0 / 214	
Goodness-of-fit on F <sup>2</sup>	1.037	
Final R indices [I > 2σ(I)]	R1 = 0.0250, wR2 = 0.0652	
R indices (all data)	R1 = 0.0295, wR2 = 0.0674	
Largest diff. peak and hole	0.710 and -0.774 e.Å <sup>-3</sup>	

**Table A.14** Crystal data and structure refinement for **4k (SR2-c)**

Identification code	ar0729m	
Empirical formula	C <sub>24</sub> H <sub>32</sub> Br <sub>2</sub> N <sub>4</sub> O <sub>6</sub>	
Formula weight	632.36	
Temperature	100(2) K	
Wavelength	0.71073 Å	
Crystal system	Triclinic	
Space group	P1	
Unit cell dimensions	a = 5.3172(2) Å	α = 101.970(2)°.
	b = 8.6548(3) Å	β = 93.037(2)°.
	c = 14.9927(6) Å	γ = 100.816(2)°.
Volume	659.92(4) Å <sup>3</sup>	
Z	1	
Density (calculated)	1.591 g/cm <sup>3</sup>	
Absorption coefficient	3.117 mm <sup>-1</sup>	
F(000)	322	
Crystal size	0.20 x 0.16 x 0.12 mm <sup>3</sup>	
Theta range for data collection	3.28 to 27.13°.	
Index ranges	-6 ≤ h ≤ 6, -11 ≤ k ≤ 11, -19 ≤ l ≤ 19	
Reflections collected	12733	
Independent reflections	2892 [R(int) = 0.0298]	
Completeness to theta = 27.13°	99.4 %	
Absorption correction	None	
Max. and min. transmission	0.7061 and 0.5703	
Refinement method	Full-matrix least-squares on F <sup>2</sup>	
Data / restraints / parameters	2892 / 0 / 170	
Goodness-of-fit on F <sup>2</sup>	1.001	
Final R indices [I > 2σ(I)]	R1 = 0.0230, wR2 = 0.0543	
R indices (all data)	R1 = 0.0283, wR2 = 0.0567	
Largest diff. peak and hole	0.285 and -0.263 e.Å <sup>-3</sup>	

**Table A.15** Crystal data and structure refinement for **4m**

Identification code	ar0713m	
Empirical formula	C <sub>20</sub> H <sub>22</sub> Br <sub>2</sub> N <sub>4</sub> O <sub>6</sub>	
Formula weight	574.24	
Temperature	120(2) K	
Wavelength	0.71073 Å	
Crystal system	Monoclinic	
Space group	P2(1)/n	
Unit cell dimensions	a = 4.8333(3) Å	α = 90°.
	b = 9.5923(5) Å	β = 90.961(2)°.
	c = 23.7901(12) Å	γ = 90°.
Volume	1102.81(11) Å <sup>3</sup>	
Z	2	
Density (calculated)	1.729 g/cm <sup>3</sup>	
Absorption coefficient	3.721 mm <sup>-1</sup>	
F(000)	576	
Crystal size	0.20 x 0.08 x 0.08 mm <sup>3</sup>	
Theta range for data collection	1.71 to 31.28°.	
Index ranges	-6 ≤ h ≤ 6, -13 ≤ k ≤ 13, -34 ≤ l ≤ 26	
Reflections collected	19971	
Independent reflections	3473 [R(int) = 0.0443]	
Completeness to theta = 31.28°	96.8 %	
Absorption correction	None	
Max. and min. transmission	0.7551 and 0.5232	
Refinement method	Full-matrix least-squares on F <sup>2</sup>	
Data / restraints / parameters	3473 / 0 / 152	
Goodness-of-fit on F <sup>2</sup>	1.037	
Final R indices [I > 2σ(I)]	R1 = 0.0296, wR2 = 0.0628	
R indices (all data)	R1 = 0.0423, wR2 = 0.0669	
Largest diff. peak and hole	0.514 and -0.395 e.Å <sup>-3</sup>	

**Table A.16** Crystal data and structure refinement for **4n (SR2-a)**

Identification code	ar0806m	
Empirical formula	C <sub>20</sub> H <sub>24</sub> Br <sub>2</sub> N <sub>4</sub> O <sub>6</sub>	
Formula weight	576.25	
Temperature	120(2) K	
Wavelength	0.71073 Å	
Crystal system	Triclinic	
Space group	P-1	
Unit cell dimensions	a = 13.8624(15) Å	α = 95.707(8)°.
	b = 13.9754(16) Å	β = 90.355(7)°.
	c = 24.726(3) Å	γ = 101.437(7)°.
Volume	4670.1(9) Å <sup>3</sup>	
Z	8	
Density (calculated)	1.639 g/cm <sup>3</sup>	
Absorption coefficient	3.515 mm <sup>-1</sup>	
F(000)	2320	
Crystal size	0.25 x 0.18 x 0.12 mm <sup>3</sup>	
Theta range for data collection	0.83 to 29.57°.	
Index ranges	-19 ≤ h ≤ 19, -19 ≤ k ≤ 18, -34 ≤ l ≤ 33	
Reflections collected	72939	
Independent reflections	26200 [R(int) = 0.1786]	
Completeness to theta = 29.57°	99.9 %	
Absorption correction	None	
Max. and min. transmission	0.6778 and 0.4736	
Refinement method	Full-matrix least-squares on F <sup>2</sup>	
Data / restraints / parameters	26200 / 0 / 457	
Goodness-of-fit on F <sup>2</sup>	1.164	
Final R indices [I > 2σ(I)]	R1 = 0.1567, wR2 = 0.3532	
R indices (all data)	R1 = 0.3711, wR2 = 0.4480	
Largest diff. peak and hole	4.708 and -2.630 e.Å <sup>-3</sup>	

**Table A.17** Crystal data and structure refinement for **4o (SR2-d)**

Identification code	ar0921m	
Empirical formula	C <sub>26</sub> H <sub>36</sub> Br <sub>2</sub> N <sub>4</sub> O <sub>6</sub>	
Formula weight	660.41	
Temperature	120(2) K	
Wavelength	0.71073 Å	
Crystal system	Triclinic	
Space group	P-1	
Unit cell dimensions	a = 5.1849(4) Å	α = 71.293(2)°.
	b = 11.4665(8) Å	β = 81.204(2)°.
	c = 12.4870(9) Å	γ = 88.593(2)°.
Volume	694.66(9) Å <sup>3</sup>	
Z	1	
Density (calculated)	1.579 g/cm <sup>3</sup>	
Absorption coefficient	2.965 mm <sup>-1</sup>	
F(000)	338	
Crystal size	0.40 x 0.20 x 0.10 mm <sup>3</sup>	
Theta range for data collection	1.88 to 31.51°.	
Index ranges	-7 ≤ h ≤ 7, -10 ≤ k ≤ 16, -15 ≤ l ≤ 18	
Reflections collected	12522	
Independent reflections	4500 [R(int) = 0.0287]	
Completeness to theta = 31.51°	97.2 %	
Absorption correction	None	
Max. and min. transmission	0.7559 and 0.3834	
Refinement method	Full-matrix least-squares on F <sup>2</sup>	
Data / restraints / parameters	4500 / 0 / 178	
Goodness-of-fit on F <sup>2</sup>	0.985	
Final R indices [I > 2σ(I)]	R1 = 0.0313, wR2 = 0.0708	
R indices (all data)	R1 = 0.0426, wR2 = 0.0758	
Largest diff. peak and hole	0.464 and -0.467 e.Å <sup>-3</sup>	

**Table A.18** Crystal data and structure refinement for **5i**

Identification code	ar0817m	
Empirical formula	C <sub>12</sub> H <sub>8</sub> Br <sub>2</sub> N <sub>4</sub> O <sub>6</sub>	
Formula weight	464.04	
Temperature	120(2) K	
Wavelength	0.71073 Å	
Crystal system	Monoclinic	
Space group	P2(1)/c	
Unit cell dimensions	a = 7.3849(5) Å	α = 90°.
	b = 31.340(2) Å	β = 90.344(3)°.
	c = 13.3082(9) Å	γ = 90°.
Volume	3080.1(4) Å <sup>3</sup>	
Z	8	
Density (calculated)	2.001 g/cm <sup>3</sup>	
Absorption coefficient	5.303 mm <sup>-1</sup>	
F(000)	1808	
Crystal size	0.22 x 0.14 x 0.08 mm <sup>3</sup>	
Theta range for data collection	1.30 to 31.51°.	
Index ranges	-10 ≤ h ≤ 10, -44 ≤ k ≤ 44, -19 ≤ l ≤ 18	
Reflections collected	35388	
Independent reflections	10050 [R(int) = 0.0333]	
Completeness to theta = 31.51°	97.9 %	
Absorption correction	None	
Max. and min. transmission	0.6763 and 0.3883	
Refinement method	Full-matrix least-squares on F <sup>2</sup>	
Data / restraints / parameters	10050 / 0 / 451	
Goodness-of-fit on F <sup>2</sup>	1.049	
Final R indices [I > 2σ(I)]	R1 = 0.0364, wR2 = 0.0866	
R indices (all data)	R1 = 0.0556, wR2 = 0.0928	
Largest diff. peak and hole	1.475 and -0.582 e.Å <sup>-3</sup>	



**Table A.19** Crystal data and structure refinement for **5m**

Identification code	ar0820m	
Empirical formula	C <sub>14</sub> H <sub>12</sub> Br <sub>4</sub> N <sub>4</sub> O <sub>4</sub>	
Formula weight	619.92	
Temperature	120(2) K	
Wavelength	0.71073 Å	
Crystal system	Monoclinic	
Space group	P2(1)/c	
Unit cell dimensions	a = 14.0298(10) Å	α = 90°.
	b = 3.8527(3) Å	β = 102.337(3)°.
	c = 17.5918(13) Å	γ = 90°.
Volume	928.92(12) Å <sup>3</sup>	
Z	2	
Density (calculated)	2.216 g/cm <sup>3</sup>	
Absorption coefficient	8.693 mm <sup>-1</sup>	
F(000)	592	
Crystal size	0.16 x 0.14 x 0.08 mm <sup>3</sup>	
Theta range for data collection	2.97 to 33.72°.	
Index ranges	-21 ≤ h ≤ 21, -6 ≤ k ≤ 6, -27 ≤ l ≤ 21	
Reflections collected	19668	
Independent reflections	3635 [R(int) = 0.0324]	
Completeness to theta = 33.72°	98.6 %	
Absorption correction	None	
Max. and min. transmission	0.5431 and 0.3368	
Refinement method	Full-matrix least-squares on F <sup>2</sup>	
Data / restraints / parameters	3635 / 0 / 127	
Goodness-of-fit on F <sup>2</sup>	1.017	
Final R indices [I > 2σ(I)]	R1 = 0.0211, wR2 = 0.0501	
R indices (all data)	R1 = 0.0268, wR2 = 0.0521	
Largest diff. peak and hole	0.688 and -0.480 e.Å <sup>-3</sup>	

**Table A.20** Crystal data and structure refinement for **6n (SR1-a)**

Identification code	ar0728m	
Empirical formula	C18 H20 Br2 N4 O6	
Formula weight	548.20	
Temperature	100(2) K	
Wavelength	0.71073 Å	
Crystal system	Triclinic	
Space group	P-1	
Unit cell dimensions	a = 4.9878(3) Å	$\alpha = 113.250(5)^\circ$ .
	b = 9.9931(7) Å	$\beta = 92.103(5)^\circ$ .
	c = 11.4625(8) Å	$\gamma = 93.352(5)^\circ$ .
Volume	522.92(6) Å <sup>3</sup>	
Z	1	
Density (calculated)	1.741 g/cm <sup>3</sup>	
Absorption coefficient	3.919 mm <sup>-1</sup>	
F(000)	274	
Crystal size	0.33 x 0.16 x 0.10 mm <sup>3</sup>	
Theta range for data collection	3.49 to 27.12°.	
Index ranges	-6<=h<=6, -12<=k<=12, -14<=l<=14	
Reflections collected	8216	
Independent reflections	2184 [R(int) = 0.0599]	
Completeness to theta = 25.00°	94.4 %	
Absorption correction	None	
Max. and min. transmission	0.6906 and 0.3561	
Refinement method	Full-matrix least-squares on F <sup>2</sup>	
Data / restraints / parameters	2184 / 0 / 143	
Goodness-of-fit on F <sup>2</sup>	0.978	
Final R indices [I>2sigma(I)]	R1 = 0.0414, wR2 = 0.0840	
R indices (all data)	R1 = 0.0784, wR2 = 0.0973	
Largest diff. peak and hole	0.772 and -0.548 e.Å <sup>-3</sup>	

**Table A.21** Crystal data and structure refinement for **10**

Identification code	ar0704m	
Empirical formula	C <sub>9</sub> H <sub>8</sub> N <sub>4</sub>	
Formula weight	172.19	
Temperature	100(2) K	
Wavelength	0.71073 Å	
Crystal system	Monoclinic	
Space group	P2(1)	
Unit cell dimensions	a = 5.2455(3) Å	α = 90°.
	b = 25.6547(15) Å	β = 98.522(3)°.
	c = 6.4584(4) Å	γ = 90°.
Volume	859.52(9) Å <sup>3</sup>	
Z	4	
Density (calculated)	1.331 Mg/m <sup>3</sup>	
Absorption coefficient	0.087 mm <sup>-1</sup>	
F(000)	360	
Crystal size	0.30 x 0.25 x 0.15 mm <sup>3</sup>	
Theta range for data collection	1.59 to 35.62°.	
Index ranges	-8 ≤ h ≤ 8, -41 ≤ k ≤ 41, -9 ≤ l ≤ 10	
Reflections collected	16192	
Independent reflections	4034 [R(int) = 0.0279]	
Completeness to theta = 35.62°	99.6 %	
Absorption correction	None	
Max. and min. transmission	0.9871 and 0.9744	
Refinement method	Full-matrix least-squares on F <sup>2</sup>	
Data / restraints / parameters	4034 / 1 / 247	
Goodness-of-fit on F <sup>2</sup>	1.046	
Final R indices [I > 2σ(I)]	R1 = 0.0436, wR2 = 0.1142	
R indices (all data)	R1 = 0.0513, wR2 = 0.1186	
Absolute structure parameter	-0.7(16)	
Largest diff. peak and hole	0.448 and -0.235 e.Å <sup>-3</sup>	

**Table A.22** Crystal data and structure refinement for **10c**

Identification code	ar1005m	
Empirical formula	C <sub>16</sub> H <sub>13</sub> Cl N <sub>4</sub> O <sub>2</sub>	
Formula weight	328.75	
Temperature	120(2) K	
Wavelength	0.71073 Å	
Crystal system	Monoclinic	
Space group	P2(1)/c	
Unit cell dimensions	a = 19.1029(12) Å	α = 90°.
	b = 7.5386(4) Å	β = 98.284(3)°.
	c = 10.6738(7) Å	γ = 90°.
Volume	1521.09(16) Å <sup>3</sup>	
Z	4	
Density (calculated)	1.436 g/cm <sup>3</sup>	
Absorption coefficient	0.267 mm <sup>-1</sup>	
F(000)	680	
Crystal size	0.36 x 0.32 x 0.08 mm <sup>3</sup>	
Theta range for data collection	1.08 to 31.51°.	
Index ranges	-28 ≤ h ≤ 15, -5 ≤ k ≤ 11, -13 ≤ l ≤ 15	
Reflections collected	15674	
Independent reflections	4844 [R(int) = 0.0286]	
Completeness to theta = 30.00°	97.9 %	
Absorption correction	Semi-empirical from equivalents	
Max. and min. transmission	0.9790 and 0.9102	
Refinement method	Full-matrix least-squares on F <sup>2</sup>	
Data / restraints / parameters	4844 / 0 / 217	
Goodness-of-fit on F <sup>2</sup>	1.054	
Final R indices [I > 2σ(I)]	R1 = 0.0481, wR2 = 0.1334	
R indices (all data)	R1 = 0.0676, wR2 = 0.1471	
Largest diff. peak and hole	0.482 and -0.384 e.Å <sup>-3</sup>	

**Table A.23 Crystal data and structure refinement for 10j**

Identification code	ar1014m	
Empirical formula	C <sub>16</sub> H <sub>9</sub> F <sub>5</sub> N <sub>4</sub> O <sub>2</sub>	
Formula weight	384.27	
Temperature	120(2) K	
Wavelength	0.71073 Å	
Crystal system	Triclinic	
Space group	P-1	
Unit cell dimensions	a = 6.0919(5) Å	α = 77.386(2)°.
	b = 7.5337(6) Å	β = 80.438(2)°.
	c = 17.0979(13) Å	γ = 81.482(2)°.
Volume	750.00(10) Å <sup>3</sup>	
Z	2	
Density (calculated)	1.702 g/cm <sup>3</sup>	
Absorption coefficient	0.157 mm <sup>-1</sup>	
F(000)	388	
Crystal size	0.32 x 0.20 x 0.08 mm <sup>3</sup>	
Theta range for data collection	2.79 to 32.57°.	
Index ranges	-9 ≤ h ≤ 7, -11 ≤ k ≤ 9, -24 ≤ l ≤ 25	
Reflections collected	19595	
Independent reflections	5166 [R(int) = 0.0242]	
Completeness to theta = 30.00°	98.9 %	
Absorption correction	Semi-empirical from equivalents	
Max. and min. transmission	0.9875 and 0.9513	
Refinement method	Full-matrix least-squares on F <sup>2</sup>	
Data / restraints / parameters	5166 / 0 / 253	
Goodness-of-fit on F <sup>2</sup>	1.072	
Final R indices [I > 2σ(I)]	R1 = 0.0422, wR2 = 0.1218	
R indices (all data)	R1 = 0.0526, wR2 = 0.1313	
Largest diff. peak and hole	0.484 and -0.313 e.Å <sup>-3</sup>	

**Table A.24** Crystal data and structure refinement for **10k**

Identification code	ar1020m	
Empirical formula	C <sub>26</sub> H <sub>30</sub> N <sub>8</sub> O <sub>4</sub>	
Formula weight	518.58	
Temperature	100(2) K	
Wavelength	0.71073 Å	
Crystal system	Triclinic	
Space group	P-1	
Unit cell dimensions	a = 5.4540(14) Å	α = 90.854(4)°.
	b = 7.0445(17) Å	β = 92.146(4)°.
	c = 17.042(4) Å	γ = 105.123(4)°.
Volume	631.4(3) Å <sup>3</sup>	
Z	1	
Density (calculated)	1.364 g/cm <sup>3</sup>	
Absorption coefficient	0.096 mm <sup>-1</sup>	
F(000)	274	
Crystal size	0.28 x 0.26 x 0.10 mm <sup>3</sup>	
Theta range for data collection	2.39 to 29.02°.	
Index ranges	-7 ≤ h ≤ 7, -9 ≤ k ≤ 9, -22 ≤ l ≤ 23	
Reflections collected	5818	
Independent reflections	3031 [R(int) = 0.0785]	
Completeness to theta = 27.50°	97.4 %	
Absorption correction	None	
Max. and min. transmission	0.9905 and 0.9737	
Refinement method	Full-matrix least-squares on F <sup>2</sup>	
Data / restraints / parameters	3031 / 0 / 181	
Goodness-of-fit on F <sup>2</sup>	1.053	
Final R indices [I > 2σ(I)]	R1 = 0.0518, wR2 = 0.1358	
R indices (all data)	R1 = 0.0598, wR2 = 0.1424	
Largest diff. peak and hole	0.310 and -0.306 e.Å <sup>-3</sup>	

**Table A.25** Crystal data and structure refinement for **10n (SR3-a)**

Identification code	ar1015m	
Empirical formula	C <sub>22</sub> H <sub>22</sub> N <sub>8</sub> O <sub>4</sub>	
Formula weight	462.48	
Temperature	120(2) K	
Wavelength	0.71073 Å	
Crystal system	Monoclinic	
Space group	P2(1)/c	
Unit cell dimensions	a = 7.2159(8) Å	α = 90°.
	b = 13.0960(14) Å	β = 98.989(4)°.
	c = 22.341(3) Å	γ = 90°.
Volume	2085.3(4) Å <sup>3</sup>	
Z	4	
Density (calculated)	1.473 g/cm <sup>3</sup>	
Absorption coefficient	0.106 mm <sup>-1</sup>	
F(000)	968	
Crystal size	0.30 x 0.22 x 0.12 mm <sup>3</sup>	
Theta range for data collection	3.11 to 30.03°.	
Index ranges	-10 ≤ h ≤ 10, -18 ≤ k ≤ 13, -31 ≤ l ≤ 31	
Reflections collected	18085	
Independent reflections	5954 [R(int) = 0.0736]	
Completeness to theta = 30.03°	97.4 %	
Absorption correction	Semi-empirical from equivalents	
Max. and min. transmission	0.9874 and 0.9688	
Refinement method	Full-matrix least-squares on F <sup>2</sup>	
Data / restraints / parameters	5954 / 0 / 325	
Goodness-of-fit on F <sup>2</sup>	1.129	
Final R indices [I > 2σ(I)]	R1 = 0.0814, wR2 = 0.1863	
R indices (all data)	R1 = 0.1344, wR2 = 0.2168	
Largest diff. peak and hole	0.597 and -0.455 e.Å <sup>-3</sup>	

**Table A.26** Crystal data and structure refinement for **10o (SR3-d)**

Identification code	ar1001m	
Empirical formula	C <sub>28</sub> H <sub>34</sub> N <sub>8</sub> O <sub>4</sub>	
Formula weight	546.63	
Temperature	120(2) K	
Wavelength	0.71073 Å	
Crystal system	Triclinic	
Space group	P-1	
Unit cell dimensions	a = 5.4295(3) Å	α = 84.697(3)°.
	b = 7.0626(4) Å	β = 89.661(4)°.
	c = 18.6385(11) Å	γ = 74.553(4)°.
Volume	685.82(7) Å <sup>3</sup>	
Z	1	
Density (calculated)	1.324 g/cm <sup>3</sup>	
Absorption coefficient	0.092 mm <sup>-1</sup>	
F(000)	290	
Crystal size	0.28 x 0.24 x 0.12 mm <sup>3</sup>	
Theta range for data collection	2.20 to 32.57°.	
Index ranges	-8 ≤ h ≤ 8, -10 ≤ k ≤ 10, -28 ≤ l ≤ 28	
Reflections collected	17030	
Independent reflections	4957 [R(int) = 0.0583]	
Completeness to theta = 32.57°	99.2 %	
Absorption correction	None	
Max. and min. transmission	0.9891 and 0.9747	
Refinement method	Full-matrix least-squares on F <sup>2</sup>	
Data / restraints / parameters	4957 / 0 / 190	
Goodness-of-fit on F <sup>2</sup>	1.073	
Final R indices [I > 2σ(I)]	R1 = 0.0522, wR2 = 0.1403	
R indices (all data)	R1 = 0.0718, wR2 = 0.1554	
Largest diff. peak and hole	0.431 and -0.285 e.Å <sup>-3</sup>	



**Table A.27** Crystal data and structure refinement for **10r**

Identification code	ar1009m	
Empirical formula	C <sub>17</sub> H <sub>13</sub> Cl N <sub>6</sub> O	
Formula weight	352.78	
Temperature	296(2) K	
Wavelength	0.71073 Å	
Crystal system	Monoclinic	
Space group	P2(1)/c	
Unit cell dimensions	a = 18.4973(11) Å	α = 90°.
	b = 7.5005(4) Å	β = 105.707(4)°.
	c = 12.5176(7) Å	γ = 90°.
Volume	1671.83(16) Å <sup>3</sup>	
Z	4	
Density (calculated)	1.402 g/cm <sup>3</sup>	
Absorption coefficient	0.247 mm <sup>-1</sup>	
F(000)	728	
Crystal size	0.28 x 0.24 x 0.14 mm <sup>3</sup>	
Theta range for data collection	2.29 to 31.00°.	
Index ranges	-26 ≤ h ≤ 26, -10 ≤ k ≤ 10, -18 ≤ l ≤ 17	
Reflections collected	19450	
Independent reflections	5301 [R(int) = 0.0647]	
Completeness to theta = 31.00°	99.6 %	
Absorption correction	None	
Max. and min. transmission	0.9663 and 0.9341	
Refinement method	Full-matrix least-squares on F <sup>2</sup>	
Data / restraints / parameters	5301 / 0 / 235	
Goodness-of-fit on F <sup>2</sup>	1.060	
Final R indices [I > 2σ(I)]	R1 = 0.0570, wR2 = 0.1668	
R indices (all data)	R1 = 0.0818, wR2 = 0.1835	
Largest diff. peak and hole	0.280 and -0.343 e.Å <sup>-3</sup>	

**Table A.28** Crystal data and structure refinement for **12**

Identification code	ar1006m	
Empirical formula	C <sub>10</sub> H <sub>10</sub> N <sub>4</sub>	
Formula weight	186.22	
Temperature	120(2) K	
Wavelength	0.71073 Å	
Crystal system	Monoclinic	
Space group	P2(1)/c	
Unit cell dimensions	a = 11.9569(9) Å	α = 90°.
	b = 7.3412(5) Å	β = 96.834(4)°.
	c = 10.2804(7) Å	γ = 90°.
Volume	895.98(11) Å <sup>3</sup>	
Z	4	
Density (calculated)	1.381 g/cm <sup>3</sup>	
Absorption coefficient	0.089 mm <sup>-1</sup>	
F(000)	392	
Crystal size	0.22 x 0.16 x 0.08 mm <sup>3</sup>	
Theta range for data collection	3.26 to 32.57°.	
Index ranges	-17 ≤ h ≤ 14, -10 ≤ k ≤ 9, -15 ≤ l ≤ 15	
Reflections collected	9469	
Independent reflections	3027 [R(int) = 0.0346]	
Completeness to theta = 30.00°	98.7 %	
Absorption correction	None	
Max. and min. transmission	0.9929 and 0.9807	
Refinement method	Full-matrix least-squares on F <sup>2</sup>	
Data / restraints / parameters	3027 / 0 / 134	
Goodness-of-fit on F <sup>2</sup>	1.038	
Final R indices [I > 2σ(I)]	R1 = 0.0514, wR2 = 0.1411	
R indices (all data)	R1 = 0.0765, wR2 = 0.1578	
Largest diff. peak and hole	0.452 and -0.272 e.Å <sup>-3</sup>	

**Table A.29** Crystal data and structure refinement for **12n**

Identification code	ar1004m	
Empirical formula	C <sub>24</sub> H <sub>26</sub> N <sub>8</sub> O <sub>4</sub>	
Formula weight	490.53	
Temperature	120(2) K	
Wavelength	0.71073 Å	
Crystal system	Monoclinic	
Space group	P2(1)/c	
Unit cell dimensions	a = 14.8427(10) Å	$\alpha = 90^\circ$ .
	b = 7.3677(5) Å	$\beta = 101.321(4)^\circ$ .
	c = 10.6264(8) Å	$\gamma = 90^\circ$ .
Volume	1139.46(14) Å <sup>3</sup>	
Z	2	
Density (calculated)	1.430 g/cm <sup>3</sup>	
Absorption coefficient	0.102 mm <sup>-1</sup>	
F(000)	516	
Crystal size	0.28 x 0.14 x 0.10 mm <sup>3</sup>	
Theta range for data collection	2.80 to 32.57°.	
Index ranges	-22 ≤ h ≤ 19, -6 ≤ k ≤ 11, -15 ≤ l ≤ 15	
Reflections collected	13858	
Independent reflections	4011 [R(int) = 0.0303]	
Completeness to theta = 32.57°	96.8 %	
Absorption correction	None	
Max. and min. transmission	0.9899 and 0.9721	
Refinement method	Full-matrix least-squares on F <sup>2</sup>	
Data / restraints / parameters	4011 / 0 / 173	
Goodness-of-fit on F <sup>2</sup>	1.060	
Final R indices [I > 2σ(I)]	R1 = 0.0544, wR2 = 0.1514	
R indices (all data)	R1 = 0.0825, wR2 = 0.1732	
Largest diff. peak and hole	0.467 and -0.311 e.Å <sup>-3</sup>	

**Table A.30** Crystal data and structure refinement for **15**

Identification code	ar1018m
Empirical formula	C <sub>9</sub> H <sub>8</sub> N <sub>4</sub>
Formula weight	172.19
Temperature	120(2) K
Wavelength	0.71073 Å
Crystal system	Monoclinic
Space group	P2(1)/n
Unit cell dimensions	a = 8.7786(8) Å                      α = 90°. b = 9.7939(8) Å                      β = 105.850(7)°. c = 9.4421(10) Å                      γ = 90°.
Volume	780.94(13) Å <sup>3</sup>
Z	4
Density (calculated)	1.465 g/cm <sup>3</sup>
Absorption coefficient	0.096 mm <sup>-1</sup>
F(000)	360
Crystal size	0.26 x 0.18 x 0.12 mm <sup>3</sup>
Theta range for data collection	2.81 to 30.60°.
Index ranges	-12 ≤ h ≤ 12, -14 ≤ k ≤ 13, -12 ≤ l ≤ 13
Reflections collected	8233
Independent reflections	2384 [R(int) = 0.0582]
Completeness to theta = 30.60°	99.4 %
Absorption correction	Semi-empirical from equivalents
Max. and min. transmission	0.9886 and 0.9755
Refinement method	Full-matrix least-squares on F <sup>2</sup>
Data / restraints / parameters	2384 / 0 / 124
Goodness-of-fit on F <sup>2</sup>	1.053
Final R indices [I > 2σ(I)]	R1 = 0.0563, wR2 = 0.1464
R indices (all data)	R1 = 0.0842, wR2 = 0.1648
Largest diff. peak and hole	0.536 and -0.220 e.Å <sup>-3</sup>

**Table A.31** Crystal data and structure refinement for **15e**

Identification code	ar1012m	
Empirical formula	C <sub>16</sub> H <sub>13</sub> N <sub>5</sub> O <sub>4</sub>	
Formula weight	339.31	
Temperature	120(2) K	
Wavelength	0.71073 Å	
Crystal system	Triclinic	
Space group	P-1	
Unit cell dimensions	a = 7.2069(12) Å	α = 97.387(9)°.
	b = 7.3475(12) Å	β = 93.282(9)°.
	c = 15.599(3) Å	γ = 116.353(7)°.
Volume	727.9(2) Å <sup>3</sup>	
Z	2	
Density (calculated)	1.548 g/cm <sup>3</sup>	
Absorption coefficient	0.115 mm <sup>-1</sup>	
F(000)	352	
Crystal size	0.36 x 0.16 x 0.08 mm <sup>3</sup>	
Theta range for data collection	3.14 to 30.87°.	
Index ranges	-10 ≤ h ≤ 10, -10 ≤ k ≤ 10, 0 ≤ l ≤ 22	
Reflections collected	9417	
Independent reflections	9417 [R(int) = 0.0000]	
Completeness to theta = 30.87°	96.5 %	
Absorption correction	Semi-empirical from equivalents	
Max. and min. transmission	0.9908 and 0.9596	
Refinement method	Full-matrix least-squares on F <sup>2</sup>	
Data / restraints / parameters	9417 / 0 / 227	
Goodness-of-fit on F <sup>2</sup>	1.798	
Final R indices [I > 2σ(I)]	R1 = 0.1692, wR2 = 0.3773	
R indices (all data)	R1 = 0.2580, wR2 = 0.4092	
Largest diff. peak and hole	0.987 and -0.570 e.Å <sup>-3</sup>	

**Table A.32** Crystal data and structure refinement for **16**

Identification code	ar0710m	
Empirical formula	C <sub>12</sub> H <sub>11</sub> N <sub>3</sub> O	
Formula weight	213.24	
Temperature	120(2) K	
Wavelength	0.71073 Å	
Crystal system	Triclinic	
Space group	P-1	
Unit cell dimensions	a = 7.2839(7) Å	α = 93.643(7)°.
	b = 10.4921(11) Å	β = 101.724(6)°.
	c = 13.8219(13) Å	γ = 97.267(7)°.
Volume	1021.63(17) Å <sup>3</sup>	
Z	4	
Density (calculated)	1.386 g/cm <sup>3</sup>	
Absorption coefficient	0.092 mm <sup>-1</sup>	
F(000)	448	
Crystal size	0.30 x 0.10 x 0.05 mm <sup>3</sup>	
Theta range for data collection	1.97 to 29.61°.	
Index ranges	-9 ≤ h ≤ 10, -14 ≤ k ≤ 14, -19 ≤ l ≤ 19	
Reflections collected	25236	
Independent reflections	25236 [R(int) = 0.0000]	
Completeness to theta = 29.61°	95.2 %	
Absorption correction	None	
Max. and min. transmission	0.9954 and 0.9728	
Refinement method	Full-matrix least-squares on F <sup>2</sup>	
Data / restraints / parameters	25236 / 0 / 292	
Goodness-of-fit on F <sup>2</sup>	0.790	
Final R indices [I > 2σ(I)]	R1 = 0.0618, wR2 = 0.1323	
R indices (all data)	R1 = 0.1865, wR2 = 0.1699	
Largest diff. peak and hole	0.527 and -0.410 e.Å <sup>-3</sup>	

**Table A.33** Crystal data and structure refinement for **16p**

Identification code	ar0702m	
Empirical formula	C <sub>20</sub> H <sub>17</sub> N <sub>5</sub> O <sub>2</sub>	
Formula weight	359.39	
Temperature	133(2) K	
Wavelength	0.71073 Å	
Crystal system	Triclinic	
Space group	P-1	
Unit cell dimensions	a = 4.8980(3) Å	α = 103.791(2)°.
	b = 11.0334(6) Å	β = 97.134(3)°.
	c = 17.2045(10) Å	γ = 100.278(2)°.
Volume	874.84(9) Å <sup>3</sup>	
Z	2	
Density (calculated)	1.364 g/cm <sup>3</sup>	
Absorption coefficient	0.092 mm <sup>-1</sup>	
F(000)	376	
Crystal size	0.25 x 0.20 x 0.20 mm <sup>3</sup>	
Theta range for data collection	1.95 to 30.47°.	
Index ranges	-6 ≤ h ≤ 6, -15 ≤ k ≤ 15, -24 ≤ l ≤ 24	
Reflections collected	34094	
Independent reflections	5216 [R(int) = 0.0353]	
Completeness to theta = 30.47°	98.6 %	
Absorption correction	None	
Max. and min. transmission	0.9818 and 0.9773	
Refinement method	Full-matrix least-squares on F <sup>2</sup>	
Data / restraints / parameters	5216 / 0 / 250	
Goodness-of-fit on F <sup>2</sup>	1.082	
Final R indices [I > 2σ(I)]	R1 = 0.0403, wR2 = 0.1102	
R indices (all data)	R1 = 0.0525, wR2 = 0.1172	
Largest diff. peak and hole	0.297 and -0.187 e.Å <sup>-3</sup>	

**Table A.34** Crystal data and structure refinement for **21**

Identification code	ar0604m	
Empirical formula	C <sub>14</sub> H <sub>11</sub> N <sub>3</sub> O	
Formula weight	237.26	
Temperature	173(2) K	
Wavelength	0.71073 Å	
Crystal system	Triclinic	
Space group	P-1	
Unit cell dimensions	a = 10.711(3) Å	α = 116.949(17)°.
	b = 11.567(3) Å	β = 109.883(18)°.
	c = 11.613(3) Å	γ = 90.970(16)°.
Volume	1180.8(5) Å <sup>3</sup>	
Z	4	
Density (calculated)	1.335 g/cm <sup>3</sup>	
Absorption coefficient	0.088 mm <sup>-1</sup>	
F(000)	496	
Crystal size	0.30 x 0.25 x 0.15 mm <sup>3</sup>	
Theta range for data collection	2.02 to 27.63°.	
Index ranges	-13 ≤ h ≤ 12, -15 ≤ k ≤ 14, -15 ≤ l ≤ 14	
Reflections collected	8761	
Independent reflections	5176 [R(int) = 0.1487]	
Completeness to theta = 27.63°	94.5 %	
Absorption correction	None	
Refinement method	Full-matrix least-squares on F <sup>2</sup>	
Data / restraints / parameters	5176 / 0 / 333	
Goodness-of-fit on F <sup>2</sup>	1.032	
Final R indices [I > 2σ(I)]	R1 = 0.0733, wR2 = 0.1876	
R indices (all data)	R1 = 0.1200, wR2 = 0.2294	
Largest diff. peak and hole	0.338 and -0.353 e.Å <sup>-3</sup>	



**Table A.35** Crystal data and structure refinement for **24**

Identification code	ar0803m	
Empirical formula	C <sub>14</sub> H <sub>13</sub> N <sub>4</sub> O <sub>1.50</sub>	
Formula weight	261.28	
Temperature	120(2) K	
Wavelength	0.71073 Å	
Crystal system	Triclinic	
Space group	P-1	
Unit cell dimensions	a = 11.4425(4) Å	α = 96.6520(10)°.
	b = 11.5867(3) Å	β = 111.7030(10)°.
	c = 12.3007(4) Å	γ = 117.1760(10)°.
Volume	1265.45(7) Å <sup>3</sup>	
Z	4	
Density (calculated)	1.371 g/cm <sup>3</sup>	
Absorption coefficient	0.094 mm <sup>-1</sup>	
F(000)	548	
Crystal size	0.20 x 0.10 x 0.05 mm <sup>3</sup>	
Theta range for data collection	1.90 to 33.14°.	
Index ranges	-17 ≤ h ≤ 16, -17 ≤ k ≤ 17, -18 ≤ l ≤ 18	
Reflections collected	25333	
Independent reflections	9499 [R(int) = 0.0252]	
Completeness to theta = 33.14°	98.4 %	
Absorption correction	None	
Max. and min. transmission	0.9953 and 0.9815	
Refinement method	Full-matrix least-squares on F <sup>2</sup>	
Data / restraints / parameters	9499 / 0 / 378	
Goodness-of-fit on F <sup>2</sup>	1.039	
Final R indices [I > 2σ(I)]	R1 = 0.0501, wR2 = 0.1393	
R indices (all data)	R1 = 0.0657, wR2 = 0.1513	
Largest diff. peak and hole	0.520 and -0.257 e.Å <sup>-3</sup>	

**Table A.36** Crystal data and structure refinement for **24h**

Identification code	ar0808m	
Empirical formula	C <sub>32</sub> H <sub>32</sub> N <sub>4</sub> O <sub>5</sub>	
Formula weight	552.62	
Temperature	120(2) K	
Wavelength	0.71073 Å	
Crystal system	Monoclinic	
Space group	P2(1)/n	
Unit cell dimensions	a = 7.2753(2) Å	$\alpha = 90^\circ$ .
	b = 51.4772(16) Å	$\beta = 113.373(2)^\circ$ .
	c = 8.4137(3) Å	$\gamma = 90^\circ$ .
Volume	2892.46(16) Å <sup>3</sup>	
Z	4	
Density (calculated)	1.269 g/cm <sup>3</sup>	
Absorption coefficient	0.087 mm <sup>-1</sup>	
F(000)	1168	
Crystal size	0.25 x 0.15 x 0.04 mm <sup>3</sup>	
Theta range for data collection	2.67 to 31.51°.	
Index ranges	-10 ≤ h ≤ 10, -74 ≤ k ≤ 72, -12 ≤ l ≤ 11	
Reflections collected	31609	
Independent reflections	9354 [R(int) = 0.0531]	
Completeness to theta = 31.51°	96.9 %	
Absorption correction	None	
Max. and min. transmission	0.9965 and 0.9786	
Refinement method	Full-matrix least-squares on F <sup>2</sup>	
Data / restraints / parameters	9354 / 0 / 390	
Goodness-of-fit on F <sup>2</sup>	1.033	
Final R indices [I > 2σ(I)]	R1 = 0.0591, wR2 = 0.1398	
R indices (all data)	R1 = 0.1092, wR2 = 0.1620	
Largest diff. peak and hole	0.485 and -0.325 e.Å <sup>-3</sup>	

**Table A.37** Crystal data and structure refinement for **24I**

Identification code	ar0809m	
Empirical formula	C <sub>36</sub> H <sub>30</sub> N <sub>8</sub> O <sub>8.40</sub>	
Formula weight	709.08	
Temperature	120(2) K	
Wavelength	0.71073 Å	
Crystal system	Triclinic	
Space group	P-1	
Unit cell dimensions	a = 8.5333(6) Å	α = 102.318(3)°.
	b = 12.6109(9) Å	β = 103.824(4)°.
	c = 17.3881(12) Å	γ = 101.808(4)°.
Volume	1709.5(2) Å <sup>3</sup>	
Z	2	
Density (calculated)	1.378 g/cm <sup>3</sup>	
Absorption coefficient	0.101 mm <sup>-1</sup>	
F(000)	738	
Crystal size	0.30 x 0.25 x 0.12 mm <sup>3</sup>	
Theta range for data collection	1.25 to 31.50°.	
Index ranges	-12 ≤ h ≤ 12, -18 ≤ k ≤ 18, -25 ≤ l ≤ 25	
Reflections collected	21749	
Independent reflections	10076 [R(int) = 0.0257]	
Completeness to theta = 25.00°	89.2 %	
Absorption correction	None	
Max. and min. transmission	0.9880 and 0.9704	
Refinement method	Full-matrix least-squares on F <sup>2</sup>	
Data / restraints / parameters	10076 / 0 / 481	
Goodness-of-fit on F <sup>2</sup>	1.414	
Final R indices [I > 2σ(I)]	R1 = 0.0749, wR2 = 0.2147	
R indices (all data)	R1 = 0.1139, wR2 = 0.2356	
Largest diff. peak and hole	0.711 and -0.533 e.Å <sup>-3</sup>	

**Table A.38** Crystal data and structure refinement for **27**

Identification code	ar0701m	
Empirical formula	C <sub>28</sub> H <sub>28</sub> N <sub>10</sub> O <sub>3</sub> S	
Formula weight	584.66	
Temperature	133(2) K	
Wavelength	0.71073 Å	
Crystal system	Monoclinic	
Space group	C2/c	
Unit cell dimensions	a = 13.553(2) Å	α = 90°.
	b = 12.1888(18) Å	β = 111.307(6)°.
	c = 18.161(3) Å	γ = 90°.
Volume	2795.1(7) Å <sup>3</sup>	
Z	4	
Density (calculated)	1.389 g/cm <sup>3</sup>	
Absorption coefficient	0.167 mm <sup>-1</sup>	
F(000)	1224	
Crystal size	0.30 x 0.20 x 0.15 mm <sup>3</sup>	
Theta range for data collection	2.32 to 36.32°.	
Index ranges	-22 ≤ h ≤ 22, -20 ≤ k ≤ 19, -30 ≤ l ≤ 28	
Reflections collected	38879	
Independent reflections	6724 [R(int) = 0.0364]	
Completeness to theta = 36.32°	99.1 %	
Absorption correction	None	
Max. and min. transmission	0.9754 and 0.9517	
Refinement method	Full-matrix least-squares on F <sup>2</sup>	
Data / restraints / parameters	6724 / 0 / 214	
Goodness-of-fit on F <sup>2</sup>	1.045	
Final R indices [I > 2σ(I)]	R1 = 0.0498, wR2 = 0.1404	
R indices (all data)	R1 = 0.0705, wR2 = 0.1543	
Largest diff. peak and hole	0.565 and -0.382 e.Å <sup>-3</sup>	

**Table A.39** Crystal data and structure refinement for **27i**

Identification code	ar0703m	
Empirical formula	C <sub>20</sub> H <sub>15</sub> N <sub>7</sub> O <sub>7</sub>	
Formula weight	465.39	
Temperature	100(2) K	
Wavelength	0.71073 Å	
Crystal system	Monoclinic	
Space group	P2(1)/n	
Unit cell dimensions	a = 4.9179(4) Å	α = 90°.
	b = 42.483(3) Å	β = 103.945(4)°.
	c = 10.0242(8) Å	γ = 90°.
Volume	2032.6(3) Å <sup>3</sup>	
Z	4	
Density (calculated)	1.521 g/cm <sup>3</sup>	
Absorption coefficient	0.119 mm <sup>-1</sup>	
F(000)	960	
Crystal size	0.25 x 0.10 x 0.08 mm <sup>3</sup>	
Theta range for data collection	1.92 to 29.57°.	
Index ranges	-6 ≤ h ≤ 4, -58 ≤ k ≤ 57, -13 ≤ l ≤ 13	
Reflections collected	29121	
Independent reflections	5619 [R(int) = 0.0529]	
Completeness to theta = 29.57°	99.0 %	
Absorption correction	None	
Max. and min. transmission	0.9906 and 0.9709	
Refinement method	Full-matrix least-squares on F <sup>2</sup>	
Data / restraints / parameters	5619 / 0 / 320	
Goodness-of-fit on F <sup>2</sup>	1.020	
Final R indices [I > 2σ(I)]	R1 = 0.0597, wR2 = 0.1298	
R indices (all data)	R1 = 0.1267, wR2 = 0.1548	
Largest diff. peak and hole	0.314 and -0.327 e.Å <sup>-3</sup>	

**Table A.40** Crystal data and structure refinement for **35**

Identification code	ar0724m	
Empirical formula	C60 H76 Br4 O12	
Formula weight	1308.85	
Temperature	120(2) K	
Wavelength	0.71073 Å	
Crystal system	Triclinic	
Space group	P-1	
Unit cell dimensions	a = 11.9718(13) Å	$\alpha = 102.441(6)^\circ$ .
	b = 14.4406(16) Å	$\beta = 104.039(6)^\circ$ .
	c = 19.602(2) Å	$\gamma = 104.479(6)^\circ$ .
Volume	3042.5(6) Å <sup>3</sup>	
Z	2	
Density (calculated)	1.429 g/cm <sup>3</sup>	
Absorption coefficient	2.703 mm <sup>-1</sup>	
F(000)	1344	
Crystal size	0.25 x 0.15 x 0.15 mm <sup>3</sup>	
Theta range for data collection	1.52 to 30.51°.	
Index ranges	-16<=h<=17, -20<=k<=20, -26<=l<=27	
Reflections collected	93764	
Independent reflections	18547 [R(int) = 0.0679]	
Completeness to theta = 30.51°	99.9 %	
Absorption correction	None	
Max. and min. transmission	0.6872 and 0.5513	
Refinement method	Full-matrix least-squares on F <sup>2</sup>	
Data / restraints / parameters	18547 / 44 / 699	
Goodness-of-fit on F <sup>2</sup>	1.042	
Final R indices [I>2sigma(I)]	R1 = 0.0478, wR2 = 0.1283	
R indices (all data)	R1 = 0.0836, wR2 = 0.1455	
Largest diff. peak and hole	0.959 and -0.601 e.Å <sup>-3</sup>	

**Table A.41 Crystal data and structure refinement for 35'**

Identification code	ar0923m	
Empirical formula	C <sub>54</sub> H <sub>66</sub> Br <sub>4</sub> O <sub>9</sub> S	
Formula weight	1210.77	
Temperature	120(2) K	
Wavelength	0.71073 Å	
Crystal system	Monoclinic	
Space group	P2(1)/c	
Unit cell dimensions	a = 18.3282(10) Å	α = 90°.
	b = 16.0987(8) Å	β = 110.518(2)°.
	c = 18.5304(10) Å	γ = 90°.
Volume	5120.7(5) Å <sup>3</sup>	
Z	4	
Density (calculated)	1.571 g/cm <sup>3</sup>	
Absorption coefficient	3.241 mm <sup>-1</sup>	
F(000)	2472	
Crystal size	0.36 x 0.28 x 0.18 mm <sup>3</sup>	
Theta range for data collection	1.73 to 32.03°.	
Index ranges	-27 ≤ h ≤ 27, -24 ≤ k ≤ 15, -17 ≤ l ≤ 27	
Reflections collected	72820	
Independent reflections	16776 [R(int) = 0.0317]	
Completeness to theta = 27.50°	98.5 %	
Absorption correction	Semi-empirical from equivalents	
Max. and min. transmission	0.5931 and 0.3883	
Refinement method	Full-matrix least-squares on F <sup>2</sup>	
Data / restraints / parameters	16776 / 0 / 613	
Goodness-of-fit on F <sup>2</sup>	1.058	
Final R indices [I > 2σ(I)]	R1 = 0.0405, wR2 = 0.0966	
R indices (all data)	R1 = 0.0697, wR2 = 0.1106	
Largest diff. peak and hole	1.298 and -1.355 e.Å <sup>-3</sup>	

**Table A.42** Crystal data and structure refinement for **36**

Identification code	ar0914m	
Empirical formula	C <sub>54</sub> H <sub>63</sub> I <sub>4</sub> N O <sub>8</sub>	
Formula weight	1361.65	
Temperature	120(2) K	
Wavelength	0.71073 Å	
Crystal system	Monoclinic	
Space group	P2(1)/c	
Unit cell dimensions	a = 19.0866(13) Å	α = 90°.
	b = 16.7107(11) Å	β = 117.933(3)°.
	c = 18.6754(12) Å	γ = 90°.
Volume	5262.6(6) Å <sup>3</sup>	
Z	4	
Density (calculated)	1.719 g/cm <sup>3</sup>	
Absorption coefficient	2.422 mm <sup>-1</sup>	
F(000)	2680	
Crystal size	0.57 x 0.28 x 0.17 mm <sup>3</sup>	
Theta range for data collection	2.46 to 30.65°.	
Index ranges	-27<=h<=22, 0<=k<=23, 0<=l<=25	
Reflections collected	14131	
Independent reflections	14131 [R(int) = 0.0000]	
Completeness to theta = 25.00°	99.0 %	
Absorption correction	None	
Max. and min. transmission	0.6836 and 0.3390	
Refinement method	Full-matrix least-squares on F <sup>2</sup>	
Data / restraints / parameters	14131 / 0 / 604	
Goodness-of-fit on F <sup>2</sup>	1.070	
Final R indices [I>2sigma(I)]	R1 = 0.0430, wR2 = 0.1153	
R indices (all data)	R1 = 0.0614, wR2 = 0.1229	
Largest diff. peak and hole	1.940 and -1.329 e.Å <sup>-3</sup>	



**Table A.43** Crystal data and structure refinement for **37**

Identification code	ar0712m	
Empirical formula	C100.60 H113.30 N8 O16.80	
Formula weight	1703.29	
Temperature	120(2) K	
Wavelength	0.71073 Å	
Crystal system	Triclinic	
Space group	P-1	
Unit cell dimensions	a = 14.7722(7) Å	$\alpha = 109.733(3)^\circ$ .
	b = 15.9370(8) Å	$\beta = 96.094(3)^\circ$ .
	c = 22.1716(11) Å	$\gamma = 93.890(3)^\circ$ .
Volume	4855.4(4) Å <sup>3</sup>	
Z	2	
Density (calculated)	1.165 Mg/m <sup>3</sup>	
Absorption coefficient	0.080 mm <sup>-1</sup>	
F(000)	1815	
Crystal size	0.30 x 0.20 x 0.10 mm <sup>3</sup>	
Theta range for data collection	0.99 to 28.40°.	
Index ranges	-19<=h<=19, -21<=k<=21, -28<=l<=29	
Reflections collected	99701	
Independent reflections	23980 [R(int) = 0.0575]	
Completeness to theta = 28.40°	98.4 %	
Absorption correction	None	
Max. and min. transmission	0.9921 and 0.9765	
Refinement method	Full-matrix least-squares on F <sup>2</sup>	
Data / restraints / parameters	23980 / 45 / 1136	
Goodness-of-fit on F <sup>2</sup>	1.806	
Final R indices [I>2sigma(I)]	R1 = 0.1055, wR2 = 0.2969	
R indices (all data)	R1 = 0.1804, wR2 = 0.3241	
Largest diff. peak and hole	1.223 and -0.708 e.Å <sup>-3</sup>	

**Table A.44** Crystal data and structure refinement for **38**

Identification code	ar0721m	
Empirical formula	C <sub>79</sub> H <sub>93</sub> Br <sub>2</sub> N <sub>4</sub> O <sub>12</sub>	
Formula weight	1450.39	
Temperature	120(2) K	
Wavelength	0.71073 Å	
Crystal system	Monoclinic	
Space group	P2(1)/m	
Unit cell dimensions	a = 13.3457(7) Å	α = 90°.
	b = 19.5826(9) Å	β = 99.793(2)°.
	c = 14.0550(8) Å	γ = 90°.
Volume	3619.7(3) Å <sup>3</sup>	
Z	2	
Density (calculated)	1.331 g/cm <sup>3</sup>	
Absorption coefficient	1.184 mm <sup>-1</sup>	
F(000)	1522	
Crystal size	0.28 x 0.24 x 0.10 mm <sup>3</sup>	
Theta range for data collection	1.47 to 29.13°.	
Index ranges	-18 ≤ h ≤ 18, -26 ≤ k ≤ 26, -14 ≤ l ≤ 19	
Reflections collected	45929	
Independent reflections	9980 [R(int) = 0.0389]	
Completeness to theta = 29.13°	99.7 %	
Absorption correction	None	
Max. and min. transmission	0.8907 and 0.7327	
Refinement method	Full-matrix least-squares on F <sup>2</sup>	
Data / restraints / parameters	9980 / 44 / 481	
Goodness-of-fit on F <sup>2</sup>	1.251	
Final R indices [I > 2σ(I)]	R1 = 0.0823, wR2 = 0.2499	
R indices (all data)	R1 = 0.1321, wR2 = 0.2791	
Largest diff. peak and hole	1.441 and -1.063 e.Å <sup>-3</sup>	

**Table A.45** Crystal data and structure refinement for **40a**

Identification code	ar0822m	
Empirical formula	C <sub>162</sub> H <sub>171.20</sub> F <sub>4</sub> I <sub>2</sub> N <sub>13.60</sub> O <sub>16.40</sub>	
Formula weight	2900.93	
Temperature	120(2) K	
Wavelength	0.71073 Å	
Crystal system	Triclinic	
Space group	P-1	
Unit cell dimensions	a = 12.2272(7) Å	α = 95.883(3)°.
	b = 13.5156(7) Å	β = 103.793(2)°.
	c = 23.4101(12) Å	γ = 100.699(3)°.
Volume	3647.9(3) Å <sup>3</sup>	
Z	1	
Density (calculated)	1.321 g/cm <sup>3</sup>	
Absorption coefficient	0.505 mm <sup>-1</sup>	
F(000)	1512	
Crystal size	0.30 x 0.25 x 0.15 mm <sup>3</sup>	
Theta range for data collection	0.91 to 32.58°.	
Index ranges	-18 ≤ h ≤ 17, -19 ≤ k ≤ 20, -32 ≤ l ≤ 34	
Reflections collected	79170	
Independent reflections	24629 [R(int) = 0.0316]	
Completeness to theta = 25.00°	99.4 %	
Absorption correction	None	
Max. and min. transmission	0.9280 and 0.8632	
Refinement method	Full-matrix least-squares on F <sup>2</sup>	
Data / restraints / parameters	24629 / 12 / 917	
Goodness-of-fit on F <sup>2</sup>	1.018	
Final R indices [I > 2σ(I)]	R1 = 0.0382, wR2 = 0.0959	
R indices (all data)	R1 = 0.0513, wR2 = 0.1031	
Largest diff. peak and hole	1.010 and -0.670 e.Å <sup>-3</sup>	

**Table A.46** Crystal data and structure refinement for **40b**

Identification code	ar0901m	
Empirical formula	C150 H147 F16 I4 N5 O20.50	
Formula weight	3159.33	
Temperature	120(2) K	
Wavelength	0.71073 Å	
Crystal system	Triclinic	
Space group	P-1	
Unit cell dimensions	a = 18.758(3) Å	$\alpha = 100.106(10)^\circ$ .
	b = 19.828(3) Å	$\beta = 98.682(10)^\circ$ .
	c = 22.558(3) Å	$\gamma = 110.342(9)^\circ$ .
Volume	7538.1(19) Å <sup>3</sup>	
Z	2	
Density (calculated)	1.392 g/cm <sup>3</sup>	
Absorption coefficient	0.911 mm <sup>-1</sup>	
F(000)	3204	
Crystal size	0.45 x 0.40 x 0.25 mm <sup>3</sup>	
Theta range for data collection	1.13 to 26.31°.	
Index ranges	-22<=h<=22, -24<=k<=23, 0<=l<=27	
Reflections collected	32547	
Independent reflections	32547 [R(int) = 0.0000]	
Completeness to theta = 26.31°	82.8 %	
Absorption correction	TWINABS	
Max. and min. transmission	0.8043 and 0.6847	
Refinement method	Full-matrix least-squares on F <sup>2</sup>	
Data / restraints / parameters	32547 / 895 / 703	
Goodness-of-fit on F <sup>2</sup>	2.282	
Final R indices [I>2sigma(I)]	R1 = 0.2143, wR2 = 0.4462	
R indices (all data)	R1 = 0.3441, wR2 = 0.4890	
Largest diff. peak and hole	2.421 and -2.276 e.Å <sup>-3</sup>	

**Table A.47** Crystal data and structure refinement for **41**

Identification code	ar0824m	
Empirical formula	C76 H86 N4 O10	
Formula weight	1215.49	
Temperature	120(2) K	
Wavelength	0.71073 Å	
Crystal system	Monoclinic	
Space group	P2(1)/c	
Unit cell dimensions	a = 24.918(2) Å	$\alpha = 90^\circ$ .
	b = 14.3312(15) Å	$\beta = 107.680(6)^\circ$ .
	c = 19.1136(19) Å	$\gamma = 90^\circ$ .
Volume	6503.2(11) Å <sup>3</sup>	
Z	4	
Density (calculated)	1.241 g/cm <sup>3</sup>	
Absorption coefficient	0.082 mm <sup>-1</sup>	
F(000)	2600	
Crystal size	0.24 x 0.20 x 0.05 mm <sup>3</sup>	
Theta range for data collection	2.14 to 28.34°.	
Index ranges	-30 ≤ h ≤ 33, -17 ≤ k ≤ 8, -24 ≤ l ≤ 25	
Reflections collected	31545	
Independent reflections	14736 [R(int) = 0.1805]	
Completeness to theta = 22.50°	96.0 %	
Absorption correction	None	
Max. and min. transmission	0.9959 and 0.9806	
Refinement method	Full-matrix least-squares on F <sup>2</sup>	
Data / restraints / parameters	14736 / 3171 / 860	
Goodness-of-fit on F <sup>2</sup>	0.945	
Final R indices [I > 2σ(I)]	R1 = 0.1099, wR2 = 0.2571	
R indices (all data)	R1 = 0.3632, wR2 = 0.3766	
Largest diff. peak and hole	0.925 and -0.545 e.Å <sup>-3</sup>	

**Table A.48** Crystal data and structure refinement for **41a**

Identification code	ar0826m	
Empirical formula	C <sub>88</sub> H <sub>82</sub> F <sub>8</sub> I <sub>4</sub> N <sub>6</sub> O <sub>8</sub>	
Formula weight	2011.20	
Temperature	120(2) K	
Wavelength	0.71073 Å	
Crystal system	Triclinic	
Space group	P-1	
Unit cell dimensions	a = 12.3175(5) Å	α = 88.893(2)°.
	b = 13.2596(6) Å	β = 88.152(2)°.
	c = 25.4769(11) Å	γ = 79.980(2)°.
Volume	4095.0(3) Å <sup>3</sup>	
Z	2	
Density (calculated)	1.631 g/cm <sup>3</sup>	
Absorption coefficient	1.601 mm <sup>-1</sup>	
F(000)	2000	
Crystal size	0.24 x 0.18 x 0.10 mm <sup>3</sup>	
Theta range for data collection	0.80 to 30.51°.	
Index ranges	-16 ≤ h ≤ 16, -18 ≤ k ≤ 15, -36 ≤ l ≤ 33	
Reflections collected	59351	
Independent reflections	22662 [R(int) = 0.0417]	
Completeness to theta = 27.50°	99.5 %	
Absorption correction	None	
Max. and min. transmission	0.8563 and 0.7000	
Refinement method	Full-matrix least-squares on F <sup>2</sup>	
Data / restraints / parameters	22662 / 36 / 1057	
Goodness-of-fit on F <sup>2</sup>	1.033	
Final R indices [I > 2σ(I)]	R1 = 0.0513, wR2 = 0.1244	
R indices (all data)	R1 = 0.0806, wR2 = 0.1412	
Largest diff. peak and hole	2.524 and -1.537 e.Å <sup>-3</sup>	

**Table A.49** Crystal data and structure refinement for **SR1-e**

Identification code	ar0916m	
Empirical formula	C <sub>26</sub> H <sub>36</sub> Br <sub>2</sub> N <sub>4</sub> O <sub>6</sub>	
Formula weight	660.41	
Temperature	120(2) K	
Wavelength	0.71073 Å	
Crystal system	Triclinic	
Space group	P-1	
Unit cell dimensions	a = 5.1413(5) Å	α = 98.672(6)°.
	b = 9.8969(10) Å	β = 90.297(6)°.
	c = 14.1428(15) Å	γ = 90.815(6)°.
Volume	711.31(13) Å <sup>3</sup>	
Z	1	
Density (calculated)	1.542 g/cm <sup>3</sup>	
Absorption coefficient	2.895 mm <sup>-1</sup>	
F(000)	338	
Crystal size	0.32 x 0.24 x 0.12 mm <sup>3</sup>	
Theta range for data collection	2.35 to 32.69°.	
Index ranges	-7 ≤ h ≤ 7, -13 ≤ k ≤ 15, -21 ≤ l ≤ 19	
Reflections collected	12441	
Independent reflections	4862 [R(int) = 0.0458]	
Completeness to theta = 27.50°	97.4 %	
Absorption correction	None	
Max. and min. transmission	0.7226 and 0.4576	
Refinement method	Full-matrix least-squares on F <sup>2</sup>	
Data / restraints / parameters	4862 / 0 / 179	
Goodness-of-fit on F <sup>2</sup>	1.058	
Final R indices [I > 2σ(I)]	R1 = 0.0596, wR2 = 0.1450	
R indices (all data)	R1 = 0.0908, wR2 = 0.1619	
Largest diff. peak and hole	2.527 and -1.450 e.Å <sup>-3</sup>	

**Table A.50** Crystal data and structure refinement for **SR2-b**

Identification code	ar0915m	
Empirical formula	C <sub>22</sub> H <sub>28</sub> Br <sub>2</sub> N <sub>4</sub> O <sub>6</sub>	
Formula weight	604.30	
Temperature	120(2) K	
Wavelength	0.71073 Å	
Crystal system	Triclinic	
Space group	P-1	
Unit cell dimensions	a = 4.7253(9) Å	α = 79.367(5)°.
	b = 10.624(2) Å	β = 84.778(5)°.
	c = 12.692(2) Å	γ = 82.062(5)°.
Volume	618.8(2) Å <sup>3</sup>	
Z	1	
Density (calculated)	1.622 g/cm <sup>3</sup>	
Absorption coefficient	3.320 mm <sup>-1</sup>	
F(000)	306	
Crystal size	0.32 x 0.24 x 0.14 mm <sup>3</sup>	
Theta range for data collection	1.97 to 31.50°.	
Index ranges	-6 ≤ h ≤ 6, -15 ≤ k ≤ 15, -17 ≤ l ≤ 17	
Reflections collected	8959	
Independent reflections	3773 [R(int) = 0.0352]	
Completeness to theta = 25.00°	95.5 %	
Absorption correction	None	
Max. and min. transmission	0.6536 and 0.4164	
Refinement method	Full-matrix least-squares on F <sup>2</sup>	
Data / restraints / parameters	3773 / 0 / 160	
Goodness-of-fit on F <sup>2</sup>	1.046	
Final R indices [I > 2σ(I)]	R1 = 0.0358, wR2 = 0.0925	
R indices (all data)	R1 = 0.0422, wR2 = 0.0973	
Largest diff. peak and hole	0.857 and -0.573 e.Å <sup>-3</sup>	



**Table A.51** Crystal data and structure refinement for **SR2-e**

Identification code	ar1003m	
Empirical formula	C <sub>28</sub> H <sub>40</sub> Br <sub>2</sub> N <sub>4</sub> O <sub>6</sub>	
Formula weight	688.46	
Temperature	120(2) K	
Wavelength	0.71073 Å	
Crystal system	Triclinic	
Space group	P-1	
Unit cell dimensions	a = 5.2550(4) Å	α = 82.638(3)°.
	b = 9.2658(7) Å	β = 80.927(2)°.
	c = 15.8434(12) Å	γ = 84.634(2)°.
Volume	753.39(10) Å <sup>3</sup>	
Z	1	
Density (calculated)	1.517 g/cm <sup>3</sup>	
Absorption coefficient	2.737 mm <sup>-1</sup>	
F(000)	354	
Crystal size	0.30 x 0.20 x 0.08 mm <sup>3</sup>	
Theta range for data collection	2.45 to 33.14°.	
Index ranges	-8 ≤ h ≤ 6, -12 ≤ k ≤ 13, -24 ≤ l ≤ 23	
Reflections collected	13430	
Independent reflections	5020 [R(int) = 0.0275]	
Completeness to theta = 30.00°	97.9 %	
Absorption correction	None	
Max. and min. transmission	0.8108 and 0.4940	
Refinement method	Full-matrix least-squares on F <sup>2</sup>	
Data / restraints / parameters	5020 / 0 / 187	
Goodness-of-fit on F <sup>2</sup>	1.082	
Final R indices [I > 2σ(I)]	R1 = 0.0359, wR2 = 0.0803	
R indices (all data)	R1 = 0.0507, wR2 = 0.0852	
Largest diff. peak and hole	0.767 and -0.651 e.Å <sup>-3</sup>	

**Table A.52** Crystal data and structure refinement for **SR3-b**

Identification code	ar1010m	
Empirical formula	C <sub>24</sub> H <sub>26</sub> N <sub>8</sub> O <sub>4</sub>	
Formula weight	490.53	
Temperature	120(2) K	
Wavelength	0.71073 Å	
Crystal system	Monoclinic	
Space group	P2(1)/c	
Unit cell dimensions	a = 15.3250(15) Å	α = 90°.
	b = 7.5844(7) Å	β = 101.884(4)°.
	c = 10.3773(10) Å	γ = 90°.
Volume	1180.3(2) Å <sup>3</sup>	
Z	2	
Density (calculated)	1.380 g/cm <sup>3</sup>	
Absorption coefficient	0.098 mm <sup>-1</sup>	
F(000)	516	
Crystal size	0.34 x 0.22 x 0.12 mm <sup>3</sup>	
Theta range for data collection	1.36 to 30.50°.	
Index ranges	-20 ≤ h ≤ 21, -10 ≤ k ≤ 6, -14 ≤ l ≤ 13	
Reflections collected	9563	
Independent reflections	3530 [R(int) = 0.0357]	
Completeness to theta = 30.50°	97.8 %	
Absorption correction	None	
Max. and min. transmission	0.9883 and 0.9674	
Refinement method	Full-matrix least-squares on F <sup>2</sup>	
Data / restraints / parameters	3530 / 0 / 172	
Goodness-of-fit on F <sup>2</sup>	1.060	
Final R indices [I > 2σ(I)]	R1 = 0.0541, wR2 = 0.1421	
R indices (all data)	R1 = 0.0772, wR2 = 0.1652	
Largest diff. peak and hole	0.404 and -0.341 e.Å <sup>-3</sup>	

**Table A.53** Crystal data and structure refinement for **SR3-e**

Identification code	ar1008m	
Empirical formula	C30 H38 N8 O4	
Formula weight	574.68	
Temperature	120(2) K	
Wavelength	0.71073 Å	
Crystal system	Triclinic	
Space group	P-1	
Unit cell dimensions	a = 5.4083(4) Å	$\alpha = 80.343(2)^\circ$ .
	b = 7.0348(5) Å	$\beta = 83.201(3)^\circ$ .
	c = 20.0745(15) Å	$\gamma = 74.450(2)^\circ$ .
Volume	723.21(9) Å <sup>3</sup>	
Z	1	
Density (calculated)	1.320 g/cm <sup>3</sup>	
Absorption coefficient	0.091 mm <sup>-1</sup>	
F(000)	306	
Crystal size	0.38 x 0.20 x 0.08 mm <sup>3</sup>	
Theta range for data collection	3.04 to 31.00°.	
Index ranges	-7 ≤ h ≤ 7, -6 ≤ k ≤ 10, -29 ≤ l ≤ 29	
Reflections collected	11245	
Independent reflections	4394 [R(int) = 0.0273]	
Completeness to theta = 30.00°	96.9 %	
Absorption correction	None	
Max. and min. transmission	0.9928 and 0.9664	
Refinement method	Full-matrix least-squares on F <sup>2</sup>	
Data / restraints / parameters	4394 / 0 / 199	
Goodness-of-fit on F <sup>2</sup>	1.109	
Final R indices [I > 2σ(I)]	R1 = 0.0501, wR2 = 0.1457	
R indices (all data)	R1 = 0.0659, wR2 = 0.1611	
Largest diff. peak and hole	0.451 and -0.261 e.Å <sup>-3</sup>	

**Table A.54** Crystal data and structure refinement for **SR4-c**

Identification code	ar0925m	
Empirical formula	C <sub>29</sub> H <sub>37</sub> Cl F N O <sub>6</sub>	
Formula weight	550.05	
Temperature	120(2) K	
Wavelength	0.71073 Å	
Crystal system	Triclinic	
Space group	P-1	
Unit cell dimensions	a = 8.5818(4) Å	α = 86.103(2)°.
	b = 8.8742(5) Å	β = 83.495(2)°.
	c = 18.3524(10) Å	γ = 73.728(2)°.
Volume	1332.07(12) Å <sup>3</sup>	
Z	2	
Density (calculated)	1.371 g/cm <sup>3</sup>	
Absorption coefficient	0.195 mm <sup>-1</sup>	
F(000)	584	
Crystal size	0.36 x 0.28 x 0.16 mm <sup>3</sup>	
Theta range for data collection	2.48 to 30.61°.	
Index ranges	-12 ≤ h ≤ 12, -12 ≤ k ≤ 12, 0 ≤ l ≤ 26	
Reflections collected	15845	
Independent reflections	15845 [R(int) = 0.0000]	
Completeness to theta = 30.61°	98.4 %	
Absorption correction	Semi-empirical from equivalents	
Max. and min. transmission	0.9694 and 0.9330	
Refinement method	Full-matrix least-squares on F <sup>2</sup>	
Data / restraints / parameters	15845 / 0 / 353	
Goodness-of-fit on F <sup>2</sup>	1.035	
Final R indices [I > 2σ(I)]	R1 = 0.0481, wR2 = 0.1305	
R indices (all data)	R1 = 0.0737, wR2 = 0.1514	
Largest diff. peak and hole	0.557 and -0.345 e.Å <sup>-3</sup>	

## Appendix B - $^1\text{H}$ , $^{13}\text{C}$ NMR, and Mass Data

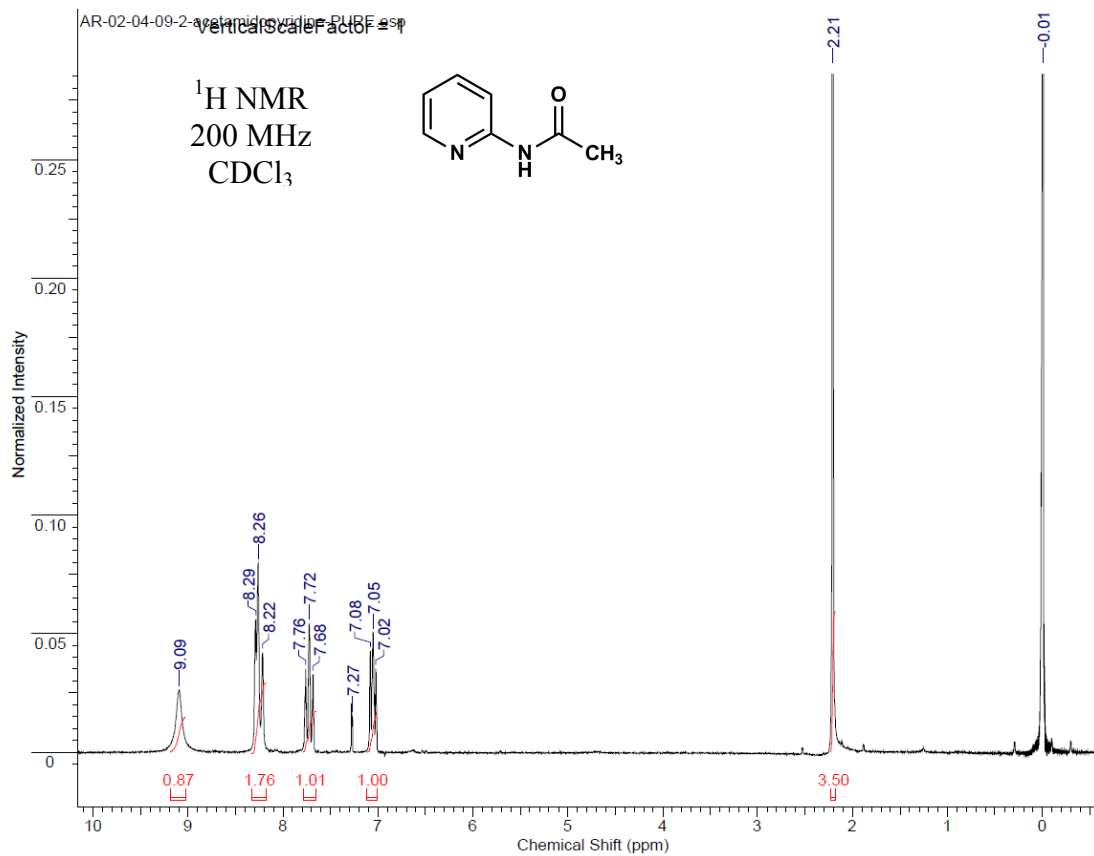


Figure B.1 2-acetamidopyridine, **3**,  $^1\text{H}$

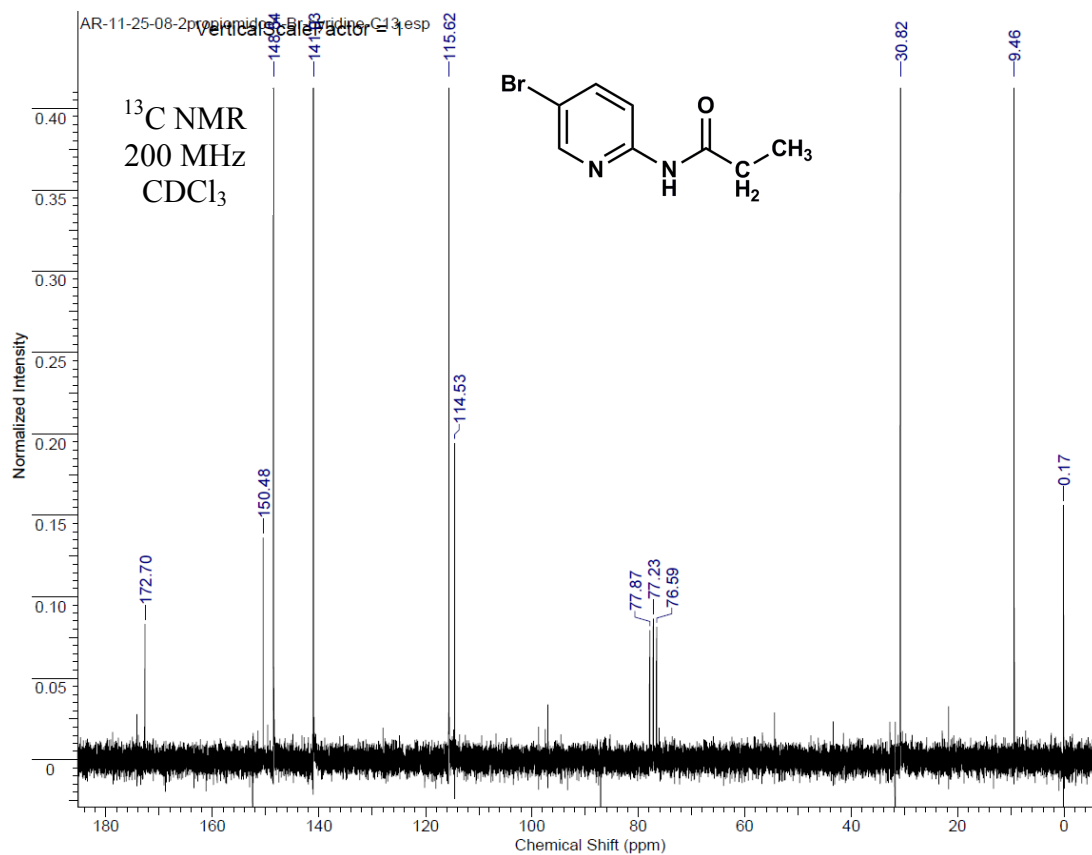
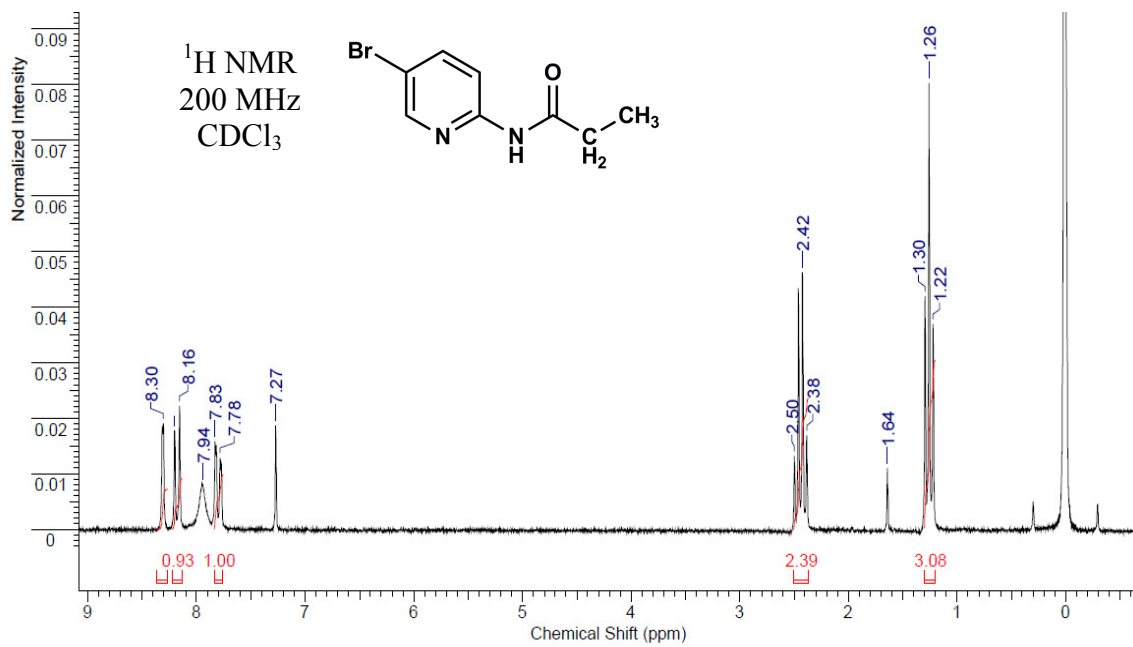


Figure B.2 2-propionamido-5-bromopyridine, 4, <sup>1</sup>H & <sup>13</sup>C

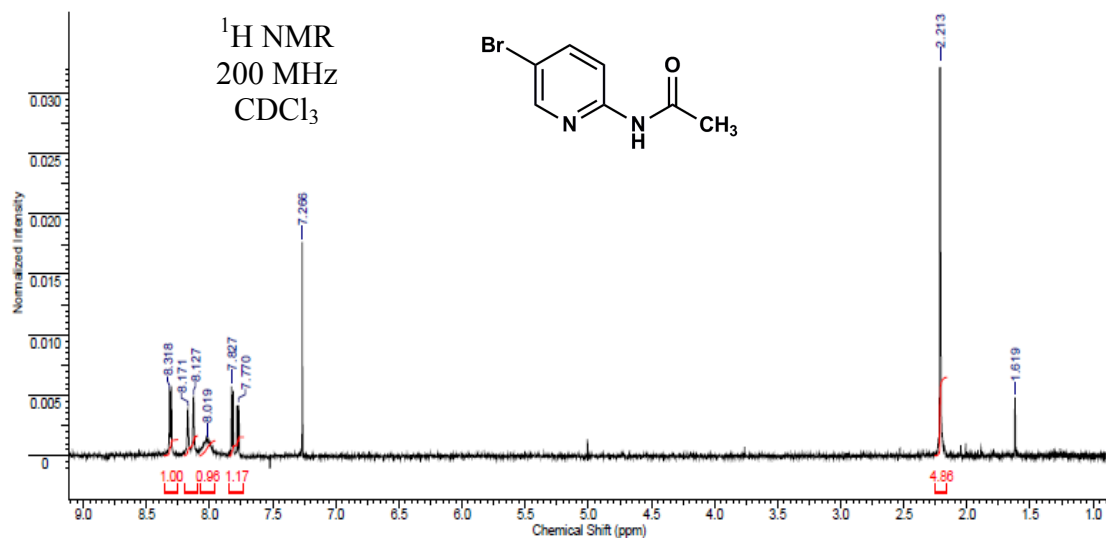


Figure B.3 2-acetamido-5-bromopyridine, **6**, <sup>1</sup>H

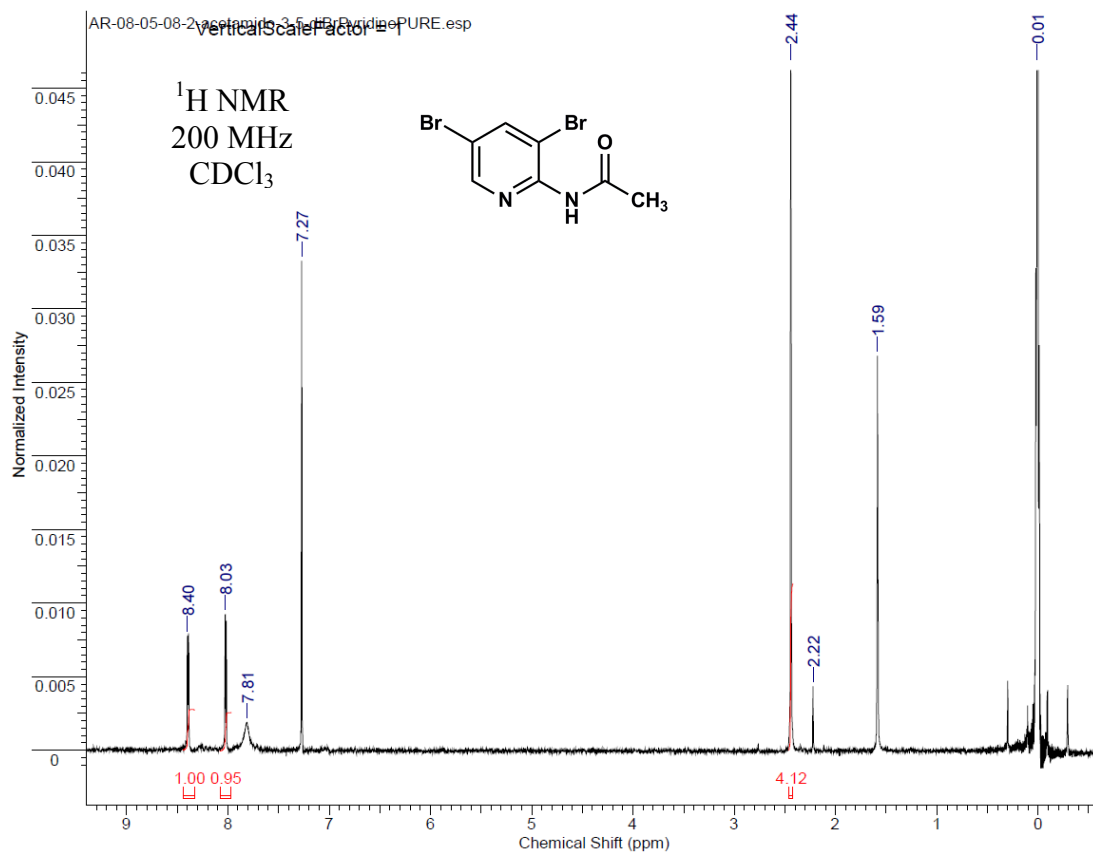


Figure B.4 2-acetamido-3,5-dibromopyridine, **7**, <sup>1</sup>H



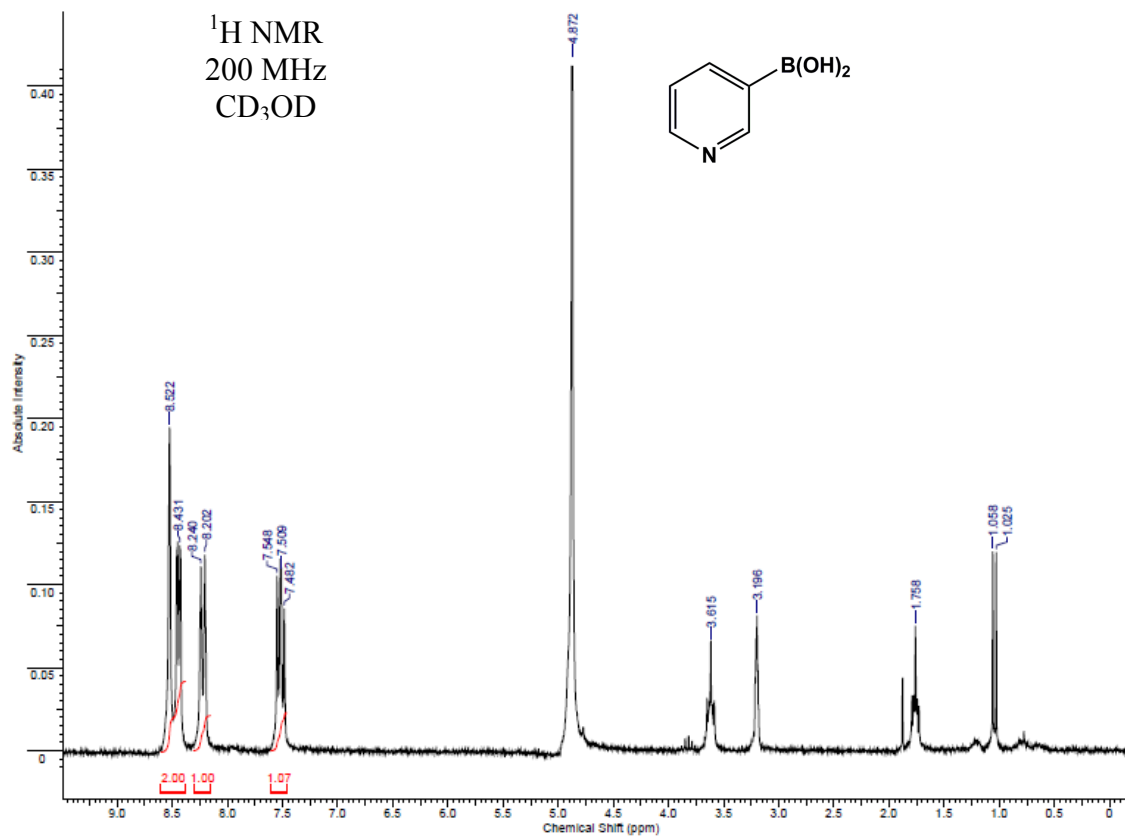
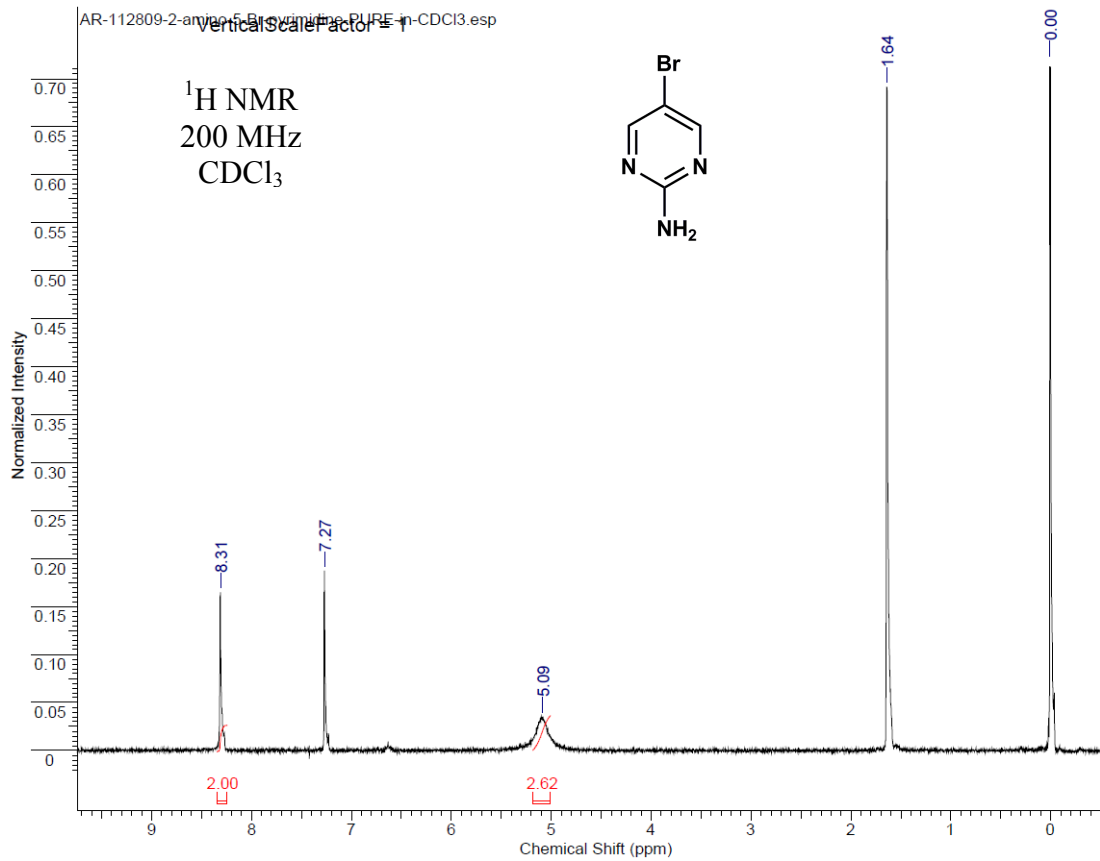


Figure B.5 3-pyridylbenzoic acid, **8**,  $^1\text{H}$



**Figure B.6** 2-amino-5-bromopyrimidine, **9**

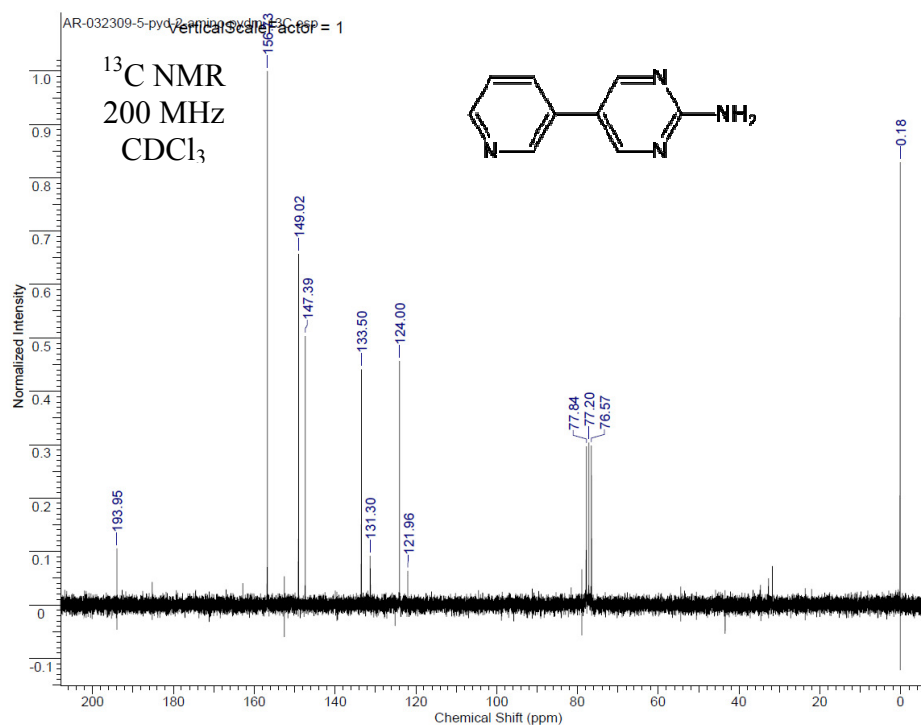
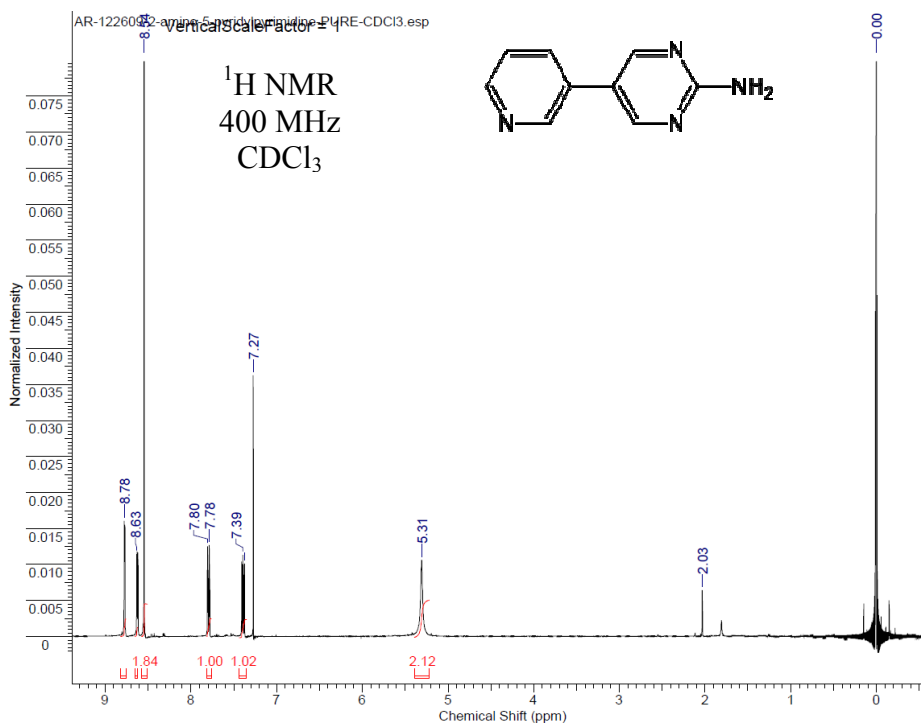


Figure B.7 2-amino-5-(3-pyridyl)pyrimidine, **10**, <sup>1</sup>H & <sup>13</sup>C

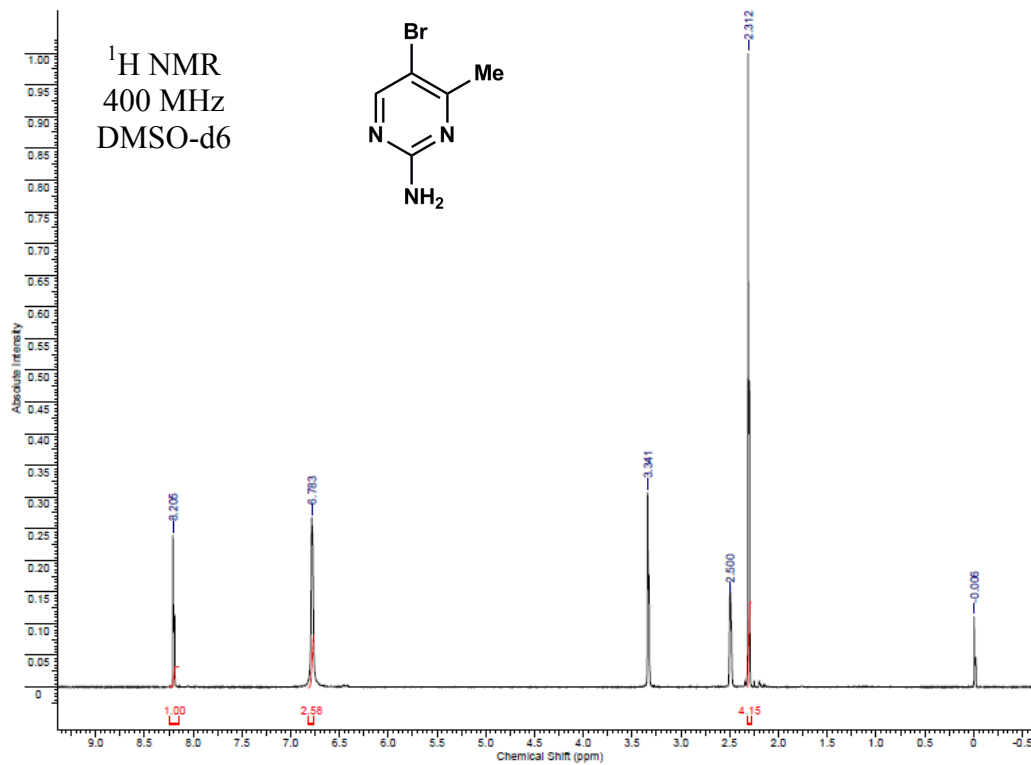


Figure B.8 2-amino-4-methyl-5-bromopyrimidine, **11**, <sup>1</sup>H

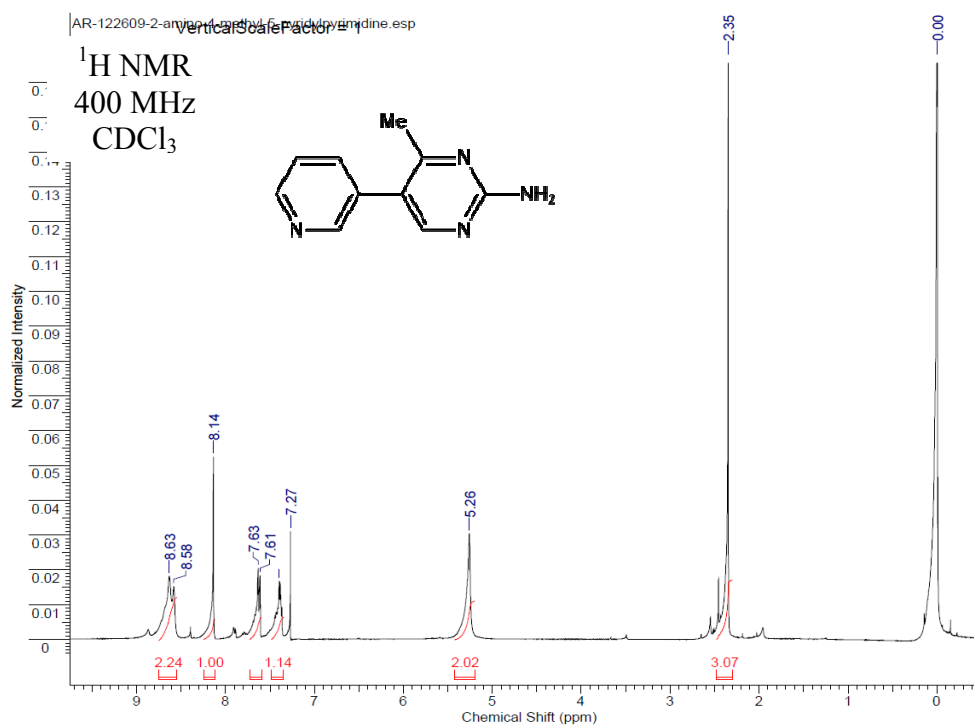
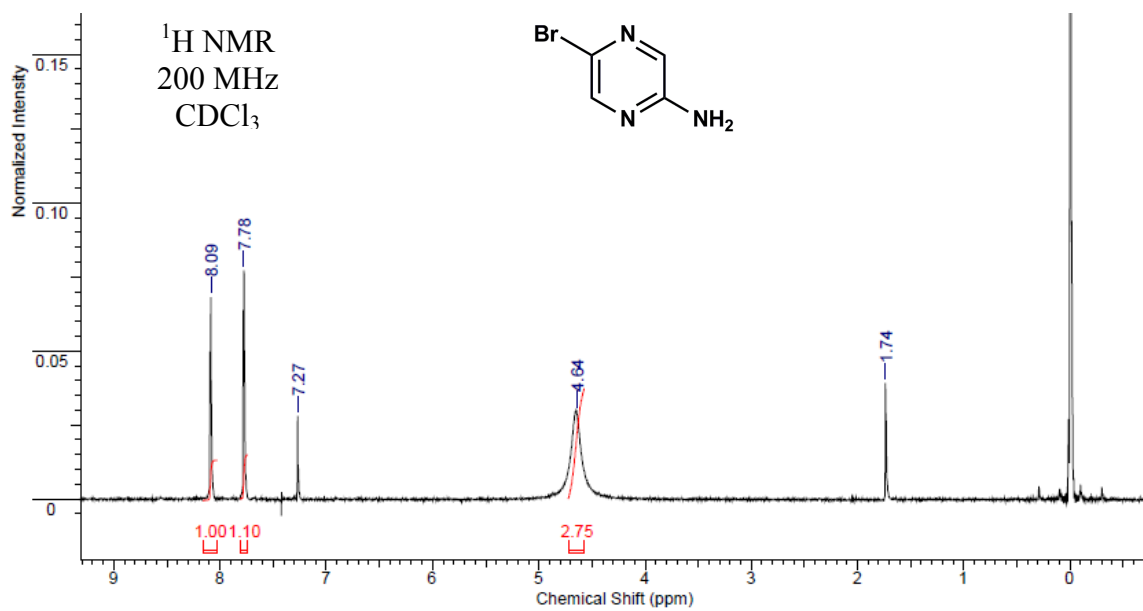
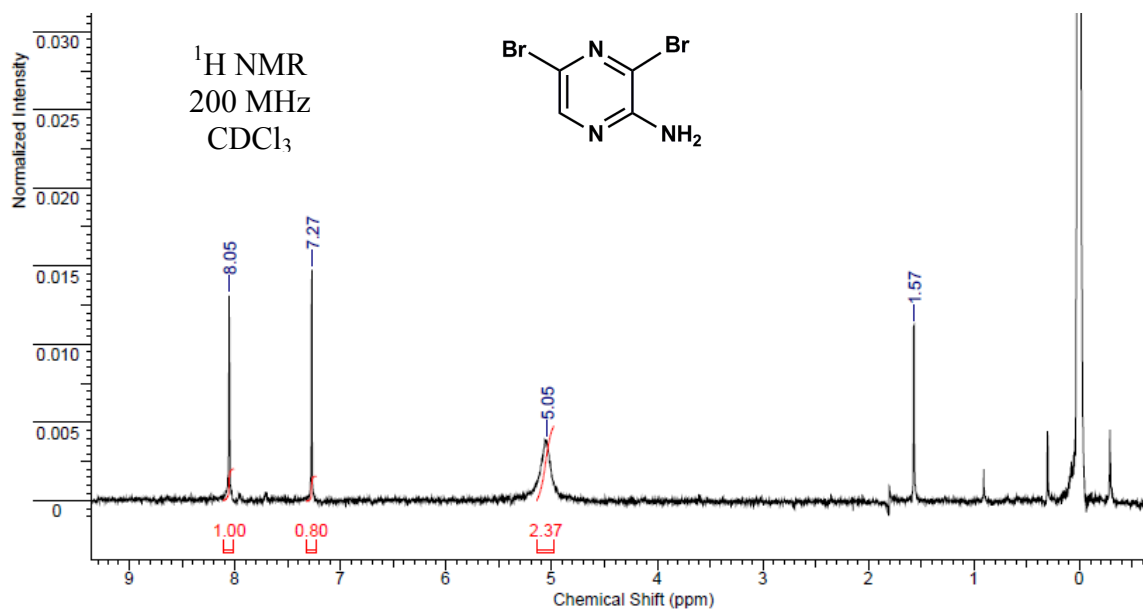


Figure B.9 2-amino-4-methyl-5-(3-pyridyl)pyrimidine, **12**, <sup>1</sup>H



**Figure B.10** 2-amino-5-bromopyrazine, **13**, <sup>1</sup>H



**Figure B.11** 2-amino-3,5-dibromopyrazine, **14**, <sup>1</sup>H

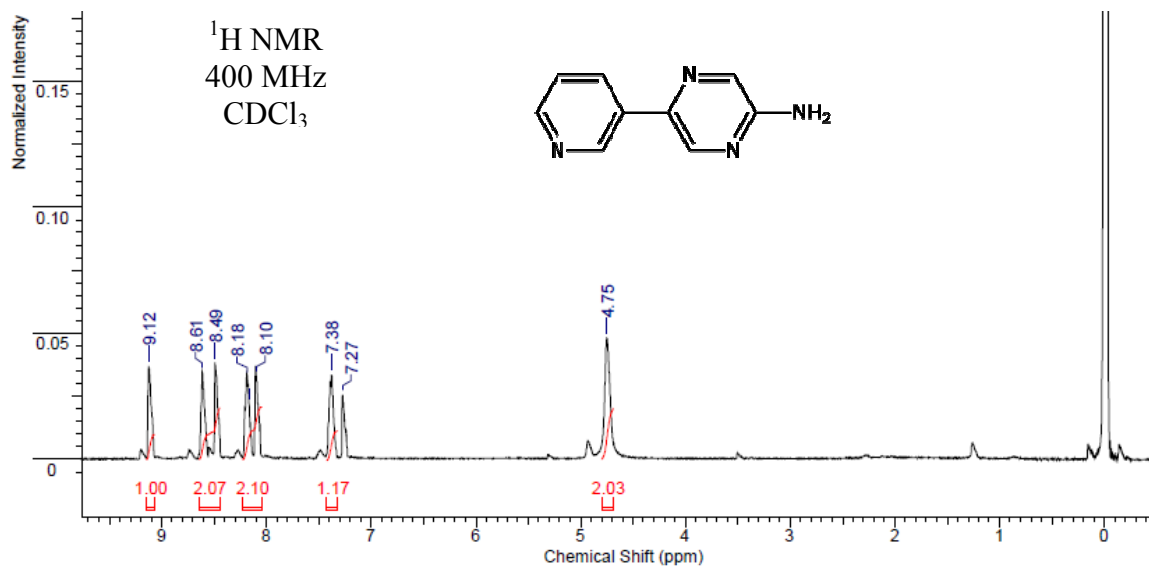


Figure B.12 2-amino-5-(3-pyridyl)pyrazine, **15**, <sup>1</sup>H

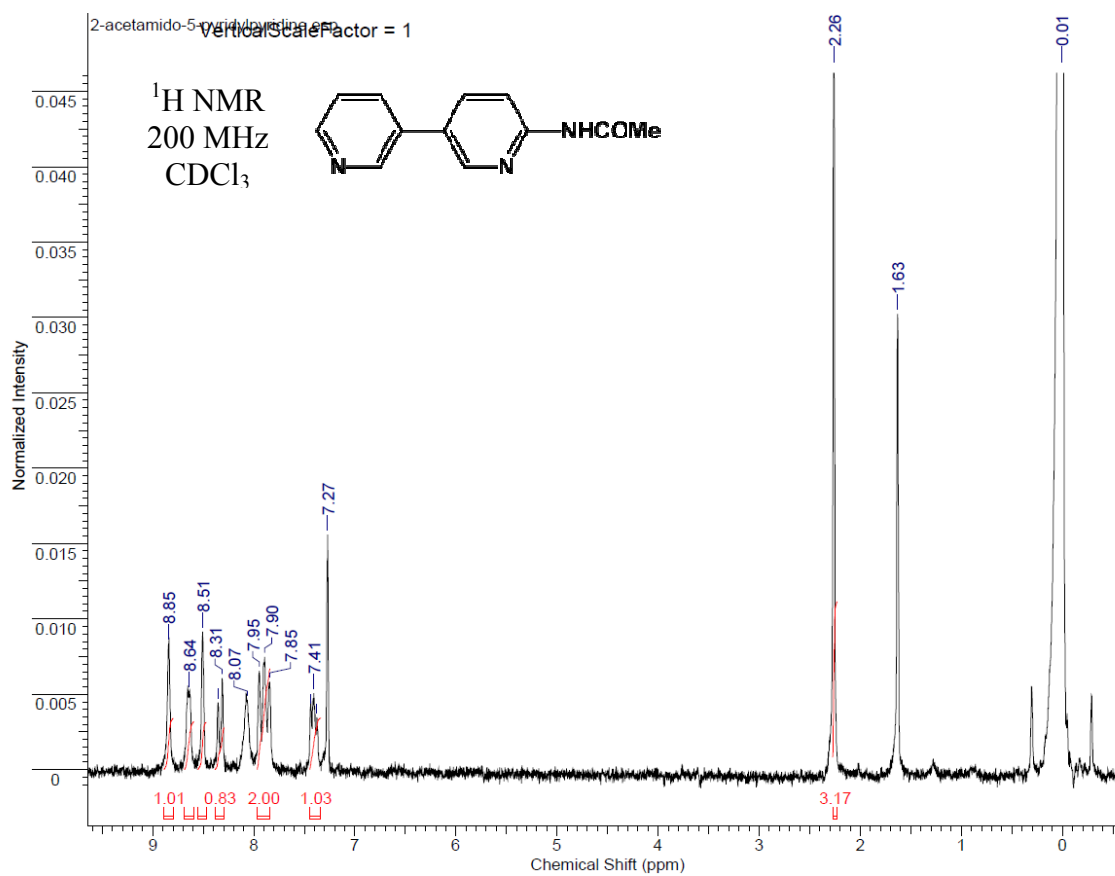


Figure B.13 2-acetamido-5-(3-pyridyl)pyridine, **16**, <sup>1</sup>H

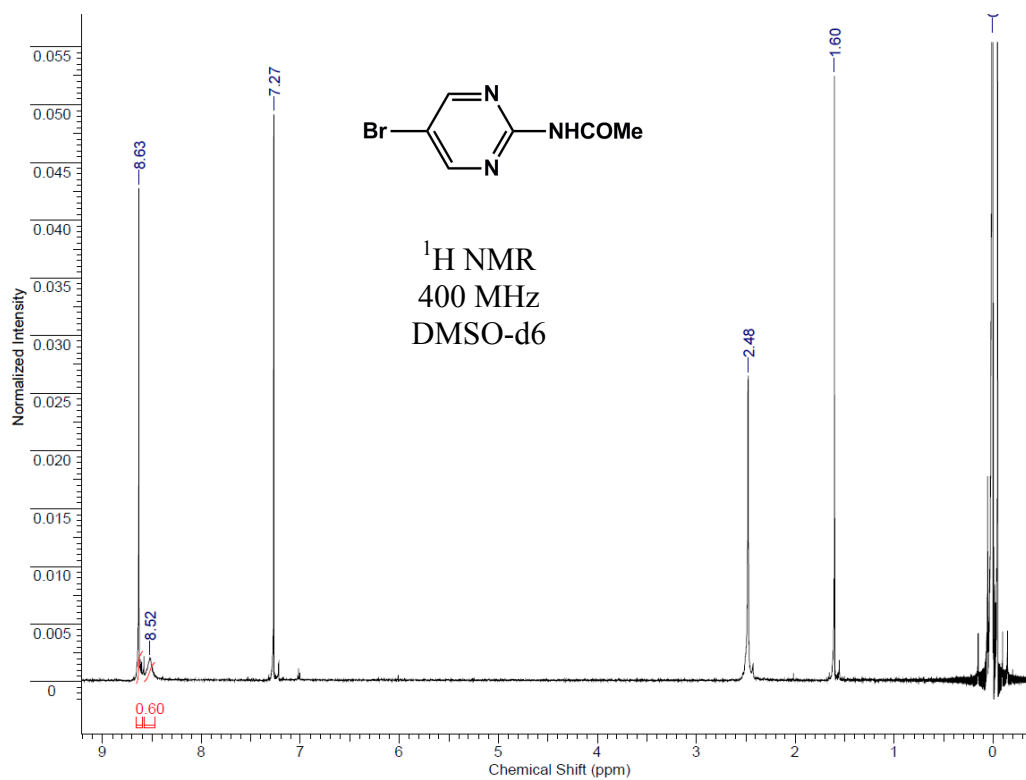


Figure B.14 2-acetamido-5-bromopyrimidine, **17**, <sup>1</sup>H

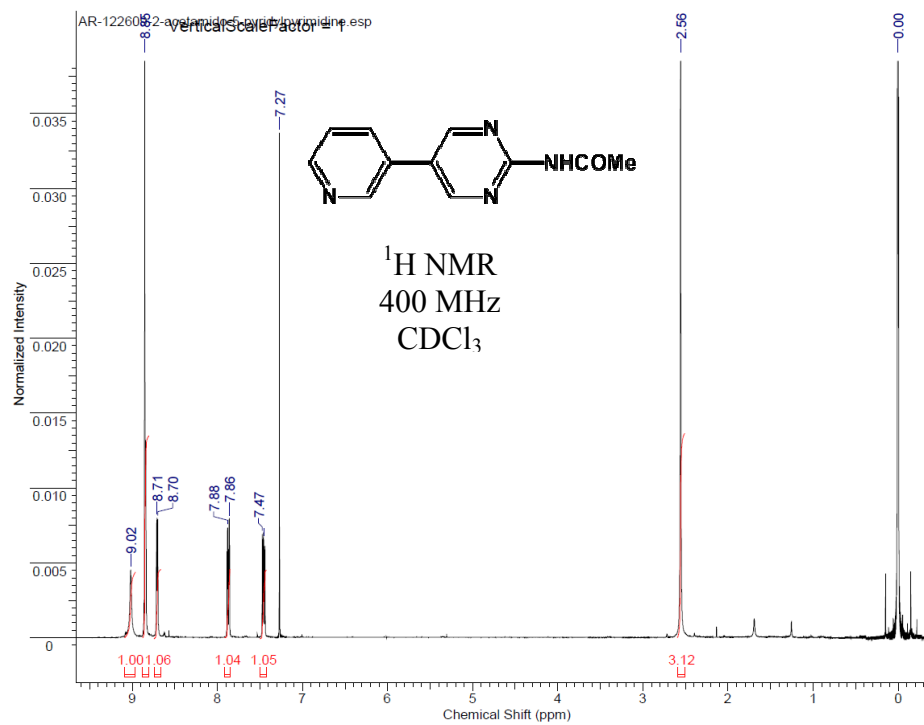


Figure B.15 2-acetamido-5-(3-pyridyl)pyrimidine, **18**

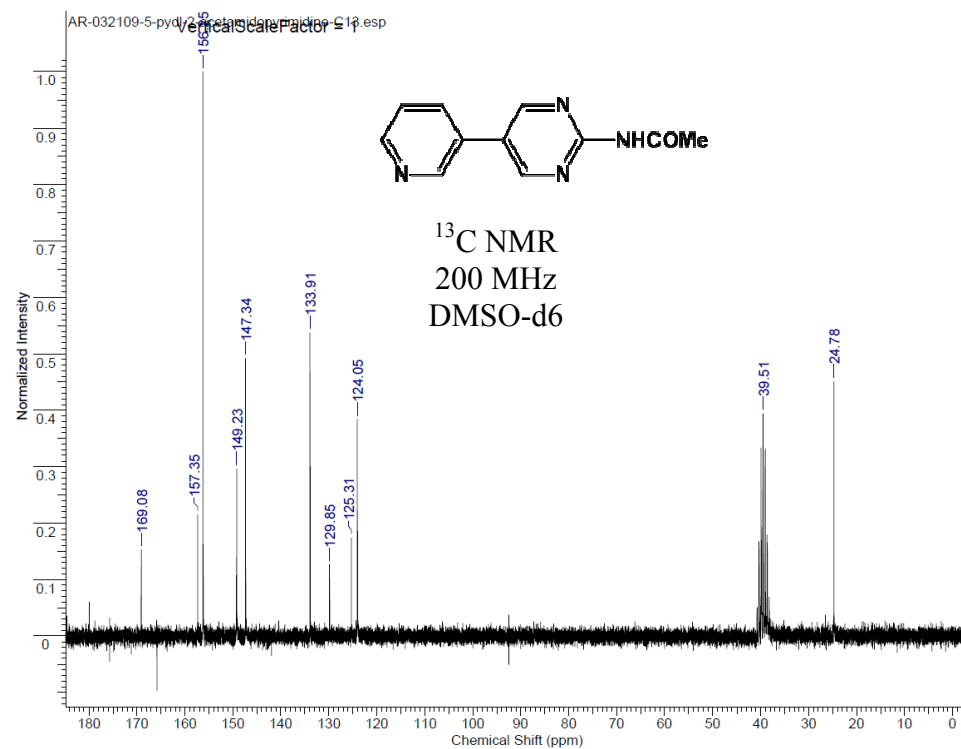
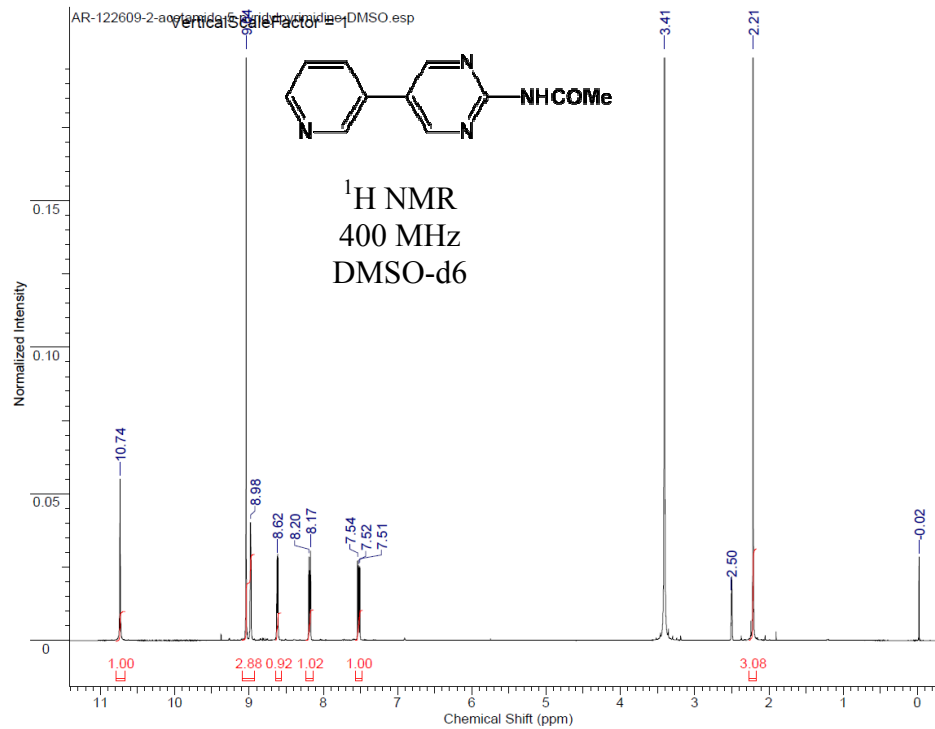


Figure B.16 2-acetamido-5-(3-pyridyl)pyrimidine, **18**,  $^1\text{H}$  &  $^{13}\text{C}$



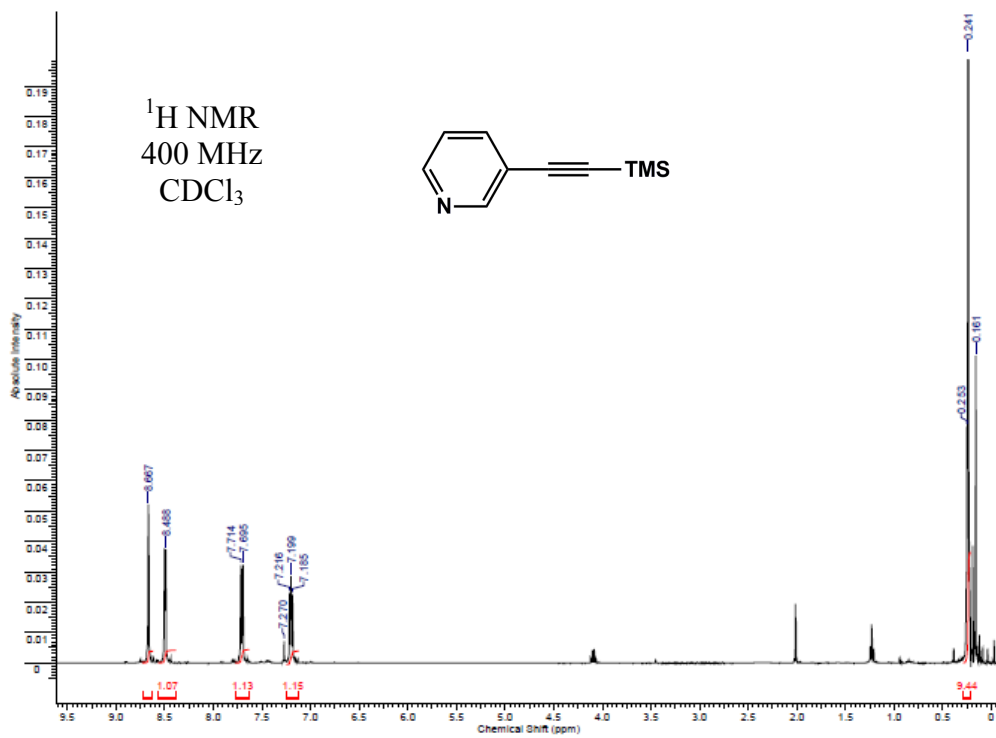


Figure B.17 TMS-protected 3-trimethylsilanylethynylpyridine, **19**, <sup>1</sup>H

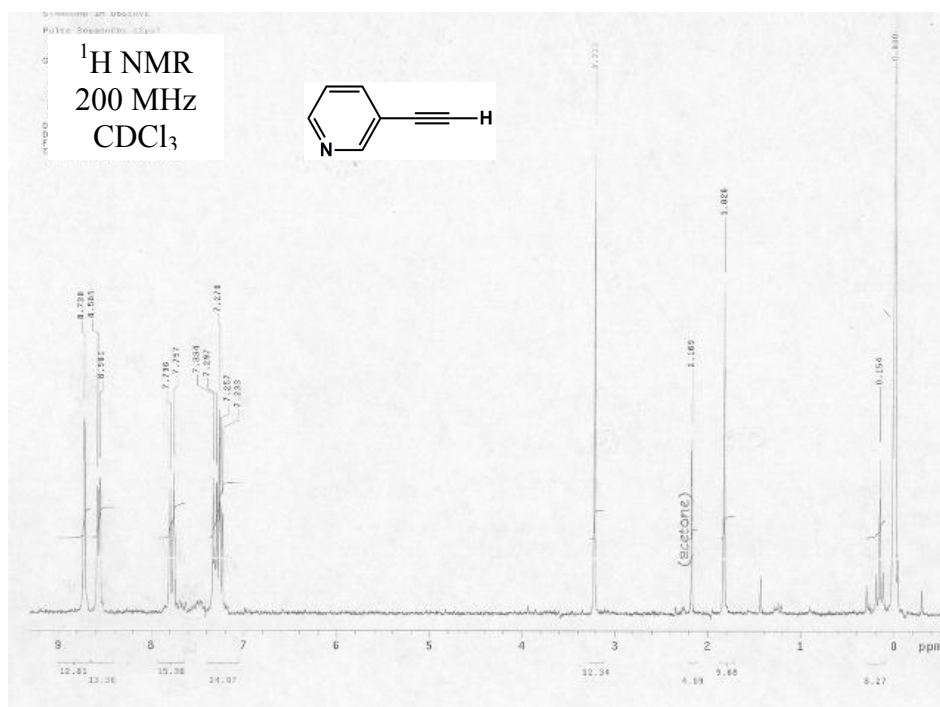


Figure B.18 3-ethynylpyridine, **20**, <sup>1</sup>H

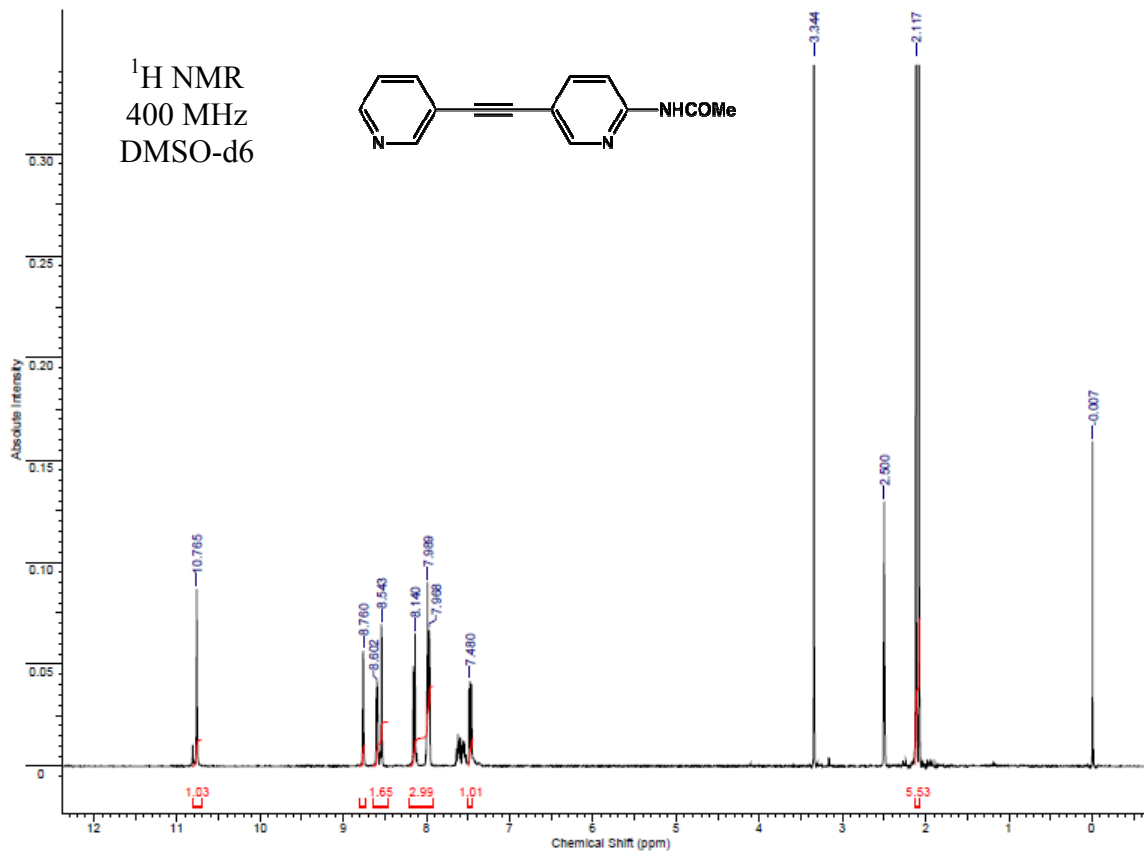


Figure B.19 2-acetamido-5-(3-pyridyl)ethynylpyridine, **21**, <sup>1</sup>H

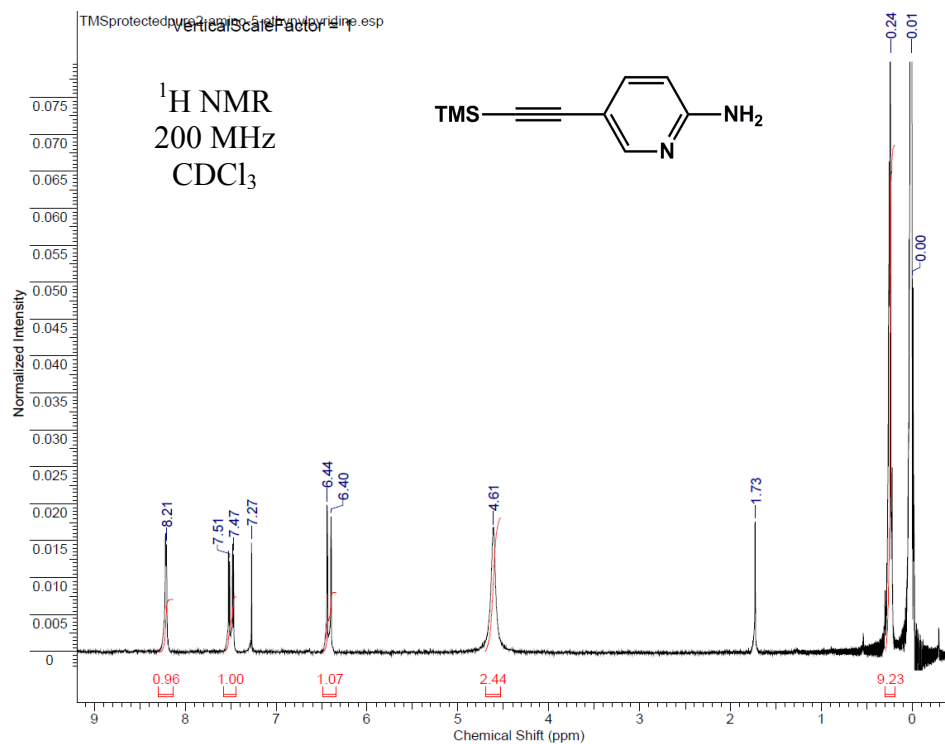


Figure B.20 2-amino-5-(trimethylsilyl)ethynylpyridine, **22**, <sup>1</sup>H

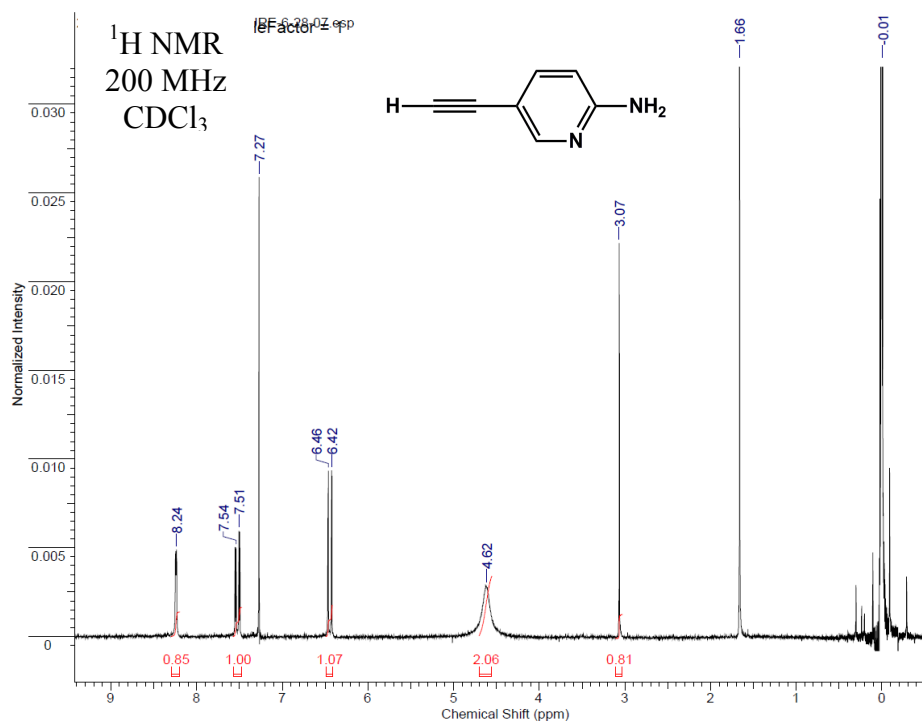


Figure B.21 2-amino-5-ethynylpyridine, **23**, <sup>1</sup>H

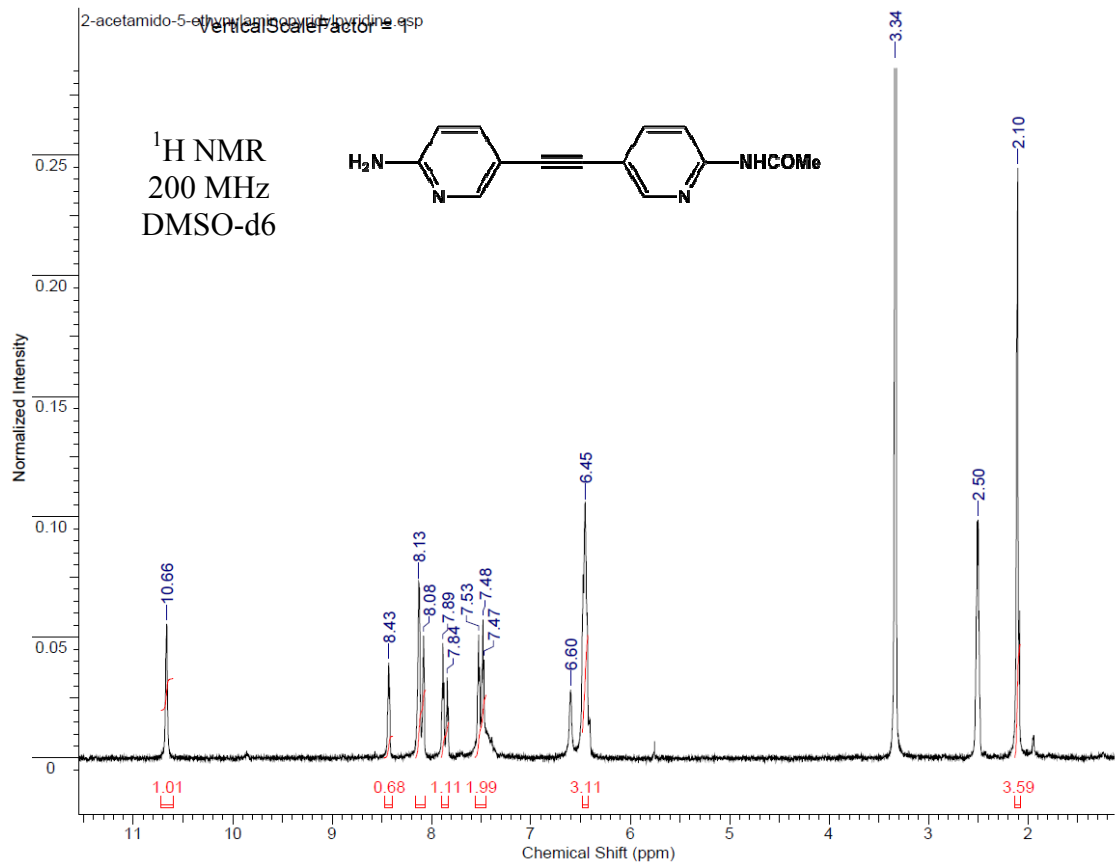


Figure B.22 2-acetamido-5-(3-(2-aminopyridyl)ethynyl)pyridine, **24**, <sup>1</sup>H

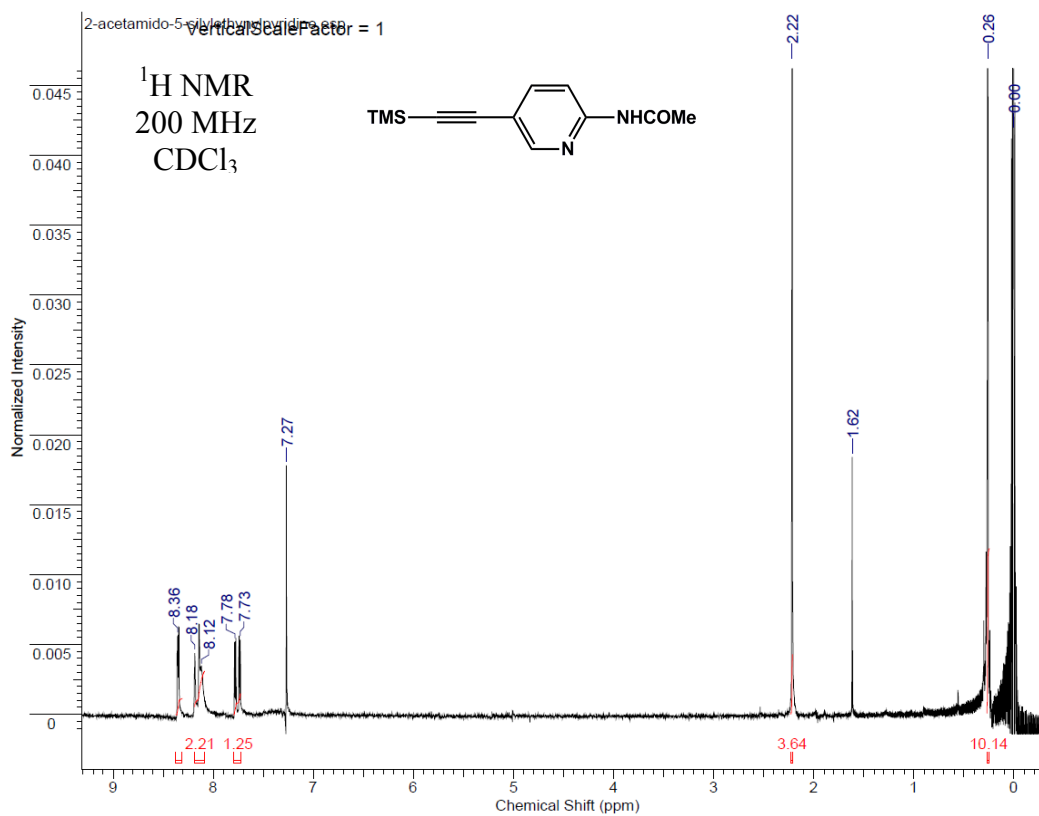


Figure B.23 2-acetamido-5-trimethylsilyl ethynylpyridine, **25**,  $^1\text{H}$

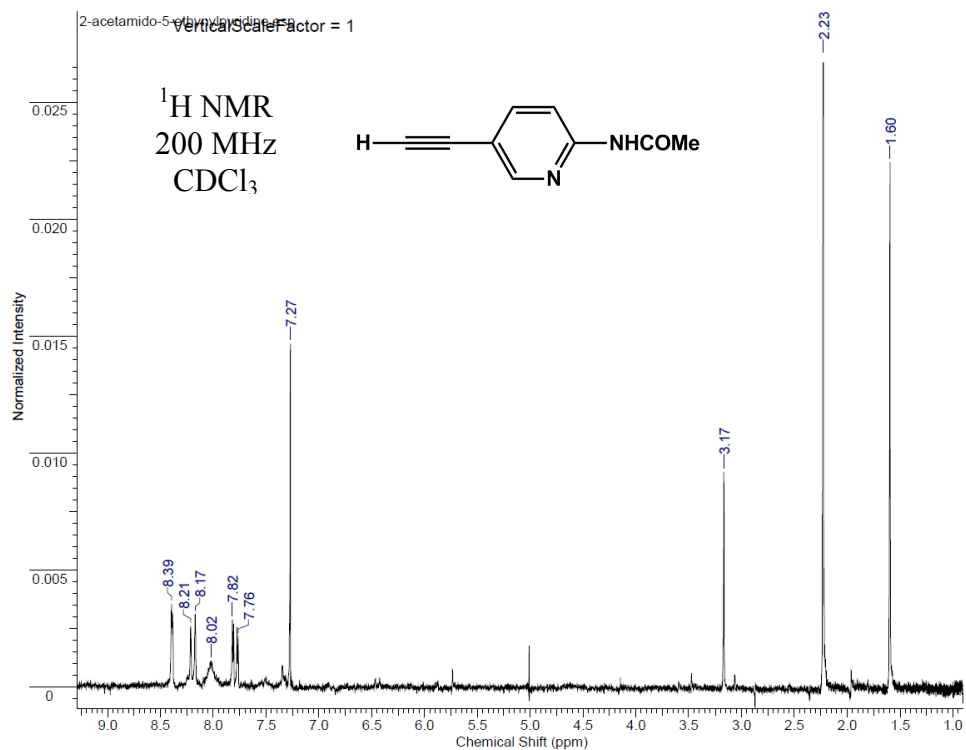


Figure B.24 2-acetamido-5-ethynylpyridine, **26**,  $^1\text{H}$

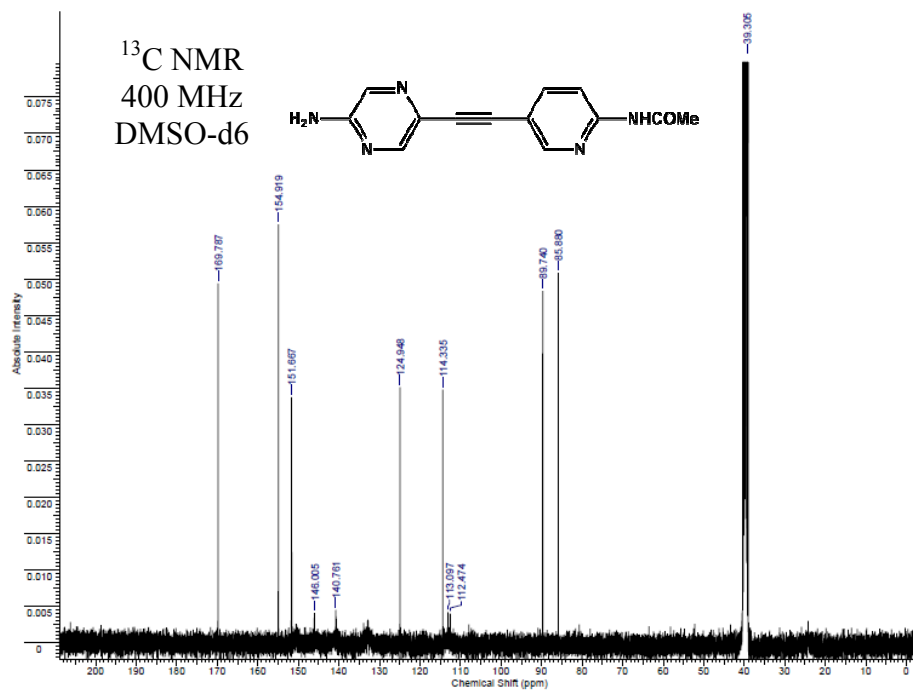
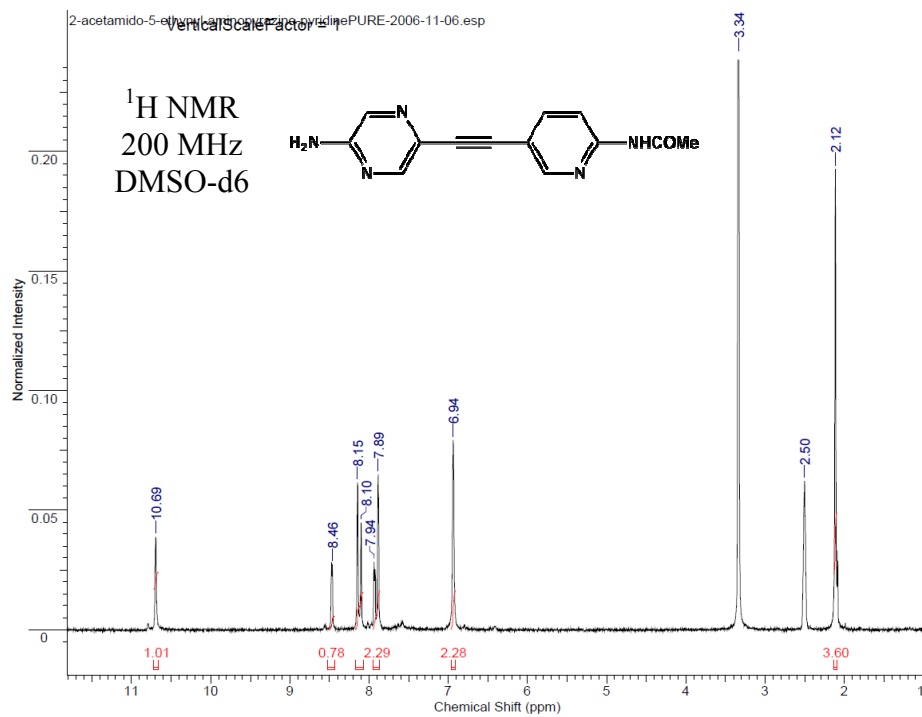


Figure B.25 2-amino-5-(3-(2-aminopyridin-5-ylethynyl)pyridine)pyridine, **27**, <sup>1</sup>H & <sup>13</sup>C

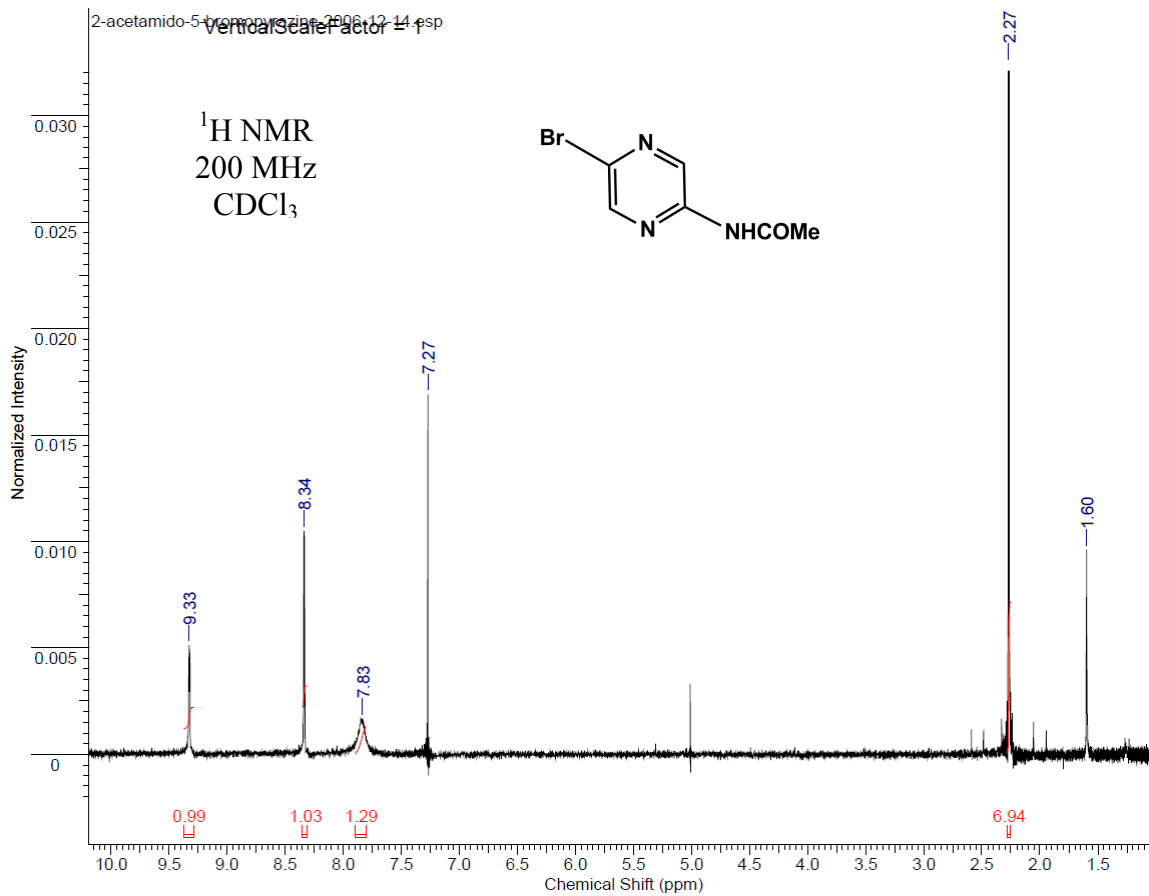


Figure B.26 2-acetamido-5-bromopyrazine, **28**, <sup>1</sup>H

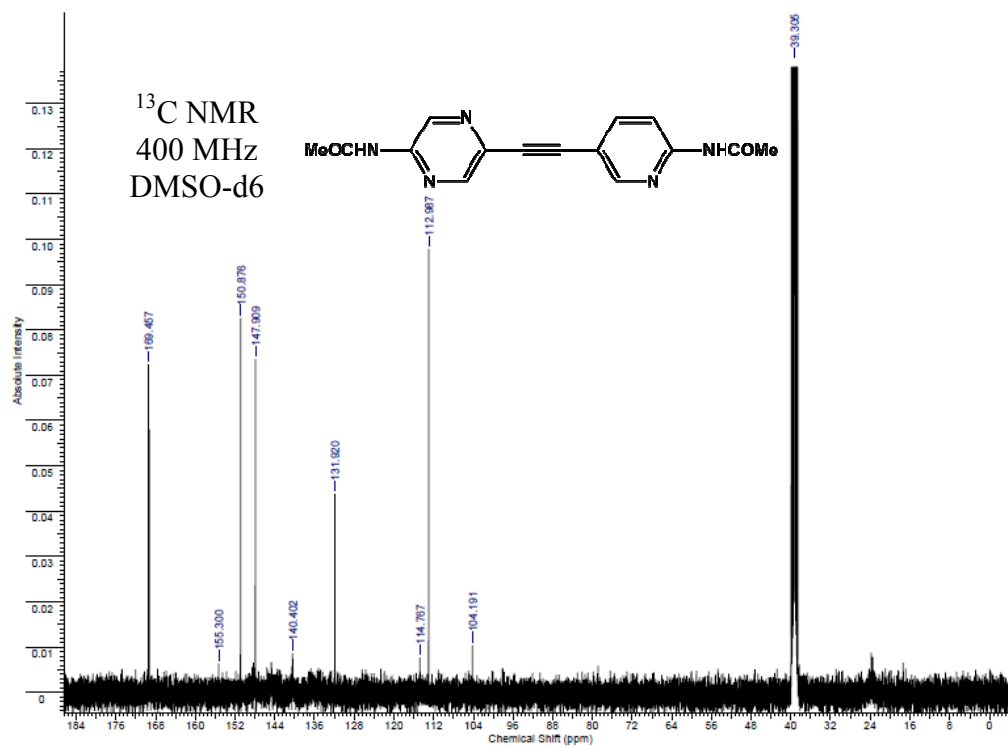
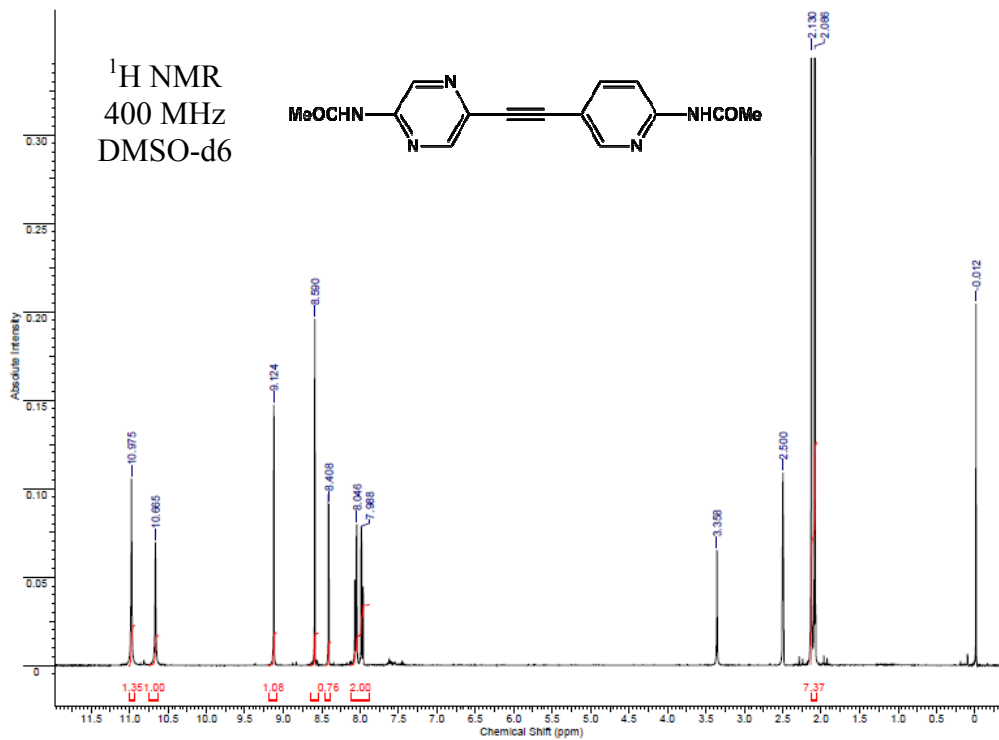


Figure B.27 2-acetamido-5-(3-(2-acetamidopyridyl)ethynyl)pyrazine, 29, <sup>1</sup>H & <sup>13</sup>C



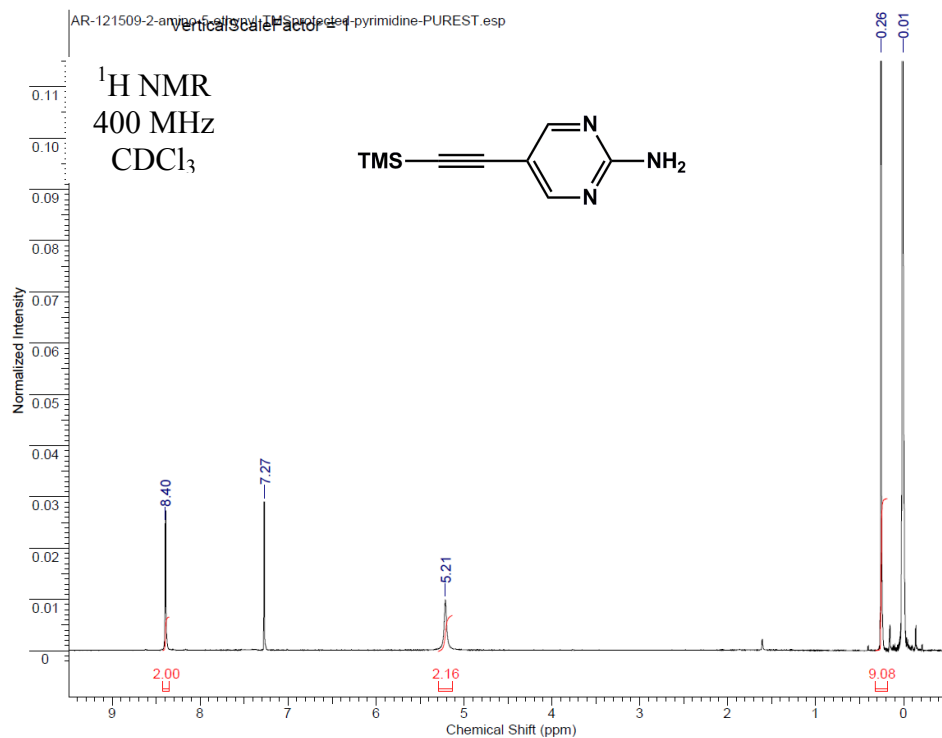


Figure B.28 2-amino-5-(trimethylsilyl)ethynylpyrimidine, **30**,  $^1\text{H}$

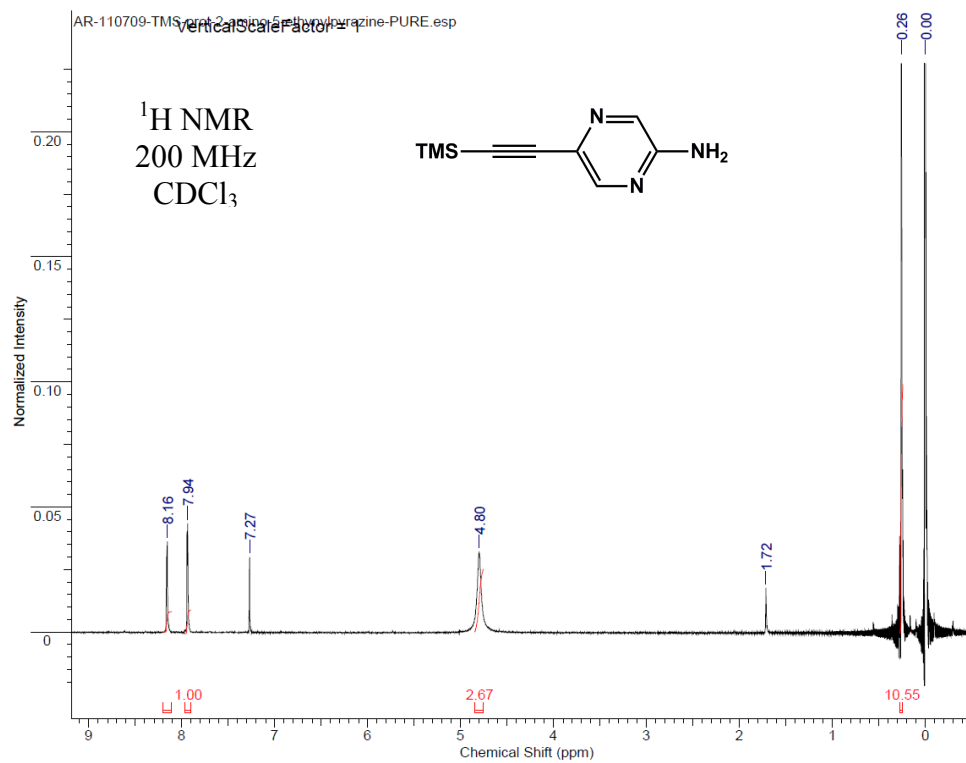


Figure B.29 2-amino-5-(trimethylsilyl)ethynylpyrazine, **31**,  $^1\text{H}$

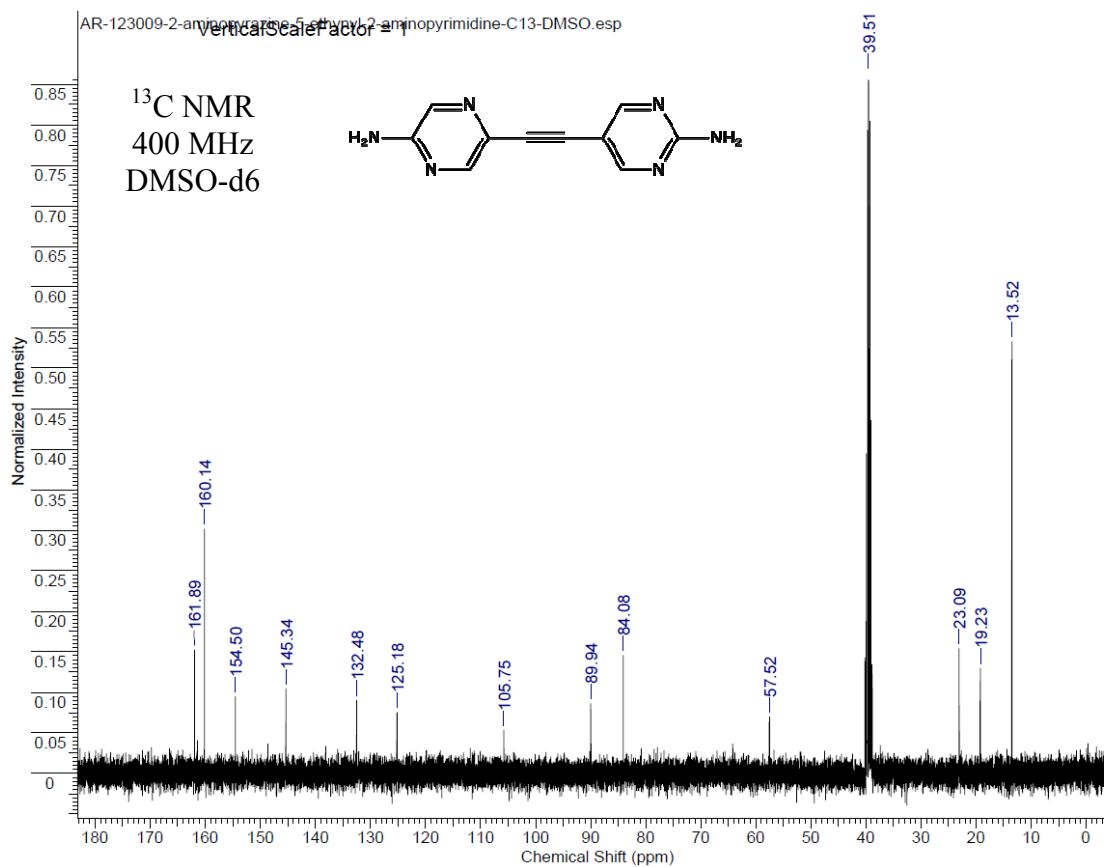
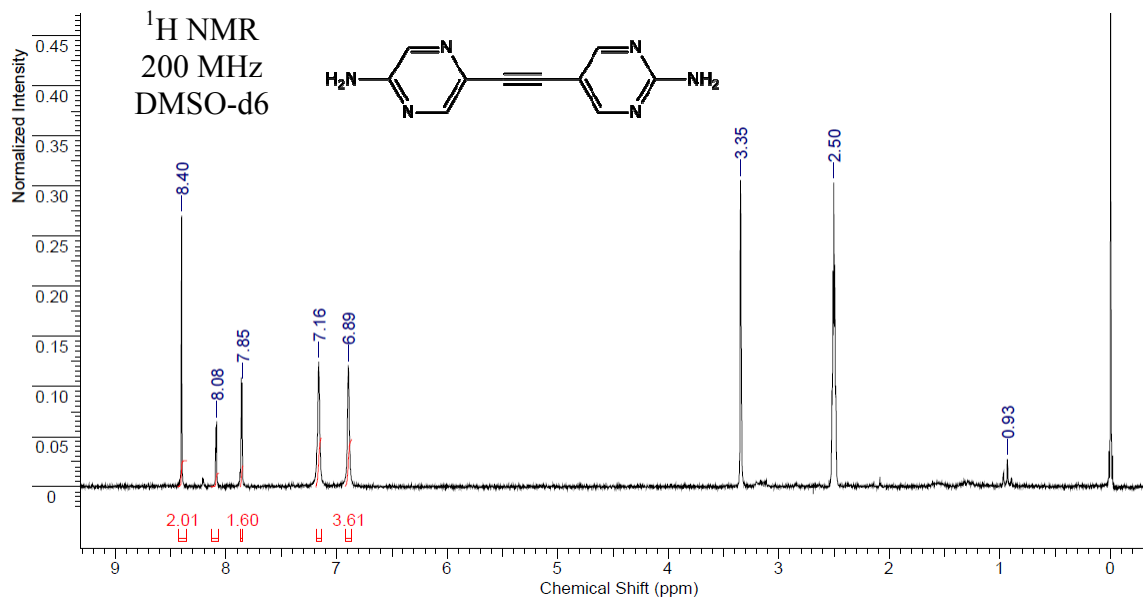
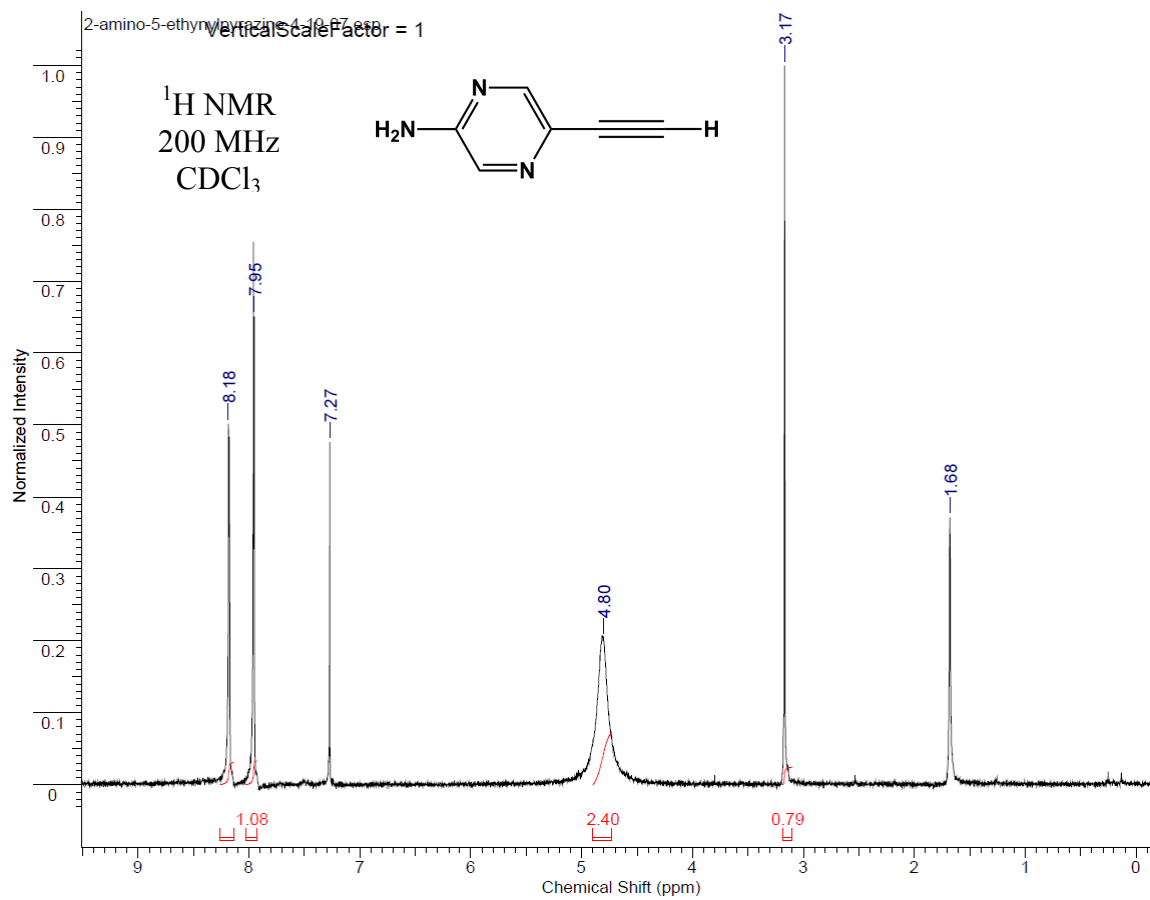
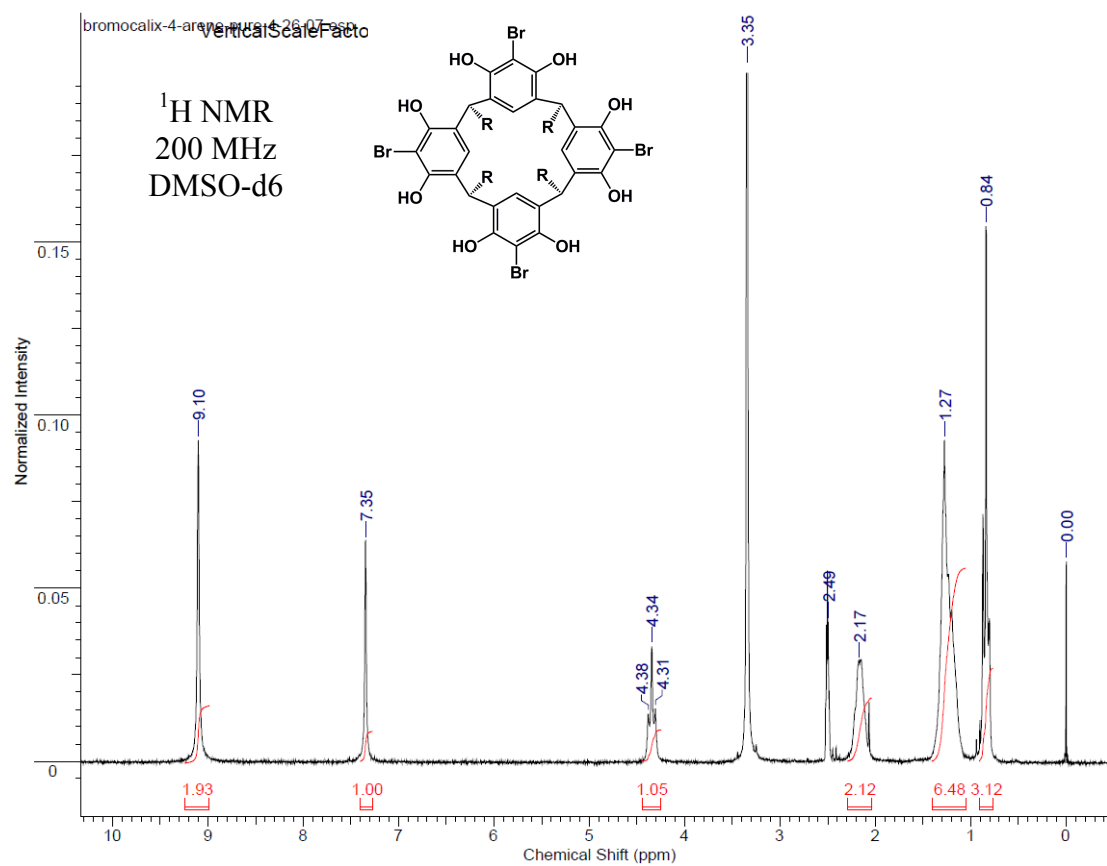


Figure B.30 2-amino-5-(3-(2-aminopyrazino))ethynylpyrimidine, **32**, <sup>1</sup>H & <sup>13</sup>C



**Figure B.31** 2-amino-5-ethynylprazine,  $^1\text{H}$



**Figure B.32** C-Pentylbromocalix[4]resorcinarene, **34**, <sup>1</sup>H

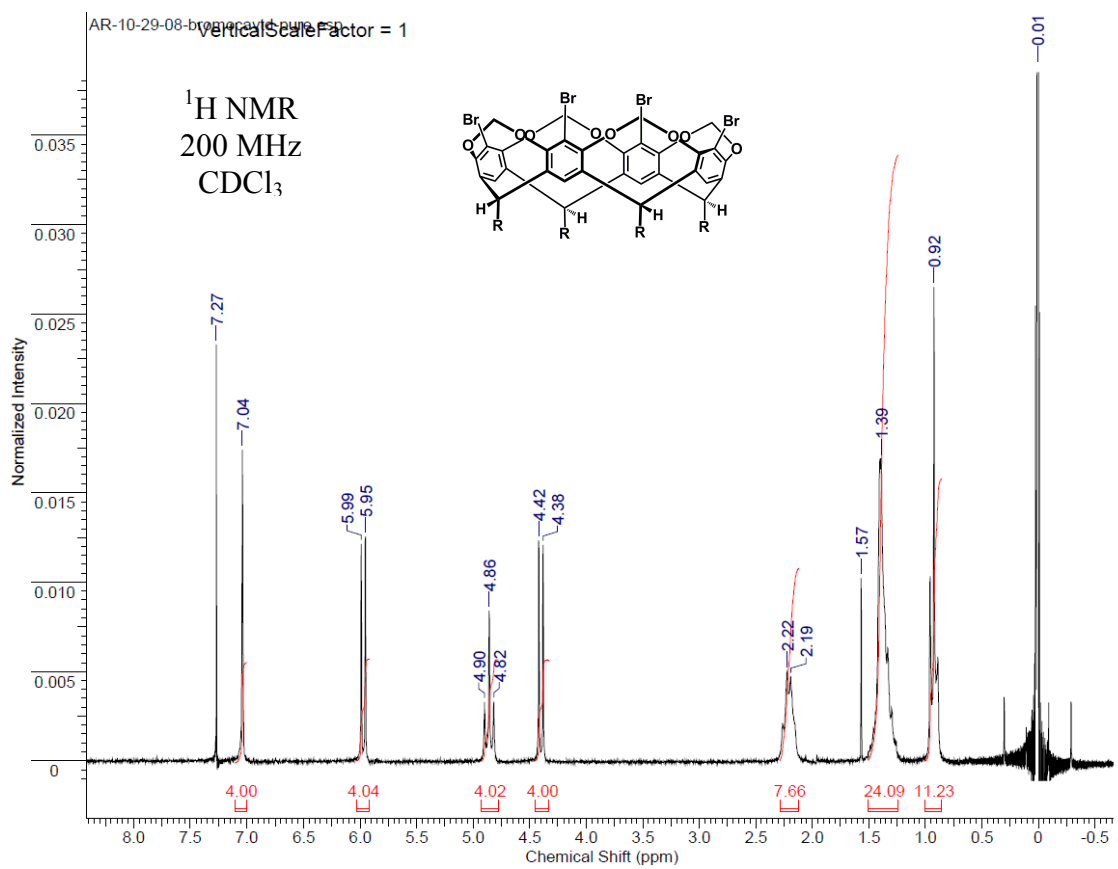


**Figure B.33** C-Pentyltetrabromocavitand, **35**, <sup>1</sup>H

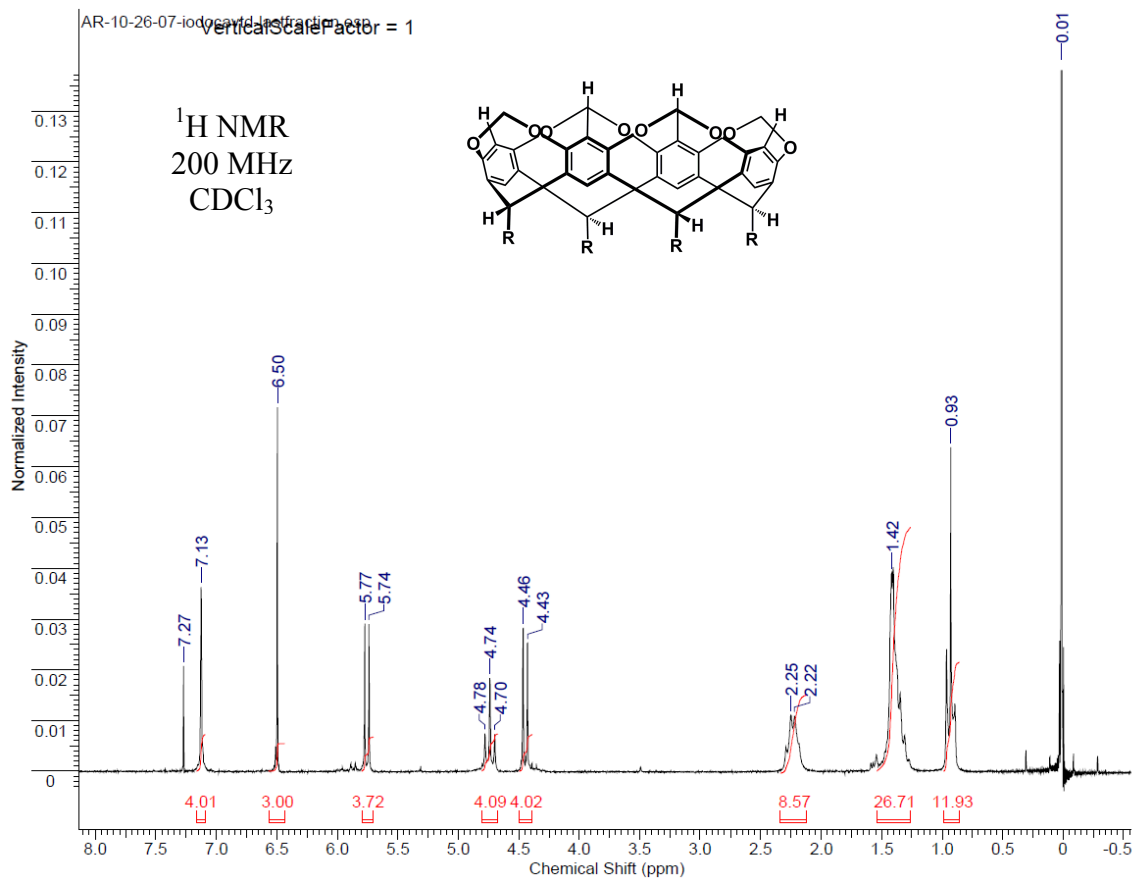


**Figure B.34** C-PentyltetraprotioCavitand, <sup>1</sup>H

35.

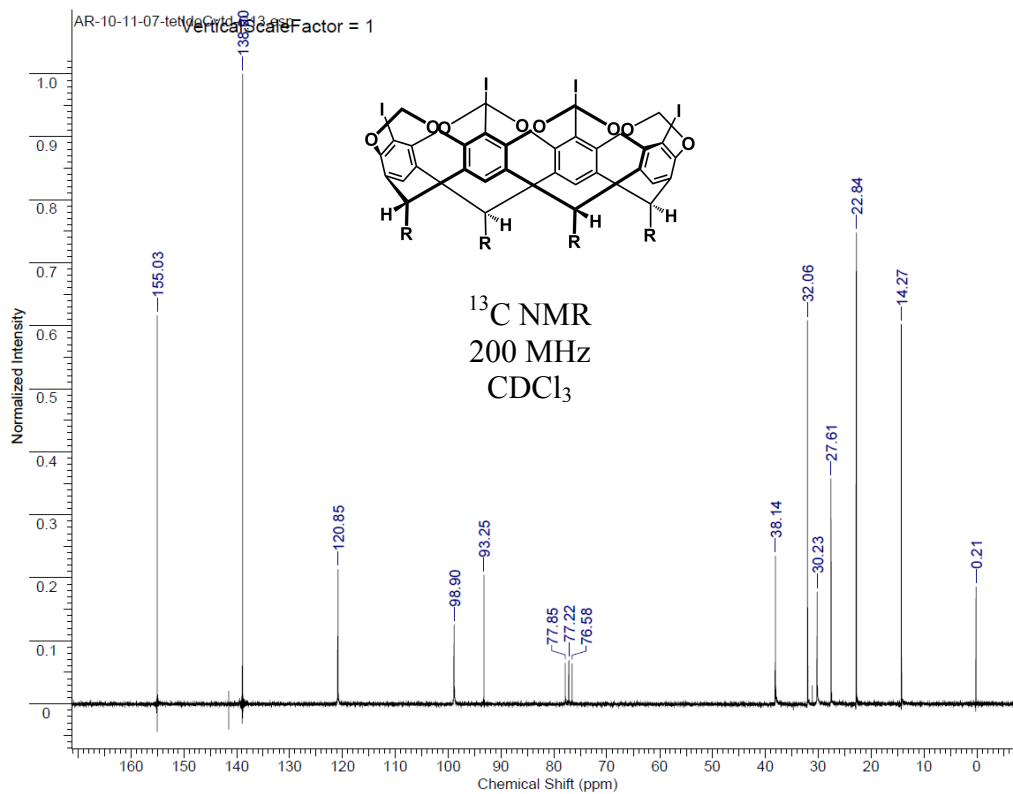
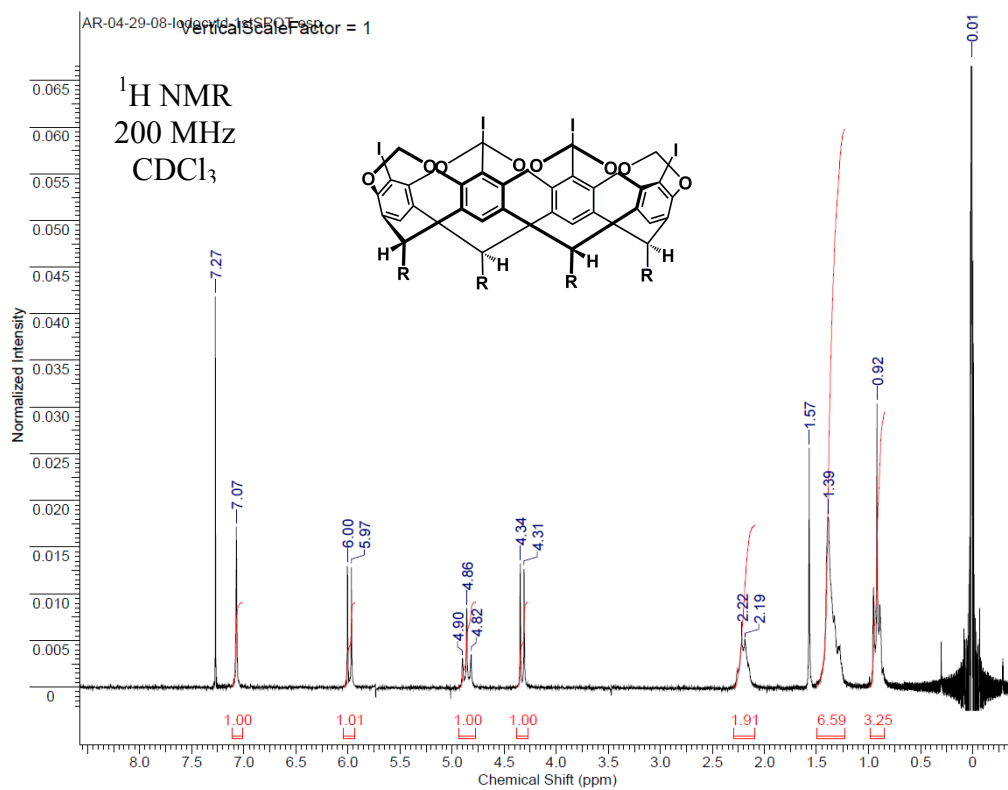
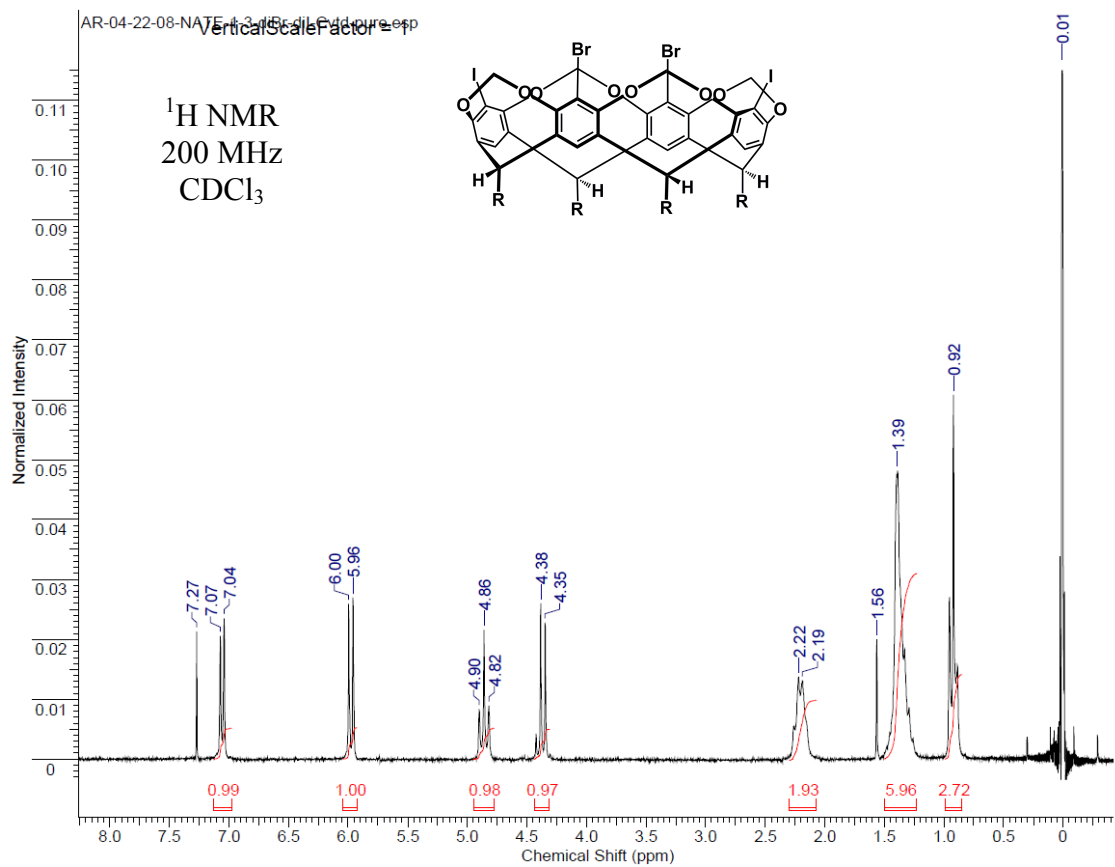
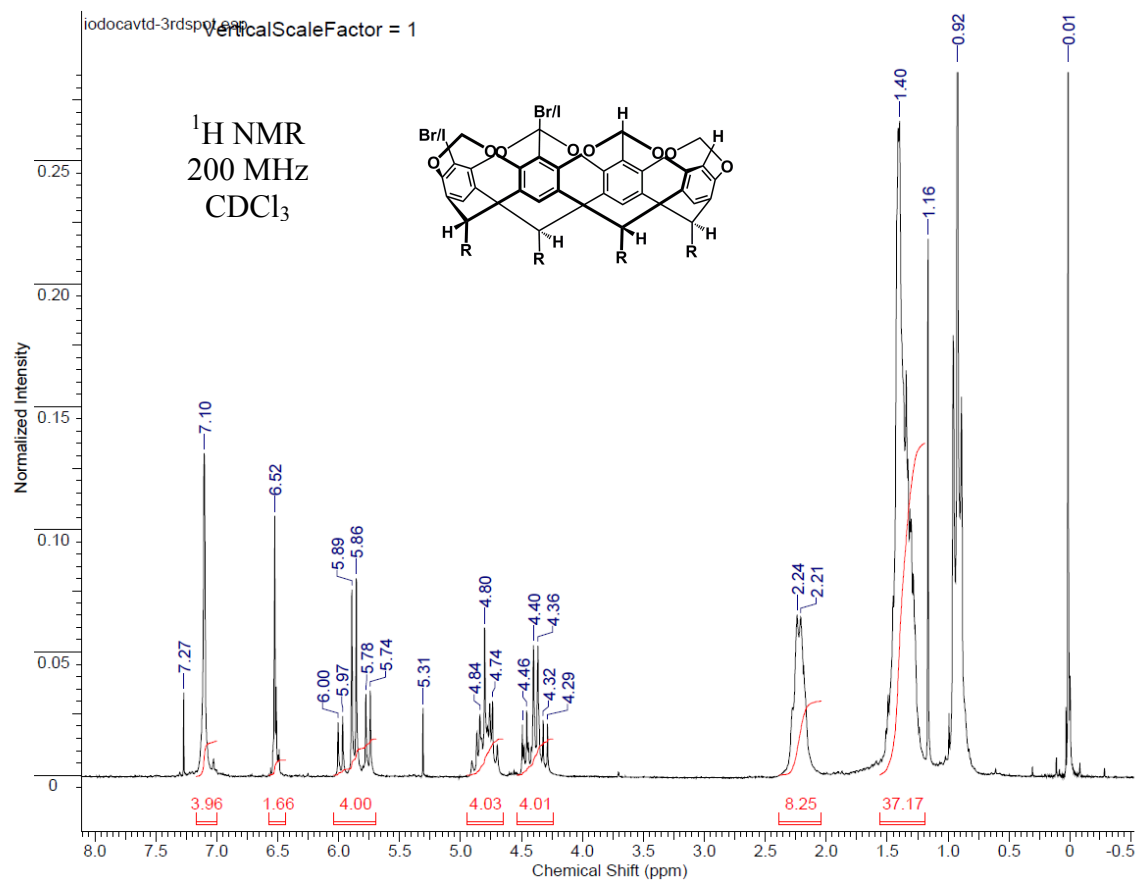


Figure B.35 C-Pentyltetraiodocavitand, **36**,  $^1\text{H}$  &  $^{13}\text{C}$



**Figure B.36** C-Pentyl-1,3-dibromo-2,4-diiodo-cavitand, **36\***,  $^1\text{H}$





**Figure B.37** C-pentyl-1,2-dibromo/diiodo-2,4-diprotiocavitand, <sup>1</sup>H

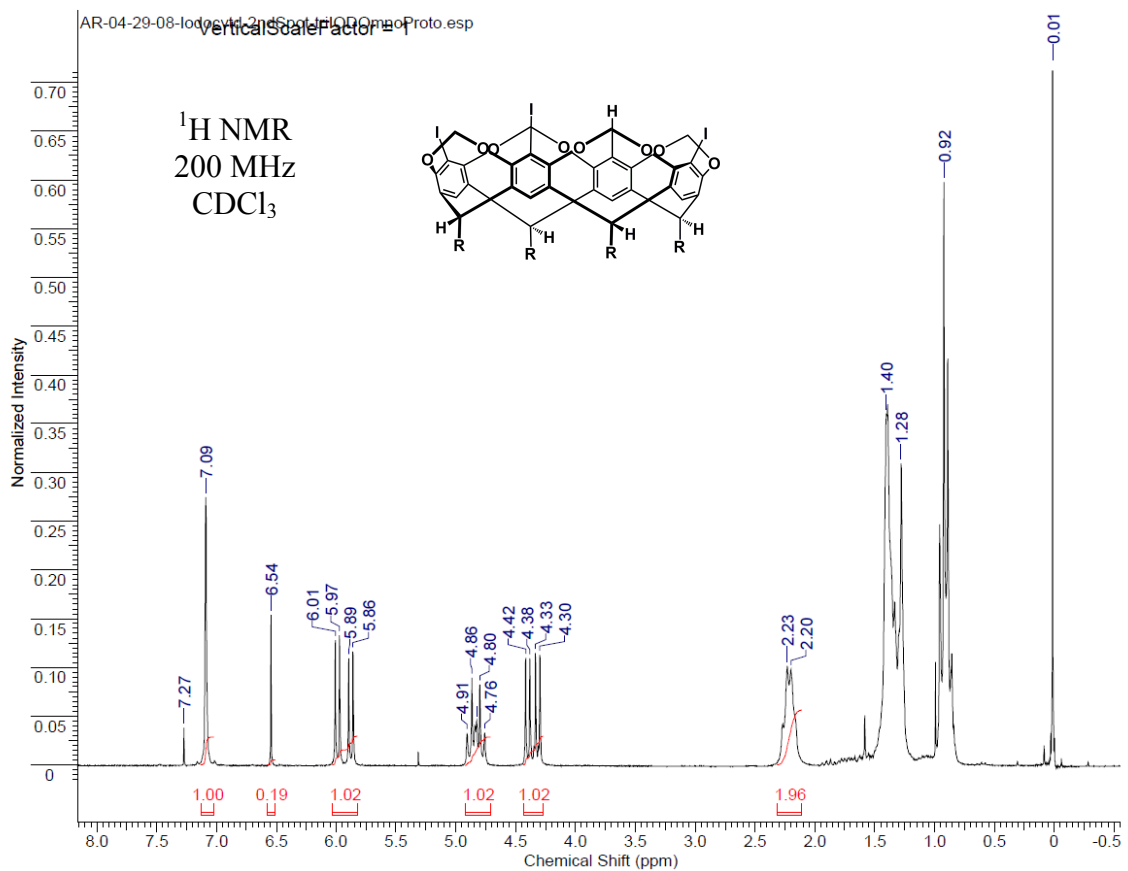


Figure B.38 C-Pentyl-triiodo-monoprotiocavitand, <sup>1</sup>H

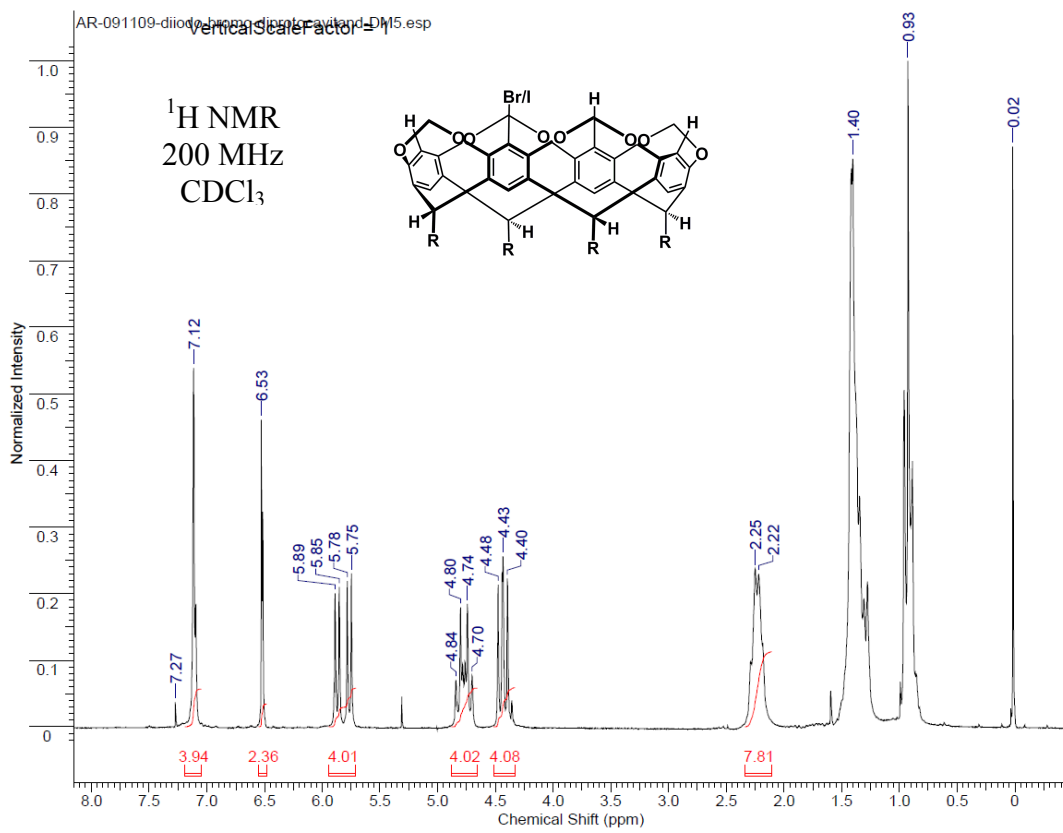
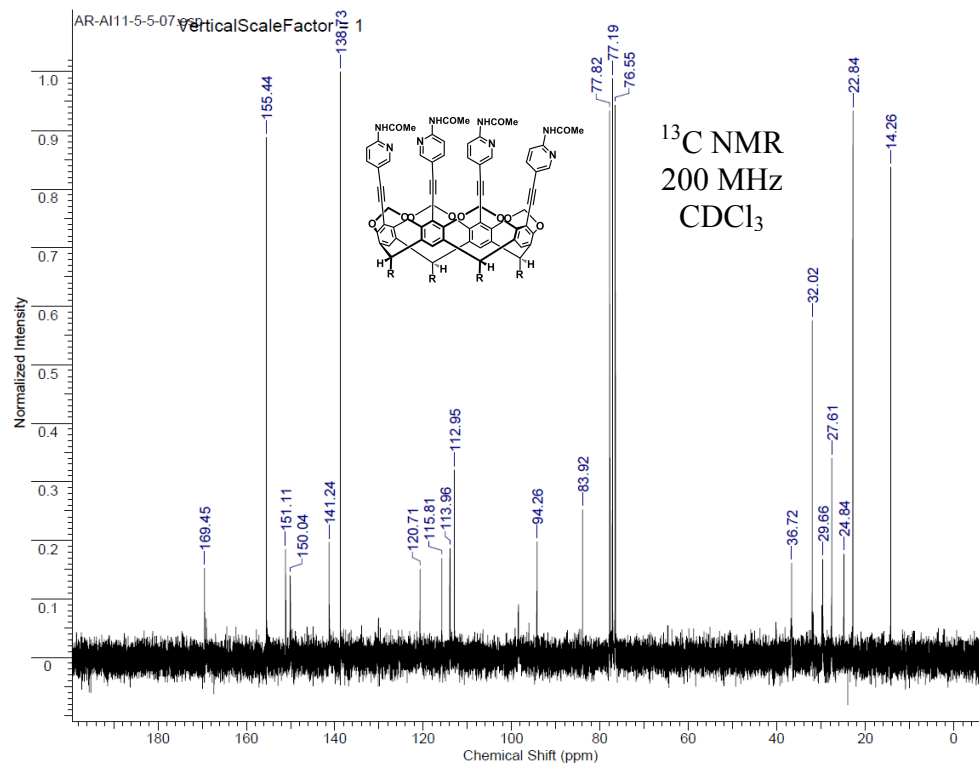
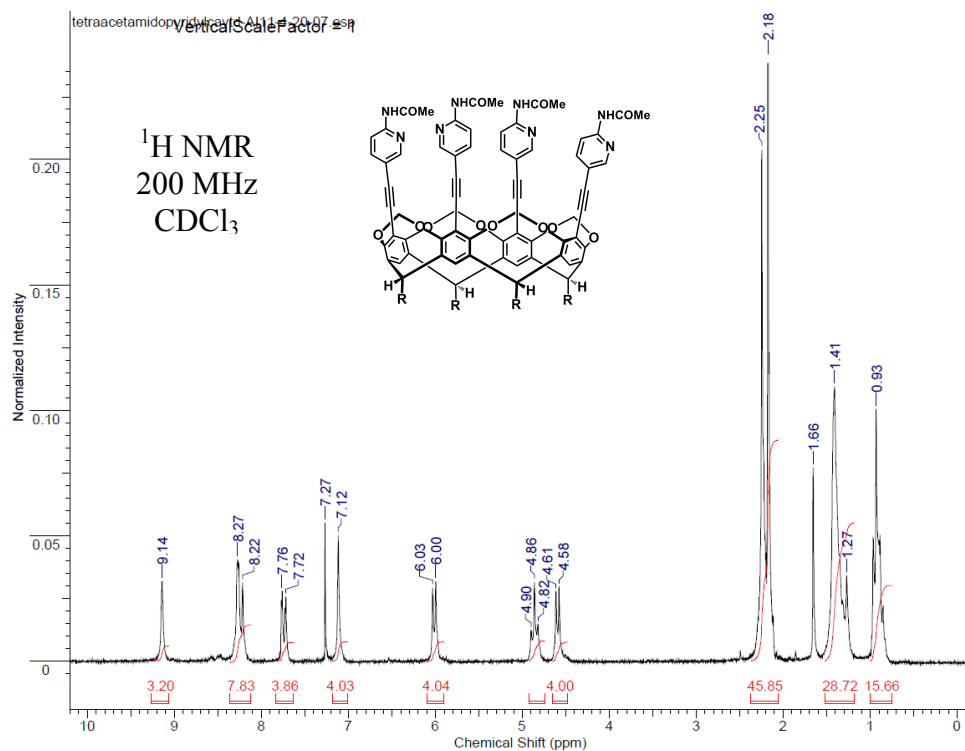
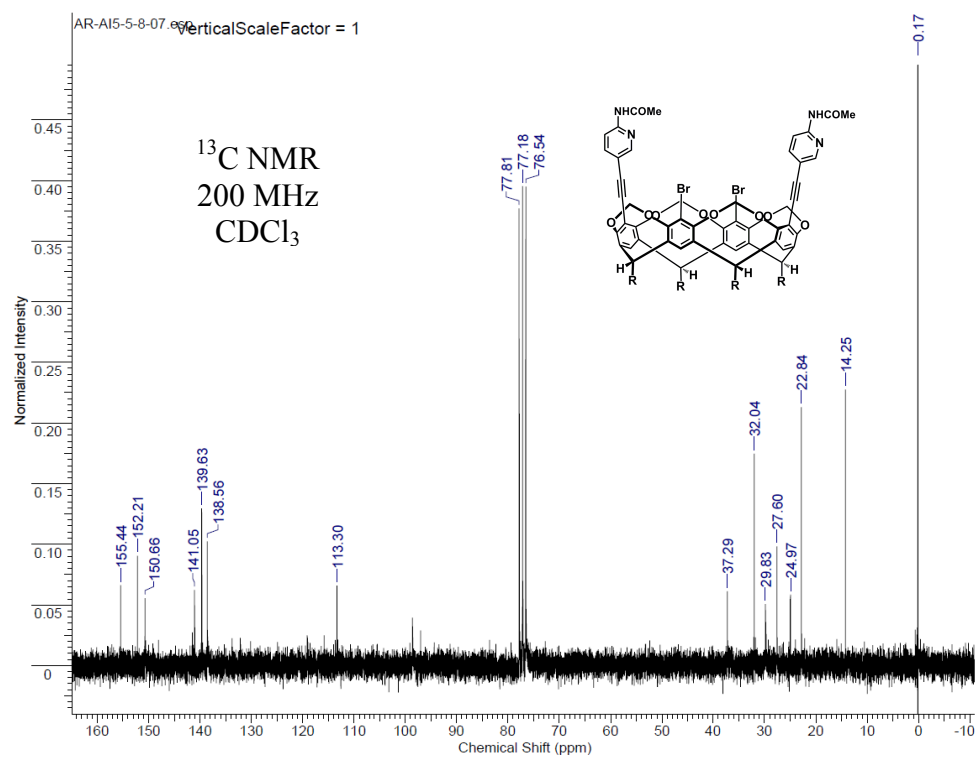
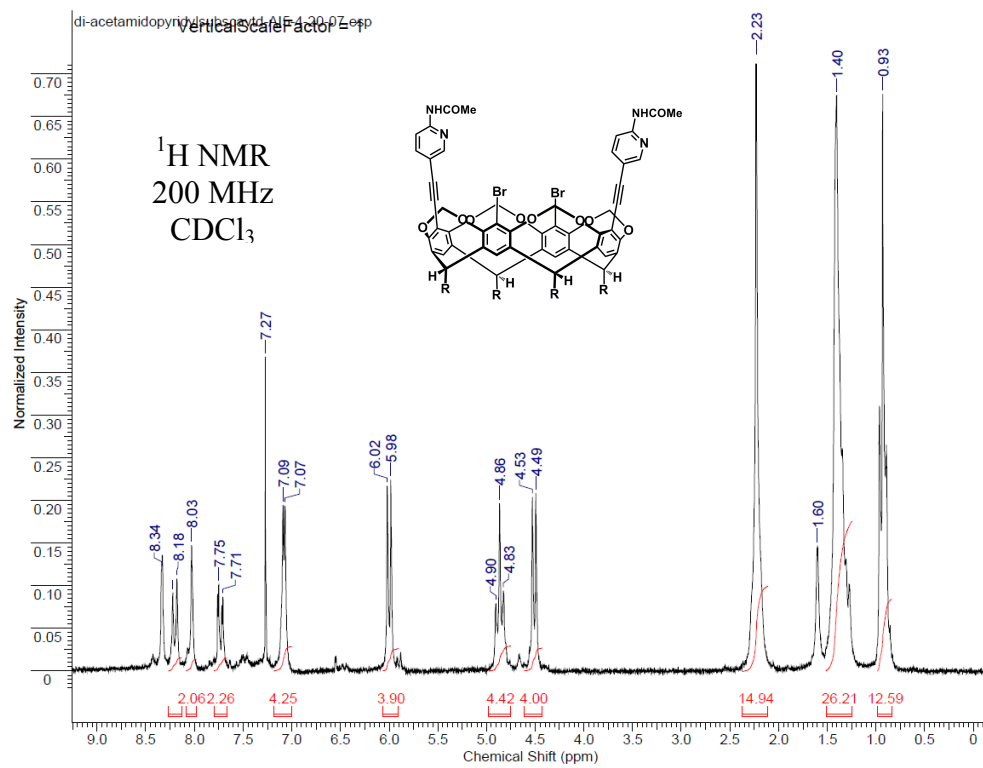


Figure B.39 C-Pentyl-monobromo/iodo-triprotiocavitand, <sup>1</sup>H



**Figure B.40** C-Pentyl-tetra-(2-acetamidopyridyl-5-ethynyl)cavitand, **37**, <sup>1</sup>H & <sup>13</sup>C



**Figure B.41** C-Pentyl-1,3-di-(2-acetamidopyridyl-5-ethynyl)-2,4-bibromocavitand, **38**,  
<sup>1</sup>H & <sup>13</sup>C

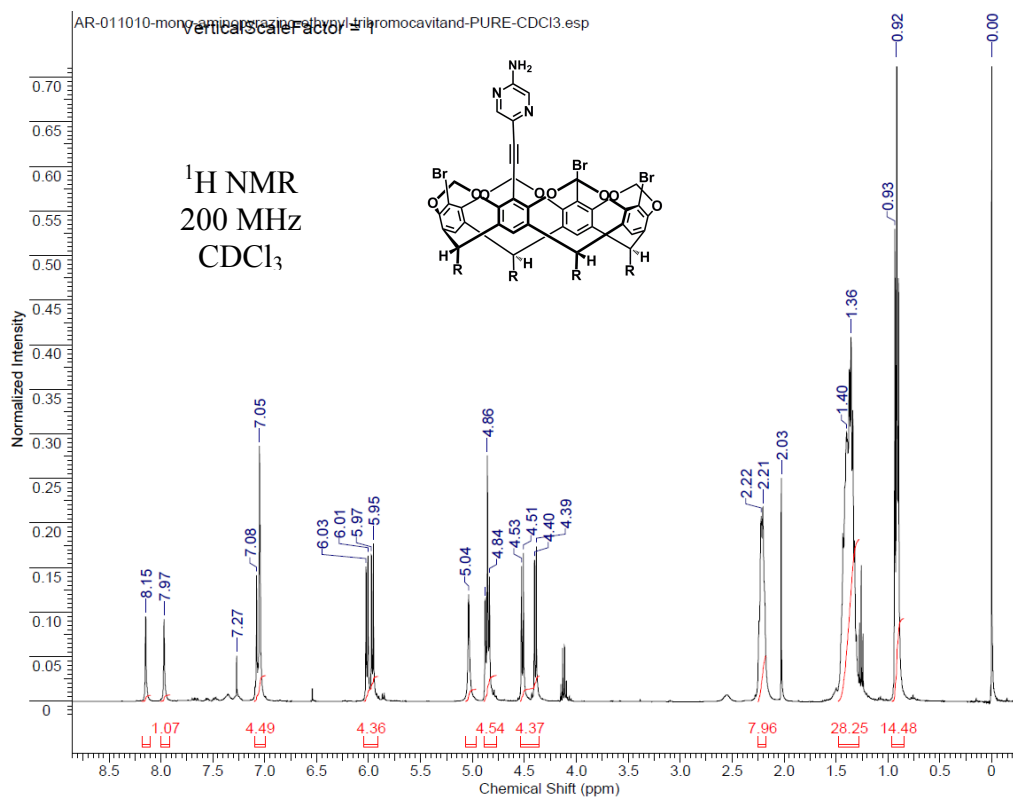


**Figure B.42** C-Pentyl-mono-(2-aminopyrazino-5-ethynyl)-tribromocavitand, <sup>1</sup>H



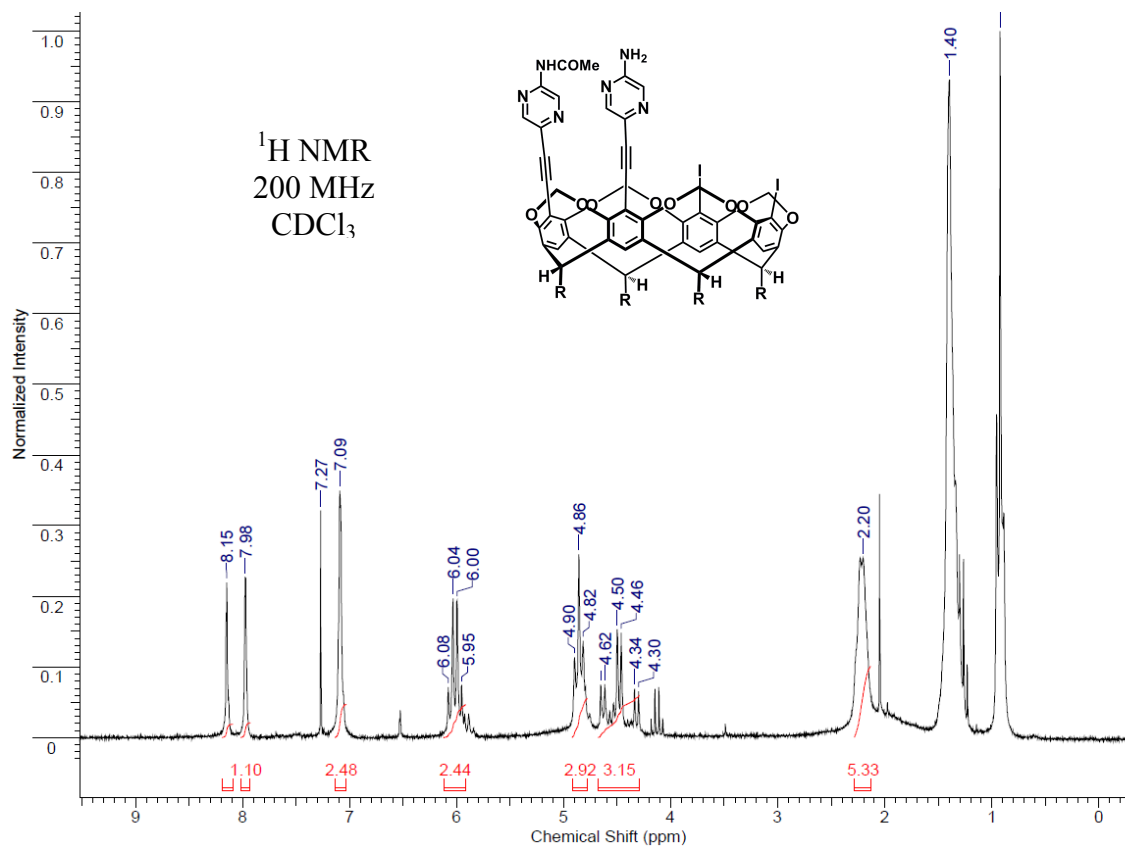


**Figure B.44** C-Pentyl-1,2-di(2-aminopyrazino-5-ethynyl)-3,4-diiodocavitand, <sup>1</sup>H



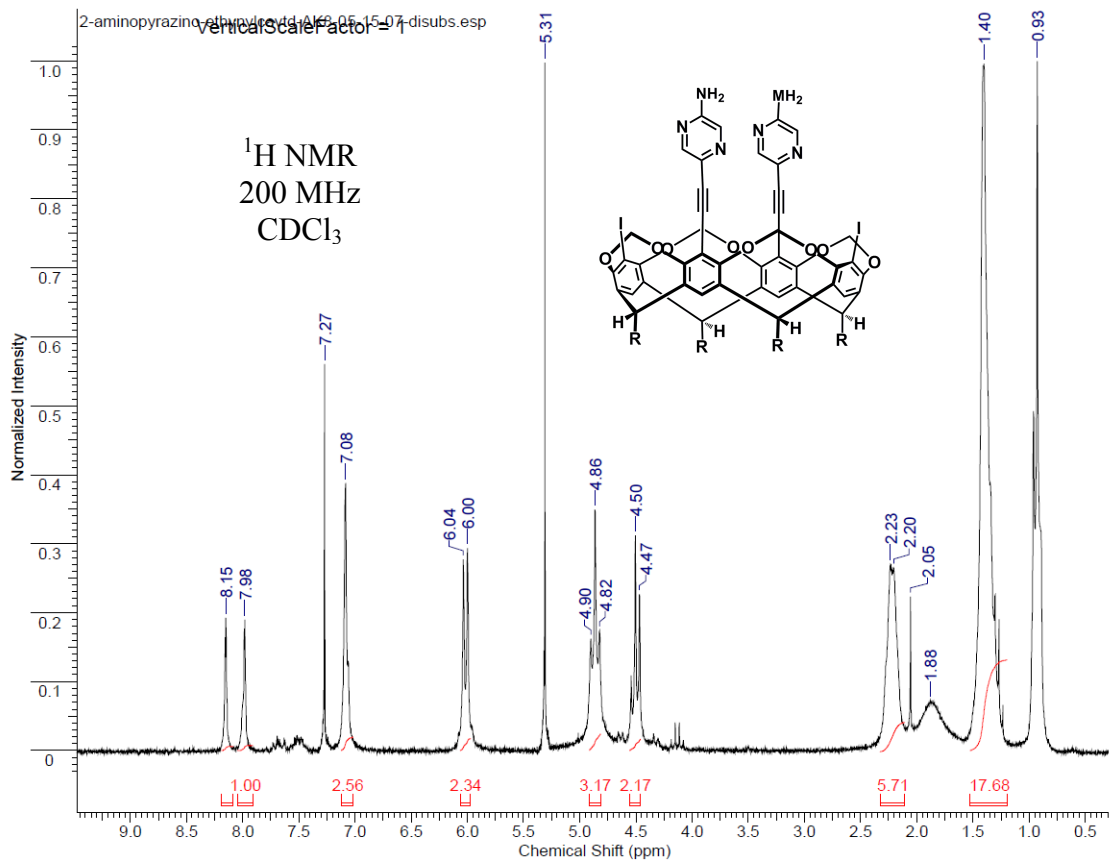


**Figure B.45** C-Pentyl-1,3-di(2-aminopyrazino-5-ethynyl)-2,4-diiodocavitand, **39**, <sup>1</sup>H

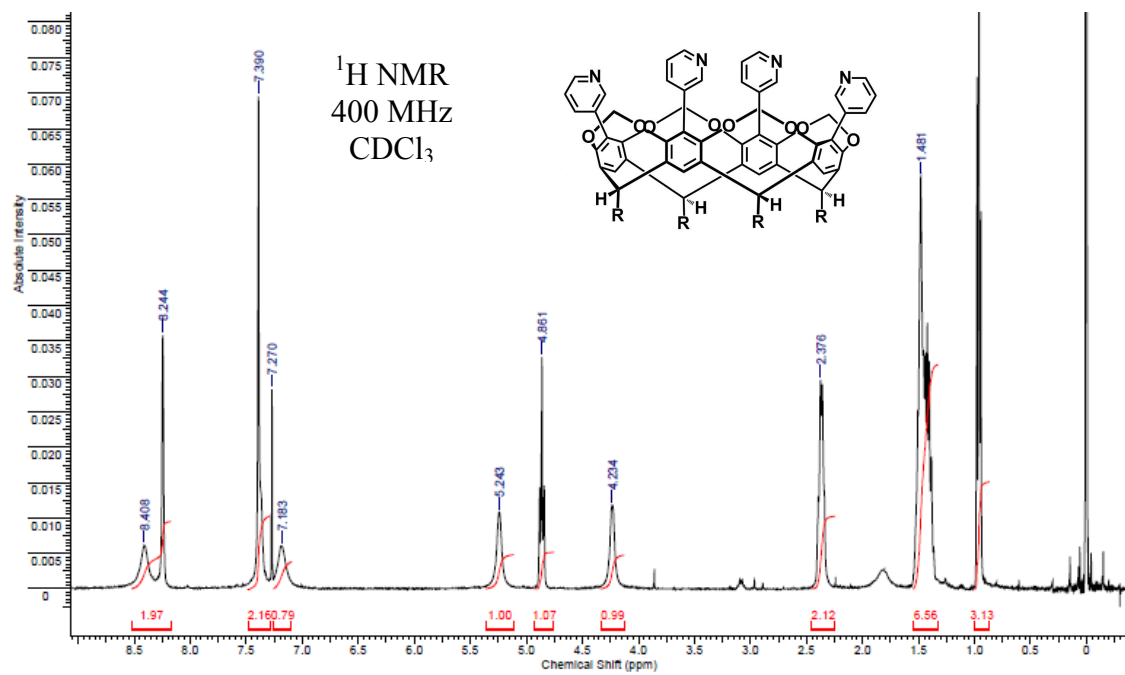


Figure B.46 C-Pentyltetra(3-pyridyl)cavitand, **40**,  $^1\text{H}$

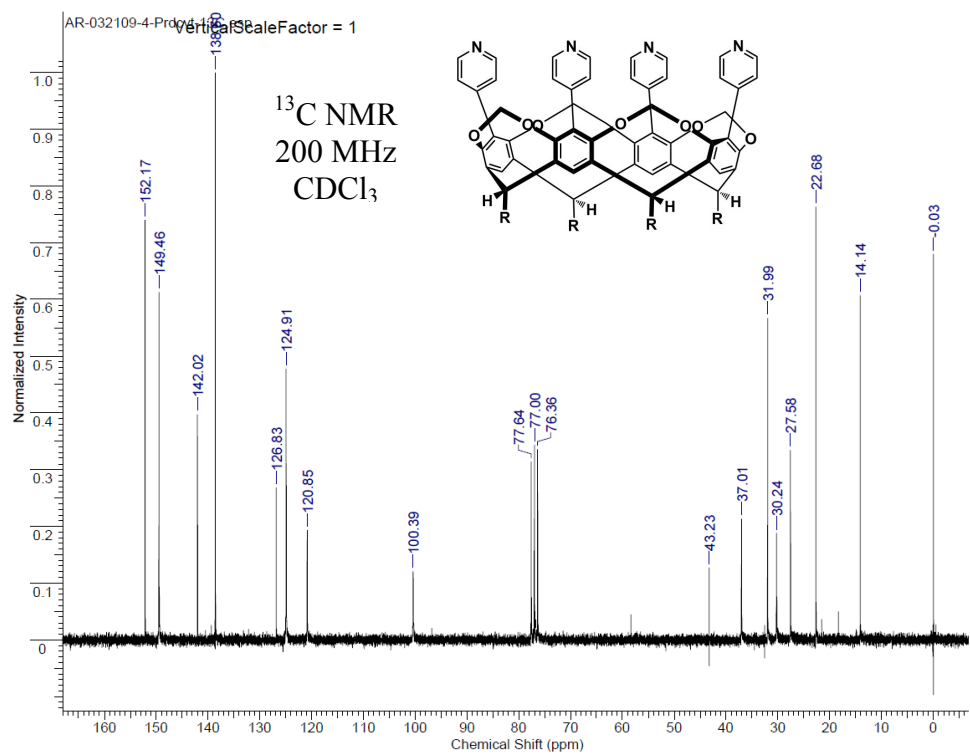
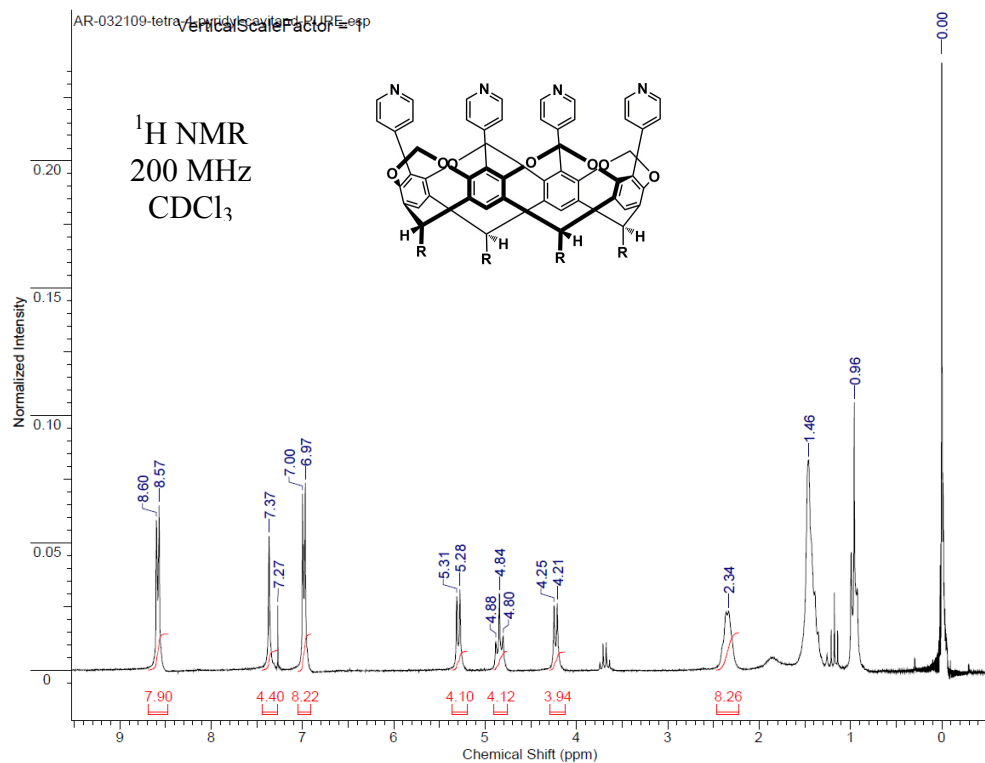


Figure 6.47 C-Pentyltetra(4-pyridyl)cavitand, **41**, <sup>1</sup>H & <sup>13</sup>C

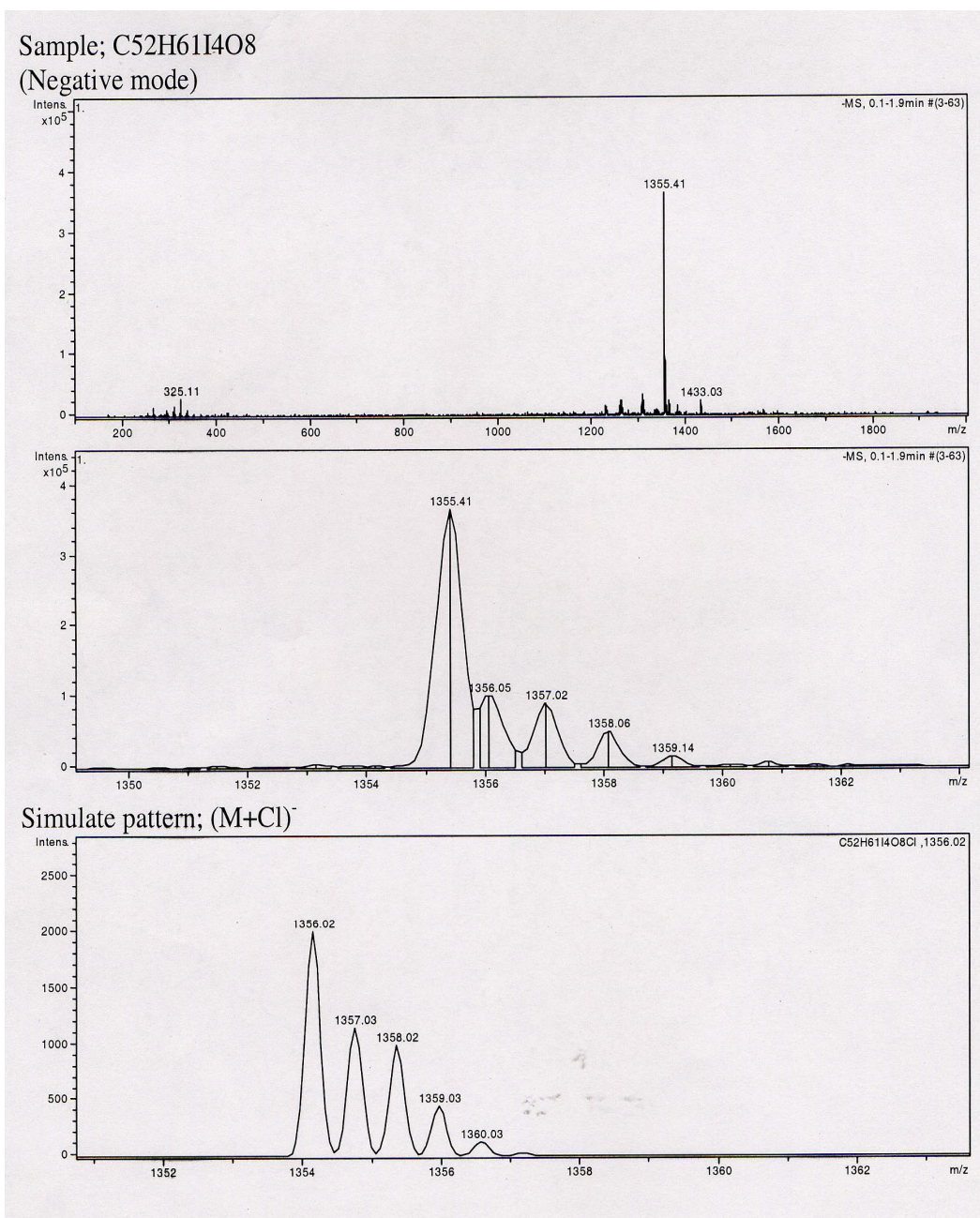
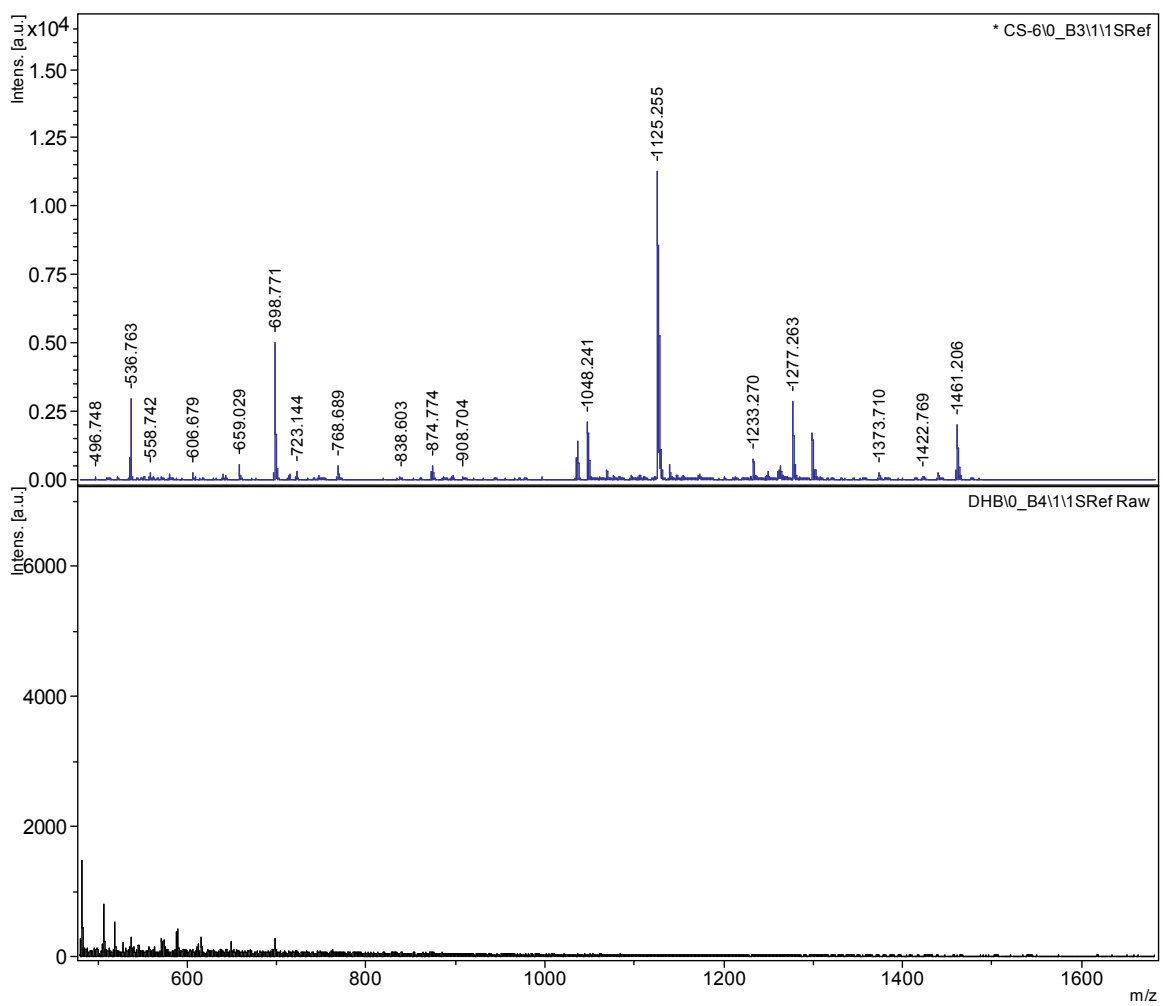


Figure B.48 Mass Spectra of C-Pentyltetraiodocavitand, **36**



**Figure B.49** Mass Spectra of C-Pentyltetra(4-pyridyl)cavitand, **41**